

AD-A171 218

DEPOLARIZATION AND SCATTERING OF ELECTROMAGNETIC WAVES
APPENDICES (U) NEBRASKA UNIV LINCOLN E SAHAR 38 JUN 86
ARO-18128.17-EL-APP DRAC29-82-K-0123

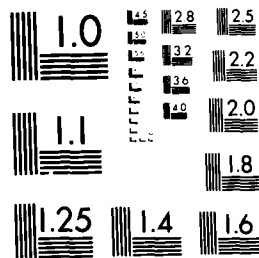
1/5

UNCLASSIFIED

F/C 20/14

NL





MICROCOPY RESOLUTION TEST CHART
NATIONAL BUREAU OF STANDARDS-1963-A

AD-A171 218

ARO 18/20.17-EL



DEPOLARIZATION AND SCATTERING
OF ELECTROMAGNETIC WAVES.

FINAL REPORT

APPENDICES

EZEKIEL BAHAR
PRINCIPAL INVESTIGATOR

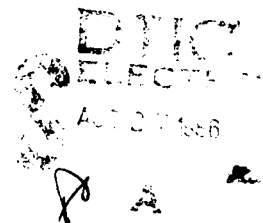
JUNE 30, 1986

U. S. ARMY RESEARCH OFFICE

CONTRACT/GRANT NUMBER
DAAG29-82-K-0123

UNIVERSITY OF NEBRASKA-LINCOLN

APPROVED FOR PUBLIC RELEASE;
DISTRIBUTION UNLIMITED.



(TWENTY COPIES REQUIRED)

1. ARO PROPOSAL NUMBER: _____
2. PERIOD COVERED BY REPORT: May 17, 1982 - Dec. 31, 1982
3. TITLE OF PROPOSAL: "Depolarization and Scattering of Electromagnetic Waves by Objects of Irregular Shape and Finite Conductivity--Full Wave Solutions"
4. CONTRACT OR GRANT NUMBER: DAAG-29-K-0123
5. NAME OF INSTITUTION: University of Nebraska-Lincoln
6. AUTHOR(S) OF REPORT: Ezekiel Bahar
7. LIST OF MANUSCRIPTS SUBMITTED OR PUBLISHED UNDER ARO SPONSORSHIP DURING THIS PERIOD, INCLUDING JOURNAL REFERENCES:
(see attached list)
8. SCIENTIFIC PERSONNEL SUPPORTED BY THIS PROJECT AND DEGREES AWARDED DURING THIS REPORTING PERIOD:
Dr. W. B. Campbell
Dr. P. F. Wahid
C. E. Grant
S. Chakrabarti
Dr. Ezekiel Bahar
University of Nebraska-Lincoln
Lincoln, Nebraska 68588-0511

7. LIST OF MANUSCRIPTS SUBMITTED OR PUBLISHED UNDER ARO SPONSORSHIP
DURING THIS PERIOD, INCLUDING JOURNAL REFERENCES:

1. Backscatter Cross Sections for Randomly Oriented Metallic Flakes at Optical Frequencies-Full Wave Approach, E. Bahar and Mary Ann Fitzwater, a full length paper submitted for internal review to the U.S. Army Armament Research and Development Command, Chemical Systems Laboratory, Aberdeen Proving Ground, Maryland.
2. Backscatter Cross Sections for Randomly Oriented Metallic Flakes at Optical Frequencies-Full Wave Approach, E. Bahar and Mary Ann Fitzwater, paper presented at the National Radio Science Meeting, Jan. 5-7, 1983, Boulder, Colorado.
3. Modulation of the Scattering Cross Sections by Arbitrarily Oriented Composite Rough Surfaces-Full Wave Approach, E. Bahar, C.F. Rufenach, D.E. Barrick and M.A. Fitzwater, a paper submitted for presentation at the International Geoscience and Remote Sensing Symposium and National Radio Science Commission F Meeting, Aug. 31-Sept. 2, 1983, San Francisco, California.



A-1

1. Backscatter Cross Sections for Randomly Oriented Metallic Flakes at Optical Frequencies.

The purpose of this investigation is to determine the average normalized backscatter cross sections for randomly oriented metallic flakes. The irregular shaped flake is characterized by its surface height spectral density function and its lateral dimension is assumed to be larger than both the wavelength of the incident electromagnetic field and the correlation distance of the rough surface.

The full wave approach which accounts for both specular point scattering and Bragg scattering in a self-consistent manner is used to express the total cross section of the flake as a weighted sum of two cross sections. The first is associated with the large scale spectral components of the surface of the flakes and the second is associated with its small scale spectral components. It is shown that the average backscatter cross section per unit volume for the arbitrarily oriented metallic flakes considered is larger than that for metallic spheres. Thus, the irregularly shaped flakes could be significantly better obscurants than metallic spheres, for a given volume of particles. The cross sections for the metallic flakes are also compared with the cross sections for similar flakes characterized by either a small scale roughness or by a large scale roughness.

2. Backscatter Cross Sections for Metallic Spheres with Rough Surfaces.

Since the small scale roughness of the surface contributes significantly to the scattering cross sections, the full wave approach described in item #1 is currently being applied to the problem of scattering by spheres with small scale rough surfaces.

3. Modulation of Scattering Cross Sections by Arbitrarily Oriented Composite Rough Surfaces.

In this work the full wave approach is used to determine the modulations of the like and cross polarized cross sections for composite models of rough surfaces illuminated by Synthetic Aperture Radars.

4. Multiple Scattering.

We have decided to analyze multiple scattering using the equation of radiative transfer with the general Stokes' parameters. Our ultimate goal is to develop codes which will allow us to compute multiple scattering for a variety of particle shapes and orientations.

PROGRESS REPORT #2
(TWENTY COPIES REQUIRED)

1. ARO PROPOSAL NUMBER: _____
2. PERIOD COVERED BY REPORT: Jan. 1, 1983--June 30, 1983
3. TITLE OF PROPOSAL: Depolarization and Scattering of Electromagnetic Waves
by Objects of Irregular Shape and Finite Conductivity-Full Wave Solution
4. CONTRACT OR GRANT NUMBER: DAAG-29-K-0123
5. NAME OF INSTITUTION: University of Nebraska-Lincoln
6. AUTHOR(S) OF REPORT: Ezekiel Bahar
7. LIST OF MANUSCRIPTS SUBMITTED OR PUBLISHED UNDER ARO SPONSORSHIP
DURING THIS PERIOD, INCLUDING JOURNAL REFERENCES:

See Attached List

8. SCIENTIFIC PERSONNEL SUPPORTED BY THIS PROJECT AND DEGREES AWARDED
DURING THIS REPORTING PERIOD:

Dr. W. B. Campbell (Faculty Associate)

Dr. P. F. Wahid (Post Doctoral Associate)

S. Chakrabarti (Graduate Assistant)

Dr. Ezekiel Bahar 18120-EL
University of Nebraska
Department of Electrical Engineering
Lincoln, NE 68588 -0511

7. LIST OF MANUSCRIPTS SUBMITTED OR PUBLISHED UNDER ARO SPONSORSHIP DURING THIS PERIOD, INCLUDING JOURNAL REFERENCES:

1. Scattering Cross Section Modulation for Arbitrarily Oriented Composite Rough Surfaces--Full Wave Solutions (E. Bahar, C. L. Rafenach, D. E. Barrick and M. A. Fitzwater, full length paper was submitted to project monitor and to Radio Science for review. This paper has been accepted for publication in Radio Science (copy enclosed).
2. Presented paper at CSL Scientific Conference on Obscuration and Aerosol Research (June 20-24, 1983). Visited Drs. E. Stuebing and J. Enbury, Chemical Systems Laboratory, Aberdeen, Maryland. Title of paper, "Scattering Cross Sections for Large Finitely Conducting Spheres with Rough Surfaces--Full Wave Solutions (copy enclosed).
3. Modulation of Scattering Cross Sections for Arbitrarily Oriented Composite Rough Surfaces--Full Wave Approach, to be published in Proceedings of the 1983 Joint Meeting of the IEEE Geoscience and Remote Sensing Society and URSI/USNC--Commission F, August 31--September 2, 1983, San Francisco, California (copy enclosed).
4. Scattering and Depolarization by Large Conducting Spheres with Very Rough Surfaces. Paper submitted for presentation at the URSI Meeting, January 1984, Boulder, Colorado (copy enclosed).
5. Optimum Backscatter Cross Section of the Ocean as Measured by Synthetic Aperture Radars. Paper submitted for presentation at the URSI (Radio Science International Union) Commission F Symposium and Workshop, Israel May 14-23, 1984 (copy enclosed).

BRIEF OUTLINE OF RESEARCH FINDINGS

1. Scattering and Depolarization by Large Conducting Spheres with Very Rough Surfaces.

The purpose of this investigation is to determine the like and cross polarized scattering cross sections for electrically large finitely conducting spheres with very rough surfaces. Perturbation theory has been used to determine electromagnetic scattering by spheres with random rough surfaces provided that the parameter $\beta = 4k_0^2 \langle h^2 \rangle$ is much smaller than unity (where k_0 is the wavenumber and $\langle h^2 \rangle$ is the mean square height of the rough surface of the sphere). However, for large conducting spheres with $\beta \ll 1$, the total scattering cross sections are not significantly different from the physical optics cross section for smooth (unperturbed) conducting spheres.

In this work the full wave approach is used to determine the scattering cross sections for large spheres with roughness scales that significantly modify the total cross sections. The full wave approach accounts for specular point scattering and Bragg scattering in a self consistent manner and the total scattering cross sections are expressed as weighted sums of two cross sections. The results are compared with earlier solutions based on the perturbation approach and a recent reformulated current method.

2. Scattering Cross Sections of Arbitrarily Oriented Composite Rough Surfaces.

This investigation is an extension of the earlier work on scattering by randomly oriented metallic flakes at optical frequencies. Full wave solutions are derived for a relatively small area or resolution cell of the rough surface that is effectively illuminated by a Synthetic Aperture Radar. The relative modulations of the like polarized cross sections are optimum for incident angles between 10° and 15° depending on the lateral dimensions of the resolution cell and the polarization.

3. Multiple Scattering.

The preliminary results obtained for multiple scattering are for (electrically) large finitely conducting spheres. The standard equation of transfer for the diffuse intensity is used in these calculations. The effects of the rough surface of the sphere has not yet been included in this analysis. This will be done upon completion of the numerical work associated with the investigation reported in item #1 above.

4. Visited U. S. Army Chemical Systems Laboratory (see Item 7.2).

PROGRESS REPORT #3

19

(TWENTY COPIES REQUIRED)

1. ARO PROPOSAL NUMBER: _____
2. PERIOD COVERED BY REPORT: July 1, 1983 - Dec. 31, 1983
3. TITLE OF PROPOSAL: Depolarization and Scattering of Electromagnetic Waves by Objects of Irregular Shape and Finite Conductivity-Full Wave Solution
4. CONTRACT OR GRANT NUMBER: DAAG-29-K-0123
5. NAME OF INSTITUTION: University of Nebraska-Lincoln
6. AUTHOR(S) OF REPORT: Ezekiel Bahar
7. LIST OF MANUSCRIPTS SUBMITTED OR PUBLISHED UNDER ARO SPONSORSHIP DURING THIS PERIOD, INCLUDING JOURNAL REFERENCES:

See Attached List

8. SCIENTIFIC PERSONNEL SUPPORTED BY THIS PROJECT AND DEGREES AWARDED DURING THIS REPORTING PERIOD:
 - Dr. L. Lipsky (Faculty Associate)
 - Dr. P. F. Wahid (Post Doctoral Associate)
 - Dr. Mary Ann Fitzwater (Post Doctoral Associate)
 - S. Chakrabarti (Graduate Assistant)

7. LIST OF MANUSCRIPTS SUBMITTED OR PUBLISHED UNDER ARO SPONSORSHIP DURING THIS PERIOD, INCLUDING JOURNAL REFERENCES:

(7.1) Journal Publications - Reprints

1. Scattering Cross Section Modulation for Arbitrarily Oriented Composite Rough Surfaces-Full Wave Approach (E. Bahar, C. L. Rufenach, D. E. Barrick and M. A. Fitzwater), Radio Science, Volume 18, Number 5, pages 675-690, September-October 1983.
2. Backscatter Cross Sections For Randomly Oriented Metallic Flakes at Optical Frequencies: Full Wave Approach (E. Bahar and M.A. Fitzwater), Applied Optics, Vol. 23, pages 3813-3819, December 1, 1983.
3. Optimum Backscatter Cross Section of the Ocean as Measured by Synthetic Aperture Radars, Paper to be presented at the URSI (Radio Science International Union) Commission F. Symposium and Workshop, Israel May 14-23, 1984.

(7.2) Papers Presented at Technical Meetings

1. Scattering and Depolarization By Large Conducting Spheres With Very Rough Surfaces (E. Bahar and Swapn Chakrabarti). Paper presented at the URSI Meeting, January 1984, Boulder, Colorado (copy enclosed).

1. Scattering and Depolarization by Large Conducting Spheres With Very Rough Surfaces

The albedo and the like and cross polarized scattering cross sections have been determined at optical frequencies for electrically large finitely conducting spheres with very rough surfaces. (The radius vector to the surface of the rough sphere is assumed to be $\mathbf{r} = \mathbf{r}_0 + \mathbf{h}$ where r_0 is the mean radius and h is a random variable.) The total scattering cross sections for slightly rough conducting spheres ($\beta \ll 1$) are not significantly different from the physical optics cross sections for smooth ($\beta = 0$) conducting spheres and perturbation theory is applicable. The roughness scale is $\beta = 4k^2 \langle h^2 \rangle$, where k is the wavenumber and $\langle h^2 \rangle$ is the mean square height of the rough surface that is superimposed on the smooth sphere of radius r_0 . However for roughness scales $\beta = k^2 \langle h^2 \rangle \gg 1$, the albedo and the like and cross polarized scattering cross sections differ significantly from their respective values for smooth spheres ($\beta = 0$). In this case the perturbation method fails and the full wave approach is used. Comparisons between the full wave solution and the perturbation solution are given for $\beta = 0.1, 0.5$ and 1.0 . The mean radius of the sphere is $r_0 = 10\lambda$ where $\lambda = 0.555 \times 10^{-4}$ cm is the electromagnetic wavelength. The relative dielectric coefficient (ϵ_r) for aluminum is assumed in this work. The albedo and scattering cross sections are currently being evaluated for other particle sizes at different frequencies. This work is being coordinated with the Aerosol/Obscuration group of the Army Chemical Systems Laboratory, Aberdeen, Maryland.

2. Scattering and Depolarization by Large Diameter Infinitely Long Conducting Cylinders with Very Rough Surfaces.

The albedo and the like and cross polarized scattering cross sections for long finitely conducting rough cylinders are evaluated at optical frequencies using the full wave approach. The radius vector to the surface of the rough cylinder is $\mathbf{r} = \mathbf{r}_0 + \mathbf{h}$ where r_0 is the mean radius ($r_0 > \lambda$) and h is the rough surface height, a random variable which depends on the azimuth angle.⁵ Both normal and oblique incidence are considered. The full wave solution which accounts for specular and diffuse scattering in a self consistent manner is compared with the perturbation solution for different roughness scales β .

3. Multiple Scattering.

Multiple scattering from slabs consisting of large conducting spherical scatterers (see item #1) is analyzed using the equation of radiative transfer with the generalized Stokes parameters. The transmitted and reflected diffuse intensities are evaluated for polarized plan waves incident upon slabs of different optical thicknesses. The effects of the rough surface of the sphere will also be included in this analysis. For smooth spherical scatterers only two elements of the Mueller matrix need to be evaluated (related to the like polarized cross sections reported in item #1). However for the spheres with rough surfaces all sixteen elements of the Mueller matrix have to be evaluated.

PROGRESS REPORT #4

(TWENTY COPIES REQUIRED)

1. ARO PROPOSAL NUMBER: _____
2. PERIOD COVERED BY REPORT: January 1, 1984 — June 30, 1984
3. TITLE OF PROPOSAL: "Depolarization and Scattering of Electromagnetic Waves by Objects of Irregular Shape and Finite Conductivity—Full Wave Solutions."
4. CONTRACT OR GRANT NUMBER: DAAG-29-82-0123
5. NAME OF INSTITUTION: University of Nebraska-Lincoln
6. AUTHOR(S) OF REPORT: Ezekiel Bahar
7. LIST OF MANUSCRIPTS SUBMITTED OR PUBLISHED UNDER ARO SPONSORSHIP DURING THIS PERIOD, INCLUDING JOURNAL REFERENCES:

(See Attached List)
8. SCIENTIFIC PERSONNEL SUPPORTED BY THIS PROJECT AND DEGREES AWARDED DURING THIS REPORTING PERIOD:
Dr. Mary Ann Fitzwater (Post Doctoral Associate)
S. Chakrabarti (Graduate Assistant)

Dr. Ezekiel Bahar 18120-EL
University of Nebraska
Department of Electrical Engineering
Lincoln, NE 68588

7. LIST OF MANUSCRIPTS SUBMITTED OR PUBLISHED UNDER ARO SPONSORSHIP DURING THIS PERIOD, INCLUDING JOURNAL REFERENCES:

(7.1) Submitted for Review:

1. "Scattering and Depolarization by Large Conducting Spheres with Rough Surfaces."
2. "Scattering by Anisotropic Models of Composite Rough Surfaces--Full Wave Solutions."

(7.2) Papers Presented at Technical Meetings:

1. Union of Radio Science Meeting, at the University of Colorado-Boulder, January 11-13, 1984, "Scattering and Depolarization by Large Conducting Spheres with Very Rough Surfaces."
2. International Union of Radio Science Meeting at Saresh, Israel, May 14-23, 1984, "Optimum Backscatter Cross Sections of the Ocean as Measured by Synthetic Aperture Radars."
3. 1984 CSL Scientific Conference on Abscuration and Aerosol Research, Aberdeen, Maryland, June 25-29, 1984, "Scattering by Finitely Conducting Cylinders with Rough Surfaces."

(7.3) Reprints of Published Papers Enclosed with Report:

1. "Backscatter Cross Sections for Randomly Oriented Metallic Flakes at Optical Frequencies--Full Wave Approach," Applied Optics, Vol. 23, pp. 3813-3819, December 1983.

1. Scattering and Depolarization by Large Conducting Spheres With Very Rough Surfaces

The initial series of computations of the like and cross polarized differential cross sections for electrically large finitely conducting smooth and rough spheres has been completed. In this work the assumed electromagnetic wavelength was $\lambda = 0.555 \mu\text{m}$ and the mean radius of the spheres $r_0 = 10\lambda$. For the wavelength considered the relative complex dielectric coefficient (aluminum) is $\epsilon_r = -40 - i12$. For the perfect spheres (with smooth surfaces) the Mie solution was used and for the spheres with random rough surfaces the full wave solutions (that account for specular and diffuse scattering) were used. The roughness scale of the surface was characterized by the parameter $\beta = 4k_0^2 \langle h_s^2 \rangle$ where $k_0 = 2\pi/\lambda$ and $\langle h_s^2 \rangle$ is the mean square height of the rough surface (measured normal to the mean surface of the sphere). Values of β considered range from 0.1 to 1.0.

The full wave solutions were compared with earlier solutions to the problem. The albedo for the rough spheres were shown to be about 10% to 15% smaller than the albedo for the smooth spheres. These values differ significantly from those obtained from perturbation solutions when $\beta > 0.1$. Following discussions with members of the Army Chemical Research Development Center (CRDC, Aberdeen, Maryland), a new series of computations were also carried out for the differential scattering cross sections. The electromagnetic wavelength assumed was $\lambda = 10 \mu\text{m}$. The values of r_0 (the mean radius of the sphere) considered range from 2λ to 7λ . The value for the complex dielectric coefficient (for $\lambda = 10 \mu\text{m}$) is $\epsilon_r = -60000(1+i)$. For the surface roughness parameter $\beta = 1.0$ several surfaces with different surface height spectral density functions $W(k)$ were considered. (The surface height spectral density function $W(k)$ is the Fourier transform of surface height autocorrelation function). For the smaller values of r_0/λ the diffuse differential scattering cross sections were found to be critically dependent upon the form of surface height spectral density function and the mean radius of the spheres.

These preliminary calculations indicate possible techniques for solving the more complicated problem of inverse scattering. Thus for instance, with an appropriate choice of the wavelength λ , the measured cross polarized differential scattering cross section $\sigma^{VH}(\theta)$ could reveal the values of the mean radius of the spheres, the roughness parameter β as well as the surface roughness spectral density function. Only a set of measurements of the cross polarized cross section for angles θ in the near forward direction would be needed for the purpose of these proposed experiments.

2. Scattering and Depolarization by Large Diameter Infinitely Long Conducting Cylinders with Very Rough Surfaces

The like and cross polarized scattering cross sections were also computed for long finitely conducting cylinders. Both electromagnetic wavelengths $\lambda = 0.555 \mu\text{m}$ and $\lambda = 10 \mu\text{m}$ were assumed and the mean diameter of the cylinders considered ranged from $d = 5\lambda$ to $d = 20\lambda$. The effect of surface roughness was also examined as in the case of the spherical particles. This work was presented at the 1984 CSL Scientific Conference on Obscuration and Aerosol Research (CRDC Aberdeen, Maryland) June 25-29. (See Item #7.2.3)

3. Multiple Scattering

Using the equation of radiative transfer for scattering by electrically large conducting spherical particles the generalized Stokes parameters have been evaluated for different thicknesses of the scattering medium. Conducting obscurants with both smooth and rough surfaces were considered. The specific diffuse intensities for vertically and horizontally polarized waves were determined for both circularly and linearly polarized incident waves. For optical thicknesses $\tau < 0.1$, effects of multiple scattering begin to become significant. The effects of particle surface roughness increase as the optical thickness τ increases and multiple scattering is not negligible. The particle surface roughness also has the effect of decreasing the degree of polarization of the scattered waves. The diffuse intensities and the degree of polarization become significantly less dependent on scatter angle when the particle surface roughness is taken into consideration.

PROGRESS REPORT

TWENTY COPIES REQUIRED

1. ARO PROPOSAL NUMBER: 18120-EL
2. PERIOD COVERED BY REPORT: 1 July 1984 - 31 December 1984
3. TITLE OF PROPOSAL: Depolarization & Scattering of
Electro-Magnetic Waves
4. CONTRACT OR GRANT NUMBER: DAAG29-82-K-0123
5. NAME OF INSTITUTION: University of Nebraska
6. AUTHORS OF REPORT: Ezekiel Bahar (Principal Investigator)
7. LIST OF MANUSCRIPTS SUBMITTED OR PUBLISHED UNDER ARO SPONSORSHIP
DURING THIS REPORTING PERIOD, INCLUDING JOURNAL REFERENCES:
See attached list.

8. SCIENTIFIC PERSONNEL SUPPORTED BY THIS PROJECT AND DEGREES AWARDED
DURING THIS REPORTING PERIOD:

In addition to Principal Investigator
Dr. Mary Ann Fitzwater (Post Doctoral Associate)
S. Chakrabarti (Graduate Assistant)

Ezekiel Bahar
Department of Electrical Engineering
University of Nebraska
Lincoln, NB 68588-0511

7. LIST OF MANUSCRIPTS SUBMITTED OR PUBLISHED UNDER ARO SPONSORSHIP
DURING THIS PERIOD, INCLUDING JOURNAL REFERENCES:

(7.1) Papers Presented at Technical Meetings

International Union of Radio Science Symposium on Radio Techniques in Planetary Exploration in Conjunction with the XXI General Assembly of URSI, Florence, Italy, August 28 - September 5, 1984. Scattering and Depolarization of Radio Waves by Rough Planetary Surfaces.

(7.2) Papers Submitted for Publication

"Scattering and Depolarization by Conducting Cylinders With Very Rough Surfaces".

(7.3) Papers Accepted for Publication

"Scattering by Anisotropic Models of Composite Rough Surfaces - Full Wave Solutions" - to be published in IEEE Transactions on Antennas and Propagation".

Scattering and Depolarization by (Electrically) Large Conducting Particles With Random Rough Surfaces

In our investigations, the irregular-shaped obscuration are assumed to have the following physical and electrical characteristics.

- (i) The deterministic (idealized) shape of the average particle is spherical or circular cylindrical.
- (ii) The actual surface of the particle is assumed to deviate from the idealized surface. The particle random rough surface is characterized by its surface height spectral density function W or the Fourier transform of W , the surface height autocorrelation function $\langle hh' \rangle$.
- (iii) The particles are characterized electrically by their relative complex dielectric coefficients ϵ_r .

The electromagnetic wavelength λ is assumed to be in the $10 \mu\text{m}$ to $0.5 \mu\text{m}$ range, and the diameter d of the (idealized) particle considered is between 5 and 15 wavelengths.

Using the full wave approach it was necessary to express the characteristic function and the joint characteristic function χ_2 of the random rough surface in terms of the roughness parameter $\beta = 4k^2 \langle h^2 \rangle$ (where $k = 2\pi/\lambda$ and $\langle h^2 \rangle$ is the mean square height of the rough surface) and a power series of the surface height autocorrelation function $\langle hh' \rangle$. For $\beta < 0.1$ only the first term of the power series expansion is significant and the diffuse scattering due to the rough surface is identified with Bragg scattering. However as the roughness parameter β increases several additional terms of the power series expansion need to be considered. (For example when β is between one and two, four terms become significant). This imposed an undesired upper bound on the value of the roughness parameter β used in our computations for the scattering cross sections of the rough particle. This limitation has now been eliminated through the use of more efficient representation of our full wave analytical results which yield algorithms that do not require power series expansions of the characteristic functions. The updated computer programs for the like and cross polarized scattering cross-sections have been tested for a family of surface height spectral density functions W with roughness parameters $\beta = 10$.

In order to compute the albedo for the irregular-shaped particles it is also necessary to evaluate the total cross sections (scattered plus absorption cross sections). For particles with relatively small roughness scales ($\beta < 1$), the surface irregularities do not significantly effect the forward scattered fields. Thus the total cross sections, for particles with small roughness scales, are essentially the same as those for the idealized (unperturbed) particles. However when $\beta > 1$, this approximation is not valid. A new approach has been developed to evaluate the albedos when β is not small. This approach exploits the fact that for large particles ($kd \gg 1$) the forward scattered field (which is related to the total cross section) is the same for all conducting particles that have the same shadow line.

During the reporting period, a copy of the manuscript on scattering and depolarization by long conducting cylinders with rough surfaces was submitted to the organizers of the 198 CLS Scientific Conference on Obscuration and Aerosol Research (CRDC Aberdeen, Maryland) (See Item #7b). The computer programs for the multiple scattering problem were updated to reflect the advances made in the computations of the scattering cross sections and the albedo of irregular particles with very large roughness scales β . Numerical results were also obtained for particles with a broad range of complex dielectric coefficients corresponding to those of artificial dielectrics such as dissipative plastic and foam materials.

PROGRESS REPORT #6

TWENTY COPIES REQUIRED

1. ARO PROPOSAL NUMBER: 18120-EL
2. PERIOD COVERED BY REPORT: 1 January 1985 - 30 June 1985
3. TITLE OF PROPOSAL: Depolarization & Scattering of
Electro-Magnetic Waves
4. CONTRACT OR GRANT NUMBER: DAAG29-82-K-0123
5. NAME OF INSTITUTION: University of Nebraska
6. AUTHORS OF REPORT: Ezekiel Bahar (Principal Investigator)

7. LIST OF MANUSCRIPTS SUBMITTED OR PUBLISHED UNDER ARO SPONSORSHIP
DURING THIS REPORTING PERIOD, INCLUDING JOURNAL REFERENCES:

See attached list.

8. SCIENTIFIC PERSONNEL SUPPORTED BY THIS PROJECT AND DEGREES AWARDED
DURING THIS REPORTING PERIOD:

In addition to Principal Investigator
Dr. Mary Ann Fitzwater (Post Doctoral Associate)
S. Chakrabarti (Graduate Assistant)

Ezekiel Bahar
Department of Electrical Engineering
University of Nebraska
Lincoln, NB 68508

7. LIST OF MANUSCRIPTS SUBMITTED OR PUBLISHED UNDER ARO SPONSORSHIP DURING THIS REPORTING PERIOD, INCLUDING JOURNAL REFERENCES:

(7.1) Papers Presented at Technical Meetings

- (i) International IEEE/APS-Symposium and 1985 North American Radio Science Meeting, Vancouver, Canada, June 17-21, 1985, "Scattering by Anisotropic Models of Composite Rough Surfaces--Full Wave Solutions."
- (ii) 1985 CRDC Scientific Conference on Obscuration and Aerosol Research, Aberdeen, Maryland, June 17-21, 1985, "Multiple Scattering in Media Consisting of Non-Spherical, Finitely Conducting Particles."

(7.2) Papers Submitted for Review by Journal Editors

- (i) "Like and Cross Polarized Scattering Cross Sections for Random Rough Surfaces--Theory and Experiment," Journal of the Optical Society of America Special Issue on "Wave Propagation and Scattering in Random Media".
- (ii) "Scattering and Depolarization by Conducting Cylinders with Rough Surfaces."

(7.3) Papers Accepted for Publication

- (i) "Scattering and Depolarization by Conducting Cylinders with Very Rough Surfaces," Proceedings of the 1984 CRDC Scientific Conference on Obscuration and Aerosol Research, DRSMC-CLJ-IV, pp. 365-371, January 1985.

(7.4) Papers Published in the Technical Literature and Submitted with This Report

- (i) "Scattering by Anisotropic Models of Composite Rough Surfaces--Full Wave Solutions," IEEE Transactions on Antennas and Propagation, Vol. AP-33, No. 1, pp. 106-112, January 1985.
- (ii) "Scattering and Depolarization by Large Conducting Spheres with Very Rough Surfaces," with S. Chakrabarti, Applied Optics, Vol. 24, No. 12, pp. 1820, June 1985.

BRIEF OUTLINE OF RESEARCH FINDINGS

Multiple Scattering by Irregular Shaped Particles of Finite Conductivity at Infrared and Optical Frequencies

The equation of transfer for a layer of randomly distributed particles has been solved for a variety of particle sizes, shapes and complex dielectric coefficients at infrared and optical frequencies. The unperturbed particle shape is assumed to be spherical and the actual random surface of the particle is characterized by its surface height spectral density function or its Fourier transform, the surface height autocorrelation function. The mean square height of the rough surface $\langle h_s^2 \rangle$ is assumed to be large ($\beta = 4k_0^2 \langle h_s^2 \rangle \gg 1$ where k_0 is the free space wavenumber). The full wave approach is used to express the scattering matrix for the irregular shaped particles as a weighted sum of two cross sections. The first is a modified contribution from the unperturbed spherical particle and the second is the diffuse contribution due to the surface roughness.

The modified Stokes parameters (incoherent specific diffuse intensities) are determined for a variety of excitations.

- (i) Circularly polarized waves normally incident upon the layer of particles. The solutions in this case are azimuthally independent.
- (ii) Linearly polarized waves normally incident upon the layer of particles.
- (iii) Vertically and horizontally polarized waves obliquely incident upon the layer of particles.

The matrix characteristic value approach was used to solve the problem. Both single scatter and multiple scatter solutions were presented and the effects of the surface roughness are demonstrated by comparing the results for irregular shaped particles with the corresponding results for smooth (spherical) particles.

Written reports on this work are currently in preparation. The principal investigator also presented a paper on "Multiple Scattering in Media Consisting of Non-Spherical, Finitely Conducting Particles" at the Chemical Research and Development Center (CRDC), Aberdeen Proving Ground Maryland, on June 21 in conjunction with the 1985 CRDC Scientific Conference on Obscuration and Aerosol Research. During this visit discussions were also held with CRDC Laboratory personnel on current and future aspects of our research program.

A list of conferences papers and journal publications during this reporting period is given in Item #7.

Enclosures: Reprints of articles: Item Nos. (7.4)(1) and (11).

PROGRESS REPORT #7

TWENTY COPIES REQUIRED

1. ARO PROPOSAL NUMBER: 18120-EL
2. PERIOD COVERED BY REPORT: 1 July 1985 - 31 December 1985
3. TITLE OF PROPOSAL: Depolarization & Scattering of
Electro-Magnetic Waves
4. CONTRACT OR GRANT NUMBER: DAAG29-82-K-0123
5. NAME OF INSTITUTION: University of Nebraska
6. AUTHORS OF REPORT: Ezekiel Bahar (Principal Investigator)
7. LIST OF MANUSCRIPTS SUBMITTED OR PUBLISHED UNDER ARO SPONSORSHIP
DURING THIS REPORTING PERIOD, INCLUDING JOURNAL REFERENCES:

See Attached List

8. SCIENTIFIC PERSONNEL SUPPORTED BY THIS PROJECT AND DEGREES AWARDED
DURING THIS REPORTING PERIOD:

In addition to Principal Investigator:
Dr. Mary Ann Fitzwater (Post Doctoral Associate)
S. Chakrabarti (Graduate Assistant)
D. Notowitz (Undergraduate Computer Programmer)

Ezekiel Bahar
Department of Electrical Engineering
University of Nebraska
Lincoln, NB 68508

7. LIST OF MANUSCRIPTS SUBMITTED OR PUBLISHED UNDER ARO SPONSORSHIP DURING THIS REPORTING PERIOD, INCLUDING JOURNAL REFERENCES:

(7.1) Papers Presented at Technical Meetings

- (i) Symposium/Workshop on Multiple Scattering of Waves in Random Media and by Random Rough Surfaces," Pennsylvania State University, University Park, Pennsylvania, July 29-August 1, 1985, "Scattering and Depolarization by Random Rough Surfaces--Unified Full Wave Approach."
- (ii) Schlumberger Workshop on Waves in Inhomogeneous Media, August 8-9, 1985, Ridgefield, Connecticut, "Unified Full Wave Solutions for Electromagnetic Scattering by Rough Surfaces--Comparison with Physical Optics, Geometric Optics and Perturbation Solutions Using Two-Scale Models of Rough Surfaces."
- (iii) 1985 Joint Meeting of the IEEE Geoscience and Remote Sensing Society and USNC/URSI Commission, October 7-9, 1985, University of Massachusetts, Amherst, Massachusetts, "Like and Cross Polarized Cross Sections for Random Rough Surfaces--Full Wave Theory and Experiment."
- (iv) International Union of Radio Science (URSI) Meeting at the University of Colorado, Boulder, Colorado, January 13-16, 1986, "Scattering and Depolarization by Conducting Cylinders with Rough Surfaces."

(7.2) Papers Submitted for Review by Journal Editors

- (i) "Scattering and Depolarization by Random Rough Surfaces, Unified Full Wave Approach - An Overview," Wave Material Interaction.
- (ii) "Full Wave Solutions for Electromagnetic Scattering and Depolarization in Irregular Stratified Media," Special Issue of Radio Science on Waves in Inhomogeneous Media.
- (iii) "Multiple Scattering by Irregular Shaped Particles of Finite Conductivity at Infrared and Optical Frequencies."
- (iv) "Backscatter Cross Sections for Normal Incidence Using a Two-Scale Full Wave Analysis of Rough Surfaces."

(7.3) Papers Accepted for Publication

- (i) "Multiple Scattering in Media Consisting of Nonspherical Finitely Conducting Particles," Proceedings of the 1985 CRDC Scientific Conference on Obscuration and Aerosol Research, in press.
- (ii) "Scattering and Depolarization by Conducting Cylinders with Rough Surfaces," Applied Optics, in press.

(7.4) Papers Published in the Technical Literature and Submitted with This Report

- (i) "Scattering and Depolarization by Conducting Cylinders with Rough Surfaces," Proceedings of the 1984 CRDC Scientific Conference on Obscuration and Aerosol Research, DRSMC-CLJ-IR, pp. 386-371, January 1985.
- (ii) "Like and Cross Polarized Scattering Cross Sections for Random Rough Surfaces--Theory and Experiment," Journal of the Optical Society of America Special Issue on "Wave Propagation and Scattering in Random Media," Vol. 2, No. 12, pp. 2295-2303, December 1985.

Multiple Scattering by Irregular Shaped Particles of Finite Conductivity
at Infrared and Optical Frequencies

The modified Stokes parameters (the incoherent specific diffuse intensities) for a layered media consisting of a random distribution of finitely conducting particles with very rough surfaces were computed for normally and obliquely incident electromagnetic waves. Both vertically and horizontally polarized excitations at infrared and optical frequencies were considered. For large angles of incidence ($\theta_0^i = 30^\circ$), it is necessary to use more than twenty-four terms of the Fourier series expansions of the Mueller matrix. The analytical solutions are based on the matrix characteristic value techniques. For these cases the principal investigator used his access to the Cyber 205 supercomputer at Colorado State University through a grant awarded by the National Science Foundation. Use of the supercomputer has enabled us to tighten the accuracy of our computations. Additional work has been done to determine the albedos and the extinction cross sections for the irregular shaped particles considered in our investigations.

It is shown that the particle surface roughness results in effectively blocking transmission windows that appear when electromagnetic waves propagate through thin layers consisting of smooth (spherical) particles. Particle surface roughness is also shown to result in a small but significant backscatter enhancement.

During this reporting period the principal investigator presented papers at four international/national conferences/workshops (see Item (7.1)). In addition, he attended the 1985 Advanced Planning Briefing for Industry (APBI) at the U. S. Army Chemical Research and Development Center, Aberdeen Proving Ground Maryland in (October 1985). He also visited with Army laboratory personnel at Aberdeen and provided an overview of his research program.

The principal investigator submitted two additional manuscripts for publication in scientific journals (see Item (7.2)). Two papers were accepted for publication (see Item (7.3)) and two papers were published in the Technical Literature (see Item (7.4)) during this reporting period.

The final report for this contract will be submitted by the next reporting period. This report will also contain documented computer codes on tape.

Scattering cross section modulation for arbitrarily oriented composite rough surfaces: Full wave approach

Ezekiel Bahar

Electrical Engineering Department, University of Nebraska

Clifford L. Rufenach and Donald E. Barrick

NOAA/ERL Wave Propagation Laboratory

Mary Ann Fitzwater

Electrical Engineering Department, University of Nebraska

As a synthetic aperture radar scans different portions of a rough surface, the direction of the unit vector normal to the mean surface of the effective illuminated area (resolution cell) fluctuates. In this paper the modulation of the like and cross polarized scattering cross sections of the resolution cell are determined as the normal to it tilts in planes that are in and perpendicular to the fixed reference plane of incidence. By using the full wave approach, the scattering cross sections are expressed as a weighted sum of two cross sections. The first cross section is associated with scales of roughness within the effective illuminated area that are large compared to the radar wavelength, and the second cross section is associated with small-scale spectral components within the resolution cell. Thus both specular point scattering and Bragg scattering are accounted for in a self-consistent manner. The results are compared with earlier solutions based on first-order Bragg scattering theory.

1. INTRODUCTION

Microwave remote sensing of rough surfaces (both land and ocean), using moving platforms (aircraft and satellite) as well as ground-based measurements, has illustrated the need for a better understanding of the interaction of the radar signals with these surfaces. This interaction is particularly important for the ocean surface where the radar modulation can yield information about the long ocean wave field. Radar modulation measurements from fixed platforms have been made in wavetanks and the open oceans. The surfaces have been described in terms of two-scale models [e.g., Wright, 1968]. The radar modulation is considered to be principally due to (1) geometrical tilt due to the slope of the long ocean waves and (2) the straining of the short waves (by hydrodynamic interaction) [e.g., Keller and Wright, 1975; Alpers and Hasselmann, 1978]. For application to moving platforms, synthetic aperture radar (SAR) and side looking airborne radar (SLAR), this modulation needs to be described in terms of a general

geometry for both like polarization and cross polarization, since the long ocean waves, in general, travel in arbitrary directions. In the present work, the finite resolution of the radar is considered for tilt modulation with hydrodynamic effects neglected.

The full wave approach is used to determine the modulation of the like and cross polarized scattering cross sections for composite models of rough surfaces illuminated by SAR. The full wave approach accounts for both specular point scattering and Bragg scattering in a self-consistent manner. Thus the total scattering cross section is expressed as a weighted sum of two cross sections [Bahar *et al.*, 1983]. The first is the scattering cross section associated with the filtered surface consisting of the large-scale specular components of the illuminated rough surface area. The second is the cross section associated with the surface consisting of the small-scale spectral components that ride on the filtered surface. The principal elements of the full wave solutions are summarized in section 2.

In section 3, full wave solutions are derived for the scattering cross sections of a relatively small area or resolution cell of the rough surface that is effectively illuminated by SAR. The normal to an arbitrarily

This paper is not subject to U.S. copyright. Published in 1983 by the American Geophysical Union.
Paper number 3S1006.

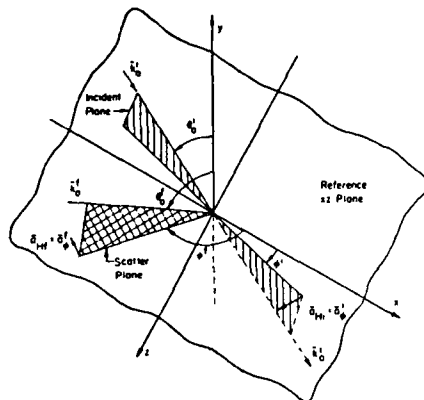


Fig. 1. Plane of incidence, scattering plane, and reference (x, z) plane.

oriented mean plane associated with the illuminated cell is characterized by tilt angles Ω and τ in and perpendicular to a fixed reference plane of incidence. It is assumed that the lateral dimension of the resolution cell L_r is much larger than both the electromagnetic wavelength and the small-scale surface height correlation distance for the cell. As the SAR scans different portions of the rough surface S , the direction of the unit vector normal to the cell F fluctuates. In this paper the "modulations" of scattering cross sections are determined as the tilt angles Ω and τ fluctuate. In a recent study of "tilt modulation" by

Alpers *et al.* [1981], first-order Bragg scatter due to capillary waves on a tilted plane is considered. It can be shown that if the large-scale spectral components of the surface within the cell are ignored, the full wave solutions derived here for tilt modulation reduce to the results obtained by Alpers *et al.* [1981] for a comprehensive review of the literature on this subject.)

For the illustrated examples presented in section 4, the scattering cross sections and their derivatives with respect to the tilt angles are evaluated for all angles of incidence. The modulation of the like cross sections near normal incidence is due primarily to fluctuations in specular point scattering, while the modulation of the like cross section for near grazing angles is due primarily to fluctuations in Bragg scattering. Thus for large angles of incidence the cross sections for the horizontally polarized waves are shown to be more strongly modulated than the cross sections for vertically polarized waves [Wright, 1968].

2. FORMULATION OF THE PROBLEM

The recently derived full wave solutions for the normalized cross sections per unit area are summarized here for composite rough surfaces (see Figure 1) that can be expressed as follows:

$$h(x, z) = h_A(x, z) + h_B(x, z) \quad (1)$$

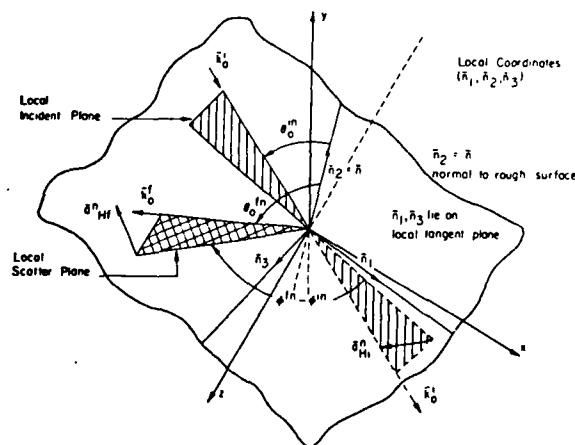


Fig. 2. Local plane of incidence and scatter and local coordinate system with unit vectors $\hat{n}_1, \hat{n}_2, \hat{n}_3$.

The surface $h_1(x, z)$ consists of the large-scale spectral components while $h_2(x, z)$ consists of the small-scale spectral components. For a homogeneous, isotropic surface height the spectral density function is the Fourier transform of the surface height autocorrelation function $\langle h(x, z), h(x', z') \rangle$ [Rice, 1951; Barrick, 1970; Ishimaru, 1978]

$$W(v_x, v_z) = \frac{1}{\pi^2} \int_{-\infty}^{\infty} \langle hh' \rangle \exp(i v_x x_d + i v_z z_d) dx_d dz_d \quad (2a)$$

where $\langle hh' \rangle$ is a function of $|\vec{r}_d| = (x_d^2 + z_d^2)^{1/2}$ and

$$x - x' = x_d \quad z - z' = z_d \quad (2b)$$

The surface $h_1(x, z)$ consists of the spectral components $k = (v_x^2 + v_z^2)^{1/2} \leq k_d$ and the remainder term $h_2(x, z)$ consists of the spectral components $k > k_d$. Since the full wave approach accounts for both specular point scattering and Bragg scattering in a self-consistent manner, the total scattering cross section can be expressed as a weighted sum of the cross section $\langle \sigma^{PQ} \rangle_1$ for the filtered surface h_1 and the cross section $\langle \sigma^{PQ} \rangle_2$ for the surface h_2 that rides on the large-scale surface h_1 [Bahar et al., 1983]

$$\langle \sigma^{PQ} \rangle = \langle \sigma^{PQ} \rangle_1 + \langle \sigma^{PQ} \rangle_2 \quad (3)$$

The angle brackets denote statistical average. The first superscript P corresponds to the polarization of the scattered wave while the second superscript Q corresponds to the polarization of the incident wave. To derive (3) by using the full wave approach, it is implicitly assumed that the large-scale surface meets the radii of curvature criteria (associated with the Kirchhoff approximations for the surface fields) as well as the condition for deep phase modulation. Thus the first term in (3) is shown to be

$$\langle \sigma^{PQ} \rangle_1 = |\chi'(\vec{v} \cdot \vec{n}_s)|^2 \langle \sigma_s^{PQ} \rangle \quad (4)$$

in which χ' is the characteristic function for the small-scale surface

$$\chi'(\vec{v} \cdot \vec{n}_s) = \chi'(v) = \langle \exp i v h_s \rangle \quad (5)$$

and

$$\vec{v} = \vec{k}^s - \vec{k}^i = k_0(\vec{n}^s - \vec{n}^i) \quad v = |\vec{v}| \quad (6)$$

The unit vectors \vec{n}^s and \vec{n}^i are in the directions of the scattered and incident wave normals, respectively; thus for backscatter $\vec{n}^s = -\vec{n}^i$. The free space radio

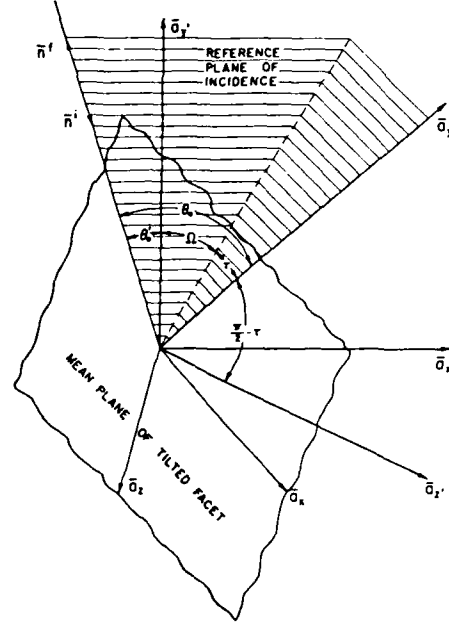


Fig. 3. The tilted cell.

wave number is k_0 . An $\exp(i\omega t)$ time dependence is assumed. The vector \vec{n} is the value of the unit vector \vec{n} normal to the surface $h(x, z)$ at the specular points. Thus

$$\vec{n} = \nabla f / |\nabla f| = (-h_x \vec{a} + \vec{a}_z - h_z \vec{a}_x) / (h_x^2 + h_z^2 + 1)^{1/2} \quad (7a)$$

where

$$f = y - h(x, z) \quad h_x = \partial h / \partial x \quad h_z = \partial h / \partial z \quad (7b)$$

and

$$\vec{n}_s = \vec{v} / v \quad (7c)$$

The expression for the physical optics (specular point) cross section for the large-scale surface h_1 is

$$\langle \sigma_s^{PQ} \rangle = \frac{4k_0^2}{v_s^2} \left[\left| \frac{D^{PQ}}{\vec{n} \cdot \vec{a}_y} \right|^2 P_2(\vec{n}^s, \vec{n}^i | \vec{n}) \rho(\vec{n}) \right]_{n_s} \quad (8)$$

in which D^{PQ} depends on \vec{n}^s , \vec{n}^i , \vec{n} , the media of propagation above and below the rough surface $h(x, z)$ and the polarization of the incident and scattered

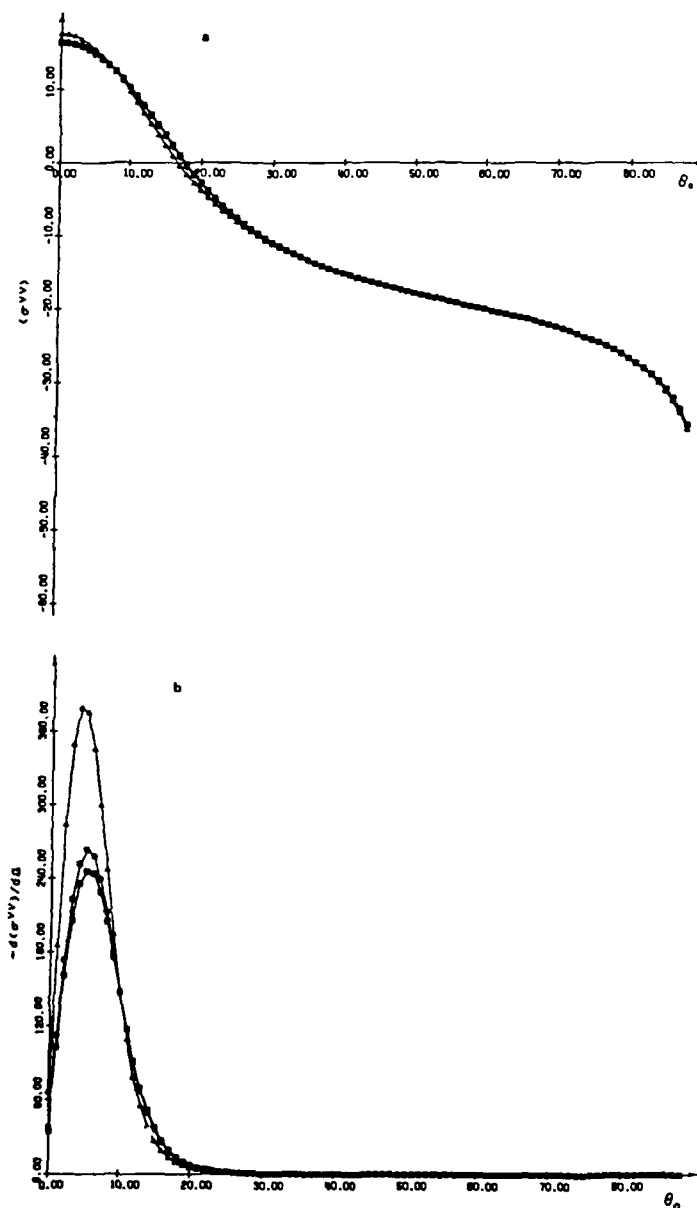


Fig. 4. (a) $\langle \sigma^{VV} \rangle$, (b) $-(d\langle \sigma^{VV} \rangle/d\Omega)$, and (c) $-(d\langle \sigma^{VV} \rangle/d\Omega)/\langle \sigma^{VV} \rangle$ for $\Omega = 0$ and $\tau = 0$ as a function of θ_0 . Triangle, $L_s = 300$ cm; octagon, $L_s = 1000$ cm; square, $L_s = 2500$ cm.

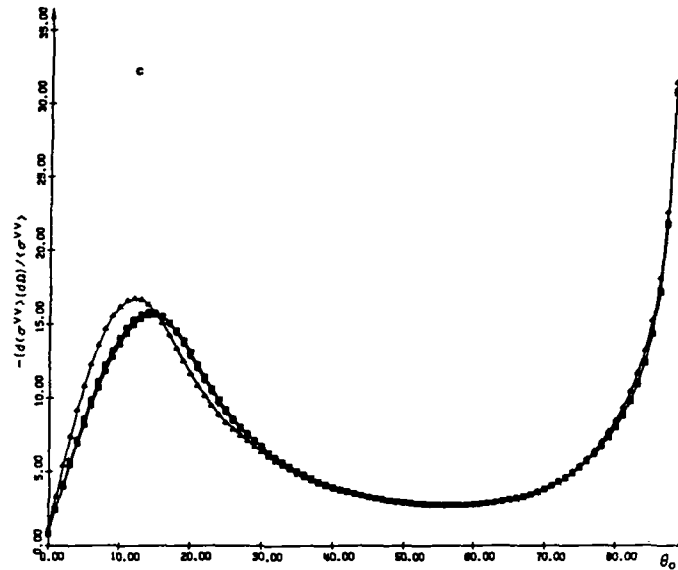


Fig. 4. (continued)

waves [Bahar, 1981a, b]. The shadow function P_2 is the probability that a point on the rough surface is both illuminated and visible, given the slopes $\tilde{n}(h_x, h_z)$, at the point [Smith, 1967; Sancer, 1969]. The probability density function for the slopes h_x and h_z is $p(\tilde{n})$. The factor $\chi^2(v)$ that multiplies $\langle \sigma_{\infty}^{PQ} \rangle$ accounts for the degradation of the contributions from the specular points due to the superimposed small-scale rough surface h_s .

Assuming a Gaussian probability density function for h_s , $\langle \sigma^{PQ} \rangle_s$ is given by the sum

$$\langle \sigma^{PQ} \rangle_s = \sum_{m=0}^{\infty} \langle \sigma^{PQ} \rangle_{sm} \quad (9)$$

where

$$\langle \sigma^{PQ} \rangle_{sm} = 4\pi k_0^2 \int \frac{|D^{PQ}|^2 P_2(\tilde{n}', \tilde{n}^i | \tilde{n})}{\tilde{n} \cdot \tilde{a}_s} \exp(-v_s^2 \langle h_s^2 \rangle) \left(\frac{v_s^2}{2}\right)^m \frac{W_m(v_s, v_s)}{m!} p(h_x, h_z) dh_x dh_z \quad (10)$$

in which $\langle h_s^2 \rangle$ is the mean square of the surface height h_s and v_x, v_y , and v_z are the components of v (equation (6) in the local coordinate system (at each point on the large-scale surface) associated with the

unit vectors \tilde{n}_1, \tilde{n}_2 , and \tilde{n}_3 (see Figure 2). Thus \tilde{v} can also be expressed as

$$\tilde{v} = v_x \tilde{n}_1 + v_y \tilde{n}_2 + v_z \tilde{n}_3 \quad (11)$$

where

$$\tilde{n}_1 = (\tilde{n} \times \tilde{a}_s) / |\tilde{n} \times \tilde{a}_s| \quad \tilde{n}_2 = \tilde{n} \quad \tilde{n}_3 = \tilde{n}_1 \times \tilde{n}_2 \quad (12)$$

The surface height h_s is measured perpendicular to h_l , i.e., along \tilde{n} . The function $W_m(v_x, v_x)/2^{2m}$ is the two-dimensional Fourier transform of $\langle h_s h_s \rangle^m$.

$$\begin{aligned} \frac{W_m(v_x, v_x)}{2^{2m}} &= \frac{1}{(2\pi)^2} \int \langle h_s h_s \rangle^m \exp(i v_x \tilde{x}_s + i v_x \tilde{z}_s) d\tilde{x}_s d\tilde{z}_s \\ &= \frac{1}{2^{2m}} \int W_{m-1}(v'_x, v'_x) W_1(v_x - v'_x, v_x - v'_x) dv'_x dv'_z \\ &= \frac{1}{2^{2m}} W_{m-1}(v_x, v_x) \otimes W_1(v_x, v_x) \end{aligned} \quad (13)$$

In (13), $|\tilde{x}_s \tilde{n}_1 + \tilde{z}_s \tilde{n}_3|$ is the distance measured along the large-scale surface h_l , and the symbol \otimes denotes the two-dimensional convolution of W_{m-1} with W_1 . The two-dimensional Fourier transform of the surface height autocorrelation function $\langle h_s h_s \rangle$ is equal to the spectral density function $W_1(v_x, v_x)/4$.

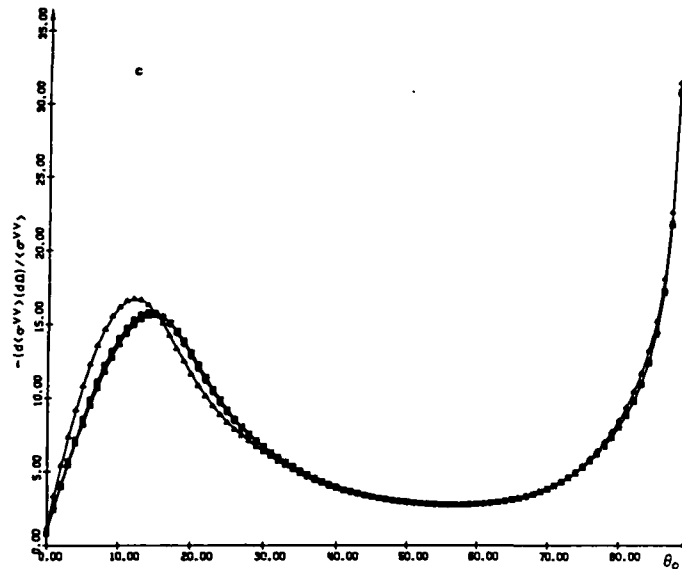


Fig. 4. (continued)

waves [Bahar, 1981a, b]. The shadow function P_2 is the probability that a point on the rough surface is both illuminated and visible, given the slopes $\tilde{n}(h_x, h_z)$, at the point [Smith, 1967; Sancer, 1969]. The probability density function for the slopes h_x and h_z is $p(\tilde{n})$. The factor $\chi(v)$ that multiplies $\langle \sigma^{sc} \rangle$ accounts for the degradation of the contributions from the specular points due to the superimposed small-scale rough surface h_s .

Assuming a Gaussian probability density function for h_s , $\langle \sigma^{sc} \rangle_s$ is given by the sum

$$\langle \sigma^{sc} \rangle_s = \sum_{m=0}^{\infty} \langle \sigma^{sc} \rangle_{sm} \quad (9)$$

where

$$\langle \sigma^{sc} \rangle_{sm} = 4\pi k_0^2 \int \frac{|D^{sc}|^2 P_2(\tilde{n}^f, \tilde{n}^i | \tilde{n})}{\tilde{n} \cdot \tilde{a}_s} \cdot \exp(-v_s^2 \langle h_s^2 \rangle) \left(\frac{v_s^2}{2} \right)^m \frac{W_m(v_s, v_s)}{m!} p(h_x, h_z) dh_x dh_z \quad (10)$$

in which $\langle h_s^2 \rangle$ is the mean square of the surface height h_s and v_s, v_y , and v_z are the components of v (equation (6) in the local coordinate system (at each point on the large-scale surface) associated with the

unit vectors \tilde{n}_1, \tilde{n}_2 , and \tilde{n}_3 (see Figure 2). Thus \tilde{v} can also be expressed as

$$\tilde{v} = v_s \tilde{n}_1 + v_y \tilde{n}_2 + v_z \tilde{n}_3 \quad (11)$$

where

$$\tilde{n}_1 = (\tilde{n} \times \tilde{a}_s) / |\tilde{n} \times \tilde{a}_s| \quad \tilde{n}_2 = \tilde{n} \quad \tilde{n}_3 = \tilde{n}_1 \times \tilde{n} \quad (12)$$

The surface height h_s is measured perpendicular to h_l , i.e., along \tilde{n} . The function $W_m(v_s, v_s)/2^{2m}$ is the two-dimensional Fourier transform of $\langle h_s h_s \rangle^m$.

$$\begin{aligned} \frac{W_m(v_s, v_s)}{2^{2m}} &= \frac{1}{(2\pi)^2} \int \langle h_s h_s \rangle^m \exp(i v_s \tilde{x}_s + i v_s \tilde{z}_s) d\tilde{x}_s d\tilde{z}_s \\ &= \frac{1}{2^{2m}} \int W_{m-1}(v'_s, v'_s) W_1(v_s - v'_s, v_s - v'_s) dv'_s dv'_s \\ &= \frac{1}{2^{2m}} W_{m-1}(v_s, v_s) \otimes W_1(v_s, v_s) \end{aligned} \quad (13)$$

In (13), $|\tilde{x}_s \tilde{n}_1 + \tilde{z}_s \tilde{n}_3|$ is the distance measured along the large-scale surface h_l , and the symbol \otimes denotes the two-dimensional convolution of W_{m-1} with W_1 . The two-dimensional Fourier transform of the surface height autocorrelation function $\langle h_s h_s \rangle$ is equal to the spectral density function $W_1(v_s, v_s)/4$.

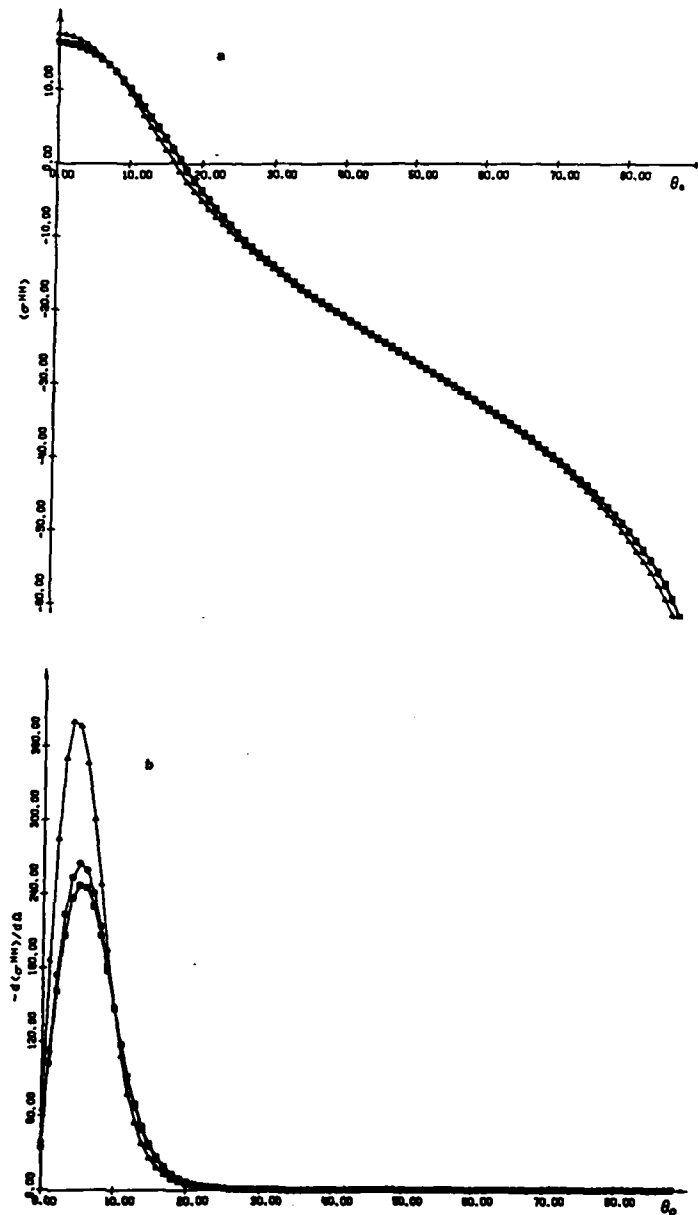


Fig. 5. (a) $\langle \sigma^{HH} \rangle$, (b) $-(d\langle \sigma^{HH} \rangle/d\Omega)$, and (c) $-(d\langle \sigma^{HH} \rangle/d\Omega)/\langle \sigma^{HH} \rangle$ for $\Omega = 0$ and $\tau = 0$ as a function of θ_0 . Triangle, $L_s = 300$ cm; octagon, $L_s = 1000$ cm; square, $L_s = 2500$ cm.

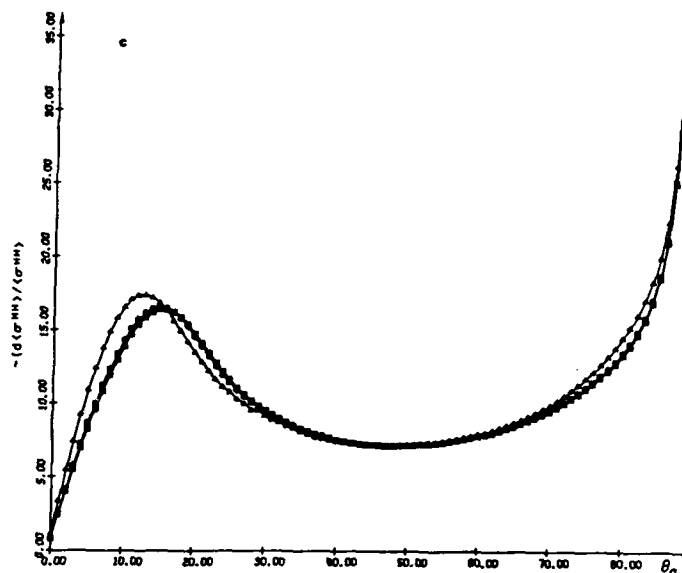


Fig. 5. (continued)

The first term in (9), $\langle\sigma^{pq}\rangle_{11}$, reduces to the first-order Bragg scattering cross section for $\beta = 4k_0^2 \langle h_z^2 \rangle \ll 1$, and $\bar{n} \rightarrow \bar{a}$, [Rice, 1941; Barrick, 1970]. In this case $p(h_x, h_z)$ is given by the Dirac delta functions $\delta(h_x)\delta(h_z)$ and (10) reduces to [Bahar, 1981a, b]

$$\langle\sigma^{pq}\rangle_{11} = \pi k_0^2 |D^{pq}|_{\bar{a}-\bar{a}}^2 v_z^2 W_1(v_x, v_z) \quad (14)$$

For $\beta \ll 1$ and arbitrary $p(h_x, h_z)$, the first term in (9), $\langle\sigma^{pq}\rangle_{11}$, is also in agreement with Valenzuela's solutions that are "mostly based on physical considerations" [Valenzuela, 1968; Valenzuela et al., 1971]. For small slopes $\bar{n} \approx \bar{a}$, and $\beta \ll 1$, the first term in (3) reduces to Brown's [1978] solution based on a combination of physical optics and perturbation theory. Since it is assumed (on deriving (3) from the full wave solutions for the scattered fields) that the surface h_i satisfies the radii of curvature criteria as well as the condition for deep phase modulation, it is necessary to choose $\beta = 4k_0^2 \langle h_z^2 \rangle \geq 1$ in order to assure that the weighted sum of cross sections (equation (3)) remains insensitive to variations in k_a , the wave number where spectral splitting is assumed to occur [Bahar et al., 1983].

In order to apply the full wave approach to SAR it is necessary to modify the results presented in this section (1) to account for the filtering of the very

large scale spectral component of the rough surface by the SAR that effectively illuminates a relatively small area of cell F of the rough surface S and (2) to account for the normal to a reference plane associated with the illuminated cell which is characterized by arbitrary tilt angles Ω and τ in and perpendicular to the reference plane of incidence (see Figure 3). It is assumed here that the lateral dimension of the cell illuminated by the SAR is much larger than the small-scale surface height correlation distance for the cell and that as the SAR scans different portions of the rough surface S , the direction of the unit vector normal to the cell F fluctuates. Our purpose is to determine the "modulation" of the backscatter cross sections $\langle\sigma^{pq}\rangle$ (equation (3)) as the tilt angles (of the normal to the cell) in and perpendicular to the reference plane of incidence fluctuate.

3. SCATTERING CROSS SECTIONS FOR ARBITRARILY ORIENTED RESOLUTION CELLS OF THE ROUGH SURFACE

Let x, y, z be the reference coordinate system associated with the surface of the cell F that is illuminated by the SAR such that the mean surface of the cell is the $y = 0$ plane (see Figure 3). Furthermore, let x', y', z' be the fixed coordinate system associated

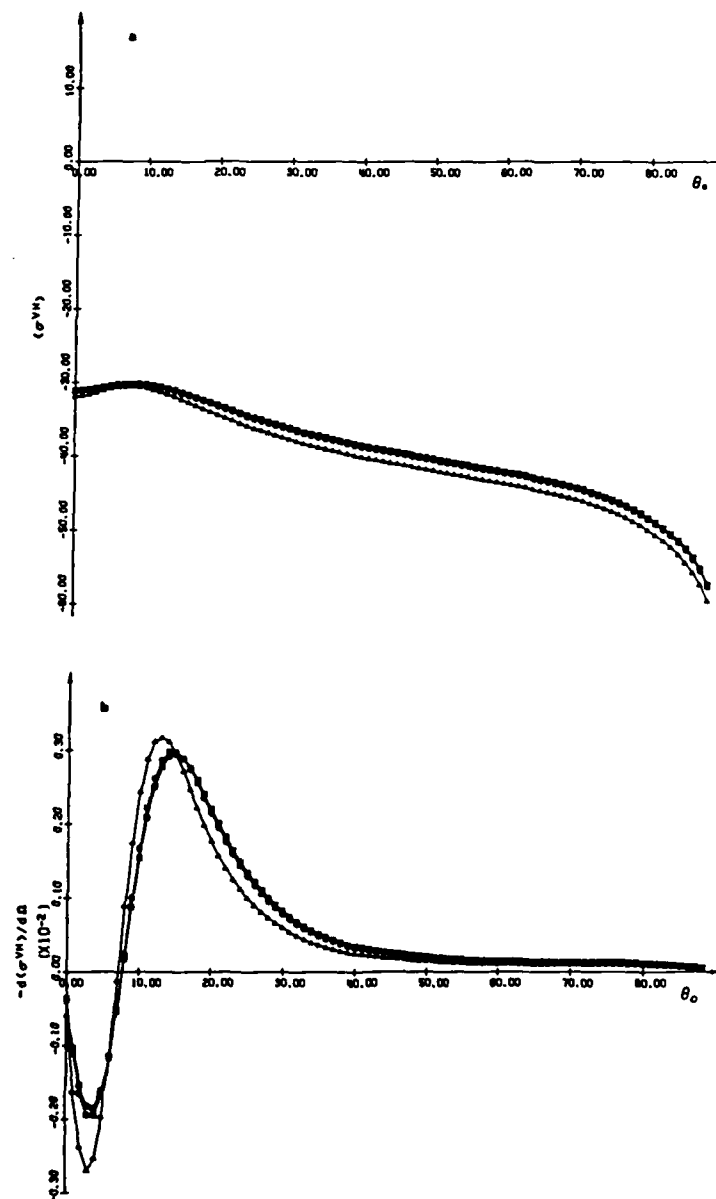


Fig. 6. (a) $\langle \sigma^{VH} \rangle$, (b) $-d\langle \sigma^{VH} \rangle / d\Omega$, and (c) $-(d\langle \sigma^{VH} \rangle / d\Omega) / \langle \sigma^{VH} \rangle$ for $\Omega = 0$ and $\tau = 0$ as a function of θ_0 . Triangle, $L_s = 300$ cm; octagon, $L_s = 1000$ cm; square, $L_s = 2500$ cm.

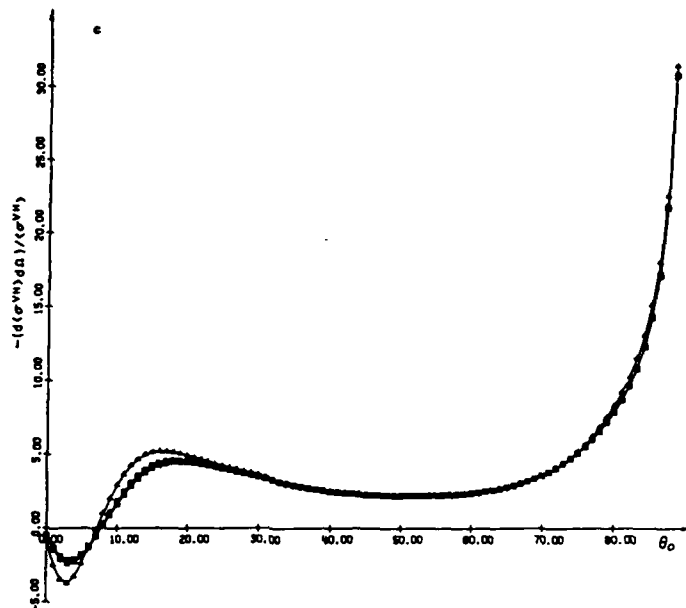


Fig. 6. (continued)

with the large surface S such that the unit vector \bar{a}'_y is normal to the mean rough surface height $h(x', z')$. The unit vector $\bar{n}^i = -\bar{n}^f$ is expressed in terms of the unit vectors of the fixed coordinate system (x', y', z') :

$$\bar{n}^i = -\bar{n}^f = \sin \theta'_0 \bar{a}'_x - \cos \theta'_0 \bar{a}'_y \quad (15)$$

The unit vector \bar{a}_y normal to the reference surface associated with the cell is expressed in terms of the tilt angles Ω and τ in and perpendicular to the fixed plane of incidence, the x', y' plane. Thus

$$\bar{a}_y = \sin \Omega \cos \tau \bar{a}'_x + \cos \Omega \cos \tau \bar{a}'_y + \sin \tau \bar{a}'_z \quad (16)$$

For convenience, \bar{a}_x and \bar{a}_z , the unit vectors associated with the cell, can be chosen such that the plane of incidence in the x, y, z coordinate system is normal to the vector \bar{a}_x . Thus

$$\bar{a}_x = (\bar{n}^i \cdot \bar{a}_y) / |\bar{n}^i \cdot \bar{a}_y| \quad \bar{a}_z = \bar{a}_y \times \bar{a}_x \quad (17)$$

and the expression for \bar{n}^i in the x, y, z coordinate system is

$$\bar{n}^i = (\bar{n}^i \cdot \bar{a}_x) \bar{a}_x + (\bar{n}^i \cdot \bar{a}_y) \bar{a}_y = \sin \theta_0 \bar{a}_x - \cos \theta_0 \bar{a}_y \quad (18)$$

where

$$\cos \theta_0 = \cos (\theta'_0 + \Omega) \cos \tau \quad (19)$$

The angle ψ'_f between the plane of incidence in the fixed coordinate system (x', y', z') and the plane of incidence in the coordinate system (x, y, z) associated with the cell is given by

$$\begin{aligned} \cos \psi'_f &= \frac{(\bar{n}^i \cdot \bar{a}_y)(\bar{n}^i \cdot \bar{a}'_y)}{|\bar{n}^i \cdot \bar{a}_y| |\bar{n}^i \cdot \bar{a}'_y|} = \frac{\bar{a}_y \cdot \bar{a}'_y - (\bar{n}^i \cdot \bar{a}_y)(\bar{n}^i \cdot \bar{a}'_y)}{|\bar{n}^i \cdot \bar{a}_y| |\bar{n}^i \cdot \bar{a}'_y|} \\ &= \frac{\cos \Omega \cos \tau - \cos \theta'_0 \cos \theta_0}{\sin \theta'_0 \sin \theta_0} = \frac{\cos \tau \sin (\theta'_0 + \Omega)}{\sin \theta_0} \quad (20) \end{aligned}$$

and

$$\begin{aligned} \sin \psi'_f &= \frac{(\bar{n}^i \cdot \bar{a}'_z)(\bar{n}^i \cdot \bar{a}_z)}{|\bar{n}^i \cdot \bar{a}'_z| |\bar{n}^i \cdot \bar{a}_z|} = \frac{[\bar{n}^i \cdot \bar{a}'_z]}{|\bar{n}^i \cdot \bar{a}_z|} \\ &= \frac{\sin \tau}{\sin \theta_0} \quad (21) \end{aligned}$$

For backscatter $\bar{n}^f = -\bar{n}^i$. Thus the angle ψ'_f between the plane of scatter in the fixed coordinate system (x', y', z') and the plane of scatter in the coor-

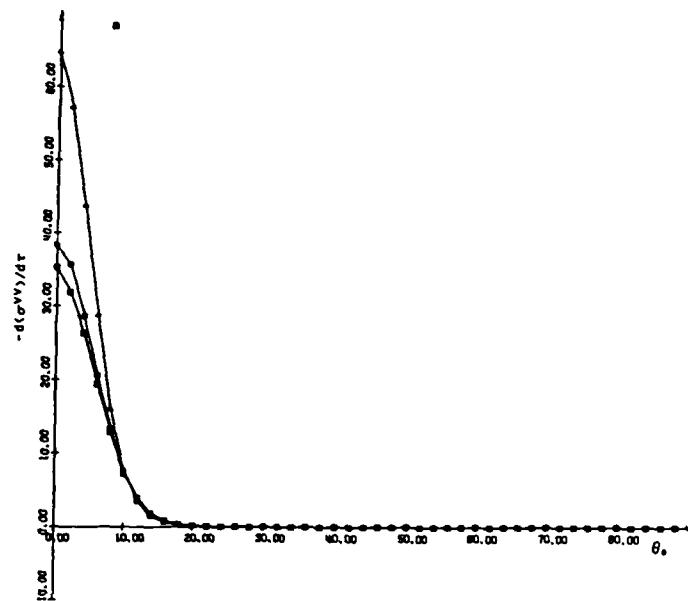


Fig. 7. (a) $-(d\langle\sigma^{VV}\rangle/d\tau)$, and (b) $-(d\langle\sigma^{VV}\rangle/d\tau)/\langle\sigma^{VV}\rangle$ for $\Omega = 0$ and $\tau = 0$ as a function of θ_0 . Triangle, $L_s = 300$ cm; octagon, $L_s = 1000$ cm; square, $L_s = 2500$ cm.

dinate system associated with the cell is

$$\psi_f^i = -\psi_f^i \quad (22)$$

The matrix that transforms the incident vertically and horizontally polarized waves in the fixed coordinate system to vertically and horizontally polarized waves in the cell coordinate system is therefore [Bahar, 1981a, b]

$$T_f^i = \begin{bmatrix} \cos \psi_f^i & \sin \psi_f^i \\ -\sin \psi_f^i & \cos \psi_f^i \end{bmatrix} \quad (23)$$

Similarly, the matrix that transforms the scattered vertically and horizontally polarized waves in the cell coordinate system back into the vertically and horizontally polarized waves in the fixed coordinate system is

$$T_f^s = \begin{bmatrix} \cos \psi_f^s & -\sin \psi_f^s \\ \sin \psi_f^s & \cos \psi_f^s \end{bmatrix} \quad (24)$$

Thus in view of (22), $T_f^s = T_f^i$. The coefficients D^{pq} in (8) are elements of a 2×2 matrix D given by

$$D = C_0^0 T^s F T^i \quad (25)$$

in which C_0^0 is the cosine of the angle between the incident wave normal \hat{n}^i and the unit vector \hat{n} normal to the rough surface of the cell $h_f(x, z)$. Thus

$$C_0^0 = -\hat{n}^i \cdot \hat{n} = \cos \theta_0^0 \quad (26)$$

where \hat{n}^i is given by (18) and \hat{n} is given by (27a) with $f_f(x, y) = y - h_f(x, y)$. The elements of the scattering matrix F in (25) are functions of the unit vectors \hat{n}^i , \hat{n}^s and \hat{n} as well as the media of propagation above and below the rough surface S [Bahar, 1981a]. The matrix T^i transforms the vertically and horizontally polarized waves in the cell coordinate system ($\hat{a}_x, \hat{a}_y, \hat{a}_z$) to vertically and horizontally polarized waves in the local coordinate system that conforms with the rough surface, $\hat{n}_1, \hat{n}_2, \hat{n}_3$ (12). Similarly, the matrix T^s transforms the vertically and horizontally polarized waves in the local coordinate system back into vertically and horizontally polarized waves in the cell coordinate system [Bahar, 1981a].

To account for the arbitrary orientation of the cell, the matrix D in (25) must be postmultiplied by T_f^s and premultiplied by T_f^i . Thus the elements of the matrix D in (8) must be replaced by the elements of

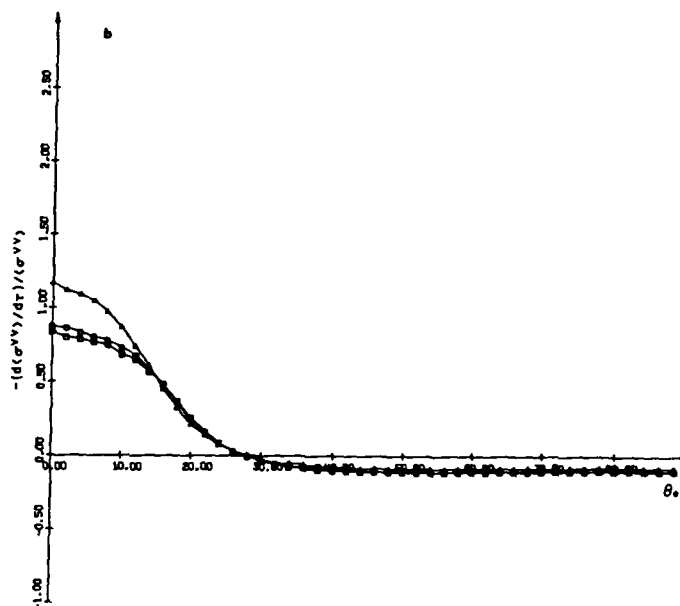


Fig. 7. (continued)

the matrix D_F where

$$D_F = T_F^T D T_F \quad (27)$$

Furthermore, in view of the effective filtering by the SAR of the very large scale spectral components of the rough surface $f(x', z') = 0$, the spectral density function for the rough surface $f_F(x, y) = 0$ associated with the resolution cell F is given by

$$\begin{aligned} W_F(v_x, v_y) &= W(v_x, v_y) & k \geq k_s \\ W_F(v_x, v_y) &= 0 & k < k_s \end{aligned} \quad (28)$$

where $W(v_x, v_y)$ is the spectral density function for the surface $S, f(x', z') = 0$. The wave number k_s is

$$k_s = 2\pi/L_s < k_d \quad (29)$$

where L_s is the width of the area of the cell illuminated by the SAR. Other models for the effective filtering of the spectral components of the rough surface by the SAR could be considered in this analysis; however, it would not change these results significantly. The very large scale surface consisting of the spectral components $0 < k < k_s$ are responsible for tilting the resolution cell with respect to the mean sea surface.

Thus on replacing the spectral density function $W(2a)$ for the surface S by the spectral density function W_F for the cell F (28) and on replacing the elements D^{pq} of the matrix D by the elements D_F^{pq} of the matrix D_F (27) the expression (3) can be used to determine the normalized backscatter cross section for an arbitrarily oriented cell F . In view of (23) and (24), the expressions for these backscatter cross sections are explicit functions of the tilt angles Ω and τ . For the special case $\tau = 0$ (tilt is in the plane of incidence), the matrices T_F^i and T_F^f reduce to identity matrices and

$$\cos \theta_0 = \cos(\theta'_0 + \Omega) \quad (30)$$

Thus for $\tau = 0$

$$\left. \frac{\partial \theta_0}{\partial \Omega} \right|_{\theta'_0 = \text{const}} = \left. \frac{\partial \theta_0}{\partial \theta'_0} \right|_{\Omega = \text{const}} \quad (31)$$

and

$$(\partial \langle \sigma^{pq} \rangle / \partial \Omega)_{\theta'_0 = \text{const}} = (\partial \langle \sigma^{pq} \rangle / \partial \theta'_0)_{\Omega = \text{const}} \quad (32)$$

Therefore to obtain $\partial \langle \sigma^{pq} \rangle / \partial \Omega$ for $\Omega = 0$ and $\tau = 0$ it is sufficient to evaluate $\langle \sigma^{pq} \rangle$ as a function of θ'_0 with both Ω and τ set equal to zero. The value for

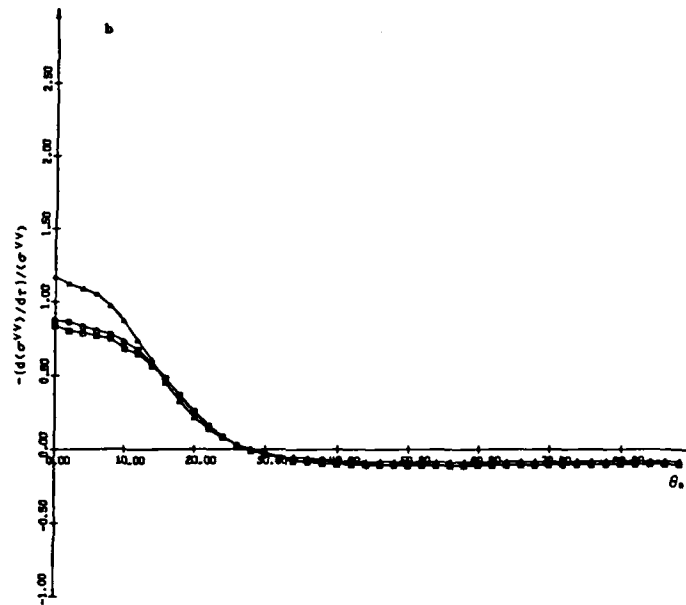


Fig. 7. (continued)

the matrix D_F where

$$D_F = T_F^i D T_F^i \quad (27)$$

Furthermore, in view of the effective filtering by the SAR of the very large scale spectral components of the rough surface $f(x', z') = 0$, the spectral density function for the rough surface $f_F(x, y) = 0$ associated with the resolution cell F is given by

$$\begin{aligned} W_F(v_x, v_y) &= W(v_x, v_y) & k \geq k_s \\ W_F(v_x, v_y) &= 0 & k < k_s \end{aligned} \quad (28)$$

where $W(v_x, v_y)$ is the spectral density function for the surface $S, f(x', z') = 0$. The wave number k_s is

$$k_s = 2\pi/L_s < k_s \quad (29)$$

where L_s is the width of the area of the cell illuminated by the SAR. Other models for the effective filtering of the spectral components of the rough surface by the SAR could be considered in this analysis; however, it would not change these results significantly. The very large scale surface consisting of the spectral components $0 < k < k_s$ are responsible for tilting the resolution cell with respect to the mean sea surface.

Thus on replacing the spectral density function $W(2a)$ for the surface S by the spectral density function W_F for the cell F (28) and on replacing the elements D^{pq} of the matrix D by the elements D_F^{pq} of the matrix D_F (27) the expression (3) can be used to determine the normalized backscatter cross section for an arbitrarily oriented cell F . In view of (23) and (24), the expressions for these backscatter cross sections are explicit functions of the tilt angles Ω and τ . For the special case $\tau = 0$ (tilt is in the plane of incidence), the matrices T_F^i and T_F^f reduce to identity matrices and

$$\cos \theta_0 = \cos(\theta'_0 + \Omega) \quad (30)$$

Thus for $\tau = 0$

$$\left. \frac{\partial \theta_0}{\partial \Omega} \right|_{\theta'_0 = \text{const}} = \left. \frac{\partial \theta_0}{\partial \theta'_0} \right|_{\Omega = \text{const}} \quad (31)$$

and

$$(\partial \langle \sigma^{pq} \rangle / \partial \Omega)_{\theta'_0 = \text{const}} = (\partial \langle \sigma^{pq} \rangle / \partial \theta'_0)_{\Omega = \text{const}} \quad (32)$$

Therefore to obtain $\partial \langle \sigma^{pq} \rangle / \partial \Omega$ for $\Omega = 0$ and $\tau = 0$ it is sufficient to evaluate $\langle \sigma^{pq} \rangle$ as a function of θ'_0 with both Ω and τ set equal to zero. The value for

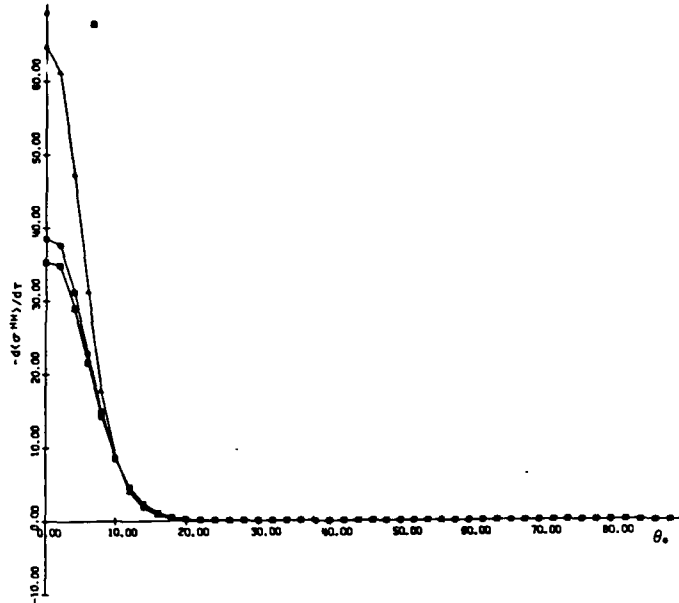


Fig. 8. (a) $-(d\langle\sigma^{HH}\rangle/d\tau)$, and (b) $-(d\langle\sigma^{HH}\rangle/d\tau)/\langle\sigma^{HH}\rangle$, for $\Omega = 0$ and $\tau = 0$ as a function of θ_0 . Triangle, $L_s = 300$ cm; octagon, $L_s = 1000$ cm; square, $L_s = 2500$ cm.

$\partial\langle\sigma^{PQ}\rangle/\partial\tau$ can either be evaluated analytically, since D_r^{PQ} (equation (27)) is an analytic function of τ , or the derivative could be evaluated numerically.

4. ILLUSTRATIVE EXAMPLES

For the illustrative examples presented in this section, the following specific form of the surface height spectral density function is selected [Brown, 1978]

$$W(v_x, v_z) = \frac{2}{\pi} S(v_x, v_z) = \begin{cases} \left(\frac{1}{\pi}\right) B k^4 / (\kappa^2 + k^2)^4 & k \leq k_c \\ 0 & k > k_c \end{cases} \quad (33)$$

where W is the notation used by Rice [1951] and S is the notation used by Brown [1978]. For the assumed isotropic model of the sea surface

$$B = 0.0046$$

$$k^2 = v_x^2 + v_z^2 \text{ (cm)}^{-2} \quad k_c = 12 \text{ (cm)}^{-1} \quad (34)$$

$$\kappa = (335.2 V^4)^{-1/2} \text{ (cm)}^{-1} \quad V = 4.3 \text{ (m/s)}$$

in which k_c is the spectral cutoff wave number

[Brown, 1978] and V is the surface wind speed. The wavelength for the electromagnetic wave is

$$\lambda_0 = 3.0 \text{ cm } (k_0 = 2\pi/3 = \text{(cm)}^{-1}) \quad (35)$$

The relative complex dielectric coefficient for the sea is

$$\epsilon_r = 48 - i35 \quad (36)$$

and the permeability for the sea is the same as for free space ($\mu_r = 1$).

The mean square height for the small scale surface h_s is given by

$$\langle h_s^2 \rangle \approx \int_0^{2\pi} \int_{k_c}^{k_0} \frac{W(k)}{4} k dk d\phi \approx \frac{B}{2} \left[\frac{1}{k_c^2} - \frac{1}{k_0^2} \right] \quad (37)$$

The mean square slope for the large-scale surface h_l within the resolution cell is

$$\sigma_h^2 = \langle h_l^2 \rangle = \int_0^{2\pi} \int_{k_c}^{k_0} \frac{W(k)}{4} k^3 dk d\phi$$

$$= B \left[\frac{1}{2} \ln \frac{k_0^2 + \kappa^2}{k_c^2 + \kappa^2} + \frac{3}{2} \kappa^2 \left(\frac{1}{k_c^2 + \kappa^2} - \frac{1}{k_0^2 + \kappa^2} \right) \right]$$

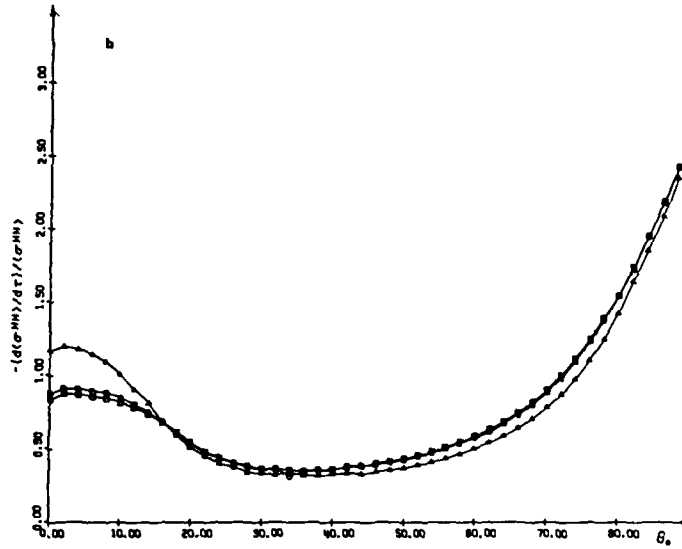


Fig. 8. (continued)

$$-\frac{3}{4}\kappa^4\left(\frac{1}{(k_s^2 + \kappa^2)^2} - \frac{1}{(k_s^2 + \kappa^2)^3}\right) + \frac{\kappa^6}{6}\left(\frac{1}{(k_s^2 + \kappa^2)^3} - \frac{1}{(k_s^2 + \kappa^2)^4}\right)$$

in which k_s is given by (29). The mean square height for the large-scale surface h_s is

$$\langle h_s^2 \rangle = \int_0^{2\pi} \int_{k_s}^{\infty} \frac{W(k)}{4} k dk d\phi = \frac{B}{2} \left[\frac{1}{k_s^2 + \kappa^2} - \frac{1}{k_s^2 + \kappa^2} + \kappa^2 \left(\frac{1}{(k_s^2 + \kappa^2)^2} - \frac{1}{(k_s^2 + \kappa^2)^3} \right) - \frac{\kappa^4}{3} \left(\frac{1}{(k_s^2 + \kappa^2)^3} - \frac{1}{(k_s^2 + \kappa^2)^4} \right) \right] \quad (39)$$

For $\beta = 4k_0^2 \langle h_s^2 \rangle = 1.0$, $k_s = 0.201$. Thus for $L_s = 300, 1000$, and 2500 cm (equation (29)), $\sigma_h^2 = 0.0102, 0.0143$, and 0.0152 , respectively, and $k_0^2 \langle h_s^2 \rangle = 21.9, 173$, and 357 , respectively. The slope probability density function within a resolution cell is assumed to be Gaussian; thus

$$p(h_s, h_s) = \frac{1}{\pi \sigma_h^2} \exp \left[-\frac{h_s^2 + h_s^2}{\sigma_h^2} \right] \quad (40)$$

and the physical optics (specular point) backscatter cross section is (equation (8)) [Bahar, 1981a]

$$\langle \sigma_{\text{po}}^{PQ} \rangle = \delta_{PQ} \frac{\sec^4 \theta_0}{\sigma_h^2} \exp \left(-\frac{\tan^2 \theta_0}{\sigma_h^2} \right) |R_P|^2 \quad (41)$$

in which δ_{PQ} is the Kronecker delta and R_P ($P = V, H$) is the Fresnel reflection coefficient for the vertically or horizontally polarized waves [Bahar, 1981a, b].

In Figures 4a, 4b, and 4c, $\langle \sigma^{VV} \rangle$, $-(d\langle \sigma^{VV} \rangle/d\Omega)$, and $-(d\langle \sigma^{VV} \rangle/d\Omega)/\langle \sigma^{VV} \rangle$ are plotted for $\Omega = 0$ and $\tau = 0$ as functions of θ_0 , the angle of incidence with respect to the fixed reference system (x', y', z'). In these figures $L_s = 300, 1000$, and 2500 cm.

In Figures 5a, 5b, and 5c and Figures 6a, 6b, and 6c, these results are repeated for $\langle \sigma^{HH} \rangle$ and $\langle \sigma^{HV} \rangle = \langle \sigma^{VH} \rangle$. It is interesting to note that the effective filtering of the very large scale spectral components of the rough surface ($0 < k < k_s$) by the SAR does not significantly change the value of σ^{PQ} unless $L_s < 300$ cm (see Figures 4a, 5a, and 6a). As one may expect, the modulation of the scattering cross sections in the plane of incidence $|d\langle \sigma^{VV} \rangle/d\Omega|$ is strongest for the SAR corresponding to the nar-

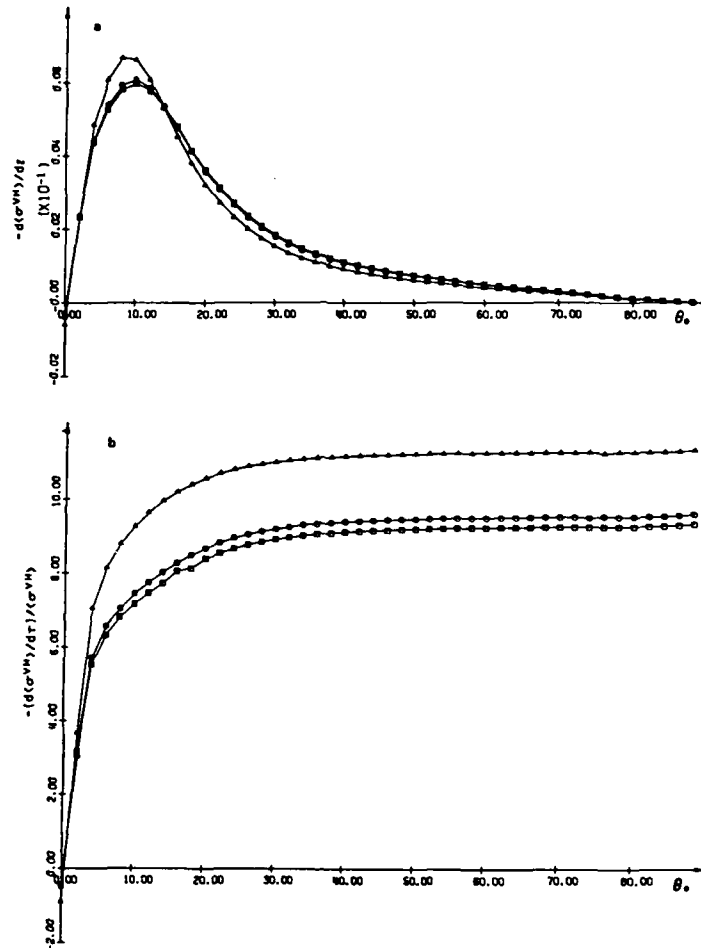


Fig. 9. (a) $-(d\langle\sigma^{VH}\rangle/d\tau)$, and (b) $-(d\langle\sigma^{VH}\rangle/d\tau)/\langle\sigma^{VH}\rangle$ for $\Omega = 0$ and $\tau = 0$ as a function of θ_0 . Triangle, $L_s = 300$ cm; octagon, $L_s = 1000$ cm; square, $L_s = 2500$ cm.

rowest effective beam width $L_s = 300$ cm (see Figures 4b, 5b, and 6b). Except for near-normal incidence the relative modulation $|d\langle\sigma^{PQ}\rangle/d\Omega|/\langle\sigma^{PQ}\rangle$ is larger for the horizontally polarized waves than for the vertically polarized waves (see Figures 4c and 5c). This is because for large angles of incidence θ_0 , the dominant term in the expression for the total cross section is (equation (3)) $\langle\sigma^{PQ}\rangle_H$, corresponding to first-order Bragg scatter. Since $|v_y D^{HH}|^2$ is proportional to $(\tilde{n}^i \cdot$

$\tilde{n})^4$ and $|v_y D^{VV}|^2$ is proportional to $|2 - (\tilde{n}^i \cdot \tilde{n})^2|^2$ for highly conducting surfaces, for large angles of incidence $|v_y D^{HH}|^2$ is more strongly dependent than $|v_y h D^{VV}|^2$ on the slopes $(\tilde{n}(h_x, h_z))$. The largest modulation of the like polarized cross sections occurs in the transition region where the contribution to the cross section due to Bragg scatter becomes larger than the contribution due to specular point scatter, namely at about 5° (see Figures 4b and 5b). The de-

polarized cross section $\langle \sigma^{PQ} \rangle$ ($P \neq Q$) does not have a contribution due to specular point scatter [Bahar, 1981a, b]. There are two peaks in the value of $|d\langle \sigma^{VH} \rangle/d\Omega|$, one at about 4° and the larger one at about 13° ; however, both peaks are much smaller than the peak value of $|d\langle \sigma^{PP} \rangle/d\Omega|$ for $P = V, H$ since the like polarized cross sections are much larger than the depolarized cross sections.

In Figures 7a and 7b, $(-d\langle \sigma^{VV} \rangle/d\tau)$ and $-(d\langle \sigma^{VV} \rangle/d\tau)/\langle \sigma^{VV} \rangle$ are plotted for $\Omega = 0$ and $\tau = 0$ as functions of the angle of incidence θ_0 . These results are repeated in Figures 8a and 8b and Figures 9a and 9b for $\langle \sigma^{HH} \rangle$ and $\langle \sigma^{VH} \rangle = \langle \sigma^{HV} \rangle$. In Figures 7–9, the width of the SAR is also $L_s = 300, 1000$, and 2500 cm. Unlike $|d\langle \sigma^{PP} \rangle/d\Omega|$ ($P = V, H$) the peak in the derivatives $|d\langle \sigma^{PP} \rangle/d\tau|$ occurs at normal incidence ($\theta_0 = 0$). For near-normal incidence the dependence of $|d\langle \sigma^{HH} \rangle/d\tau|/\langle \sigma^{HH} \rangle$ on the angle of incidence θ_0 is very similar to that of $|d\langle \sigma^{VV} \rangle/d\tau|/\langle \sigma^{VV} \rangle$. However, the modulations of the vertically and horizontally polarized waves differ significantly for near-grazing incidence. As noted above, since $\langle \sigma^{HH} \rangle$ is more sensitive than $\langle \sigma^{VV} \rangle$ to slope variations, the relative modulation of the horizontally polarized backscatter cross sections $\langle \sigma^{HH} \rangle$ is significantly larger than the relative modulation of $\langle \sigma^{VV} \rangle$. The physical optics contribution to the depolarized backscatter cross section is zero, and the derivative $|d\langle \sigma^{VH} \rangle/d\tau|$ peaks at about 10° rather than at normal incidence as in the case of the like-polarized backscatter cross sections. The relative modulation of the depolarized cross section $|d\langle \sigma^{VH} \rangle/d\tau|/\langle \sigma^{VH} \rangle$ increases rapidly near normal incidence and remains practically constant for large angle of incidence θ_0 .

5. CONCLUDING REMARKS

The full wave approach is used to determine the scattering cross sections for arbitrarily oriented resolution cells on random rough surfaces illuminated by synthetic aperture radars. The purpose of this analysis is to determine the modulation of the like and cross polarized scattering cross sections as the normal to the cells tilt in and perpendicular to the plane of incidence. The full wave approach accounts for shadowing and both specular point scattering as well as Bragg scattering in a self-consistent manner. Thus the scattering cross sections are expressed as weighted sums of two cross sections. The first cross section is associated with the filtered surface consisting of the large-scale spectral components of the rough surface. The second cross section is associated

with the surface consisting of the small-scale spectral components. It can be shown that if the large-scale spectral components of the surface of the cell are neglected, the second cross section accounts for first-order Bragg scattering and the results are in agreement with earlier published results [Alpers et al., 1981]. However, for typical terrain or sea surfaces, the large-scale spectral components are not negligible.

By using the full wave analysis, the modulation of the like-polarized and cross-polarized cross sections can be determined for all angles of incidence and tilt angles. On the other hand, first-order Bragg scatter theory does not account for backscattering near normal to the surface of the cell [Alpers et al., 1981]. The results based on the two-scale model indicate that the relative modulation of the like-polarized backscatter cross section is maximum for angles of incidence between 10° and 15° (depending on polarization and effective width of the resolution cell L_s). The analyses based on first-order Bragg scatter do not provide these results. It is also shown that as the angle of incidence approaches zero, the modulation of the scattering cross sections in and perpendicular to the plane of incidence becomes comparable.

When the normal to the cell is tilted in the direction normal to the plane of incidence ($\tau \neq 0$), the full wave analysis not only accounts for the change in the local angle of incidence θ_0 (equation (19)), but also takes into account the fact that the local planes of incidence (or scatter) are not parallel to the reference planes of incidence (or scatter), namely, $\psi_i = -\psi_s \neq 0$ (equations (20)–(22)). Since Alpers et al. [1981] do not account for the effects of the large-scale spectral components of the surface within the resolution cell the results presented here for the modulation of the like-polarized scattering cross sections near normal incidence are significantly different from those given by Alpers et al. The cross-polarized backscattering cross sections based on the first-order Bragg scattering theory used by Alpers et al. [1981] are not published.

Acknowledgments. This paper was sponsored by the U.S. Army Research Office, contract DAAG-29-82-K-0123, and the Wave Propagation Laboratory, NOAA.

REFERENCES

- Alpers, W., and K. Hasselmann, The two-frequency microwave technique for measuring ocean wave spectra from an airplane or satellite, *Boundary Layer Meteorol.*, 13, 215–230, 1978.
- Alpers, W. R., D. B. Ross, and C. L. Rufenach, On the detectabil-

- ity of ocean surface waves by real and synthetic aperture radar, *J. Geophys. Res.*, **86**(C7), 6481-6498, 1981.
- Bahar, E., Scattering cross sections from rough surfaces: Full wave analysis, *Radio Sci.*, **16**(3), 331-341, 1981a.
- Bahar, E., Scattering cross sections for composite random surfaces: Full wave analysis, *Radio Sci.*, **16**(6), 1327-1335, 1981b.
- Bahar, E., D. E. Barrick, and M. A. Fitzwater, Computations of scattering cross sections for composite surfaces and the specification of the wave-number where spectral splitting occurs, *IEEE Trans. Antennas Propag.*, in press, 1983.
- Barrick, D. E., Rough surfaces, in *Radar Cross Section Handbook*, pp. 671-770, Plenum, New York, 1970.
- Brown, G. S., Backscattering from a Gaussian-distributed perfectly conducting rough surface, *IEEE Trans. Antennas Propag.*, **AP 26**(3), 472-482, 1978.
- Ishimaru, A., Wave propagation and scattering in random media, in *Multiple Scattering, Turbulence, Rough Surfaces and Remote Sensing*, vol. 2, pp. 463-492, Academic, New York, 1978.
- Keller, W. C., and J. W. Wright, Microwave scattering and straining of wind-generated waves, *Radio Sci.*, **10**, 139-147, 1975.
- Rice, S. O., Reflection of electromagnetic waves from a slightly rough surface, *Commun. Pure Appl. Math.*, **4**, 351-378, 1951.
- Sancer, M. I., Shadow-corrected electromagnetic scattering from a randomly rough surface, *IEEE Trans. Antennas Propag.*, **AP 17**(5), 577-585, 1969.
- Smith, B. G., Geometrical shadowing of a randomly rough surface, *IEEE Trans. Antennas Propag.*, **AP 15**(5), 668-671, 1967.
- Valenzuela, G. R., Scattering of electromagnetic waves from a tilted slightly rough surface, *Radio Sci.*, **3**, 1051-1066, 1968.
- Valenzuela, G. R., M. B. Laing, and J. C. Daley, Ocean sea spectra for the high frequency waves as determined from airborne radar measurements, *J. Mar. Res.*, **29**, 69-84, 1971.
- Wright, J. W., A new model for sea clutter, *IEEE Trans. Antennas Propag.*, **AP 16**(2), 217-223, 1968.

E. Bahar and M. A. Fitzwater, Electrical Engineering Department, University of Nebraska, Lincoln, NE 68588.

C. L. Rufenach and D. E. Barrick, NOAA/ERL Wave Propagation Laboratory, Boulder, CO 80303.

Reprinted from Applied Optics, Vol. 23, page 3813, December 1, 1983
Copyright © 1983 by the Optical Society of America and reprinted by permission of the copyright owner.

Backscatter cross sections for randomly oriented metallic flakes at optical frequencies: full wave approach

Ezekiel Bahar and Mary Ann Fitzwater

The backscatter cross sections for randomly oriented metallic flakes are derived using the full wave approach. The metallic flakes are characterized by their surface height spectral density function. Both specular point and Bragg scattering at optical frequencies are accounted for in a self-consistent manner. It is shown that the average normalized backscatter cross sections (per unit volume) for the randomly oriented metallic flakes are larger than that of metallic spheres.

I. Introduction

The purpose of this investigation is to determine the average normalized backscatter cross sections for randomly oriented metallic flakes. The irregular-shaped flake is characterized by its surface height spectral density function, and its lateral dimension is assumed to be larger than both the wavelength of the incident electromagnetic field and the correlation distance of the random rough surface. Thus, scattering by the edges of the metallic flakes is ignored.¹

The full wave approach which accounts for both specular point scattering and Bragg scattering in a self-consistent manner is used to express the total cross section of the flake as a weighted sum of two cross sections (see Sec. II). The first is associated with the large-scale spectral components of the surface of the flakes, and the second is associated with its small-scale spectral components. The unit vector normal to the mean surface of the flake is characterized by the polar angle θ_F and azimuth angle ϕ_F (see Sec. III). Through a suitable choice of the coordinate system, the average with respect to the azimuth angle ϕ_F is evaluated analytically, while the average over the polar angle θ_F is evaluated numerically (see illustrative examples Sec. IV). It is shown that the average backscatter cross section/unit volume for the arbitrarily oriented metallic flakes considered is larger than that for metallic spheres. In Sec. IV the cross section of the metallic flake is also compared with the cross sections of similar flakes characterized by either small-scale or large-scale roughness.

II. Formulation of the Problem

To determine the scattering cross section for arbitrarily oriented metallic flakes at optical frequencies, it is convenient to use a two-scale model of the rough surface of the flakes. Thus, \vec{r}_s , the position vector to a point on the surface of the flake, is expressed as follows (see Fig. 1)

$$\vec{r}_s = \vec{r}_l(x, y, z) + \vec{n} \vec{h}_s \quad (1)$$

In Eq. (1), $y = h_l(x, z)$ is the equation of the surface consisting of the large-scale spectral components, and \vec{h}_s is the height of the small-scale surface measured in the direction of the normal (\vec{n}) to the large-scale surface. It is assumed that the lateral dimensions of the flake L_F are much larger than both the wavelength of the electromagnetic waves and the correlation distance of the random rough surface \vec{h}_s [Eq. (1)]. For a homogeneous isotropic surface height, the spectral density function²⁻⁴ is the Fourier transform of the surface height autocorrelation function $\langle h(x, z) h'(x', z') \rangle$

$$W(u_x, u_z) = \frac{1}{\pi^2} \int \langle h h' \rangle \exp(i u_x x_d + i u_z z_d) dx_d dz_d \quad (2)$$

where the symbol $\langle \cdot \rangle$ implies statistical average, and $\langle h h' \rangle$ is a function of $|\vec{r}_d|$:

$$\vec{r}_d = (x - x') \vec{e}_x + (z - z') \vec{e}_z = x_d \vec{e}_x + z_d \vec{e}_z \quad (3)$$

The surface h_l is assumed to consist of the spectral components

$$k_F < k = (u_x^2 + u_z^2)^{1/2} < k_d \quad (4)$$

where $k_F = 2\pi/L_F$ is the smallest wave number characterizing the surface of the flake, and k_d is the wave number where spectral splitting (between the large- and small-scale surface) is assumed to occur. The surface \vec{h}_s consists of the small-scale spectral components

$$k_d < k = (u_x^2 + u_z^2)^{1/2} < k_c \quad (5)$$

The authors are with University of Nebraska-Lincoln, Department of Electrical Engineering, Lincoln, Nebraska 68588-0511.

Received 3 June 1983.

0003-6935/83/233813-07\$01.00/0.

© 1983 Optical Society of America.

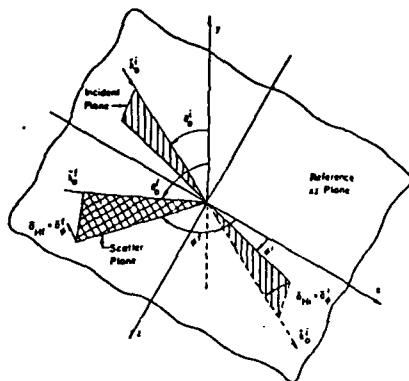


Fig. 1. Plane of incidence, scattering plane, and reference (x,z) plane.

where k_c , the spectral cutoff wave number⁵ is the largest wave number characterizing the flake.

The full wave approach, which accounts for both specular point scattering as well as Bragg scattering in a self-consistent manner, is used in this work to determine the scattering cross section of the composite model of an arbitrarily oriented flake.⁶ Thus, the total normalized scattering cross section/unit area $\langle \sigma^{PQ} \rangle$ is expressed as a weighted sum of two cross sections

$$\langle \sigma^{PQ} \rangle = \langle \sigma^{PQ} \rangle_l + \langle \sigma^{PQ} \rangle_s, \quad (6)$$

in which $\langle \sigma^{PQ} \rangle_l$ is the cross section associated with the large-scale filtered surface h_l , and the cross section $\langle \sigma^{PQ} \rangle_s$ is associated with the small-scale surface h_s that rides on the large-scale surface h_l . The first superscript P corresponds to the polarization of the scattered wave, while the second superscript Q corresponds to the polarization of the incident wave.

On deriving the full wave solution it is implicitly assumed that the wave number where spectral splitting occurs, k_d , is chosen so that the large-scale surface h_l satisfies the radii of curvature criteria (associated with the Kirchhoff approximations of the surface fields) and the condition for deep-phase modulation. The scattering cross section $\langle \sigma^{PQ} \rangle_l$ is given by^{7,8}

$$\langle \sigma^{PQ} \rangle_l = |\chi^*(\bar{v} \cdot \bar{n}_s)|^2 \langle \sigma_s^{PQ} \rangle \quad (7)$$

in which χ^* is the characteristic function for the small-scale surface

$$\chi^*(\bar{v} \cdot \bar{n}_s) = \chi^*(v) = \langle \exp i v \bar{h}_s \rangle, \quad (8)$$

$$\bar{v} = \bar{k}' - \bar{k} = k_0(\bar{n}' - \bar{n}) \quad v = |\bar{v}|. \quad (9)$$

The unit vectors \bar{n}' and \bar{n} are in the directions of the incident and scattered waves, and $k_0 = \omega(\mu_0 \epsilon_0)^{1/2}$ is the free-space wave number for the electromagnetic waves (μ_0 and ϵ_0 are the free-space permittivity and permeability). An $\exp(i\omega t)$ time dependence is assumed in this work. The vector \bar{n}_s is the value of the unit vector \bar{n} normal to the surface $h(x,z)$ at the specular points. Thus,

$$\bar{n} = \nabla f / |\nabla f| = (-h_x \bar{a}_x + \bar{a}_y - h_z \bar{a}_z) / (h_x^2 + 1 + h_z^2)^{1/2} \\ = \sin \gamma \cos \delta \bar{a}_x + \cos \gamma \bar{a}_y + \sin \gamma \sin \delta \bar{a}_z, \quad (10)$$

where

$$f = y - h(x,z), \quad h_x = \partial h / \partial x, \quad h_z = \partial h / \partial z, \quad (11)$$

$$\bar{a}_y = \bar{v} / v. \quad (12)$$

The expression for the physical optics cross section $\langle \sigma_s^{PQ} \rangle$ for the surface h_l is

$$\langle \sigma_s^{PQ} \rangle = \frac{4\pi}{v^2} k_0^2 \left| \frac{D^{PQ}}{\bar{n} \cdot \bar{a}_y} \right|^2 P_2(\bar{n}', \bar{n} | \bar{n}) p(\bar{n}), \quad (13)$$

in which D^{PQ} depends on the polarization of the incident and scattered waves, the unit vectors \bar{n}' , \bar{n} , and \bar{a}_y and the relative complex permittivities and permeabilities of the flake. The shadow function P_2 is the probability that a point on the rough surface is both illuminated by the source and visible to the observer given the slopes $\bar{n}(h_x, h_z)$ at the point.^{9,10} The function $p(\bar{n})$ is the probability density of the slopes h_x and h_z . The coefficient $|\chi^*|^2$ that multiplies $\langle \sigma_s^{PQ} \rangle$ is a weighting function that accounts for the degradation of the specular point scattering cross section due to the superimposed small-scale rough surface h_s .⁸ Thus, as $\bar{h}_s \rightarrow 0$, $|\chi^*|^2 \rightarrow 1$.

The scattering cross section $\langle \sigma^{PQ} \rangle_s$ for the Gaussian surface h_s that rides the large-scale surface h_l is given by the sum⁶

$$\langle \sigma^{PQ} \rangle_s = \sum_{m=1}^{\infty} \langle \sigma^{PQ} \rangle_{sm}, \quad (14a)$$

where

$$\langle \sigma^{PQ} \rangle_{sm} = 4\pi k_0^2 \int \frac{|D^{PQ}|^2 P_2(\bar{n}', \bar{n} | \bar{n})}{\bar{n} \cdot \bar{a}_y} \\ \times \exp \left(-v^2 \langle \bar{h}_s^2 \rangle \right) \left[\frac{v^2}{2} \right]^{2m} \frac{W_m(v \bar{h}_s, v \bar{h}_z)}{m!} p(h_x, h_z) dh_x dh_z. \quad (14b)$$

In Eq. (14) $\langle \bar{h}_s^2 \rangle$ is the mean square of the surface height \bar{h}_s , and v_x , v_y , and v_z are the components of \bar{v} [Eq. (9)] in the local coordinate system associated with the unit vectors \bar{n}_1 , \bar{n}_2 , and \bar{n}_3 (at each point on the large-scale surface h_l , see Fig. 2). Thus, \bar{v} is also expressed as

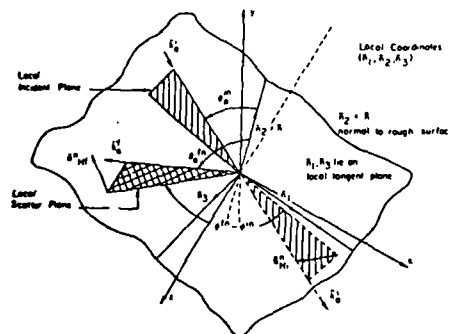


Fig. 2. Local plane of incidence and scatter and local coordinate system with unit vectors $\bar{n}_1, \bar{n}_2, \bar{n}_3$.

$$\bar{v} = v_x \bar{n}_1 + v_y \bar{n}_2 + v_z \bar{n}_3, \quad (15)$$

where

$$\bar{n}_1 = (\bar{n} \times \bar{a}_x) / |\bar{n} \times \bar{a}_x|, \bar{n}_2 = \bar{n}_3 \times \bar{n}_1, \bar{n}_3 = \bar{n}_1 \times \bar{n}_2. \quad (16)$$

The function $W_m(v_x, v_z)/2^m$ is the 2-D Fourier transform of $(\bar{h}_x \bar{h}_z)^m$:

$$\begin{aligned} \frac{W_m(v_x, v_z)}{2^m} &= \frac{1}{(2\pi)^2} \int (\bar{h}_x \bar{h}_z)^m \exp(i v_x \bar{x}_d + i v_z \bar{z}_d) d\bar{x}_d d\bar{z}_d \\ &= \frac{1}{2^m} \int W_{m-1}(v_x, v_z) W_1(v_x - v_x', v_z - v_z') dv_x' dv_z' \\ &= \frac{1}{2^m} W_{m-1}(v_x, v_z) \otimes W_1(v_x, v_z). \end{aligned} \quad (17)$$

In Eq. (17) the symbol \otimes denotes the 2-D convolution of W_{m-1} with W_1 . The surface height \bar{h}_x is measured normal to the surface $y = h_i$, and $|\bar{x}_d \bar{n}_1 + \bar{z}_d \bar{n}_3|$ is the distance measured along the large-scale surface h_i . The 2-D Fourier transforms of the surface height autocorrelation function $\langle \bar{h}_x \bar{h}_z \rangle$ is equal to the spectral density function $W_1(v_x, v_z)/4$. When the parameter $4k_0^2 \langle \bar{h}_x^2 \rangle \equiv \beta < 1$ and $\bar{n} \approx \bar{a}_y$, the first term in (14) accounts for first-order Bragg scattering, and the higher-order terms $m \geq 2$ may be neglected. In this case, the full wave solution Eq. (14) is in agreement with Brown's solution⁵ based on a combination of physical optics and perturbation theory. However, since it is assumed using the full wave approach that the condition for deep-phase modulation is satisfied, it is necessary to choose $\beta = 4k_0^2 \langle \bar{h}_x^2 \rangle \geq 1$. Since fewer terms in Eq. (14) need to be evaluated for smaller values of β , in this work the value assumed for β is 1.0.

While the perturbed-physical optics solutions^{5,11,12} for the cross sections critically depend on the choice of k_d (the wave number where spectra splitting is assumed to occur), the full wave approach is insensitive to variations in k_d for $\beta \geq 1$.⁶

Since the metallic flakes are randomly oriented with respect to the fixed observer, in Sec. III the analytical results presented are modified to account for arbitrary orientation of the normal to the mean surface of the flake.

III. Scattering Cross Sections for Arbitrarily Oriented Metallic Flakes

Let x', y', z' be a fixed reference coordinate system, and let x, y, z be a rotated coordinated system so that the unit vector \bar{a}_y is normal to the mean surface of the flake ($y = 0$) (see Fig. 3). For backscatter it is convenient to choose the unit vectors $\bar{n}' = -\bar{n}$ so that

$$\bar{n}' = -\bar{n} = -\bar{a}_y. \quad (18)$$

The unit vector \bar{a}_y normal to the mean surface of the flake can be expressed as follows in terms of the fixed reference coordinate system

$$\bar{a}_y = \sin\theta_F \cos\phi_F \bar{a}_x + \cos\theta_F \bar{a}_z + \sin\theta_F \sin\phi_F \bar{a}_y. \quad (19)$$

For convenience the two orthogonal unit vectors \bar{a}_x and \bar{a}_z in the mean plane of the flake are chosen so that the plane of incidence in the flake coordinate system is the x, y plane (normal to \bar{a}_z). Thus,

$$\bar{a}_x = (\bar{n}' \times \bar{a}_y) / |\bar{n}' \times \bar{a}_y| \text{ and } \bar{a}_z = \bar{a}_y \times \bar{a}_x. \quad (20)$$

The expression for \bar{n}' in the flake coordinate system is, therefore,

$$\bar{n}' = (\bar{n}' \cdot \bar{a}_x) \bar{a}_x + (\bar{n}' \cdot \bar{a}_y) \bar{a}_y = \sin\theta_F \bar{a}_x - \cos\theta_F \bar{a}_y, \quad (21)$$

where

$$\cos\theta_F = -\bar{n}' \cdot \bar{a}_y = \cos\theta_F. \quad (22)$$

The angle ψ_F between the reference plane of incidence (normal to \bar{a}_z in the fixed coordinate system), and the plane of incidence in the flake coordinate system (normal to $\bar{n}' \times \bar{a}_y$) is

$$\cos\psi_F = \frac{\bar{a}_z \cdot (\bar{n}' \times \bar{a}_y)}{|\bar{n}' \times \bar{a}_y|} = \frac{-(\bar{a}_z \cdot \bar{a}_y)}{|\bar{n}' \times \bar{a}_y|} = \cos\phi_F, \quad (23)$$

thus

$$\sin\psi_F = \frac{\bar{a}_z \times (\bar{n}' \times \bar{a}_y) \cdot \bar{n}'}{|\bar{n}' \times \bar{a}_y|} = \sin\phi_F. \quad (24)$$

Since $\bar{n}' = -\bar{n}$ for backscatter, the angle ψ_F between the plane of scatter in the fixed (x', y', z') coordinate system and the plane of scatter in the flake coordinate system (x, y, z) is

$$\psi_F = -\psi_F. \quad (25)$$

Thus, the matrix that transforms the vertically and horizontally polarized incident waves of the fixed coordinate system to the vertically and horizontally polarized incident waves of the flake coordinate system is^{7,8}

$$T_F = \begin{bmatrix} \cos\psi_F & \sin\psi_F \\ -\sin\psi_F & \cos\psi_F \end{bmatrix}. \quad (26)$$

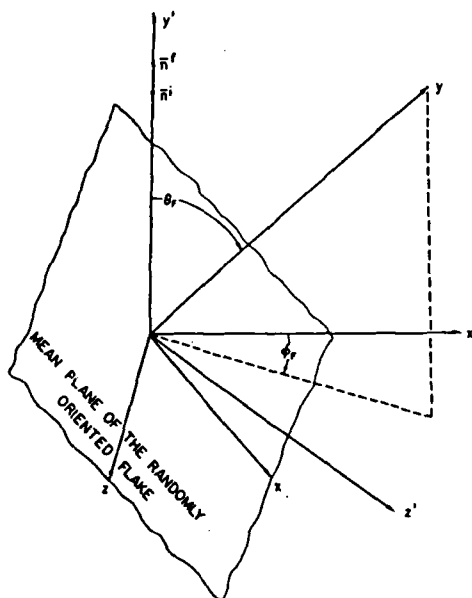


Fig. 3. Randomly oriented flake.

Similarly, the matrix that transforms the vertically and horizontally polarized scattered waves in the flake coordinate system back into vertically and horizontally polarized scattered waves of the fixed coordinate system is

$$T_F' = \begin{bmatrix} \cos\psi_F' & -\sin\psi_F' \\ \sin\psi_F' & \cos\psi_F' \end{bmatrix}. \quad (27)$$

Thus, in view of Eq. (25) for backscatter,

$$T_F' = T_F. \quad (28)$$

The coefficients D^{PQ} in Eq. (14) are elements of the 2×2 matrix D given by^{7,8}

$$D = C_0^0 T' F T_i. \quad (29)$$

in which C_0^0 is the cosine of the angle between the incident wave normal \bar{n}^i [Eq. (21)] and the unit vector \bar{n} normal to the rough surface of the flake [Eq. (10)]. Thus,

$$C_0^0 = -\bar{n}^i \cdot \bar{n} = \cos\gamma \cos\theta_F - \sin\gamma \sin\theta_F \cos\delta. \quad (30)$$

The elements F^{PQ} of the scattering matrix F in Eq. (29) are functions of the unit vectors $\bar{n}^i, \bar{n}', \bar{n}$ and the relative permittivity and permeability of the flakes.⁷ The matrix T_i transforms the vertically and horizontally polarized incident waves of the x, y, z coordinate system to vertically and horizontally polarized waves of the local coordinate system $(\bar{n}_1, \bar{n}_2, \bar{n}_3)$ associated with the rough surface of the flake [Eq. (16)]. Similarly, the matrix T' transforms the vertically and horizontally polarized scattered waves of the local coordinate system back into vertically and horizontally polarized waves of the x, y, z coordinate system.^{7,8}

To account for the arbitrary orientation of the flake with respect to the fixed (x', y', z') coordinate system [Eq. (29)] must be postmultiplied by T_F' and premultiplied by T_F . Therefore, in the expressions for the scattering cross sections [Eq. (6)], the elements of matrix D must be replaced by the elements of matrix D_F given by

$$D_F = T_F' D T_F = C_0^0 T_F' T' F T_i T_F = C_0^0 T_F' F T_i T_F, \quad (31)$$

where

$$T_F' = T_F T_i = \begin{bmatrix} \cos(\psi^i + \phi_F) & \sin(\psi^i + \phi_F) \\ -\sin(\psi^i + \phi_F) & \cos(\psi^i + \phi_F) \end{bmatrix} = \begin{bmatrix} C_T & S_T \\ -S_T & C_T \end{bmatrix}. \quad (32)$$

In Eq. (32)

$$\cos\psi^i = [\cos\gamma \sin\theta_F + \sin\gamma \cos\theta_F \cos\delta]/S_0^0, \quad (33)$$

$$\sin\psi^i = \sin\gamma \sin\delta/S_0^0, \quad (34)$$

where

$$S_0^0 = [1 - (C_0^0)^2]^{1/2}. \quad (35)$$

For backscatter $T_F' = T_F$ and $F^{VH} = F^{HV} = 0$, thus,

$$D_F = C_0^0 \begin{bmatrix} C_T^2 F^{VV} - S_T^2 F^{HH} & C_T S_T (F^{VV} + F^{HH}) \\ -C_T S_T (F^{VV} + F^{HH}) & C_T^2 F^{HH} - S_T^2 F^{VV} \end{bmatrix}. \quad (36)$$

Neglecting multiple scatter and assuming that the phase of the scattered signals from the individual flakes are

uniformly distributed in the interval $[0, 2\pi]$ the backscatter cross section for an ensemble of randomly located flakes is given by the sum of the individual backscatter cross sections.¹ Thus, accounting for the random orientation of each individual flake, the average backscatter cross section of a single scatterer in the ensemble of flakes is

$$\begin{aligned} \langle \sigma^{PQ} \rangle &= \int_0^{\pi/2} \int_0^{2\pi} \langle \sigma^{PQ} \rangle p(\theta_F, \phi_F) d\phi_F d\theta_F \\ &= \int_0^{\pi/2} \langle \sigma^{PQ} \rangle_{OP}(\theta_F) d\theta_F, \end{aligned} \quad (37)$$

in which it is assumed that the unit vector normal to the mean surface of the flake is uniformly directed in the half-space $0 \leq \theta_F \leq \pi/2$, $0 < \phi_F < 2\pi$ and

$$p(\theta_F, \phi_F) = \frac{\sin\theta_F}{2\pi} = \frac{p(\theta_F)}{2\pi}. \quad (38)$$

Since $\langle \sigma^{PQ} \rangle$ is dependent on ϕ_F only through the sines and cosines of the angles $(\psi^i + \phi_F)$ [Eq. (36)], it is convenient to evaluate the average of $\langle \sigma^{PQ} \rangle$ with respect to the angle ϕ_F analytically by first evaluating the average of $|D_F^{PQ}|^2$ with respect to ϕ_F . Thus, for $P \neq Q$,

$$\begin{aligned} \overline{|D_F^{PQ}|^2} &= \frac{1}{2\pi} \int_0^{2\pi} |D_F^{PQ}|^2 d\phi_F = \frac{(C_0^0)^2}{2\pi} \int_0^{2\pi} C_T^2 S_T^2 |F^{VV} \\ &\quad + F^{HH}|^2 d\phi_F \\ &= \frac{(C_0^0)^2}{8} |F^{VV} + F^{HH}|^2, \end{aligned} \quad (39)$$

and for $P = V, H$

$$\begin{aligned} \overline{|D_F^{PP}|^2} &= \frac{1}{2\pi} \int_0^{2\pi} |D_F^{PP}|^2 d\phi_F = \frac{(C_0^0)^2}{2\pi} \int_0^{2\pi} [C_T^2 |F^{VV}|^2 \\ &\quad + S_T^2 |F^{HH}|^2 - 2C_T S_T \operatorname{Re}(F^{VV} F^{HH*})] d\phi_F \\ &= \frac{1}{8} (C_0^0)^2 [3|F^{VV}|^2 + 3|F^{HH}|^2 - 2\operatorname{Re}(F^{VV} F^{HH*})] \\ &= \frac{1}{8} (C_0^0)^2 (4|F^{VV}|^2 + 4|F^{HH}|^2 - |F^{VV} + F^{HH}|^2), \end{aligned} \quad (40)$$

in which the symbol $*$ denotes the complex conjugate.

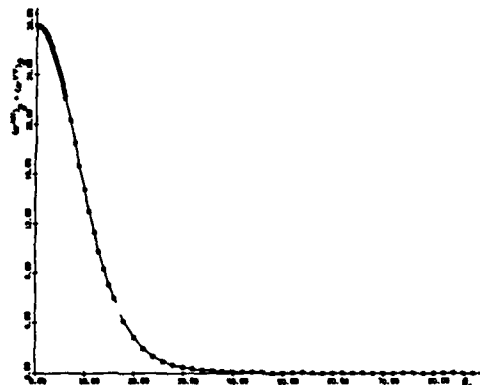


Fig. 4. $(\sigma^{HH})_0 = (\sigma^{VV})_0$ for the composite surface h as a function of θ_F .

The expressions for F^{VV} and F^{HH} are complicated functions of θ_F . Thus, the integrals with respect to θ_F are not evaluated analytically. Instead, $\langle \sigma^{PQ} \rangle_\theta$ [Eq. (37)], is evaluated numerically using Eq. (14) with $|D^{PQ}|^2$ ($P, Q = V, H$) replaced by $|D_F^{PQ}|^2$ [Eqs. (39) and (49)]. To obtain the ensemble average for the scattering cross sections $\langle \sigma^{PQ} \rangle$ [Eq. (37)], the result from the previous integration $\langle \sigma^{PQ} \rangle_\theta$ is multiplied by $p(\theta_F) = \sin\theta_F$ and integrated with respect to θ_F . Thus, summing up, the integral (37) is performed analytically with respect to ϕ_F and numerically with respect to θ_F . The integrations with respect to k_x, k_z [Eq. (14)] are also performed numerically.

IV. Illustrative Examples

The specific form of the surface height spectral density function [Eq. (2)] selected for the illustrative examples presented in this section is

$$W(u_x, u_z) = \begin{cases} \frac{2}{\pi} B/k^4, & k_F \leq k \leq k_c \\ 0, & k > k_c \text{ and } k < k_F, \end{cases} \quad (41)$$

in which

$$\left. \begin{aligned} B &= 0.016 \\ k^2 &= u_x^2 + u_z^2 \text{ (cm)}^{-2} \\ k_F &= 2\pi/L_F \text{ and } L_F = 0.002 \text{ cm} \\ k_c &= 0.45 \times 10^6 \text{ cm}^{-1} \end{aligned} \right\} \quad (42)$$

[For naturally generated surfaces, W can be approximated by k^{-n} , where n is between 3 and 4.⁴] The wavelength of the electromagnetic wave is

$$\lambda_0 = 0.555 \times 10^{-4} \text{ cm} \left(k_0 = \frac{2\pi}{\lambda_0} = 1.132 \times 10^5 \text{ cm}^{-1} \right). \quad (43)$$

The relative complex dielectric coefficient for the aluminum flakes at the assumed optical frequency is¹³

$$\epsilon_r = -40 - i12, \quad (44)$$

and the permeability of the flake is assumed to be that of free space ($\mu_r = 1$).

The mean square height for the small-scale surface \bar{h}_s ($k_d < k \leq k_c$) is given by

$$\begin{aligned} \langle \bar{h}_s^2 \rangle &\approx \int_0^{2\pi} \int_{k_d}^{k_c} \frac{W(k)}{4} k dk d\phi \\ &\approx \frac{B}{2} \left(\frac{1}{k_d^2} - \frac{1}{k_c^2} \right) = 0.195 \times 10^{-10} \text{ cm}^2 = \frac{1}{4k_d^2} \end{aligned} \quad (45)$$

since in this work $\beta = 4k_d^2 \langle \bar{h}_s^2 \rangle = 1.0$. The wave number where spectral splitting (between the small and large roughness scales) is assumed to occur is

$$k_d = [2Bk_c^2/(k_c^2 + 2Bk_d^2)]^{1/2} = 0.202 \times 10^5 \text{ (cm)}^{-1}. \quad (46)$$

For Gaussian surface heights,

$$|\chi^*(u_x)|^2 = \exp(-u_x^2 \langle \bar{h}_s^2 \rangle), \text{ and } \chi^*(u) = \exp(-\beta). \quad (47)$$

The mean square height for the large-scale surface \bar{h}_l is

$$\begin{aligned} \langle \bar{h}_l^2 \rangle &= \int_0^{2\pi} \int_{k_F}^{k_c} \frac{W(k)}{4} k dk d\phi = \frac{B}{2} \left(\frac{1}{k_F^2} - \frac{1}{k_c^2} \right) \\ &= 0.791 \times 10^{-9} \text{ cm}^2. \end{aligned} \quad (48)$$

Thus, $k_d^2 \langle \bar{h}_l^2 \rangle \gg 1$ and the physical optics treatment of scattering by the large scale structure is justified. The total mean square slope of the large-scale surface \bar{h}_l is

$$\begin{aligned} \sigma_k^2 &= \langle \bar{h}_l^2 \rangle = \int_0^{2\pi} \int_{k_F}^{k_c} \frac{W(k)}{4} k^3 dk d\phi \\ &= B \ln \left(\frac{k_c}{k_F} \right) = 0.298 \times 10^{-1}. \end{aligned} \quad (49)$$

The slope probability density is assumed to be Gaussian, thus,

$$p(\bar{\mathbf{s}}) = \frac{1}{\pi \sigma_k^2} \exp \left(-\frac{\bar{\mathbf{s}}^2}{\sigma_k^2} \right). \quad (50)$$

In Figs. 4 through 8, the backscatter cross section $\langle \sigma^{PQ} \rangle_\theta$ averaged over the range of the azimuth angle ϕ_F is plotted as a function of the polar angle θ_F (see Fig. 3). This is formally given by

$$\langle \sigma^{PQ} \rangle_\theta = \frac{1}{2\pi} \int_0^{2\pi} \langle \sigma^{PQ} \rangle d\phi_F. \quad (51)$$

However, in Sec. IV it is shown that Eq. (51) can be evaluated directly on replacing $|D^{PQ}|^2$ in Eq. (14) by its average value $|D_F^{PQ}|^2$ [Eqs. (39) and (40)].

In Fig. 4, $\langle \sigma^{PP} \rangle_\theta$ ($P = V, H$) is plotted as a function of θ_F for the composite surface characterized by the spectral density function [Eq. (41)]. This cross section includes the effects of both the small and large roughness scales of the surface of the flake. Thus, it takes into account both specular point scattering and Bragg scattering. In view of Eq. (40), the average cross section is the same for vertically and horizontally polarized waves. The average cross section of a single scatterer in the ensemble of randomly oriented flakes is $\langle \sigma^{PP} \rangle = 0.77$ [Eq. (37)]. For a conducting sphere of radius a_F , the normalized cross section is 0.92 provided that $k_0 a_F \gg 1$ and ϵ_r is given by Eq. (44).

In Fig. 5, $\langle \sigma^{PP} \rangle_\theta$ ($P = V, H$) is plotted as a function

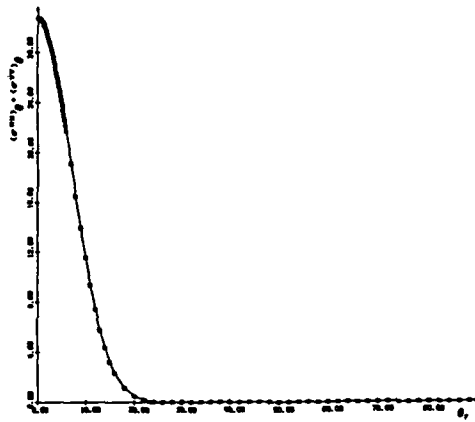


Fig. 5. $\langle \sigma^{HH} \rangle_\theta = \langle \sigma^{VV} \rangle_\theta$ for the large-scale filtered surface \bar{h}_l as a function of θ_F .

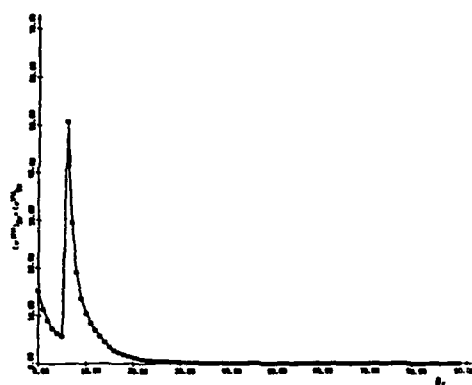


Fig. 6. $\langle \sigma^{HH} \rangle_\theta = \langle \sigma^{VV} \rangle_\theta$ for the small-scale surface h_s as a function of θ_F .

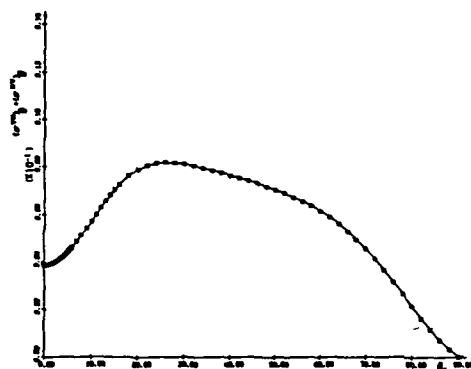


Fig. 7. $\langle \sigma^{VH} \rangle_\theta = \langle \sigma^{HV} \rangle_\theta$ for the composite surface h as a function of θ_F .

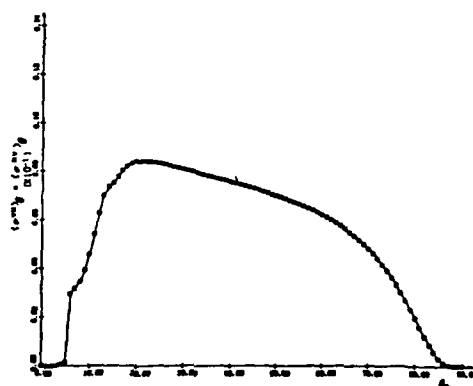


Fig. 8. $\langle \sigma^{VH} \rangle_\theta = \langle \sigma^{HV} \rangle_\theta$ for the small-scale surface h_s as a function of θ_F .

of θ_F for the large-scale filtered surface only ($k_F \leq k < k_d$). Thus, only specular point scattering is considered here. In this case $\langle \sigma^{PP} \rangle = 0.47$. In Fig. 6, $\langle \sigma^{PP} \rangle_\theta$ ($P = V, H$) is plotted as a function of θ_F for the small-scale surface only ($k_d \leq k \leq k_c$). Since $\sigma_{li}^2 \rightarrow 0$ for this case, to evaluate $\langle \sigma^{PQ} \rangle_s$ using Eq. (14), $p(h_x, h_z)$ is set equal to the product of the Dirac delta functions $\delta(h_x)\delta(h_z)$. Thus,

$$\langle \sigma^{PQ} \rangle_{sm} \rightarrow 4\pi k_0^2 \frac{|D^{PQ}|^2}{|\mathbf{u} \cdot \mathbf{u}_y|} \times \exp(-u_y^2 < k_c^2) \left(\frac{u_y}{2} \right)^{2m} \frac{W_m(u_y, u_y)}{m!} \Big|_{\mathbf{u}=\mathbf{u}_y}, \quad (52)$$

and the leading term in the sum $\langle \sigma^{PQ} \rangle_s$ (i.e., $m = 1$) reduces to the first-order Bragg scattering cross section. For this case, $\langle \sigma^{PP} \rangle_s = 0.5$. The corresponding coherent scattering term for a smooth flat flake³ is $\langle \sigma^{PP} \rangle = 0.32$. A flake with a two-scale roughness has, on the average, a larger backscatter cross section than a corresponding flake with no small-scale roughness. Since, for the randomly oriented flakes, $\langle \sigma^{PP} \rangle = 0.77$, their backscatter cross sections are on the average smaller than the cross sections for spheres with a cross-sectional area $\pi a_F^2 = L_F^2$ ($\langle \sigma^{PP} \rangle = 0.92$). However, considering the fact that a volume of nine flakes each of thickness $d \approx L_F/12$ is approximately equal to the volume of a sphere of radius a_F , for a given volume of particles the backscatter cross section for the flakes is 7.5 times larger than the cross section for the spheres. In Fig. 7 the cross-polarized backscatter cross section (averaged over θ_F) $\langle \sigma^{VH} \rangle_\theta = \langle \sigma^{HV} \rangle_\theta$ is plotted as a function of θ_F . The value of $\langle \sigma^{VH} \rangle$ (0.522×10^{-2}) is significantly smaller than the average backscatter cross sections for the like polarized case $\langle \sigma^{PP} \rangle$. In Fig. 8, $\langle \sigma^{PQ} \rangle_\theta$ ($P \neq Q$) is plotted as a function of θ_F for the small-scale surface only ($k_d \leq k < k_c$) [Eq. (52)]. At near-normal incidence the cross section $\langle \sigma^{VH} \rangle_\theta$ is very small since $|D^{VH}|_{\mathbf{u}_y}^2$ is very small for backscatter when $\theta_F \ll 1$. Furthermore, since $W_1 = 0$ for $k < k_d$, therefore, $\langle \sigma^{VH} \rangle_{s1} \rightarrow 0$ for $\theta_F \rightarrow 0$. For grazing angles, higher-order Bragg terms become very small and $\langle \sigma^{VH} \rangle_s \approx \langle \sigma^{VH} \rangle_{s1}$ in Eq. (14). For the flake with the small-scale roughness, $\langle \sigma^{VH} \rangle = 0.52 \times 10^{-2}$.

V. Concluding Remarks

The average normalized backscatter cross sections for arbitrarily oriented metallic flakes are derived using the full wave approach. Thus, the total backscatter cross section is expressed as a weighted sum of two cross sections. The first is associated with the filtered surface consisting of the large-scale spectral components of the composite rough surface, while the second is associated with the surface consisting of its small-scale spectral components that ride on the large-scale surface.¹⁴⁻¹⁶ These backscatter cross sections are compared with those of similar flakes having either a large- or a small-scale surface roughness.

It is shown that the average normalized backscatter cross section (per unit volume) for the flake with the composite surface is larger than the backscatter cross sections for metallic spheres.

This paper was sponsored by the U.S. Army Research Office, Contract DAAG-29-82-K-0123. The manuscript was typed by E. Everett.

VI. References

1. P. Beckmann and A. Spizzichino, *The Scattering of Electromagnetic Waves from Rough Surfaces* (McMillan, New York, 1963).
2. S. O. Rice, *Commun. Pure Appl. Math.* 4, 351 (1951).
3. D. E. Barrick, "Rough Surfaces" in *Radar Cross Section Handbook* (Plenum, New York, 1970), Chap. 9.
4. A. Ishimaru, *Wave Propagation and Scattering in Random Media in Multiple Scattering, Turbulence, Rough Surfaces and Remote Sensing, Vol. 2* (Academic, New York, 1978).
5. G. S. Brown, *IEEE Trans. Antennas Propag.* AP-26, 472 (1978).
6. E. Bahar, D. E. Barrick, and M. A. Fitzwater, *IEEE Trans. Antennas Propag.* AP-31, 698 (1983).
7. E. Bahar, *Radio Sci.* 16, 331 (1981a).
8. E. Bahar, *Radio Sci.* 16, 1327 (1981b).
9. B. G. Smith, *IEEE Trans. Antennas Propag.* AP-15, 668 (1967).
10. M. I. Sancer, *IEEE Trans. Antennas Propag.* AP-17, 577 (1969).
11. T. Hagfors, *J. Geophys. Res.* 71, 279 (1966).
12. G. L. Tyler, *Radio Sci.* 11, 83 (1976).
13. H. Ehrenreich, *IEEE Spectrum* 2, 162 (1965).
14. J. W. Wright, *IEEE Trans. Antennas Propag.* AP-14, 749 (1966).
15. J. W. Wright, *IEEE Trans. Antennas Propag.* AP-16, 217 (1968).
16. G. R. Valenzuela, *Radio Sci.* 3, 1051 (1968).

SCATTERING CROSS SECTIONS FOR PARTICLES OF IRREGULAR SHAPE

Ezekiel Bahar
Electrical Engineering Department
University of Nebraska-Lincoln, Lincoln, Nebraska 68588-0511

ABSTRACT

The full wave approach recently applied to the problem of electromagnetic scattering by a two scale model of random rough surfaces has been shown to account for both Bragg scattering and Specular Point scattering in a self-consistent manner. Thus scattering cross sections can be expressed as weighted sums of two cross sections. The first is associated with a smooth, filtered surface consisting of the large scale spectral components of the rough surface and the second is associated with its small scale spectral components.

In a similar manner the scattering cross sections for a particle of irregular shape can be characterized by weighted sums of two cross sections. The first is related to the cross section for a "smooth" particle of arbitrary shape and the second accounts for the small scale surface roughness of the particle. To apply such an approach to the scattering problem, it is necessary to assume that the principal dimensions of the particle are larger than both the wavelength of the scattered fields and the small scale surface height correlation distance.

Both the depolarized and like polarized components of the scattered fields are accounted for in the full wave analysis. These solutions are consistent with reciprocity and realizability relationships in electromagnetic theory and they are invariant to coordinate transformations.

1. Introduction

The purpose of this investigation is to determine the average normalized backscatter cross sections for randomly oriented metallic flakes. The irregular shaped flake is characterized by its surface height spectral density function and its lateral dimension is assumed to be larger than both the wavelength of the incident electromagnetic field and the correlation distance of the rough surface.

The full wave approach which accounts for both specular point scattering and Bragg scattering in a self-consistent manner is used to express the total cross section of the flake as a weighted sum of two cross sections (see Section 2). The first is associated with the large scale spectral components of the surface of the flakes and the second is associated with its small scale spectral components. The unit vector normal to the surface of the flake is characterized by the polar angle θ_f and azimuth angle ϕ_f (see Section 3). Through a suitable choice of the coordinate system, the average with respect to the azimuth angle is evaluated analytically while the average over the polar angle θ_f can be evaluated numerically.

2. Formulation of the Problem

To determine the scattering cross section for arbitrarily oriented metallic flakes at optical frequencies, it is convenient to use a two-scale model of the rough surface of the flakes. Thus, the composite surface of the flake is expressed as follows (see Fig. 1)

$$h(x,z) = h_L(x,z) + h_s(x,z) \quad (2.1)$$

In equation (2.1), h_L consists of the large scale spectral components of h while h_s consists of its small scale spectral components. It is assumed that the lateral dimensions of the flake L_F are much larger than both the wavelength of the electromagnetic waves and the correlation distance of the rough surface h , (2.1). For a homogeneous isotropic surface height, the spectral density function (Rice 1951, Barrick 1970, Ishimaru 1978), is the Fourier transform of the surface height autocorrelation

$$\langle h(x,z)h'(x',z') \rangle \quad W(v_x, v_z) = \frac{1}{\pi^2} \int \langle hh' \rangle \exp(i v_x \bar{x}_d + i v_z \bar{z}_d) dx_d dz_d \quad (2.2)$$

where the symbol $\langle \rangle$ implies statistical average and $\langle hh' \rangle$ is a function of $|\bar{r}_d|$.

$$\bar{r}_d = (x-x')\bar{a}_x + (z-z')\bar{a}_z = x_d\bar{a}_x + z_d\bar{a}_z \quad (2.3)$$

Thus, the surface h_L consists of the spectral components

$$k_F < k = (v_x^2 + v_z^2)^{1/2} < k_d \quad (2.4)$$

where $k_F = 2\pi/L_F$ is the largest wavenumber characterizing the surface of the flake and k_d is the wavenumber where spectral splitting (between the large and small scale surface) is assumed to occur. The surface h_s consists of the small scale spectral components

$$k_d < k = (v_x^2 + v_z^2)^{1/2} < k_c \quad (2.5)$$

where k_c , the spectral cutoff wavenumber (Brown 1978) is the smallest wavenumber characterizing the flake.

The full wave approach which accounts for both specular point scattering as well as Bragg scattering in a self-consistent manner is used in this work to determine the scattering cross section of the composite model of an arbitrarily oriented flake (Bahar, et al. 1982). Thus, the total normalized scattering cross section per unit area $\langle \sigma^{PQ} \rangle$ as a weighted sum of two cross sections

$$\langle \sigma^{PQ} \rangle = \langle \sigma^{PQ} \rangle_L + \langle \sigma^{PQ} \rangle_s \quad (2.6)$$

in which $\langle \sigma^{PQ} \rangle_L$ is the cross section associated with the large scale filtered surface h_L and the cross section $\langle \sigma^{PQ} \rangle_s$ is associated with the small scale surface h_s that rides on the large scale surface h_L . The first superscript, P , corresponds to the polarization of the scattered wave while the second superscript corresponds to the polarization of the incident wave.

On deriving the full wave solution it is implicitly assumed that the wavenumber where spectral splitting occurs, k_d , is chosen such that the large scale surface h_L satisfies the radii of curvature criteria associated with the Kirchhoff approximations of the surface fields and the condition for deep phase modulation. The scattering cross section $\langle \sigma_m^{PQ} \rangle_L$ is given by (Bahar 1981a,b)

$$\langle \sigma_m^{PQ} \rangle_L = |\chi^s(\vec{v} \cdot \vec{n})|^2 \langle \sigma_m^{PQ} \rangle \quad (2.7)$$

in which χ^s is the characteristic function for the small scale surface

$$\chi^s(\vec{v} \cdot \vec{n}_s) = \chi^s(v) = \langle \exp i v h_s \rangle \quad (2.8)$$

and

$$\vec{v}_0 = \vec{k}^f - \vec{k}_i = k_0 (\vec{n}^f - \vec{n}^i), \quad \vec{v} = |\vec{v}| \quad (2.9)$$

The unit vectors \vec{n}^i and \vec{n}^f are in the directions of the incident and scattered waves and $k_0 = \omega(\mu_0 \epsilon_0)^{1/2}$ is the free space wavenumber for the electromagnetic waves (μ_0 and ϵ_0 are the free space permeability and permittivity). An $\exp(i\omega t)$ time dependence is assumed in this work. The vector \vec{n}_s is the value of the unit vector \vec{n} normal to the surface $h(x,z)$ at the specular points. Thus

$$\begin{aligned} \vec{n} &= \nabla f / |\nabla f| = (-h_x \vec{a}_x + \vec{a}_y - h_z \vec{a}_z) / (h_x^2 + 1 + h_z^2)^{1/2} \\ &\equiv \sin \gamma \cos \delta \vec{a}_x + \cos \gamma \vec{a}_y + \sin \gamma \sin \delta \vec{a}_z \end{aligned} \quad (2.10)$$

where

$$f = y - h(x,z), \quad h_x = \partial h / \partial x, \quad h_z = \partial h / \partial z \quad (2.11)$$

and

$$\vec{n}_s = \vec{v} / v \quad (2.12)$$

The expression for the physical optics cross section $\langle \sigma_m^{PQ} \rangle$, for the surface h_L is

$$\langle \sigma_m^{PQ} \rangle = \frac{4\pi}{v} k_0^2 \left[\frac{D^{PQ}}{|\vec{n} \cdot \vec{a}_y|} \right]^2 P_2(\vec{n}^f, \vec{n}^i | \vec{n}) p(\vec{n}) \bigg|_{\vec{n}_s} \quad (2.13)$$

in which D^{PQ} depends on the polarization of the incident and scattered waves, the unit vectors \vec{n}^i, \vec{n}^f and \vec{n} and the relative complex permittivities and permeabilities of the flake. The shadow function P is the probability that a point on the rough surface is both illuminated by the source and visible by the observer given the slopes, $\vec{n}(h_x, h_z)$, at the point (Smith 1967, Sancer 1969). The function $p(\vec{n})$ is the probability density of the slopes h_x and h_z . The coefficient $|\chi^s|^2$ that multiplies $\langle \sigma_m^{PQ} \rangle$ is a weighting function that accounts for the degradation of the specular point scattering cross section due to the superimposed small scale rough surface h_s (Bahar 1981b). Thus, as $h_s \rightarrow 0$ $|\chi^s|^2 \rightarrow 1$.

The scattering cross section $\langle \sigma_m^{PQ} \rangle_s$ for the Gaussian surface h_s that rides the large scale surface h_L is given by the sum, (Bahar et al. 1982)

$$\langle \sigma_m^{PQ} \rangle_s = \sum_{m=1}^{\infty} \langle \sigma_m^{PQ} \rangle_{sm} \quad (2.14a)$$

where

$$\langle \sigma^{PQ} \rangle_m = 4\pi k_0^2 \int \frac{|D^{PQ}|^2 P_2(\bar{n}^f, \bar{n}^i | \bar{n})}{\bar{n} \cdot \bar{a}_y} \cdot \exp\left[-v_y^2 \langle h_s^2 \rangle\right] \left[\frac{v_y}{2}\right]^{2m} \frac{W_m(v_x, v_z)}{n!} p(h_x, h_z) dh_x dh_z \quad (2.14)$$

In (2.14) $\langle h_s^2 \rangle$ is the mean square of the surface height h_s and v_x, v_y and v_z are the components of \bar{v} (2.9) in the local coordinate system associated with the unit vectors \bar{n}_1, \bar{n}_2 and \bar{n}_3 (at each point on the large scale surface h_1 , see Fig. 2). Thus \bar{v} is also expressed as

$$\bar{v} = v_x \bar{n}_1 + v_y \bar{n}_2 + v_z \bar{n}_3 \quad (2.15)$$

where

$$\bar{n}_1 = (\bar{n} \times \bar{a}_z) / |\bar{n} \times \bar{a}_z|, \quad \bar{n}_2 = \bar{n}, \quad \bar{n}_3 = \bar{n}_1 \times \bar{n} \quad (2.16)$$

The function $W_m(v_x, v_z) 2^{2m}$ is the two dimensional Fourier transform of $\langle h_s h_s' \rangle^m$

$$\begin{aligned} \frac{W_m(v_x, v_z)}{2^{2m}} &= \frac{1}{(2\pi)^2} \int \langle h_s h_s' \rangle^m \exp(i v_x \bar{x}_d + i v_z \bar{z}_d) d\bar{x}_d d\bar{z}_d \\ &= \frac{1}{2^{2m}} \int W_{m-1}(v_x', v_z') W_1(v_x - v_x', v_z - v_z') dv_x' dv_z' \\ &= \frac{1}{2^{2m}} W_{m-1}(v_x, v_z) \otimes W_1(v_x, v_z) \end{aligned} \quad (2.17)$$

In (2.17) the symbol \otimes denotes the two dimensional convolution of W_{m-1} with W_1 and $|x_d \bar{n}_1 + \bar{z}_d \bar{n}_3|$ is the distance measured along the large scale surface h_1 . The two dimensional Fourier transforms of the surface height autocorrelation function $\langle h_s h_s' \rangle$ is equal to the spectral density function $W_1(v_x, v_z)/4$. When the parameter $4k_0^2 \langle h_s^2 \rangle \equiv \beta \ll 1$ and $\bar{n} = \bar{a}_y$ the first term in (2.14) accounts for first order Bragg scattering and the higher order terms $m \geq 2$ may be neglected. In this case, the full wave solution (2.14) is in agreement with Brown's solution (1978) based on a combination of physical optics and perturbation theory. However, since it is assumed using the full wave approach that the condition for deep phase modulation is satisfied, it is necessary to choose $\beta = 4k_0^2 \langle h_s^2 \rangle \geq 1$ in order to assure that the weighted sum (2.14) remains insensitive to variations in k_d (the wavenumber where spectral splitting is assumed to occur, (Bahar et al. 1982)). Since fewer terms in (2.14) need to be evaluated for smaller values of β , it is appropriate to assume $\beta = 1.0$.

Since the metallic flakes are randomly oriented with respect to the fixed observer, in Section 3, the analytical results presented in this section are modified to account for arbitrary orientation of the normal to the mean surface of the flake.

3. Scattering Cross Sections for Arbitrarily Oriented Metallic Flakes

Let x', y', z' be a fixed reference coordinate system and let x, y, z be a rotated coordinated system such that the unit vector \bar{a}_y is normal to the mean surface of the flake ($y=0$) (see Fig. 3). For backscatter it is convenient to choose the unit vectors $\bar{n}^f = -\bar{n}^i$ such that

$$\bar{n}^f = -\bar{n}^i = \bar{a}_y \quad (3.1)$$

The unit vector \bar{a}_y normal to the mean surface of the flake can be expressed as follows in terms of the fixed reference coordinate system

$$\bar{a}_y = \sin\theta_F \cos\phi_F \bar{a}_x' + \cos\theta_F \bar{a}_y' + \sin\theta_F \sin\phi_F \bar{a}_z' \quad (3.2)$$

For convenience the two orthogonal unit vectors \bar{a}_x and \bar{a}_z in the mean plane of the flake are chosen such that the plane of incidence in the flake coordinate system is the x, y plane (normal to \bar{a}_z). Thus

$$\bar{a}_z = (\bar{n}^i \times \bar{a}_y) / |\bar{n}^i \times \bar{a}_y| \text{ and } \bar{a}_x = \bar{a}_y \times \bar{a}_z \quad (3.3)$$

The expression for \bar{n}^i in the flake coordinate system is therefore

$$\bar{n}^i = (\bar{n}^i \cdot \bar{a}_x) \bar{a}_x + (\bar{n}^i \cdot \bar{a}_y) \bar{a}_y = \sin\theta_o^i \bar{a}_x - \cos\theta_o^i \bar{a}_y \quad (3.4)$$

where

$$\cos\theta_o^i = -\bar{n}^i \cdot \bar{a}_y = \cos\theta_F \quad (3.5)$$

The angle ψ_F^i between the reference plane of incidence (normal to \bar{a}_z' in the fixed coordinate system) and the plane of incidence in the flake coordinate system (normal to $\bar{n}^i \times \bar{a}_y$) is

$$\cos\psi_F^i = \frac{\bar{a}_z' \cdot (\bar{n}^i \times \bar{a}_y)}{|\bar{n}^i \times \bar{a}_y|} = \frac{-[\bar{a}_z' \cdot \bar{a}_y \bar{a}_x]}{|\bar{n}^i \times \bar{a}_y|} = \frac{\bar{a}_z' \cdot \bar{a}_x}{|\bar{n}^i \times \bar{a}_y|} = \cos\phi_F \quad (3.6)$$

thus

$$\sin\psi_F^i = \frac{\bar{a}_z' \times (\bar{n}^i \times \bar{a}_y) \cdot \bar{n}^i}{|\bar{n}^i \times \bar{a}_y|} = \sin\phi_F \quad (3.7)$$

Since $\bar{n}^f = -\bar{n}^i$ for backscatter, the angle ψ_F^f between the plane of scatter in the fixed (x', y', z') coordinate system and the plane of scatter in the flake coordinate system (x, z, z) is

$$\psi_F^f = -\psi_F^i \quad (3.8)$$

Thus the matrix that transforms the vertically and horizontally polarized incident waves of the fixed coordinate system to the vertically and horizontally polarized incident waves of the flake coordinate system is (Bahar 1981a,b)

$$T_F^i = \begin{bmatrix} \cos\psi_F^i & \sin\psi_F^i \\ -\sin\psi_F^i & \cos\psi_F^i \end{bmatrix} \quad (3.9)$$

Similarly, the matrix that transforms the vertically and horizontally polarized scattered waves in the flake coordinate system back into vertically and horizontally polarized scattered waves of the fixed coordinate system is

$$T_F^f = \begin{bmatrix} \cos \psi_F^f & -\sin \psi_F^f \\ \sin \psi_F^f & \cos \psi_F^f \end{bmatrix} \quad (3.10)$$

Thus, in view of (3.8) for backscatter

$$T_F^f = T_F^i \quad (3.11)$$

The coefficients D^{PQ} in (2.14) are elements of the 2×2 matrix D given by (Bahar 1981a,b)

$$D = C_0^{in} T_F^f T_I^i \quad (3.12)$$

in which C_0^{in} is the cosine of the angle between the incident wave normal \bar{n}^i (3.4) and the unit vector \bar{n} normal to the rough surface of the flake (2.10). Thus,

$$C_0^{in} = -\bar{n}^i \cdot \bar{n} = \cos \gamma \cos \theta_F - \sin \gamma \sin \theta_F \cos \delta \quad (3.13)$$

The elements F^{PQ} of the scattering matrix F in (3.12) are functions of the unit vectors $\bar{n}^i, \bar{n}^f, \bar{n}$ and the relative permittivity and permeability of the flakes (Bahar 1981a). The matrix T^i transforms the vertically and horizontally polarized incident waves of the x, y, z coordinate system to vertically and horizontally polarized waves of the local coordinate system $(\bar{n}_1, \bar{n}_2, \bar{n}_3)$ associated with the rough surface of the flake (3.16). Similarly, the matrix T^f transforms the vertically and horizontally polarized scattered waves of the local coordinate system back into vertically and horizontally polarized waves of the x, y, z coordinate system (Bahar 1981a,b).

To account for the arbitrary orientation of the flake with respect to the fixed (x', y', z') coordinate system (3.12) must be post-multiplied by T_I^i and pre-multiplied by T_F^f . Therefore, in the expressions for the scattering cross sections (2.6), the elements of the matrix D must be replaced by the elements of the matrix D_F given by

$$D_F = T_F^f D T_I^i = C_0^{in} T_F^f T_I^i D T_I^i T_F^i \quad (3.14)$$

where

$$T_I^i \equiv T_I^i T_F^i = \begin{bmatrix} \cos(\psi^i + \phi_F) & \sin(\psi^i + \phi_F) \\ -\sin(\psi^i + \phi_F) & \cos(\psi^i + \phi_F) \end{bmatrix} \equiv \begin{bmatrix} C_I & S_I \\ -S_I & C_I \end{bmatrix} \quad (3.15)$$

In (3.15)

$$\cos \psi^i = [\cos \gamma \sin \theta_F + \sin \gamma \cos \theta_F \cos \delta] / S_0^{in} \quad (3.16)$$

where

$$\sin \psi^i = \sin \gamma \sin \delta / S_0^{in} \quad (3.16)$$

$$S_0^{in} = [1 - (C_0^{in})^2]^{1/2} \quad (3.16)$$

For backscatter $T_I^f = T_I^i$ and $F^{VH} = F^{HV} = 0$ thus,

$$D_F = C_o^{in} \begin{bmatrix} C_T^2 F^{VV} - S_T^2 F^{HH} & C_T S_T (F^{VV} + F^{HH}) \\ -C_T S_T (F^{VV} + F^{HH}) & C_T^2 F^{HH} - S_T^2 F^{VV} \end{bmatrix} \quad (3.18)$$

Neglecting multiple scatter and assuming that the phase of the scattered signals from the individual flakes are uniformly distributed in the interval $[0, 2\pi]$ the backscatter cross section for an ensemble of randomly located flakes is given by the sum of the individual backscatter cross sections (Beckmann and Spizzichino 1964). Thus, accounting for the random orientation of each individual flake, the average cross backscatter cross section of the ensemble of flakes is

$$\langle \sigma^{PQ} \rangle = \int_0^{\pi/2} \int_0^{2\pi} \langle \sigma^{PQ} \rangle_P(\theta_F, \phi_F) d\phi_F d\theta_F \equiv \int_0^{\pi/2} \langle \sigma^{PQ} \rangle_\theta p(\theta_F) d\theta_F \quad (3.19a)$$

in which

$$\langle \sigma^{PQ} \rangle_\theta = \frac{1}{2\pi} \int_0^{2\pi} \langle \sigma^{PQ} \rangle d\phi \quad (3.19b)$$

and it is assumed that the unit vector normal to the mean surface of the flake is uniformly directed in the half space $0 \leq \theta_F \leq \pi/2$, $0 < \phi_F < 2\pi$. Thus,

$$p(\theta_F, \phi_F) = \frac{\sin \theta_F}{2\pi} \equiv \frac{p(\theta_F)}{2\pi} \quad (3.20)$$

Since $\langle \sigma^{PQ} \rangle$ is dependent on ϕ_F only through the sines and cosines of the angles $(\psi^1 + \phi_F)$ (3.18), it is convenient to evaluate the average of $\langle \sigma^{PQ} \rangle$ with respect to the angle ϕ_F analytically by first evaluating the average of $|D_F^{PQ}|^2$ with respect to ϕ_F . Thus for $P \neq Q$

$$\begin{aligned} \overline{|D_F^{PQ}|^2} &\equiv \frac{1}{2\pi} \int_0^{2\pi} |D_F^{PQ}|^2 d\phi_F = \frac{(C_o^{in})^2}{2\pi} \int_0^{2\pi} C_T^2 S_T^2 |F^{VV} + F^{HH}|^2 d\phi_F \\ &= \frac{(C_o^{in})^2}{8} |F^{VV} + F^{HH}|^2 \end{aligned} \quad (3.21)$$

and for $P = V, H$

$$\begin{aligned} \overline{|D_F^{PP}|^2} &\equiv \frac{1}{2\pi} \int_0^{2\pi} |D_F^{PP}|^2 d\phi_F = \frac{(C_o^{in})^2}{2\pi} \int_0^{2\pi} C_T^4 |F^{VV}|^2 + S_T^4 |F^{HH}|^2 - 2C_T^2 S_T^2 \operatorname{Re}(F^{VV} F^{HH*}) d\phi_F \\ &= \frac{1}{8} (C_o^{in})^2 [3|F^{VV}|^2 + 3|F^{HH}|^2 - 2 \operatorname{Re} F^{VV} F^{HH*}] \\ &= \frac{1}{2} (C_o^{in})^2 (4|F^{VV}|^2 + 4|F^{HH}|^2 - |F^{VV} + F^{HH}|^2) \end{aligned} \quad (3.22)$$

in which the symbol * denotes the complex conjugate.

The expression for F^{VV} and F^{HH} are complicated functions of θ_F . Thus, the integrals with respect to θ_F are not evaluated analytically. Instead $\langle \sigma^{PQ} \rangle_\theta$ (3.19), must be evaluated numerically using (2.14)

with $|D^{PQ}|^2$ ($P, Q=V, H$) replaced by $|\overline{D_F^{PQ}}|^2$ (3.2) and (3.22). To obtain the ensemble average for the scattering cross sections $\langle \sigma^{PQ} \rangle$ (3.19) the result from the previous integration, $\langle \sigma^{PQ} \rangle_\theta$, is multiplied by $p(\theta_F) = \sin \theta_F$ and integrated with respect to θ_F . Thus summing up, the integral (3.19) is performed analytically with respect to ϕ_F , however it must be performed numerically with respect to θ_F . The integrations with respect to $h_x h_z$ (2.14) must also be performed numerically.

4. Concluding Remarks

Expressions for the average normalized backscatter cross sections for arbitrarily oriented metallic flakes are derived using the full wave approach. Thus, the total backscatter cross section is expressed as a weighted sum of two cross sections. The first is associated with the filtered surface consisting of the large scale spectral components of the composite rough surface while the second is associated with the surface consisting of its small scale spectral components that ride on the large scale surface.

To obtain numerical values for the average normalized backscatter cross sections, using the full wave approach presented in this paper, it is necessary to know the surface height spectral density $W(v_x, v_y)$ (2.2) and the complex dielectric constant of the metallic flake. Several models of metallic flakes are currently under investigation.

Acknowledgments

This paper was sponsored by the U. S. Army Research Office, Contract No. DAAG-29-82-K-0123.

The manuscript was typed by Mrs. E. Everett.

5. References

1. Bahar, E. (1981a), "Scattering Cross Sections from Rough Surfaces—Full Wave Analysis," *Radio Science*, 16(3), pp. 331-341.
2. Bahar, E. (1981b), "Scattering Cross Sections for Composite Random Surfaces—Full Wave Analysis," *Radio Science*, 16(6), pp. 1327-1335.
3. Bahar, E., D. E. Barrick and M. A. Fitzwater (1982), "Computations of Scattering Cross Sections for Composite Surfaces and the Specification of the Wavenumber Where Spectral Splitting Occurs," (submitted for review).
4. Barrick, D. E. (1970), *Rough Surfaces*, in *Radar Cross Section Handbook*, Chapter 9, Plenum Press, New York.
5. Beckmann, P., and A. Spizzichino (1963), *The Scattering of Electromagnetic Waves from Rough Surfaces*, McMillan, New York.
6. Brown, G. S. (1978), "Backscattering from a Gaussian-Distributed Perfectly Conducting Rough Surface," *IEEE Transactions on Antennas and Propagation*, AP-26(3), pp. 472-482.
7. Ishimaru, A. (1978), *Wave Propagation and Scattering in Random Media in Multiple Scattering, Turbulence, Rough Surfaces and Remote Sensing*, Vol. 2, Academic Press, New York.
8. Rice, S. O. (1951), "Reflection of Electromagnetic Waves from a Slightly Rough Surface," *Communication of Pure and Applied Math*, Vol. 4, pp. 351-378.
9. Sancer, M. I. (1969), "Shadow-Corrected Electromagnetic Scattering from a Randomly Rough Surface," *IEEE Transactions on Antennas and Propagation*, AP-17(5), pp. 577-585.
10. Smith, B. G. (1967), "Geometrical Shadowing of a Randomly Rough Surface," *IEEE Transactions on Antennas and Propagation*, AP-15(5), pp. 668-671.

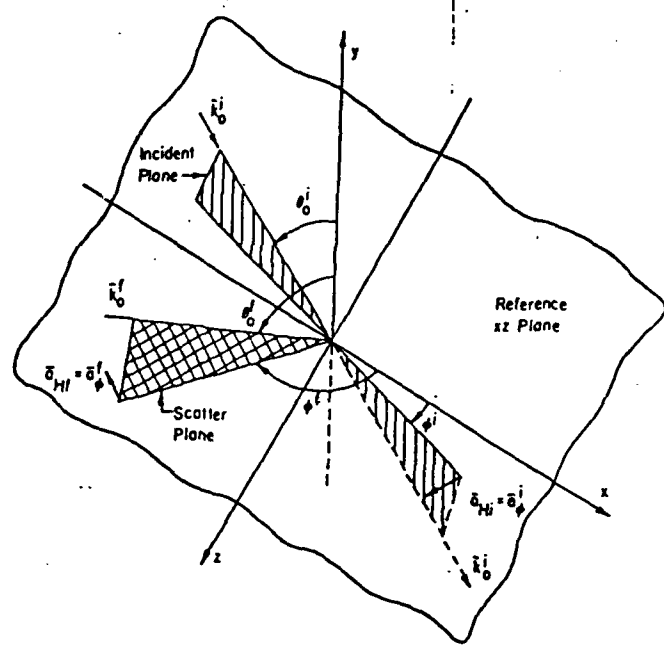


Figure 1. Plane of incidence, scattering plane, and reference (x,y) plane.

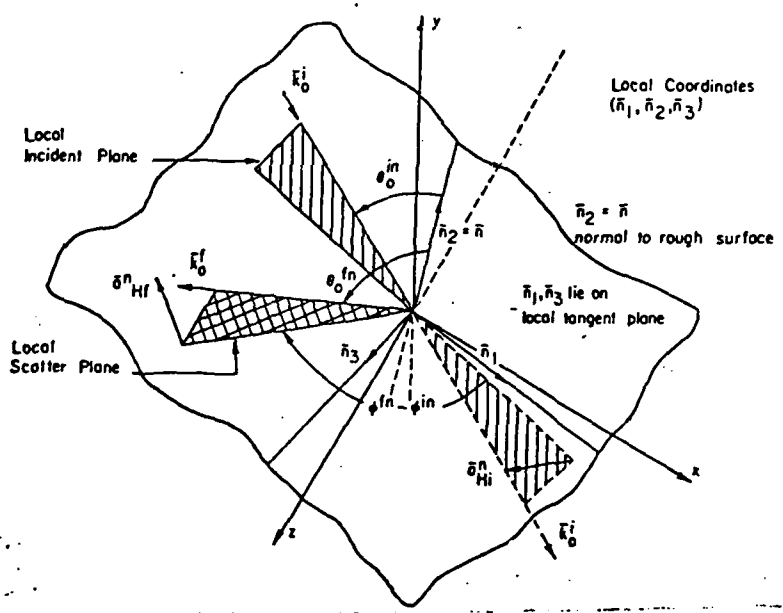


Figure 2. Local plane of incidence and scatter and local coordinate system with unit vectors $\bar{n}_1, \bar{n}_2, \bar{n}_3$.

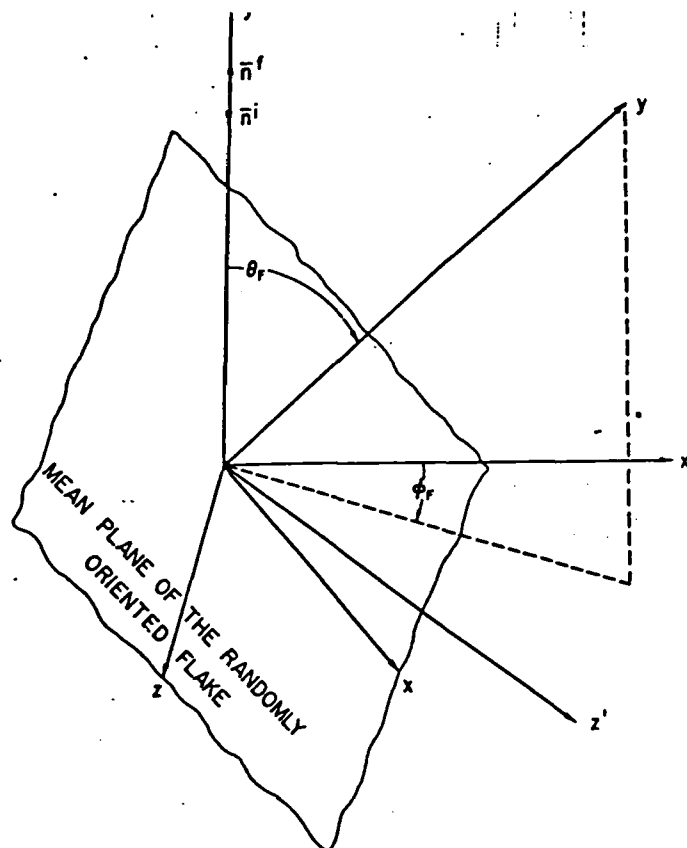


Figure 3. The randomly oriented flake.

MODULATION OF SCATTERING CROSS SECTIONS FOR ARBITRARILY ORIENTED
COMPOSITE ROUGH SURFACES--FULL WAVE APPROACH

Ezekiel Bahar
Electrical Engineering Department
University of Nebraska, Lincoln, Nebraska 68588
Clifford L. Rufenach and Donald E. Barrick
NOAA/ERL/Wave Propagation Laboratory
Boulder, Colorado 80303
and

Mary Ann Fitzwater
Electrical Engineering Department
University of Nebraska, Lincoln, Nebraska 68588

ABSTRACT

As a synthetic aperture radar scans different portions of a rough surface, the direction of the unit vector normal to the mean surface of the effective illuminated area (resolution cell) fluctuates. In this paper the modulations of the scattering cross sections of the resolution cell are determined as the normal to it tilts in planes that are in and perpendicular to the fixed reference plane of incidence. Using the full wave approach, the scattering cross sections are expressed as a weighted sum of two cross sections. The first cross section is associated with scales of roughness within the resolution cell that are large compared to the radar wavelength, and the second cross section is associated with small-scale spectral components within the resolution cell. Thus, both specular point scattering and Bragg scattering are accounted for in a self-consistent manner. The results are compared with earlier solutions based on first order Bragg scattering theory.

Formulation of the Problem

The recently derived full wave solutions for the normalized cross sections per unit area are summarized here for composite rough surfaces. Let the position vector to a point on the rough surface be expressed as follows:

$$\vec{r}_s = \vec{r}_L(x, h_L, z) + \vec{n}_s h_s \quad (1)$$

in which $y = h_L(x, z)$ is the filtered surface consisting of the large scale spectral components and h_s the small scale surface height is measured in the direction of the normal (\vec{n}) to the large scale surface $y = h_L$. For a homogeneous, isotropic surface height the spectral density function is the Fourier transform of the surface height autocorrelation function $\langle h(x, z)h'(x', z') \rangle$

$$W(v_x, v_z) = \frac{1}{\pi^2} \int_{-\infty}^{\infty} \langle hh' \rangle \exp(i v_x x_d + i v_z z_d) dx_d dz_d \quad (2a)$$

where $\langle hh' \rangle$ is a function of $|\vec{r}_d| = (x_d^2 + z_d^2)^{1/2}$ and

$$x - x' = x_d \text{ and } z - z' = z_d. \quad (2b)$$

The surface $h_L(x, z)$ consists of the spectral components $k = (v_x^2 + v_z^2)^{1/2} \leq k_d$ and the remainder term h_s consists of the spectral components $k > k_d$. Since the full wave approach accounts for both specular point scattering and Bragg scattering in a self-consistent manner, the total scattering cross section can be expressed as a weighted sum of the cross section $\langle \sigma^{PQ} \rangle_L$ for the filtered surface h_L and the cross section $\langle \sigma^{PQ} \rangle_s$ for the surface h_s that rides on the large-scale surface h_L

$$\langle \sigma^{PQ} \rangle = \langle \sigma^{PQ} \rangle_L + \langle \sigma^{PQ} \rangle_s \quad (3)$$

The symbol $\langle \rangle$ denotes statistical average. The first superscript P corresponds to the polarization of the scattered wave while the second superscript Q corresponds to the polarization of the incident wave. To derive (3) using the full wave approach it is implicitly assumed that the large scale surface meets the radii

of curvature criteria (associated with the Kirchhoff approximations for the surface fields) as well as the condition for deep phase modulation. Thus the first term in (3) is shown to be

$$\langle \sigma^{PQ} \rangle_L = |\chi^s(\vec{v} \cdot \vec{n}_s)|^2 \langle \sigma^{PQ} \rangle_m \quad (4)$$

in which χ^s is the characteristic function for the small scale surface

$$\chi^s(\vec{v} \cdot \vec{n}_s) = \chi^s(v) = \langle \exp i v h_s \rangle \quad (5)$$

where $\vec{v} = \vec{k}^f - \vec{k}^i = k_0(\vec{n}^f - \vec{n}^i)$, $v = |\vec{v}|$.

The unit vectors \vec{n}^f and \vec{n}^i are in the directions of the scattered and incident wave normals respectively; thus for backscatter $\vec{n}^f = -\vec{n}^i$. The free space radio wavenumber is k_0 . An $\exp(i\omega t)$ time dependence is assumed. The vector \vec{n}_s is the value of the unit vector \vec{n} normal to the surface $h(x, z)$ at the specular points. Thus

$$\vec{n} = \nabla f / |\nabla f|, \quad f(x, y, z) = y - h(x, z) \quad (7a)$$

and $\vec{n}_s = \vec{v} / v$.

The expression for the physical optics (specular point) cross section for the large-scale surface h_L is

$$\langle \sigma^{PQ} \rangle_m = \frac{4k_0^2}{v^2} \left[\frac{D^{PQ}}{|\vec{n} \cdot \vec{a}_y|} \right]^2 P_2(\vec{n}^f, \vec{n}^i | \vec{n}) p(\vec{n}) \quad (8)$$

in which D^{PQ} depends on \vec{n}^i , \vec{n}^f , \vec{n} , the media of propagation above and below the rough surface $h(x, z)$ and the polarization of the incident and scattered waves.^{2,3} The shadow function P_2 is the probability that a point on the rough surface h_L is both illuminated and visible, given the slopes $\vec{n}(h_L, h_s)$, at the point. The probability density function for the slopes h_L and h_s is $p(\vec{n})$. The factor $\chi^s(v)$ that multiplies $\langle \sigma^{PQ} \rangle_m$ accounts for the degradation of the contributions from the specular points due to the superimposed small scale rough surface h_s .

Assuming a Gaussian probability density function for h_s , $\langle \sigma^{PQ} \rangle_s$ is given by the sum

$$\langle \sigma^{PQ} \rangle_s = \sum_{m=1}^{\infty} \langle \sigma^{PQ} \rangle_{sm} \quad (9)$$

where

$$\langle \sigma^{PQ} \rangle_{sm} = 4vk_0^2 \int \frac{|D^{PQ}|^2}{|\vec{n} \cdot \vec{a}_y|} P_2(\vec{n}^f, \vec{n}^i | \vec{n}) \cdot \exp(-v^2 \chi_s^2) \left(\frac{v^2}{2} \right)^{2m} \frac{W(v_x, v_z)}{m!} p(h_L, h_s) dh_L dh_s \quad (10)$$

in which χ_s^2 is the mean square of the surface height h_s and v_x , v_y and v_z are the components of \vec{v} (6) in the local coordinate system (at each point on the large scale surface) associated with the unit vectors

\bar{n}_1, \bar{n}_2 and \bar{n}_3 . The function $W(v_x, v_y)/2^{1/2}$ is the two-dimensional Fourier transform of $\langle h(x, y) \rangle^2$.

The first term in (9) $\propto \rho_{01}^{PQ}$ reduces to the first order Bragg scattering cross section for $\beta = 4k_0^2 \langle h^2 \rangle \ll 1$, and $\bar{n} \rightarrow \bar{n}_y$.

In order to apply the full wave approach to SAR it is necessary to modify the results presented in this section (a) to account for the filtering of the very large scale spectral component of the rough surface by the SAR that effectively illuminates a relatively small area of cell F of the rough surface S and (b) to account for the normal to a reference plane associated with the illuminated cell which is characterized by arbitrary tilt angles θ and τ in and perpendicular to the reference plane of incidence (see Fig. 1). It is assumed here that the lateral dimension of the cell illuminated by the SAR is much larger than the small scale surface height correlation distance for the cell and that as the SAR scans different portions of the rough surface S the direction of the unit vector normal to the cell F fluctuates.

Scattering Cross Sections for Arbitrarily Oriented Resolution Cells of the Rough Surface

Let x, y, z be the reference coordinate system associated with the surface of the cell F that is illuminated by the SAR such that the mean surface of the cell is the $y=0$ plane (see Fig. 1). Furthermore, let x', y', z' be the fixed coordinate system associated with the large surface S such that the unit vector \bar{n}^i is normal to the mean rough surface height $h(x', z')$. The unit vector $\bar{n}^i = -\bar{n}^i$ is expressed in terms of the unit vectors of the fixed coordinate system (x', y', z') :

$$\bar{n}^i = -\bar{n}^i \sin \theta \bar{a}_x - \cos \theta \bar{a}_z \quad (11)$$

The unit vector \bar{a}_y normal to the reference surface associated with the cell is expressed in terms of the tilt angles θ and τ in and perpendicular to the fixed plane of incidence, the x', y' plane. Thus

$$\bar{a}_y = \sin \theta \cos \tau \bar{a}_x + \cos \theta \cos \tau \bar{a}_z + \sin \tau \bar{a}_y \quad (12)$$

For convenience \bar{a}_x and \bar{a}_z , the unit vectors associated with the cell, can be chosen such that the plane of incidence in the x, y, z coordinate system is normal to the vector \bar{a}_z . Thus

$$\bar{a}_z = (\bar{n}^i \times \bar{a}_y) / |\bar{n}^i \times \bar{a}_y|, \quad \bar{a}_x = \bar{a}_y \times \bar{a}_z \quad (13)$$

and the expression for \bar{n}^i in the x, y, z coordinate system is

$$\bar{n}^i = \sin \theta \bar{a}_x - \cos \theta \bar{a}_y \quad (14a)$$

where

$$\cos \theta = \cos(\theta' + \theta) \cos \tau \quad (14b)$$

The angle θ' between the plane of incidence in the fixed coordinate system (x', y', z') and the plane of incidence in the coordinate system (x, y, z) associated with the cell is given by

$$\cos \theta' = \frac{\cos \sin(\theta' + \theta)}{\sin \theta} \quad (15)$$

For backscatter $\bar{n}^i = -\bar{n}^i$. Thus the angle θ' between the plane of scatter in the fixed coordinate system (x', y', z') and the plane of scatter in the coordinate system associated with the cell is

$$\theta' = -\theta \quad (16)$$

The matrix that transforms the incident vertically and horizontally polarized waves in the fixed coordinate

system to vertically and horizontally polarized waves in the cell coordinate system is therefore^{2,3}

$$T_F^i = \begin{bmatrix} \cos \theta_F^i & \sin \theta_F^i \\ -\sin \theta_F^i & \cos \theta_F^i \end{bmatrix} \quad (17)$$

Similarly, the matrix that transforms the scattered vertically and horizontally polarized waves in the cell coordinate system back into the vertically and horizontally polarized waves in the fixed coordinate system is

$$T_F^f = \begin{bmatrix} \cos \theta_F^f & -\sin \theta_F^f \\ \sin \theta_F^f & \cos \theta_F^f \end{bmatrix} \quad (18)$$

Thus in view of (16), $T_F^f = T_F^i$. The coefficients D^{PQ} in (8) are elements of a 2×2 matrix D given by

$$D = C_0^{in} T_F^i T_F^f \quad (19)$$

in which C_0^{in} is the cosine of the angle between the incident wave normal \bar{n}^i and the unit vector \bar{n} normal to the rough surface of the cell $h(x, z)$. Thus

$$C_0^{in} = -\bar{n}^i \cdot \bar{n} = \cos \theta_0^{in} \quad (20)$$

where \bar{n}^i is given by (14) and \bar{n} is given by (7) with $f(x, z) = y - h(x, z)$. The elements of the scattering matrix F in (19) are functions of the unit vectors \bar{n}^i, \bar{n}^f and \bar{n} as well as the media of propagation above and below the rough surface S.² The matrix T_F^i transforms the vertically and horizontally polarized waves in the cell coordinate system $(\bar{a}_x, \bar{a}_y, \bar{a}_z)$ to vertically and horizontally polarized waves in the local coordinate system that conforms with the rough surface, $\bar{n}_1, \bar{n}_2, \bar{n}_3$. Similarly, the matrix T_F^f transforms the vertically and horizontally polarized waves in the local coordinate system back into vertically and horizontally polarized waves in the cell coordinate system.²

To account for the arbitrary orientation of the cell, the matrix D in (19) must be post-multiplied by T_F^i and pre-multiplied by T_F^f . Thus the elements of the matrix D in (8) must be replaced by the elements of the matrix D_F

$$D_F = T_F^f D T_F^i \quad (21)$$

Furthermore, in view of the effective filtering by the SAR of the very large scale spectral components of the rough surface $f(x', z') = 0$, the spectral density function for the rough surface $f(x, z) = 0$ associated with the resolution cell F is given by

$$W_F(v_x, v_z) = \begin{cases} W(v_x, v_z), & k \geq k_0 = 2\pi/L_0 \\ 0, & k < k_0 = 2\pi/L_0 \end{cases} \quad (22)$$

where $W(v_x, v_z)$ is the spectral density function for the surface S, $f(x', z') = 0$, and L_0 is the width of the resolution cell.

Illustrative Examples

For the illustrative examples presented in this section, the following specific form of the surface height spectral density function is selected⁵

$$W(v_x, v_z) = \begin{cases} (2/L_0)^{1/2} / (\epsilon^2 + k^2)^4, & k \leq k_c \\ 0, & k > k_c \end{cases} \quad (23)$$

For the assumed isotropic model of the sea surface

$$B = 0.0046$$

$$\left. \begin{aligned} k^2 &= v_x^2 + v_y^2 \text{ (cm)}^{-2}, \quad k_c = 12 \text{ (cm)}^{-1} \\ \kappa &= (335.2 V^4)^{-1/2} \text{ (cm)}^{-1}, \quad V = 4.3 \text{ (m/s)} \end{aligned} \right\} \quad (24)$$

in which k_c is the spectral cutoff wavenumber⁵ and V is the surface wind speed. The wavelength for the electromagnetic wave is

$$\lambda_0 = 3.0 \text{ cm } (k_0 = 2\pi/3 = \text{(cm)}^{-1}). \quad (25)$$

The relative complex dielectric coefficient for the sea is

$$\epsilon_r = 48 - 135i \quad (26)$$

and the permeability for the sea is the same as for free space ($\mu_r = 1$). The slope probability density function within a resolution cell is assumed to be Gaussian.

In Figs. 2a and 2b, $\langle \sigma^{VV} \rangle$, and $-(d\langle \sigma^{VV} \rangle / d\Omega) / \langle \sigma^{VV} \rangle$ are plotted for $\Omega = 0$ and $\tau = 0$ as functions of θ'_0 , the angle of incidence with respect to the fixed reference system (x', y', z'). In these figures $L_s = 300, 1000$ and 2500 cm .

In Figs. 3a and 3b these results are repeated for $\langle \sigma^{HH} \rangle$. It is interesting to note that the effective filtering of the very large scale spectral components of the rough surface ($0 < k < k_c$) by the SAR does not significantly change the value of σ^{PP} unless $L_s < 300 \text{ cm}$. As one may expect, the modulation of the scattering cross sections in the plane of incidence $|d\langle \sigma^{VV} \rangle / d\Omega|$ is strongest for the SAR corresponding to the narrowest effective beam width $L_s = 300 \text{ cm}$.

In Fig. 4 $-(d\langle \sigma^{VV} \rangle / d\Omega) / \langle \sigma^{VV} \rangle$ is plotted for $\Omega = 0$ and $\tau = 0$ as a function of the angle of incidence θ'_0 . These results are repeated in Fig. 5 for $\langle \sigma^{HH} \rangle$. In Figs. 4 and 5 the width of the SAR is also $L_s = 300, 1000$ and 2500 cm . Unlike $|d\langle \sigma^{PP} \rangle / d\Omega|$ ($P=V, H$) the peak in the derivatives $|d\langle \sigma^{PP} \rangle / d\Omega|$ occurs at normal incidence ($\theta'_0 = 0$).

Acknowledgments

This paper was sponsored by the U. S. Army Research Office, Contract No. DAAG-29-82-K-0123 and the Wave Propagation Laboratory, NOAA.

References

1. Alpers, W. R., D. B. Ross and C. L. Rufenach (1981): On the detectability of ocean surface waves by real and synthetic aperture radar, *J. Geophys. Res.*, **86**(C7), 6481-6498.
2. Bahar, E. (1981a): Scattering cross sections from rough surfaces—full wave analysis, *Radio Sci.*, **16**(3), 331-341.
3. Bahar, E. (1981b): Scattering cross sections for composite random surfaces—full wave analysis, *Radio Sci.*, **16**(6), 1327-1335.
4. Bahar, E., D. E. Barrick and M. A. Fitzwater (1982): Computations of scattering cross sections for composite surfaces and the specification of the wavenumber where spectral splitting occurs, *IEEE Transactions on Antennas and Propagation*, to be published.

5. Brown, C. S. (1978): Backscattering from a Gaussian-distributed perfectly conducting rough surface, *IEEE Transactions on Antennas and Propagation*, **AP-26**(3), 472-482.
6. Valenzuela, G. R. (1968): Scattering of electromagnetic waves from a tilted slightly rough surface, *Radio Sci.*, **3**, 1051-1066.
7. Wright, J. W. (1968): A new model for sea clutter, *IEEE Transactions on Antennas and Propagation*, **AP-16**(2), 217-223.

Illustrations

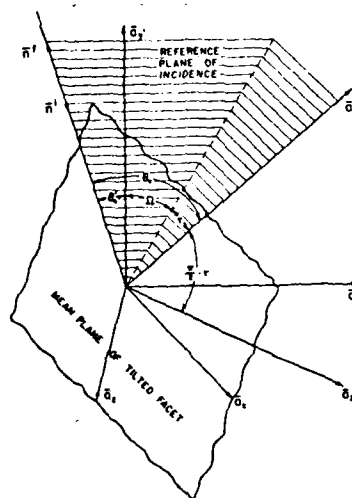


Fig. 1. The tilted resolution cell.

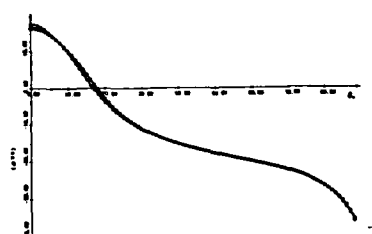


Fig. 2a. $\langle \sigma^{VV} \rangle$, for $\Omega = 0$ and $\tau = 0$ as a function of θ_0^1 . (Δ) $L_g = 300$ cm, (\circ) $L_g = 1000$ cm, (\square) $L_g = 2500$ cm.

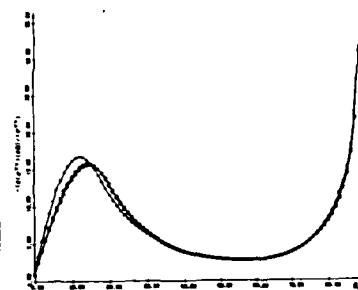


Fig. 2b. $-(d\langle \sigma^{VV} \rangle / d\Omega) / \langle \sigma^{VV} \rangle$ for $\Omega = 0$ and $\tau = 0$ as a function of θ_0^1 . (Δ) $L_g = 300$ cm, (\circ) $L_g = 1000$ cm, (\square) $L_g = 2500$ cm.

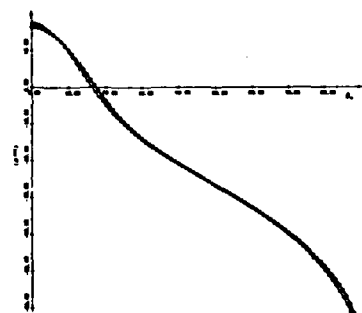


Fig. 3a. $\langle \sigma^{RH} \rangle$, for $\Omega = 0$ and $\tau = 0$ as a function of θ_0^1 . (Δ) $L_g = 300$ cm, (\circ) $L_g = 1000$ cm, (\square) $L_g = 2500$ cm.

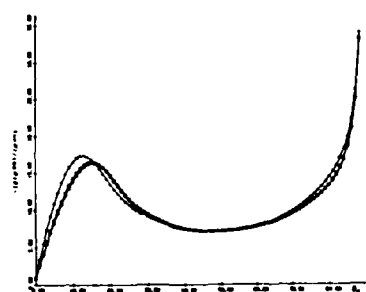


Fig. 3b. $-(d\langle \sigma^{RH} \rangle / d\Omega) / \langle \sigma^{RH} \rangle$ for $\Omega = 0$ and $\tau = 0$ as a function of θ_0^1 . (Δ) $L_g = 300$ cm, (\circ) $L_g = 1000$ cm, (\square) $L_g = 2500$ cm.

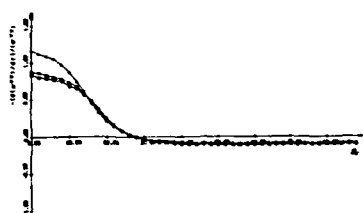


Fig. 4. $-(d\langle\sigma^{VV}\rangle_O/d\tau)/\langle\sigma^{VV}\rangle$ for $\Omega = 0$ and $\tau = 0$ as a function of θ_O^1 . (Δ) $L_g = 300$ cm, (\circ) $L_g = 1000$ cm, (\square) $L_g = 2500$ cm.

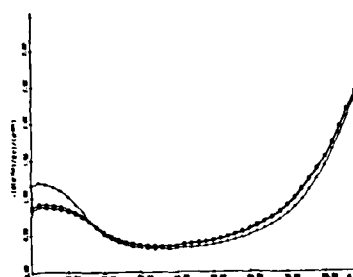


Fig. 5. $-(d\langle\sigma^{HH}\rangle_O/d\tau)/\langle\sigma^{HH}\rangle$ for $\Omega = 0$ and $\tau = 0$ as a function of θ_O^1 . (Δ) $L_g = 300$ cm, (\circ) $L_g = 1000$ cm, (\square) $L_g = 2500$ cm.

Scattering Cross Sections for Composite Rough Surfaces Using the Unified Full Wave Approach

EZEKIEL BAHAR, SENIOR MEMBER, IEEE, AND MARY ANN FITZWATER

Abstract—The full wave approach is used to derive a unified formulation for the like and cross polarized scattering cross sections of composite rough surfaces for all angles of incidence. Earlier solutions for electromagnetic scattering by composite random rough surfaces are based on two-scale models of the rough surface. Thus, on applying a hybrid approach physical optics theory is used to account for specular scattering associated with a filtered surface (consisting of the large scale spectral components of the surface) while perturbation theory is used to account for Bragg scattering associated with the surface consisting of the small scale spectral components. Since the full wave approach accounts for both specular point scattering and Bragg scattering in a self-consistent manner, the two-scale model of the rough surface is not adopted in this work. These unified full wave solutions are compared with the earlier solutions and the simplifying assumptions that are common to all the earlier solutions are examined. It is shown that while the full wave solutions for the like polarized scattering cross sections based on the two-scale model are in reasonably good agreement with the unified full wave solutions, the two solutions for the cross polarized cross sections differ very significantly.

Manuscript received August 12, 1983; revised November 7, 1983. This work was supported by the U.S. Air Force under Contract F19628-81-K-0025. The authors are with the Department of Electrical Engineering, University of Nebraska, Lincoln, NE 68588.

1. INTRODUCTION

Traditionally physical optics and perturbation theories have been used to drive the like and cross polarized scattering cross sections for composite random rough surfaces. Beckmann [6], Rice [13]. To this end two-scale models have been adopted and the rough surfaces are regarded as small scale surface perturbations that are superimposed on large scale, filtered surfaces (Wright [7], Valenzuela [17], Barrick and Peake [5]). Thus the scattering cross sections are expressed as sums of two cross sections. The first accounts for specular point scattering. It is given by the physical optics cross section for the filtered surface consisting of the large scale spectral components. The second accounts for Bragg scattering. It is given by the perturbation cross section for the surface consisting of the small scale spectral components that ride on the filtered surface.

On applying the perturbed-physical optics approaches it is necessary to specify the wavenumber k_d where spectral splitting is assumed to occur between the large and small scale spectral components of the rough surface. Thus Brown [7] who applied a combination of Burrows' perturbation theory [8] and physical optics (Beckmann [6]), to obtain the scattering cross sections for perfectly conducting random rough surfaces, specified k_d on the basis of the characteristics of the small scale surface ($\beta \equiv 4k_0^2 \langle h_s^2 \rangle = 0.1$, where k_0 is the electromagnetic wavenumber and $\langle h_s^2 \rangle$ in the mean square height of the small scale surface). However, using the approaches of Hagfors [9] and Tyler [16], the specification of k_d is assumed to be based on the characteristics of the large scale surface. In general the restrictions on both the large and small scale surfaces cannot be satisfied simultaneously and, using the perturbed-physical optics approaches, the evaluation of the scattering cross sections critically depend on the specifications of k_d (Brown [7]).

More recently the full wave approach has been used to determine the scattering cross sections for composite random rough surfaces of finite conductivity (Bahar [2], Bahar and Barrick [3]). Since the full wave solutions account for Bragg scattering and specular point scattering in a self-consistent manner, it is not necessary to decompose the surface into two surfaces with small and large roughness scales. However, when such a decomposition is feasible, the full wave solutions for the scattering cross sections can be expressed in terms of a *weighted* sum of two cross sections (Bahar [2], Bahar and Barrick [3]). Thus on adopting a two-scale model, the full wave solution resolves the discrepancies between Valenzuela's [17] solution (mostly based on physical considerations) and Brown's solution [7]. Furthermore, in an attempt to draw more definite conclusions regarding the choice of k_d , it was varied over a wide range of values (Bahar *et al.* [4]). It was shown that while, as expected, the cross section associated with the individual large and small scale surfaces critically depend upon the choice of k_d , the *weighted* sum of the like polarized cross sections remain practically insensitive to variations in k_d for $\beta > 1.0$. Thus, provided that the large scale surface satisfies the radii of curvature criteria (associated with the Kirchhoff approximations for the surface fields) and the condition for deep phase modulation, the full wave solutions for the like polarized scattering cross sections based on the two-scale model is practically independent of the specified value of k_d . However, on applying the full wave approach to evaluate the like and cross polarized scattering cross polarized scattering cross sections for two-scale models of composite rough surfaces, several assumptions were made to facilitate the computations.

The first assumption was that the large and small scale surfaces were statistically independent (Brown [7]). It would seem reasonable to make such an assumption if the two surfaces are results of independent processes. For the general case, however, one cannot assume statistical independence of the large and small scale surfaces.

The second simplifying assumption that was made was that the mean square slope σ_s^2 for the total surface was approximately equal to the mean square slope σ_{FS}^2 for the filtered large scale surface.

The third assumption was that the mean square height of the total rough surface was large compared to a wavelength, and the surface height characteristic function for the total surface was negligibly small compared to unity.

Finally, the physical optics approximation for the cross polarized backscatter cross section is zero (Brown [7]). As a result, the cross polarized backscatter cross section for the filtered surface is set equal to zero when the two-scale model is used. However, for backscatter, only the specular points on the rough surface do not depolarize the incident wave.

In this communication the full wave approach is used to derive a unified formulation for the like and cross polarized cross sections for all angles of incidence. These solutions are compared with earlier solutions based on a two-scale model of the random rough surface (Bahar *et al.* [4]). Thus, the simplifying assumptions, that are common to all the earlier solutions based on two-scale models of the rough surface, are carefully examined. It is shown that while the full wave solutions for the like polarized scattering cross sections based on the two-scale model are in reasonably good agreement with the unified full wave solutions, the two solutions for the cross polarized cross sections differ very significantly.

II. APPLICATION OF THE FULL WAVE SOLUTION WITHOUT SURFACE DECOMPOSITION

The starting point for this analysis is the full wave expression for the like and cross polarized scattering cross sections of the rough surface $y = h(x, z)$ (Bahar *et al.* [4])

$$\langle \sigma^P \sigma^Q \rangle = \frac{k_0^2}{\pi} \int_{-\infty}^{\infty} \langle \langle S^P Q \exp \{ i v_y (h - h') \} \rangle \rangle - \left| \left\langle \frac{D^P Q P_2(\vec{n}', \vec{n}^i | \vec{n})}{\vec{n} \cdot \vec{a}_y} \right\rangle \chi(v) \right|^2 \cdot \exp \{ i v_x x_d + i v_z z_d \} dx_d dz_d \quad (1)$$

in which

$$\vec{r}_d = (x - x')\vec{a}_y + (z - z')\vec{a}_z = x_d \vec{a}_x + z_d \vec{a}_z \quad (2)$$

is the radius vector between two points on the reference plane (x, z) . The vector \vec{v} is

$$\vec{v} = k_0(\vec{n}' - \vec{n}^i) = v_x \vec{a}_x + v_y \vec{a}_y + v_z \vec{a}_z \quad (3)$$

where k_0 is the free space wavenumber for the electromagnetic wave and \vec{n}^i and \vec{n}' are unit vectors in the directions of the incident and scattered wave normals, respectively. As $\exp(i\omega t)$ time dependence is assumed in this work. The symbol $\langle \cdot \rangle$ denotes

the statistical average and

$$\begin{aligned} & \frac{k_0^2}{\pi} \langle S^P Q \exp [i v_y (h - h')] \rangle \\ &= \frac{k_0^2}{\pi} \int \left| \frac{D^P Q(\vec{n})}{\vec{n} \cdot \vec{a}_y} \right|^2 P_2(\vec{n}^f, \vec{n}^i | \vec{n}) p(h_x, h_z) dh_x dh_z \\ & \cdot \chi_2(v_y, -v_y) \equiv I^P Q(\vec{n}^f, \vec{n}^i) \chi_2(v_y, -v_y) \end{aligned} \quad (4)$$

in which $\vec{n}(h_x, h_z)$ is the unit vector normal to the rough surface

$$f(x, y, z) = y - h(x, z) = 0. \quad (5)$$

Thus,

$$\nabla f = \vec{n} | \nabla f | = \nabla(y - h(x, z)) = (-h_x \vec{a}_x + \vec{a}_y - h_z \vec{a}_z) \quad (6)$$

in which the components of the gradient of $h(x, z)$

$$h_x = \partial h / \partial x, \quad h_z = \partial h / \partial z \quad (7)$$

are the random variables and $p(h_x, h_z)$ is the probability density function for the slopes h_x and h_z . The expression for the scattering cross sections $\langle \sigma^P Q \rangle$, (1) accounts for shadowing; thus $P_2(\vec{n}^f, \vec{n}^i | \vec{n})$ is the probability that a point on the rough surface is both illuminated and visible given the value of the slopes at the point (Sancer [14]). The characteristic and joint characteristic functions for the surface height h are $\chi(v_y)$ and $\chi_2(v_y, -v_y)$. It is assumed in this work that the probability density function for the surface height is jointly Gaussian. Thus

$$\begin{aligned} | \chi(v_y) |^2 &= \exp(-v_y^2 \langle h^2 \rangle), \\ \chi_2(v_y, -v_y) &= \exp(-v_y^2 \langle h^2 \rangle + v_y^2 \langle h h' \rangle) \end{aligned} \quad (8)$$

where $\langle h^2 \rangle$ is the mean square height and $\langle h h' \rangle$ is the surface height autocorrelation function. The coefficients $D^P Q$ depend explicitly upon the polarization of the incident wave (second superscript $Q = V$ -vertical, $Q = H$ -horizontal) and the polarization of the scattered wave (first superscript $P = V, H$) the direction of the incident and scattered wave normals \vec{n}^i and \vec{n}^f , respectively, the unit vector \vec{n} normal to the rough surface and the complex permeability and permittivity of the medium of propagation, respectively (Bahar [1]). On deriving (4), it is assumed that the rough surface is Gaussian and stationary, thus the surface height h and slopes (h_x, h_z) are statistically independent (Brown [7], Longuet-Higgins [11]). It is also assumed that for distances $| \vec{r}_d |$ less than the surface height correlation distance, l_c , $\vec{n}(h_x, h_z) \cong \vec{n}(h'_x, h'_z)$. It has been shown that if the principal contributions to the scattered fields come from specular points on the rough surface ($\vec{n} = \vec{n}_s$), (1) reduces to the physical optics solution for the scattering cross section. If, however, the roughness scale of the surface is small compared to the wavelength ($k_0^2 \langle h^2 \rangle \ll 1$) and the surface slopes h_x and h_z are very small, (1) reduces to the perturbation solution for the scattering cross sections (Rice [13]). Thus, in this case Bragg scattering is accounted for and the backscatter cross sections for grazing angles are strongly dependent on polarization. Recently a two-scale model was adopted to determine the corresponding full wave solution for the scattering cross sections (Bahar and Barrick [3]). To facilitate the application of the two-scale model it is assumed that the small scale surface h_s and the large scale filtered surface h_F are statistically independent (Valenzuela [17]; Wright [18]; Brown [7]). In the general case however, if the two-scale model is used to analyze the problem

it would be necessary to know the large and small scale surface height joint probability density function for two adjacent points on the rough surface to determine χ_2 , (8) alone.

Since the full wave solutions account for both Bragg scatter and specular point scatter in a unified, self-consistent manner in this communication solutions for (1) are developed without adopting a two-scale model of the rough surface.

It has been noted in the introduction that the physical optic approximation for the cross polarized backscatter cross section is zero ($\langle \sigma^P Q \rangle_F = 0$ for $P \neq Q$) (Brown [7]). However, even the large scale filtered surface will depolarize the backscattered field at nonspecular points on the surface. Therefore the present analysis should shed more light on the evaluation of the like and cross polarized backscatter cross sections and the suitability of the two-scale model even if it can be assumed that the large and small scale surfaces are statistically independent.

Assuming that $k_0^2 \langle h^2 \rangle \gg 1$ and $| \chi |^2 \ll 1$, the scattering cross section (1) can be expressed as follows:

$$\langle \sigma^P Q \rangle = I^P Q(\vec{n}^f, \vec{n}^i) Q(\vec{n}^f, \vec{n}^i, R) \quad (9a)$$

in which $I^P Q$ is defined by (4) and

$$Q = \int_{-\infty}^{\infty} (\chi_2 - | \chi |^2) \exp [i v_x x_d + i v_z z_d] dx_d dz_d, \quad (9b)$$

is the two-dimensional Fourier transform of $(\chi_2 - | \chi |^2)$ (8). It therefore depends on the surface height correlation coefficient R

$$R \equiv \langle h h' \rangle / \langle h^2 \rangle. \quad (10)$$

The surface height spectral density function $W(v_x, v_z)$ is related to the two-dimensional Fourier transform of the surface height autocorrelation function.

$$W(v_x, v_z) = \frac{1}{\pi^2} \int \langle h h' \rangle \exp [i v_x x_d + i v_z z_d] dx_d dz_d. \quad (11)$$

Thus assuming that the rough surface is Gaussian and stationary, to compute the scattering cross sections (9) it is necessary to prescribe the two-dimensional slope probability density function $p(h_x, h_z)$, (4) and the surface height autocorrelation function or its Fourier transform (the surface height spectral density function). Since it is assumed in this work that the surface is isotropic, $\langle h h' \rangle$ depends only on the distance $r_d = | \vec{r}_d |$ between the two points (x, h, z) and (x', h', z') on the rough surface. Thus

$$\langle h h' \rangle = 2\pi \int \frac{W(v_{xz})}{4} J_0(v_{xz} r_d) v_{xz} dv_{xz} \quad (12)$$

in which J_0 is the Bessel function of order zero and

$$v_{xz}^2 = v_x^2 + v_z^2 \quad (13)$$

$$\langle h^2 \rangle = 2\pi \int \frac{W(v_{xz})}{4} v_{xz} dv_{xz} \quad (14)$$

and the total mean square slope is

$$\sigma_s^2 = 2\pi \int \frac{W(v_{xz})}{4} v_{xz}^2 dv_{xz}. \quad (15)$$

III. ILLUSTRATIVE EXAMPLES

For the following illustrative examples the special form of the surface height spectral density function is chosen (Brown

[7])

$$W(u_x, u_z) = \left(\frac{2}{\pi} \right) S(u_x, u_z) \\ = \begin{cases} \left(\frac{2}{\pi} \right) B k^4 / (k^2 + \kappa^2)^4, & k \leq k_c \\ 0, & k > k_c \end{cases} \quad (16)$$

where W is the spectral density function (16) and S is the corresponding quantity used by Brown [7]. For the above isotropic model of the ocean surface

$$k^2 = u_x^2 + u_z^2 \text{ (cm)}^{-2}, \quad k_c = 12 \text{ (cm)}^{-1}, \quad B = 0.0046 \\ \kappa = (335.2 V^4)^{-1/2} \text{ (cm)}^{-1}, \quad V = 4.3 \text{ (m/s)}, \quad (17)$$

in (17) V is the surface wind speed. The wavelength for the electromagnetic wave is

$$\lambda_0 = 2 \text{ (cm)}, \quad (k_0 = 3.1416 \text{ (cm)}^{-1}). \quad (18)$$

Equation (14) for the mean square height of the rough surface yields

$$\langle h^2 \rangle = \frac{B k_c^6}{6 \kappa^2 (\kappa^2 + k_c^2)^3} \cong \frac{B}{6 \kappa^2} = 87.9 \text{ cm}^2. \quad (19)$$

The surface height autocorrelation function $\langle hh' \rangle$ (12) can be expressed in closed form for $k_c \rightarrow \infty$. Thus the surface height correlation coefficient $R(r_d)$ (10) is given by (Miller *et al.* [12])

$$R(r_d) = \left[1 + \frac{1}{8} (\kappa r_d)^2 \right] (\kappa r_d) K_1(\kappa r_d) - (\kappa r_d)^2 K_0(\kappa r_d) \quad (20)$$

in which K_0 and K_1 are the modified Bessel functions of the second kind and of order zero and one, respectively. Since $k_c \gg \kappa$ and $k_c > k_0$ the above closed form expression is used for R in this illustrative example. The total mean square slope of the rough surface is obtained on substituting (16) into (15).

$$\sigma_S^2 = B \left[\frac{1}{2} \ln \frac{k_c^2 + \kappa^2}{\kappa^2} - \frac{k_c^2 (6 \kappa^2 + 15 \kappa^2 k_c^2 + 11 k_c^4)}{12 (\kappa^2 + k_c^2)^3} \right] \\ = 0.034. \quad (21)$$

For typical sea surfaces the relative complex dielectric coefficient at 15 GHz is given by (Stogryn [15])

$$\epsilon_r = 42 - i39. \quad (22)$$

The slope probability density function $p(h_x, h_z)$ is assumed to be Gaussian. In Fig. 1, the like polarized backscatter cross section $\langle \sigma^{VV} \rangle$ is plotted as a function of the angle of incidence θ_0^i using the expression derived in Section II. These results are compared with the two-scale full wave results (Bahar *et al.* [4]) based on the choice of k_d (the wavenumber where spectral splitting occurs) corresponding to $\beta = 1$. Both results yield the same general dependence of $\langle \sigma^{VV} \rangle$ on the angle of incidence. The small difference in level is primarily due to the fact that in (3) the mean square slope σ_S^2 of the total (unfiltered) surface is used, while for the solution based on the two-scale model the mean square slope σ_{FS}^2 for the filtered surface h_F is used (Bahar *et al.* [4]). It should be noted that in deriving the expressions for the scattering cross sections based on the two-scale model, it was assumed that $\sigma_{FS}^2 \cong \sigma_S^2$. Thus the results based on (3) are

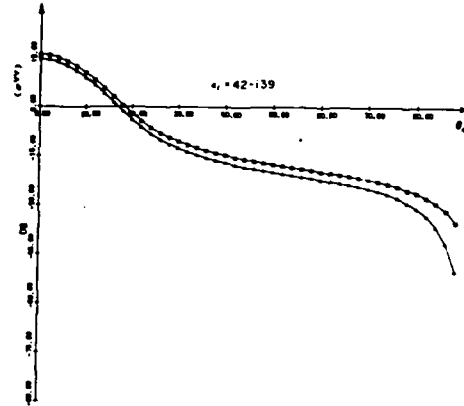


Fig. 1. Backscatter cross sections $\langle \sigma^{VV} \rangle$ for rough surfaces characterized by $W(u_x, u_z)$ given by (16). (□) Two-scale model and (△) unified full wave solution (4). Relative complex permittivity is $\epsilon_r = 42 - i39$.

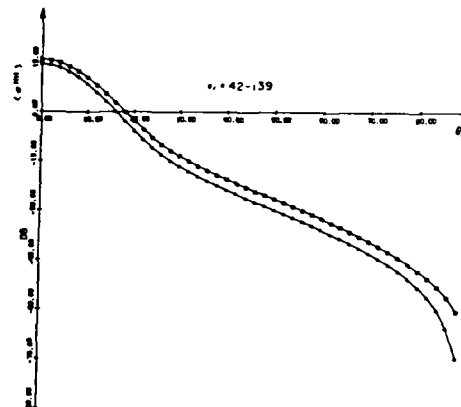


Fig. 2. Backscatter cross sections $\langle \sigma^{HH} \rangle$ for rough surfaces characterized by $W(u_x, u_z)$ given by (16). (□) Two-scale model and (△) unified full wave solution (4). Relative complex permittivity is $\epsilon_r = 42 - i39$.

more accurate. Furthermore, on deriving the solution based on the two-scale model, the quantity $\chi(u_y)$ (8) is assumed to be negligible compared to $\chi_2(u_y, -u_y)$ (8) for $r_d < l_c$. Since $4k_0^2 \langle h^2 \rangle = 3468$ for this illustrative example, the resulting approximation is very good except very near grazing angles. In Fig. 2, the corresponding results are given for the horizontally polarized backscatter cross sections $\langle \sigma^{HH} \rangle$. It is interesting to note that the full wave solution (3) yields the proper polarization dependence of the scattering cross sections for all angles of incidence without use of a two-scale model since it accounts for specular point and Bragg scattering in a unified, self consistent manner. In Fig. 3 the cross polarized backscatter cross sections $\langle \sigma^{VH} \rangle = \langle \sigma^{HV} \rangle$ are plotted as functions of the angle of incidence. Here too, both the solutions based on the two-scale model as well as the solution derived in this section are presented. Unlike the solutions for the like polarized backscatter cross sections $\langle \sigma^{PP} \rangle$ ($P = V, H$), the solutions for the cross polarized backscatter cross sections

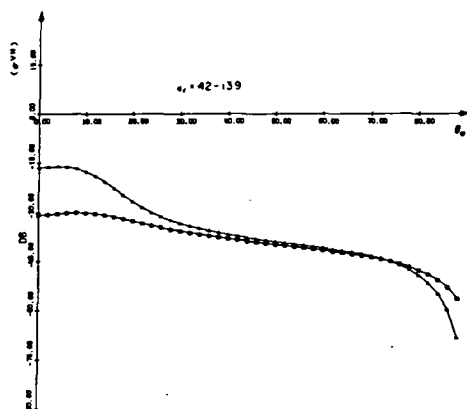


Fig. 3. Backscatter cross sections $\langle \sigma^{VH} \rangle = \langle \sigma^{HV} \rangle$ for rough surfaces characterized by $W(u, v)$ given by (16). (□) Two-scale model and (Δ) unified full wave solution (4). Relative complex permittivity is $\epsilon_r = 42 - j39$.

differ significantly, especially near normal incidence where the difference in level is about 15 dB. This very significant difference is due to the fact that the physical optics approximations for the cross polarized backscatter cross section is zero (Brown [7], Bahar *et al.* [4]). For backscatter the surface at the specular points is normal to the incident wave. At these stationary phase points no depolarization occurs. However, since depolarization occurs at the nonspecular points of the filtered surface, the physical optics approximations for the cross polarized backscatter cross section is not valid. It is interesting to note that for the two-scale model at normal incidence $\langle \sigma^{PP} \rangle / \langle \sigma^{PQ} \rangle \approx 47$ dB ($P \neq Q$). However, using the full wave solution (3), $\langle \sigma^{PP} \rangle / \langle \sigma^{PQ} \rangle \approx 31$ dB ($P \neq Q$). The latter results are significantly more in line with published experimental results¹ (Long [10]).

IV. CONCLUDING REMARKS

It is shown in this section that two-scale models of rough surfaces can be adopted to obtain solutions for the like polarized backscatter cross sections that are in reasonably good agreement with the full wave solutions derived in this section. However, the two-scale model cannot be used to evaluate the cross polarized backscatter cross sections. The significant differences between the solutions derived in this paper and those based on the two-scale models are primarily due to the fact that the physical optics approximation for the cross polarized backscatter cross section (associated with the large scale filtered surface) is zero. For backscatter, the specular points lie on portions of the rough surfaces that are perpendicular to the incident wave normal $\vec{n}'(\vec{n}_s = \vec{n}' = -\vec{n}_i)$. At these specular points, the backscattered waves are not depolarized. However, at nonspecular points of the rough surface, the backscattered waves are depolarized (Bahar [2]). Thus, it is important to note that even if a surface satisfies the radii of curvature criteria (associated with the

Kirchhoff approximations for the surface fields), the physical optics approximations for the scattered fields may not be valid unless for the given incident and scatter angles specular points exist on the surface and significant contributions to the scattered fields come from these stationary phase (specular-points) of the surface. This explains why the physical optics approximations for the like polarized backscattered cross sections are not suitable for grazing angles even if the surface meets the radii of curvature criteria associated with the Kirchhoff approximations.

There are additional important reasons for preferring to use the analysis developed in this section over those that are based on two-scale models of rough surfaces. Firstly, if the two-scale model is used, it is necessary to assume that the large and small scale surfaces are statistically independent (Brown [7]). Secondly, even if the assumption of statistical independence is acceptable, when the two scale model is used, it is still necessary to judiciously specify k_d (where spectral splitting is assumed to occur). These problems do not arise when the unified full wave formulation is used to evaluate the scattering cross sections.

ACKNOWLEDGMENT

The manuscript was prepared by E. Everett.

REFERENCES

- [1] E. Bahar, "Scattering cross sections from rough surfaces—full wave analysis," *Radio Sci.*, vol. 16, no. 3, pp. 331-341, 1981.
- [2] —, "Scattering cross sections for composite random surfaces—full wave analysis," *Radio Sci.*, vol. 16, no. 6, pp. 1327-1335, 1981.
- [3] E. Bahar and D. E. Barrick, "Scattering cross sections for composite surfaces that cannot be treated as perturbed physical optics problems," *Radio Sci.*, vol. 18, no. 2, pp. 129-137, 1983.
- [4] E. Bahar, D. E. Barrick, and M. A. Fitzwater, "Computations of scattering cross sections for composite surfaces and the specification of the wavenumber where spectral splitting occurs," *IEEE Trans. Antennas Propagat.*, vol. AP-31, no. 5, pp. 698-709, Sept. 1983.
- [5] D. E. Barrick and W. H. Peake, "A review of scattering from surfaces with different roughness scales," *Radio Sci.*, vol. 3, no. 8, pp. 865-868, 1968.
- [6] P. Beckmann, *The Depolarization of Electromagnetic Waves*. Boulder, CO: Golem, 1968.
- [7] G. S. Brown, "Backscattering from a Gaussian distributed perfectly conducting rough surface," *IEEE Trans. Antennas Propagat.*, vol. AP-26, no. 3, pp. 472-482, May 1978.
- [8] M. L. Burrows, "On the composite model for rough surface scattering," *IEEE Trans. Antennas Propagat.*, vol. AP-21, pp. 241-243, 1967.
- [9] T. Hagfors, "Relationship of geometric optics and autocorrelation approach to the analysis of lunar and planetary radar," *J. Geophys. Res.*, vol. 71, pp. 379-383, 1966.
- [10] M. W. Long, *Radar Reflectivity of Land and Sea*. Lexington, MA: D.C. Heath and Co., 1975.
- [11] M. S. Longuet-Higgins, "The statistical analysis of a random moving surface," *Phil. Trans. Royal Soc. London*, vol. A249, pp. 321-387, 1957.
- [12] L. S. Miller, G. S. Brown, and G. S. Hayne, "Analysis of satellite altimeter signal characteristics and investigation of sea-truth data requirements," NASA CR-137465, Res. Triangle Inst., Durham, NC, Apr. 1972.
- [13] S. O. Rice, "Reflection of electromagnetic waves from a slightly rough surface," *Commun. Pure Appl. Math.*, vol. 4, pp. 351-378, 1951.
- [14] M. I. Sancer, "Shadow-corrected electromagnetic scattering from a randomly rough surface," *IEEE Trans. Antennas Propagat.*, vol. AP-17, no. 5, pp. 577-585, 1968.
- [15] A. Stogryn, "Equations for calculating the dielectric constant of saline water," *IEEE Trans. Microwave Theory Tech.*, vol. MTT-19, no. 8, pp. 734-736, 1971.
- [16] G. L. Tyler, "Wavelength dependence in radio-wave scattering and specular point theory," *Radio Sci.*, vol. 11, no. 2, pp. 83-91, 1976.
- [17] G. R. Valenzuela, "Scattering of electromagnetic waves from a tilted slightly rough surface," *Radio Sci.*, vol. 3, no. 11, pp. 1051-1066, 1968.
- [18] J. W. Wright, "A new model for sea clutter," *IEEE Trans. Antennas Propagat.*, vol. AP-16, no. 2, pp. 217-223, Mar. 1968.

¹ See also NRL report on "Airborne radar backscatter study at four frequencies," NRL Prob ROZ-37, SER: 8560, Aug. 1966, by J. C. Daley.

Frontiers of Remote Sensing of the Oceans and Troposphere from Air and Space Platforms

*Proceedings of the URSI Commission F
Symposium and Workshop
Shoresh, Israel
May 14-23, 1984*

NASA

OPTIMUM BACKSCATTER CROSS SECTION OF THE OCEAN
AS MEASURED BY SYNTHETIC APERTURE RADARS

Ezekiel Bahar

Electrical Engineering Department
University of Nebraska-Lincoln, NE 68588-0511

Clifford L. Rufenach and Donald E. Barrick
NOAA/ERL/Wave Propagation Laboratory, Boulder, CO 80303

Mary Ann Fitzwater
Electrical Engineering Department
University of Nebraska-Lincoln, NE 68588-0511

ABSTRACT

Microwave remote sensing of rough surfaces (both land and ocean), using moving platforms (aircraft and satellite), as well as ground based measurements has illustrated the need for a better understanding of the interaction of the radar signals with these surfaces. This interaction is particularly important for the ocean surface where the radar modulation can yield information about the long ocean wave field. Radar modulation measurements from fixed platforms have been made in wavetanks and the open oceans. The surfaces have been described in terms of two-scale models. The radar modulation is considered to be principally due to: (1) geometrical tilt due to the slope of the long ocean waves and (2) the straining of the short waves (by hydrodynamic interaction). For application to moving platforms, Synthetic Aperture Radar (SAR) and Side Looking Airborne Radar (SLAR), this modulation needs to be described in terms of a general geometry for both like- and cross-polarization since the long ocean waves, in general, travel in arbitrary directions. In the present work, the finite resolution of the radar is considered for tilt modulation with hydrodynamic effects neglected.

1. INTRODUCTION

The full wave approach is used to determine the modulation of the like- and cross-polarized scattering cross sections for composite models of rough surfaces illuminated by SAR. The full wave approach accounts for both specular point scattering and Bragg scattering in a self-consistent manner. Thus, the total scattering cross section is expressed as a weighted sum of two cross sections (Bahar et al., 1983). The first is the scattering cross section associated with the filtered surface consisting of the large-scale specular components of the illuminated rough surface area. The second is the cross section associated with the surface consisting of the small-scale spectral components that ride on the filtered surface.

Full wave solutions are derived for the scattering cross sections of a relatively small area or resolution cell of the rough surface that is effectively illuminated by SAR. The normal to an arbitrarily oriented mean plane associated with the illuminated cell is characterized by tilt angles Ω and τ in and perpendicular to a fixed reference plane of incidence. It is assumed that the lateral dimension of the resolution cell L_s is much larger than both the electromagnetic wavelength and the surface height correlation distance for the cell. As the SAR scans different portions of the rough surface S , the direction of the unit vector normal to the cell F fluctuates. In this paper the "modulations" of scattering cross sections are determined as the tilt angles Ω and τ fluctuate. In a recent study of "tilt modulation" by Alpers et al. (1981), first-order Bragg scatter due to capillary waves on a tilted plane is considered. It can be shown that if the large scale spectral components of the surface within the cell are ignored, the full wave solutions derived here for tilt modulation reduce to the results obtained by Alpers et al.

$$\bar{n} = \nabla f / |\nabla f| = (-h_x \bar{a}_x + \bar{a}_y - h_z \bar{a}_z) / (h_x^2 + h_z^2 + 1)^{1/2} \quad (7a)$$

$$\text{where} \quad f = y - h(x, z), \quad h_x = \partial h / \partial x, \quad h_z = \partial h / \partial z \quad (7b)$$

$$\text{and} \quad \bar{n}_s = \bar{v} / v. \quad (7c)$$

The expression for the physical optics (specular point) cross section for the large-scale surface h_s is

$$\langle \sigma_{\text{po}}^{PQ} \rangle = \frac{4k_o^2}{v_y^2} \left[\frac{|D^{PQ}|^2}{\bar{n} \cdot \bar{a}_y} P_2(\bar{n}^f, \bar{n}^i | \bar{n}) p(\bar{n}) \right] \bar{n}_s \quad (8)$$

in which D^{PQ} depends on \bar{n}^i , \bar{n}^f , \bar{n} , the media of propagation above and below the rough surface $h(x, z)$ and the polarization of the incident and scattered waves (Bahar, 1981a, b). The shadow function P_2 is the probability that a point on the rough surface is both illuminated and visible, given the slopes $\bar{n}(h_x, h_z)$, at the point (Smith, 1967; Sancer, 1969). The probability density function for the slopes h_x and h_z is $p(\bar{n})$. The factor $\chi^s(v)$ that multiplies $\langle \sigma_{\text{po}}^{PQ} \rangle$ accounts for the degradation of the contributions from the specular points due to the superimposed small scale rough surface h_s .

Assuming a Gaussian probability density function for h_s , $\langle \sigma^{PQ} \rangle_s$ is given by the sum

$$\langle \sigma^{PQ} \rangle_s = \sum_{m=1}^{\infty} \langle \sigma^{PQ} \rangle_{sm} \quad (9)$$

where

$$\begin{aligned} \langle \sigma^{PQ} \rangle_{sm} &= 4\pi k_o^2 \int \frac{|D^{PQ}|^2 P_2(\bar{n}^f, \bar{n}^i | \bar{n})}{\bar{n} \cdot \bar{a}_y} \\ &\cdot \exp(-v_y^2 \langle h_s^2 \rangle) \left(\frac{v_y^2}{2} \right)^{2m} \frac{W_m(v_x, v_z)}{m!} p(h_x, h_z) dh_x dh_z \end{aligned} \quad (10)$$

in which $\langle h_s^2 \rangle$ is the mean square of the surface height h_s and v_x, v_y and v_z are the components of \bar{v} (6) in the local coordinate system (at each point on the large scale surface) associated with the unit vectors \bar{n}_1, \bar{n}_2 and \bar{n}_3 . Thus \bar{v} can also be expressed as

$$\bar{v} = v_x \bar{n}_1 + v_y \bar{n}_2 + v_z \bar{n}_3 \quad (11)$$

where

$$\bar{n}_1 = (\bar{n} \times \bar{a}_z) / |\bar{n} \times \bar{a}_z|, \quad \bar{n}_2 = \bar{n}, \quad \bar{n}_3 = \bar{n}_1 \times \bar{n}. \quad (12)$$

The function $W_m(v_x, v_z) / 2^{2m}$ is the two-dimensional Fourier transform of $\langle h_s h_s' \rangle^m$.

For $\beta \ll 1$ and arbitrary $p(h_x, h_z)$ the first term in (9), $\langle \sigma^{PQ} \rangle_{s1}$ is also in agreement with Valenzuela's solutions that are "mostly based on physical considerations" (Valenzuela, 1968, Valenzuela et al., 1971). For small slopes $\bar{n} = \bar{a}_y$ and $\beta \ll 1$ the first term in (3) reduces to Brown's solution (1978) based on a combination of physical optics and perturbation theory. Since it is assumed (on deriving (3) from the full wave solutions for the scattered fields) that the surface h_s satisfies the radii of curvature criteria as well as the condition for deep phase modulation, it is necessary to choose $\beta = 4k_o^2 \langle h_s^2 \rangle \geq 1$ in order to assure that the weighted sum of cross sections (3) remains insensitive to variations in k_d , the wavenumber where spectral splitting is assumed to occur (Bahar et al., 1983).

In order to apply the full wave approach to SAR it is necessary to modify the results presented in this section (a) to account for the filtering of the very

For the illustrated examples presented, the scattering cross sections and their derivatives with respect to the tilt angles are evaluated for all angles of incidence. The modulation of the like cross sections near normal incidence is due primarily to fluctuations in specular point scattering while the modulation of the like cross section for near grazing angles is due primarily to fluctuations in Bragg scattering. Thus, for large angles of incidence the cross sections for the horizontally polarized waves are shown to be more strongly modulated than the cross sections for vertically polarized waves. The relative modulations of the like polarized backscatter cross sections are optimum for incident angles between 10° and 15° depending upon the lateral dimension of the resolution cell and the polarization.

2. FORMULATION OF THE PROBLEM

The full wave solutions for the normalized cross sections per unit area are summarized here for composite rough surfaces. The position vector to a point on the rough surface is expressed as follows:

$$\vec{r}_s = \vec{r}_l(x, h_l, z) + \vec{n}h_s \quad (1)$$

in which $y=h_l(x, z)$ is the filtered surface consisting of the large scale spectral components of the rough surface and h_s , the small scale surface height is measured in the direction of the normal (\vec{n}) to the large scale surface $y=h_l$. For a homogenous, isotropic surface height the spectral density function is the Fourier transform of the surface height autocorrelation function $\langle h(x, z), h'(x', z') \rangle$.

$$W(\vec{v}_x, \vec{v}_z) = \frac{1}{2} \int_{-\infty}^{\infty} \langle hh' \rangle \exp(i\vec{v}_x \cdot \vec{x}_d + i\vec{v}_z \cdot \vec{z}_d) d\vec{x}_d d\vec{z}_d \quad (2a)$$

where $\langle hh' \rangle$ is a function of distance $|\vec{r}_d| = (x_d^2 + z_d^2)^{1/2}$ and

$$x - x' = x_d \text{ and } z - z' = z_d. \quad (2b)$$

The surface $h_l(x, z)$ consists of the spectral components $k = (v_x^2 + v_z^2)^{1/2} \leq k_d$ and the remainder term $h_s(x, z)$ consists of the spectral components $k > k_d$. The full wave approach accounts for both specular point scattering and Bragg scattering in a self-consistent manner the total scattering cross section can be expressed as a weighted sum of the cross section $\langle \sigma^{PQ} \rangle_l$ for the filtered surface h_l and the cross section $\langle \sigma^{PQ} \rangle_s$ for the surface h_s that rides on the large-scale surface h_l (Bahar et al., 1983)

$$\langle \sigma^{PQ} \rangle = \langle \sigma^{PQ} \rangle_l + \langle \sigma^{PQ} \rangle_s. \quad (3)$$

The symbol $\langle \rangle$ denotes statistical average. The first superscript P corresponds to the polarization of the scattered wave while the second superscript Q corresponds to the polarization of the incident wave. To derive (3) using the full wave approach it is implicitly assumed that the large scale surface meets the radii of curvature criteria (associated with the Kirchhoff approximations for the surface fields) as well as the condition for deep phase modulation. Thus the first term in (3) is

$$\langle \sigma^{PQ} \rangle_l = |\chi^S(\vec{v} \cdot \vec{n}_s)|^2 \langle \sigma^{PQ} \rangle_s \quad (4)$$

in which χ^S is the characteristic function for the small scale surface

$$\chi^S(\vec{v} \cdot \vec{n}_s) = \chi^S(v) = \langle \exp i\vec{v} \cdot \vec{h}_s \rangle \quad (5)$$

and

$$\vec{v} = \vec{k}^f - \vec{k}^i = k_0(\vec{n}^f - \vec{n}^i), \quad v = |\vec{v}|. \quad (6)$$

The unit vectors \vec{n}^f and \vec{n}^i are in the directions of the scattered and incident wave normals respectively; thus for backscatter $\vec{n}^i = -\vec{n}^f$. The free space radio wavenumber is k_0 . An $\exp(i\omega t)$ time dependence is assumed. The vector \vec{n}_s is the value of the unit vector \vec{n} normal to the surface $h(x, z)$ at the specular points. Thus

large scale spectral component of the rough surface by the SAR that effectively illuminates a relatively small area of cell F of the rough surface S and (b) to account for the normal to a reference plane associated with the illuminated cell which is characterized by arbitrary tilt angles Ω and τ in and perpendicular to the reference plane of incidence. It is assumed here that the lateral dimension of the cell illuminated by the SAR is much larger than the surface height correlation distance for the cell and that as the SAR scans different portions of the rough surface S the direction of the unit vector normal to the cell F fluctuates. Our purpose is to determine the "modulation" of the backscatter cross sections $\langle \sigma^{PQ} \rangle$ (3) as the tilt angles (of the normal to the cell) in and perpendicular to the reference plane of incidence fluctuate.

3. SCATTERING CROSS SECTIONS FOR ARBITRARILY ORIENTED RESOLUTION CELLS OF THE ROUGH SURFACE

Let x, y, z be the reference coordinate system associated with the surface of the cell F that is illuminated by the SAR such that the mean surface of the cell is the $y=0$ plane. Furthermore, let x', y', z' be the fixed coordinate system associated with the large surface S such that the unit vector \bar{a}'_y is normal to the mean rough surface height $h(x', z')$. The unit vector $\bar{n}^i = -\bar{n}^f$ is expressed in terms of the unit vectors of the fixed coordinate system (x', y', z') :

$$\bar{n}^i = -\bar{n}^f = \sin\theta'_0 \bar{a}'_x - \cos\theta'_0 \bar{a}'_y. \quad (13)$$

The unit vector \bar{a} normal to the reference surface associated with the cell is expressed in terms of the tilt angles Ω and τ in and perpendicular to the fixed plane of incidence, the x', y' plane. Thus

$$\bar{a}_y = \sin\Omega \cos\tau \bar{a}'_x + \cos\Omega \cos\tau \bar{a}'_y + \sin\tau \bar{a}'_z. \quad (14)$$

For convenience \bar{a}_x and \bar{a}_z , the unit vectors associated with the cell, can be chosen such that the plane of incidence in the x, y, z coordinate system is normal to the vector \bar{a}_z . Thus

$$\bar{a}_z = (\bar{n}^i \times \bar{a}_y) / |\bar{n}^i \times \bar{a}_y|, \quad \bar{a}_x = \bar{a}_y \times \bar{a}_z \quad (15)$$

and the expression for \bar{n}^i in the x, y, z coordinate system is

$$\begin{aligned} \bar{n}^i &= (\bar{n}^i \cdot \bar{a}_x) \bar{a}_x + (\bar{n}^i \cdot \bar{a}_y) \bar{a}_y \\ &= \sin\theta_0 \bar{a}_x - \cos\theta_0 \bar{a}_y \end{aligned} \quad (16a)$$

where

$$\cos\theta_0 = \cos(\theta'_0 + \Omega) \cos\tau. \quad (16b)$$

The angle ψ_F^i between the plane of incidence in the fixed coordinate system (x', y', z') and the plane of incidence in the coordinate system (x, y, z) associated with the cell is given by

$$\cos\psi_F^i = \frac{\cos\tau \sin(\theta'_0 + \Omega)}{\sin\theta_0} \quad (17a)$$

and

$$\sin\psi_F^i = \frac{\sin\tau}{\sin\theta_0}. \quad (17b)$$

For backscatter $\bar{n}^f = -\bar{n}^i$. Thus the angle ψ_F^f between the plane of scatter in the fixed coordinate system (x', y', z') and the plane of scatter in the coordinate system associated with the cell is

$$\psi_F^f = -\psi_F^i. \quad (18)$$

The matrix that transforms the incident vertically and horizontally polarized waves in the fixed coordinate system to vertically and horizontally polarized waves in the cell coordinate system is therefore (Bahar, 1981a,b)

$$T_F^i = \begin{bmatrix} \cos \psi_F^i & \sin \psi_F^i \\ -\sin \psi_F^i & \cos \psi_F^i \end{bmatrix} \quad (19)$$

Similarly, the matrix that transforms the scattered vertically and horizontally polarized waves in the cell coordinate system back into the vertically and horizontally polarized waves in the fixed coordinate system is

$$T_F^f = \begin{bmatrix} \cos \psi_F^f & -\sin \psi_F^f \\ \sin \psi_F^f & \cos \psi_F^f \end{bmatrix} \quad (20)$$

Thus in view of (18), $T_F^f = T_F^i$. The coefficients D^{PQ} in (8) are elements of a 2×2 matrix D given by

$$D = C_o^{in} T^f T^i \quad (21)$$

in which C_o^{in} is the cosine of the angle between the incident wave normal \bar{n}^i and the unit vector \bar{n} normal to the rough surface of the cell $h_F(x, z)$. Thus

$$C_o^{in} = -\bar{n}^i \cdot \bar{n} = \cos \theta_o^{in} \quad (22)$$

where \bar{n}^i is given by (16) and \bar{n} is given by (7a) with $f_F(x, y) = y - h_F(x, y)$. The elements of the scattering matrix F in (21) are functions of the unit vectors \bar{n}^i, \bar{n}^f and \bar{n} as well as the media of propagation above and below the rough surface S (Bahar, 1981a). The matrix T^i transforms the vertically and horizontally polarized waves in the cell coordinate system $(\bar{a}_x, \bar{a}_y, \bar{a}_z)$ to vertically and horizontally polarized waves in the local coordinate system that conforms with the rough surface, $\bar{n}_1, \bar{n}_2, \bar{n}_3$ (12). Similarly, the matrix T^f transforms the vertically and horizontally polarized waves in the local coordinate system back into vertically and horizontally polarized waves in the cell coordinate system (Bahar, 1981a).

To account for the arbitrary orientation of the cell, the matrix D in (21) must be post-multiplied by T_F^i and pre-multiplied by T_F^f . Thus the elements of the matrix D in (8) must be replaced by the elements of the matrix D_F where

$$D_F = T_F^f D T_F^i \quad (23)$$

Furthermore, in view of the effective filtering by the SAR of the very large scale spectral components of the rough surface $f(x', z') = 0$, the spectral density function for the rough surface $f_F(x, y) = 0$ associated with the resolution cell F is given by

$$W_F(v_{\bar{x}}, v_{\bar{z}}) = \begin{cases} W(v_{\bar{x}}, v_{\bar{z}}) & , k \geq k_s \\ 0 & , k < k_s \end{cases} \quad (24)$$

where $W(v_{\bar{x}}, v_{\bar{z}})$ is the spectral density function for the surface S , $f(x', z') = 0$. The wavenumber k_s is

$$k_s = 2\pi/L_s < k_d \quad (25)$$

where L_s is the width of the area of the cell illuminated by the SAR. The very large scale surface consisting of the spectral components $0 < k < k_s$ are responsible for tilting the resolution cell with respect to the mean sea surface.

Thus on replacing the spectral density function W (2a) for the surface S by the spectral density function W_F for the cell F (24) and on replacing the elements D^{PQ} of the matrix D by the elements D_F^{PQ} of the matrix D_F (23) the expression (3) can be used to determine the normalized backscatter cross section for an arbitrarily oriented cell F . In view of (19) and (20) the expressions for these backscatter cross sections are explicit functions of the tilt angles Ω and τ . For the special

case $\tau = 0$ (tilt is in the plane of incidence) the matrices T_F^i and T_F^f reduce to identity matrices and

$$\cos \theta_0 = \cos(\theta'_0 + \Omega) . \quad (26)$$

Thus for $\tau = 0$

$$\left. \frac{\partial \theta_0}{\partial \Omega} \right|_{\theta'_0 = \text{const}} = \left. \frac{\partial \theta_0}{\partial \theta'_0} \right|_{\Omega = \text{const}} \quad (27)$$

and

$$(\partial \langle \sigma^{PQ} \rangle / \partial \Omega)_{\theta'_0 = \text{const}} = (\partial \langle \sigma^{PQ} \rangle / \partial \theta'_0)_{\Omega = \text{const}} . \quad (28)$$

Therefore to obtain $\partial \langle \sigma^{PQ} \rangle / \partial \Omega$ for $\Omega = 0$ and $\tau = 0$ it is sufficient to evaluate $\langle \sigma^{PQ} \rangle$ as a function of θ'_0 with both Ω and τ set equal to zero. The value for $\partial \langle \sigma^{PQ} \rangle / \partial \tau$ can either be evaluated analytically since D_F^{PQ} (23) is an analytic function of τ , or the derivative could be evaluated numerically.

4. ILLUSTRATIVE EXAMPLES

For the illustrative examples presented in this section, the following specific form of the surface height spectral density function is selected (Brown, 1978)

$$W(v_{\bar{x}}, v_{\bar{z}}) = \frac{2}{\pi} S(v_{\bar{x}}, v_{\bar{z}}) = \begin{cases} \left(\frac{2}{\pi}\right) B k^4 / (\kappa^2 + k^2)^4 & k \leq k_c \\ 0 & k > k_c \end{cases} \quad (29)$$

where W is the notation used by Rice (1951) and S is the notation used by Brown (1978). For the assumed isotropic model of the sea surface

$$\begin{aligned} B &= 0.0046 \\ k^2 &= v_{\bar{x}}^2 + v_{\bar{z}}^2 \text{ (cm)}^{-2}, \quad k_c = 12 \text{ (cm)}^{-1} \\ \kappa &= (335.2 \text{ V}^4)^{-1/2} \text{ (cm)}^{-1}, \quad V = 4.3 \text{ (m/s)} \end{aligned} \quad (30)$$

in which k_c is the spectral cutoff wavenumber (Brown 1978) and V is the surface wind speed. The wavelength for the electromagnetic wave is

$$\lambda_0 = 3.0 \text{ cm } (k_0 = 2\pi/3 \text{ (cm)}^{-1}) . \quad (31)$$

The relative complex dielectric coefficient for the sea is

$$\epsilon_r = 48 - 135i \quad (32)$$

and the permeability for the sea is the same as for free space ($\mu_r = 1$).

The mean square height for the small scale surface h_s is given by

$$\langle h_s^2 \rangle = \int_0^{2\pi} \int_{k_d}^{k_c} \frac{W(k)}{4} k dk d\phi = \frac{B}{2} \left[\frac{1}{k_d^2} - \frac{1}{k_c^2} \right] . \quad (33)$$

The mean square slope for the large scale surface h_l within the resolution cell, is

$$\sigma_{ls}^2 = \langle h_{ls}^2 \rangle = \int_0^{2\pi} \int_{k_s}^{k_d} \frac{W(k)}{4} k^3 dk d\phi \quad (34)$$

in which k_s is given by (25). The mean square height for the large scale surface h_l is

$$\langle h_L^2 \rangle = \int_0^{2\pi} \int_0^{k_d} \frac{W(k)}{4} k dk d\phi \quad (35)$$

For $\beta = 4k_o^2 \langle \tilde{h}_s^2 \rangle = 1.0$, $k_d = 0.201$. For $L_s = 300, 1000$ and 2500 cm (25)

$$\sigma_{ls}^2 = 0.0102, 0.0143 \text{ and } 0.0152 \text{ respectively}$$

and

$$k_o^2 \langle h_L^2 \rangle = 21.9, 173 \text{ and } 357 \text{ respectively. The slope probability}$$

density function within a resolution cell is assumed to be Gaussian; thus

$$p(h_x, h_z) = \frac{1}{\pi \sigma_{ls}^2} \exp \left[-\frac{h_x^2 + h_z^2}{\sigma_{ls}^2} \right] \quad (36)$$

and the physical optics (specular point) backscatter cross section is (8) (Bahar, 1981a)

$$\langle \sigma_{PQ} \rangle_B = \delta_{PQ} \frac{\sec^4 \theta_o}{\sigma_{ls}^2} \exp \left[-\frac{\tan^2 \theta_o}{\sigma_{ls}^2} \right] |R_P|^2 \quad (37)$$

in which δ_{PQ} is the Kronecker delta and $R_P(P=V,H)$ is the Fresnel reflection coefficient for the vertically or horizontally polarized waves (Bahar, 1981a,b).

In Fig. 1a, and b $\langle \sigma^{VV} \rangle$, and $-(d\langle \sigma^{VV} \rangle / d\Omega) / \langle \sigma^{VV} \rangle$ are plotted for $\Omega = 0$ and $\tau = 0$ as functions of θ_o' the angle of incidence with respect to the fixed reference system (x', y', z') . In these figures $L_s = 300, 1000$ and 2500 cm.

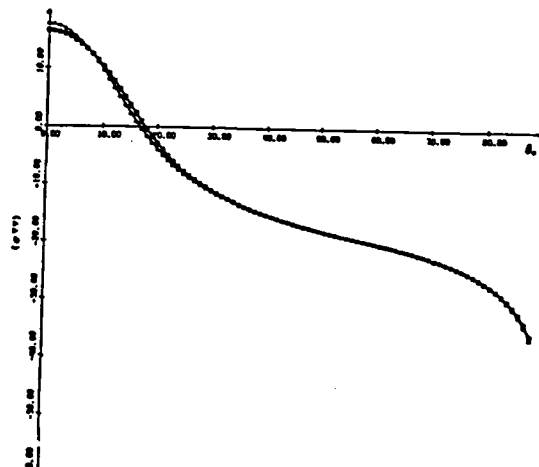


Figure 1a. $\langle \sigma^{VV} \rangle$, for $\Omega = 0$ and

$\tau = 0$ as a function of θ_o' .

(Δ) $L_s = 300$ cm, (\circ) $L_s = 1000$ cm,

(\square) $L_s = 2500$ cm.

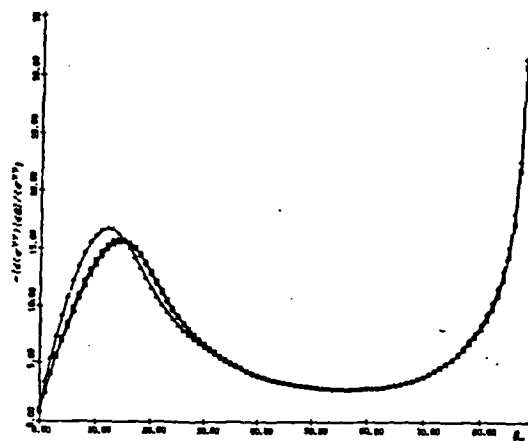


Figure 1b. $-(d\langle\sigma^{VV}\rangle/d\Omega)/\langle\sigma^{VV}\rangle$ for $\Omega = 0$ and $\tau = 0$ as a function of θ'_0 . (Δ) $L_s = 300$ cm, (\circ) $L_s = 1000$ cm, (\square) $L_s = 2500$ cm.

In Fig. 2a, and b these results are repeated for $\langle\sigma^{HH}\rangle$. It is interesting to note that the effective filtering of the very large scale spectral components of the rough surface ($0 < k < k_s$) by the SAR does not significantly change the value of σ^{PQ} unless $L_s < 300$ cm. As one may expect, the modulation of the scattering cross sections in the plane of incidence $|d\langle\sigma^{VV}\rangle/d\Omega|$ is strongest for the SAR corresponding to the narrowest effective beam width $L_s = 300$ cm. Except for near-normal incidence the relative modulation $|d\langle\sigma^{PQ}\rangle/d\Omega|/\langle\sigma^{PQ}\rangle$ is larger for the horizontally polarized waves than for the vertically polarized waves. The largest relative modulation of the like polarized cross sections occurs in the transition region where the contribution to the cross section due to Bragg scatter becomes larger than the contribution due to specular point scatter namely at about 10° - 15° (see Figs. 1b and 2b).

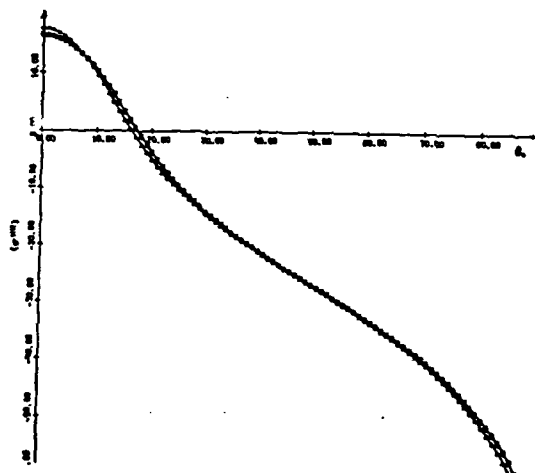


Figure 2a. $\langle\sigma^{HH}\rangle$, for $\Omega = 0$ and $\tau = 0$ as a function of θ'_0 . (Δ) $L_s = 300$ cm, (\circ) $L_s = 1000$ cm, (\square) $L_s = 2500$ cm.

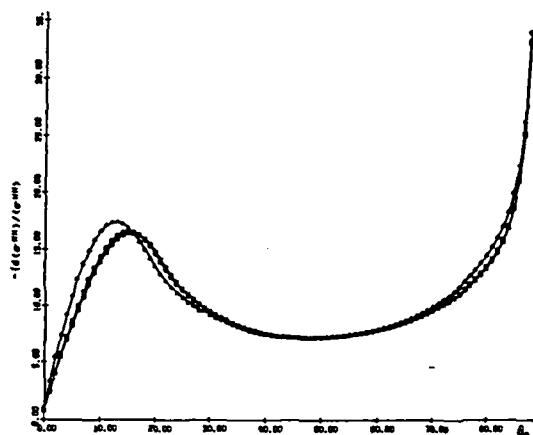


Figure 2b. $-(\langle \sigma^{HH} \rangle / d\Omega) / \langle \sigma^{HH} \rangle$ for $\Omega = 0$ and $\tau = 0$ as a function of θ_o' . (Δ) $L_s = 300$ cm, (\circ) $L_s = 1000$ cm, (\square) $L_s = 2500$ cm.

5. CONCLUDING REMARKS

The full wave approach is used to determine the scattering cross sections for arbitrarily oriented resolution cells on random rough surfaces illuminated by synthetic aperture radars. The purpose of this analysis is to determine the modulation of the like polarized scattering cross sections as the normal to the cells tilt in and perpendicular to the plane of incidence. The full wave approach accounts for shadowing and both specular point scattering as well as Bragg scattering in a self-consistent manner. Thus, the scattering cross sections are expressed as weighted sums of two cross sections. The first cross section is associated with the filtered surface consisting of the large-scale spectral components of the rough surface. The second cross section is associated with the surface consisting of the small-scale spectral components. It can be shown that if the large-scale spectral components of the surface of the cell are neglected, the second cross section accounts for first order Bragg scattering and the results are in agreement with earlier published results (Alpers et al., 1981). However, for typical terrain or sea surfaces, the large-scale spectral components are not negligible.

By using the full wave analysis, the modulation of the like and cross polarized cross sections can be determined for all angles of incidence and tilt angles. On the other hand, first order Bragg scatter theory does not account for backscattering near normal to the surface of the cell (Alpers et al., 1981). The results based on the two-scale model indicate that the relative modulation of the like polarized backscatter cross section is maximum for angles of incidence between 10° and 15° (depending on polarization and effective width of the resolution cell, L_s). The analyses based on first order Bragg scatter do not provide these results. It is also shown that as the angle of incidence approaches zero, the modulation of the scattering cross sections in and perpendicular to the plane of incidence becomes comparable.

When the normal to the cell is tilted in the direction normal to the plane of incidence ($\tau \neq 0$), the full wave analysis not only accounts for the change in the local angle of incidence θ_o' but also takes into account the fact that the local planes of incidence (or scatter) are not parallel to the reference planes of incidence for scatter, namely $\psi_F^i = -\psi_F^f \neq 0$.

Since Alpers et al. (1981) do not account for the effects of the large scale spectral components of the surface within the resolution cell the results presented here for the modulation of the like polarized scattering cross sections near normal incidence are significantly different from those given by Alpers et al.

6. REFERENCES

- Alpers, W. R., D. B. Ross and C. L. Rugenach (1981): On the detectability of ocean surface waves by real and synthetic aperture radar, J. Geophys. Res., 86(C7), 6481-6498.
- Bahar, E. (1981a): Scattering cross sections from rough surfaces--full wave analysis, Radio Sci., 16(3), 331-341.
- Bahar, E. (1981b): Scattering cross sections for composite random surfaces--full wave analysis, Radio Sci., 16(6), 1327-1335.
- Bahar, E., D. E. Barrick and M. A. Fitzwater (1983): Computations of scattering cross sections for composite surfaces and the specification of the wavenumber where spectral splitting occurs, IEEE Transactions on Antennas and Propagation, to be published.
- Barrick, D. E. (1970): Rough surfaces, in Radar Cross Section Handbook, Chapter 9, Plenum Press, New York.
- Brown, G. S. (1978): Backscattering from a Gaussian-distributed perfectly conducting rough surface, IEEE Transactions on Antennas and Propagation, AP-26(3), 472-482.
- Rice, S. O. (1951): Reflection of electromagnetic waves from a slightly rough surface, Communication of Pure and Applied Math, 4, 351-378.
- Sancer, M. I. (1969): Shadow-corrected electromagnetic scattering from a randomly rough surface, IEEE Transactions on Antennas and Propagation, AP-17(5), 577-585.
- Smith, B. G. (1967): Geometrical shadowing of a randomly rough surface, IEEE Transactions on Antennas and Propagation, AP-15(5), 668-671.
- Valenzuela, G. R. (1968): Scattering of electromagnetic waves from a tilted slightly rough surface, Radio Sci., 3, 1051-1066.
- Valenzuela, G. R., M. B. Laing and J. C. Daley (1971): Ocean sea spectra for the high frequency waves as determined from airborne radar measurements, J. Marine Res., 29, 69-84.

This paper was sponsored by the U. S. Army Research Office, Contract No. DAAG-29-82-K-0123 and the Wave Propagation Laboratory, NOAA. The text of the full paper will be published in Radio Science.

AD



CHEMICAL
RESEARCH &
DEVELOPMENT
CENTER

CRDC-SP-84009

PROCEEDINGS OF THE
1983 SCIENTIFIC CONFERENCE
ON
OBSCURATION AND AEROSOL RESEARCH

Edited by JAN FARMER
RONALD H. KOHL

RONALD H. KOHL & ASSOCIATES
Tullahoma, TN 37388

JULY 1984

US Army Armament, Munitions & Chemical Command
Aberdeen Proving Ground, Maryland 21010

SCATTERING CROSS SECTIONS FOR LARGE FINITELY CONDUCTING SPHERES
WITH ROUGH SURFACES-FULL WAVE SOLUTIONS

Ezekiel Bahar
and
Swapn Chakrabarti
Electrical Engineering Department
University of Nebraska-Lincoln
Lincoln, NE 68588-0511

ABSTRACT

The scattering cross sections for large finitely conducting spheres with very rough surfaces are determined for optical frequencies using the full wave approach. For the roughness scales considered the scattering cross sections differ significantly from those of smooth conducting spheres. Several illustrative examples are presented and the results are compared with earlier solutions to the problem.

1. Introduction

The purpose of this investigation is to determine the like and cross polarized scattering cross sections for electrically large finitely conducting spheres with very rough surfaces. Perturbation theory has been used to determine electromagnetic scattering by spheres with random rough surfaces provided that the parameter $\beta = 4k_0^2 \langle h_s^2 \rangle$ is much smaller than unity (where k_0 is the wavenumber and $\langle h_s^2 \rangle$ is the mean square height of the rough surface of the sphere, Barrick 1970). However, for large conducting spheres with $\beta \ll 1$, the total scattering cross sections are not significantly different from the physical optics cross section for smooth (unperturbed) conducting spheres.

In this paper the full wave approach is used to determine the scattering cross sections for large spheres with roughness scales that significantly modify the total cross sections. The full wave approach accounts for specular point scattering and Bragg scattering in a self consistent manner and the total scattering cross sections are expressed as weighted sums of two cross sections (Bahar and Barrick 1983). In Section 2 the problem is formulated and the principal elements of the full wave solution are presented. Illustrative examples at optical frequencies are presented in Section 3 and the results are compared with earlier solutions based on the perturbation approach (Barrick 1970) and a recent reformulated current method (Abdelazeez 1983).

2. Formulation of the Problem

The purpose of this investigation is to determine the like and cross polarized scattering cross sections at optical frequencies for large conducting spheres with very rough surfaces. The position vector \vec{r}_s to a point on the rough surface of the sphere is (see Fig. 1)

$$\vec{r}_s = h_0 \vec{a}_r + h_s \vec{a}_r \quad (2.1)$$

in which \vec{a}_r is the radius vector in the spherical coordinate system, h_0 , the radius of the unperturbed sphere, is large compared to the wavelength λ_0 of the electromagnetic wave, and h_s is the random surface

height measured along the radius vector \bar{a}_r . For a homogeneous isotropic rough surface height h_s , the spectral density function (Rice 1951, Barrick 1970, Ishimaru 1978) is the Fourier transform of the surface height autocorrelation function $\langle h(x,z), h'(x',z') \rangle$

$$W(v_x, v_z) = \frac{1}{2} \int \langle h_s h'_s \rangle \exp(iv_x x_d + iv_z z_d) dx_d dz_d \quad (2.2)$$

in which the symbol $\langle \rangle$ denotes statistical average and $\langle h_s h'_s \rangle$ is a function of distance measured along the surface of the sphere. It is assumed that the correlation distance l_c for the rough surface height h_s is very small compared to the circumference of the sphere. The unit vectors \bar{n}^i and \bar{n}^f are in the directions of the incident and scattered waves and the vector \bar{v} is given by

$$\bar{v} = k_0 (\bar{n}^f - \bar{n}^i) \quad (2.3)$$

where k_0 is the electromagnetic wavenumber ($k_0 = 2\pi/\lambda_0$).

$$\bar{n}^i = -\bar{a}_{y0} \quad (2.4)$$

$$\bar{n}^f = \sin \theta_0^f \bar{a}_{x0} + \cos \theta_0^f \bar{a}_{y0} \quad (2.5)$$

in which \bar{a}_{x0} , \bar{a}_{y0} and \bar{a}_{z0} are unit vectors in the reference coordinate system (see Fig. 1). Associated with a point on the surface of the unperturbed sphere is a local coordinate system x, y, z whose unit vectors are

$$\bar{n}_1 = (\bar{n} \times \bar{a}_{z0}) / |\bar{n} \times \bar{a}_{z0}|, \bar{n}_2 = \bar{n} - \bar{a}_r, \bar{n}_3 = \bar{n}_1 \times \bar{n} \quad (2.6)$$

Thus \bar{n}_2 is in the direction normal to the surface of the sphere and \bar{n}_1 and \bar{n}_2 are tangent to the surface of the sphere. When the distance r_d measured along the surface of the sphere is commensurate with the correlation distance l_c

$$r_d = [(x-x')^2 + (z-z')^2]^{1/2} = (x_d^2 + z_d^2)^{1/2} \quad (2.7)$$

Thus for points on the surface of the sphere at a distance $r_d = l_c$, the surface height autocorrelation function is $\langle h_s h'_s \rangle = \langle h_s^2 \rangle / e$ (where $\langle h_s^2 \rangle$ is the mean square height and e is the Neperian number). The surface h_s consists of the spectral components

$$k_d < k = (v_x^2 + v_z^2)^{1/2} < k_c \quad (2.8)$$

where $k_d = 2\pi/d$ is the smallest wavenumber characterizing the rough surface of the sphere ($d = 2h_0$) and k_c is the spectral cutoff wavenumber (Brown 1978). Perturbation theory has been used to determine electromagnetic scattering by rough surfaces (Rice 1951, Burrows 1967, Valenzuela 1968, Barrick 1970, Brown 1978). To apply perturbation theory, it is necessary to assume that $\beta = 4k_0^2 \langle h_s^2 \rangle \ll 1$. For large conducting spheres, the scattered fields are primarily due to specular point scattering. Thus, if the mean square height $\langle h_s^2 \rangle$ of the rough surface is restricted by the perturbation condition $\beta \ll 1$, the

total scattering cross sections for spheres with rough surfaces is not significantly different from those of unperturbed conducting spheres.

Since the full wave approach (Bahar 1981, 1982, Bahar and Barrick 1983) accounts for specular point scattering and Bragg scattering in a self consistent manner, the perturbation restriction need not be imposed on the mean square height $\langle h_s^2 \rangle$ of the rough surface. In this work we consider spheres with large roughness scales whose scattering cross sections differ significantly from the cross sections of unperturbed spheres. Thus using the full wave approach the total normalized scattering cross sections per unit area $\langle \sigma^{PQ} \rangle$ is expressed as a weighted sum of two cross sections

$$\langle \sigma^{PQ} \rangle = \langle \sigma^{PQ} \rangle_L + \langle \sigma^{PQ} \rangle_s \quad (2.9)$$

in which $\langle \sigma^{PQ} \rangle_L$ is the cross section associated with the large scale unperturbed surface and $\langle \sigma^{PQ} \rangle_s$ is the cross section associated with the small scale surface h_s that is superimposed on the large scale surface. The first superscript P corresponds to the polarization of the scattered wave while the second superscript Q corresponds to the polarization of the incident wave. The scattering cross section $\langle \sigma^{PQ} \rangle_L$ is given by (Bahar 1981)

$$\langle \sigma^{PQ} \rangle_L = |\chi^s(v)|^2 \langle \sigma^{PQ} \rangle \quad (2.10)$$

in which χ^s is the characteristic function for the surface h_s

$$\chi^s(v) = \langle \exp i v h_s \rangle \quad (2.11)$$

and v is the magnitude of the vector \bar{v} (2.3). Thus the weighting function $|\chi^s|^2$ is less than unity.

It approaches unity for $\langle h_s^2 \rangle \rightarrow 0$. For Gaussian rough surfaces h_s ,

$$|\chi^s|^2 = e^{-4k_o^2 \langle h_s^2 \rangle \cos^2(\theta_o^f/2)} = e^{-v_y^2 \langle h_s^2 \rangle} \quad (2.12)$$

Since in this work the unperturbed surface is assumed to be the surface of a large conducting sphere ($d \gg \lambda_o$), the cross section $\langle \sigma^{PQ} \rangle$ is given by the physical optics expression (Barrick 1970)

$$\langle \sigma^{PQ} \rangle = \delta_{PQ} |R_p|^2 \quad (2.13)$$

in which R_p is the Fresnel reflection coefficient for vertically (P=V) or horizontally (P=H) polarized waves and δ_{PQ} is the Kronecker delta. For Gaussian rough surfaces h_s , the term $\langle \sigma^{PQ} \rangle_s$ can be expressed as

$$\langle \sigma^{PQ} \rangle_s = \sum_{m=1}^{\infty} \langle \sigma^{PQ} \rangle_{sm} \quad (2.14)$$

where

$$\begin{aligned} \langle \sigma^{PQ} \rangle_{sm} = & 4\pi k_o^2 \int \frac{|D^{PQ}|^2 P_2(\bar{n}^f, \bar{n}^i | \bar{n})}{\bar{n} \cdot \bar{a}_y} \\ & \cdot \exp(-v_y^2 \langle h_s^2 \rangle) \left(-\frac{v_y}{2}\right)^{\frac{2m}{m!}} \frac{W(v_x, v_z)}{m!} p(h_x, h_z) dh_x dh_z \end{aligned} \quad (2.15)$$

In (2.15) v_x, v_y and v_z are the components of \vec{v} (2.3) in the local coordinate system (2.6)

$$\vec{v} = v_x \vec{n}_1 + v_y \vec{n}_2 + v_z \vec{n}_3 \quad (2.16)$$

The shadow function $P_2(\vec{n}^f, \vec{n}^i | \vec{n})$ is the probability that a point on the rough surface is both illuminated by the source and visible to the observer given the slopes $\vec{n}(h_x, h_z)$ at the point (Smith 1967, Sanar 1969). The function $p(\vec{n}) = p(h_x, h_z)$ is the two-dimensional probability density of the slopes h_x and h_z . The expression D^{PQ} depends on the polarization of the incident and scattered waves, the unit vectors \vec{n}^i, \vec{n}^f and \vec{n} , and the relative complex permittivity ϵ_r of the conducting sphere. The function $W_m(v_x, v_z)/2^{2m}$ is the two-dimensional Fourier transform of $\langle h_s h_s' \rangle^m$. It can be expressed as follows

$$\begin{aligned} \frac{W_m(v_x, v_z)}{2^{2m}} &= \frac{1}{(2\pi)^2} \int \langle h_s h_s' \rangle^m \exp(i v_x x_d + i v_z z_d) dx_d dz_d \\ &= \frac{1}{2^{2m}} \int W_{m-1}(x'_x, v'_z) W_1(v_x - v'_x, v_z - v'_z) dv'_x dv'_z, \\ &= \frac{1}{2^{2m}} W_{m-1}(v_x, v_z) \otimes W_1(v_x, v_z) \end{aligned} \quad (2.17)$$

In (2.17) the symbol \otimes denotes the two-dimensional convolution of W_{m-1} with W_1 .

It should be noted that for $\beta \rightarrow 0$ the scattering cross section (2.9) reduces to the scattering cross sections for large conducting spheres; for $\beta \ll 1$, it reduces to the perturbation solution (Burrows 1967) since in this case $|\chi^s| = 1$ and (2.14) reduces to the leading term $m = 1$ (Bragg scatter). In a recent analysis of wave scattering from a large sphere with rough surface (using a reformulated current method), Abdelazez (1983) obtains a solution which corresponds to the first term in (2.9). Barrick (1970), who considered backscatter by spheres with small scale roughness, presents a solution that accounts for $\langle \sigma_m^{PQ} \rangle_s$ and the first term in (2.14). The weighting function $|\chi^s|^2$ that multiplies $\langle \sigma_m^{PQ} \rangle_s$ accounts for the degradation of the specular point scattering cross section due to the superimposed rough surface h_s . The second term in (2.9), $\langle \sigma_m^{PQ} \rangle_s$, accounts for diffuse scatter due to the rough surface h_s . The leading term in $\langle \sigma_m^{PQ} \rangle_s$ ($m=1$) corresponds to Bragg scatter (Rice 1951, Valenzuela 1968, Barrick 1970, Brown 1978). In the next section illustrative examples of spheres with very rough surfaces are considered. The significance of the different terms of the solution (2.9) are considered in detail and the results are compared to earlier solutions. On replacing $\langle \sigma_m^{PQ} \rangle_s$ (2.15) by the expression for large scatterers of arbitrary shape (such as ellipsoids), one can obtain the effects of surface roughness on large scatterers of any desired shape.

3. Illustrative Examples

Assuming a homogeneous isotropic random rough surface h_s , the surface height spectral density function (2.2) (Rice 1951) considered for the illustrative examples is

$$W(v_x, v_z) = W(k) = \begin{cases} \frac{2}{\pi} B/k^4 & k_d < k < k_c \\ 0 & k > k_c \text{ and } k < k_d \end{cases} \quad (3.1)$$

in which

$$k^2 = v_x^2 + v_z^2 \quad (\text{cm})^{-2} \quad (3.2)$$

The smallest wavenumber characterizing the rough surface h_s is

$$k_d = \frac{2\pi}{d} \quad (3.3)$$

where

$$d = 20 \lambda_0$$

is the diameter of the sphere and λ_0 is the wavelength of the electromagnetic wave

$$\lambda_0 = 0.555 \times 10^{-4} \text{ cm} \quad (k_0 = \frac{2\pi}{\lambda_0} = 1.132 \times 10^5 \text{ cm}^{-1}). \quad (3.4)$$

The spectral cutoff number is (Brown 1978)

$$k_c = 4.5 \times 10^5 \text{ cm}^{-1} \quad (3.5)$$

The mean square height of the rough surface h_s is

$$\langle h_s^2 \rangle = \int_0^{2\pi} \int_{k_d}^{k_c} \frac{W(k)}{4} k_d k_c d\phi = \frac{B}{2} \left[\frac{1}{k_d^2} - \frac{1}{k_c^2} \right] \quad (3.6)$$

Thus the value of B (3.1) in terms of the parameter $\beta = 4k_0^2 \langle h_s^2 \rangle$ is

$$B = \frac{\beta k_c^2 k_d^2}{2k_0^2 (k_c^2 - k_d^2)} \quad (3.7)$$

For $\beta = 1.0$

(3.8)

the corresponding value of the mean square height is

$$\langle h_s^2 \rangle = 0.195 \times 10^{-10} \text{ cm}^2 \quad (3.9)$$

thus

$$B = 0.125 \times 10^{-2} \quad (3.10)$$

At optical frequencies the relative dielectric coefficient of aluminum is (Ehrenreich 1965)

$$\epsilon_r = -40 - i12 \quad (3.11)$$

The permeability of the sphere is assumed to be that of free space $\mu_0 = 1$. For the unperturbed sphere, the probability density function of the slopes (2.15) is given by

$$p(h_x, h_z) dh_x dh_z = p(\gamma, \delta) d\gamma d\delta = \frac{\sin \gamma d\gamma d\delta}{2\pi} \quad (3.12)$$

where γ and δ are the latitude and azimuth angles in the spherical coordinate system.

In Fig. 2 the vertically polarized scattering cross section $\langle \sigma^{VV} \rangle$ (2.9) is plotted as a function of the scatter angle θ_0^f (see Fig. 1). The parameter $\beta = 4k_0^2 \langle h_s^2 \rangle = 1.0$. In addition to the plot of $\langle \sigma^{VV} \rangle$ (2.9) (the total cross section), plots are also given for the individual terms in (2.9); $\langle \sigma^{VV} \rangle_1 = |R_V X^s|^2$, $\langle \sigma^{VV} \rangle_{s1}$ and $\langle \sigma^{VV} \rangle_{s2}$. The terms $\langle \sigma^{VV} \rangle_{sm}$ for $m \geq 3$ are negligible. The value of $\langle \sigma^{VV} \rangle = |R_V|^2$ (corresponding to the physical optics cross section for the unperturbed sphere) is also given for the purpose of comparison. Note that the total scattering cross section $\langle \sigma^{VV} \rangle$ for the rough sphere is significantly smaller than that of the unperturbed sphere $\langle \sigma^{VV} \rangle$. Furthermore, for $\beta = 1.0$ the contribution of the term $\langle \sigma^{VV} \rangle_s$ (2.9) is not negligible and $\langle \sigma^{VV} \rangle$ cannot be approximated by the first term $\langle \sigma^{VV} \rangle_1 = |R_V X^s|^2$. The corresponding results ($\beta = 1.0$) for the horizontally polarized scattering cross sections $\langle \sigma^{HH} \rangle$ are presented in Fig. 3. These results are similar to the results for the vertically polarized waves except near the quasi-Brewster angle.

The cross-polarized section $\langle \sigma^{HV} \rangle = \langle \sigma^{VH} \rangle$ is presented in Fig. 4 for $\beta = 1.0$. In view of (2.13) there is no physical optics contribution to the cross-polarized cross section. Note also that for backscatter, $\theta_0^f = 0$, $\langle \sigma^{HV} \rangle$ becomes vanishingly small. For $\beta < 0.1$, the terms $\langle \sigma \rangle_{sm}$ for $m \geq 2$ are negligible. Furthermore since $e^{-\beta} = 0.9$ for $\beta = 0.1$, the perturbation solution (Barrick 1970) is approximately equal to the full wave solution. For very small values of β the full wave solutions equal those of the reformulated current method (Abdelazeez 1983) since the second term in (2.9), $\langle \sigma^{PQ} \rangle_s$ becomes very small compared to $\langle \sigma^{PQ} \rangle_1$. However, when the scale of the roughness is very small ($\beta < 0.1$), the scattering cross sections of rough spheres are not significantly different from that of unperturbed spheres. As β (the roughness of the surface) increases, the weighting function $|X^s|^2$ decreases and the contribution of the term $\langle \sigma^{PQ} \rangle_s$ increases. Furthermore, an increasing number of terms $\langle \sigma^{PQ} \rangle_{sm}$ ($m=1,2,3,\dots$) need to be evaluated as β increases.

4. Concluding Remarks

The full wave approach has been used to determine the scattering cross sections for electrically large conducting spheres ($d \gg \lambda_0$) with very rough surfaces. The total scattering cross sections are significantly modified by the rough surface when the parameter $\beta = 4k_0^2 \langle h_s^2 \rangle > 1$. In these cases the perturbation solutions are not valid. For $\beta \ll 1$ the full wave solutions reduce to the perturbation solution (Barrick 1970); however, for $\beta \ll 1$, the modification of the total scattering cross section is not very significant. The full wave solutions are compared with the perturbation solutions (Barrick 1970) and a recent solution based on the reformulated current method (Abdelazeez 1983). The full wave solutions presented here can also be used to determine the effects of surface roughness on the scattering cross sections for large conductors of different shapes such as ellipsoids.

Acknowledgments

This investigation was sponsored by the U. S. Army Research Office, Contract No. DAAG-29-82-K-0123.

The manuscript was typed by Mrs. E. Everett.

5. References

1. Abdelazeez, M. K. (1983), "Wave Scattering from a Large Sphere with Rough Surface," IEEE Transactions on Antennas and Propagation, Vol. AP-31, No. 2, pp. 375-377.
2. Bahar, E. (1981), "Scattering Cross Sections for Composite Random Surfaces--Full Wave Analysis," Radio Science, 16(6), pp. 1327-1335.
3. Bahar, E. (1982), "Scattering Cross Sections for Composite Surfaces with Large Mean Square Slopes--Full Wave Solution," International Journal of Remote Sensing, Vol. 3, No. 3, pp. 327-337.
4. Bahar, E., D. E. Barrick (1982), "Scattering Cross Sections for Composite Surfaces that Cannot be Treated as Perturbed Physical Optics Problems," Radio Science, Vol. 18, No. 2, pp. 129-137.
5. Barrick, D. E. (1970), Rough Surfaces, in Radar Cross Section Handbook, Chapter 9, Plenum Press, New York.
6. Brown, G. S. (1978), "Backscattering from Gaussian-Distributed Perfectly Conducting Rough Surfaces," IEEE Transactions on Antennas and Propagation, AP-26(3), pp. 472-482.
7. Burrows, M. L. (1967), "On the Composite Model for Rough Surface Scattering," IEEE Transactions on Antennas and Propagation, Vol. AP-21, pp. 241-243.
8. Ehrenreich, H. (1965), "The Optical Properties of Metals," IEEE Spectrum 2(3), pp. 162-170.
9. Ishimaru, A. (1978), "Wave Propagation and Scattering in Random Media in Multiple Scattering, Turbulence, Rough Surfaces and Remote Sensing," Vol. 2, Academic Press, New York.
10. Rice, S. O. (1951), "Reflection of Electromagnetic Waves from a Slightly Rough Surface," Communication of Pure and Applied Math, Vol. 4, pp. 351-378.
11. Sancer, M. K. (1969), "Shadow-Corrected Electromagnetic Scattering from a Randomly Rough Surface," IEEE Transactions on Antennas and Propagation, AP-17(5), pp. 577-585.
12. Smith, B. G. (1967), "Geometrical Shadowing of a Randomly Rough Surface," IEEE Transactions on Antennas and Propagation, AP-15(5), pp. 668-671.
13. Valenzuela, G. R. (1968), "Scattering of Electromagnetic Waves from a Tilted Slightly Rough Surface," Radio Science, Vol. 3, No. 11, pp. 1051-1066.

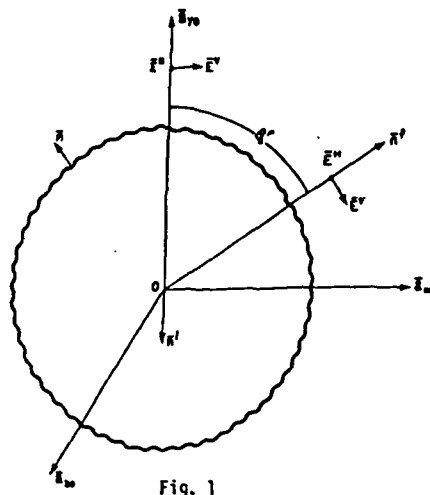


Fig. 1

Scattering of electromagnetic waves from a rough conducting sphere.

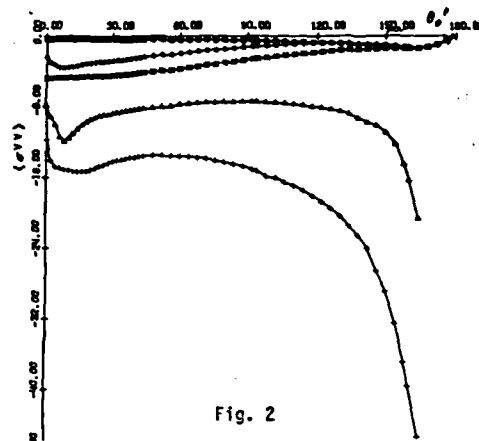


Fig. 2

Vertically polarized scattering cross section. $\beta = 1.0$ (\diamond) total cross section $\langle \sigma^{VV} \rangle$, (\circ) $\langle \sigma^{VV} \rangle = |R^{VV}|^2$, (\times) $\langle \sigma^{VV} \rangle_L = |R^{VV}_L|^2$, (Δ) $\langle \sigma^{VV} \rangle_{s1}$, (+) $\langle \sigma^{VV} \rangle_{s2}$.

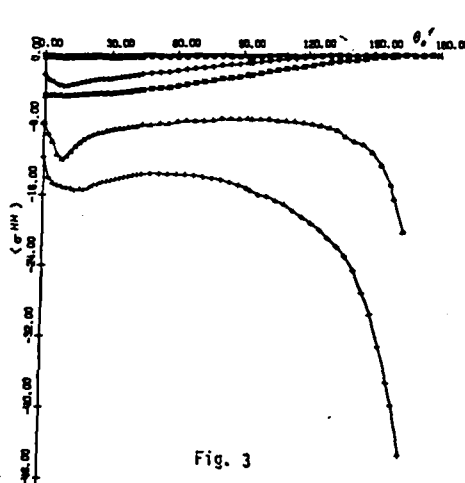


Fig. 3

Horizontally polarized cross section $\beta = 1.0$ (\diamond) total cross section $\langle \sigma^{HH} \rangle$, (\circ) $\langle \sigma^{HH} \rangle = |R^{HH}|^2$, (\times) $\langle \sigma^{HH} \rangle_L = |R^{HH}_L|^2$, (Δ) $\langle \sigma^{HH} \rangle_{s1}$, (+) $\langle \sigma^{HH} \rangle_{s2}$.

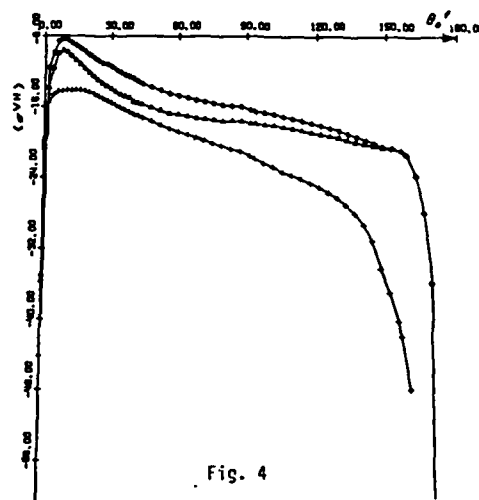


Fig. 4

Cross polarized cross section. $\beta = 1.0$ (\diamond) total cross section $\langle \sigma^{HV} \rangle = \langle \sigma^{VH} \rangle$, (Δ) $\langle \sigma^{HV} \rangle_{s1}$, (+) $\langle \sigma^{HV} \rangle_{s2}$.

Scattering by Anisotropic Models of Composite Rough Surfaces—Full Wave Solution

EZEKIEL BAHAR, FELLOW, IEEE

Abstract—Expressions for the scattering cross sections of anisotropic models of composite random rough surfaces are derived using the full wave approach that accounts for specular point scattering and Bragg scattering in a self-consistent manner. Backscatter cross sections are evaluated for vertically and horizontally polarized waves as a function of angle of incidence for cross wind, up wind, and down wind directions. The cross sections are most sensitive to wind direction for angles of incidence around 40° .

I. INTRODUCTION

Various combinations of physical optics theory and perturbation theory have been used to determine the scattering cross sections for composite models of rough surfaces [13], [12]. These solutions are based on a two-scale model of the rough surface. Physical optics [7] accounts for specular point scattering from the large scale surface while perturbation theory [11] accounts for Bragg scattering from the small scale surface. However, the results based on the perturbed-physical optics approach [8] critically depend upon the manner in which the composite surface is decomposed into a large and a small scale surface.

Since the full wave approach accounts for specular point scattering and Bragg scattering in a unified self-consistent manner, the solutions for the scattering cross sections can be derived from a single integral. However, the two-scale model can also be adopted when the full wave approach is used and the results are shown to be independent of the wavenumber k_d where spectral splitting is assumed to occur, provided that the large scale surface satisfies the criteria for deep phase modulation [5].

In this work, the full wave approach is applied to a rough surface characterized by an anisotropic slope probability density function. In Section II the full wave solutions based on the unified and two-scale model are presented, and in Section III illustrative examples are presented. Backscatter cross sections for both vertically and horizontally polarized waves are evaluated for all angles of incidence, and it is shown that the results are most sensitive to wind direction for angles of incidence around 40° . On examining the individual terms for the total cross sections based on the two-scale model, it is shown that the cross sections become insensitive to wind direction for near grazing incidence.

II. FORMULATION OF THE PROBLEM

In this section full wave analytical solutions are derived for the like and cross polarized cross sections for composite models of rough surfaces characterized by non-Gaussian surface slope probability density functions. As an illustrative example, the analysis is applied to rough surfaces with slope probability densities that can be adequately represented by the Gram Charlier expression [9], [10]. For these surfaces the surface height and slope probability densities are close to Gaussian. The deviation of the slope probability density from the Gaussian probabil-

Manuscript received May 2, 1984; revised August 15, 1984. This work was supported in part by the U.S. Army Research Office under Contract DAAG-29-82-K-0123 and the Wave Propagation Laboratory, NOAA.

The author is with the Electrical Engineering Department, University of Nebraska, Lincoln, NE 68588.

ity density is characterized by a set of skewness and peakedness coefficients [9], [10].

Assuming that $k_0^2 \langle h^2 \rangle \gg 1$ where k_0 is the free space wave-number and $\langle h^2 \rangle$ is the mean square height of the rough surface (see Fig. 1), the full wave solution for the normalized scattering cross sections per unit area is given by [4], [3].

$$\langle \sigma^{PQ} \rangle = \frac{k_0^2}{\pi} \left\langle \int \left| \frac{D^{PQ}}{\bar{n} \cdot \bar{a}_y} \right|^2 P_2(\bar{n}^i, \bar{n}^f | \bar{n}) \cdot \exp[i\bar{v} \cdot (\bar{r} - \bar{r}')] dx_d dz_d \right\rangle. \quad (1)$$

In (1) D^{PQ} depends explicitly upon the polarization of incident wave (second superscript $Q = V$ -vertical, or H -horizontal) and the polarization of the scattered wave (first superscript $P = V, H$) the direction of the incident and scattered wave normals \bar{n}^i and \bar{n}^f , respectively, the complex permittivity ϵ and permeability μ of the medium of propagation, and the unit vector $\bar{n}(h_x, h_z)$ normal to the rough surface [1], [2]. For a random rough surface

$$f(x, y, z) = y - h(x, z) = 0 \quad (2a)$$

the unit vector \bar{n} is

$$\bar{n} = \nabla f / |\nabla f| \quad (2b)$$

where

$$\nabla f = (-h_x \bar{a}_x + \bar{a}_y - h_z \bar{a}_z) \quad (3a)$$

$$h_x \equiv \partial h / \partial x, \quad h_z \equiv \partial h / \partial z \quad (3b)$$

and $\bar{a}_x, \bar{a}_y, \bar{a}_z$ are unit vectors in the reference coordinate system (see Figs. 1 and 2). The plane $y = 0$ is chosen to be the reference plane. The function $P_2(\bar{n}^i, \bar{n}^f | \bar{n})$ is the probability that a point on the rough surface is both illuminated and visible given the value of the slopes $\bar{n}(h_x, h_z)$ at the point. The vector \bar{v} is given by

$$\begin{aligned} \bar{v} &= \bar{k}^f - \bar{k}^i = k_0(\bar{n}^f - \bar{n}^i) \equiv v_x \bar{a}_x + v_y \bar{a}_y + v_z \bar{a}_z \\ &= k_0[(\sin \theta_0^f \cos \phi^f - \sin \theta_0^i \cos \phi^i) \bar{a}_x + (\cos \theta_0^f \\ &\quad + \cos \theta_0^i) \bar{a}_y + (\sin \theta_0^f \sin \phi^f - \sin \theta_0^i \sin \phi^i) \bar{a}_z] \end{aligned} \quad (4)$$

and

$$\begin{aligned} \bar{r} - \bar{r}' &= (x - x') \bar{a}_x + (h - h') \bar{a}_y + (z - z') \bar{a}_z \\ &= x_d \bar{a}_y + (h - h') \bar{a}_y + z_d \bar{a}_z \end{aligned} \quad (5)$$

is the vector joining two points (x, h, z) and (x', h', z') on the rough surface. The symbol $\langle \cdot \rangle$ denotes the statistical average over the slopes and height of the rough surface. For convenience the position vectors (from the origin to points on the rough surface) are expressed as follows (see Fig. 3):

$$\bar{r} = \bar{r}_F + \bar{r}_R \quad (6)$$

in which

$$\bar{r}_F = x \bar{a}_x + h \bar{a}_y + z \bar{a}_z \quad (7)$$

is the position vector to a point on the large scale (filtered) surface [4]. Associated with the large scale surface is a local coordinate system $(\bar{x}, \bar{y}, \bar{z})$ (see Figs. 2 and 3) with unit vector \bar{n}_1, \bar{n}_2 and \bar{n}_3 such that

$$\bar{n}_1 = (\bar{n} \times \bar{a}_z) / |\bar{n} \times \bar{a}_z|, \quad \bar{n}_2 = \bar{n}, \quad \bar{n}_3 = \bar{n}_1 \times \bar{n}_2 \quad (8)$$

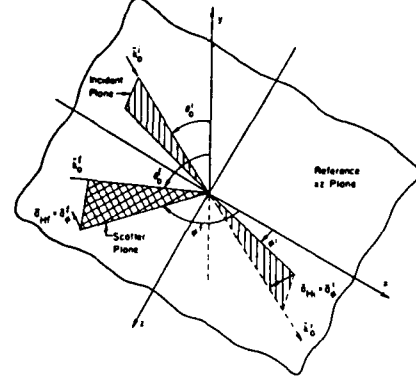


Fig. 1. Planes of incidence and scatter and the reference plane (x, z) .

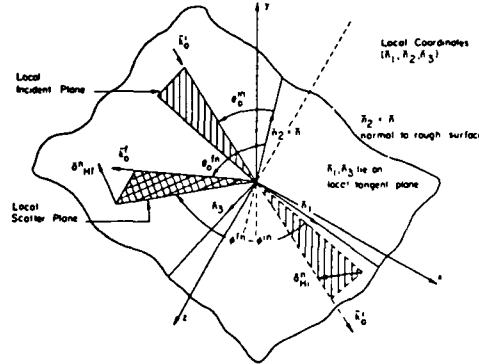


Fig. 2. Local planes of incidence and scatter and the local coordinate system.

Thus in (6)

$$\bar{r}_R = \bar{h}_R \bar{n}, \quad \nabla(y - h_F) / |\nabla(y - h_F)| \equiv \nabla f / |\nabla f| = \bar{n} \quad (9)$$

where $\bar{h}_R(\bar{x}, \bar{z})$ is the displacement of the small scale surface from the large scale (filtered) surface. The distance vector $\bar{r} - \bar{r}'$ can also be expressed as

$$\begin{aligned} \bar{r} - \bar{r}' &= (x - x') \bar{a}_x + (z - z') \bar{a}_z + (h_F - h'_F) \bar{a}_y + (\bar{h}_R - \bar{h}'_R) \bar{n} \\ &\equiv (x - x') \bar{a}_x + (z - z') \bar{a}_z + [h_x^F(x - x') + h_z^F(z - z')] \bar{a}_y \\ &\quad + (\bar{h}_R - \bar{h}'_R) \bar{n} \equiv \bar{r}_d + (\bar{h}_R - \bar{h}'_R) \bar{n} \end{aligned} \quad (10)$$

where

$$h_x^F = \partial h_F / \partial x \approx h_x \quad \text{and} \quad h_z^F = \partial h_F / \partial z \approx h_z. \quad (11)$$

Thus \bar{r}_d is the distance vector measured in the plane tangent to the large scale surface

$$y = h_F(x, z) = 0. \quad (12)$$

$$\begin{aligned} \bar{r}_d &= (x - x') \bar{a}_x + (z - z') \bar{a}_z + [h_x^F(x - x') + h_z^F(z - z')] \bar{a}_y \\ &= \bar{x}_d \bar{n}_1 + \bar{z}_d \bar{n}_3 \end{aligned} \quad (13)$$

in which \bar{x}_d and \bar{z}_d are distances measured along the unit vectors

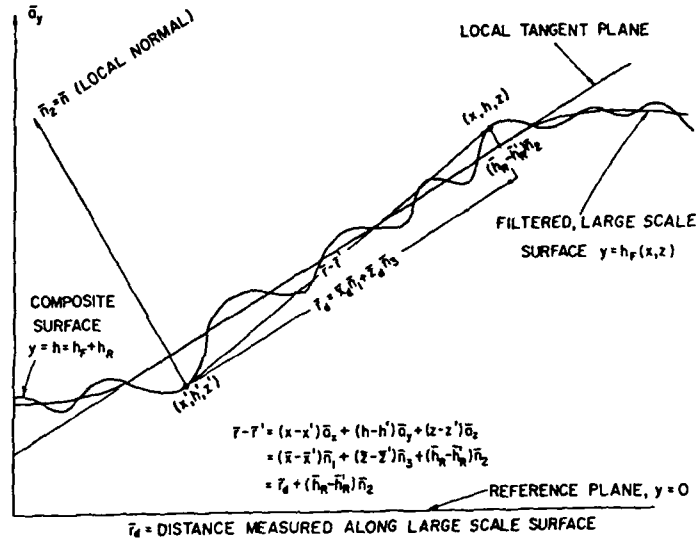


Fig. 3. Decomposition of the composite rough surface.

\bar{n}_1 and \bar{n}_3 in the plane tangent to the large scale surface. Thus

$$\begin{aligned}\bar{v} \cdot (\bar{r} - \bar{r}') &= (v_x + v_y h_x) x_d + (v_z + v_y h_z) z_d + v_y (\bar{h} - \bar{h}') \\ &= (v_x \bar{x}_d + v_z \bar{z}_d) + v_y (\bar{h} - \bar{h}') \\ &= \bar{v} \cdot \bar{r}_d + v_y (\bar{h} - \bar{h}')\end{aligned}\quad (14)$$

in which v_x and v_z are components of the vector \bar{v} (4) in the local coordinate system.

$$v_x = \bar{v} \cdot \bar{n}_1, v_z = \bar{v} \cdot \bar{n}_3 \quad \text{and} \quad v_y = \bar{v} \cdot \bar{n}_2. \quad (15)$$

The scattering cross sections $\langle \sigma^P Q \rangle$, (1) for composite rough surfaces can therefore be expressed as follows:

$$\begin{aligned}\langle \sigma^P Q \rangle &= \frac{k_0^2}{\pi} \left\langle \int \left| \frac{D^P Q}{\bar{n} \cdot \bar{a}_y} \right|^2 P_2(\bar{n}', \bar{n}' | \bar{n}) \exp[i\bar{v} \cdot \bar{r}_d] \right. \\ &\quad \cdot [|\chi^R|^2 + \chi_2^R - |\chi^R|^2] dx_d dz_d \Big\rangle.\end{aligned}\quad (16)$$

In (16) the term

$$|\chi^R|^2 \equiv |\langle \exp(i v_y \bar{h}_R) \rangle|^2 \quad (17)$$

has been added and subtracted for convenience. The expectation of $\exp(i v_y \bar{h}_R)$ is the small scale surface characteristic function and

$$\chi_2^R = \langle \exp[i v_y (\bar{h}_R - \bar{h}_R')] \rangle \quad (18)$$

is the joint characteristic function for the small scale surface. It is assumed in (16) that the small scale surface height is independent of the surface slopes $\bar{n}(h_x, h_z)$. Thus the scattering cross section for composite surfaces can be expressed as a weighted sum of two cross sections [4]

$$\langle \sigma^P Q \rangle = \langle \sigma^P Q \rangle_F + \langle \sigma^P Q \rangle_R \quad (19)$$

in which

$$\begin{aligned}\langle \sigma^P Q \rangle_F &= \frac{k_0^2}{\pi} \int \left| \frac{D^P Q}{\bar{n} \cdot \bar{a}_y} \right|^2 P_2(\bar{n}', \bar{n}' | \bar{n}) |\chi^R|^2 p(h_x, h_z) \\ &\quad \cdot \exp[i(v_x + v_y h_x)x_d + i(v_z + v_y h_z)z_d] \\ &\quad \cdot dx_d dz_d dh_x dh_z\end{aligned}\quad (20)$$

$$\begin{aligned}\langle \sigma^P Q \rangle_R &= \frac{k_0^2}{\pi} \int \left| \frac{D^P Q}{\bar{n} \cdot \bar{a}_y} \right|^2 P_2(\bar{n}', \bar{n}' | \bar{n}) [|\chi_2^R| - |\chi^R|^2] p(h_x, h_z) \\ &\quad \cdot \exp[i v_y \bar{x}_d + v_y \bar{z}_d] d\bar{x}_d d\bar{z}_d dh_x dh_z\end{aligned}\quad (21)$$

and $p(h_x, h_z)$ is the two-dimensional probability density of the slopes. Note that in (20) the integration is with respect to x_d and z_d (distances in the reference plane) while in (21) the integration is with respect to \bar{x}_d and \bar{z}_d (distances along the large scale surface). Thus in (21) use has been made of the relationship

$$\frac{dx_d dz_d}{\bar{n} \cdot \bar{a}_y} = d\bar{x}_d d\bar{z}_d. \quad (22)$$

To evaluate (20) use is made of the integral representation of the Dirac delta functions

$$\begin{aligned}\int \exp[i(v_x + v_y h_x)x_d + i(v_z + v_y h_z)z_d] dx_d dz_d \\ = 4\pi^2 \delta(v_x + v_y h_x) \delta(v_z + v_y h_z).\end{aligned}\quad (23)$$

Thus on integrating with respect to the slopes h_x and h_z (20) reduces to

$$\begin{aligned}\langle \sigma^P Q \rangle_F &= \frac{4\pi k_0^2}{v_y^2} \left[\int \left| \frac{D^P Q}{\bar{n} \cdot \bar{a}_y} \right|^2 P_2(\bar{n}', \bar{n}' | \bar{n}) p(\bar{n}) |\chi^R(v_y \bar{h}_R)|^2 \right]_{\bar{n}=\bar{n}_2} \\ &= \langle \sigma_{\text{smooth}}^P Q \rangle |\chi^R|^2\end{aligned}\quad (24)$$

in which \bar{n}_s is the value of the unit vector normal to the surface \bar{n} at the specular points.

$$\bar{n}_s = \bar{v}/v = (\bar{n}^f - \bar{n}^i)/|\bar{n}^f - \bar{n}^i|. \quad (25)$$

In (24) $\langle \sigma^P Q \rangle$ is the physical optics scattering cross section for the filtered surface $y = h_F(x, z)$. It is multiplied by the coefficient $|\chi^R|^2$. This weighting function which is less than unity accounts for the degradation of the physical optics cross section due to the effects of the small scale surface that rides on the filtered surface.

To evaluate the cross section associated with the small scale surface, it is assumed that the surface \bar{h}_R is Gaussian. Thus $\langle \sigma^P Q \rangle_R$ can be expressed as follows [4]:

$$\langle \sigma^P Q \rangle_R = \sum_{m=1}^{\infty} \langle \sigma^P Q \rangle_{Rm} \quad (26)$$

where

$$\langle \sigma^P Q \rangle_{Rm} = 4\pi k_0^2 \int \frac{|D^P Q|^2 P_2(\bar{n}^f, \bar{n}^i | \bar{n})}{\bar{n} \cdot \bar{a}_y} \exp(-v_y^2 \langle h_R^2 \rangle) \cdot \left(\frac{v_y}{2} \right)^{2m} \frac{W_m(v_x, v_z)}{m!} p(h_x, h_z) dh_x dh_z \quad (27)$$

and $W_m(v_x, v_z)/2^{2m}$ is the dimensional Fourier transform of $\langle (\bar{h}_R \bar{h}_R') \rangle^m$ [4]. Thus W_1 is the surface height spectral density function and

$$\begin{aligned} \frac{W_m(v_x, v_z)}{2^{2m}} &= \frac{1}{(2\pi)^2} \int \langle (\bar{h}_R \bar{h}_R') \rangle^m \exp(i v_x \bar{x}_d + i v_z \bar{z}_d) d\bar{x}_d d\bar{z}_d \\ &\cdot \frac{1}{2^{2m}} \int W_{m-1}(v'_x, v'_z) W_1(v_x - v'_x, v_z - v'_z) dv'_x dv'_z \\ &= \frac{1}{2^{2m}} W_{m-1}(v_x, v_z) \otimes W_1(v_x, v_z). \end{aligned} \quad (28)$$

In (28) the symbol \otimes denotes the two-dimensional convolution of W_{m-1} with W_1 .

III. ILLUSTRATIVE EXAMPLES

For the illustrative examples considered in this section, the two dimensional slope probability density function is given by [9]

$$\begin{aligned} p(\bar{n}) = p(h_x, h_z) &= \frac{1}{2\pi\sigma_c\sigma_u} \exp \left[-\frac{1}{2} (\xi^2 + \eta^2) \right] \\ &\cdot \left[1 - \frac{1}{2} C_{21}(\xi^2 - 1)\eta - \frac{1}{6} C_{03}(\eta^2 - 3)\eta \right. \\ &+ \frac{1}{24} C_{40}(\xi^4 - 6\xi^2 + 3) - \frac{1}{4} C_{22}(\xi^2 - 1)(\eta^2 - 1) \\ &\left. + \frac{1}{24} C_{04}(\eta^4 - 6\eta^2 + 3) \right] \end{aligned} \quad (29)$$

where for a wind speed $V = 14$ m/s, the skewness coefficients are

$$C_{21} = -0.1404, \quad C_{03} = -0.542 \quad (30)$$

and the peakedness coefficients are

$$C_{40} = 0.40, \quad C_{22} = 0.12, \quad C_{04} = 0.23. \quad (31)$$

The cross wind and up/down wind mean square slopes are

$$\sigma_c^2 = 0.02988 \quad \text{and} \quad \sigma_u^2 = 0.04824. \quad (32)$$

In (29) the dimensionless quantities ξ and η are

$$\xi = h_x/\sigma_c \quad \text{and} \quad \eta = h_z/\sigma_u. \quad (33)$$

The surface of the sea is assumed to be perfectly conducting for simplicity. The frequency of the radar is

$$f = 15 \text{ GHz} (\lambda_0 = 2 \text{ cm}). \quad (34)$$

The spectral density function W_1 for the small scale surface is given by

$$W_1 = \frac{2}{\pi} B/k^4 \quad k_d \leq k \leq k_c \quad (35)$$

in which

$$B = 0.012 \quad k_c = 12 \text{ (cm)}^{-1} \quad (36)$$

and the wavenumber k_d where spectral splitting (between the large and small scale surfaces) is assumed to occur is chosen such that [5]

$$\beta = 4k_0^2 \langle h_R^2 \rangle = 1.0 = 2k_0^2 B \left[\frac{1}{k_d^2} - \frac{1}{k_c^2} \right]. \quad (37)$$

Thus

$$k_d = 0.485 \text{ (cm)}^{-1}. \quad (38)$$

In Fig. 4 $\langle \sigma^{VV} \rangle$ the backscatter cross section for vertically polarized waves is plotted as a function of the angle of incidence θ_0^i for the cross wind, up wind, and down wind directions. The corresponding result for the horizontally polarized backscatter cross section $\langle \sigma^{HH} \rangle$ is given in Fig. 5. For normal incidence ($\theta_0^i = 0$) there is no difference between the backscatter cross sections for cross wind, up wind, and down wind. This is because for normal incidence, specular point scattering (which is polarization independent) dominates. To notice significant differences in the backscatter cross sections at normal incidence, it is necessary to consider surfaces with considerably larger skewness and mean square slopes. Furthermore, all three cases merge for grazing angles. This is because, the principal contribution to backscatter for near grazing angles is due to Bragg scatter which is given by the term $\langle \sigma^P Q \rangle_{R1}$ (27). In this term the effects of the anisotropic slope distribution are averaged out and the dependence on wind direction becomes small for grazing angles. The anisotropic effects of the slope distribution are most pronounced around $\theta_0^i = 40^\circ$. This is shown in Fig. 6 in which $\langle \sigma^{VV} \rangle$ and $\langle \sigma^{HH} \rangle$ are plotted as functions of the azimuth angle $90^\circ \leq \phi \leq 270^\circ$ with the angle of incidence $\theta_0 = 40^\circ$. The up wind and down wind directions correspond to $\phi = 90^\circ$ and $\phi = 270^\circ$, respectively, and cross wind corresponds to 0° and 180° .

For the illustrative examples considered here, the terms $\langle \sigma^P Q \rangle_{Rm}$ can be neglected for $m \geq 4$. Individual terms for the total cross section $\langle \sigma^{VV} \rangle$ are shown in Fig. 7 for the cross wind case.

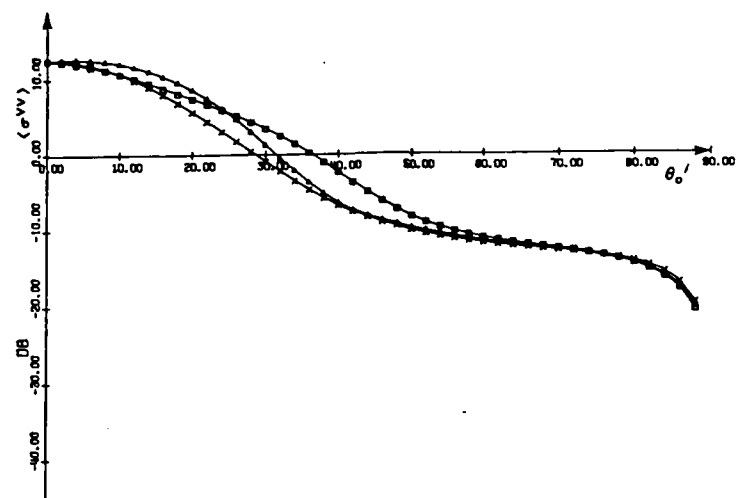


Fig. 4. Backscatter cross section for vertically polarized waves. (X) Cross wind, (□) up wind, (Δ) down wind.

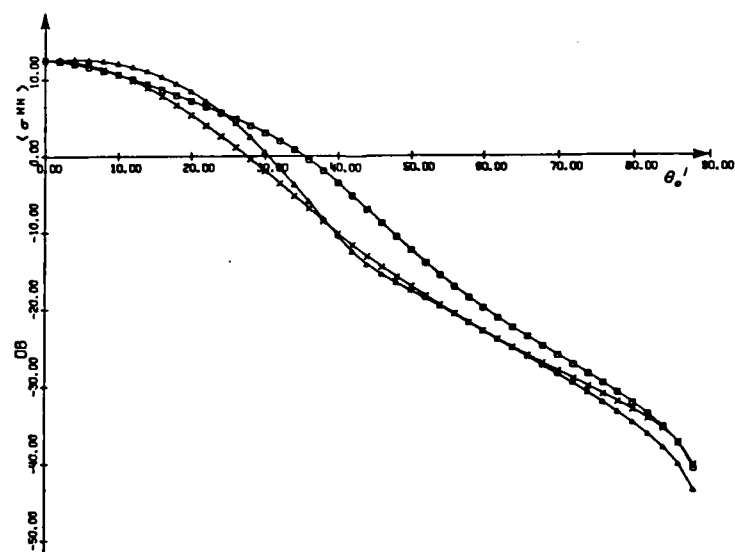


Fig. 5. Backscatter cross section for horizontally polarized waves. (X) Cross wind, (□) up wind, (Δ) down wind.

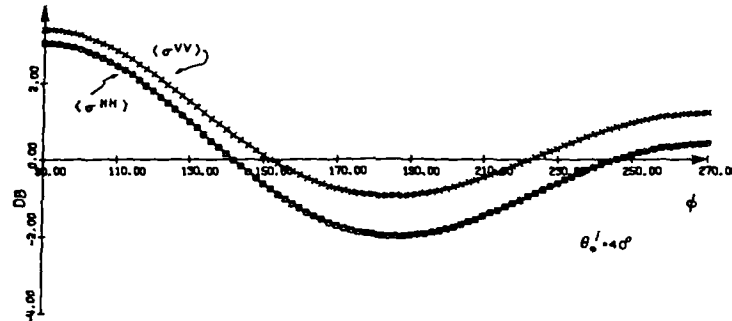


Fig. 6. Plots of the backscatter cross sections (σ^{VV}) (X) and (σ^{HH}) (□) as a function of the azimuth angle. The angle of incidence is $\theta_i = 30^\circ$.

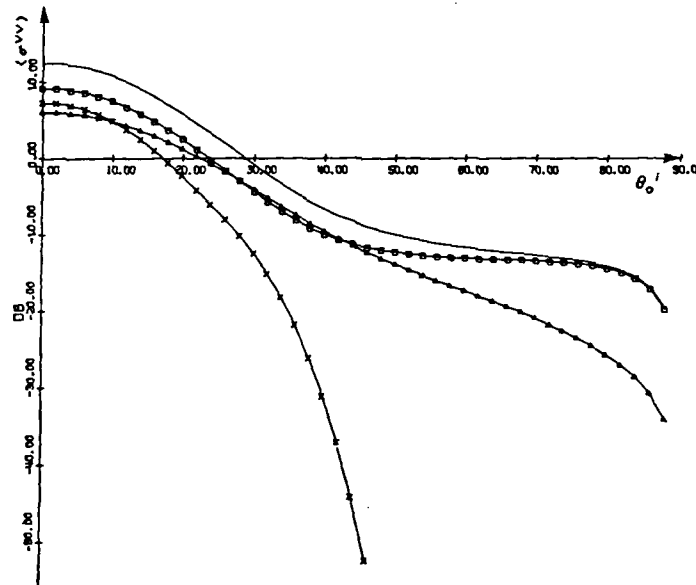


Fig. 7. Individual terms of the total cross sections. Total (σ^{VV}) solid line, $(\sigma^{VV})_R$ (X), $(\sigma^{VV})_{R1}$ (□), $(\sigma^{VV})_{R2} + (\sigma^{VV})_{R3}$ (Δ).

IV. CONCLUDING REMARKS

The full wave approach has been used to determine the scattering cross sections for composite rough surfaces characterized by anisotropic slope distribution functions. A two-scale model of the rough surface was adopted and the large scale surface is assumed to satisfy the radii of curvature criteria and the condition for deep phase modulation. For the illustrative examples the large scale slope probability density function is given by the Gram Charlier expression [9]. The small scale surface \bar{h}_R is characterized by its surface height spectral density function. The random rough surface height \bar{h}_R is assumed to be stationary and Gaussian. Thus it is assumed that the slopes $p(\vec{n})$ and the small scale surface heights \bar{h}_R are statistically independent. The like polarized backscatter cross sections based on the two-scale model were shown to be independent of the choice of k_d (spectral

splitting wavenumber) provided that $\beta \geq 1.0$. On the other hand the perturbed-physical optics solution for the backscatter cross sections [8] is very sensitive to the choice of k_d .

The examples in Section III illustrate the polarization dependence of the backscatter cross sections for all angles of incidence. The results are given for the cross wind, up wind and down wind directions. It is shown that the backscatter cross sections are insensitive to wind direction for near grazing and near normal angles of incidence. They are most sensitive to wind direction for angles of incidence around 40° (see Fig. 6).

The full wave approach can be applied to a wide class of anisotropic rough surfaces for which the perturbed-physical optics approach is not suitable. Furthermore, since the full wave approach accounts for specular point scatter and Bragg scatter in a unified self-consistent manner (1), it is not necessary

to adopt a two-scale model of the surface and spectral splitting can be avoided.

ACKNOWLEDGMENT

The author wishes to thank W. Warnsholz and M. A. Fitzwater for the computational work. The manuscript was prepared by Mrs. E. Everett.

REFERENCES

- [1] E. Bahar, "Scattering cross sections for random rough surfaces: full wave analysis," *Radio Sci.*, vol. 16, no. 3, pp. 331-341, 1981.
- [2] —, "Scattering cross sections for composite random surfaces: Full wave analysis," *Radio Sci.*, vol. 16, no. 6, pp. 1327-1335, 1981.
- [3] —, "Full wave solutions of the depolarization of the scattered radiation fields by rough surfaces of arbitrary slope," *IEEE Trans. Antennas Propagat.*, vol. AP-29, no. 3, pp. 443-454, 1981.
- [4] E. Bahar and D. E. Barrick, "Scattering cross sections for composite surfaces that cannot be treated as perturbed-physical optics problems," *Radio Sci.*, vol. 18, no. 2, pp. 129, 137, 1983.
- [5] E. Bahar, D. E. Barrick, and M. A. Fitzwater, "Computations of the scattering cross sections for composite surfaces and the specification of the wavenumber where spectral splitting occurs," *IEEE Trans. Antennas Propagat.*, vol. AP-31, no. 5, pp. 698-709, 1983.
- [6] D. E. Barrick and W. H. Peake, "A review of scattering from surfaces with different roughness scales," *Radio Sci.*, vol. 3, no. 8, pp. 865-868, 1968.
- [7] P. Beckmann, *The Depolarization of Electromagnetic Waves*. Boulder, CO: Golem, 1968.
- [8] G. S. Brown, "Backscattering from a Gaussian-distributed perfectly conducting rough surface," *IEEE Trans. Antennas Propagat.*, vol. AP-26, no. 3, pp. 472-482, 1978.
- [9] C. Cox and W. Munk, "Measurement of the roughness of the sea surfaces from photographs of the sun's glitter," *J. Opt. Soc. Am.*, vol. 44, no. 11, pp. 838-850, 1954.
- [10] B. Kinsman, *Wind Waves—Their Generation and Propagation on the Ocean Surface*. Englewood Cliffs, NJ: Prentice Hall, 1965.
- [11] S. O. Rice, "Reflection of electromagnetic waves from a slightly rough surface," *Commun. Pure Appl. Math.*, vol. 4, pp. 351-378, 1951.
- [12] G. R. Valenzuela, "Scattering of electromagnetic waves from a tilted slightly rough surface," *Radio Sci.*, vol. 3, no. 11, pp. 1051-1066, 1968.
- [13] J. W. Wright, "A new model for sea clutter," *IEEE Trans. Antennas Propagat.*, vol. AP-16, no. 2, pp. 217-223, 1968.

Reprinted from Applied Optics, Vol. 24, page 1820, June 15, 1985
 Copyright © 1985 by the Optical Society of America and reprinted by permission of the copyright owner.

Scattering and depolarization by large conducting spheres with rough surfaces

Ezekiel Bahar and Swapan Chakrabarti

The scattering cross sections for large finitely conducting spheres with rough surfaces are determined for optical frequencies using the full wave approach. For the roughness scales considered the scattering cross sections differ significantly from those of smooth conducting spheres. Several illustrative examples are presented, and the results are compared to earlier solutions to the problem.

I. Introduction

The purpose of this investigation is to determine the like- and cross-polarized scattering cross sections for electrically large finitely conducting spheres with rough surfaces. Perturbation theory has been used to determine electromagnetic scattering by spheres with random rough surfaces provided that the parameter $\beta = 4k_0^2 \langle h_s^2 \rangle$ is much smaller than unity (where k_0 is the wave number, and $\langle h_s^2 \rangle$ is the mean square height of the rough surface of the sphere¹). However, for large conducting spheres with $\beta \ll 1$, the total scattering cross sections are not significantly different from the physical optics cross section for smooth (unperturbed) conducting spheres.

In this paper the full wave approach is used to determine the scattering cross sections for large spheres with roughness scales that significantly modify the total cross sections. The full wave approach accounts for specular point scattering and Bragg scattering in a self-consistent manner, and the total scattering cross sections are expressed as weighted sums of two cross sections.² In Sec. II the problem is formulated, and the principal elements of the full wave solution are presented. Several illustrative examples at optical frequencies are presented in Sec. III, and the results are compared to earlier solutions based on the perturbation approach¹ and a recent reformulated current method.³

II. Formulation of the Problem

The purpose of this investigation is to determine the like- and cross-polarized scattering cross sections at optical frequencies for large conducting spheres with very rough surfaces. The position vector \mathbf{r}_s to a point on the rough surface of the sphere is (see Fig. 1)

$$\mathbf{r}_s = h_0 \hat{\mathbf{a}}_r + h_s \hat{\mathbf{a}}_r, \quad (1)$$

in which $\hat{\mathbf{a}}_r$ is the radius vector in the spherical coordinate system, h_0 , the radius of the unperturbed sphere, is large compared with the wavelength λ_0 of the electromagnetic wave, and h_s is the random surface height measured along the radius vector $\hat{\mathbf{a}}_r$. For a homogeneous isotropic rough surface height h_s the spectral density function^{1,4,5} is the Fourier transform of the surface height autocorrelation function $\langle h(x,z)h'(x',z') \rangle$:

$$W(v_x, v_z) = \frac{1}{\pi^2} \int_{-\infty}^{\infty} \int_{-\infty}^{\infty} \langle h_s h'_s \rangle \exp(i v_x x_d + i v_z z_d) dx_d dz_d, \quad (2)$$

in which the symbol $\langle \cdot \rangle$ denotes statistical average, and $\langle h_s h'_s \rangle$ is a function of distance measured along the surface of the sphere. It is assumed that the correlation distance l_c for the rough surface height h_s is very small compared with the circumference of the sphere. The unit vectors $\hat{\mathbf{n}}^i$ and $\hat{\mathbf{n}}^s$ are in the directions of the incident and scattered waves, and the vector \mathbf{v} is given by

$$\mathbf{v} = k_0(\hat{\mathbf{n}}^i - \hat{\mathbf{n}}^s), \quad (3)$$

where k_0 is the electromagnetic wave number ($k_0 = 2\pi/\lambda_0$):

$$\hat{\mathbf{n}}^i = -\hat{\mathbf{d}}_{y0} \quad (4)$$

$$\hat{\mathbf{n}}^s = \sin \theta \hat{\mathbf{d}}_{x0} + \cos \theta \hat{\mathbf{d}}_{y0}, \quad (5)$$

in which $\hat{\mathbf{d}}_{x0}$, $\hat{\mathbf{d}}_{y0}$, and $\hat{\mathbf{d}}_{z0}$ are unit vectors in the reference coordinate system (see Fig. 1). Associated with a point on the surface of the unperturbed sphere is a local coordinate system x, y, z whose unit vectors are

The authors are with University of Nebraska-Lincoln, Electrical Engineering Department, Lincoln, Nebraska 68588-0511.

Received 9 March 1984.

0003-6935/85/121820-06\$02.00/0.

© 1985 Optical Society of America.

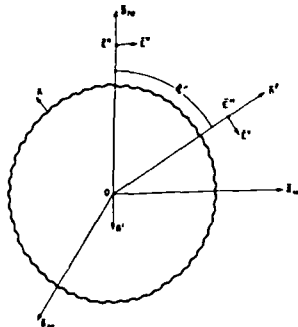


Fig. 1. Scattering of electromagnetic waves from a rough conducting sphere.

$$\hat{n} = (\hat{n} \times \hat{e}_{z0}) / |\hat{n} \times \hat{e}_{z0}|, \hat{n}_2 = \hat{n} = \hat{e}_r, \hat{n}_3 = \hat{n}_1 \times \hat{n}. \quad (6)$$

Thus $\hat{n}_2 = \hat{n}$ is in the direction normal to the surface of the sphere, and \hat{n}_1 and \hat{n}_3 are tangent to the surface of the sphere. When the distance r_d measured along the surface of the sphere is commensurate with the correlation distance l_c ,

$$r_d \approx [(x-x')^2 + (z-z')^2]^{1/2} = (x_d^2 + z_d^2)^{1/2} \ll \pi h_0 \quad (7)$$

For points on the surface of the sphere at a distance $r_d = l_c$, the surface height autocorrelation function is $\langle h_s h_s \rangle = \langle h_s^2 \rangle / e$ (where $\langle h_s^2 \rangle$ is the mean square height, and e is the Neperian number). The surface h_s consists of the spectral components

$$h_d < h = (v_s^2 + v_z^2)^{1/2} < k_c, \quad (8)$$

where $k_d = 2\pi/d$ is the smallest wave number characterizing the rough surface of the sphere ($d = 2h_0$), and k_c is the spectral cutoff wave number.⁶ Perturbation theory has been used to determine electromagnetic scattering by rough surfaces.^{1,4,6-8} To apply perturbation theory, it is necessary to assume that $\beta = 4k_0^2 \langle h_s^2 \rangle \ll 1$. For large conducting spheres, the scattered fields are primarily due to specular point scattering. Thus, if the mean square height $\langle h_s^2 \rangle$ of the rough surface is restricted by the perturbation condition $\beta \ll 1$, the total scattering cross sections for spheres with rough surfaces is not significantly different from those of unperturbed conducting spheres.

Since the full wave approach^{2,9,10} accounts for specular point scattering and Bragg scattering in a self-consistent manner, the perturbation restriction need not be imposed on the mean square height $\langle h_s^2 \rangle$ of the rough surface. In this work we consider spheres with large roughness scales whose scattering cross sections differ significantly from the cross sections of unperturbed spheres. Thus using the full wave approach the total normalized scattering cross sections per unit projected area $\langle \sigma^{PQ} \rangle$ is expressed as a weighted sum of two cross sections:

$$\langle \sigma^{PQ} \rangle = \langle \sigma^{PQ} \rangle_l + \langle \sigma^{PQ} \rangle_s, \quad (9)$$

in which $\langle \sigma^{PQ} \rangle_l$ is the cross section associated with the large scale unperturbed surface, and $\langle \sigma^{PQ} \rangle_s$ is the cross section associated with the small scale surface h_s that is superimposed on the large scale surface. The first superscript P corresponds to the polarization of the scattered wave, while the second superscript Q corresponds to the polarization of the incident wave. The scattering cross section $\langle \sigma^{PQ} \rangle_l$ is given by⁹

$$\langle \sigma^{PQ} \rangle_l = |\chi^*(v)|^2 \langle \sigma_s^{PQ} \rangle, \quad (10)$$

in which χ^* is the characteristic function for the surface h_s :

$$\chi^*(v) = \langle \exp(i\mathbf{v} \cdot \mathbf{h}_s) \rangle, \quad (11)$$

and v is the magnitude of the vector \mathbf{v} [Eq. (3)]. Thus the weighting function $|\chi^*|^2$ is less than unity. It approaches unity for $\langle h_s^2 \rangle \rightarrow 0$. For Gaussian rough surfaces h_s ,

$$|\chi^*|^2 = \exp[-4k_0^2 \langle h_s^2 \rangle \cos^2(\theta_0/2)] = \exp(-v^2 \langle h_s^2 \rangle) \quad (12)$$

Since in this work the unperturbed surface is assumed to be the surface of a large conducting sphere ($d \gg \lambda_0$), the cross section $\langle \sigma_s^{PQ} \rangle$ is given by the physical optics expression¹

$$\langle \sigma_s^{PQ} \rangle = \delta_{PQ} |R_P|^2, \quad (13)$$

in which R_P is the Fresnel reflection coefficient for vertically ($P = V$) or horizontally ($P = H$) polarized waves, and δ_{PQ} is the Kronecker delta. For Gaussian

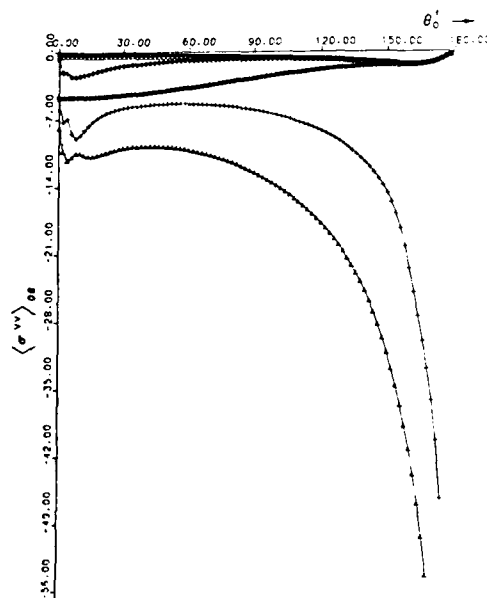


Fig. 2. Vertically polarized scattering cross section: $\beta = 1.0$, \circ , total cross section $\langle \sigma^{VV} \rangle$; \circ , $\langle \sigma_s^{VV} \rangle = |R_V|^2$; \times , $\langle \sigma^{VV} \rangle_l = |R_V \chi^*|^2$; $+$, $\langle \sigma^{VV} \rangle_{s1}$; Δ , $\langle \sigma^{VV} \rangle_{s2}$.

AD-A171 218

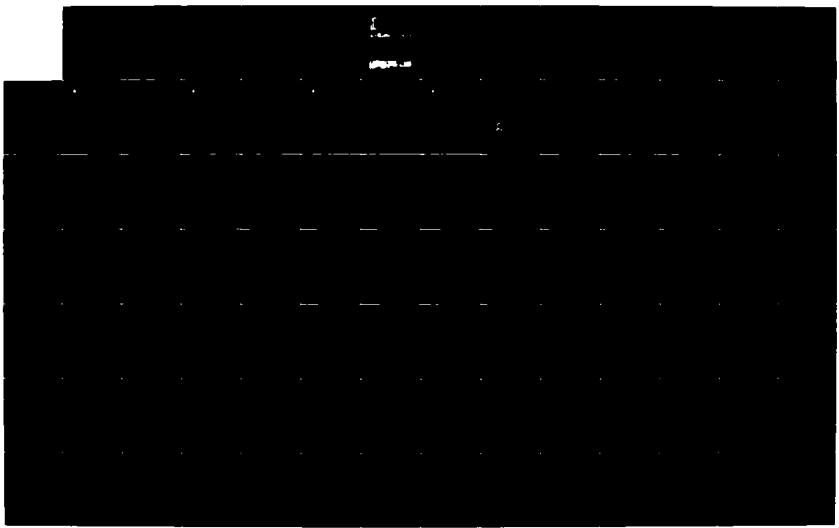
DEPOLARIZATION AND SCATTERING OF ELECTROMAGNETIC WAVES
APPENDICES (U) NEBRASKA UNIV LINCOLN 1 BANAR 30 JUN 86
ARO-18120.17-EL-APP DAAG29-82-K-0123

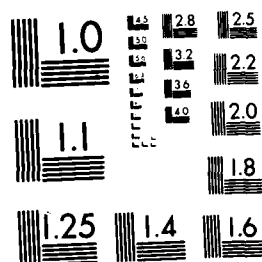
2/3

UNCLASSIFIED

F/G 28/14

NL





MICROCOPY RESOLUTION TEST CHART
NATIONAL BUREAU OF STANDARDS-1963-A

rough surfaces h , the term $(\sigma^{PQ})_s$ can be expressed as

$$(\sigma^{PQ})_s = \sum_{m=1}^{\infty} (\sigma^{PQ})_{sm}, \quad (14)$$

where

$$(\sigma^{PQ})_{sm} = 4\pi k_0^2 \int \frac{|D^{PQ}|^2 P_2(A', A'') |A|}{A \cdot d_y} \cdot \exp(-v_y^2 (h_z^2)) \left(\frac{v_x}{2} \right)^{2m} \frac{W_m(v_x, v_z)}{m!} p(h_x, h_z) dh_x dh_z. \quad (15)$$

In Eq. (15) v_x, v_y , and v_z are the components \mathbf{v} [Eq. (3)] in the local coordinate system [Eq. (6)]

$$\mathbf{v} = v_x \hat{A}_1 + v_y \hat{A}_2 + v_z \hat{A}_3. \quad (16)$$

The shadow function $P_2(\hat{A}', \hat{A}'') |A|$ is the probability that a point on the rough surface is both illuminated by the source and visible to the observer given the slopes $\hat{A}(h_x, h_z)$ at the point.^{11,12} The function $p(\hat{A}) = p(h_x, h_z)$ is the 2-D probability density of the slopes h_x and h_z . The expression D^{PQ} depends on the polarization of the incident and scattered waves, the unit vectors \hat{A}', \hat{A} , and \hat{n} and the relative complex permittivity ϵ_r of the conducting sphere. The function $W_m(v_x, v_z)$, 2^{2m} is the 2-D Fourier transform of $\langle h_x h_z \rangle^m$. It can be expressed as follows:

$$\begin{aligned} \frac{W_m(v_x, v_z)}{2^{2m}} &= \frac{1}{(2\pi)^2} \int \langle h_x h_z \rangle^m \exp(i v_x x_d + i v_z z_d) dx_d dz_d \\ &= \frac{1}{2^{2m}} \int W_{m-1}(x'_x, v'_z) W_1(v_x - v'_x, v_z - v'_z) dv'_x dv'_z \\ &= \frac{1}{2^{2m}} W_{m-1}(v_x, v_z) \otimes W_1(v_x, v_z). \end{aligned} \quad (17)$$

In Eq. (17) \otimes denotes the 2-D convolution of W_{m-1} with W_1 .

It should be noted that for $\beta \rightarrow 0$ the scattering cross section [Eq. (9)] reduces to the scattering cross sections for large conducting spheres, for $\beta \ll 1$, it reduces to the perturbation solution,⁷ since in this case $|\chi'| \approx 1$, and Eq. (14) reduces to the leading term $m = 1$ (Bragg scatter). In a recent analysis of wave scattering from a large sphere with rough surface (using a reformulated current method) Abdelazeez³ obtained a solution which corresponds to the first term in Eq. (9). Barrick,¹ who considered backscatter by spheres with small scale roughness, presents a solution that accounts for $(\sigma^{PQ})_1$ and the first term in Eq. (14). The weighting function $|\chi'|^2$ that multiplies (σ^{PQ}) accounts for the degradation of the specular point scattering cross section due to the superimposed rough surface h_s . The second term in Eq. (9), $(\sigma^{PQ})_s$, accounts for diffuse scattering due to the rough surface h_s . The leading term in $(\sigma^{PQ})_s$ ($m = 1$) corresponds to Bragg scatter.^{1,6,4,8} In the next section illustrative examples of spheres with very rough surfaces are considered. The significance of the different terms of the solution (9) are considered in detail, and the results are compared to earlier solutions. On replacing (σ^{PQ}) [Eq. (15)] by the expression for large scatterers of arbitrary shape (such as ellipsoids) one can obtain the effects of surface roughness on large scatterers of any desired shape.

III. Illustrative Examples

Assuming a homogeneous isotropic random rough surface h_s , the surface height spectral density function (2) (Ref. 4) considered for the illustrative examples is

$$W(v_x, v_z) = W(k) = \begin{cases} \frac{2}{\pi} B/k^4 & k_d < k < k_c, \\ 0 & k > k_c \text{ and } k < k_d, \end{cases} \quad (18)$$

in which

$$k^2 = v_x^2 + v_z^2 \text{ (cm)}^{-2}. \quad (19)$$

The smallest wave number characterizing the rough surface h_s is

$$k_d = (2\pi)/d, \quad (20)$$

where $d = 20\lambda_0$ is the diameter of the sphere, and λ_0 is the wavelength of the electromagnetic wave:

$$\lambda_0 = 0.555 \times 10^{-4} \text{ cm} \left\{ k_0 = \frac{2\pi}{\lambda_0} = 1.132 \times 10^5 \text{ cm}^{-1} \right\}. \quad (21)$$

The spectral cutoff number is⁶

$$k_c = 4.5 \times 10^5 \text{ cm}^{-1}. \quad (22)$$

The mean square height of the rough surface h_s is

$$\langle h_s^2 \rangle = \int_0^{2\pi} \int_{k_d}^{k_c} \frac{W(k)}{4} k dk d\phi = \frac{B}{2} \left(\frac{1}{k_d^2} - \frac{1}{k_c^2} \right). \quad (23)$$

Thus the value of B [Eq. (18)] in terms of the parameter $\beta = 4k_0^2 \langle h_s^2 \rangle$ is

$$B = \frac{\beta k_0^2 k_c^2}{2k_0^2(k_c^2 - k_d^2)}. \quad (24)$$

For $\beta = 2.0$ (case a), $\beta = 1.0$ (case b), $\beta = 0.5$ (case c), and $\beta = 0.1$ (case d) the corresponding values of the mean square height are

$$\langle h_s^2 \rangle = \begin{cases} 0.390 \times 10^{-10} \text{ cm}^2, \beta = 2.0, \\ 0.195 \times 10^{-10} \text{ cm}^2, \beta = 1.0, \\ 0.975 \times 10^{-11} \text{ cm}^2, \beta = 0.5, \\ 0.195 \times 10^{-11} \text{ cm}^2, \beta = 0.1. \end{cases} \quad (25)$$

Thus

$$B = \begin{cases} 0.250 \times 10^{-2}, \beta = 2.0, \\ 0.125 \times 10^{-2}, \beta = 1.0, \\ 0.625 \times 10^{-3}, \beta = 0.5, \\ 0.125 \times 10^{-3}, \beta = 0.1. \end{cases} \quad (26)$$

For $\lambda_0 = 0.555 \times 10^{-4} \text{ cm}$ the relative dielectric coefficient of aluminum is¹³

$$\epsilon_r = -40 - i12. \quad (27)$$

The permeability of the sphere is assumed to be that of free space $\mu_0 = 1$. For all the cases considered here, the mean square slope of the rough surface h_s (with respect to the surface of the unperturbed sphere) is <0.02 . The projection (in the $\hat{A}_{x0}, \hat{A}_{z0}$ plane) of an elementary area of the sphere oriented in the direction \hat{n} is $h_0^2 \cos \gamma \sin \gamma d\gamma d\delta$, where γ and δ are the latitudinal and azimuthal angles in the spherical coordinate system. Therefore in Eq. (15)

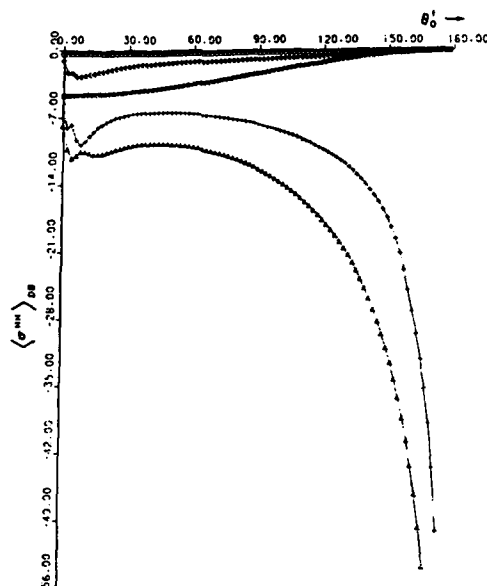


Fig. 3. Horizontally polarized cross section $\beta = 1.0$, ϕ , total cross section $\langle \sigma^{HH} \rangle$; O, $\langle \sigma^{HH} \rangle_l = |R_H|^2$; X, $\langle \sigma^{HH} \rangle_l = |R_H|^2$; +, $\langle \sigma^{HH} \rangle_{s1}$; Δ, $\langle \sigma^{HH} \rangle_{s2}$.

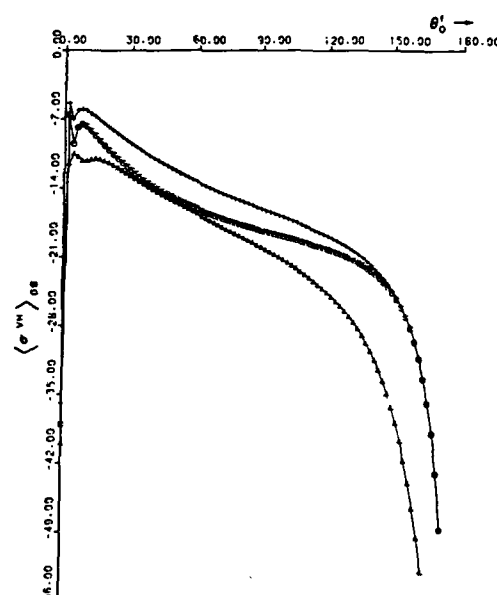


Fig. 4. Cross-polarized cross section, $\beta = 1.0$, ϕ , total cross section $\langle \sigma^{VH} \rangle = \langle \sigma^{HV} \rangle$; O, $\langle \sigma^{VH} \rangle_l = \langle \sigma^{HV} \rangle_l$; X, $\langle \sigma^{VH} \rangle_l = \langle \sigma^{HV} \rangle_l$; +, $\langle \sigma^{VH} \rangle_{s1}$; Δ, $\langle \sigma^{VH} \rangle_{s2}$.

$$p(h_x, h_z) dh_x dh_z \rightarrow p(\gamma, \delta) d\gamma d\delta = \frac{\sin \gamma \cos \gamma d\gamma d\delta}{\pi}, \quad (28)$$

$$0 < \delta < \frac{\pi}{2}, \quad 0 < \gamma < 2\pi.$$

In Fig. 2 the vertically polarized scattering cross section $\langle \sigma^{VV} \rangle$ [Eq. (9)] is plotted as a function of the scatter angle θ_0' (see Fig. 1). The parameter $\beta = 4k_0^2 \langle h_z^2 \rangle = 1.0$. In addition to the plot of $\langle \sigma^{VV} \rangle$ (Eq. (9)) (the total cross-section) plots are also given for the individual terms in Eq. (9): $\langle \sigma^{VV} \rangle_l = |R_V|^2$, $\langle \sigma^{VV} \rangle_{s1}$, and $\langle \sigma^{VV} \rangle_{s2}$. For $\beta = 1$, the terms $\langle \sigma^{VV} \rangle_{sm}$ for $m \geq 3$ are negligible. The value of $\langle \sigma^{VV} \rangle_l = |R_V|^2$ (corresponding to the physical optics cross section for the unperturbed sphere) is also given for the purpose of comparison. Note that the total scattering cross section $\langle \sigma^{VV} \rangle$ for the rough sphere is significantly smaller than that of the unperturbed sphere $\langle \sigma^{VV} \rangle_l$. Furthermore, for $\beta = 1.0$ the contribution of the term $\langle \sigma^{VV} \rangle_s$ [Eq. (9)] is not negligible, and $\langle \sigma^{VV} \rangle$ cannot be approximated by the first term $\langle \sigma^{VV} \rangle_l = |R_V|^2$, which corresponds to the solution based on Abdelazeez's reformulated current method.³ The corresponding results ($\beta = 1.0$) for the horizontally polarized scattering cross sections $\langle \sigma^{HH} \rangle$ are presented in Fig. 3. These results are similar to the results for the vertically polarized waves except near the quasi-Brewster angle.

The cross-polarized cross section $\langle \sigma^{VH} \rangle = \langle \sigma^{HV} \rangle$ is presented in Fig. 4 for $\beta = 1.0$. In view of Eq. (13) there

is no physical optics contribution to the cross-polarized cross section. Note also that for backscatter, $\theta_0' = 0$, $\langle \sigma^{VH} \rangle$ becomes vanishingly small. The like- and cross-polarized cross sections for $\beta = 2.0$ (case a), $\beta = 1.0$ (case b), $\beta = 0.5$ (case c), and $\beta = 0.1$ (case d) are presented in Figs. 5 and 6. Thus one finds that for $\beta < 0.1$, the terms $\langle \sigma \rangle_{sm}$ for $m \geq 2$ are negligible. Furthermore, since $e^{-\beta} \approx 0.9$ for $\beta = 0.1$, the perturbation solution¹ is approximately equal to the full wave solution. For small values of β the full wave solutions are also approximately equal to the solutions obtained using the reformulated current method³ since the second term in Eq. (9) $\langle \sigma^{VV} \rangle_s$ becomes very small compared with $\langle \sigma^{VV} \rangle_l$. However, Abdelazeez's solution for $\langle \sigma^{VH} \rangle = \langle \sigma^{HV} \rangle_s$ is zero. When the scale of the roughness is very small ($\beta < 0.1$), the scattering cross sections of rough spheres are not significantly different from that of unperturbed spheres. As β (the roughness of the surface) increases, the weighting function $|\chi^s|^2$ decreases, and the contribution of the term $\langle \sigma^{PQ} \rangle_s$ increases. Furthermore, an increasing number of terms $\langle \sigma^{PQ} \rangle_{sm}$ ($m = 1, 2, 3, \dots$) needs to be evaluated as β increases. (For $\beta = 2.0$, $m = 1, 2, 3$ is used). In Figs. 5(a)-(d) the differences between the full wave solution, Barrick's solution, and Abdelazeez's solution for $\langle \sigma^{VV} \rangle$ are shown to increase progressively as β increases from 0.1 to 2.0. In Figs. 6(a)-(d), the full wave solution and Barrick's solution for $\langle \sigma^{VH} \rangle$ are compared for β between 0.1 and 2.0.

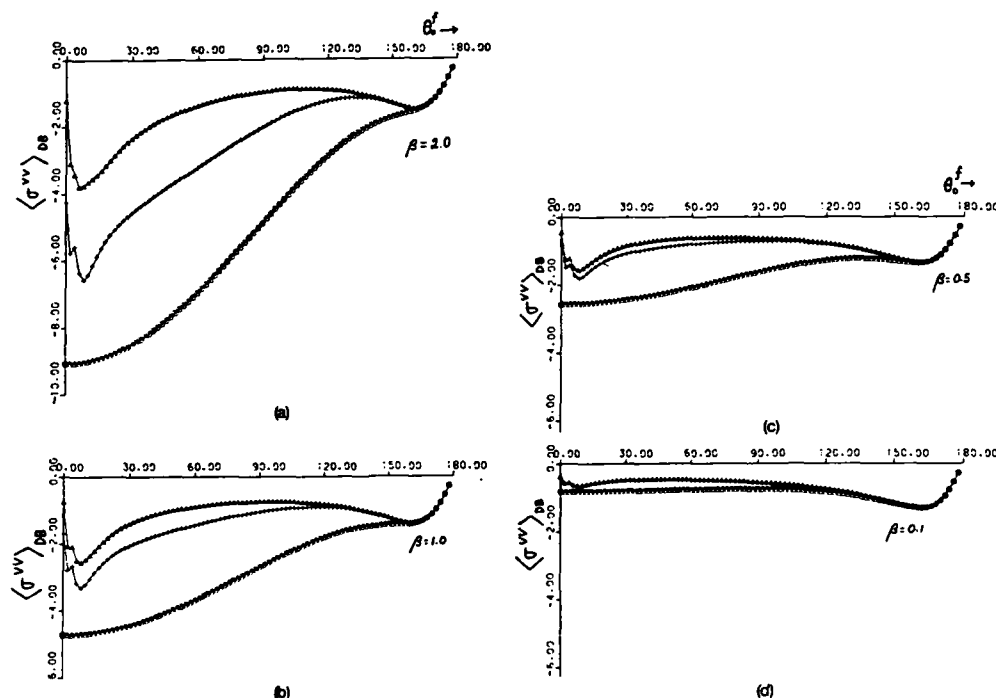


Fig. 5. Vertically polarized scattering cross section for (a) $\beta = 2.0$, (b) $\beta = 1.0$, (c) $\beta = 0.5$, (d) $\beta = 0.1$; Δ , $\langle \sigma^{VV} \rangle$ total cross-section, +, $\langle \sigma^{VV} \rangle_i + \langle \sigma^{VV} \rangle_{s1}$ (Barrick's solution), O, $\langle \sigma^{VV} \rangle_i = |R_V \chi^*|^2$ (Abdelazeez's solution).

IV. Concluding Remarks

The full wave approach has been used to determine the scattering cross sections for electrically large conducting spheres ($d \gg \lambda_0$) with rough surfaces. The total scattering cross sections are significantly modified by the rough surface when the parameter $\beta = 4k_0^2 \langle h^2 \rangle > 1$. In these cases the perturbation solutions are not valid. For $\beta \ll 1$ the full wave solutions reduce to the perturbation solution¹; however, for $\beta \ll 1$, the modification of the total scattering cross section is not very significant. The full wave solutions are compared with the perturbation solutions¹ and a recent solution based on the reformulated current method.³ The full wave solutions presented here can also be used to determine the effects of surface roughness on the scattering cross sections for large conductors of different shapes (such as ellipsoids or cylinders).

For the purpose of analysis, the surface roughness is characterized by its spectral density function W or by its autocorrelation function $\langle hh' \rangle$. A detailed study of the like- and cross-polarized scattering cross sections at different frequencies could shed light on the surface roughness of the conducting particles (the inverse scattering problem).

This investigation was sponsored by the U.S. Army Research Office contract DAAG-29-82-K-0123. The manuscript was typed by E. Everett.

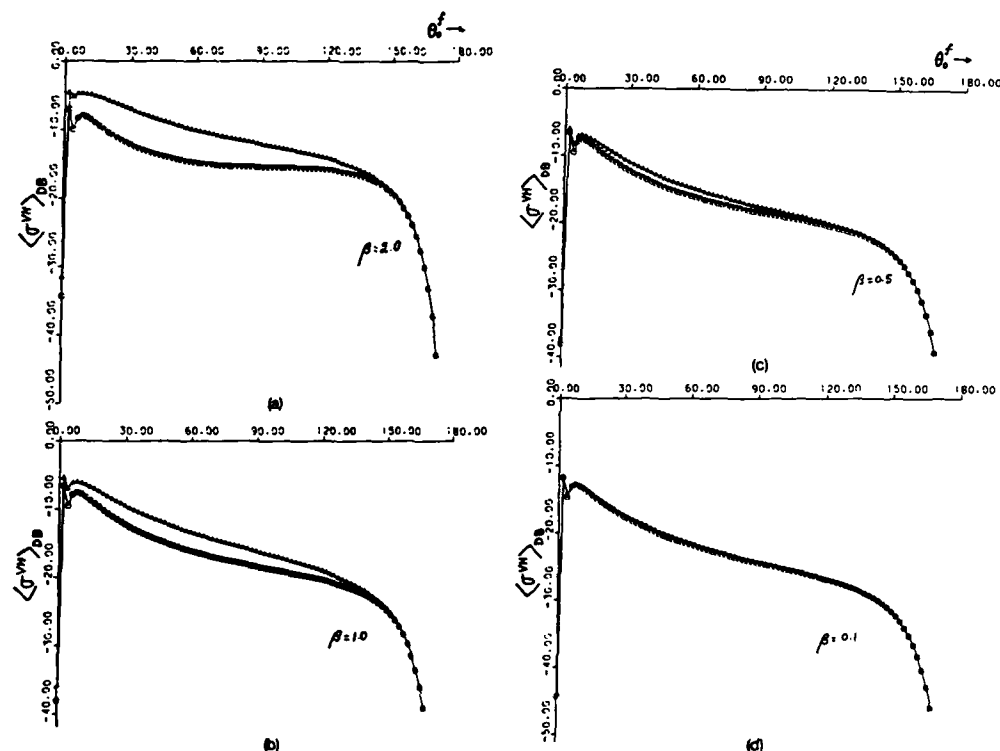
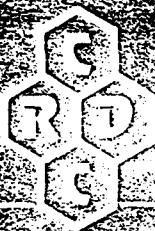


Fig. 6. Cross-polarized cross section for (a) $\beta = 2.0$, (b) $\beta = 1.0$, (c) $\beta = 0.5$, (d) $\beta = 0.1$; Δ , $\langle \sigma^{VH} \rangle_{\text{DB}} = \langle \sigma^{NV} \rangle_{\text{DB}}$, total cross-section, O, $\langle \sigma^{VH} \rangle_{\text{DB}} = \langle \sigma^{NV} \rangle_{\text{DB}}$ (Barrick's solution).

References

1. D. E. Barrick, *Rough Surfaces, in Radar Cross Section Handbook* (Plenum, New York, 1970), Chap. 9.
2. E. Bahar, and D. E. Barrick, "Scattering Cross Sections for Composite Surfaces that Cannot be Treated as Perturbed Physical Optics Problems," *Radio Sci.*, **18**, 129 (1983).
3. M. K. Abdelazeez, "Wave Scattering from a Large Sphere with Rough Surface," *IEEE Trans. Antennas Propag.* AP-31, 375 (1983).
4. S. O. Rice, "Reflection of Electromagnetic Waves from a Slightly Rough Surface," *Commun. Pure Applied Math.* **4**, 351 (1951).
5. A. Ishimaru, *Wave Propagation and Scattering in Random Media in Multiple Scattering, Turbulence, Rough Surfaces and Remote Sensing*, Vol. 2 (Academic, New York, 1978).
6. G. S. Brown, "Backscattering from Gaussian-Distributed Perfectly Conducting Rough Surfaces," *IEEE Trans. Antennas Propag.* AP-26, 472 (1978).
7. M. L. Burrows, "On the Composite Model for Rough Surface Scattering," *IEEE Trans. Antennas Propag.* AP-21, (1967).
8. G. R. Valenzuela, "Scattering of Electromagnetic Waves from a Tilted Slightly Rough Surface," *Radio Sci.*, **3**, 1051 (1968).
9. E. Bahar, "Scattering Cross Sections for Composite Random Surfaces—Full Wave Analysis," *Radio Sci.* **16**, 1327 (1981).
10. E. Bahar, "Scattering Cross Sections for Composite Surfaces with Large Mean Square Slopes—Full Wave Solution," *Int. J. Remote Sensing* **3**, 327 (1982).
11. M. K. Sancer, "Shadow-Corrected Electromagnetic Scattering from a Randomly Rough Surface," *IEEE Trans. Antennas Propag.* AP-17, 577 (1969).
12. B. G. Smith, "Geometrical Shadowing of a Randomly Rough Surface," *IEEE Trans. Antennas Propag.* AP-15, 668 (1967).
13. H. Ehrenreich, "The Optical Properties of Metals," *IEEE Spectrum* **2**, 162 (1965).



CHEMICAL
RESEARCH &
DEVELOPMENT
CENTER

CRDC-SP-85007

**PROCEEDINGS OF THE
CHEMICAL RESEARCH AND DEVELOPMENT
CENTER'S 1984 SCIENTIFIC CONFERENCE
ON OBSCURATION AND AEROSOL
RESEARCH**

Edited by Ronald H. Kohl
Deborah Stroud

RONALD H. KOHL & ASSOCIATES
Tullahoma, Tennessee 37388

June 1985

Approved for Release by the Chemical Command
Gordon, Maryland 21010-5425

SCATTERING AND DEPOLARIZATION BY CONDUCTING CYLINDERS
WITH VERY ROUGH SURFACES

113

Ezekiel Bahar
and
Mary Ann Fitzwater
Electrical Engineering Department
University of Nebraska—Lincoln
Lincoln, NE 68588-0511

ABSTRACT

Like- and cross-polarized scattering cross sections are determined at optical frequencies for conducting cylinders with very rough surfaces. Both normal and oblique incidence with respect to the cylinder axis are considered. The full-wave approach is used to account for both the specular point scattering and the diffuse scattering. For the roughness scales considered, the scattering cross sections differ significantly from those derived for smooth conducting cylinders. Several illustrative examples are presented.

1. Introduction

The problem of electromagnetic scattering by finitely conducting circular cylinders or spheres has been dealt with extensively in the technical literature. Perturbation theory has been used to extend these results to scattering by slightly rough circular cylinders or spheres (Barrick 1970). However, perturbation theory is limited to surfaces for which the roughness parameter $\beta = 4k_0^2 \langle h_s^2 \rangle < 0.1$ (k_0 is the electromagnetic wavenumber and $\langle h_s^2 \rangle$ is the mean square height of the rough surface, Brown 1978). For $\beta < 0.1$ the scattering cross sections are not significantly different from those for smooth conducting circular cylinders.

In this work the full-wave approach is used to determine the like- and cross-polarized scattering cross sections at optical frequency for finitely conducting cylinders with roughness scales that significantly modify the scattering cross sections. The radii of curvature of the unperturbed cylinders considered are large compared to wavelength λ . (However, the cross section of the unperturbed cylinder need not be circular). Both specular point scattering and diffuse scattering are accounted for in the analysis in a self consistent manner and the cross sections are expressed as a weighted sum of two cross sections.

In Section 2 the special forms of full-wave solutions are presented for long cylinders with mean circular cross sections and both the specular point and diffuse contributions are identified. In Section 3 several illustrative examples are considered for cylinders with roughness parameter $\beta = 1$. The rough surface is characterized by its surface-height spectral-density function. The results are compared with solutions based on the perturbation approach.

2. Formulation of the Problem

The scattered radiation fields for two dimensionally rough surfaces can be expressed in matrix form as follows (Bahar 1981)

$$\begin{pmatrix} G^{Vf} \\ G^{Hf} \end{pmatrix} = G_o \begin{pmatrix} D^{VV} & D^{VH} \\ D^{HV} & D^{HH} \end{pmatrix} \begin{pmatrix} G^{Vi} \\ G^{Hi} \end{pmatrix} \exp[i\vec{v} \cdot \vec{r}_s] dS \quad (2.1)$$

in which G^{Vf} and G^{Hf} are the vertically and horizontally polarized (electric or magnetic) fields scattered at a distance r in the direction of the unit vector \vec{n}^f . Similarly G^{Vi} and G^{Hi} are the vertically and horizontally polarized fields incident (at the origin) in the direction of the unit vector \vec{n}^i . The scattering matrix D is given by

$$D = C_o^{in} T^f F T^i \quad (2.2)$$

in which the transformation matrices T^f and T^i relate the scattered and incident waves in the local planes of scatter and incidence to reference planes of scatter and incidence while F is the scattering matrix defined in the local planes of incidence and scatter. The coefficient C_o is

$$C_o = -ik \exp(-ikr)/2\pi r \quad (2.3)$$

the vector \vec{v} is

$$\vec{v} = k_o (\vec{n}^f - \vec{n}^i) = v_x \vec{a}_x + v_y \vec{a}_y + v_z \vec{a}_z \quad (2.4)$$

and

$$C_o^{in} = -\vec{n}^i \cdot \vec{n} \quad (2.5)$$

where \vec{n} is the unit vector normal to the rough surface S . The position vector to a point on the rough surface is \vec{r}_s and for a reference cross sectional area in the x, z plane

$$dS = dx dz / (\vec{n} \cdot \vec{a}_y) \quad (2.6)$$

The expression (2.1) is invariant to coordinate transformations. For very (infinitely) long cylinders the surface integral (2.1) can be reduced to a line integral by noting that

$$\int_{-\infty}^{\infty} \exp(i v_z z) dz = 2\pi \delta(v_z) \quad (2.7)$$

On evaluating the expressions for the radiation (far) fields from the expressions for their transforms (using the steepest descent method, Bahar and Rajan (1979) it can be shown that

$$G^f = G_o^i \int D G^i \exp[i\vec{v} \cdot (x \vec{a}_x + y \vec{a}_y)] dx / (\vec{n} \cdot \vec{a}_y) \quad (2.8)$$

in which

$$G_o^i = - \left[\frac{k_o}{2\pi \rho \cos \theta_o^i} \right]^{1/2} \exp(i\pi/4) \exp \left[-ik_o (\rho \cos \theta_o^i + z \sin \theta_o^i) \right] \quad (2.9)$$

and for oblique incidence (with respect to the z axis) the direction of the incident plane wave is

$$\vec{n}^i = -\cos \theta_o^i \vec{a}_y + \sin \theta_o^i \vec{a}_z \quad (2.10)$$

The direction of the scattered wave is (Bahar 1981)

115

$$\bar{n}^f = \sin\theta_0^f \cos\phi^f \bar{a}_x + \cos\theta_0^f \bar{a}_y + \sin\theta_0^f \sin\phi^f \bar{a}_z \quad (2.11)$$

(where the polar angle is measured with respect to the y axis, see Figs. 1 and 2). In view of (2.7)

$$\sin\theta_0^f \sin\phi^f = \sin\theta_0^i \quad (2.12)$$

Thus (2.11) can also be expressed as

$$\bar{n}^f = \cos\theta_0^i (\sin\phi^i \bar{a}_x + \cos\phi^i \bar{a}_y) + \sin\theta_0^i \bar{a}_z \quad (2.13)$$

where the azimuth angle ϕ^i is measured in the xy plane with $\phi^i = 0$ on the y axis (see Figs. 1 and 2).

The explicit expression for the scattering coefficients D (2.2) have been presented earlier when the

reference incident plane is normal to $\bar{n}^i \times \bar{a}_y$ and the reference scatter plane is normal to $\bar{n}^f \times \bar{a}_y$.

However, if the plane of incidence (and scatter) is taken to be the plane normal to \bar{n}^i and \bar{n}_s (the normal to the cylinder at the specular point) (Barrick 1970), in these expressions for T^f and T^i the unit vector \bar{u}_y must be replaced by the unit vector

$$\begin{aligned} \bar{n}_s &= \bar{v}/v = \sin(\phi^i/2) \bar{a}_x + \cos(\phi^i/2) \bar{a}_y = \bar{a}_x \\ &= \frac{\sin\theta_0^f \cos\phi^f \bar{a}_x + (\cos\theta_0^f + \cos\theta_0^i) \bar{a}_y}{[2 \cos\theta_0^i (\cos\theta_0^i + \cos\theta_0^f)]^{1/2}} \end{aligned} \quad (2.14)$$

The normalized scattering cross sections (or scattering width) are for P, Q = V, H

$$\begin{aligned} \langle \sigma^{PQ} \rangle &= \frac{\langle |G^{Pf}|^2 \rangle}{|G^{Qi}|^2} \frac{2\pi p}{ka} \\ &= \langle \chi_2 \frac{k_0}{na \cos\theta_0^i} \int \frac{D^{PQ} D^{PQ*} \exp[iv_x(x-x') + iv_y(y-y')]}{(\bar{n} \cdot \bar{a}_y)(\bar{n}^i \cdot \bar{a}_y)} dx dx' \rangle \end{aligned} \quad (2.15)$$

where the radius vector to the surface of the cylinder is

$$\bar{r}_s = (a+h_s) \bar{a}_r = (a+h_s) \frac{(x \bar{a}_x + y \bar{a}_y)}{a} \quad (2.16)$$

and $a = (x^2 + y^2)^{1/2}$ is the radius of the unperturbed cylinder. The characteristic function χ and the joint characteristic function χ_2 for the random rough-surface height h_s are

$$\chi = \langle \exp(iv h_s) \rangle \quad (2.17)$$

where

$$v = 2k_0 \cos(\phi^i/2) \quad (2.18)$$

and

$$\chi_2 = \langle \exp[iv(h_s - h_s')] \rangle \quad (2.19)$$

For Gaussian distributions

$$|\chi|^2 = \exp[-\beta \cos^2(\phi^i/2)] \quad (2.20)$$

and

$$\chi_2 = |\chi|^2 \exp(v^2 \langle h_s h_s' \rangle) \quad (2.21)$$

where

$$\beta = 4k_o^2 \langle h_s^2 \rangle \quad (2.22)$$

and the surface-height autocorrelation function $\langle hh' \rangle$ is the Fourier transform of the surface height spectral density function W

$$\frac{W(k)}{4} = \frac{1}{2\pi} \int_{-\infty}^{\infty} \langle h_s h'_s \rangle \exp(ik\tau) d\tau. \quad (2.23)$$

In (2.23) $\langle h_s h'_s \rangle$ is assumed to be a function of the distance measured along the cylinder's circumference.

The normalized scattering cross section (2.15) is expressed as a weighted sum of two cross sections

(Bahar 1981, Bahar and Barrick 1982)

$$\langle \sigma^{PQ} \rangle = |\chi|^2 \langle \sigma_{\infty}^{PQ} \rangle + \langle \sigma^{PQ} \rangle_R. \quad (2.24)$$

The first term in (2.24) is the physical optics contribution $\langle \sigma_{\infty}^{PQ} \rangle$ modified by the coefficient $|\chi|^2$.

It can be shown (using the steepest descent method) that for a conducting circular cylinder

$$\langle \sigma_{\infty}^{PQ} \rangle = \frac{k_o}{\pi a \cos \theta_o^i} \left| \int_{-a}^a \frac{D^{PQ}}{(\bar{n} \cdot \bar{a}_y)} \exp(i v_x x + i v_y y) dx \right|^2 = \frac{\cos(\phi'/2)}{\cos^2 \theta_o^i} \left| \frac{D^{PQ}}{\bar{n} \cdot \bar{a}_y} \right|_{\bar{n}=\bar{n}_s}^2. \quad (2.25)$$

When the plane of incidence is taken to the normal to $\bar{n}^i \times \bar{n}_s$,

$$\langle \sigma_{\infty}^{PQ} \rangle = \cos(\phi'/2) |R_P|^2 \delta_{PQ} \quad (2.26)$$

in which R_P is the Fresnel reflection coefficient and δ_{PQ} is the Kronicker delta.

Due to the surface roughness the contribution due to specular scattering is decreased by the factor $|\chi|^2$ (2.20). The surface roughness also gives rise to the diffuse scattering term

$$\langle \sigma^{PQ} \rangle_R = \sum_{m=1}^{\infty} \langle \sigma^{PQ} \rangle_{Rm}$$

$$= \sum_{m=1}^{\infty} \frac{2k_o}{\cos \theta_o^i} \int_{-\pi/2}^{\pi/2} \left| D^{PQ} \right|^2 P_2(\bar{n}^f, \bar{n}^i | \bar{n}) \cdot \exp(-v_n^2 \langle h_s^2 \rangle \left(\frac{v_n}{2}\right)^{2m} \frac{W_m(v_T)}{m!} dy \quad (2.27)$$

where

$$\frac{W_m(v_T)}{2^{2m}} = \frac{1}{2\pi} \int_{-\infty}^{\infty} \langle h h' \rangle^m \exp(ik\tau) d\tau \quad (2.28)$$

in which v_n and v_T are the components of \bar{v} (2.7) normal and tangential to the surface of the unperturbed circular cylinder and $P_2(\bar{n}^f, \bar{n}^i | \bar{n})$ is the shadow function (Bahar and Barrick 1982).

3. Illustrative Examples

Assuming that the random rough (homogeneous and isotropic) surface height autocorrelation function $\langle hh' \rangle$ is a function of distance measured around the circumference of the unperturbed cylinder, we consider in the following examples the surface-height spectral density function $W(k)$ (2.23) given by (Rice 1951)

$$W(k) = \frac{2B(k-k_d)^4}{\pi[(k-k_d)^2 + \kappa^2]^4} \quad , \quad k_d < k < k_c \quad (3.1)$$

where

$$k_d = 2/a \quad k_c = 4 k_0 \quad (3.2)$$

and $W(k)$ peaks for $k - k_d = \kappa = 0.3k_d$. The electromagnetic wavelength is

$$\lambda_0 = 10 \mu m \quad (3.3)$$

and the corresponding relative (complex) dielectric coefficient for aluminum is

$$\epsilon_r = -6000(1 + i) \quad (3.4)$$

(where an $\exp(i\omega t)$ time dependence for the fields is assumed). The radius of the unperturbed cylinder is

$$a = 2.5 \lambda_0 \quad (3.5)$$

The shadow function is a product of the unit step functions u

$$P_2(\vec{n}^f, \vec{n}^i | \vec{n}) = u(\vec{n}^f \cdot \vec{n}) u(-\vec{n}^i \cdot \vec{n}) \quad (3.6)$$

The constant B in (3.1) is determined by the surface roughness parameter

$$\beta = 4k_0^2 \langle h_s^2 \rangle = 1 \quad .$$

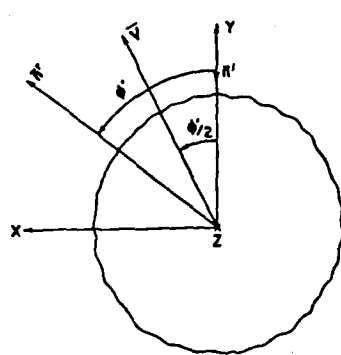
In Figures 3, 4 and 5 $\langle \sigma^{VV} \rangle$, $\langle \sigma^{HH} \rangle$ and $\langle \sigma^{HV} \rangle = \langle \sigma^{VH} \rangle$ are plotted for $\theta_0^i = 30^\circ$ as functions of ϕ' for cylinders with smooth (unperturbed) surfaces, (+) and random rough surfaces, (\square). The incident and scatter planes are normal to $-\vec{n}^i \cdot \vec{a}_y$ and $\vec{n}^f \cdot \vec{a}_y$ respectively. Note that for finitely conducting smooth cylinders $\langle \sigma^{VV} \rangle$ and $\langle \sigma^{HH} \rangle$ are very small for $\phi' = \pi/2$, and for $\phi' = 0$ these normalized cross sections are near unity. For the corresponding rough cylinder, the cross sections do not display the sharp minima and near normal incidence they are significantly less than unity. The cross-polarized cross sections $\langle \sigma^{VH} \rangle = \langle \sigma^{HV} \rangle$ are significantly different near normal incidence. For the smooth cylinder $\langle \sigma^{VH} \rangle$ vanishes for $\phi' = 0$, while it is about -5db for the rough cylinder. Thus as the surface roughness increases all three plots of the cross sections tend to flatten out (as functions of ϕ') except near grazing angles $\phi' \rightarrow \pi$ where the cross sections for the smooth and rough surfaces merge.

In conclusion, therefore, even a surface roughness corresponding to $\beta = 4k_0^2 \langle h_s^2 \rangle = 1$ cannot be ignored since it has the effect of making the scattered fields more isotropic and unpolarized. Using a perturbation approach to solve the problem one is restricted to values of $\beta < 0.1$ (Brown 1978). In this case the perturbation diffuse scattering term can be shown to correspond to the first term $\langle \sigma_{RI}^{PQ} \rangle$ in the expression for $\langle \sigma_{RI}^{PQ} \rangle$. In this case, however, the effects of surface roughness are practically insignificant.

This investigation was sponsored by the U. S. Army Research Office, Contract No. DAAG-29-82-K-0123.

References

1. Bahar, E. (1981), "Scattering Cross Sections for Composite Random Surfaces—Full Wave Analysis," Radio Science, 16 (6), pp. 1327-1335.
2. Bahar, E., D. E. Barrick (1982), "Scattering Cross Sections for Composite Surfaces that Cannot be Treated as Perturbed Physical Optics Problems," Radio Science, Vol. 18, No. 2, pp. 129-137.
3. Bahar, E., G. G. Rajan (1979), "Depolarization and Scattering of Electromagnetic Waves by Irregular Boundaries for Arbitrary Indicated and Scatter Angles Full Wave Solutions," IEEE Transactions on Antennas and Propagation, AP-27 (2), pp. 214-225.
4. Barrick, D. E. (1970), "Rough Surfaces in Radar Cross Section Handbook," Chapter 8, Plenum Press, New York.
5. Brown, G. S. (1978), "Backscattering From Gaussian-Distributed Perfectly Conducting Rough Surfaces," IEEE Transactions on Antennas and Propagation, AP-26 (3), pp. 472-482.
6. Rice, S. O. (1951), "Reflection of Electromagnetic Waves From a Slightly Rough Surface," Communication of Pure and Applied Math, Vol. 4, pp. 351-378.



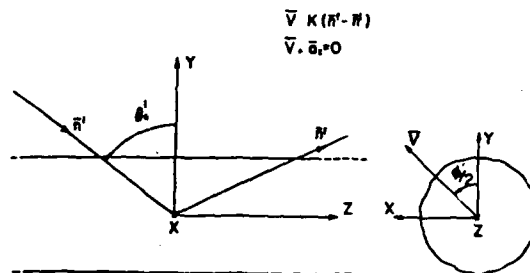
INCIDENT AND SCATTERED WAVES IN THE X-Y PLANE

Fig. 1

$$\theta_i = 0^\circ$$

$$\nabla = K(K' - K)$$

$$\nabla \cdot \vec{a}_s = 0$$



PLANE WAVE INCIDENT IN THE Y-Z PLANE

Fig. 2

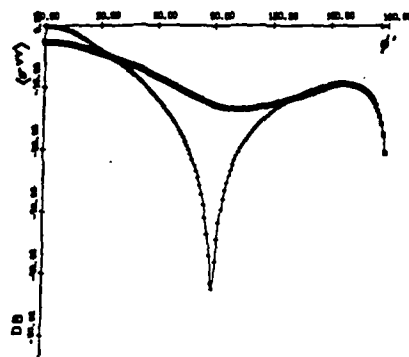


Fig. 3. $\langle \sigma^{VV} \rangle$, (2.24) smooth cylinder (+), rough cylinder (□)

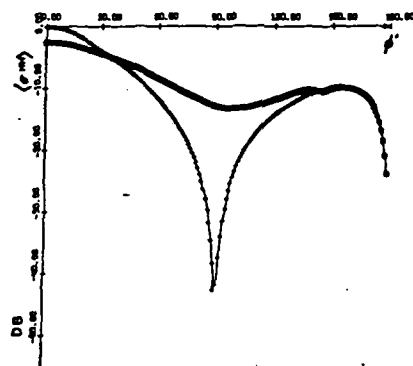


Fig. 4. $\langle \sigma^{HH} \rangle$, (2.24) smooth cylinder (+), rough cylinder (□)

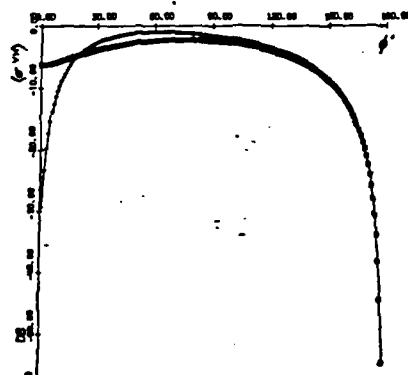


Fig. 5. $\langle \sigma^{VH} \rangle$, (2.24) smooth cylinder (+), rough cylinder (□)

Reprinted from *Journal of the Optical Society of America A*, Vol. 2, page 2295, December 1985
Copyright © 1985 by the Optical Society of America and reprinted by permission of the copyright owner.

Like- and cross-polarized scattering cross sections for random rough surfaces: theory and experiment

Ezekiel Bahar and Mary Ann Fitzwater

Electrical Engineering Department, University of Nebraska-Lincoln, Lincoln, Nebraska 68588-0511

Received April 16, 1985; accepted July 8, 1985

The unified full-wave solutions for the vertically and horizontally polarized scattered radiation fields and the like- and cross-polarized scattering cross sections for random rough surfaces are presented in this paper. They are compared with the corresponding physical-optics, geometric-optics, and perturbation solutions that are obtained on adopting a two-scale model of the composite rough surface. Computations based on the unified full-wave solution (which accounts for both specular point scattering and diffuse scattering in a self-consistent manner) as well as those based on the two-scale representation of the rough surface are provided for several illustrative examples. It is shown that the two solutions for the cross-polarized backscatter cross sections differ significantly for near-normal incidence. The solution based on the unified approach is consistent with experimental data.

1. INTRODUCTION

Solutions for the like- and cross-polarized scattered radiation fields are presented for rough surfaces using the full-wave approach.¹⁻³ The full-wave solutions account for specular point scattering and diffuse scattering in a self-consistent manner. Unified full-wave expressions for the like- and cross-polarized cross sections are also presented for random rough surfaces. In addition, on adopting a two-scale model of the rough surface, the cross sections are expressed as a weighted sum of two cross sections. The first accounts for specular point scattering from the large-scale filtered surface h_L , and the second accounts for diffuse scattering from the small-scale surface h_s that rides on the large-scale surface h_L . The solutions based on the two-scale model are shown to be consistent with the corresponding perturbation, physical-optics, and geometric-optics solutions.

In Section 4 several illustrative examples are presented that use both the unified full-wave expressions and those based on the two-scale model. The discrepancies between the two solutions for the like- and cross-polarized backscatter cross sections are examined in detail. In particular, near normal incidence ($\theta_0 = 15^\circ$) there is a difference of about 15 dB between the two computed values of the ratio of the like- to cross-polarized cross sections (σ^{HH}/σ^{VH}) (V and H correspond to vertical and horizontal, respectively). The unified full-wave solution for the ratio is consistent with experimental data.

2. FORMULATION OF THE PROBLEM

The full-wave solution for the radiation fields scattered by two-dimensionally rough surfaces $f(x, z) = y - h(x, z) = 0$ is expressed as follows in matrix notation (see Fig. 1):

$$G^i = G_0 \int_{A_w} D(A^i, \hat{r}) \exp[i\mathbf{v} \cdot \mathbf{r}] dA G^i = S G^i, \quad (2.1)$$

in which \hat{r} and A^i are unit vectors in the directions of the incident and scattered fields, and the vector \mathbf{v} is

$$\mathbf{v} = (\hat{r}^i - \hat{r}^s) \mathbf{k}_0 = v_x \hat{a}_x + v_y \hat{a}_y + v_z \hat{a}_z \equiv \mathbf{k}_0^i - \mathbf{k}_0^s, \quad (2.2)$$

where $\mathbf{k}_0 = \omega(\mu_0 \epsilon_0)^{1/2}$ is the free-space wave number of the electromagnetic wave. The integration is over A_w , the illuminated and visible portions of the rough surface, and

$$\int dA = \int_{-L_x}^{L_x} \int_{-L_y}^{L_y} dx dz / \hat{n} \cdot \hat{a}_y = A_y, \quad \int \cdot dA = \int_{A_w} \cdot dA, \quad (2.3)$$

where \hat{n} is the unit vector normal to the surface $f(x, z) = 0$,

$$\hat{n} = \nabla f / |\nabla f| = \frac{-h_x \hat{a}_x + \hat{a}_y - h_z \hat{a}_z}{(1 + h_x^2 + h_z^2)^{1/2}},$$

$$h_x = \frac{\partial h}{\partial x}, \quad h_z = \frac{\partial h}{\partial z}, \quad (2.4)$$

and \mathbf{r} is the position vector to a point on the rough surface. The elements of the 2×1 column matrix G^i are the incident vertically and horizontally polarized complex-wave amplitudes G^{Vi} and G^{Hi} at the origin with $\hat{r}^i \times \hat{a}_y$ defined as the vector normal to the plane of incidence. Similarly, G^s is a 2×1 column matrix whose elements are the vertically and horizontally polarized complex-wave amplitudes G^{Vs} and G^{Hs} (with $\hat{r}^s \times \hat{a}_y$ defined as the vector normal to the scatter plane) at the point given by the position vector

$$\mathbf{r}^s = x^s \hat{a}_x + y^s \hat{a}_y + z^s \hat{a}_z = \mathbf{r}^s \cdot \hat{r}^s. \quad (2.5)$$

Thus

$$G^i = \begin{pmatrix} G^{Vi} \\ G^{Hi} \end{pmatrix} = \begin{pmatrix} E^{Vi} \\ E^{Hi} \end{pmatrix} = \eta_0 \begin{pmatrix} H^{Vi} \\ H^{Hi} \end{pmatrix} \quad (2.6a)$$

and

$$G^s = \begin{pmatrix} G^{Vs} \\ G^{Hs} \end{pmatrix} = \begin{pmatrix} E^{Vs} \\ E^{Hs} \end{pmatrix} = \eta_0 \begin{pmatrix} H^{Vs} \\ H^{Hs} \end{pmatrix}, \quad (2.6b)$$

where $\eta_0 = (\mu_0/\epsilon_0)^{1/2}$ is the free-space wave impedance. The coefficient G_0 is given by

$$G_0 = k_0^2 \exp[-ik_0 r^i] / 2\pi i k_0 r^s, \quad (2.7)$$

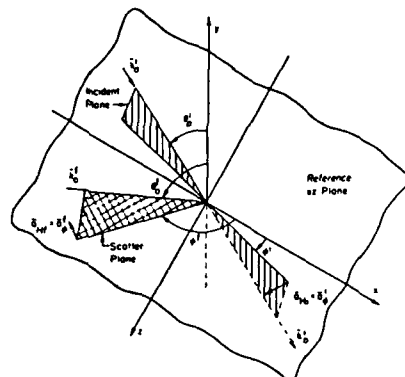


Fig. 1. Planes of incidence and scatter with respect to the reference-coordinate system. (Mean reference plane for rough surface is $y = 0$).

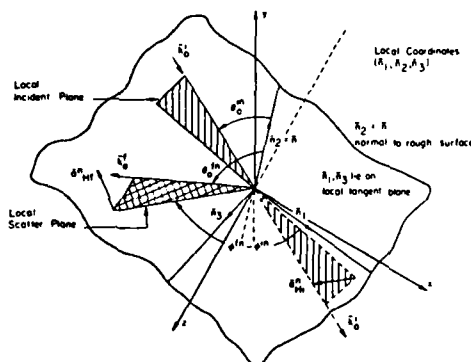


Fig. 2. Local planes of incidence and scatter and local-coordinate system $(\hat{a}_1, \hat{a}_2, \hat{a}_3)$.

and a suppressed $\exp(i\omega t)$ time dependence is assumed in this work.

The like- and cross-polarized local scattering matrix

$$D(\hat{n}', \hat{n}) = \begin{pmatrix} D^{VV} & D^{VH} \\ D^{HV} & D^{HH} \end{pmatrix} = (-\hat{n}' \cdot \hat{A}) T^i F T^i \quad (2.8)$$

is derived by (1) using the 2×2 matrix $T^i(\hat{n}', \hat{n})$ to transform the incident vertically and horizontally polarized wave from its representation in the fixed reference coordinate system $(\hat{a}_x, \hat{a}_y, \hat{a}_z)$ to its representation with respect to the local coordinate system $(\hat{a}_1, \hat{a}_2, \hat{a}_3)$ [the unit vector \hat{a}^{in} is the representation of the vector \hat{n} in the local coordinate system (see Fig. 2)], (2) using the 2×2 local scattering matrix $(-\hat{n}' \cdot \hat{A}) F(\hat{n}', \hat{n}) dA$ to account for like- and cross-polarized scattering by an element dA of the rough surface (\hat{A}^{in} is the representation of the vector \hat{n} in the local coordinate system), and finally, (3) using the 2×2 matrix $T^i(\hat{n}', \hat{n})$ to transform the scattered vertically and horizontally polarized wave from its representation in the local coordinate system to its representation in the reference coordinate system. The full-wave solutions [Eq. (2.1)] are invariant to

coordinate transformations, and they satisfy the duality and reciprocity relationships in electromagnetic theory. In Eq. (2.1) multiple scattering and the contributions from shadow regions of the rough surface are neglected. Explicit expressions for the local scattering matrix $D(\hat{n}', \hat{n})$ [Eq. (2.8)] are found in the published literature.¹

The full-wave solution for the scattered field can be applied to random rough surfaces.² Thus the scattering cross sections per unit projected area A_y for an incident wave with polarization $Q = V$ or H and a scattered wave with polarization $P = V$ or H are given by

$$\langle \sigma^{PQ} \rangle = \left\langle \frac{k_0^2}{\pi} \int \left| \frac{D^{PQ}}{\hat{n} \cdot \hat{a}_y} \right|^2 P_2(\hat{n}', \hat{n}) n \right. \\ \left. \times \exp[i\mathbf{v} \cdot (\mathbf{r} - \mathbf{r}')] \frac{d\mathbf{r} d\mathbf{r}' dz}{A_y} \right\rangle, \quad (2.9)$$

in which the symbol $\langle \cdot \rangle$ denotes the statistical average over the heights h, h' and the slopes \hat{n}, \hat{n}' . The probability-density functions for the random slopes \hat{n}, \hat{n}' and random heights h, h' are assumed to be independent. In addition, it is assumed that the slopes are more strongly correlated than the heights $[p(\hat{n}, \hat{n}') \rightarrow p(\hat{n})\delta(\hat{n}' - \hat{n})]$. In this paper the rough surface is assumed to be isotropic (independent of direction), and its characteristics are independent of position (\mathbf{r}). Thus the rough-surface height characteristic function

$$\chi(v, h) = \langle \exp(i\mathbf{v} \cdot \mathbf{h}) \rangle = \int \exp(i\mathbf{v} \cdot \mathbf{h}) p(h) dh \quad (2.10)$$

is independent of position, whereas the rough-surface-height joint characteristic function

$$\chi_2(v, h - v, h') = \langle \exp[i\mathbf{v} \cdot (\mathbf{h} - \mathbf{h}')] \rangle \\ = \int \exp[i\mathbf{v} \cdot (\mathbf{h} - \mathbf{h}')] p(h, h') dh dh' \quad (2.11)$$

is only a function of distance τ measured in the (x, z) reference plane

$$\mathbf{r}_d = (x - x')\hat{a}_x + (z - z')\hat{a}_z, \\ |\mathbf{r}_d| = \tau = [(x - x')^2 + (z - z')^2]^{1/2}. \quad (2.12)$$

In Eqs. (2.9) $P_2(\hat{n}', \hat{n})$ is the probability that a point on the rough surface is both illuminated (\hat{n}') and visible (\hat{n}), given the value of the slope (\hat{n}) at that point.⁴

Since the full-wave solution [Eq. (2.9)] accounts for both specular point (physical optics) scattering as well as diffuse scattering in a self-consistent manner, there is no need to adopt an artificial two-scale model. To use the two-scale model, it is assumed that the surface $h(x, z)$ consisting of the large-scale components of the surface-height spectral-density function $W(v_x, v_z)$ is independent of the surface $h_s(x, z)$ consisting of the small-scale components of the surface-height spectral-density function. The surface-height spectral-density function is the two-dimensional Fourier transform of the rough-surface-height autocorrelation function $\langle hh' \rangle$. Thus

$$\frac{W(v_x, v_z)}{4} = \frac{1}{4\pi^2} \int_{-\infty}^{\infty} \langle hh' \rangle \exp(i\mathbf{v} \cdot \mathbf{r}_d) d\mathbf{r}_d \\ = \frac{1}{2\pi} \int_0^{\infty} \langle hh' \rangle J_0(kr) r dr, \quad (2.13a)$$

where J_0 is the Bessel function of order zero and the spatial wave number k is

$$k = v_{xz} = (v_x^2 + v_z^2)^{1/2}, \quad (2.13b)$$

in which use has been made of the fact that $\langle hh' \rangle$ is only a function of τ . Similarly,

$$\begin{aligned} \langle hh' \rangle &= \int_{-\infty}^{\infty} \frac{W(v_x, v_z)}{4} \exp(-iv \cdot \mathbf{r}_d) dv_x dv_z \\ &= 2\pi \int_0^{\infty} \frac{W(k)}{4} J_0(k\tau) k dk = R(\tau) \langle h^2 \rangle, \end{aligned} \quad (2.14)$$

in which $|R(\tau)| \leq 1$ is the normalized correlation coefficient and $\langle h^2 \rangle$ is the mean-square height

$$\langle h^2 \rangle = \langle hh' \rangle_{\tau=0} = 2\pi \int_0^{\infty} \frac{W(k)}{4} k dk. \quad (2.15)$$

Thus, using the two-scale model, it is assumed that the large-scale surface h_l is associated with the surface-height spectral-density function $W(k)U(k_d - k)$ and the small-scale surface h_s is associated with the surface-height spectral-density function $W(k)U(k - k_d)$ in which $U(\cdot)$ is the unit step function and k_d is some arbitrary value of k where spectral splitting is assumed to occur.⁵ Brown chooses k_d such that the parameter

$$\beta = 4k_d^2 \langle h_s^2 \rangle = 0.1 \quad (2.16)$$

satisfies the perturbation condition for the small-scale surface. However, he shows that the computed value of the scattering cross sections critically depends on the choice of β and therefore on the specified value of k_d . Bahar and Barick⁶ considered the two-scale model using the full-wave approach. It is shown that if k_d is chosen such that deep phase modulation occurs, it is necessary to choose $\beta > 1$. For a range of values of k_d corresponding to β between 1 and 2 it is shown⁷ that the values of the scattering cross sections do not depend on k_d . For problems of scattering by random surfaces the dimensions of the projected area $A_y = 4L_x L_z$ are such that $L_x \gg \tau_c$ and $L_z \gg \tau_c$ [where $R(\tau_c) = \exp(-1)$ and τ_c is the correlation length]. For distances $\tau \gg \tau_c$, $x_2 \rightarrow |x|^2$, since $\langle hh' \rangle \rightarrow \langle h^2 \rangle$. Thus, assuming statistical independence between the surfaces h_l and h_s , $[p(h_l, h_s)] = p(h_l)p(h_s)$, the characteristic and the joint characteristic functions of the total surface are expressed as

$$\begin{aligned} x &= x^l x^s, & x^s &= x^s(\mathbf{v} \cdot \hat{\mathbf{n}}), & x^l &= x^l(v_z), \\ x_2^s &= x_2^s(\mathbf{v} \cdot \hat{\mathbf{n}}), & x_2^l &= x_2^l(v_z), \\ x_2 &= x_2^l x_2^s = (x_2^l - |x|^2) |x|^2 + (x_2^s - |x|^2) x_2^l + |x|^2 x^2, \end{aligned} \quad (2.17a)$$

$$(2.17b)$$

in which the superscripts l and s denote quantities associated with the large- and small-scale surfaces, respectively. Using the two-scale model, it is also assumed that the slopes for the small-scale (perturbation) surface are small such that the slope probability-density function for the total surface is equal to the slope probability function for the large-scale surface $p(\hat{\mathbf{n}}) \approx p(\hat{\mathbf{n}}_l)(\hat{\mathbf{n}}_l = \nabla f_l / |\nabla f|)$ and $f_l = y - h_l$. Thus the unified and two-scale expressions for the scattering cross sections [Eq. (2.9)] are, respectively,

$$\begin{aligned} \langle \sigma^{PQ} \rangle_U &= \int A^{PQ}(\hat{\mathbf{n}}^l, \hat{\mathbf{n}}^s, \hat{\mathbf{n}}) p(\hat{\mathbf{n}}) d\hat{\mathbf{n}} \left[Q(\hat{\mathbf{n}}^l, \hat{\mathbf{n}}^s) \right. \\ &\quad \left. + \frac{1}{A_y} |v_y x| \int \exp(i v_x x + i v_z z) dx dz \right] \end{aligned} \quad (2.18a)$$

where

$$Q(\hat{\mathbf{n}}^l, \hat{\mathbf{n}}^s) = v_y^2 \int (x_2^l - |x|^2) \exp(i \mathbf{v} \cdot \mathbf{r}_d) dx_d dz_d, \quad (2.18b)$$

$$A^{PQ}(\hat{\mathbf{n}}^l, \hat{\mathbf{n}}^s, \hat{\mathbf{n}}) = \frac{1}{\pi} \left| \frac{k_0 D^{PQ}}{v_y \hat{\mathbf{n}} \cdot \hat{\mathbf{a}}_y} \right|^2 P_2, \quad (2.18c)$$

$$p(\hat{\mathbf{n}}) d\hat{\mathbf{n}} = p(h_x, h_z) dh_x dh_z, \quad (2.18d)$$

and

$$\begin{aligned} \langle \sigma^{PQ} \rangle_T &= |x|^2 A^{PQ}(\hat{\mathbf{n}}^l, \hat{\mathbf{n}}^s, \hat{\mathbf{n}}) [Q(\hat{\mathbf{n}}^l, \hat{\mathbf{n}}^s) \\ &\quad + \frac{1}{A_y} |v_y x| \exp(i v_x x + i v_z z) dx dz]^2 \\ &\quad + \int A^{PQ}(\hat{\mathbf{n}}^l, \hat{\mathbf{n}}^s, \hat{\mathbf{n}}) \hat{\mathbf{n}} \cdot \hat{\mathbf{a}}_y Q_s(\hat{\mathbf{n}}^l, \hat{\mathbf{n}}^s, \hat{\mathbf{n}}) p(\hat{\mathbf{n}}) d\hat{\mathbf{n}} \\ &= |x|^2 \langle \sigma^{PQ} \rangle_l + \langle \sigma^{PQ} \rangle_s, \end{aligned} \quad (2.19a)$$

where

$$Q_l(\hat{\mathbf{n}}^l, \hat{\mathbf{n}}^s) = v_y^2 \int (x_2^l - |x|^2) \exp(i \mathbf{v} \cdot \mathbf{r}_d) dx_d dz_d, \quad (2.19b)$$

$$Q_s(\hat{\mathbf{n}}^l, \hat{\mathbf{n}}^s, \hat{\mathbf{n}}) = v_y^2 \int (x_2^s - |x|^2) \exp(i \mathbf{v} \cdot \mathbf{r}_{ld}) dx_{ld} dz_{ld}. \quad (2.19c)$$

In Eqs. (2.18b), (2.19b), and (2.19c) the integration limits are $(-\infty, \infty)$ since $L_x, L_z \gg \tau_c$ and $A^{PQ}(\hat{\mathbf{n}}^l, \hat{\mathbf{n}}^s, \hat{\mathbf{n}})$ is defined in Eq. (2.18c).

To derive the first term in Eq. (2.19a), the slope-dependent function $A^{PQ}(\hat{\mathbf{n}}^l, \hat{\mathbf{n}}^s, \hat{\mathbf{n}})$ is replaced by its value at the specular point where

$$\hat{\mathbf{n}} \rightarrow \hat{\mathbf{n}}_s = \mathbf{v}/v, \quad v = |\mathbf{v}| = \mathbf{v} \cdot \hat{\mathbf{n}}_s. \quad (2.20)$$

For surface-height probability-density functions that are Gaussian

$$|x|^2 = \exp(-v_y^2 \langle h^2 \rangle) \ll 1, \quad (2.21)$$

$$x_2^l = \exp(-v_y^2 \langle h_l^2 \rangle) + v_y^2 \langle h_l h_l' \rangle = \exp(v_y^2 \langle h_l h_l' \rangle) |x|^2. \quad (2.22)$$

Thus for $k_0^2 \langle h^2 \rangle \gg 1$ it can be shown that the two-dimensional Fourier transform [Eq. (2.19b)] is given by

$$Q_l(\hat{\mathbf{n}}^l, \hat{\mathbf{n}}^s) = 4\pi^2 p(\hat{\mathbf{n}}_s), \quad (2.23)$$

in which $p(\hat{\mathbf{n}}_s)$ is the slope probability-density function at the stationary phase points³

$$\begin{aligned} P(\hat{\mathbf{n}}_s) &= p(h_x, h_z) = \frac{1}{2\pi\sigma_n^2} \exp\left[-\frac{v_{xz}^2}{2\sigma_n^2 v_y^2}\right] \\ &= \frac{1}{2\pi\sigma_n^2} \exp\left[-\frac{(h_x^2 + h_z^2)}{2\sigma_n^2}\right]_{A_s}, \end{aligned} \quad (2.24)$$

in which the value of the slope at the specular point is

$$\begin{aligned} (h_x^2 + h_z^2)_{A_s} &= \tan^2 \gamma_s = v_{xz}^2 / v_y^2, \\ \hat{\mathbf{n}}_s \cdot \hat{\mathbf{a}}_y &= \cos \gamma_s, \end{aligned} \quad (2.25a)$$

and the mean-square slope σ_n^2 is

$$\sigma_n^2 = \frac{\pi}{2} \int_0^{\infty} W(k) k^3 dk. \quad (2.25b)$$

Thus the first term in Eq. (2.19a) is given by

$$|x|^2 \langle \sigma^{PQ} \rangle_l = |x|^2 A^{PQ}(\hat{n}', \hat{n}', \hat{n}_s) [4\pi^2 p(\hat{n}_s) + A_s |v_y x|^2 \text{sinc}^2(v_x L_x) \text{sinc}^2(v_z L_z)], \quad (2.26)$$

in which $\text{sinc}(\alpha) = \sin(\alpha)/\alpha$, and $A_s = 4L_x L_z$ is the projected area of the rough surface on the x, z plane. In Eq. (2.26) $\langle \sigma^{PQ} \rangle_l$ is precisely the physical-optics solution for scattering by the large scale (filtered surface). Thus the coefficient $|x|^2 < 1$ accounts for the degradation of the physical-optics (specular point) contribution that is due to the small-scale surface.

To derive the second term in Eqs. (2.19), it is assumed that over a correlation length of the small-scale surface, the large-scale surface is approximately flat and that the small-scale (perturbed) surface height is measured normal to the large-scale surface. Thus

$$\begin{aligned} \mathbf{v} \cdot (\mathbf{r} - \mathbf{r}') &= \mathbf{v} \cdot (\mathbf{r}_l - \mathbf{r}_l') + \mathbf{v} \cdot (\mathbf{h} - \mathbf{h}') \hat{\mathbf{a}}_y \\ &= \mathbf{v} \cdot \mathbf{r}_{ld} + \mathbf{v} \cdot \hat{\mathbf{h}}(\mathbf{h} - \mathbf{h}'), \end{aligned} \quad (2.27)$$

in which the distance \mathbf{r}_{ld} is measured along the large-scale surface in the local coordinate system $(\hat{\mathbf{h}}_1, \hat{\mathbf{h}}_2 = \hat{\mathbf{h}}, \hat{\mathbf{h}}_3)$:

$$\mathbf{r}_{ld} = x_{ld} \hat{\mathbf{h}}_1 + z_{ld} \hat{\mathbf{h}}_3, \quad |\mathbf{r}_{ld}| = r_l = (x_{ld}^2 + z_{ld}^2)^{1/2}. \quad (2.28)$$

Thus, in the expression for $\langle \sigma^{PQ} \rangle_s$, the integration is, with respect to distances, measured along the large-scale surface and not the reference surface. This is in agreement with the expressions obtained intuitively by Wright and Valenzuela^{8,9} "mostly based on physical considerations." Thus $\langle \sigma^{PQ} \rangle_s$ can be regarded as an average of the scattered power from patches of slightly rough surfaces that ride the large-scale surface. Brown's⁵ solutions, which are based on a combination of Burrows's perturbation theory¹⁰ and physical optics,¹¹ are in agreement with the full-wave expressions for $\langle \sigma^{PQ} \rangle_s$ only in the limit of small-scale slopes, since in his work \mathbf{h}_s is measured normal to the reference plane. However, in Burrows's perturbation theory the small-scale surface height \mathbf{h}_s is measured normal to the large-scale surface \mathbf{h}_l .

The two-dimensional Fourier transform [Eq. (2.18b)] can be expressed as

$$Q(\hat{n}', \hat{n}') = 2\pi v_y^2 \int_0^\infty (x_2(v_y) - |x(v_y)|^2) J_0(v_{zz} \tau) \tau d\tau, \quad (2.29)$$

since the surface-height correlation function $\langle \mathbf{h} \mathbf{h}' \rangle$ is only a function of $\tau = r_d = |\mathbf{r}_d|$. The corresponding expression for the Fourier transform [Eq. (2.19c)] is dependent on the slope. Thus

$$\begin{aligned} Q_s(\hat{n}', \hat{n}', \hat{n}) &= 2\pi v_y^2 \int_0^\infty (x_2^s(\mathbf{v} \cdot \hat{\mathbf{h}}) - |x^s(\mathbf{v} \cdot \hat{\mathbf{h}})|^2) J_0(v_{zz} \tau) \tau d\tau, \\ &= [x^s(\mathbf{v} \cdot \hat{\mathbf{h}})]^2 J_0(v_{zz} \tau) \tau d\tau, \end{aligned} \quad (2.30)$$

in which

$$\mathbf{v} \cdot \mathbf{r}_{ld} = \mathbf{v} \cdot (x_{ld} \hat{\mathbf{h}}_1 + z_{ld} \hat{\mathbf{h}}_3) = v_{xld} x_{ld} + v_{zld} z_{ld}, \quad (2.31a)$$

$$\mathbf{v} \cdot \hat{\mathbf{h}} = v_{xld} v_{xld} + v_{zld} v_{zld} = [v_{xld}^2 + v_{zld}^2]^{1/2}, \quad (2.31b)$$

and v_{xld} , v_{yld} , and v_{zld} are the components of \mathbf{v} in the local coordinate system $(\hat{\mathbf{h}}_1, \hat{\mathbf{h}}_2 = \hat{\mathbf{h}}, \hat{\mathbf{h}}_3)$. Thus the scattering cross sections can be expressed as follows for the unified and two-scale models:

$$\begin{aligned} \langle \sigma^{PQ} \rangle_l &= \int A^{PQ}(\hat{n}', \hat{n}', \hat{n}) p(\hat{n}) d\hat{n} [Q(\hat{n}', \hat{n}') \\ &+ A_s |v_y x|^2 \text{sinc}^2(v_x L_x) \text{sinc}^2(v_z L_z)] \end{aligned} \quad (2.32)$$

and

$$\begin{aligned} \langle \sigma^{PQ} \rangle_s &= |x|^2 A^{PQ}(\hat{n}', \hat{n}', \hat{n}_s) [Q_l(\hat{n}', \hat{n}') \\ &+ A_s |v_y x|^2 \text{sinc}^2(v_x L_x) \text{sinc}^2(v_z L_z)] \\ &+ \int A^{PQ}(\hat{n}', \hat{n}', \hat{n}) \hat{\mathbf{n}} \cdot \hat{\mathbf{a}}_y Q_s(\hat{n}', \hat{n}', \hat{n}) p(\hat{n}) d\hat{n}. \end{aligned} \quad (2.33)$$

To facilitate the computations in Eq. (2.33), in which Q_s is a function of \hat{n} for a given \mathbf{v} and $R(\tau)$, a set of values of Q_s/v_y^2 is first computed and stored as a function of

$$\mathbf{v} \hat{\mathbf{n}} = (-v_x h_x + v_y - v_z h_z)/(1 + h_x^2 + h_z^2)^{1/2}. \quad (2.34)$$

The integration with respect to $d\hat{n} = dh_x dh_z$ is performed using values of Q_s interpolated from the stored set. For Gaussian surface-height probability-density functions,

$$\begin{aligned} Q_s(\hat{n}', \hat{n}', \hat{n}) &= 2\pi v_y^2 \int_0^\infty \exp(-v_{xld}^2 (h_x^2)) \\ &\times [\exp(v_{zld}^2 (h_z^2) R(\tau))] - 1] \\ &\times J_0(v_{zz} \tau) \tau d\tau \\ &\rightarrow \pi^2 v_y^2 v_{xld}^2 \chi^s(\mathbf{v} \cdot \hat{\mathbf{h}})^2 W(v_{zz}), \end{aligned} \quad (2.35)$$

Thus for $\hat{n} \rightarrow \mathbf{a}$, and $\beta \ll 1$ the last term in Eq. (2.33), $\langle \sigma^{PQ} \rangle_s$, reduces to the perturbation solution³

$$\langle \sigma^{PQ} \rangle_s \rightarrow \langle \sigma^{PQ} \rangle_P = \pi k_0^2 v_y^2 \chi^s(\mathbf{v}) (-\hat{n}' \cdot \hat{\mathbf{n}}) F(\hat{n}', \hat{n}') W(v_{zz}). \quad (2.36)$$

Note that Eq. (2.33) reduces to Eq. (2.32) if we set $\langle h_x^2 \rangle \rightarrow 0$ and that Eq. (2.32) reduces to Eq. (2.33) if we set $\langle h_z^2 \rangle \rightarrow 0$ and replace $A^{PQ}(\hat{n}', \hat{n}', \hat{n})$ by $A^{PQ}(\hat{n}', \hat{n}', \hat{n}_s)$. The term containing the product of the sinc functions is the coherent scattered field. This term vanishes as $|x(v_y)|^2 \rightarrow 0$.

For cases in which the physical-optics solutions are valid, the corresponding geometrical-optics expressions for $\langle \sigma^{PQ} \rangle_l$ are obtained by replacing \hat{n} by \hat{n}_s in Eq. (2.1) and integrating over the area A_{sc} (using the stationary phase method) before the expectations $\langle \cdot \rangle$ are evaluated. Thus in the neighborhood of a stationary phase point $\mathbf{r} = \mathbf{r}_{sp}$, where $v_x + v_z h_x = 0$ and $v_z + v_y h_z = 0$,^{2,12} it can be shown that

$$\begin{aligned} \int \exp[i\mathbf{v} \cdot \mathbf{r}] \frac{dx dz}{\hat{\mathbf{n}} \cdot \hat{\mathbf{a}}_y} &= \int \exp[i\mathbf{v} \cdot \mathbf{r}_{sp}] \\ &\times \exp\left\{\frac{i\mathbf{v} \cdot \hat{\mathbf{n}}_s}{2} [h_{xx} r_{sp}^2 + h_{zz} v_z^2]\right\} dx dz \\ &\rightarrow \frac{\exp(i\mathbf{v} \cdot \mathbf{r}_{sp}) (2\pi i)}{\mathbf{v} \cdot \hat{\mathbf{n}}_s (h_{xx} h_{zz})^{1/2}}, \quad \mathbf{v} \cdot \hat{\mathbf{n}}_s = 2k_0 (-\hat{n}' \cdot \hat{\mathbf{n}}_s), \end{aligned} \quad (2.37)$$

in which the integral has been expressed in terms of the local coordinates at the stationary plane point (x_{sp}, y_{sp}, z_{sp}) associated with the unit vectors $(\hat{\mathbf{h}}_1, \hat{\mathbf{h}}_2 = \hat{\mathbf{h}}, \hat{\mathbf{h}}_3)$, $\hat{\mathbf{h}}_1$, and $\hat{\mathbf{h}}_3$, the vectors in the tangent plane, are chosen such that the principal radii of curvature $r_{xp} = |1/h_{xx}|$ and $r_{zp} = |1/h_{zz}|$ are measured along the $\hat{\mathbf{h}}_1$ and $\hat{\mathbf{h}}_3$ directions. As seen by an observer in the region $y > h(x, z)$, the curvatures h_{xx} and h_{zz} are positive when the surface is concave. They are negative when the surface is convex. When h_{xx} or h_{zz} is negative, the curvatures are expressed as $(h_{xx})^{1/2} = i/(r_{xp})^{1/2}$

and $(h_{z,p})^{1/2} = i/(r_{z,p})^{1/2}$. Thus the geometric-optics contribution to the normalized cross section from N randomly located specular points per unit surface area is

$$(\sigma^{PQ})_{op} = \pi r_{z,p}^2 N |T^T F T|_{\hat{h}_s}^{PQ} P_2(\hat{h}', \hat{h}^q \hat{h}_s), \quad (2.38)$$

in which

$$F(\hat{h}', \hat{h}^q)_{\hat{h}_s} = \begin{bmatrix} R_V(\theta_{op}) & 0 \\ 0 & R_H(\theta_{op}) \end{bmatrix}, \quad (2.39)$$

and $R_V(\theta_{op})$ are the Fresnel reflection coefficients at the specular points where the local angles of incidence and scatter are $-\hat{h}' \cdot \hat{h}_s = \hat{h}^q \cdot \hat{h}_s = \cos \theta_{op}$. Note however, that the surface will depolarize the incident wave if the triple products $(\hat{n} \cdot \hat{n}' \cdot \hat{a}_y)$ and $(\hat{n} \hat{n}' \cdot \hat{a}_y)$ do not vanish. [When $(\hat{n} \hat{n}' \cdot \hat{a}_y)$ and $(\hat{n} \hat{n}' \cdot \hat{a}_y)$ vanish, T and T^T become identity matrices.]

The expectation of $(r_{z,p}^2 N)$ in Eq. (2.38)^{13,14} is

$$\langle r_{z,p}^2 N \rangle = p(\hat{h}_s)/(\hat{h}_s \cdot \hat{a}_y)^4, \quad \hat{h}_s \cdot \hat{a}_y = v_y/(v \cdot \hat{h}_s); \quad (2.40)$$

thus

$$\langle \sigma^{PQ} \rangle = \frac{\pi}{(\hat{h}_s \cdot \hat{a}_y)^4} p(\hat{h}_s) |T^T F T|_{\hat{h}_s}^{PQ} P_2(\hat{h}', \hat{h}^q \hat{h}_s), \quad (2.41)$$

in agreement with $(\sigma^{PP})_i$. Thus for backscatter the geometric-optics theory predicts no depolarization:

$$\langle \sigma^{PP}(\hat{h}' = -\hat{h}) \rangle = \frac{\pi}{(\hat{h}_s \cdot \hat{a}_y)^4} p(\hat{h}_s) P_2(-\hat{h}', \hat{h}^q \hat{h}_s) R_p(\theta_0 = 0). \quad (2.42)$$

In the following illustrative examples the unified full-wave solution is compared with the solution based on the two-scale model. In addition, the computed ratios of the like- to cross-polarized cross sections $(\sigma^{HH})/(\sigma^{VH})$ are compared with the experimental data.^{15,16}

3. ILLUSTRATIVE EXAMPLES

The illustrative examples considered are at X band 8.91 GHz; thus the wavelength λ_0 and wave number k_0 are

$$\lambda_0 = 3.367 \text{ cm}, \quad k_0 = 1.87 \text{ cm}^{-1}. \quad (3.1)$$

The wind velocity assumed is $V = 24$ m/sec, the relative complex-dielectric coefficient for the sea is $\epsilon_r = 55 - i37$,¹⁷ and the relative permeability $\mu_r = 1$. The surface-height spectral-density function is assumed to be⁵

$$W(k) = W(v_x, v_z) = \frac{2}{\pi} S(v_x, v_z) \\ = \begin{cases} \frac{2}{\pi} B v_{xz}^4 / (v_{xz}^2 + \kappa^2)^4 & k \leq k_c \\ 0 & k > k_c \end{cases} \quad (3.2)$$

in which S is the corresponding quantity defined by Brown.⁵ In Eq. (3.2)

$$k_c = 12 \text{ cm}^{-1}, \quad \kappa = (335.2 \text{ V}^4)^{1/2} = 0.948 + 10^{-4} \text{ cm}^{-1}. \quad (3.3)$$

The surface-height autocorrelation coefficient $R(r)$ corresponding to $W(k)$ [Eq. (3.2)] is given in closed form for $\kappa \ll k_c \rightarrow \infty$ (Ref. 18):

$$R(r) = \left[1 + \frac{1}{8} (\kappa r)^2 \right] (\kappa r) K_1(\kappa r) - (\kappa r)^2 K_0(\kappa r), \quad (3.4)$$

in which K_0 and K_1 are the modified Bessel functions of the second kind and of order zero and one, respectively.¹⁹ The mean-square height of the rough surface is

$$\langle h^2 \rangle = B/[6\kappa^2(1 + \kappa^2/k_c^2)^3] \approx \frac{B}{6\kappa^2}, \quad (3.5)$$

and the mean-square slope is

$$\sigma_n^2 = B \left[\frac{1}{2} \ln \frac{k_c^2 + \kappa^2}{\kappa^2} - \frac{k_c^2(6\kappa^4 + 15\kappa^2 k_c^2 + 11k_c^4)}{12(\kappa^2 + k_c^2)^3} \right] \\ \approx B(\ln k_c/\kappa - 11/12), \quad (3.6)$$

and the slope probability-density function is assumed to be Gaussian. Two values of B are assumed in this work. The corresponding values for $\langle h^2 \rangle$ and σ_n^2 and for k_d , with $\beta = 1$ for the two-scale model, are given below:

case (a)	case (b)
$B = 0.0046$	$B = 0.0092$
$\langle h^2 \rangle = 0.853 \times 10^5 \text{ cm}^2$	$\langle h^2 \rangle = 0.171 \times 10^6 \text{ cm}^2$
$\sigma_n^2 = 0.0498$	$\sigma_n^2 = 0.0997$
$k_d = 0.179 \text{ cm}^{-1}$	$k_d = 0.253 \text{ cm}^{-1}$

In Fig. 3 the normalized spectral-density function $W(k/\kappa)/W_{max}$ is plotted as a function of $v_{xz}/\kappa = k/\kappa$ ($W = W_{max}$ at $v_{xz} = \kappa$). The corresponding surface-height correlation coefficient $R(\kappa r)$ is plotted in Fig. 4 as a function of the dimensionless quantity κr . The above parameters approximate the range of conditions prevailing during the measurements conducted by Daley *et al.*¹⁶ [wind speed 24 m/sec ($\sigma_1 \approx 0.05$); average wave height 650 cm ($\langle h^2 \rangle = 1.05 \times 10^5 \text{ cm}^2$)]. In Figs. 5-7, the like- and cross-polarized backscatter cross sections $\langle \hat{h}' = -\hat{h} \rangle (\langle \sigma^{VV} \rangle, \langle \sigma^{HH} \rangle, \text{ and } \langle \sigma^{VH} \rangle = \langle \sigma^{HV} \rangle)$ are plotted as functions of the angle of incidence θ_0 using the unified and two-scale approaches [Eqs. (2.32) and (2.33)] for case (a). The corresponding quantities are plotted in Figs. 8-10 for case (b). The most significant differences between the results based on the unified and two-scale approaches occur near normal incidence for the cross-polarized back-

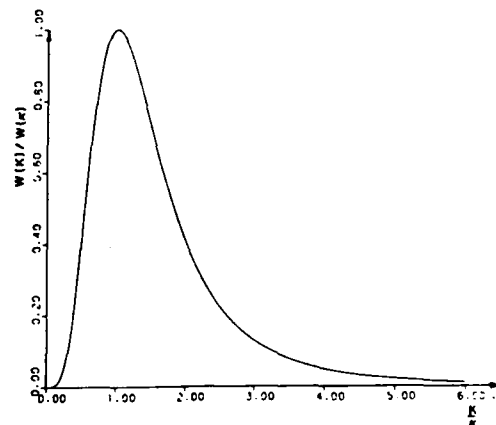


Fig. 3. The normalized surface-height spectral-density function $W(k)/W(k_c)$.

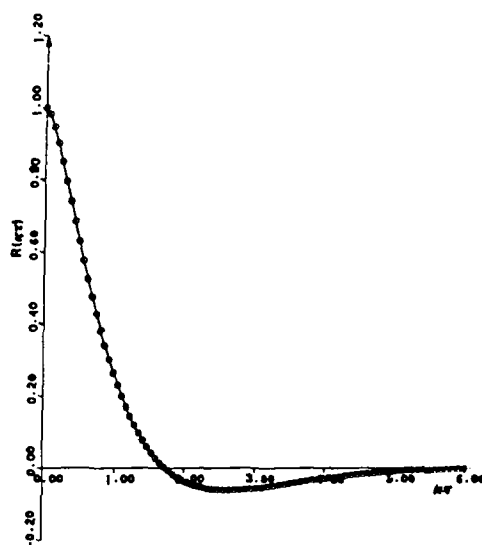


Fig. 4. The surface-height correlation coefficient $R(r)$.

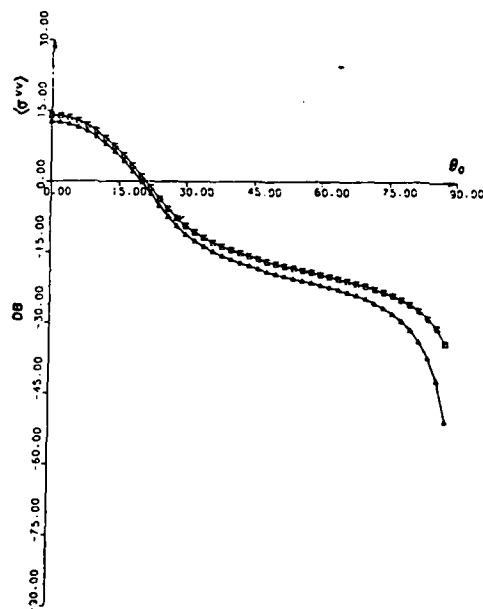


Fig. 5. The backscatter scattering cross section $\langle \sigma^{VV} \rangle$ for case (a). Δ , Unified full-wave solution; \square , two-scale model.

scatter cross sections. In Figs. 11 and 12 the like- to cross-polarized backscatter cross-section ratio $\langle \sigma^{HH} \rangle / \langle \sigma^{VH} \rangle$ is plotted for cases (a) and (b), respectively, using both analytical approaches. In these figures the symbol x corresponds

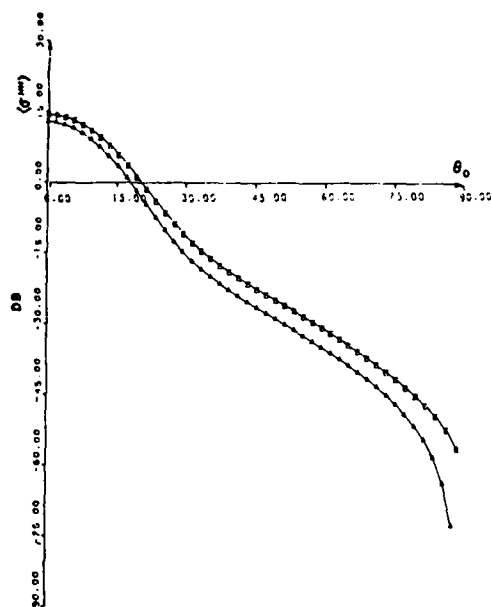


Fig. 6. The backscatter scattering cross section $\langle \sigma^{HH} \rangle$ for case (a). Δ , Unified full-wave solution; \square , two-scale model.

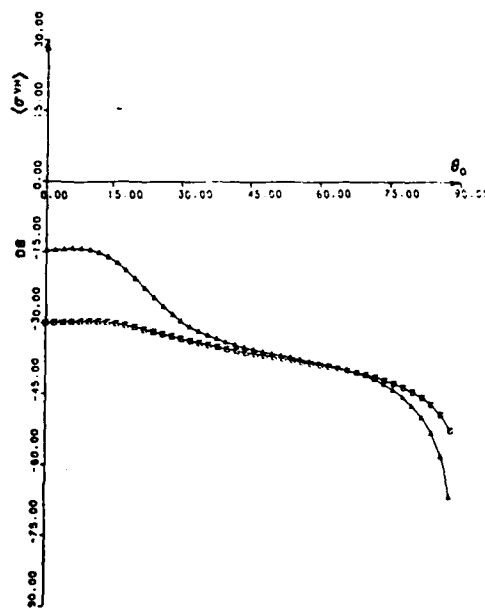


Fig. 7. The backscatter scattering cross section $\langle \sigma^{HV} \rangle = \langle \sigma^{VH} \rangle$ for case (a). Δ , Unified full-wave solution; \square , two-scale model.

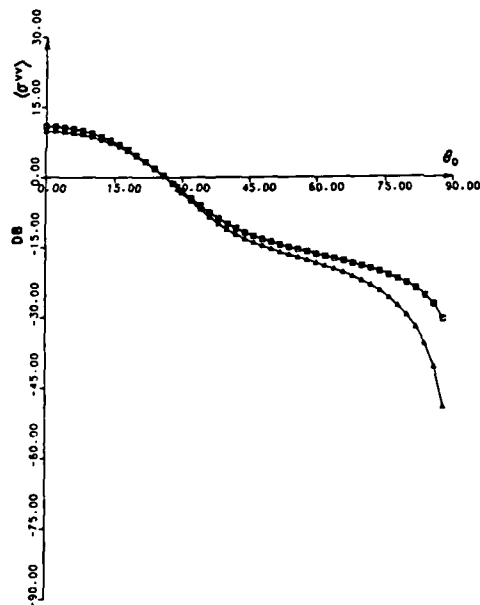


Fig. 8. The backscatter scattering cross section $\langle \sigma^{VV} \rangle$ for case (b). Δ , Unified full-wave solution; \square , two-scale model.

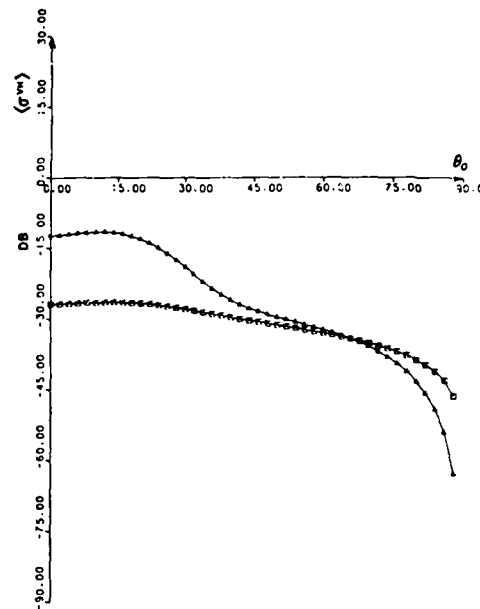


Fig. 10. The backscatter scattering cross section $\langle \sigma^{HV} \rangle \approx \langle \sigma^{VH} \rangle$ for case (b). Δ , Unified full-wave solution; \square , two-scale model.

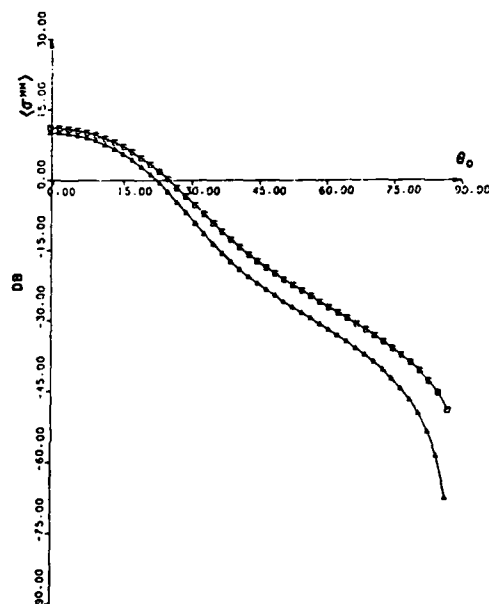


Fig. 9. The backscatter scattering cross section $\langle \sigma^{HH} \rangle$ for case (b). Δ , Unified full-wave solution; \square , two-scale model.

to the measurement taken by Daley *et al.* (For large wind speeds few data are given for the like- and cross-polarized cross sections near normal incidence at X band.) To understand the significant difference between the solutions based on the unified and two-scale approaches for the cross-polarized backscatter cross section, it is necessary to note that for backscatter at the specular points, $T^i = T^s$ are identity matrices, and for $|x|^2 \ll 1$ the contribution to $\langle \sigma^{PQ} \rangle_T$ [Eq. (2.33)] from the large-scale surface h_1 reduces to³

$$\langle \sigma^{PQ} \rangle_I = \frac{\pi}{(\hat{h}^i \cdot \hat{a}_y)^4} |x|^2 R_P \delta_{PQ}, \quad P, Q = V, H, \quad (3.8)$$

in which $\delta_{VH} = \delta_{HV} = 0$, $\delta_{HH} = \delta_{VV} = 1$ and R_V and R_H are the Fresnel reflection coefficients at normal incidence for vertically and horizontally polarized waves. Thus, as is expected, physical-optics theory predicts no cross polarization for backscatter by the large-scale surface h_1 . However, the local scattering matrix D^{PQ} becomes diagonal only at the specular point, and the contributions to $\langle \sigma^{VH} \rangle$ come from the neighborhood of the specular points. Physical-optics techniques fail to predict backscatter cross-polarized cross sections since the integrand $A^{PQ}(\hat{h}', \hat{h}', \hat{h})$ [Eqs. (2.18)] ($P \neq Q$) vanishes at the stationary phase points where $\hat{h} = \hat{h}_s$. For the like-polarized case, or for bistatic scattering in general when $A^{PQ}(\hat{h}', \hat{h}', \hat{h}_s) \neq 0$, the physical-optics solutions are suitable for the large-scale filtered surface. Furthermore, for scattering at grazing angles ($-\hat{h}' \cdot \hat{h} \rightarrow 0$ and $\hat{h}' \cdot \hat{h} \rightarrow 0$) except forward scattering in the specular direction, the coefficient $A^{PQ}(\hat{h}', \hat{h}', \hat{h})$ has a pole near the stationary phase points, and the physical-optics solution $\langle \sigma^{PQ} \rangle_I$ [Eq. (2.33)] is

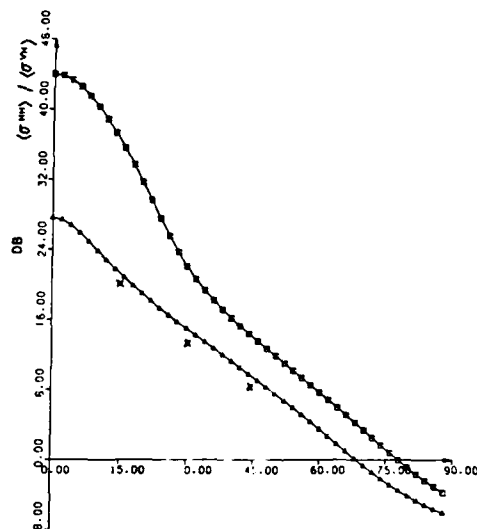


Fig. 11. The ratio $\langle \sigma^{HH} \rangle / \langle \sigma^{VH} \rangle$ for case (a); the symbol x corresponds to experimental data.¹⁶ Δ , Unified full-wave solution; O , two-scale model.

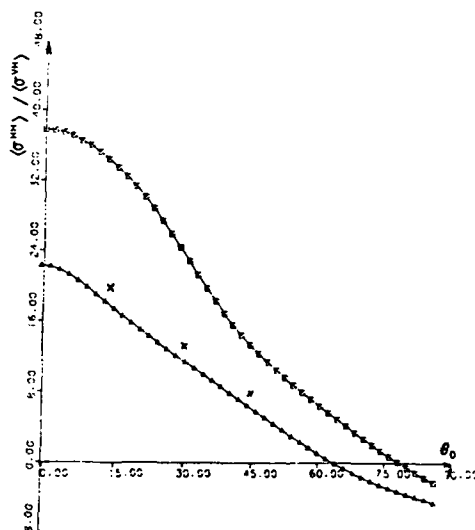


Fig. 12. The ratio $\langle \sigma^{HH} \rangle / \langle \sigma^{VH} \rangle$ for case (b); the symbol x corresponds to experimental data.¹⁶ Δ , Unified full-wave solution; O , two-scale model.

not suitable. In this case the full-wave (complete spectral) approach can be used to account for the pole in the vicinity of the stationary phase points ($\hat{n} \rightarrow \hat{n}_s$).²⁰

There are other reasons for the discrepancies between the solutions based on the unified and the two-scale model. To facilitate spectral splitting of the surface, it is assumed that

$p(h_s, h_i) = p(h_s)p(h_i)$. However, in general, statistical independence cannot be assumed between the large- and small-scale surfaces. Using the two-scale model, it is also assumed that $\hat{n} \approx \hat{n}_i$ and that $p(\hat{n}) \approx p(\hat{n}_i)$. Thus the slopes of the small-scale surface are totally ignored when the two-scale model is used. In order to derive the expression for scattering by the large-scale surface, it is assumed that the major contributions to the scattered fields come from the vicinity of specular points and that $A^{PQ}(\hat{n}', \hat{n}, \hat{n}) \rightarrow A^{PQ}(\hat{n}', \hat{n}, \hat{n}_s)$. However, for backscatter near grazing angles, specular points are practically nonexistent unless the surface is very rough. Thus, for the like- and cross-polarized backscatter cross section, the discrepancies between the two solutions increase as the angle of incidence θ_0 approaches 90° .

Finally, with reference to Figs. 11 and 12, it is seen from the published experimental results marked x that for $\theta_0 = 15^\circ$, $\langle \sigma^{HH} \rangle / \langle \sigma^{VH} \rangle \approx 20$ dB. Using the unified approach, this ratio is 21.5 dB for case (a) and 18 dB for case (b). However, using the two-scale model, $\langle \sigma^{HH} \rangle / \langle \sigma^{VH} \rangle = 36$ dB for case (a) and 34 dB for case (b). Recently designed dual-polarized receivers with significantly improved performance make it more feasible to use both like- and cross-polarized data for the purposes of remote sensing. To this end, additional measurements are needed to make more extensive comparisons between theory and experiment.

4. CONCLUDING REMARKS

In this paper the solutions for the backscatter like- and cross-polarized cross sections based on the unified full-wave solutions have been compared with the solution based on the two-scale model. For the two-scale model the wave number k_d where spectral splitting is assumed to occur is chosen such that $\beta = 4k_0^2(h_s^2) = 1.7$. It is also assumed that the two surfaces h_i and h_s are statistically independent and that the slope of the small-scale surface was neglected ($\hat{n} \approx \hat{n}_i$). It is shown that for the like-polarized case, the difference between the two solutions increases as $\theta_0 \rightarrow \pi/2$. However, except for near-grazing angles, the two solutions for the like-polarized cross sections are separated by about 3 dB. For the cross-polarized case, the difference between the two solutions is most significant near normal incidence $\theta_0 < 40^\circ$. For normal incidence ($\theta_0 = 0$), the two-scale solution for the cross-polarized cross section is about 15 dB below the unified solution. As the angle of incidence increases, the difference decreases and the two solutions cross over at $\theta_0 \approx 65^\circ$. As in the case of the like-polarized cross sections, the difference between the two solutions increases as $\theta_0 \rightarrow \pi/2$. The large discrepancy near normal incidence occurs because elements of the rough surface that are oriented specularly do not depolarize the backscattered wave. The depolarization comes from the neighborhood of these specular points, and even the filter 1 large-scale surface depolarizes the incident waves.²¹ However, the physical-optics contribution to cross polarization is zero. The discrepancy near grazing angles occurs because as $\theta_0 \rightarrow \pi/2$, for backscatter there are practically no specular points on the surface and again the physical-optics approximations are invalid. The solutions based on the unified approach are in agreement with experimental data for near-normal incidence. Finally, it should be recalled that the assumption $p(\hat{n}, \hat{n}') = p(\hat{n})\delta(\hat{n}, \hat{n}')$ is valid only if most of the scattering comes from the neighborhood of the stationary phase points $\hat{n} = \hat{n}_s$. For near-grazing

angles this assumption is not valid, since there are practically no stationary phase points as $\theta_0 \rightarrow \pi/2$. Thus, for near-grazing angles, the solution can be improved provided that it is possible to determine the slope joint probability-density function $p(\hat{n}, \hat{n}') = p(\hat{n})p(\hat{n}'|\hat{n})$ and the joint probability that two points on the rough surface are both illuminated and visible given the slopes \hat{n} and \hat{n}' at the points $P_2(\hat{n}', \hat{n}|\hat{n}, \hat{n}')$. This, however, is not necessary if $|x|^2 \rightarrow 0$ and if it can be assumed that $\hat{n} \approx \hat{n}'$ for distances r less than r_c (the correlation length for the surface heights).

ACKNOWLEDGMENTS

This investigation was sponsored by the U.S. Army Research Office under contract DAAG-29-82-K-0123 and the U.S. Air Force under contract F19628-81-K-0025.

REFERENCES

1. E. Bahar, "Full-wave solutions for the depolarization of the scattered radiation fields by rough surfaces of arbitrary slope," *IEEE Trans. Antennas Propag.* AP-29, 443-454, (1981).
2. E. Bahar, "Scattering cross sections from rough surfaces—full wave analysis," *Radio Sci.* 16, 331-341 (1981).
3. E. Bahar, "Scattering cross sections for composite random surfaces—full wave analysis," *Radio Sci.* 16, 1327-1335 (1981).
4. M. I. Sancer, "Shadow-corrected electromagnetic scattering from a randomly rough surface," *IEEE Trans. Antennas Propag.* AP-17, 577-585 (1968).
5. G. S. Brown, "Backscattering from a Gaussian-distributed perfectly conducting rough surfaces," *IEEE Trans. Antennas Propag.* AP-28, 943-946 (1978).
6. E. Bahar and D. E. Barrick, "Scattering cross sections for composite rough surfaces that cannot be treated as perturbed physical optics problems," *Radio Sci.* 18, 129-137 (1983).
7. E. Bahar, D. E. Barrick, and M. A. Fitzwater, "Computations of scattering cross sections for composite surfaces and the specification of the wavenumber where spectral splitting occurs," *IEEE Trans. Antennas Propag.* AP-31, 698-709 (1983).
8. J. W. Wright, "A new model for sea clutter," *IEEE Trans. Antennas Propag.* AP-16, 217-223 (1968).
9. G. R. Valenzuela, (1968), "Scattering of electromagnetic waves from a tilted slightly rough surface," *Radio Sci.* 3, 1051-1060 (1968).
10. M. L. Burrows, "On the composite model for rough surface scattering," *IEEE Trans. Antennas Propag.* AP-21, 241-243 (1967).
11. P. Beckmann and A. Spizzichino, *The Scattering of Electromagnetic Waves from Rough Surfaces* (Macmillan, New York, 1963).
12. D. E. Barrick, "Rough surfaces," in *Radar Cross Section Handbook* (Plenum, New York, 1970), Chap. 9.
13. D. E. Barrick, "Remote sensing of sea state by radar," in *Remote Sensing of the Troposphere*, V. E. Derr, ed. (U. S. Government Printing Office, Washington, D.C., 1972), pp. 12.1-12.24.
14. D. E. Barrick and E. Bahar, "Rough surface scattering using specular theory," *IEEE Trans. Antennas Propag.* AP-29, 798-800 (1981).
15. M. W. Long, *Radar Reflectivity of Land and Sea* (Heath, Lexington, Mass., 1975).
16. J. C. Daley, W. T. Davis, and N. R. Mills, "Radar sea return in high sea states," *Naval Research Laboratory Rep.* 7142, (U. S. Government Printing Office, Washington, D.C., 1970).
17. A. Stogryn, "Equations for calculating the dielectric constant of saline water," *IEEE Trans. Microwave Theory Tech.* MTT-19, 734-736 (1971).
18. L. S. Miller, G. S. Brown, and G. S. Hayne, "Analysis of satellite altimeter signal characteristics and investigation of sea-truth data requirements," *NASA Rep. No. CR-137465* (Research Triangle Institute, Durham, N. C., 1972).
19. M. Abramowitz and I. A. Stegun, *Handbook of Mathematical Functions* (U. S. Printing Office, Washington, D.C., 1964).
20. E. Bahar, "Scattering and depolarization by rough surfaces near grazing angle—null wave solutions," *IEEE Trans. Antennas Propag.* AP-30, 712-719 (1982).
21. E. Bahar and M. A. Fitzwater, "Scattering cross sections for composite rough surfaces using the unified full wave approach," *IEEE Trans. Antennas Propag.* AP-32, 730-734 (1984).

Ezekiel Bahar



Ezekiel Bahar received the B.Sc. and M.Sc. degrees in electrical engineering from the Technion-Israel Institute of Technology, Haifa, in 1958 and 1960, respectively, and the Ph.D. degree from the University of Colorado, Boulder, in 1964. From 1958 to 1962 he was a research assistant and an instructor at the Technion-Israel Institute of Technology. In 1962 he joined the Department of Electrical Engineering, University of Colorado, as a research associate and from 1964 to 1967 was an assistant professor. In 1967 he joined the Department of Electrical Engineering, University of Nebraska, Lincoln, as an associate professor and in 1971 became professor of electrical engineering. He is the Durham Professor of Electrical Engineering. His field of research is electromagnetic theory, propagation, and microwave theory. He has employed EM model studies to investigate the problem of propagation in nonuniform terrestrial waveguides. He has developed transform techniques to obtain full-wave solutions to problems of depolarization, diffraction, and scattering of radio waves in nonuniform layered structures. He has employed generalized characteristic vectors and developed generalized WKB techniques to solve problems of propagation in inhomogeneous anisotropic media. Dr. Bahar is a member of Commissions B, C, and F of the International Union of Radio Science and is a member of the Institute of Electrical and Electronics Engineers Society on Antennas and Propagation and the Society on Microwave Theory and Techniques.

Mary Ann Fitzwater

Mary Ann Fitzwater received the B.Sc. and M.Sc. degrees in electrical engineering and the Ph.D. degree in engineering, all from the University of Nebraska, Lincoln, in 1971, 1975, and 1978, respectively. She was a postdoctoral fellow in the Department of Mechanical Engineering, University of Nebraska, Lincoln, for one year followed by a year as assistant professor in the Department of Engineering Mechanics. Since 1980 she has been a research associate in the Department of Electrical Engineering.

SCATTERING AND DEPOLARIZATION BY RANDOM ROUGH SURFACES

UNIFIED FULL WAVE APPROACH--AN OVERVIEW

Ezekiel Bahar

Department of Electrical Engineering

University of Nebraska--Lincoln

Lincoln, NE 68588-0511

Abstract

In this paper the principal elements of the full wave approach to problems of scattering and depolarization by nonuniform stratified media are summarized. Scattering by random rough surfaces is considered in detail and the full wave solutions are compared with earlier solutions based on physical optics and perturbation theories. It is shown that since the full wave approach accounts for both specular point scattering as well as Bragg scattering in a self-consistent manner, it resolves the discrepancies between the physical optics and perturbation solutions and bridges the wide gap between them. Thus, on applying the full wave approach to scattering by composite random rough surfaces it is not necessary to adapt a two-scale model of the rough surface.

The full wave solutions satisfy duality, reciprocity and realizability relations in electromagnetic theory and the results are invariant to coordinate transformations. The full wave approach also accounts for coupling between the radiation fields, the lateral waves and the surface waves that constitute the complete expansions of the fields and it can be applied directly to problems of scattering at near grazing angles.

1. Introduction and Overview

Rigorous closed form solutions for the reflection and transmission of electromagnetic waves have been derived for multilayered dielectric structures of uniform thickness (Wait 1962). (See Fig. 1). However, in a large variety of pertinent radio wave propagation problems the thicknesses of the layers are nonuniform and the height of the interface between two adjacent dielectric layers is a random function. (See Fig. 2). In these cases the incident waves are depolarized and scattered into both propagating and evanescent waves. Furthermore, an incident plane wave may be coupled into guided surface waves and lateral waves of the structure.

Often the problem that is actually solved is a highly idealized version of the original problem and concepts such as "effective dielectric coefficient" and "effective surface impedance" are introduced in order to make the solution of the original problem more tractable. However, the validity of such approximations is very limited and often questionable and they do not necessarily satisfy reciprocity (Schlak and Wait 1967, 1968).

Using a full wave approach it is possible to analyze more realistic models of the original physical structure without introducing simplifying approximations that cannot be justified a priori (Bahar 1973c,d).

The principal properties of the full wave solution and its relationships to earlier solutions of scattering problems are also summarized here (Bahar 1981a). This summary is also presented schematically in Figs. 3 and 4. The reader of this manuscript who is not familiar with the full wave approach will find this summary useful even though the details of the full wave method have been reported earlier (Bahar. 1973c,d, 1974, 1981a).

A. Principal Elements of the Full Wave Approach (See Fig. 3)

(a) The electromagnetic fields are expressed in terms of complete expansions of vertically and horizontally polarized waves. These include the radiation fields, the lateral waves and the surface waves (Bahar 1973c,d, 1974).

(b) Exact boundary conditions are imposed at the irregular surface.

(c) Using the orthogonal properties of the basis functions appearing in the complete expansions of the fields, Maxwell's equations are integrated over the transverse plane (y,z) (Bahar 1973c,d, 1974). Green's theorems are used to avoid term-by-term differentiation of the field expansions.

(d) Maxwell's equations for the electromagnetic fields are converted into coupled first order ordinary differential equations for the forward and backward traveling wave amplitudes which are only functions of the variable x (Bahar 1973c,d, 1974). (In view of the integration in the transverse plane (y,z) the telegraphists' equations are only functions of x). The coupled equations for the wave amplitudes are referred to the generalized telegraphists' equations (Bahar 1981a).

(e) A variable coordinate system that conforms with the local features of the irregular boundary is introduced and the resulting solutions for the scattered fields are shown to be invariant to coordinate transformations.

(f) Closed form second order iterative solutions for the radiation fields are obtained from the telegraphists' equations on neglecting multiple scattering from the rough surface. These second order iterative solutions account for wave scattering in arbitrary directions.

(g) The full wave solutions are compared with earlier geometric optics physical optics and perturbation solutions. The suitability of the two-scale model is investigated.

B. Principal Properties of the Full Wave Approach (See Fig. 4)

(a) The full wave solutions are shown to satisfy the reciprocity realizability and duality relationships in electromagnetic theory.

(b) The full wave approach not only accounts for scattering and depolarization of the radiation fields but also accounts for coupling between the surface waves, the lateral waves and the radiation fields.

(c) The versatility of the full wave approach is demonstrated by determining its relationship to earlier solutions. Thus, on using a stationary phase approach to evaluate the integrals for the scattered fields, the full wave approach is shown to reduce to the geometric optics solutions (Bahar, 1981a).

(d) If the vector \bar{n} normal to the rough surface is replaced by its value at the specular points \bar{n}_s , the full wave expressions for the scattered fields are shown to reduce to the Physical Optics solutions. Thus the Physical Optics approach is valid only if the contributions to the scattered fields come primarily from the neighborhood of specular points on the rough surface.

(e) In a survey of the technical literature one finds several different forms of Physical Optics solutions. The discrepancies between the different Physical Optics solutions and the appearance of the so-called "edge effect" have been shown to be the result of premature truncation of the closed surface integrals.

(f) If one assumes that the scale and the slopes of the rough surface are small, it is shown that the full wave solutions reduce to the perturbation solutions.

(g) The Physical Optics solutions for the backscattered fields become singular for near grazing angles. Thus in this case, even if the rough surface satisfies the radii of curvature criteria (associated with the

Kirchhoff approximations of the surface fields), the Physical Optics solutions cannot be used and the far fields cannot be represented by plane waves at grazing angles. This is because at near grazing angles, the principal contributions to the backscattered fields do not come from specular points of the rough surface. (In this case specular points, if they existed, would be on vertical portions of the rough surface). It is shown that the full wave solutions for the backscattered fields remain valid as one approaches grazing angles (Bahar 1982).

(h) The full wave solutions have been compared with the hybrid perturbed-physical optics solutions (Bahar and Barrick 1983, Bahar et al 1983) based on a two-scale model of the rough surface. It is shown that while the solutions based on the perturbed-physical optics approach critically depend upon the wavenumber k_d where spectral splitting is assumed to occur, the solutions based on the full wave approach are relatively insensitive to the choice of k_d for the like polarized case (Brown 1978). However, for the cross polarized case, the results based on the two-scale model are incorrect (particularly for backscatter for near normal incidence). This is because the physical optics contribution to backscatter from the large scale surface is assumed to be zero.

2. Formulation of the Problem

For the convenience of the reader the principal steps in the derivation of the full wave approach are summarized in this section. It is assumed that both electric and magnetic sources (\bar{J}, ρ and \bar{M}, ρ_m) are present in any of the $m+1$ layers of the structure. A suppressed $\exp(i\omega t)$ time dependence is assumed in this work. The i th layer of the structure is characterized by the complex electromagnetic parameters ϵ_i and μ_i and the interface between medium i and $i+1$ is given by the surface (See Fig. 2).

$$y = h_{i,i+1} \quad (1)$$

Maxwell's equations for the transverse components of the electric and magnetic fields, \bar{E}_T and \bar{H}_T respectively are (Bahar 1973c,d).

$$-\frac{\partial \bar{E}_T}{\partial x} = i\omega\mu(\bar{H}_T \times \bar{a}_x) - \frac{1}{i\omega\epsilon} \nabla_T \nabla_T \cdot (\bar{H}_T \times \bar{a}_x) + \bar{M}_T \times \bar{a}_x + \frac{1}{i\omega\epsilon} \nabla_T J_x \quad (2)$$

and

$$-\frac{\partial \bar{H}_T}{\partial x} = i\omega\epsilon(\bar{a}_x \times \bar{E}_T) - \frac{1}{i\omega\mu} \nabla_T \nabla_T \cdot (\bar{a}_x \times \bar{E}_T) + \bar{a}_x \times \bar{J}_T + \frac{1}{i\omega\mu} \nabla_T M_x, \quad (3)$$

in which the operator ∇_T is given by

$$\nabla_T = \bar{a}_y \frac{\partial}{\partial y} + \bar{a}_z \frac{\partial}{\partial z} \quad (4)$$

and the transverse vectors are

$$\bar{A}_T = \bar{a}_y A_y + \bar{a}_z A_z, \quad \bar{A} = \bar{E}, \bar{H}, \bar{J} \text{ or } \bar{M} \quad (5)$$

The following field transform pairs provide the basis for the complete expansion of the transverse electric and magnetic fields into vertically (V) and horizontally (H) polarized waves:

$$\bar{E}_T(x, y, z) = \int_V \int_{-\infty}^{\infty} [E^V(x, v, w) \bar{e}_T^V + E^H(x, v, w) \bar{e}_T^H] dw, \quad (6)$$

where

$$E^P(x, v, w) = \int_{-\infty}^{\infty} \bar{E}_T(x, y, z) \cdot (\bar{h}_P^T \times \bar{a}_x) dy dz, \quad P=V \text{ or } H, \quad (7)$$

$$\bar{H}_T(x, y, z) = \int_V \int_{-\infty}^{\infty} [H^V(x, v, w) \bar{h}_T^V + H^H(x, v, w) \bar{h}_T^H] dw, \quad (8)$$

where

$$H^P(x, v, w) = \int_{-\infty}^{\infty} \bar{H}_T(x, y, z) \cdot (\bar{a}_x \times \bar{e}_P^T) dy dz, \quad P=V \text{ or } H, \quad (9)$$

The basis functions for the vertically polarized waves are

$$\bar{e}_T^V = 2^V (\bar{a}_y \psi^V(v, y) - \frac{\bar{a}_z i w}{u^2 + w^2} \frac{\partial \psi^V(v, y)}{\partial y}) \phi(w, z) \quad (10)$$

and

$$\bar{h}_T^V = \bar{a}_z \psi^V(v, y) \phi(w, z) \quad (11)$$

and the complementary basis functions for the vertically polarized waves

are

$$\bar{e}_V^T = Z^V N^V (\bar{a}_y \psi^V(v, y) + \frac{\bar{a}_z i w}{u^2 + w^2} \frac{\partial \psi^V(v, y)}{\partial y} \phi^C(w, z) \quad (12)$$

and

$$\bar{h}_V^T = \bar{a}_z N^V \psi^V(v, y) \phi^C(w, z). \quad (13)$$

For the horizontally polarized waves, the basis functions and the complementary basis functions are respectively,

$$\bar{e}_T^H = \bar{a}_z \psi^H(v, y) \phi(w, z), \quad (14)$$

$$\bar{h}_T^H = Y^H (-\bar{a}_y \psi^H(v, y) + \frac{\bar{a}_z i w}{u^2 + w^2} \frac{\partial \psi^H(v, y)}{\partial y}) \phi(w, z), \quad (15)$$

and

$$\bar{e}_H^T = \bar{a}_z N^H \psi^H(v, y) \phi^C(w, z), \quad (16)$$

$$\bar{h}_H^T = Y^H N^H (-\bar{a}_y \psi^H(v, y) - \frac{\bar{a}_z i w}{u^2 + w^2} \frac{\partial \psi^H(v, y)}{\partial y}) \phi^C(w, z). \quad (17)$$

in which N^P are normalization coefficients, Z^P and Y^P are the wave impedance and admittance and

$$\phi(w, z) = \exp(-i w z) \text{ and } \phi^C(w, z) = 0/2\pi \exp(i w z) \quad (18)$$

The scalar basis functions are

$$R_{PO}^{Dh} \psi_O^P(v, y) = \begin{cases} \exp(i v_O y) + R_{PO}^{Dh} \exp(-i v_O y). \\ \text{for medium 0,} \\ \prod_{q=1}^r \frac{T_{Pq-1}^D}{T_{Pq}^{DH}} \exp\left(i \sum_{q=1}^r v_{p-1,q} h_{q-1,q}\right) \\ \times [\exp(i v_r y) + R_{Pr}^{Dh} \exp(-i v_r y)], \\ \text{for medium } r = 1, 2, 3, \dots, m, \end{cases} \quad (19)$$

$$\begin{aligned}
 R_{Pm}^{UH} \psi_m^P(v, y) &= \left\{ \prod_{q=1}^{m-r} \frac{T_{Pm+1-q}^U}{T_{Pm-q}^{UH}} \exp \left(i \sum_{q=1}^{m-r} v_{m-q, m+1-q}^v h_{m-q, m+1-q}^h \right) \right. \\
 &\quad \times [\exp(-iv_r y) + R_{Pr}^{UH} \exp(iv_r y)] \text{ for medium } r=0, 1, 2, \dots, m-1 \\
 &\quad \left. \exp(-iv_m y) + R_{Pm}^{UH} \exp(iv_m y), \text{ for medium } m, \right. \quad (20) \\
 \psi_s^{Pn}(v, y) &= \psi_s^{Pn}(v, h_{o,1}) \left\{ \begin{aligned} &\exp[-iv_o^n(y-h_{o,1})], \text{ for medium } 0, \\ &\frac{1}{T_{P1}^{DH}} \exp(-iv_1^n h_{o,1}) [\exp(iv_1^n y) + R_{P1}^{DH} \exp(-iv_1^n y)], \\ &\quad \text{for medium } 1, \\ &\frac{1}{T_{P1}^{DH}} \exp(-iv_1^n h_{o,1}) \prod_{q=2}^r \frac{T_{Pq-1}^{DH}}{T_{Pq}^{DH}} \\ &\quad \times \exp \left(i \sum_{q=2}^r v_{q-1, q}^n h_{q-1, q}^h \right) [\exp(iv_r^n y) + R_{Pr}^{DH} \exp(-iv_r^n y)], \\ &\quad \text{for medium } r=2, 3, \dots, m, \end{aligned} \right. \quad (21)
 \end{aligned}$$

where

$$[\psi_s^{Pn}(v, h_{o,1})]^2 = \left[u / i Z_o^P v_o \frac{d}{du} \frac{1}{R_{PO}^D} \right]_{v=v_n} \quad (22)$$

The scalar functions for vertically and horizontally polarized waves $\psi^V(v, y)$ and $\psi^H(v, y)$, are given by (19), (20), and (21), on replacing the letter P in all the expressions by V and H respectively. The reflection coefficient at the $i, i+1$ interface for waves incident from above is R_{Pi}^D and R_{Pi}^U is the reflection coefficient at the $i-1, i$ interface for waves incident from below (See Fig. 1). Thus, for $P = V$ or H ,

$$R_{Pm}^D = 0, \quad R_{Pi}^D = \frac{(R_{i+1,i}^P + R_{Pi+1}^{DH})}{(1 + R_{i+1,i}^P R_{Pi+1}^{DH})}, \quad i = 0, 1, \dots, m-1,$$

and

$$R_{PO}^U = 0, \quad R_{Pi}^U = \frac{(R_{i-1,i}^P + R_{Pi-1}^{UH})}{(1 + R_{i-1,i}^P R_{Pi-1}^{UH})}, \quad i = 1, 2, \dots, m, \quad (23)$$

where $R_{1,i+1}^V$ and $R_{1,i+1}^H$ are the two medium Fresnel reflection coefficients for vertically and horizontally polarized waves respectively, and

$$\begin{aligned} R_{P1}^{DH} &= R_{P1}^D \exp(-i2v_i H_i), & R_{P1}^{Dh} &= R_{P1}^D \exp(i2v_i h_{i,i+1}), \\ R_{P1}^{UH} &= R_{P1}^U \exp(-i2v_i H_i), & R_{P1}^{Uh} &= R_{P1}^U \exp(-i2v_i h_{i-1,i}). \end{aligned} \quad (24)$$

The transmission coefficients are

$$\begin{aligned} T_{P1}^D &= 1 + R_{P1}^D, & T_{P1}^U &= 1 + R_{P1}^U, \\ T_{P1}^{DH} &= 1 + R_{P1}^{DH}, & T_{P1}^{UH} &= 1 + R_{P1}^{UH} \end{aligned} \quad (25)$$

and N^P are normalization coefficients. The symbol Σ_v denotes summation over the entire wavenumber spectrum v . The generalized Fourier transform consists of two infinite integrals (continuous parts of the wavenumber spectrum) which are associated with the radiation and the lateral wave terms and a finite set of surface wave terms (discrete part of the wavenumber spectrum). The infinite integrals in the v plane are associated with branch cut integrals $\text{Im}(v_0) = 0$ and $\text{Im}(v_m) = 0$ in the complex v plane, while the surface wave terms are associated with the residues of the poles at $1/R_{P0}^D = 0$ (or $1/R_{Pm}^U = 0$). The modal equation which determines the surface wave parameters $v^n(\text{Im}(v) \leq 0)$ is given by

$$1 - R_{P1}^U R_{P1}^D \exp(-i2v_i H_i) = 0, \quad v_i \equiv (k_1^2 - u^2 - w^2)^{1/2}, \quad v_{i-1,i} = v_{i-1} - v_i \quad (26)$$

for P equals V or H and $i = 1, 2, 3, \dots, \text{or } m - 1$.

The irregular interfaces $y = h_{i,i+1}$ are assumed here to be continuous functions of x only. Thus the exact boundary conditions at $y = h_{i,i+1} = h(x)$ can be expressed exclusively in terms of the transverse field components

$$\left[\frac{1}{i\omega\epsilon} \nabla_T \cdot (\bar{H}_T \times \bar{a}_x) - E_y \frac{dh}{dx} \right]_{h^-}^{h^+}, \left[E_z \right]_{h^-}^{h^+} = 0 \quad (27)$$

$$\left[\frac{1}{i\omega\mu} \nabla_T \cdot (\bar{a}_x \times \bar{E}_T) - H_y \frac{dh}{dx} \right]_{h^-}^{h^+}, \left[H_z \right]_{h^-}^{h^+} = 0. \quad (28)$$

The complete field expansions are substituted into Maxwell's equations for the transverse field components and use is made of the orthogonality relationship, Green's theorem, and the exact boundary conditions, to obtain the differential equations for the field transforms E^P and H^P . These may be expressed in terms of the forward and backward wave amplitudes a^P and b^P , respectively, as follows:

$$H^P = a^P + b^P \text{ and } E^P = a^P \mp b^P, \quad P = \begin{cases} V, & \text{upper sign} \\ H, & \text{lower sign} \end{cases} \quad (29)$$

Thus Maxwell's equations are converted into the following generalized telegraphists' equations for $P=V$ or H (Bahar, 1973c,d)

$$-\frac{da^P}{dx} - iua^P = \sum_Q \sum_V \int (S_{PQ}^{BA} a^Q + S_{PQ}^{BB} b^Q) dw' - A^P, \quad (30)$$

and

$$-\frac{db^P}{dx} + iub^P = \sum_Q \sum_V \int (S_{PQ}^{AA} a^Q + S_{PQ}^{AB} b^Q) dw' + B^P. \quad (31)$$

Explicit closed form expressions for the reflection and the transmission scattering coefficients have been derived (Bahar 1973d).

Excitations of vertically and horizontally polarized waves (with respect to the reference (x,z) plane) are considered. The terms A^P and B^P appearing in (30) and (31) account for the electric and magnetic sources \bar{J}, ρ and \bar{M}, ρ_m .

The first-order iterative solutions for the wave amplitudes a^P and b^P are obtained by neglecting the transmission and reflection scattering coefficients in (30) and (31). These first-order solutions are substituted on the right side of (30) and (31), and the resulting equations are solved to obtain the second-order iterative solution for the wave amplitudes. These second-order iterative solutions are used in the complete expansions for the electromagnetic fields to obtain the desired iterative solutions for the scattered radiation fields through the use of the steepest descent method. Thus the first-order solutions to (30) and (31) are the unperturbed vertically and horizontally polarized fields excited by the vertical electric and magnetic dipoles respectively. The second-order iterative solutions which account for depolarization and scattering in arbitrary directions are suitable when multiple scattering can be ignored. Since the full wave expressions for the fields (6), (8) are valid for all points in space, they can also be used to determine the surface fields. The above iterative procedure can be extended to account for multiple scattering. In Section 3 we consider the specific case of scattering and depolarization by a random rough interface between two semi-infinite media.

3. Scattering by Rough Surfaces— Unified and Two-Scale Formulation

The full wave solution for the radiation fields scattered by two dimensionally rough surfaces $f(x,z) = y - h(x,z) = 0$ (see Fig. 5) is expressed as follows in matrix notation

$$G^f = G_o \int_{A_{iv}} D(\vec{n}^f, \vec{n}^i) \exp[i\vec{v} \cdot \vec{r}] dA \quad G^i \equiv S G^f \quad (32)$$

in which \bar{n}^i and \bar{n}^f are unit vectors in the directions of the incident and scattered fields and the vector \bar{v} is

$$\bar{v} = (\bar{n}^f - \bar{n}^i)k_0 = v_x \bar{a}_x + v_y \bar{a}_y + v_z \bar{a}_z \quad (33)$$

where $k_0 = \omega \sqrt{\mu_0 \epsilon_0}$ is the free space wavenumber of the electromagnetic wave.

The integration is over A_{iv} the illuminated and visible portions of the rough surface and

$$\int dA = \int_{-L_z}^{L_z} \int_{-L_x}^{L_x} dx dz / \bar{n} \cdot \bar{a}_y = A_y, \quad \int \cdot dA = \int_{A_{iv}} \cdot dA \quad (34)$$

where \bar{n} is the unit vector normal to the surface $f(x, z) = 0$

$$\bar{n} = \nabla f / |\nabla f| = \frac{-h_x \bar{a}_x + \bar{a}_y - h_z \bar{a}_z}{(1 + h_x^2 + h_z^2)^{1/2}}; \quad h_x = \frac{\partial f}{\partial x}, \quad h_z = \frac{\partial f}{\partial z} \quad (35)$$

and \bar{r} is the position vector to a point on the rough surface. The elements of the 2×1 column matrix G^i are the incident vertically and horizontally polarized complex wave amplitudes G^{Vi} and G^{Hi} at the origin with $\bar{n}^i \times \bar{a}_y$ defined as the vector normal to the plane of incidence.

Similarly G^f is a 2×1 column matrix whose elements are the vertically and horizontally polarized complex wave amplitudes G^{Vf} and G^{Hf} (with $\bar{n}^f \times \bar{a}_y$ defined as the vector normal to the scatter plane) at the point given by the position vector (see Fig. 5)

$$\bar{r}^f = x \bar{a}_x + y \bar{a}_y + z \bar{a}_z = r \bar{n}^f \quad (36)$$

Thus

$$G^i = \begin{pmatrix} G^{Vi} \\ G^{Hi} \end{pmatrix} = \begin{pmatrix} E^{Vi} \\ E^{Hi} \end{pmatrix} = \eta_0 \begin{pmatrix} H^{Vi} \\ H^{Hi} \end{pmatrix} \quad (37a)$$

and

$$G^f = \begin{pmatrix} G^{Vf} \\ G^{Hf} \end{pmatrix} = \begin{pmatrix} E^{Vf} \\ E^{Hf} \end{pmatrix} = \eta_0 \begin{pmatrix} H^{Vf} \\ H^{Hf} \end{pmatrix} \quad (37b)$$

where $\eta_0 = \sqrt{\mu_0 \epsilon_0}$ is the free space wave impedance. The coefficient G_0 is given by

$$G_0 = k_0^2 \exp[-ik_0 r^f] / 2\pi i k_0 r^f \quad (38)$$

and a suppressed $\exp(i\omega t)$ time dependence is assumed in this work. The like and cross polarized local scattering matrix $D(\bar{n}^f, \bar{n}^i)$

$$D(\bar{n}^f, \bar{n}^i) = \begin{pmatrix} D^{VV} & D^{VH} \\ D^{HV} & D^{HH} \end{pmatrix} = (-\bar{n}^i \cdot \bar{n}) T^f F T^i \quad (39)$$

is derived by (a) using the 2×2 matrix $T^i(\bar{n}^{in}, \bar{n}^i)$ to transform the incident vertically and horizontally polarized wave from its representation in the fixed reference coordinate system $(\bar{a}_x, \bar{a}_y, \bar{a}_z)$ to its representation with respect to the local coordinate system $(\bar{n}_1, \bar{n}_2 = \bar{n}, \bar{n}_3)$ (the unit vector \bar{n}^{in} is the representation of the vector \bar{n}^i in the local coordinate system (see Fig. 6)), (b) using the 2×2 local scattering matrix $(-\bar{n}^i \cdot \bar{n}) \cdot F(\bar{n}^{fn}, \bar{n}^{in}) dA$ to account for like and cross polarized scattering by an element dA of the rough surface (\bar{n}^{fn} is the representation of the vector \bar{n}^f in the local coordinate system) and finally (c) using the 2×2 matrix $T^f(\bar{n}^f, \bar{n}^{fn})$ to transform the scattered vertically and horizontally polarized wave from its representation in the local coordinate system to its representation in the reference coordinate system. The full wave solutions (32) are invariant to coordinate transformations and they satisfy the duality and reciprocity relationships in electromagnetic theory. In (32) multiple scattering by the rough surface is neglected. Explicit expressions for the local scattering matrix $D(\bar{n}^f, \bar{n}^i)$ (39) are found in the published literature (Bahar 1981a).

The full wave solution for the scattered field can be applied to random rough surfaces (Bahar 1981b). Thus the scattering cross sections per unit projected area A_y for an incident wave with polarization $Q=V$ or H and scattered wave with polarization $P=V$ or H are given by

$$\langle \sigma^{PQ} \rangle = \langle \frac{k_o^2}{\pi} \left| \frac{p^{PQ}}{\bar{n} \cdot \bar{a}_y} \right|^2 P_2(\bar{n}^f, \bar{n}^i | \bar{n}) \exp(i\bar{v} \cdot (\bar{r} - \bar{r}')) \frac{dx dx' dz dz'}{A_y} \rangle \quad (40)$$

in which the symbol $\langle \cdot \rangle$ denotes the statistical average over the heights h, h' and the slopes \bar{n}, \bar{n}' . The probability density functions for the random slopes \bar{n}, \bar{n}' and random heights h, h' are assumed to be independent. In addition it is assumed that the slopes are more strongly correlated than the heights ($p(\bar{n}, \bar{n}') \rightarrow p(\bar{n})\delta(\bar{n}' - \bar{n})$). In this work the rough surface is assumed to be isotropic (independent of direction) and its characteristics are independent of position (\bar{r}). Thus the rough surface height characteristic function

$$\chi(v_y, h) = \langle \exp(i v_y h) \rangle = \int \exp(i v_y h) p(h) dh \quad (41)$$

is independent of position while the rough surface height joint characteristic function

$$\begin{aligned} \chi_2(v_y h - v_y h') &= \langle \exp[i v_y (h - h')] \rangle \\ &= \int \exp[i v_y (h - h')] p(h, h') dh dh' \end{aligned} \quad (42)$$

is only a function of distance τ measured in the (x, z) reference plane

$$\bar{r}_d = (x - x')\bar{a}_x + (z - z')\bar{a}_z, \quad |\bar{r}_d| = \tau = [(x - x')^2 + (z - z')^2]^{1/2} \quad (43)$$

In (40) $P_2(\bar{n}^f, \bar{n}^i | \bar{n})$ is the probability that a point on the rough surface is both illuminated (\bar{n}^i) and visible (\bar{n}^f) given the value of the slope (\bar{n}) at that point (Sancer, 1968).

Since the full wave solution (40) accounts for both specular point (physical optics) scattering as well as diffuse scattering in a self-consistent

manner there is no need to adopt an artificial two-scale model. To use the two-scale model, it is assumed that the surface $h_L(x, z)$ consisting of the large scale components of the surface height spectral density function $W(v_x, v_z)$ is independent of the surface $h_s(x, z)$ consisting of the small scale components of the surface height spectral density function. The surface height spectral density function is the two dimensional Fourier transform of the rough surface height autocorrelation function $\langle hh' \rangle$. Thus

$$\begin{aligned} \frac{W(v_x, v_z)}{4} &= \frac{1}{4\pi^2} \int_{-\infty}^{\infty} \langle hh' \rangle \exp(i\bar{v} \cdot \bar{r}_d) dx_d dz_d \\ &= \frac{1}{2\pi} \int_0^{\infty} \langle hh' \rangle J_0(k\tau) \tau d\tau \end{aligned} \quad (44a)$$

where J_0 is the Bessel function of order zero and the spatial wavenumber k is

$$k = v_{xz} = \sqrt{v_x^2 + v_z^2} \quad (44b)$$

in which use has been made of the fact that $\langle hh' \rangle$ is only a function of τ .

Similarly,

$$\begin{aligned} \langle hh' \rangle &= \int_{-\infty}^{\infty} \frac{W(v_x, v_z)}{4} \exp(-i\bar{v} \cdot \bar{r}_d) dv_x dv_z \\ &= 2\pi \int_0^{\infty} \frac{W(k)}{4} J_0(k\tau) k dk = R(\tau) \langle h^2 \rangle \end{aligned} \quad (45)$$

in which $|R(\tau)| \leq 1$ is the normalized correlation coefficient and $\langle h^2 \rangle$ is the mean square height

$$\langle h^2 \rangle = \langle hh' \rangle_{\tau=0} = 2\pi \int_0^{\infty} \frac{W(k)}{4} k dk \quad (46)$$

Thus using the two-scale model, it is assumed that the large scale surface h_L is associated with the surface height spectral density function $W(k)U(k_d - k)$ and the small scale surface h_s is associated with the surface height spectral density function $W(k)U(k - k_d)$ in which $U(\cdot)$ is the unit

step function and k_d is some arbitrary value of k where spectral splitting is assumed to occur (Brown 1978). Brown chooses k_d such that the parameter

$$\beta = 4k_0^2 \langle h_s^2 \rangle = 0.1 \quad (47)$$

satisfies the perturbation condition for the small scale surface. However, he shows that the computed value of the scattering cross sections critically depends on the choice of β and therefore the specified value of k_d . Bahar and Barrick (1983) considered the two-scale model using the full wave approach. It is shown that if k_d is chosen such that deep phase modulation occurs it is necessary to choose $\beta \approx 1$. For a range of values of k_d corresponding to β between 1 and 2 it is shown (Bahar et al. 1983) that the values of the scattering cross sections do not depend on k_d .

For problems of scattering by random rough surfaces the dimensions of the projected area $A_y = 4L_x L_z$ are such that $L_x \gg \tau_c$ and $L_z \gg \tau_c$ (where $R(\tau_c) = \exp(-1)$ and τ_c is the correlation length). For distances $\tau \gg \tau_c$; $\chi_2 \rightarrow |\chi|^2$ since $\langle hh' \rangle \rightarrow \langle h^2 \rangle$. Thus assuming statistical independence between the surface h_l and h_s ($p(h_l, h_s) = p(h_l)p(h_s)$) the characteristic and the joint characteristic functions of the total surface are expressed as

$$\chi = \chi^l \chi^s; \chi^s \equiv \chi^s(\vec{v} \cdot \vec{n}), \chi^l \equiv \chi^l(v_y), \chi_2^s \equiv \chi_2^s(\vec{v} \cdot \vec{n}), \chi_2^l \equiv \chi_2^l(v_y) \quad (48a)$$

$$\chi_2 = \chi_2^l \chi_2^s = (\chi_2^l - |\chi^l|^2) |\chi^s|^2 + (\chi_2^s - |\chi^s|^2) \chi_2^l + |\chi^l \chi^s|^2 \quad (48b)$$

in which the superscripts l and s denote quantities associated with the large and small scale surfaces, respectively. Using the two-scale model, it is also assumed that the slopes for the small scale (perturbation) surface are small such that slope probability density function for the total surface is equal to the slope probability function for the large scale surface $p(\vec{n}) = p(\vec{n}_l)(\vec{n}_l = \nabla f_l / |\nabla f| \text{ and } f_l = y - h_l)$. Thus the unified (U) and two-scale (T) expressions for the scattering cross sections (40) are respectively,

$$\langle \sigma^{PQ} \rangle_U = \int A^{PQ}(\bar{n}^f, \bar{n}^i, \bar{n}) p(\bar{n}) d\bar{n} \left[Q(\bar{n}^f, \bar{n}^i) + \frac{1}{A_y} |v_y \chi| \exp(i v_x x + i v_z z) dx dz \right]^2 \quad (49a)$$

where

$$Q(\bar{n}^f, \bar{n}^i) = \frac{1}{v_y^2} (\chi_2^2 - |\chi|^2) \exp(i \bar{v} \cdot \bar{r}_d) dx_d dz_d \quad (49b)$$

$$A^{PQ}(\bar{n}^f, \bar{n}^i, \bar{n}) = \frac{1}{\pi} \left| \frac{k_o D^{PQ}}{v_y \bar{n} \cdot \bar{a}_y} \right|^2 P_2 \quad (49c)$$

$$p(\bar{n}) d\bar{n} = p(h_x, h_z) dh_x dh_z \quad (49d)$$

and

$$\begin{aligned} \langle \sigma^{PQ} \rangle_T &= |\chi^S|^2 A^{PQ}(\bar{n}^f, \bar{n}^i, \bar{n}_s) \left[Q_L(\bar{n}^f, \bar{n}^i) + \frac{1}{A_y} |v_y \chi^L| \exp(i v_x x + i v_z z) dx dz \right]^2 \\ &+ \int A^{PQ}(\bar{n}^f, \bar{n}^i, \bar{n}) \bar{n} \cdot \bar{a}_y Q_s(\bar{n}^f, \bar{n}^i, \bar{n}) p(\bar{n}) d\bar{n} \\ &\equiv |\chi^S|^2 \langle \sigma^{PQ} \rangle_L + \langle \sigma^{PQ} \rangle_s \end{aligned} \quad (50a)$$

where

$$Q_L(\bar{n}^f, \bar{n}^i) = \frac{1}{v_y^2} (\chi_L^2 - |\chi|^2) \exp(i \bar{v} \cdot \bar{r}_d) dx_d dz_d \quad (50b)$$

$$Q_s(\bar{n}^f, \bar{n}^i, \bar{n}) = \frac{1}{v_y^2} (\chi_s^2 - |\chi^S|^2) \exp(i \bar{v} \cdot \bar{r}_{Ld}) dx_{Ld} dz_{Ld} \quad (50c)$$

In (49b), (50b) and (50c) the integration limits are $(-\infty, \infty)$ since $L_x, L_z \gg \tau_c$ and $A^{PQ}(\bar{n}^f, \bar{n}^i, \bar{n})$ is defined in (49c).

To derive the first term in (50a), the slope dependent function $A^{PQ}(\bar{n}^f, \bar{n}^i, \bar{n})$ is replaced by its value at the specular point where

$$\bar{n} \rightarrow \bar{n}_s = \bar{v}/v, \quad v = |\bar{v}| = \bar{v} \cdot \bar{n}_s \quad (51)$$

For surface height probability density functions that are Gaussian

$$|\chi^L|^2 = \exp(-v_y^2 \langle h^2 \rangle) \ll 1 \quad (52)$$

$$\chi_2^L = \exp(-v_y^2 \langle h_L^2 \rangle + v_y^2 \langle h_L h_L' \rangle) = \exp(v_y^2 \langle h_L h_L' \rangle) |\chi^L|^2 \quad (53)$$

Thus for $v_y^2 \langle h^2 \rangle \gg 1$ it can be shown that the two dimensional Fourier transform (50b) is given

$$Q_L(\bar{n}^f, \bar{n}^i) = 4\pi^2 p(\bar{n}_s) \quad (54)$$

in which $p(\bar{n}_s)$ is the slope probability density function at the stationary phase points (Bahar 1981c)

$$\begin{aligned}
 p(\bar{n}_s) = p(h_x, h_z) &= \frac{1}{2\pi\sigma_n^2} \exp \left[-\frac{v_{xz}^2}{2\sigma_n^2 v_y^2} \right] \\
 &= \frac{1}{2\pi\sigma_n^2} \exp \left[-\frac{(h_x^2 + h_z^2)}{2\sigma_n^2} \right]_{\bar{n}_s}
 \end{aligned} \quad (55)$$

in which the value of the slope at the specular point is

$$(h_x^2 + h_z^2)_{\bar{n}_s} = \tan^2 \gamma_s = v_{xz}^2 / v_y^2, \quad \bar{n}_s \cdot \bar{a}_y = \cos \gamma_s \quad (56a)$$

and the mean square slope σ_n^2 is

$$\sigma_n^2 = \frac{\pi}{4} \int_0^\infty W(k) k^3 dk \quad (56b)$$

Thus the first term in (50a) is given by

$$|\chi^s|^2 \langle \sigma^{PQ} \rangle_{\bar{\ell}} = |\chi^s|^2 A_y^{PQ}(\bar{n}^f, \bar{n}^i, \bar{n}_s) \left[4\pi^2 p(\bar{n}_s) + A_y |v_y \chi^{\bar{\ell}}|^2 \text{sinc}^2(v_x L_x) \text{sinc}^2(v_z L_z) \right] \quad (57)$$

in which $\text{sinc} \alpha = \sin(\alpha)/\alpha$ and $A_y = 4L_x L_z$ is the projected area of the rough surface on the x, z plane. In (57) $\langle \sigma^{PQ} \rangle_{\bar{\ell}}$ is precisely the physical optics solution for scattering by the large scale (filtered surface). Thus the coefficient $|\chi^s| < 1$ accounts for the degradation of the physical optics (specular point) contribution due to the small scale surface.

To derive the second term in (50), it is assumed that over a correlation length of the small scale surface, the large scale surface is approximately flat and that the small scale (perturbed) surface height is measured normal to the large scale surface. Thus,

$$\bar{v} \cdot (\bar{r} - \bar{r}') = \bar{v} \cdot (\bar{r}_{\bar{\ell}} - \bar{r}'_{\bar{\ell}}) + \bar{v} \cdot (h - h') \bar{a}_y = \bar{v} \cdot \bar{r}_{\bar{\ell}d} + \bar{v} \cdot \bar{n} (h - h') \quad (58)$$

in which the distance $\bar{r}_{\bar{\ell}d}$ is measured along the large scale surface in the local coordinate system $(\bar{n}_1, \bar{n}_2 = \bar{n}, \bar{n}_3)$

$$\bar{r}_{\bar{\ell}d} = x_{\bar{\ell}d} \bar{n}_1 + z_{\bar{\ell}d} \bar{n}_3, \quad |\bar{r}_{\bar{\ell}d}| = r_{\bar{\ell}} = (x_{\bar{\ell}d}^2 + z_{\bar{\ell}d}^2)^{1/2} \quad (59)$$

Thus in the expression for $\langle \sigma^{PQ} \rangle_s$, the integration is with respect to distances measured along the large scale surface and not the reference surface. This is in agreement with the expressions obtained intuitively by Wright and Valenzuela "mostly based on physical considerations" (Wright, 1968; Valenzuela, 1968). Thus $\langle \sigma^{PQ} \rangle_s$ can be regarded as an average of the scattered power from patches of slightly rough surfaces that ride the large scale surface. Brown's (1978) solutions which are based on a combination of Burrows' perturbation theory (Burrows 1967) and physical optics (Beckmann 1963) are in agreement with the full wave expressions for $\langle \sigma^{PQ} \rangle_s$ only in the limit of small scale slopes since in his work h_s is measured normal to the reference plane. However, in Burrows' perturbation theory the small scale surface height h_s is measured normal to the large scale surface h_L .

The two-dimensional Fourier transform (49b) can be expressed as

$$Q(\bar{n}^f, \bar{n}^i) = 2\pi v_y^2 \int_0^\infty (\chi_2(v_y) - |\chi(v_y)|^2) J_0(v_{xz}\tau) \tau d\tau \quad (60)$$

since the surface height correlation function $\langle hh' \rangle$ is only a function of

$\tau = r_d = |\bar{r}_d|$. The corresponding expression for the Fourier transform

(50c) is dependent on the slope. Thus

$$Q_s(\bar{n}^f, \bar{n}^i, \bar{n}) = 2\pi v_y^2 \int_0^\infty (\chi_2^s(\bar{v} \cdot \bar{n}) - |\chi^s(\bar{v} \cdot \bar{n})|^2) J_0(v_{xzl}\tau_l) \tau_l d\tau_l \quad (61)$$

in which

$$\bar{v} \cdot \bar{r}_{ld} = \bar{v} \cdot (x_{ld}\bar{n}_1 + z_{ld}\bar{n}_3) = v_{xl} x_{ld} + v_{zl} z_{ld} \quad (62a)$$

$$\bar{v} \cdot \bar{n} \equiv v_{yl}, \quad v_{xzl} = [v_{xl}^2 + v_{zl}^2]^{1/2} \quad (62b)$$

and v_{xl} , v_{zl} and v_{yl} are the components of \bar{v} in the local coordinate system

$(\bar{n}_1, \bar{n}_2 \approx \bar{n}, \bar{n}_3)$. Thus the scattering cross sections can be expressed as

follows for the unified and two-scale models

$$\langle \sigma^{PQ} \rangle_U = \int A^{PQ}(\bar{n}^f, \bar{n}^i, \bar{n}) P(\bar{n}) d\bar{n} [Q(\bar{n}^f, \bar{n}^i) + A_y |v_y \chi|^2 \text{sinc}^2(v_x L_x) \text{sinc}^2(v_z L_z)] \quad (63)$$

and

$$\begin{aligned} \langle \sigma^{PQ} \rangle_T = & \int_{\bar{n}_s} |\chi^s|^2 A^{PQ}(\bar{n}^f, \bar{n}^i, \bar{n}_s) [Q_\ell(\bar{n}^f, \bar{n}^i) + A_y |v_y \chi^\ell|^2 \text{sinc}^2(v_x L_x) \text{sinc}^2(v_z L_z)] \\ & + \int A^{PQ}(\bar{n}^f, \bar{n}^i, \bar{n}) \bar{n} \cdot \bar{a}_y Q_s(\bar{n}^f, \bar{n}^i, \bar{n}) p(\bar{n}) d\bar{n} \end{aligned} \quad (64)$$

To facilitate the computations in (64) in which Q_s is a function of \bar{n} , for a given \bar{v} and $R(\tau)$, a set of values of Q_s/v_y^2 are first computed and stored as a function of

$$\bar{v} \cdot \bar{n} = (-v_x h_x + v_y - v_z h_z) / (1 + h_x^2 + h_z^2)^{1/2} \quad (65)$$

The integration with respect to $d\bar{n} = dh_x dh_z$ is performed using values of Q_s interpolated from the stored set. For Gaussian surface height probability density functions (52) and (53)

$$\begin{aligned} Q_s(\bar{n}^f, \bar{n}^i, \bar{n}) &= 2\pi v_y^2 \int \exp(-v_y^2 \langle h_s^2 \rangle) \left[\exp[v_y^2 \langle h_s^2 \rangle R(\tau_\ell)] - 1 \right] J_0(v_{xz} \ell \tau_\ell) \tau_\ell d\tau_\ell \\ &= v_y^2 f(\bar{n}^f, \bar{n}^i, \bar{v} \cdot \bar{n}) \xrightarrow{\beta \ll 1} \pi^2 v_y^2 |\chi^s(\bar{v} \cdot \bar{n})|^2 W(v_{xz} \ell) \end{aligned} \quad (66)$$

Thus for $\bar{n} \rightarrow \bar{a}_y$ and $\beta \ll 1$ the last term in (64) $\langle \sigma^{PQ} \rangle_s$ reduces to the perturbation solution (Bahar 1981c)

$$\langle \sigma^{PQ} \rangle_s \rightarrow \langle \sigma^{PQ} \rangle_P = \pi k_o^2 v_y^2 |\chi^s(v_y) (-\bar{n}^i \bar{n}) F(\bar{n}^f, \bar{n}^i)|^2 W(v_{xz}) \quad (67)$$

Note that (64) reduces to (63) if we set $\langle h_\ell^2 \rangle \rightarrow 0$ and (63) reduces to (64) if we set $\langle h_s^2 \rangle \rightarrow 0$ and replace $A^{PQ}(\bar{n}^f, \bar{n}^i, \bar{n})$ by $A^{PQ}(\bar{n}^f, \bar{n}^i, \bar{n}_s)$. The term containing the product of the sinc functions is the coherent scattered field. This term vanishes as $|\chi(v_y)|^2 \rightarrow 0$.

For cases in which the physical optics solutions are valid the corresponding geometrical optics expressions for $\langle \sigma^{PQ} \rangle_\ell$ are obtained by replacing \bar{n} by \bar{n}_s in (32) and integrating over the area A_{iv} (using the stationary phase method) before the expectations $\langle \cdot \rangle$ are evaluated. Thus in the neighborhood of a stationary phase point $\bar{r} = \bar{r}_{op}$, where $v_x + v_y h_x$ and $v_z + v_y h_z = 0$ (Barrick 1970, Bahar 1981b) it can be shown

that

$$\int \exp[i\vec{v} \cdot \vec{r}] \frac{dx dz}{\vec{n} \cdot \vec{a}_y} = \int \exp[i\vec{v} \cdot \vec{r}_{op}] \exp\left\{\frac{i\vec{v} \cdot \vec{n}_s}{2} [h_{xxo} x_p^2 + h_{zzo} z_p^2]\right\} dx_p dz_p$$

$$\longrightarrow \frac{\exp[i\vec{v} \cdot \vec{r}_{op}]}{\vec{v} \cdot \vec{n}_s} \frac{(2\pi i)}{\sqrt{h_{xxp} h_{zzp}}}, \quad \vec{v} \cdot \vec{n}_s = 2k_o (-\vec{n}^i \cdot \vec{n}_s) \quad (68)$$

in which the integral has been expressed in terms of the local coordinates at the stationary plane point (x_p, y_p, z_p) associated with the unit vectors $(\vec{n}_1, \vec{n}_2 = \vec{n}, \vec{n}_3)$ and \vec{n}_1 and \vec{n}_3 , the vectors in the tangent plane, are chosen such that the principal radii of curvature $r_{xp} = |1/h_{xxs}|$ and $r_{zp} = |1/h_{zzs}|$ are measured along the \vec{n}_1 and \vec{n}_3 directions. As seen by an observer in the region $y > h(x, z)$, the curvatures h_{xxp} and h_{zzp} are positive when the surface is concave. They are negative when the surface is convex. When h_{xxp} or h_{zzp} are negative, they are expressed $\sqrt{h_{xxp}} = i/\sqrt{r_{xp}}$ and $\sqrt{h_{zzp}} = i/\sqrt{r_{zp}}$. Thus the geometric optics contribution to the normalized cross section from N randomly located specular points per unit surface area is

$$(\sigma^{PQ})_{op} = \pi r_{xp} r_{zp} N \left| [T^f_F T^i]_{\vec{n}_s}^{PQ} \right|_{P_2}^2 (\vec{n}^f, \vec{n}^i | \vec{n}_s) \quad (69)$$

in which

$$F(\vec{n}^f, \vec{n}^i)_{\vec{n}_s} = \begin{bmatrix} R_V(\theta_{op}^i) & 0 \\ 0 & R_H(\theta_{op}^i) \end{bmatrix} \quad (70)$$

and $R_V(\theta_{op}^i)$ and $R_H(\theta_{op}^i)$ are the Fresnel reflection coefficients at the specular points where the local angles of incidence and scatter are $-\vec{n}^i \cdot \vec{n}_s = \vec{n}^f \cdot \vec{n}_s = \cos \theta_{op}^i$. Note however, that the surface will depolarize the incident wave if the triple products $(\vec{n} \cdot \vec{n}^i \cdot \vec{a}_y)$ and $(\vec{n} \cdot \vec{n}^f \cdot \vec{a}_y)$ do not vanish. (When $(\vec{n} \cdot \vec{n}^i \cdot \vec{a}_y)$ and $(\vec{n} \cdot \vec{n}^f \cdot \vec{a}_y)$ vanish T^i and T^f become identity matrices).

The expectation of $(r_{xp} r_{zp} N)$ in (64) (Barrick, 1972, Barrick and

Bahar 1981) is

$$\langle r_{xp} r_{zp} N \rangle = p(\bar{n}_s) / (\bar{n}_s \cdot \bar{a}_y) \quad , \quad \bar{n}_s \cdot \bar{a}_y = v_y / (\bar{v} \cdot \bar{n}_s) \quad (71)$$

thus

$$\langle \sigma^{PQ} \rangle_\infty = \frac{\pi}{(\bar{n}_s \cdot \bar{a}_y)^4} p(\bar{n}_s) \left[T^f T^i \right]_{\bar{n}_s}^{PQ} P_2(\bar{n}^f, \bar{n}^i | \bar{n}_s) \quad (72)$$

in agreement with $\langle \sigma^{PQ} \rangle_\ell$. Thus for backscatter geometric optics theory predicts no depolarization and for the like polarized case

$$\langle \sigma^{PP}(\bar{n}^f = -\bar{n}^i) \rangle_\infty = \frac{\pi}{(\bar{n}_s \cdot \bar{a}_y)^4} p(\bar{n}_s) P_2(-\bar{n}^i, \bar{n}^i | \bar{n}_s) \left| R_p(\theta_o=0) \right|^2 \quad (73)$$

4. Concluding Remarks

The solutions for the backscatter like and cross polarized cross sections based on the unified full wave solutions has been compared with the solution based on the two-scale model. For the two-scale model the wavenumber k_d where spectral splitting is assumed to occur is chosen such that $\beta = 4k_o^2 \langle h_s^2 \rangle = 1$, (Bahar et al. 1983). It is also assumed that the two surfaces h_ℓ and h_s are statistically independent, and the slope of the small scale surface was neglected ($\bar{n} = \bar{n}_\ell$). Except for near grazing angles the two solutions for the like polarized cross sections are in good agreement. For the cross polarized case, the difference between the two solutions is most significant near normal incidence. The large discrepancy near normal incidence is due to the fact that elements of the rough surface that are oriented specularly do not depolarize the backscattered wave. The depolarization comes from the neighborhood of these specular points and even the filtered large scale surface depolarizes the incident waves (Bahar and Fitzwater 1984). However, the physical optics contribution to cross polarization is zero.

The discrepancy near grazing angles is due to the fact that for $\theta_o^i \rightarrow \pi/2$, there are practically no specular points on the surface and again the physical optics approximations are invalid.

Acknowledgments

This investigation was sponsored by the U.S. Army Research Office
Contract DAAG-29-82-K-0123.

5. References

1. Bahar, E., (1973a), "Electromagnetic Wave Propagation in Inhomogeneous Multilayered Structures of Arbitrary Thickness-Generalized Field Transforms," J. Math. Phys., Vol. 14, No. 8, pp. 1024-1029.
2. Bahar, E., (1973b), "Electromagnetic Wave Propagation in Inhomogeneous Multilayered Structures of Arbitrary Thickness-Full Wave Solutions," J. Math. Phys., Vol. 14, No. 8, pp. 1030-1036.
3. Bahar, E., (1973c), "Depolarization of Electromagnetic Waves Excited by Distributions of Electric and Magnetic Sources in Inhomogeneous Multilayered Structures of Arbitrarily Varying Thickness--Generalized Field Transforms," J. Math. Phys., Vol. 14, No. 11, pp. 1502-1509.
4. Bahar, E., (1973d), "Depolarization of Electromagnetic Waves Excited by Distributions of Electric Magnetic Sources in Inhomogeneous Multilayered Structures of Arbitrarily Varying Thickness--Full Wave Solutions," J. Math. Phys., Vol. 14, No. 11, pp. 1510-1515.
5. Bahar, E., "Depolarization in Nonuniform Multilayered Structures--Full Wave Solutions," J. Math. Phys., Vol. 15, No. 2, pp. 202-208, 1974.
6. Bahar, E. (1981a), "Full-Wave Solutions for the Depolarization of the Scattered Radiation Fields by Rough Surfaces of Arbitrary Slope," IEEE Transactions on Antennas and Propagation, Vol. AP-29, No. 3, May 1981.
7. Bahar, E. (1981b), "Scattering Cross Sections from Rough Surfaces--Full Wave Analysis," Radio Science, Vol. 16, No. 3, pp. 331-341.
8. Bahar, E. (1981c), "Scattering Cross Sections for Composite Random Surfaces--Full Wave Analysis," Radio Science, Vol. 16, No. 6, pp. 1327-1335.
9. Bahar, E., (1982), "Scattering and Depolarization by Rough Surfaces Near Grazing Angles--Full Wave Solutions," IEEE Transactions on Antennas and Propagation, Vol. AP-30, No. 4, pp. 712-719.
10. Bahar, E. and D. E. Barrick (1983), "Scattering Cross Sections for Composite Rough Surfaces that Cannot be Treated as Perturbed Physical Optics Problems," Radio Science, Vol. 18, No. 2, pp. 129-137.
11. Bahar, E., D. E. Barrick and M. A. Fitzwater (1983), "Computations of Scattering Cross Sections for Composite Surfaces and the Specification of the Wavenumber Where Spectral Splitting Occurs," IEEE Transactions on Antennas and Propagation, Vol. AP-31, No. 5, pp. 698-709.
12. Bahar, E. and M. A. Fitzwater (1984), "Scattering Cross Sections for Composite Rough Surfaces Using the Unified Full Wave Approach," IEEE Transactions on Antennas and Propagation, Vol. AP-32, No. 7, pp. 730-734.

13. Barrick, D. E. (1970), "Rough Surfaces," in Radar Cross Section Handbook, Chapter 9, Plenum Press, New York.
14. Barrick, D. E. (1981), "Remote Sensing of Sea State by Radar," in Remote Sensing of the Troposphere, V. E. Derr, Ed., Washington, D.C.: U. S. Government Printing Office, pp. 12.1-12.24.
15. Barrick, D. E. and E. Bahar, (1981), "Rough Surface Scattering Using Specular Theory," IEEE Transactions on Antennas and Propagation, Vol. AP-29, No. 5, pp. 798-800.
16. Beckmann, P., and A. Spizzichino, (1963), The Scattering of Electromagnetic Waves from Rough Surfaces, MacMillan, New York.
17. Brown, G. S., (1978), "Backscattering from a Gaussian-Distributed Perfectly Conducting Rough Surface," IEEE Transactions on Antennas and Propagation, Vol. AP-26, No. 3, pp. 472-482.
18. Burrows, M. L., (1967), "On the Composite Model for Rough Surface Scattering," IEEE Transactions on Antennas and Propagation, Vol. AP-21, No. 2, pp. 241-243.
19. Sancer, M. I. (1968), "Shadow-Corrected Electromagnetic Scattering from a Randomly Rough Surface," IEEE Transactions on Antennas and Propagation, Vol. AP-17, No. 5, pp. 577-585.
20. Schlak, G. A., and J. R. Wait (1967), "Electromagnetic Wave Propagation Over a Nonparallel Stratified Conducting Medium," Can. J. Phys., Vol. 45, pp. 3697-3720.
21. Schlak, G. A., and J. R. Wait (1968), "Attenuation Function for Propagation Over a Nonparallel Stratified Ground," Can. J. Phys., Vol. 46, pp. 1135-1136.
22. Valenzuela, G. R. (1968), "Scattering of Electromagnetic Waves from a Tilted Slightly Rough Surface," Radio Science, Vol. 3, No. 11, pp. 1051-1066.
23. Wright, J. W. (1968), "A New Model for Sea Clutter," IEEE Transactions on Antennas and Propagation, Vol. AP-16, No. 2, pp. 217-223.
24. Wait, J. R., (1962), Electromagnetic Waves in Stratified Media, MacMillan, New York.

6. Figure Captions

1. Electric and magnetic sources distributed in the layers of a uniform multilayered structure.
2. Electric and magnetic sources distributed in the layers of a nonuniform multilayered structure.
3. Principal elements of the full wave approach.
4. Principal properties of full wave approach.
5. Planes of incidence and scatter with respect to the reference coordinate system. Mean (reference plane for rough surface is $y = 0$).
6. Local planes of incidence and scatter and local coordinate system $(\bar{n}^1, \bar{n}_2, \bar{n}_3)$.

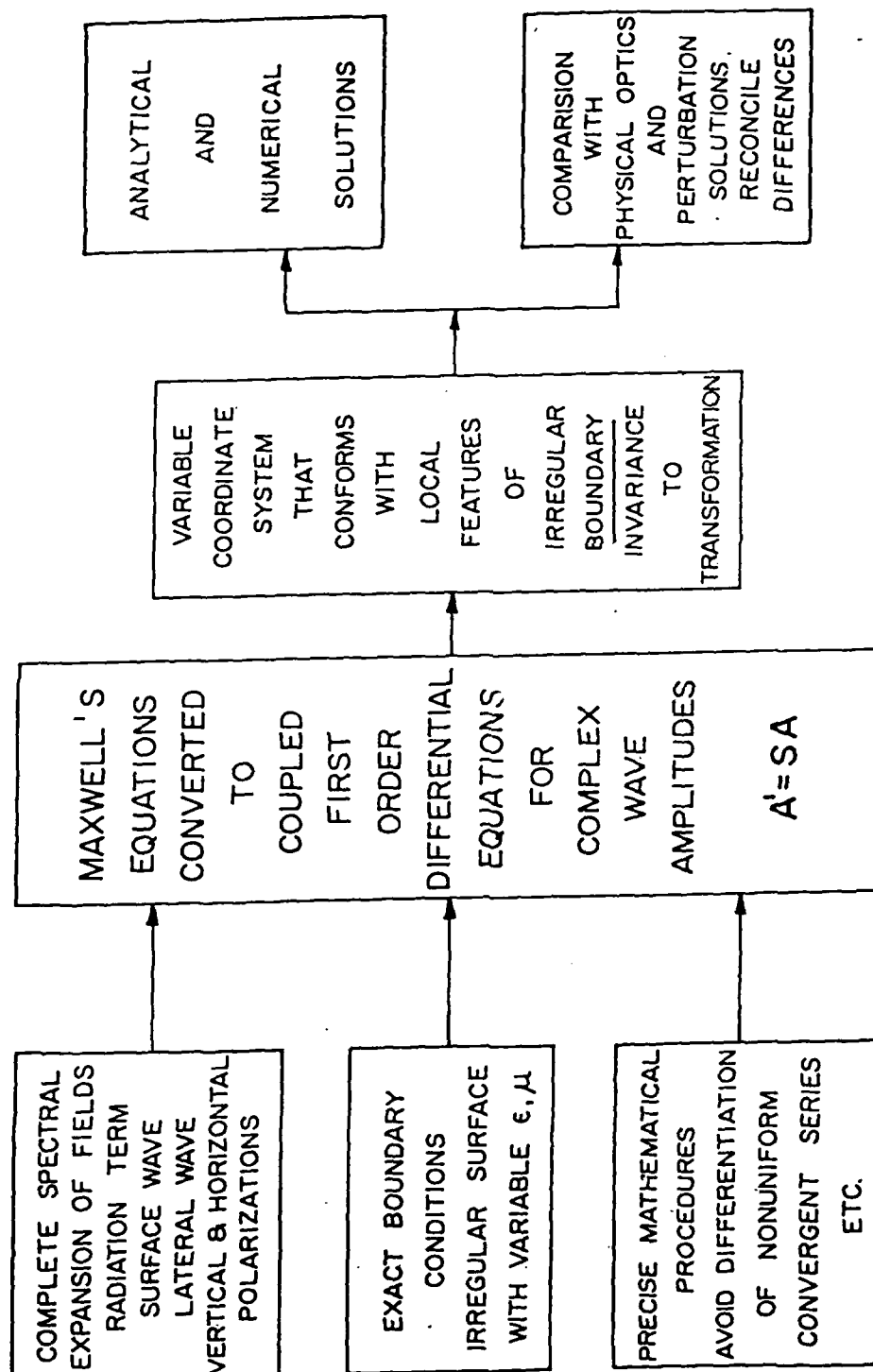


FIG. 3. Principal elements of the full wave approach.

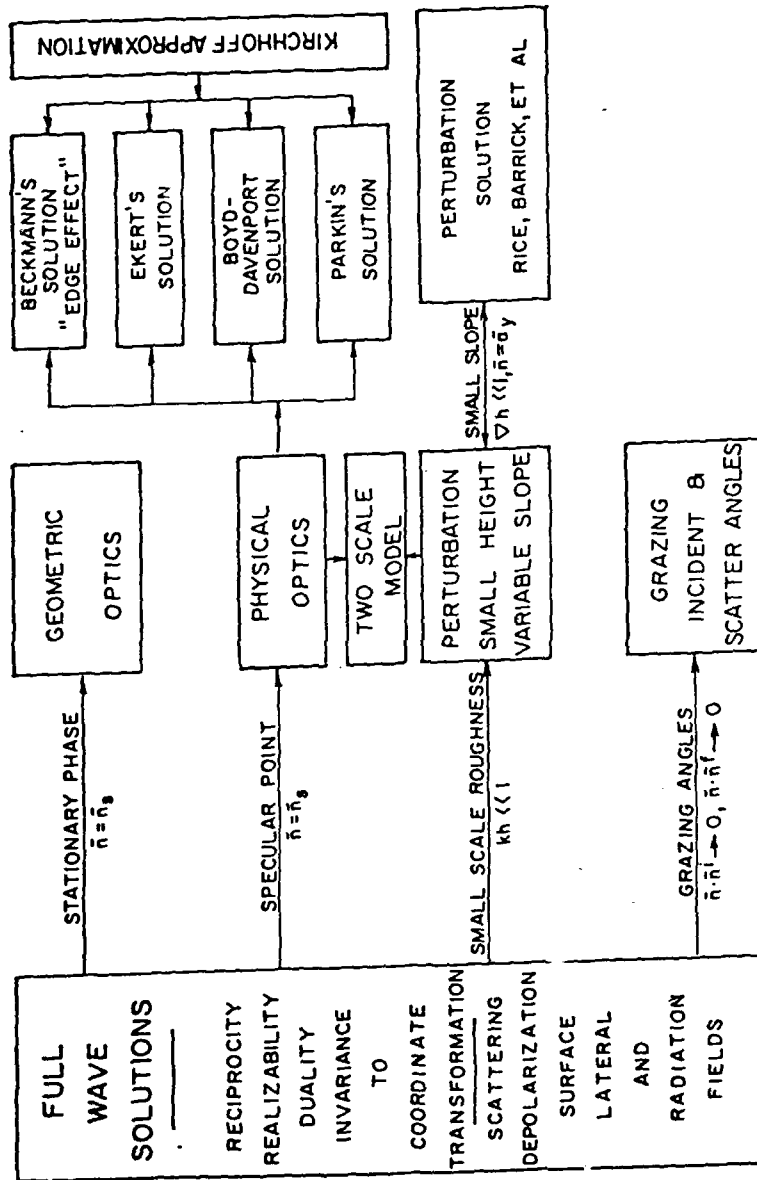


FIG. 4. Principal properties of full wave approach.

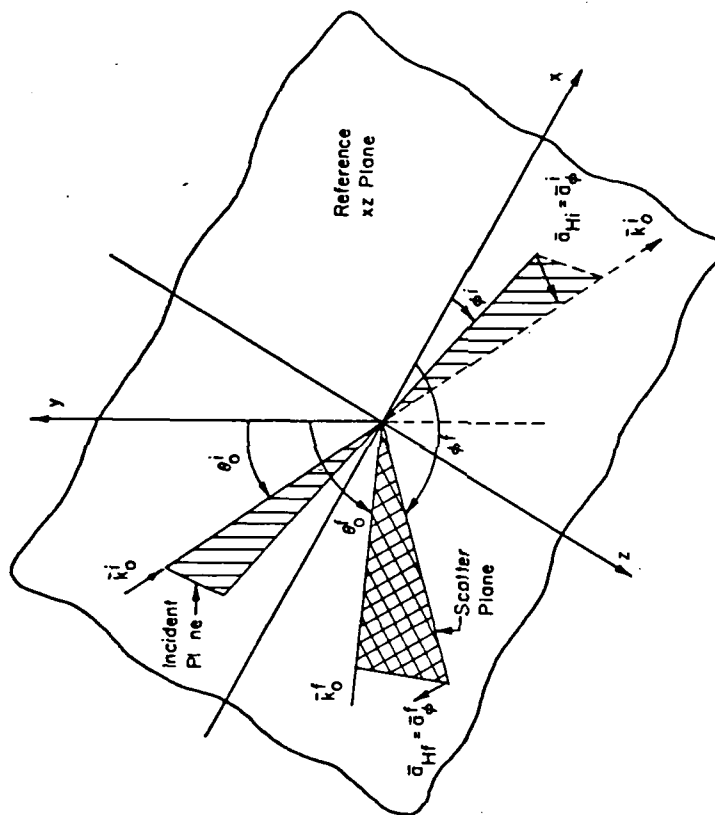


Figure 5. Planes of incidence and scatter with respect to the reference coordinate system. Mean (reference) plane for rough surface is $y = 0$.

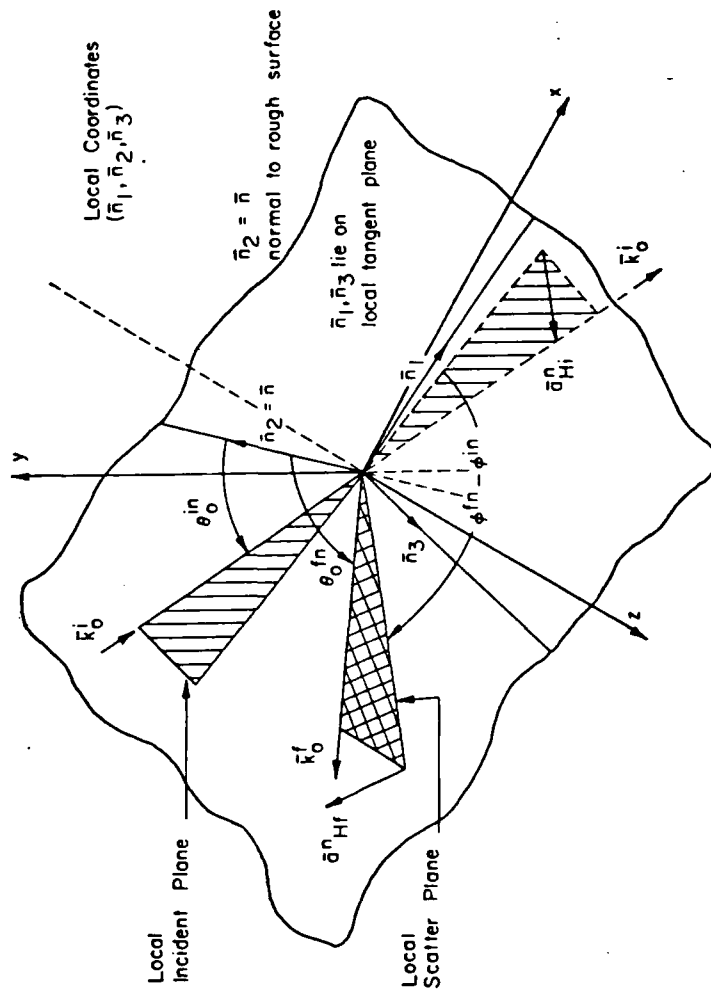


Figure 6. Local planes of incidence and scatter and local coordinate system with vectors \bar{n}_1 , \bar{n}_2 and \bar{n}_3 .

MULTIPLE SCATTERING IN MEDIA CONSISTING OF NONSPHERICAL
FINITELY CONDUCTING PARTICLES

Ezekiel Bahar and Mary Ann Fitzwater
Electrical Engineering Department
University of Nebraska--Lincoln
Lincoln, Nebraska 68588-0511

RECENT PUBLICATIONS, SUBMITTALS FOR PUBLICATION AND PRESENTATIONS:

- A) E. Bahar, "Scattering and Depolarization by Very Long Finitely Conducting Cylinders with Rough Surfaces," 1984 CRDC Scientific Conference on Obscuration and Aerosol Research, Aberdeen, Maryland, June 25-29, 1984.
- B) E. Bahar, "Scattering and Depolarization of Radio Waves by Rough Planetary Surfaces," International Union of Radio Science Symposium on Radio Techniques in Planetary Exploration, in conjunction with the XXI General Assembly of URSI, Florence, Italy, August 26-September 6, 1984.
- C) E. Bahar and M. A. Fitzwater, "Scattering Cross Sections for Composite Rough Surface Using the Unified Full Wave Approach," IEEE Transactions on Antennas and Propagation, Vol. AP-32, No. 7, pp. 730-734, July 1984.
- D) E. Bahar, "Scattering by Anisotropic Models of Composite Rough Surface-Full Wave Solutions," IEEE Transactions on Antennas and Propagation, Vol. AP-33, No. 1, pp. 106-112, January 1985.
- E) E. Bahar and S. Chakrabarti, "Scattering and Depolarization by Large Conducting Spheres with Very Rough Surfaces," Applied Optics, Vol. 24, No. 12, pp. 1820-1825, June 1985.
- F) E. Bahar, "Scattering by Anisotropic Models of Composite Rough Surfaces--Full Wave Solutions," International IEEE/APS-Symposium and 1985 North American Radio Science Meeting, Vancouver, Canada, June 17-21, 1985.
- G) E. Bahar, "Multiple Scattering in Media Consisting of Nonspherical, Finitely Conducting Particles, 1985 CRDC Scientific Conference on Obscuration and Aerosol Research, Aberdeen, Maryland, June 17-21, 1985.
- H) E. Bahar, "Scattering and Depolarization by Random Rough Surfaces--Unified Full Wave Approach," Symposium/Workshop on Multiple Scattering of Waves in Random Media and by Random Rough Surfaces," Pennsylvania State University, University Park, Pennsylvania, July 29-August 1, 1985.
- I) E. Bahar, "Unified Full Wave Solutions for Electromagnetic Scattering by Rough Surfaces--Comparison with Physical Optics, Geometric Optics and Perturbation Solutions Using Two-Scale Models of Rough Surfaces," Schlumberger Doll Research Workshop on Waves in Inhomogeneous Media, August 8-9, 1985.
- J) E. Bahar, "Scattering and Depolarization by Conducting Cylinders with Rough Surfaces," DRSMC-CLJ-IR, pp. 365-371, January 1985.
- K) E. Bahar and M. A. Fitzwater, "Like and Cross Polarized Scattering Cross Sections for Random Rough Surfaces--Theory and Experiment," Journal of the Optical Society of America Special Issue on Wave Propagation and Scattering in Random Media--in press.
- L) E. Bahar and M. A. Fitzwater, "Scattering and Depolarization by Conducting Cylinders with Rough Surfaces," submitted for review.
- M) E. Bahar and M. A. Fitzwater, "Multiple Scattering by Irregular Shaped Particles of Finite Conductivity at Infrared and Optical Frequencies," submitted for review.

ABSTRACT

The incoherent specific intensities for the waves scattered by a random distribution of particles with rough surfaces are derived. Since large roughness scales are considered, the diffuse scattering contributions to the like and cross polarized scattering cross sections are given by the full wave solutions. The scattering matrix in the expression for the equation of transfer is given by a weighted sum of the scattering matrix for the smooth particle and the diffuse contribution due to the rough surface of the particle. Illustrative examples are presented for the propagation of a circularly polarized wave normally incident upon a parallel layer of particles. Particles with different surface height spectral density functions, roughness scales, complex permittivities and sizes are considered. Both first order (single scatter) and multiple scatter solutions are provided and the results for particles with smooth and rough surfaces are compared.

1. INTRODUCTION

Scattering of electromagnetic waves in media consisting of random distributions of particles has been investigated extensively using the equation of transfer (Chandrasekhar 1950, Ishimaru 1978). The main difficulty in setting up the equation of transfer lies in the determination of the elements of the 4×4 scattering matrix for the individual particles. Thus most of the work has been done for particles of idealized shapes such as spheres.

In this work a method is presented for the modification of the results derived for particles with idealized shapes to account for the random surface roughness of the particles. To this end the full wave approach was used to determine the rough surface contributions to the like and cross polarized scattering cross sections and the elements of the scattering matrix are given in terms of a weighted sum of the Mie solutions and the diffuse scattering terms due to the particle surface roughness (See Section 2). For convenience in this work a circularly polarized wave is assumed to be normally incident upon a parallel layer consisting of a random distribution of irregular shaped particles.

For the illustrative examples presented in Section 3 both first order (single scatter) and multiple scatter results are presented for smooth particles and for particles with rough surfaces. The matrix characteristic value technique is used to account for multiple scattering (Ishimaru and Cheung 1980).

2. FORMULATION OF THE PROBLEM

In this section the principal elements of the full wave solutions for the like and cross polarized differential scattering cross sections of nonspherical particles are summarized. The contributions of these cross sections to the familiar equation of transfer (Ishimaru 1978), in a medium consisting of a random distribution of nonspherical particles are also indicated explicitly.

The radius vector from the center to the irregular surface of the particle is given by (see Fig. 1)

$$\vec{r}_s = h_0 \vec{a}_r + h_s \vec{a}_r \quad (2.1)$$

in which \vec{a}_r is the unit vector in the direction of the radius vector, h_0 is the radius of the unperturbed sphere and h_s is the random rough surface height measured in the direction normal to the surface of the unperturbed sphere. In this work it is assumed that the mean square of the rough surface height, $\langle h_s^2 \rangle$, can be sufficiently large such that standard perturbation techniques are not applicable (Barrick 1970). Thus the rough surface parameter, $\beta = 4h_0^2 \langle h_s^2 \rangle$, considered in this work is in the range $0 < \beta < 10$.

The full wave solutions for the normalized scattering cross sections $\langle \sigma^{ij} \rangle$ per unit cross sectional area ($A_y = \pi h_0^2$) are expressed as a weighted sum (Babar and Chakrabarti 1985)

$$\langle \sigma^{ij} \rangle = \langle \sigma^{ij} \rangle_L + \langle \sigma^{ij} \rangle_R \quad (2.2)$$

the symbol $\langle \cdot \rangle$ denotes the statistical average. In the above expression the first and second superscripts indicate the polarizations of the scattered and incident waves respectively. Thus $i, j = 1$ denotes Vertical polarization and $i, j = 2$ denotes Horizontal polarization. The cross section $\langle \sigma^{ij} \rangle_s$ is the modified cross section associated with the unperturbed sphere.

$$\langle \sigma^{ij} \rangle_s = |\chi^s(v)|^2 \langle \sigma^{ij} \rangle_{\text{Mie}} \quad (2.3)$$

In (2.3) $\langle \sigma^{ij} \rangle_{\text{Mie}}$ is the Mie solution (Ishimaru 1978), for the like and cross polarized cross sections of the unperturbed sphere. For large spheres, $k_0 a_0 > 20$, (k_0 is the free space wavenumber), the most significant parts of the solution are the specularly reflected wave and the shadow forming wave (Morse and Feshbach 1954). The coefficient of $\langle \sigma^{ij} \rangle_{\text{Mie}}$ is the rough surface height characteristic function

$$\chi^s(v) = \langle \exp i v h_s \rangle \quad (2.4)$$

in which v is the magnitude of the vector

$$\vec{v} = k_0 (\vec{n}^f - \vec{n}^i) \quad (2.5)$$

where \vec{n}^f and \vec{n}^i are unit vectors in the direction of the scattered and incident wave normals. The coefficient $|\chi^s|^2$ accounts for the degradation of the reflected wave due to surface roughness. The coefficient is minimum for backscatter and approaches unity for forward scattering.

The second term in (2.2) $\langle \sigma^{ij} \rangle_s$ is the contribution to the total scattering cross section due to the surface roughness. It is expressed as (Bahar and Chakrabarti 1985)

$$\langle \sigma^{ij} \rangle_s = \int A^{ij}(\vec{n}^f, \vec{n}^i, \vec{n}) (\vec{n} \cdot \vec{a}_y) Q_s(\vec{n}^f, \vec{n}^i, \vec{n}) p(\vec{n}) d\vec{n} \quad (2.6)$$

in which \vec{n} is a unit vector normal to the surface of the scatterer,

$$A^{ij}(\vec{n}^f, \vec{n}^i, \vec{n}) = \frac{1}{\pi} \left| \frac{k_0 p^{ij}}{(\vec{v} \cdot \vec{a}_x)(\vec{a}_y \cdot \vec{n})} \right|^2 P_2(\vec{n}^f, \vec{n}^i | \vec{n}) \quad (2.7)$$

$$Q_s(\vec{n}^f, \vec{n}^i, \vec{n}) = (\vec{v} \cdot \vec{a}_x)^2 \int_{-\infty}^{\infty} (\chi_2^s(\vec{v} \cdot \vec{a}_x) - |\chi^s(\vec{v} \cdot \vec{a}_x)|^2) \exp(i \vec{v} \cdot \vec{r}_d) dx_d dz_d \quad (2.8)$$

and $p(\vec{n})$ is the probability density function for the slope of the surface of the scatterer. In (2.7), P_2^{ij} is the scattering coefficient which depends on the polarizations and the directions of the wave normals for the incident and scattered waves as well as the complex electromagnetic parameters (ϵ, μ) of the scatterers. The term $P_2(\vec{n}^f, \vec{n}^i | \vec{n})$ is the probability that a point on the rough surface is both illuminated by the source and visible to the observer given the slopes (\vec{n}) of the surface of the scatterer (Smith 1967, Sancer 1969). Since $\vec{n} = \vec{a}_x$, $P_2 = u(-\vec{n}^i \cdot \vec{n}) u(\vec{n}^f \cdot \vec{n})$ where $u(\cdot)$ is the unit step function.

In (2.8) $\chi_2^s(\vec{v} \cdot \vec{a}_x)$ is the rough surface height joint characteristic function

$$\chi_2^s(\vec{v} \cdot \vec{a}_x) = \langle \exp[i v_x (h_s - h_s')] \rangle \quad (2.9)$$

in which $v_x = \vec{v} \cdot \vec{a}_x$.

With the above expressions for the scattering cross sections (2.2), the general expression for the equation of transfer (Ishimaru 1978) can be written as follows for a plane parallel slab consisting of rough spherical particles (see Fig. 2)

$$\mu \frac{d[I]}{dz} = -[I] + \int [S][I'] d\mu' d\phi' + [I_1] \quad (2.10)$$

In (2.10) τ is the optical distance in the z direction (normal to the plane parallel slab)

$$\tau = \rho[\sigma_t]z \equiv \int \sigma_t n(D) dD z, \quad D = 2h_0 \quad (2.11)$$

where $n(D)$ is the particle size distribution and σ_t is the extinction coefficient. Since $\langle \sigma^{1j} \rangle$ vanishes in the forward direction, the extinction matrix (Ishimaru and Cheung 1980) for the rough sphere, can be represented by a scalar quantity. The matrices $[I]$ and $[I']$ are the (4×1) incoherent specific diffuse intensity matrices for waves scattered from the particles in the direction $\theta = \cos^{-1}\mu$ and ϕ and for waves incident in the direction $\theta' = \cos^{-1}\mu'$ and ϕ' , respectively. The elements of $[I]$ are the modified Stokes' parameters. The (4×4) scattering matrix $[S]$ in the reference coordinate system can be expressed in terms of the scattering matrix $[S']$ in the scattering plane as follows:

$$[S] = [\mathcal{L}(-\mu + \alpha)][S'][\mathcal{L}(\alpha')] \quad (2.12)$$

in which

$$[S'] = \chi^2 (\vec{v} \cdot \vec{a}_r)^2 [S_{Mie}] + [S_s] \quad (2.13)$$

In (2.13) $[S_{Mie}]$ is given by

$$[S_{Mie}] = \frac{1}{\rho[\sigma_t]} \begin{bmatrix} \rho[|f_{11}|^2] & \rho[|f_{12}|^2] & \rho \text{Re}[f_{11}^* f_{12}] & -\rho \text{Im}[f_{11}^* f_{12}] \\ \rho[|f_{21}|^2] & \rho[|f_{22}|^2] & \rho \text{Re}[f_{21}^* f_{22}] & -\rho \text{Im}[f_{21}^* f_{22}] \\ \rho 2 \text{Re}[f_{11}^* f_{21}] & \rho 2 \text{Re}[f_{12}^* f_{22}] & \rho \text{Re}[f_{11}^* f_{22} + f_{12}^* f_{21}] & -\rho \text{Im}[f_{11}^* f_{22} - f_{12}^* f_{21}] \\ \rho 2 \text{Im}[f_{11}^* f_{21}] & \rho 2 \text{Im}[f_{12}^* f_{22}] & \rho \text{Im}[f_{11}^* f_{22} + f_{12}^* f_{21}] & \rho \text{Re}[f_{11}^* f_{22} - f_{12}^* f_{21}] \end{bmatrix} \quad (2.14)$$

where f_{ij} are elements of the 2×2 scattering amplitude matrix $[f]$ and $\rho[\cdot]$ denotes integration over the particle size distribution $n(D)$ (2.12)

$$\begin{bmatrix} E_h \\ E_r \end{bmatrix} = \begin{bmatrix} f_{11} & f_{12} \\ f_{21} & f_{22} \end{bmatrix} \begin{bmatrix} E'_h \\ E'_r \end{bmatrix} \frac{\exp(-ik_0 r)}{r} \quad (2.15)$$

In (2.15) E_h and E_r are the vertically and horizontally polarized field components in the scattering plane and r is the distance from the center of the sphere to the field point. An $\exp(i\omega t)$ time dependence is assumed in this work.

For a smooth sphere the elements f_{ij} are given by the Mie solution for a smooth sphere (Barrick 1970, Ishimaru 1978). The transformation matrices $[\mathcal{L}]$ in (2.12) account for the angles of rotation between the reference planes of incidence and scatter and the scattering plane containing \vec{n}^i and \vec{n}^f .

In (2.13) the coefficient $|\chi^2 (\vec{v} \cdot \vec{a}_r)|^2$ accounts for the fact that the specular point contributions to the scattering cross sections are decreased because of the rough surface ($|\chi^2| \leq 1$ and

$|X^s|^2 \rightarrow 1$ as $\beta \rightarrow 0$). The diffuse scattering matrix $[S_s]$ due to the random rough surface h_s is given by

$$\rho[S_s] = \begin{bmatrix} \rho[S_{11}^s] & [S_{12}^s] & 0 & 0 \\ \rho[S_{21}^s] & [S_{22}^s] & 0 & 0 \\ 0 & 0 & 0 & 0 \\ 0 & 0 & 0 & 0 \end{bmatrix} \quad (2.16)$$

where

$$\rho[S_{ij}^s] = \frac{A_y}{4\pi\rho(\sigma_c)} \cdot \rho[\langle \sigma^{ij} \rangle_s] \quad (2.17)$$

and $\rho[\cdot]$ denotes integration with respect to the particle distribution $n(D)$. For the contributions due to the random rough surface h_s , the only nonvanishing terms are of the form $\rho[|f_{ij}|^2]$ (see equation (2.14), the expectations of the phasor quantities vanish).

In order to simplify the solution of the transfer equation (2.10), it is assumed in this work that the normally incident wave is circularly polarized. Thus the incident Stokes matrix at $z = 0$ is given by

$$[I_{inc}] = \begin{bmatrix} 1 \\ 1 \\ 0 \\ \sqrt{2} \end{bmatrix} \delta(\mu'-1)\delta(\phi') \equiv I_0 \delta(\mu'-1)\delta(\phi') \quad (2.18)$$

where the $-$ and $+$ signs correspond to the right and left circularly polarized waves and $\mu' = \cos\theta'$.

The reduced incident intensity is therefore,

$$[I_{r1}] = [I_{inc}] \exp(-\tau) \quad (2.19)$$

In (2.10) the (4×1) excitation matrix $[I_i]$ is given by

$$[I_i] = \int [S][I_{r1}] d\mu' d\phi' = \left[[S][I_0] \right]_{\substack{\mu'=1 \\ \phi'=0}} \cdot \exp(-\tau) \quad (2.20)$$

where I_0 , the incident Stokes' matrix is defined by (2.18).

Since the normally incident circularly polarized wave is independent of the azimuth angle ϕ , the Stokes' matrices for the incoherent specific intensities are also independent of ϕ . And there is no coupling between I_1, I_2 and U, V in (2.10) and the equation of transfer for the normally incident, circularly polarized wave decouples into the following two matrix equations

$$\mu \frac{d}{d\tau} \begin{bmatrix} I_1 \\ I_2 \end{bmatrix} = - \begin{bmatrix} I_1 \\ I_2 \end{bmatrix} + \int \begin{bmatrix} S_{11} & S_{12} \\ S_{21} & S_{22} \end{bmatrix} \begin{bmatrix} I_1' \\ I_2' \end{bmatrix} d\mu' + \begin{bmatrix} I_{11} \\ I_{12} \end{bmatrix} \quad (2.21a)$$

and

$$\mu \frac{d}{d\tau} \begin{bmatrix} U \\ V \end{bmatrix} = - \begin{bmatrix} U \\ V \end{bmatrix} + \int \begin{bmatrix} S_{33} & S_{34} \\ S_{43} & S_{44} \end{bmatrix} \begin{bmatrix} U' \\ V' \end{bmatrix} d\mu' + \begin{bmatrix} U_1 \\ V_1 \end{bmatrix} \quad (2.21b)$$

in which I_{11} and I_{12} are the first two elements of the excitation matrix $[I_1]$ (2.20) while U_1 and V_1 are the third and fourth elements of the excitation matrix.

3. ILLUSTRATIVE EXAMPLES

For the illustrative examples considered in this section, the random rough surface height h_s (measured normal to the surface of the unperturbed spherical particle of diameter $D = 2h_0$) is assumed to be homogeneous and isotropic. The surface height spectral density function $W(v_x, v_z)$ (which is the two dimensional Fourier Transform of the surface height autocorrelation function $\langle h_s h_s' \rangle$) is

$$\begin{aligned} W(v_T) = W(v_x, v_z) &= \frac{1}{\pi^2} \int_{-\infty}^{\infty} \int_{-\infty}^{\infty} \langle h_s h_s' \rangle \exp(i v_x x_d + i v_z z_d) dx_d dz_d \\ &= \frac{2}{\pi} \int_0^{\infty} \langle h_s h_s' \rangle J_0(v_T r_d) r_d dr_d \end{aligned} \quad (3.1)$$

where $J_0(v_T r_d)$ is the Bessel function of the first kind and v_x and v_z are components of \vec{v} in the direction of the unit vectors \vec{n}_1, \vec{n}_3 tangent to the surface of the unperturbed sphere. Thus

$$v_T = (v_x^2 + v_z^2)^{1/2} = (v^2 - v_r^2)^{1/2} \quad (3.2)$$

Similarly the surface height autocorrelation function $\langle h_s h_s' \rangle$ is given by the inverse formula

$$\begin{aligned} \langle h_s h_s' \rangle &= \int_{-\infty}^{\infty} \int_{-\infty}^{\infty} \frac{W(v_x, v_z)}{v_T} \exp(-i v_x x_d - i v_z z_d) dv_x dv_z \\ &= \frac{\pi}{2} \int_0^{\infty} W(v_T) J_0(v_T r_d) v_T dv_T \end{aligned} \quad (3.3)$$

The specific expression for the surface height spectral density function is

$$\begin{aligned} W(v_T) &= \frac{2C}{\pi} \left[\frac{(v_T - v_d)}{(v_T - v_d)^2 + v_m^2} \right]^n \quad v_d < v_T < v_c \\ &= 0 \quad \text{elsewhere} \end{aligned} \quad (3.4)$$

In (3.4) the smallest spatial wavenumber is

$$v_d = 4/D \quad (3.5a)$$

and the cutoff wavenumber is

$$v_c = 4k_0 \quad (3.5b)$$

where k_0 is the wavenumber for the electromagnetic wave. The constant C is chosen such that the scale of the random rough surface is

$$\beta = 4k_0^2 \langle h_s^2 \rangle = 1 \quad (3.6)$$

In (3.6) $\langle h_s^2 \rangle$ is the mean square height

$$\langle h_s^2 \rangle = \frac{\pi}{2} \int_0^{\infty} W(v_T) v_T dv_T \quad (3.7)$$

The corresponding value for the mean square slope

$$\sigma_s^2 = \frac{\pi}{2} \int_0^\infty W(v_T) v_T^3 dv_T \quad (3.8)$$

is $\sigma_s^2 = 0.013$. The parameter v_m where $W(v_T)$ is maximum is $v_m = 1.2/D$. The exponent in (3.4) is $n = 4$ and the material of the particle is aluminum. For wavelength $\lambda = 10 \mu\text{m}$ the relative (complex) dielectric coefficient is $\epsilon_r = -6000(1+i)$ (Ehrenreich 1965). The diameter of the unperturbed spherical particle is $D = 5\lambda$ and its total (extinction) cross section is $\sigma_T = 2.059$.

For surfaces with small scale roughnesses $B \ll 1$, the contribution (2.6) to the total scattering cross sections due to surface roughness b_s can also be expressed as a series

$$\begin{aligned} \langle \sigma^{ij} \rangle_s &= \int_m k_0^2 \left\langle \frac{|D^{ij}|^2 P_2(\hat{n}^f, \hat{n}^{-1}|\hat{n})}{(\hat{a}_x \cdot \hat{a}_y)} \left(\frac{r}{2}\right)^{2m} \frac{W(v_T)}{m!} \chi(v_T) \right\rangle \\ &= \int_m k_0^2 \int_0^{2\pi} \int_0^{\pi/2} |D^{ij}|^2 P_2(\hat{n}^f, \hat{n}^{-1}|\hat{n}) \left(\frac{r}{2}\right)^{2m} \frac{W(v_T) \chi(v_T)}{m!} \sin y dy d\delta \end{aligned} \quad (3.9)$$

in which $W_m(v_T)/2^{2m}$ is the two dimensional Fourier transform of $\langle b_s b_s' \rangle^{2m}$ and the integration is over the polar angle y and azimuthal angle δ . For $B \ll 1$ only the first term in (3.9) is non-negligible. This term corresponds to first order Bragg scattering from rough surfaces (Bahar 1981). For $B = 1$, it is necessary to evaluate only two terms of the series in (3.9). For large values of roughness scales ($B > 1$) it is more convenient to evaluate $\langle \sigma^{ij} \rangle_s$ using (2.6).

For the illustrative examples, it is assumed that a right circularly polarized wave is normally incident at $\tau = 0$ ($z = 0$) upon a parallel layer of optical thickness τ_0 (see Fig. 2). The equation of transfer for the azimuthally independent modified Stokes' parameters (2.21) are solved using the matrix characteristic (eigen) value technique (Ishimaru and Cheung 1980) subject to the boundary conditions for the incoherent specific diffuse intensities

$$[I] = 0 \quad \text{for } 0 \leq \mu \leq 1 \quad \text{at } \tau = 0$$

(forward scattered incoherent diffuse intensities are zero at $\tau = 0$) and

$$[I] = 0 \quad \text{for } 0 \geq \mu \geq -1 \quad \text{at } \tau = \tau_0$$

(backward scattered incoherent diffuse intensities are zero at $\tau = \tau_0$).

In Figs. 3 and 4 I_1 (vertical polarization) and I_2 (horizontal polarization) are plotted respectively, as functions of the scatter angle θ ($0, 90^\circ$) (forward scattering) for $\tau_0 = 10$. The solid curves correspond to first order scattering solutions only (Ishimaru 1978) for the smooth (unperturbed spherical) particles and particles with rough surfaces. The surface roughness of the particles tends to smooth out the incoherent diffuse intensities as functions of θ . Note that the vertically polarized intensity is more oscillatory than the horizontally polarized intensity.

The corresponding solutions that account for multiple scatter are also given for the smooth (+) and rough (Δ) particles. We note that since the albedos for the rough particles are slightly lower than the albedos for the smooth particles (see Table I), the incoherent diffuse intensities are somewhat lower for the rough particles. For optically very thick layers of particles, the diffuse intensities I_1 and I_2 are practically equal and rather flat functions of θ . Multiple scattering cannot be neglected in these cases.

4. CONCLUDING REMARKS

In this work scattering of electromagnetic waves by particles with moderate to very large roughness scales (that cannot be accounted for using the standard perturbation methods) has been considered. The incoherent diffuse scattering intensities for the rough particles have been compared with the corresponding results for smooth particles. Both first order (single scatter) and multiple scatter results have been presented for the case listed in Table I.

As the scale of roughness $\beta = k_0^2 \langle h^2 \rangle$ increases, the scattering coefficients as well as the incoherent diffuse scattering intensities become practically independent of the scattering angle. In addition, for large τ_0 the incoherent scattering intensities decrease as the roughness scale increases. As the optical thickness of the layer increases, the incoherent diffuse scattering intensities become less dependent on scatter angle.

5. REFERENCES

1. Bahar, E. (1981), "Scattering Cross Sections for Composite Random Surfaces-Full Wave Analysis," Radio Sci., 16, 1327.
2. Bahar, E., and Swapn Chakrabarti (1985), "Scattering and Depolarization by Large Conducting Spheres with Rough Surfaces," Applied Optics, Vol. 24, No. 12, 1820.
3. Barrick, D. E. (1970), Rough Surfaces, in Radar Cross Section Handbook (Plenum, New York), Chap. 9.
4. Chandrasekhar, S. (1960), Radiative Transfer. Dover, Publ., New York.
5. Ehrenreich, E. (1965), "The Optical Properties of Metals," IEEE Spectrum 2, 162.
6. Ishimaru, E. (1978), Wave Propagation and Scattering in Random Media, Academic, New York.
7. Ishimaru, A., and R. L.-T. Cheung (1980), "Multiple Scattering Effects in Wave Propagation Due to Rain," Ann. Telecommun., 35, 373.
8. Morse, P. M., and H. Feshbach (1953), Methods of Theoretical Physics, McGraw-Hill, New York.
9. Sancer, M. E. (1969), "Shadow-Corrected Electromagnetic Scattering from a Randomly Rough Surface," IEEE Trans. Antennas Propag. AP-17, 577.
10. Smith, B. G. (1965), "Geometrical Shadowing of a Randomly Rough Surface," IEEE Trans. Antennas and Propag. AP-15, 668.

ACKNOWLEDGMENTS

This investigation is sponsored by the U. S. Army Research Offices, Contract No. DAAG-29-82-K-0123.

The authors wish to thank S. Chakrabarti for his assistance in documenting the computer programs.

TABLE I: ALBEDO FOR SMOOTH AND ROUGH PARTICLES

Smooth 0.9885: Rough 0.9732

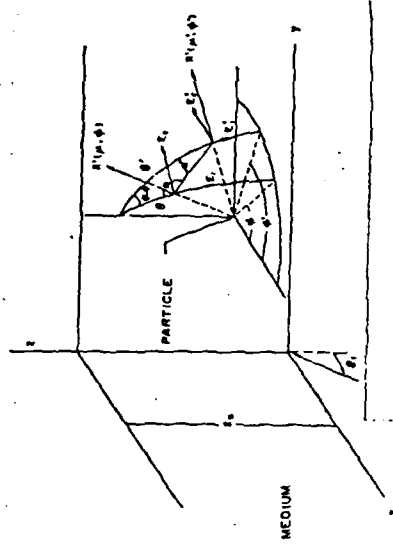


FIGURE 2. Scattering geometry indicating incident and scattering wave normals \hat{n} and \hat{n}' and corresponding field components E_1 parallel (vertical) and E_2 perpendicular (horizontal) polarizations.

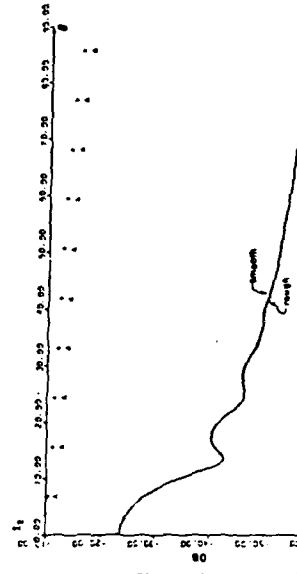


FIGURE 4. Specific incoherent intensity I_2 for a right circularly polarized wave normal incidence, $B=1$, $k=1.2/D$, $\lambda=10\mu$, $\epsilon=6000(1+i)(AL)$, $D=5\lambda$, transmitted, $T_0=10$. First order (—), smooth and rough particles. Multiple scatter: (+) smooth, (Δ) rough.

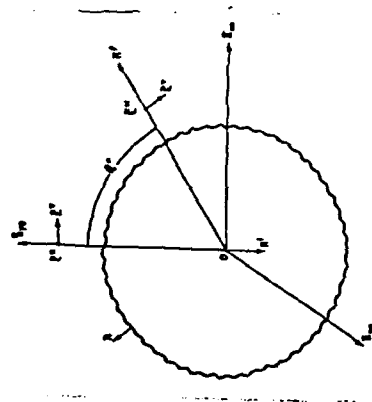


FIGURE 3. Scattering geometry for a rough conducting sphere.

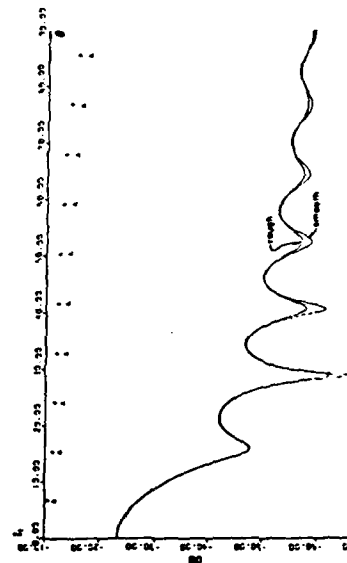


FIGURE 3. Specific incoherent intensity I_1 for a right circularly polarized wave normal incidence, $B=1$, $k=1.2/D$, $\lambda=10\mu$, $\epsilon=6000(1+i)(AL)$, $D=5\lambda$, transmitted, $T_0=10$. First order (—), smooth and rough particles. Multiple scatter: (+) smooth, (Δ) rough.

MULTIPLE SCATTERING IN MEDIA CONSISTING OF NONSPHERICAL
FINITELY CONDUCTING PARTICLES

Ezekiel Bahar and Mary Ann Fitzwater
Electrical Engineering Department
University of Nebraska--Lincoln
Lincoln, Nebraska 68588-0511

RECENT PUBLICATIONS, SUBMITTALS FOR PUBLICATION AND PRESENTATIONS:

- A) E. Bahar, "Scattering and Depolarization by Very Long Finitely Conducting Cylinders with Rough Surfaces," 1984 CRDC Scientific Conference on Obscuration and Aerosol Research, Aberdeen, Maryland, June 25-29, 1984.
- B) E. Bahar, "Scattering and Depolarization of Radio Waves by Rough Planetary Surfaces," International Union of Radio Science Symposium on Radio Techniques in Planetary Exploration, in conjunction with the XXI General Assembly of URSI, Florence, Italy, August 26-September 6, 1984.
- C) E. Bahar and M. A. Fitzwater, "Scattering Cross Sections for Composite Rough Surface Using the Unified Full Wave Approach," IEEE Transactions on Antennas and Propagation, Vol. AP-32, No. 7, pp. 730-734, July 1984.
- D) E. Bahar, "Scattering by Anisotropic Models of Composite Rough Surface--Full Wave Solutions," IEEE Transactions on Antennas and Propagation, Vol. AP-33, No. 1, pp. 106-112, January 1985.
- E) E. Bahar and S. Chakrabarti, "Scattering and Depolarization by Large Conducting Spheres with Very Rough Surfaces," Applied Optics, Vol. 24, No. 12, pp. 1820-1825, June 1985.
- F) E. Bahar, "Scattering by Anisotropic Models of Composite Rough Surfaces--Full Wave Solutions," International IEEE/APS-Symposium and 1985 North American Radio Science Meeting, Vancouver, Canada, June 17-21, 1985.
- G) E. Bahar, "Multiple Scattering in Media Consisting of Nonspherical, Finitely Conducting Particles, 1985 CRDC Scientific Conference on Obscuration and Aerosol Research, Aberdeen, Maryland, June 17-21, 1985.
- H) E. Bahar, "Scattering and Depolarization by Random Rough Surfaces--Unified Full Wave Approach," Symposium/Workshop on Multiple Scattering of Waves in Random Media and by Random Rough Surfaces," Pennsylvania State University, University Park, Pennsylvania, July 29-August 1, 1985.
- I) E. Bahar, "Unified Full Wave Solutions for Electromagnetic Scattering by Rough Surfaces--Comparison with Physical Optics, Geometric Optics and Perturbation Solutions Using Two-Scale Models of Rough Surfaces," Schlumberger Doll Research Workshop on Waves in Inhomogeneous Media, August 8-9, 1985.
- J) E. Bahar, "Scattering and Depolarization by Conducting Cylinders with Rough Surfaces," DRSMC-CLJ-IR, pp. 365-371, January 1985.
- K) E. Bahar and M. A. Fitzwater, "Like and Cross Polarized Scattering Cross Sections for Random Rough Surfaces--Theory and Experiment," Journal of the Optical Society of America Special Issue on Wave Propagation and Scattering in Random Media--in press.
- L) E. Bahar and M. A. Fitzwater, "Scattering and Depolarization by Conducting Cylinders with Rough Surfaces," submitted for review.
- M) E. Bahar and M. A. Fitzwater, "Multiple Scattering by Irregular Shaped Particles of Finite Conductivity at Infrared and Optical Frequencies," submitted for review.

ABSTRACT

The incoherent specific intensities for the waves scattered by a random distribution of particles with rough surfaces are derived. Since large roughness scales are considered, the diffuse scattering contributions to the like and cross polarized scattering cross sections are given by the full wave solutions. The scattering matrix in the expression for the equation of transfer is given by a weighted sum of the scattering matrix for the smooth particle and the diffuse contribution due to the rough surface of the particle. Illustrative examples are presented for the propagation of a circularly polarized wave normally incident upon a parallel layer of particles. Particles with different surface height spectral density functions, roughness scales, complex permittivities and sizes are considered. Both first order (single scatter) and multiple scatter solutions are provided and the results for particles with smooth and rough surfaces are compared.

1. INTRODUCTION

Scattering of electromagnetic waves in media consisting of random distributions of particles has been investigated extensively using the equation of transfer (Chandrasekhar 1950, Ishimaru 1978). The main difficulty in setting up the equation of transfer lies in the determination of the elements of the 4×4 scattering matrix for the individual particles. Thus most of the work has been done for particles of idealized shapes such as spheres.

In this work a method is presented for the modification of the results derived for particles with idealized shapes to account for the random surface roughness of the particles. To this end the full wave approach was used to determine the rough surface contributions to the like and cross polarized scattering cross sections and the elements of the scattering matrix are given in terms of a weighted sum of the Mie solutions and the diffuse scattering terms due to the particle surface roughness (See Section 2). For convenience in this work a circularly polarized wave is assumed to be normally incident upon a parallel layer consisting of a random distribution of irregular shaped particles.

For the illustrative examples presented in Section 3 both first order (single scatter) and multiple scatter results are presented for smooth particles and for particles with rough surfaces. The matrix characteristic value technique is used to account for multiple scattering (Ishimaru and Cheung 1980).

2. FORMULATION OF THE PROBLEM

In this section the principal elements of the full wave solutions for the like and cross polarized differential scattering cross sections of nonspherical particles are summarized. The contributions of these cross sections to the familiar equation of transfer (Ishimaru 1978), in a medium consisting of a random distribution of nonspherical particles are also indicated explicitly.

The radius vector from the center to the irregular surface of the particle is given by (see Fig. 1)

$$\vec{r}_s = h_0 \vec{a}_r + h_s \vec{a}_r \quad (2.1)$$

in which \vec{a}_r is the unit vector in the direction of the radius vector, h_0 is the radius of the unperturbed sphere and h_s is the random rough surface height measured in the direction normal to the surface of the unperturbed sphere. In this work it is assumed that the mean square of the rough surface height, $\langle h_s^2 \rangle$, can be sufficiently large such that standard perturbation techniques are not applicable (Barrick 1970). Thus the rough surface parameter, $\beta = kh_0^2 \langle h_s^2 \rangle$, considered in this work is in the range $0 < \beta < 10$.

The full wave solutions for the normalized scattering cross sections $\langle \sigma^{ij} \rangle$ per unit cross sectional area ($A_y = \pi h_0^2$) are expressed as a weighted sum (Bahar and Chakrabarti 1981)

$$\langle \sigma^{ij} \rangle = \langle \sigma^{ij} \rangle_s + \langle \sigma^{ij} \rangle_r \quad (2.2)$$

the symbol $\langle \cdot \rangle$ denotes the statistical average. In the above expression the first and second superscripts indicate the polarizations of the scattered and incident waves respectively. Thus $i, j = 1$ denotes Vertical polarization and $i, j = 2$ denotes Horizontal polarization. The cross section $\langle \sigma^{ij} \rangle_s$ is the modified cross section associated with the unperturbed sphere.

$$\langle \sigma^{ij} \rangle_s = |\chi^s(v)|^2 \langle \sigma^{ij} \rangle_{\text{Mie}} \quad (2.3)$$

In (2.3) $\langle \sigma^{ij} \rangle_{\text{Mie}}$ is the Mie solution (Ishimaru 1978), for the like and cross polarized cross sections of the unperturbed sphere. For large spheres, $k_0 b_0 > 20$, (k_0 is the free space wavenumber), the most significant parts of the solution are the specularly reflected wave and the shadow forming wave (Morse and Feshbach 1954). The coefficient of $\langle \sigma^{ij} \rangle_{\text{Mie}}$ is the rough surface height characteristic function

$$\chi^s(v) = \langle \exp i v h_s \rangle \quad (2.4)$$

in which v is the magnitude of the vector

$$\vec{v} = k_0 (\vec{n}^f - \vec{n}^i) \quad (2.5)$$

where \vec{n}^f and \vec{n}^i are unit vectors in the direction of the scattered and incident wave normals. The coefficient $|\chi^s|^2$ accounts for the degradation of the reflected wave due to surface roughness. The coefficient is minimum for backscatter and approaches unity for forward scattering.

The second term in (2.2) $\langle \sigma^{ij} \rangle_s$ is the contribution to the total scattering cross section due to the surface roughness. It is expressed as (Bahar and Chakrabarti 1985)

$$\langle \sigma^{ij} \rangle_s = \int A^{ij}(\vec{n}^f, \vec{n}^i, \vec{n}) (\vec{n} \cdot \vec{a}_y) Q_s(\vec{n}^f, \vec{n}^i, \vec{n}) p(\vec{n}) d\vec{n} \quad (2.6)$$

in which \vec{n} is a unit vector normal to the surface of the scatterer,

$$A^{ij}(\vec{n}^f, \vec{n}^i, \vec{n}) = \frac{1}{\pi} \left| \frac{k_0 D^{ij}}{(\vec{v} \cdot \vec{a}_x)(\vec{a}_y \cdot \vec{n})} \right|^2 P_2(\vec{n}^f, \vec{n}^i | \vec{n}) \quad (2.7)$$

$$Q_s(\vec{n}^f, \vec{n}^i, \vec{n}) = (\vec{v} \cdot \vec{a}_x)^2 \int_{-\infty}^{\infty} (\chi_2^s(\vec{v} \cdot \vec{a}_x) - |\chi^s(\vec{v} \cdot \vec{a}_x)|^2) \exp(i \vec{v} \cdot \vec{r}_d) dx_d dz_d \quad (2.8)$$

and $p(\vec{n})$ is the probability density function for the slope of the surface of the scatterer. In (2.7), D^{ij} is the scattering coefficient which depends on the polarizations and the directions of the wave normals for the incident and scattered waves as well as the complex electromagnetic parameters (ϵ, μ) of the scatterers. The term $P_2(\vec{n}^f, \vec{n}^i | \vec{n})$ is the probability that a point on the rough surface is both illuminated by the source and visible to the observer given the slopes (\vec{n}) of the surface of the scatterer (Smith 1967, Sancer 1969). Since $\vec{n} = \vec{a}_x$, $P_2 = u(-\vec{n}^i \cdot \vec{n}) u(\vec{n}^f \cdot \vec{n})$ where $u(\cdot)$ is the unit step function.

In (2.8) $\chi_2^s(\vec{v} \cdot \vec{a}_x)$ is the rough surface height joint characteristic function

$$\chi_2^s(\vec{v} \cdot \vec{a}_x) = \langle \exp[i v_x (h_s - h_s')] \rangle \quad (2.9)$$

in which $\vec{v}_x = \vec{v} \cdot \vec{a}_x$.

With the above expressions for the scattering cross sections (2.2), the general expression for the equation of transfer (Ishimaru 1978) can be written as follows for a plane parallel slab consisting of rough spherical particles (see Fig. 2)

$$\mu \frac{d[I]}{dz} = -[I] + \int [S][I'] d\mu' d\phi' + [I_1] \quad (2.10)$$

In (2.10) τ is the optical distance in the z direction (normal to the plane parallel slab)

$$\tau = \rho[\sigma_t]z \equiv \int \sigma_t n(D) dD z, \quad D = 2h_0 \quad (2.11)$$

where $n(D)$ is the particle size distribution and σ_t is the extinction coefficient. Since $\langle \sigma^{ij} \rangle_s$ vanishes in the forward direction, the extinction matrix (Ishimaru and Cheung 1980) for the rough sphere, can be represented by a scalar quantity. The matrices $[I]$ and $[I']$ are the (4×1) incoherent specific diffuse intensity matrices for waves scattered from the particles in the direction $\theta = \cos^{-1}\mu$ and ϕ and for waves incident in the direction $\theta' = \cos^{-1}\mu'$ and ϕ' , respectively. The elements of $[I]$ are the modified Stokes' parameters. The (4×4) scattering matrix $[S]$ in the reference coordinate system can be expressed in terms of the scattering matrix $[S']$ in the scattering plane as follows:

$$[S] = [\mathcal{L}(-\pi + \alpha)][S'][\mathcal{L}(\alpha)] \quad (2.12)$$

in which

$$[S'] = \chi^2 (\vec{v} \cdot \vec{a}_x)^2 [S_{Mie}] + [S_s] \quad (2.13)$$

In (2.13) $[S_{Mie}]$ is given by

$$[S_{Mie}] = \frac{1}{\rho[\sigma_t]} \begin{bmatrix} \rho[|f_{11}|^2] & \rho[|f_{12}|^2] & \rho\text{Re}[f_{11}^* f_{12}] & -\rho\text{Im}[f_{11}^* f_{12}] \\ \rho[|f_{21}|^2] & \rho[|f_{22}|^2] & \rho\text{Re}[f_{21}^* f_{22}] & -\rho\text{Im}[f_{21}^* f_{22}] \\ \rho 2\text{Re}[f_{11}^* f_{21}] & \rho 2\text{Re}[f_{12}^* f_{22}] & \rho\text{Re}[f_{11}^* f_{22}^* + f_{12}^* f_{21}] & -\rho\text{Im}[f_{11}^* f_{22}^* - f_{12}^* f_{21}] \\ \rho 2\text{Im}[f_{11}^* f_{21}] & \rho 2\text{Im}[f_{12}^* f_{22}] & \rho\text{Im}[f_{11}^* f_{22}^* + f_{12}^* f_{21}] & \rho\text{Re}[f_{11}^* f_{22}^* - f_{12}^* f_{21}] \end{bmatrix} \quad (2.14)$$

where f_{ij} are elements of the 2×2 scattering amplitude matrix $[f]$ and $\rho[\cdot]$ denotes integration over the particle size distribution $n(D)$ (2.12)

$$\begin{bmatrix} E_k \\ E_r \end{bmatrix} = \begin{bmatrix} f_{11} & f_{12} \\ f_{21} & f_{22} \end{bmatrix} \begin{bmatrix} E_k^i \\ E_r^i \end{bmatrix} \frac{\exp(-ikr)}{r} \quad (2.15)$$

In (2.15) E_k and E_r are the vertically and horizontally polarized field components in the scattering plane and r is the distance from the center of the sphere to the field point. An $\exp(i\omega t)$ time dependence is assumed in this work.

For a smooth sphere the elements f_{ij} are given by the Mie solution for a smooth sphere (Barrick 1970, Ishimaru 1978). The transformation matrices $[\mathcal{L}]$ in (2.12) account for the angles of rotation between the reference planes of incidence and scatter and the scattering plane containing \vec{n}^i and \vec{n}^f .

In (2.13) the coefficient $|\chi^2 (\vec{v} \cdot \vec{a}_x)^2|$ accounts for the fact that the specular point contributions to the scattering cross sections are decreased because of the rough surface ($|\chi^2| \leq 1$ and

$|X^s|^2 \rightarrow 1$ as $\beta \rightarrow 0$). The diffuse scattering matrix $[S_s]$ due to the random rough surface h_s is given by

$$\rho[S_s] = \begin{bmatrix} \rho[S_{11}^s] & [S_{12}^s] & 0 & 0 \\ \rho[S_{21}^s] & [S_{22}^s] & 0 & 0 \\ 0 & 0 & 0 & 0 \\ 0 & 0 & 0 & 0 \end{bmatrix} \quad (2.16)$$

where

$$\rho[S_{ij}^s] = \frac{A}{4\pi\rho\sigma_t} \rho[\langle \sigma^{ij} \rangle_s] \quad (2.17)$$

and $\rho[\cdot]$ denotes integration with respect to the particle distribution $n(D)$. For the contributions due to the random rough surface h_s , the only nonvanishing terms are of the form $\rho[|f_{ij}|^2]$ (see equation (2.14), the expectations of the phasor quantities vanish).

In order to simplify the solution of the transfer equation (2.10), it is assumed in this work that the normally incident wave is circularly polarized. Thus the incident Stokes matrix at $z = 0$ is given by

$$[I_{inc}] = \begin{bmatrix} 1 \\ 1 \\ 0 \\ 0 \end{bmatrix} \delta(\mu'-1)\delta(\phi') \equiv I_0 \delta(\mu'-1)\delta(\phi') \quad (2.18)$$

where the - and + signs correspond to the right and left circularly polarized waves and $\mu' = \cos\theta'$.

The reduced incident intensity is therefore,

$$[I_{r1}] = [I_{inc}] \exp(-\tau) \quad (2.19)$$

In (2.10) the (4×1) excitation matrix $[I_i]$ is given by

$$[I_i] = \int [S][I_{r1}] d\mu' d\phi' = \left[[S][I_0] \right]_{\substack{\mu'=1 \\ \phi'=0}} \exp(-\tau) \quad (2.20)$$

where I_0 , the incident Stokes' matrix is defined by (2.18).

Since the normally incident circularly polarized wave is independent of the azimuth angle ϕ , the Stokes' matrices for the incoherent specific intensities are also independent of ϕ . And there is no coupling between I_1, I_2 and U, V in (2.10) and the equation of transfer for the normally incident, circularly polarized wave decouples into the following two matrix equations

$$\mu \frac{d}{d\tau} \begin{bmatrix} I_1 \\ I_2 \end{bmatrix} = - \begin{bmatrix} I_1 \\ I_2 \end{bmatrix} + \int \begin{bmatrix} S_{11} & S_{12} \\ S_{21} & S_{22} \end{bmatrix} \begin{bmatrix} I_1' \\ I_2' \end{bmatrix} d\mu' + \begin{bmatrix} I_{11} \\ I_{12} \end{bmatrix} \quad (2.21a)$$

and

$$\mu \frac{d}{d\tau} \begin{bmatrix} U \\ V \end{bmatrix} = - \begin{bmatrix} U \\ V \end{bmatrix} + \int \begin{bmatrix} S_{33} & S_{34} \\ S_{43} & S_{44} \end{bmatrix} \begin{bmatrix} U' \\ V' \end{bmatrix} d\mu' + \begin{bmatrix} U_1 \\ V_1 \end{bmatrix} \quad (2.21b)$$

in which I_{11} and I_{12} are the first two elements of the excitation matrix $[I_i]$ (2.20) while U_1 and V_1 are the third and fourth elements of the excitation matrix.

3. ILLUSTRATIVE EXAMPLES

For the illustrative examples considered in this section, the random rough surface height h_s (measured normal to the surface of the unperturbed spherical particle of diameter $D = 2h_0$) is assumed to be homogeneous and isotropic. The surface height spectral density function $W(v_x, v_z)$ (which is the two dimensional Fourier Transform of the surface height autocorrelation function $\langle h_s h_s' \rangle$) is

$$\begin{aligned} W(v_x, v_z) &= W(v_x, v_z) = \frac{1}{\pi^2} \int_{-\infty}^{\infty} \int_{-\infty}^{\infty} \langle h_s h_s' \rangle \exp(iv_x x_d + iv_z z_d) dx_d dz_d \\ &= \frac{2}{\pi} \int_0^{\infty} \langle h_s h_s' \rangle J_0(v_T r_d) r_d dr_d \end{aligned} \quad (3.1)$$

where $J_0(v_T r_d)$ is the Bessel function of the first kind and v_x and v_z are components of \bar{v} in the direction of the unit vectors \bar{n}_1, \bar{n}_3 tangent to the surface of the unperturbed sphere. Thus

$$v_T = (v_x^2 + v_z^2)^{1/2} = (v^2 - v_r^2)^{1/2} \quad (3.2)$$

Similarly the surface height autocorrelation function $\langle h_s h_s' \rangle$ is given by the inverse formula

$$\begin{aligned} \langle h_s h_s' \rangle &= \int_{-\infty}^{\infty} \int_{-\infty}^{\infty} \frac{W(v_x, v_z)}{v_T} \exp(-iv_x x_d - iv_z z_d) dv_x dv_z \\ &= \frac{\pi}{2} \int_0^{\infty} W(v_T) J_0(v_T r_d) v_T dv_T \end{aligned} \quad (3.3)$$

The specific expression for the surface height spectral density function is

$$\begin{aligned} W(v_T) &= \frac{2C}{\pi} \left[\frac{(v_T - v_d)}{(v_T - v_d)^2 + v_m^2} \right]^n \quad v_d < v_T < v_c \\ &= 0 \quad \text{elsewhere} \end{aligned} \quad (3.4)$$

In (3.4) the smallest spatial wavenumber is

$$v_d = 4/D \quad (3.5a)$$

and the cutoff wavenumber is

$$v_c = 4k_0 \quad (3.5b)$$

where k_0 is the wavenumber for the electromagnetic wave. The constant C is chosen such that the scale of the random rough surface is

$$\beta = 4k_0^2 \langle h_s^2 \rangle = 1 \quad (3.6)$$

In (3.6) $\langle h_s^2 \rangle$ is the mean square height

$$\langle h_s^2 \rangle = \frac{\pi}{2} \int_0^{\infty} W(v_T) v_T dv_T \quad (3.7)$$

The corresponding value for the mean square slope

$$\sigma_s^2 = \frac{\pi}{2} \int_0^{\infty} W(v_T) v_T^3 dv_T \quad (3.8)$$

is $\sigma_s^2 = 0.013$. The parameter v_m where $W(v_T)$ is maximum is $v_m = 1.2/D$. The exponent in (3.4) is $n = 4$ and the material of the particle is aluminum. For wavelength $\lambda = 10 \mu\text{m}$ the relative (complex) dielectric coefficient is $\epsilon_r = -6000(1+i)$ (Ehrenreich 1965). The diameter of the unperturbed spherical particle is $D = 5\lambda$ and its total (extinction) cross section is $\sigma_T = 2.059$.

For surfaces with small scale roughnesses $B \leq 1$, the contribution (2.6) to the total scattering cross sections due to surface roughness h_s can also be expressed as a series

$$\begin{aligned} \langle \sigma^{ij} \rangle_s &= \sum_m 4\pi k_o^2 \left\langle \frac{|p^{ij}|^2 P_2(\hat{n}^f, \hat{n}^i | \hat{n})}{(\hat{s}_x \cdot \hat{s}_y)} \left(\frac{v_r}{2} \right)^{2m} \frac{W_m(v_T)}{m!} \chi(v_r) \right\rangle \\ &= \sum_m 4k_o^2 \int_0^{2\pi} \int_0^{\pi/2} |p^{ij}|^2 P_2(\hat{n}^f, \hat{n}^i | \hat{n}) \left(\frac{v_r}{2} \right)^{2m} \frac{W_m(v_T) \chi(v_r)}{m!} \sin \gamma d\gamma d\delta \end{aligned} \quad (3.9)$$

in which $W_m(v_T)/2^{2m}$ is the two dimensional Fourier transform of $\langle h_s h_s' \rangle^{2m}$ and the integration is over the polar angle γ and azimuthal angle δ . For $B \ll 1$ only the first term in (3.9) is non-negligible. This term corresponds to first order Bragg scattering from rough surfaces (Bahar 1981). For $B = 1$, it is necessary to evaluate only two terms of the series in (3.9). For large values of roughness scales ($B > 1$) it is more convenient to evaluate $\langle \sigma^{ij} \rangle_s$ using (2.6).

For the illustrative examples, it is assumed that a right circularly polarized wave is normally incident at $\tau = 0$ ($z = 0$) upon a parallel layer of optical thickness τ_o (see Fig. 2). The equation of transfer for the azimuthally independent modified Stokes' parameters (2.21) are solved using the matrix characteristic (eigen) value technique (Ishimaru and Cheung 1980) subject to the boundary conditions for the incoherent specific diffuse intensities

$$[I] = 0 \quad \text{for} \quad 0 \leq \mu \leq 1 \quad \text{at} \quad \tau = 0$$

(forward scattered incoherent diffuse intensities are zero at $\tau = 0$) and

$$[I] = 0 \quad \text{for} \quad 0 \geq \mu \geq -1 \quad \text{at} \quad \tau = \tau_o$$

(backward scattered incoherent diffuse intensities are zero at $\tau = \tau_o$).

In Figs. 3 and 4 I_1 (vertical polarization) and I_2 (horizontal polarization) are plotted respectively, as functions of the scatter angle θ ($0, 90^\circ$) (forward scattering) for $\tau_o = 10$. The solid curves correspond to first order scattering solutions only (Ishimaru 1978) for the smooth (unperturbed spherical) particles and particles with rough surfaces. The surface roughness of the particles tends to smooth out the incoherent diffuse intensities as functions of θ . Note that the vertically polarized intensity is more oscillatory than the horizontally polarized intensity.

The corresponding solutions that account for multiple scatter are also given for the smooth (+) and rough (Δ) particles. We note that since the albedos for the rough particles are slightly lower than the albedos for the smooth particles (see Table I), the incoherent diffuse intensities are somewhat lower for the rough particles. For optically very thick layers of particles, the diffuse intensities I_1 and I_2 are practically equal and rather flat functions of θ . Multiple scattering cannot be neglected in these cases.

4. CONCLUDING REMARKS

In this work scattering of electromagnetic waves by particles with moderate to very large roughness scales (that cannot be accounted for using the standard perturbation methods) has been considered. The incoherent diffuse scattering intensities for the rough particles have been compared with the corresponding results for smooth particles. Both first order (single scatter) and multiple scatter results have been presented for the case listed in Table I.

As the scale of roughness $\beta = k_0^2 \langle h_s^2 \rangle$ increases, the scattering coefficients as well as the incoherent diffuse scattering intensities become practically independent of the scattering angle. In addition, for large τ_0 the incoherent scattering intensities decrease as the roughness scale increases. As the optical thickness of the layer increases, the incoherent diffuse scattering intensities become less dependent on scatter angle.

5. REFERENCES

1. Bahar, E. (1981), "Scattering Cross Sections for Composite Random Surfaces-Full Wave Analysis," *Radio Sci.*, 16, 1327.
2. Bahar, E., and Suman Chakrabarti (1985), "Scattering and Depolarization by Large Conducting Spheres with Rough Surfaces," *Applied Optics*, Vol. 24, No. 12, 1820.
3. Barrick, D. E. (1970), *Rough Surfaces*, in *Radar Cross Section Handbook* (Plenum, New York), Chap. 9.
4. Chandrasekhar, S. (1960), *Radiative Transfer*. Dover, Publ., New York.
5. Ehrenreich, H. (1965), "The Optical Properties of Metals," *IEEE Spectrum* 2, 162.
6. Ishimaru, E. (1978), *Wave Propagation and Scattering in Random Media*, Academic, New York.
7. Ishimaru, A., and R. L.-T. Cheung (1980), "Multiple Scattering Effects in Wave Propagation Due to Rain," *Ann. Telecommun.*, 35, 373.
8. Morse, P. M., and H. Feshbach (1953), *Methods of Theoretical Physics*, McGraw-Hill, New York.
9. Sancer, M. H. (1969), "Shadow-Corrected Electromagnetic Scattering from a Randomly Rough Surface," *IEEE Trans. Antennas Propag.* AP-17, 577.
10. Smith, B. G. (1965), "Geometrical Shadowing of a Randomly Rough Surface," *IEEE Trans. Antennas and Propag.* AP-13, 668.

ACKNOWLEDGMENTS

This investigation is sponsored by the U. S. Army Research Offices, Contract No. DAAG-29-82-K-0123. The authors wish to thank S. Chakrabarti for his assistance in documenting the computer programs.

TABLE I: ALBEDO FOR SMOOTH AND ROUGH PARTICLES

Smooth	0.9885;	Rough	0.9732
--------	---------	-------	--------

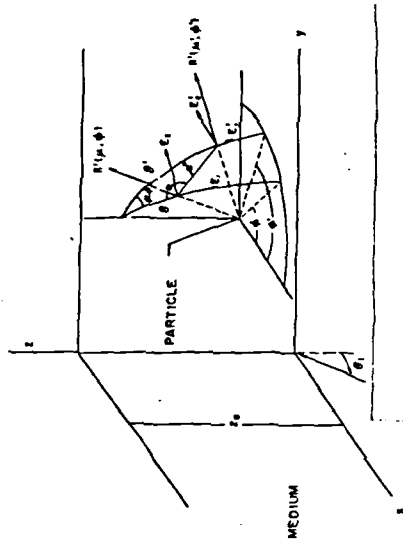


FIGURE 2. Scattering geometry indicating incident and scattering wave normals \hat{n} and \hat{n}' and corresponding field components E_1 parallel (vertical) and E_2 perpendicular (horizontal) polarizations.

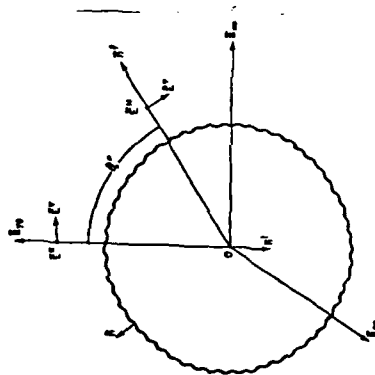


FIGURE 3. Scattering geometry for a rough conducting sphere.

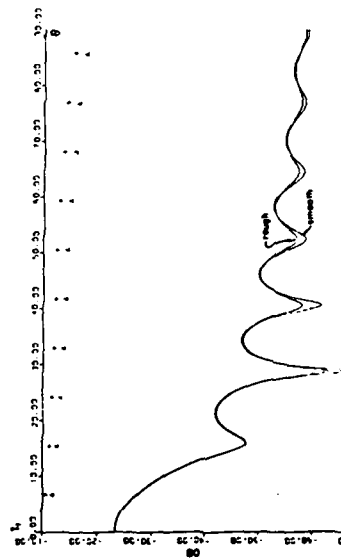


FIGURE 3. Specific incoherent intensity I_1 for a right circularly polarized wave normal incidence, $\beta=1$, $\kappa=1.2/D$, $\lambda=10D$, $\epsilon=600(1+i)(AL)$, $D=5\lambda$, transmitted, $T_0=10$. First order (—), smooth and rough particles. Multiple scatter: (+) smooth, (Δ) rough.

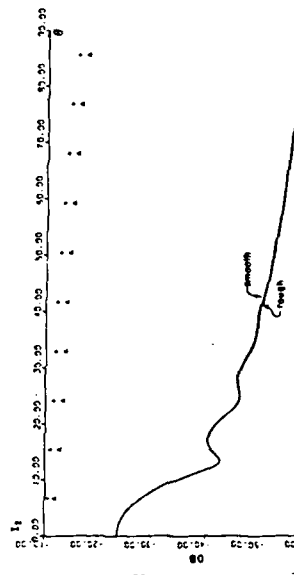


FIGURE 4. Specific incoherent intensity I_2 for a right circularly polarized wave normal incidence, $\beta=1$, $\kappa=1.2/D$, $\lambda=10D$, $\epsilon=600(1+i)(AL)$, $D=5\lambda$, transmitted, $T_0=10$. First order (—), smooth and rough particles. Multiple scatter: (+) smooth, (Δ) rough.

Full Wave Solutions for Electromagnetic Scattering
and Depolarization in Irregular Stratified Media⁺

E. Bahar

Electrical Engineering Department
University of Nebraska-Lincoln 68588-0511

Abstract

Using the complete expansions of the fields and on imposing the exact boundary conditions at the interfaces of an irregular stratified medium, Maxwell's equations are transformed into a rigorous set of coupled first order differential equations for the wave amplitudes. This full wave approach is applied to a large class of propagation problems. Since these solutions account for specular point as well as diffuse scattering in a unified self-consistent manner, it is not necessary to apply a hybrid physical optics-perturbation approach to problems of rough surface scattering. The full wave solutions satisfy realizability, duality and reciprocity relationships in electromagnetic theory. They are invariant to coordinate transformations.

⁺Presented at the Workshop on Waves in Inhomogeneous Media, Schlumberger-Doll Research, Ridgefield, Connecticut, August 8-9, 1985.

1. Introduction

In this paper the principal elements of the full wave approach to problems of radio wave propagation in irregular multilayered media are summarized. The relationships between the full wave solutions and earlier solutions to scattering problems are also presented. To demonstrate the versatility of the full wave approach, three broad classes of propagation problems are considered in some detail. In Section 3, the full wave approach is applied to problems of scattering and depolarization by a random rough interface that separates two media with different (complex) electromagnetic parameters. In Section 4, radio wave propagation in a three layer structure is considered. The thickness of the intermediate layer is assumed to vary in thickness. Finally, in Section 5, the boundaries of the irregular structure are assumed to be highly reflecting, thus the exact continuity conditions for the electric and magnetic fields are replaced by the approximate impedance boundary conditions. In this case, the fields in the layered structure are expressed in terms of trapped waveguide modes.

The Principal Elements of the Full Wave Approach are (Bahar 1973a,b):

- (a) The electromagnetic fields are expressed in terms of complete expansions of vertically and horizontally polarized waves. These include the radiation fields, the lateral waves and the surface waves.
- (b) Exact boundary conditions are imposed at the irregular surfaces.
- (c) Using the orthogonal properties of the basis functions appearing in the complete expansions of the fields, Maxwell's equations are integrated over the transverse plane. Green's theorems are used to avoid term-by-term differentiation of the field expansions.

(d) Maxwell's equations for the electromagnetic fields are converted into coupled first order ordinary differential equations for the forward and backward traveling wave amplitudes. The coupled equations for the wave amplitudes are referred to as the generalized telegraphists' equations. (Section 2), (Bahar 1974).

2. The Generalized Telegraphists' Equations

For horizontally stratified media (see Fig. 1) the following field transform pairs provide the basis for the complete expansion of the transverse (y,z) components of the electric and the magnetic fields \vec{E}_T and \vec{H}_T respectively in terms of the vertically (V) and horizontally (H) polarized field transforms (Bahar 1973a,b):

$$\vec{E}_T(x,y,z) = \sum_v \int_{-\infty}^{\infty} [E^V(x,v,w)\vec{e}_T^V + E^H(x,v,w)\vec{e}_T^H]dw, \quad (1)$$

where

$$E^P(x,v,w) = \int_{-\infty}^{\infty} \vec{E}_T(x,y,z) \cdot (\vec{h}_P^T \times \vec{a}_x) dydz, \quad P=V \text{ or } H, \quad (2)$$

$$\vec{H}_T(x,y,z) = \sum_v \int_{-\infty}^{\infty} [H^V(x,v,w)\vec{h}_T^V + H^H(x,v,w)\vec{h}_T^H]dw, \quad (3)$$

where

$$H^P(x,v,w) = \int_{-\infty}^{\infty} \vec{H}_T(x,y,z) \cdot (\vec{a}_x \times \vec{e}_P^T) dydz, \quad P=V \text{ or } H, \quad (4)$$

In the above expressions E^P and H^P ($P=V,H$) are the electric and magnetic field transforms and \vec{e}_T^P and \vec{h}_T^P are the electric and magnetic field basis function while \vec{e}_P^T and \vec{h}_P^T are the reciprocal basis functions for horizontally stratified media. The symbol, \sum_v , denotes summation over the entire wavenumber spectrum v. The generalized Fourier transform consists of two infinite integrals (continuous part of the wavenumber spectrum) which are associated with the radiation and the lateral wave terms and a finite set of surface wave terms (discrete part of the wavenumber spectrum).

The basis functions for the vertically polarized waves are

$$\bar{e}_T^V = Z^V (\bar{a}_y \psi^V(v, y) - \frac{\bar{a}_z i w}{u^2 + w^2} \frac{\partial \psi^V(v, y)}{\partial y}) \phi(w, z) \quad (5)$$

and

$$\bar{h}_T^V = \bar{a}_z \psi^V(v, y) \phi(w, z) \quad (6)$$

and the complementary basis functions for the vertically polarized waves are

$$\bar{e}_V^T = Z^V N^V (\bar{a}_y \psi^V(v, y) + \frac{\bar{a}_z i w}{u^2 + w^2} \frac{\partial \psi^V(v, y)}{\partial y}) \phi^C(w, z) \quad (7)$$

and

$$\bar{h}_V^T = \bar{a}_z N^V \psi^V(v, y) \phi^C(w, z). \quad (8)$$

For the horizontally polarized waves, the basis functions and the complementary basis functions are respectively,

$$\bar{e}_T^H = \bar{a}_z \psi^H(v, y) \phi(w, z), \quad (9)$$

$$\bar{h}_T^H = Y^H (-\bar{a}_y \psi^H(v, y) + \frac{\bar{a}_z i w}{u^2 + w^2} \frac{\partial \psi^H(v, y)}{\partial y}) \phi(w, z), \quad (10)$$

and

$$\bar{e}_H^T = \bar{a}_z N^H \psi^H(v, y) \phi^C(w, z), \quad (11)$$

$$\bar{h}_H^T = Y^H N^H (-\bar{a}_y \psi^H(v, y) - \frac{\bar{a}_z i w}{u^2 + w^2} \frac{\partial \psi^H(v, y)}{\partial y}) \phi^C(w, z). \quad (12)$$

in which N^P are normalization coefficients, Z^P and Y^P are the wave impedance and admittance and

$$\phi(w, z) = \exp(-i w z) \text{ and } \phi^C(w, z) = (1/2\pi) \exp(i w z). \quad (13)$$

The scalar basis functions for the radiation fields and the lateral waves are

$$R_{PO}^{Dh, P}(v, y) = \begin{cases} \exp(i v_0 y) + R_{PO}^{Dh} \exp(-i v_0 y), \\ \text{for medium 0,} \\ \frac{\bar{r}}{\bar{l}} \frac{T_{Pq-1}^D}{T_{Pq}^{DH}} \exp(i \sum_{q=1}^{\bar{r}} v_{p-1, q}^h) \\ \times [\exp(i v_r y) + R_{Pr}^{Dh} \exp(-i v_r y)], \\ \text{for medium } r = 1, 2, 3, \dots, m, \end{cases} \quad (14)$$

$$R_{Pm}^{Uh} \psi_m^P(v, y) = \begin{cases} \prod_{q=1}^{m-r} \frac{T_{Pm+1-q}^U}{T_{Pm-q}^{UH}} \exp(i \sum_{q=1}^{m-r} v_{m-q, m+1-q} h_{m-q, m+1-q}) \\ \times [\exp(-iv_r y) + R_{Pr}^{Uh} \exp(iv_r y)], \text{ for medium } r=0, 1, 2, \dots, m-1 \\ \exp(-iv_m y) + R_{Pm}^{Uh} \exp(iv_m y), \text{ for medium } m, \end{cases} \quad (15)$$

For the surface wave

$$\psi_s^{Pn}(v, y) = \psi_s^{Pn}(v, h_{0,1}) \begin{cases} \exp[-iv_0^n(y - h_{0,1})], \text{ for medium } 0, \\ \frac{1}{T_{P1}^{DH}} \exp(-iv_1^n h_{0,1}) [\exp(iv_1^n y) + R_{P1}^{Dh} \exp(-iv_1^n y)], \\ \text{for medium } 1, \\ \frac{1}{T_{P1}^{DH}} \exp(-iv_1^n h_{0,1}) \prod_{q=2}^r \frac{T_{Pq-1}^D}{T_{Pq}^{DH}} \\ \times \exp(i \sum_{q=2}^r v_{q-1,q}^n h_{q-1,q}) [\exp(iv_r^n y) + R_{Pr}^{Dh} \exp(-iv_r^n y)], \\ \text{for medium } r=2, 3, \dots, m, \end{cases} \quad (16)$$

where

$$[\psi_s^{Pn}(v, h_{0,1})]^2 = \left[u / i Z_0^P v_0 \frac{d}{du} \frac{1}{R_{P0}^D} \right]_{v=v_n} \quad (17)$$

The scalar functions for vertically and horizontally polarized waves $\psi^V(v, y)$ and $\psi^H(v, y)$, are given by (14), (15), and (16), on replacing the letter P in all the expressions by V and H respectively. The reflection coefficient at the $i, i+1$ interface for waves incident from above is R_{Pi}^D and R_{Pi}^U is the reflection coefficient at the $i-1, i$ interface for waves incident from below.

The transmission coefficients are

$$\begin{aligned} T_{Pi}^D &= 1 + R_{Pi}^D, & T_{Pi}^U &= 1 + R_{Pi}^U, \\ T_{Pi}^{DH} &= 1 + R_{Pi}^{DH}, & T_{Pi}^{UH} &= 1 + R_{Pi}^{UH}. \end{aligned} \quad (18)$$

The modal equation which determines the surface wave parameters $v^n (\text{Im}(v) \leq 0)$,

is given by

$$1 - R_{Pi}^U R_{Pi}^D \exp(-i2v_i h_i) = 0, \quad v_i \equiv (k_i^2 - u^2 - w^2)^{\frac{1}{2}}, \quad v_{i-1, i} = v_{i-1} - v_i \quad (19)$$

where P equals V or H and $i=1, 2, 3, \dots$, or $m-1$ and $k_i = \omega(\mu_i \epsilon_i)^{\frac{1}{2}}$

The basis functions satisfy the biorthogonal relationships for P and Q equal to V or H

$$\left. \begin{aligned} \int_{-\infty}^{\infty} \bar{e}_T^P \cdot (\bar{h}_Q^T \times \bar{a}_x) dy dz \\ \int_{-\infty}^{\infty} \bar{h}_T^Q \cdot (\bar{a}_x \times \bar{e}_P^T) dy dz \end{aligned} \right\} = \delta_{P,Q} \Delta(v-v') \Delta(w-w') \quad (20)$$

in which, for the primed quantities the variables are u' , v' , and w' and

$$\Delta(v-v') = \delta_{q,r} \times \begin{cases} \delta(v-v'), & v' \neq v_s \\ \delta_{v,v_s}, & v' = v_s \end{cases} \quad (21)$$

The complete field expansions are substituted into Maxwell's equations for the transverse field components and use is made of the orthogonality relationship, Green's theorem, and the exact boundary conditions for irregular stratified media (for example see Fig. 1) to obtain the differential equations for the field transforms E^P and H^P . These may be expressed in terms of the forward and backward wave amplitudes a^P and b^P , respectively, as follows:

$$H^P = a^P \pm b^P \text{ and } E^P = a^P \mp b^P, \quad P = \begin{cases} V, & \text{upper sign} \\ H, & \text{lower sign} \end{cases} \quad (22)$$

Thus Maxwell's equations are converted into the following generalized telegraphists' equations for $P=V$ or H (Bahar 1973a,b):

$$-\frac{da^P}{dx} - iua^P = \sum_Q \int_v \int (S_{PQ}^{BA} a^Q + S_{PQ}^{BB} b^Q) dw' - A^P, \quad (23)$$

and

$$-\frac{db^P}{dx} + iub^P = \sum_Q \int_v \int (S_{PQ}^{AA} a^Q + S_{PQ}^{AB} b^Q) dw' + B^P. \quad (24)$$

Explicit closed form expressions for the reflection and the transmission scattering coefficients S_{PQ}^{AA} , S_{PQ}^{BB} , S_{PQ}^{BA} and S_{PQ}^{AB} have been derived (Bahar 1973b). Thus, for instance, $S_{VH}^{AA}(v,w,v',w')$ accounts for coupling of the incident horizontally polarized forward wave amplitude $a^H(v',w')$ into the reflected vertically polarized wave amplitude $b^V(v,w)$. Similarly, $S_{HV}^{BA}(v,w,v',w')$ accounts for coupling of the incident vertically polarized forward wave

amplitude $a^V(v', w')$ into the forward scattered horizontally polarized wave amplitude $a^H(v, w)$. In (23) and (24), the terms A^P and B^P account for the electromagnetic source excitation in any of the layers of the structure and (u', v', w') , (u, v, w) are the orthogonal components of the vector wavenumbers \bar{k}' and \bar{k} in the directions of the incident and scattered waves. The incident and scattered wave vectors \bar{k}' and \bar{k} are in general associated with either the radiation fields, the lateral waves or the guided waves of the structure. Thus, the scattering coefficients account for coupling between components of the entire wavenumber spectrum. The derivations of the generalized telegraphists' equations (23), (24) is rigorous. They can be solved rigorously using numerical techniques (for example the eigenvalue-eigenvector technique (Ishimaru et al. 1982)).

In the following specific applications some simplifying assumptions are made to facilitate the solution of these coupled first order differential equations. Thus for instance, if multiple scattering between different portions of the rough surface is neglected, the far fields can be expressed in closed form as integrals that can be readily evaluated numerically.

3. Scattering and Depolarization by Random Rough Surfaces

In order to account for specular point scattering as well as diffuse scattering by random rough surfaces, a two-scale model of the rough surface was adopted (Wright 1968, Valenzuela 1968, Brown 1978). Thus, on applying the physical optics approach (Beckmann and Spizzichino 1963) the surface h_L consisting of the large scale components ($k < k_d$) of the surface height spectral density function $W(k)$, accounts for specular point scattering. Similarly on applying the perturbation approach (Rice 1951) the surface h_s consisting of the small scale components ($k > k_d$) of the surface height spectral density function $W(k)$ accounts for diffuse scattering. On adopting the two-scale approach it is assumed that the large scale surface h_L and the small scale surface h_s are statistically independent.

Several questions arise as a result of the use of the two-scale, hybrid, physical optics-perturbation approach to problems of scattering by random rough surfaces. In particular there are conflicting constraints on the choice of the wavenumber k_d where spectral splitting of the rough surface spectral density function is assumed to occur (Brown 1978, Bahar and Barrick 1983, Bahar et al 1983). Moreover, since the physical optics solution for the cross polarized backscatter cross section is zero, the solution based on the two-scale perturbed-physical optics model does not correctly predict the cross polarized backscatter cross section particularly for near normal incidence (Bahar and Fitzwater 1984).

Since the full wave solution is valid in both the high frequency (physical optics) limit as well as the low frequency perturbation limit $\beta = 4k_0^2 \langle h_s^2 \rangle \ll 1$, it accounts for specular point and diffuse scattering in a unified self-consistent manner. Thus it is not necessary to artificially decompose the random surface into two presumably uncorrelated surfaces when the full wave approach (Sec. 2) is used. The solutions for the like and cross polarized scattering cross sections per unit area, that follow from the full wave approach, upon neglecting multiple scattering between different patches of the rough surface) can be expressed as follows (Bahar and Fitzwater 1985)

$$\langle \sigma^{PQ} \rangle = \frac{1}{\pi} \int \left| \frac{k_0^D}{\bar{n} \cdot \bar{a}_y} \right|^2 P_2^P(\bar{n}) d\bar{n} \left[Q(\bar{n}^f, \bar{n}^i) + \frac{1}{A_y} \left| \chi(\exp(i v_x x + i v_z z)) dx dz \right|^2 \right] \quad (25)$$

in which \bar{a}_y is the unit vector normal to the unperturbed reference plane (x, z) , \bar{n} is the unit vector normal to the rough surface and A_y is the area of its projection in the reference (x, z) plane. In (25) the superscripts PQ correspond to the polarizations of the scattered and incident waves respectively $\{P, Q = V \text{ (vertical), } H \text{ (horizontal)}\}$. The unit vectors \bar{n}^i and \bar{n}^f are in the direction of the incident and scattered wave normals, k_0 is the free space electromagnetic wavenumber and the vector \bar{v} is

$$\bar{v} = k_0 (\bar{n}^f \cdot \bar{n}^i) = v_x \bar{a}_x + v_y \bar{a}_y + v_z \bar{a}_z \quad (26)$$

The coupling coefficients D^{PQ} depend on the polarizations and the directions of propagation of the incident and scattered waves as well as the complex electromagnetic parameters of the medium of propagation. The slope probability density function for the rough surface is $p(\bar{n})$, $\int p(\bar{n} \cdot \bar{a}_y + 0) d\bar{n} = \sin \gamma dy d\delta$ is the differential (solid) angle and P_2 is the shadow function derived by Sancer (1968). The coefficient $Q(\bar{n}^f, \bar{n}^i)$ is given by

$$Q(\bar{n}^f, \bar{n}^i) = \int (\chi_2 - |\chi|^2) \exp(i\bar{v} \cdot \bar{r}_d) d\chi_d dz_d \quad (27)$$

in which χ_2 and χ are the joint characteristic function and the characteristic function for the rough surface and

$$\bar{r}_d = x_d \bar{a}_x + z_d \bar{a}_z \quad (28)$$

is the distance measured in the unperturbed reference plane. The first term in (25) accounts for both specular point as well as diffuse scattering while the second term is the coherent scattering term. This second term becomes very small as the mean square rough surface height $\langle h^2 \rangle$ becomes very large since for a Gaussian surface $|\chi|^2 = \exp(-4v_y^2 \langle h^2 \rangle)$. The unified full wave solutions for the ratio of the like to cross polarized scattering cross sections are shown to be in good agreement with experimental results (Bahar and Fitzwater 1985), however additional measurements are needed to make more extensive comparisons between theory and experiment.

4. Propagation in Nonuniform Stratified Structures

Propagation of radio waves in nonuniform stratified structures is of interest in a large variety of technical problems. For instance, Schlak and Wait (1967, 1968) treated the problem of propagation over a nonparallel stratified earth using a geometrical optical approach to derive an equivalent surface impedance at the air-earth interface (see Fig. 1). The resulting mixed path propagation problem was solved through a judicious use of the compensation theorem. The realization of the salient features of the solution to this problem led Schlak and Wait to submit their solution to a critical reciprocity test which pointed out several restrictions on the geometrical optical approach.

Wave coupling in a variety of nonuniform layered structures is also of special interest for the design of a variety of devices in optical waveguide systems (R. G. Hunsperger 1982). The full wave solutions (23), (24) explicitly account for coupling between the different spectral components of the complete expansions. Thus, these solutions can be used to design nonuniform layered structures that effectively couple electromagnetic signals into and out of optical waveguides.

The full wave solutions are shown to satisfy the duality, realizability and reciprocity relationships in electromagnetic theory. Thus for the vertically polarized case (see Fig. 1) for example, the radiation (magnetic) field scattered by the nonuniform stratified structure shown in Fig. 1 is expressed as follows (Bahar and Fitzwater 1978a,b)

$$H_z^f(x,y) = (2\pi/k_0 \rho)^{1/2} \exp(-ik_0 \rho) \exp(i\pi/4) P(v^f, v^i) H_m^i \quad (29)$$

in which H_m^i is the magnitude of the incident magnetic field at the origin, ρ is the radial distance from the z axis and $P(v^f, v^i)$ is the radiation pattern:

$$P(v^f, v^i) = P_0(v^f, v^i) \sum_{p,q} I_{p,q}(v^f, v^i) \quad (30)$$

where

$$P_0(v^f, v^i) = (1 - S_1^f S_1^i - z_s^2) T_{21}(v^f) T_{21}(v^i) T_{10}(v^f) T_{10}(v^i) / 4\pi \epsilon_r \quad (31)$$

In (31) ϵ_r is the relative complex dielectric coefficient for the overburden and z_s is the normalized surface impedance of the substratum. The complex angles

for the incident and scattered waves in free space (subscript o) and the overburden (subscript 1) are related by Snell's law and $S_1^i = \sin \theta_1^i, S_1^f = \sin \theta_1^f$. The transmission coefficients from the overburden to the substratum are $T_{21}(v^i)$ and $T_{21}(v^f)$ for the incident and scatter angles θ_1^i and θ_1^f respectively, while the corresponding transmission coefficients from the air to the overburden are $T_{10}(v)$ and $T_{10}(v^f)$. The terms in the double infinite sum are

$$I_{p,q}(v^f, v^i) = \frac{[R_{01}(v^f)R_{21}(v^f)]^{p-1}[R_{01}(v^i)R_{21}(v^i)]^{q-1}}{(2p-1)C_1^f + (2q-1)C_1^i} \cdot \int_{-L}^L k_o \exp[i(u^f - u^i)x - i\{(2p-1)v_1^f + (2q-1)v_1^i\}h(x)] dx \quad (32)$$

in which R_{21} and R_{01} are the overburden to substrate and overburden to air Fresnel reflection coefficients respectively, while $C_1^i = \cos \theta_1^i = u^i/k_1$ and $C_1^f = \cos \theta_1^f = u^f/k_1$. The arbitrarily varying height of the overburden substratum interface is $h(x)$. It is interesting to note that while the solution based on the geometrical-optics approach involves a single summation (that depends on the direction of propagation of the incident wave), the full wave solution involves double infinite sums that satisfy the reciprocity relations in electromagnetic theory. For the special case when $k_o = k_1$ (no overburden) and $h=0$, the full wave solution (29) reduces to the physical optics expression for diffuse scattering in the specular direction

$$H_z^f(x, y) = (i/2\pi k_o \rho)^{1/2} \exp(-ik_1 \rho) 2k_o L C_1^i R_{21}^i H_m^i \quad (33)$$

5. Waveguides with Irregular Boundaries

When the boundary conditions for the electromagnetic fields at the uppermost interface and the lowermost interface of the irregular stratified structure can be approximated by a surface impedance condition, namely

$$\vec{E} = \vec{Z} \cdot \vec{H} \times \vec{n} \quad (34)$$

in which \vec{Z} is an impedance diadic (Gallawa 1964), (as in the case of highly reflecting boundaries such as good conductors), the electromagnetic fields may be expanded completely in terms of waveguide modes. The wave spectrum in this case is discrete (the radiation fields and lateral wave contributions

vanish). The resulting telegraphists' equation (23),(24) for the coupled forward and backward propagating waveguide modes of the irregular structure can be readily solved numerically using the Runge-Kutta method (Abramowitz and Stegun 1964).

The full wave approach can also be applied to problems of propagation in irregular stratified cylindrical and spheroidal structures (Bahar 1975, 1980; Bahar and Fitzwater 1983). For these structures, the contribution from the continuous portion of the wave spectrum vanishes if the electromagnetic fields at the innermost interface of the structure can be characterized by a surface impedance condition (34).

6. Concluding Remarks

An interesting feature of the full wave solution is that by avoiding the imposition of simplifying assumptions (such as Kirchhoff or perturbation approximations) at the outset of the analysis, it is possible to demonstrate succinctly the limitations of the earlier solutions and the relationships between them. Thus for instance, by simply replacing \bar{n} in (25) by its value at the specular points $\bar{n} = \bar{v}/v$ ($v^2 = \bar{v} \cdot \bar{v}$) one obtains the physical optics solutions. Furthermore by replacing \bar{n} by \bar{a}_y and assuming that $\beta \equiv 4k_0^2 \langle n^2 \rangle \ll 1$, the expression for Q (27) becomes $Q = |\pi v_y \chi(v_y)|^2 W(k)$ and (25) reduces to the perturbation solution (Rice 1951).

7. References

1. Abramowitz, M. and A. Stegun (1964) Handbook of Mathematical Functions, U.S. Government Printing Office, Washington, D.C.
2. Bahar, E., (1973a), "Electromagnetic Wave Propagation in Inhomogeneous Multilayered Structures of Arbitrary Thickness-Generalized Field Transforms," J. Math. Phys., Vol. 14, No. 8, pp. 1024-1029.
3. Bahar, E., (1973b), "Electromagnetic Wave Propagation in Inhomogeneous Multilayered Structures of Arbitrary Thickness-Full Wave Solutions," J. Math. Phys., Vol. 14, No. 8, pp. 1030-1036.
4. Bahar, E., (1974), "Depolarization in Nonuniform Multilayered Structures--Full Wave Solutions," J. Math. Phys., Vol. 15, No. 2, pp. 202-208.
5. Bahar, E., (1975), "Propagation in Irregular Multilayered Cylindrical Structures of Finite Conductivity--Full Wave Solutions," Canadian Journal of Physics, Vol. 53, No. 11, pp. 1088-1096.
6. Bahar, E., (1980), "Computations of the Transmission and Reflection Scattering Coefficients in an Irregular Spheroidal Model of the Earth-Ionosphere Waveguide," Radio Science, Vol. 15, No. 5, pp. 987-1000.

7. Bahar, E. and D. E. Barrick (1983), "Scattering Cross Sections for Composite Rough Surfaces that Cannot be Treated as Perturbed Physical Optics Problems," Radio Science, Vol. 18, No. 2, pp. 129-137.
8. Bahar, E., D. E. Barrick and M. A. Fitzwater (1983), "Computations of Scattering Cross Sections for Composite Surfaces and the Specification of the Wavenumber Where Spectral Splitting Occurs," IEEE Transactions on Antennas and Propagation, Vol. AP-31, No. 5, pp. 698-709.
9. Bahar, E. and M. Fitzwater (1978a), "Transient Electromagnetic Response from Nonparallel Stratified Models of the Earth's Crust, 1, Scattered Radiation Field," Radio Science, Vol. 13, No. 1, pp. 1-10.
10. Bahar, E. and M. Fitzwater (1978b), "Transient Electromagnetic Response from Nonparallel Stratified Models of the Earth's Crust, 2, The Scattered Surface Wave," Radio Science, Vol. 13, No. 1, pp. 11-20.
11. Bahar, E. and M. A. Fitzwater (1983), "Scattering and Depolarization of Electromagnetic Waves in Irregular Stratified Spheroidal Structures of Finite Conductivity-Full Wave Analysis," Canadian Journal of Physics, Vol. 61, No. 1, pp. 128-139.
12. Bahar, E. and M. A. Fitzwater (1984), "Scattering Cross Sections for Composite Rough Surfaces Using the Unified Full Wave Approach," IEEE Transactions on Antennas and Propagation, Vol. AP-32, No. 7, pp. 730-734.
13. Bahar, E. and M. A. Fitzwater (1985), "Like and Cross Polarized Scattering Cross Sections for Random Rough Surfaces; theory and experiment," Journal of Optical Society of America, Vol. 2, No. 12, pp. 2295-2303.
14. Beckmann, P., and A. Spizzichino (1963), The Scattering of Electromagnetic Waves from Rough Surfaces, MacMillan, New York.
15. Brown, G. S., (1978), "Backscattering from a Gaussian-Distributed Perfectly Conducting Rough Surface," IEEE Transactions on Antennas and Propagation, Vol. AP-26, No. 3, pp. 472-482.
16. Gallawa, R. L., (1964), "Propagation in Nonuniform Waveguides with Impedance Walls," J. Research NBS (Radio Propagation), Vol. 68D, pp. 1201-1213.
17. Hunsperger, R. G., (1982), Integrated Optics: Theory and Technology, Springer-Verlag, New York.
18. Ishimaru, A., R. Woo, J. W. Armstrong and D. C. Blackman (1982), "Multiple Scattering Calculations of Rain Effects," Radio Science, Vol. 17, No. 6, pp. 1425-1433.
19. Rice, O. (1951), "Reflection of Electromagnetic Waves from a Slightly Rough Surface," Communicat. Appl. Matl., Vol. 4, pp. 351-378.
20. Sancer, M. I. (1968), "Shadow-Corrected Electromagnetic Scattering from a Randomly Rough Surface," IEEE Transactions on Antennas and Propagation, Vol. AP-17, No. 5, pp. 577-585.
21. Schlak, G. A., and J. R. Wait (1967), "Electromagnetic Wave Propagation Over a Nonparallel Stratified Conducting Medium," Can. J. Phys., Vol. 45, pp. 3697-3720.
22. Schlak, G. A., and J. R. Wait (1968), "Attenuation Function for Propagation Over a Nonparallel Stratified Ground," Can J. Phys., Vol. 46, pp. 1135-1136.
23. Valenzuela, G. R. (1968), "Scattering of Electromagnetic Waves from a Tilted Slightly Rough Surface," Radio Science, Vol. 3, No. 11, pp. 1051-1066.
24. Wright, G. R. (1968), "A New Model for Sea Clutter," IEEE Transactions on Antennas and Propagation, Vol. AP-16, No. 2, pp. 217-223.

SCATTERING AND DEPOLARIZATION BY CONDUCTING CYLINDERS
WITH ROUGH SURFACES

Ezekiel Bahar
and
Mary Ann Fitzwater
Electrical Engineering Department
University of Nebraska--Lincoln
Lincoln, NE 68588-0511

ABSTRACT

Like and cross polarized scattering cross sections are determined at optical frequencies for conducting cylinders with rough surfaces. Both normal and oblique incidence with respect to the cylinder axis are considered. The full wave approach is used to account for both the specular point scattering and the diffuse scattering. For the roughness scales considered, the scattering cross sections differ significantly from those derived for smooth or slightly rough conducting cylinders. Several illustrative examples are presented and the albedos for smooth and rough cylinders are compared.

1. Introduction

The problem of electromagnetic scattering by finitely conducting cylinders or spheres has been dealt with extensively in the technical literature. Perturbation theory has been used to extend these results to scattering by circular cylinders or spheres with slightly rough surfaces (Barrick 1970). However, perturbation theory is limited to surfaces for which the roughness parameter $\beta = 4k_0^2 \langle h_s^2 \rangle < 0.1$ (k_0 is the electromagnetic wavenumber and $\langle h_s^2 \rangle$ is the mean square height of the rough surface, Brown 1978). For the low frequency limit, ($\beta \ll 1$), the scattering cross sections are not significantly different from those for smooth conducting circular cylinders. On the other hand, in the high frequency limit when the scales of the surface roughness are large such that the radii of curvature of the surface are large compared to a wavelength λ_0 and the major contributions to the scattered fields come from the neighborhood of the stationary phase (specular) points on the surface of the scatterer, the Kirchhoff approximations for the surface fields may be used to yield the physical optics solutions (Beckmann and Spizzichino 1963; Barrick 1970). For the general case however, when the high or low frequency approximations are not applicable, the physical optics or perturbation methods cannot be used.

In this work the full wave approach is used to determine the like and cross polarized scattering cross sections at optical frequencies for finitely conducting cylinders with roughness scales that significantly modify the scattering cross sections ($\beta=1$). While the radii of curvature of the unperturbed cylinders considered are large compared to the wavelength λ_0 , the radii of curvature of the rough

surfaces are not. The cross section of the unperturbed cylinder need not be circular. Both specular point scattering and diffuse scattering are accounted for in the analysis in a self-consistent manner and the cross sections are expressed as a weighted sum of two cross sections. Multiple scattering from the surface of the cylinder however, is neglected.

In Section 2 the special forms of full wave solutions are presented for long cylinders with mean circular cross sections and both the specular point and diffuse contributions are identified. The solutions are given in matrix form to include both the like and cross polarized contributions. The solutions are presented as closed form integrals (not integral equations) involving the scattering surface. Thus, although they remain valid for large and small roughness scales, they are no more difficult for a user to employ, than the corresponding physical optics or perturbation expressions. In Section 3 several illustrative examples are considered for cylinders with roughness parameter $\beta=1$. The random rough surface (assumed here to have Gaussian statistics) is characterized by its surface height (isotropic) spectral density function and a corresponding non-Gaussian autocorrelation function. The like and cross polarized cross sections as well as the albedos for smooth and rough cylinders are compared. To facilitate the analysis, it is assumed here that the radius of the cylinder is not only large compared to the wavelength but also large compared to the rough surface height correlation length.

The scattered radiation fields for two-dimensionally rough surfaces can be expressed in matrix form as follows (Bahar 1981a)

$$\begin{pmatrix} G^{Vf} \\ G^{Hf} \end{pmatrix} = G_o \begin{pmatrix} D^{VV} & D^{VH} \\ D^{HV} & D^{HH} \end{pmatrix} \begin{pmatrix} G^{Vi} \\ G^{Hi} \end{pmatrix} \exp[i\vec{v} \cdot \vec{r}_s] dS \quad (2.1)$$

in which G^{Vf} and G^{Hf} are the vertically and horizontally polarized (electric or magnetic) fields scattered at a distance r in the direction of the unit vector \vec{n}^f . Similarly, G^{Vi} and G^{Hi} are the vertically and horizontally polarized fields incident (at the origin) in the direction of the unit vector \vec{n}^i . The scattering matrix D is a function of the direction of the incident and scattered waves \vec{n}^i and \vec{n}^f , the unit vector \vec{n} normal to the rough surface and the complex permittivity ϵ and permeability μ of the medium. It is expressed as (Bahar 1981a, 1982)

$$D = C_o^{in} T^f F T^i U(-\vec{n}^i \cdot \vec{n}) U(\vec{n}^f \cdot \vec{n}) \quad (2.2)$$

in which the transformation matrices T^f and T^i relate the scattered and incident waves in the local planes of scatter and incidence to reference planes of scatter and incidence while F is the scattering matrix defined in the local planes of incidence and scatter. The coefficient G_o is

$$G_o = -ik_o \exp(-ik_o r) / 2\pi r \quad (2.3)$$

An $\exp(i\omega t)$ time dependence is assumed in this work and $U(\alpha)$ is the unit step function. The vector \vec{v} is

$$\vec{v} = k_o (\vec{n}^f - \vec{n}^i) = v_x \vec{a}_x + v_y \vec{a}_y + v_z \vec{a}_z \quad (2.4)$$

and

$$C_o^{in} = -\vec{n}^i \cdot \vec{n} \quad (2.5)$$

where \vec{n} is the unit vector normal to the rough surface S . The position vector to a point on the rough surface is \vec{r}_s . In view of the unit step functions appearing in (2.2), the integration in (2.1) is over the surface that is illuminated and visible. Thus (2.2) does not include the shadow forming wave (Morse and Feshbach 1953). The differential cross sectional area is

$$dS = dx dz / (\vec{n} \cdot \vec{a}_y) \quad (2.6)$$

In order to derive the full wave expression (2.1) complete spectral expansions of the electric and magnetic fields are used, exact boundary conditions are imposed and Maxwell's equations are converted into rigorous sets of telegraphists' equations (Bahar 1973a,b). The far field approximations (2.1) are obtained from these telegraphists' equations on neglecting multiple scattering from one element of the rough surface to another and on employing suitable coordinate transformations (Bahar 1981a). The expression (2.1) is invariant to coordinate transformations and it satisfies duality and reciprocity relationships in electromagnetic theory. For very (infinitely) long one-dimensionally rough surfaces, the integral (2.1) can be reduced to a line integral by noting the integral expression for the Dirac delta function

$$\int_{-\infty}^{\infty} \exp(iv_z z) dz = 2\pi\delta(v_z) \quad (2.7)$$

On evaluating the expressions for the radiation (far) fields from the expressions for their transforms (using the steepest descent method, Bahar and Rajan (1979)), it can be shown that

$$G^i = G_o^i \int DG^i \exp[i\vec{v} \cdot (x \vec{a}_x + y \vec{a}_y)] dx / (\vec{n} \cdot \vec{a}_y) \quad (2.8)$$

in which

$$G_o^i = - \left[\frac{k_o}{2\pi\rho \cos\theta_o^i} \right]^{1/2} \exp(i\pi/4) \exp \left[-ik_o (\rho \cos\theta_o^i + z \sin\theta_o^i) \right] \quad (2.9)$$

and for oblique incidence (with respect to the z axis) the direction of the incident plane wave is

$$\vec{n}^i = -\cos\theta_o^i \vec{a}_y + \sin\theta_o^i \vec{a}_z \quad (2.10)$$

The direction of the scattered wave is (Bahar 1981a)

$$\vec{n}^f = \sin\theta_o^f \cos\phi^f \vec{a}_x + \cos\theta_o^f \vec{a}_y + \sin\theta_o^f \sin\phi^f \vec{a}_z \quad (2.11)$$

(where the polar angle is measured with respect to the y axis, see Figs. 1 and 2). In view of (2.7)

$$\sin\theta_0^f \sin\phi^f = \sin\theta_0^i \quad (2.12)$$

Thus (2.11) can also be expressed as

$$\bar{n}^f = \cos\theta_0^i (\sin\phi^i \bar{a}_x + \cos\phi^i \bar{a}_y) + \sin\theta_0^i \bar{a}_z \quad (2.13)$$

where the azimuth angle ϕ^i is measured in the x-y plane with $\phi^i = 0$ along the y axis (see Figs. 1 and 2). The explicit expressions for the scattering coefficients D (2.2) have been presented earlier when the reference incident plane is normal to $\bar{n}^i \times \bar{a}_y$ and the reference scatter plane is normal to $\bar{n}^f \times \bar{a}_y$. However, if the planes of incidence and scatter are taken to be the planes normal to $\bar{n}^i \times \bar{n}_s$ (\bar{n}_s is the normal to the cylinder at the specular point) (Barrick 1970) in the expressions for T^f and T^i , the unit vector \bar{a}_y must be replaced by the unit vector .

$$\begin{aligned} \bar{n}_s &= \bar{v}/v = \sin(\phi'/2) \bar{a}_x + \cos(\phi'/2) \bar{a}_y = \bar{a}_r \\ &= \frac{\sin\theta_0^f \cos\phi^f \bar{a}_x + (\cos\theta_0^f + \cos\theta_0^i) \bar{a}_y}{[2 \cos\theta_0^i (\cos\theta_0^i + \cos\theta_0^f)]^{1/2}} \end{aligned} \quad (2.14)$$

To facilitate the derivation of the scattering cross sections for cylinders with rough surfaces from (2.8), it is assumed that the radius of the cylinder is large compared to the wavelength and the rough surface height correlation length. In view of the conductivity of the cylinders, transmission through its cross section is negligible. Thus the normalized scattering cross sections (or scattering widths) for cylinders with rough surfaces are for P,Q=V,H

$$\begin{aligned} \langle \sigma^{PQ} \rangle &= \frac{\langle |G^{Pf}|^2 \rangle}{|G^{Qi}|^2} \frac{2\pi\rho}{\pi a} \\ &= \frac{k_0}{\pi a \cos\theta_0^i} \int \frac{D^{PQ} D^{PQ*} \exp[i v_x (x-x') + i v_y (y-y')]}{(\bar{n} \cdot \bar{a}_y) (\bar{n}' \cdot \bar{a}_y)} \chi_2 dx dx' \end{aligned} \quad (2.15)$$

where the radius vector to the surface of the rough cylinder is

$$\bar{r}_s = (a+h_s) \bar{a}_r = (a+h_s) \frac{(x \bar{a}_x + y \bar{a}_y)}{a} \quad (2.16)$$

and $a = (x^2 + y^2)^{1/2}$ is the radius of the unperturbed cylinder. The characteristic function χ and the joint characteristic function χ_2 for the random rough surface height h_s are the expectations

$$\chi = \langle \exp(iv_n h_s) \rangle \quad (2.17)$$

where

$$\bar{v} = 2k_o \cos \theta_o^i \cos(\phi'/2) \bar{n}_s, \quad v_n = \bar{v} \cdot \bar{n} \quad (2.18)$$

and

$$\chi_2 = \langle \exp[iv_n (h_s - h'_s)] \rangle \quad (2.19)$$

For Gaussian rough surface height probability density functions $p(h_s)$ and $p(h'_s, h'_s)$

$$|\chi|^2 = \exp[-v_n^2 \langle h_s^2 \rangle] \quad (2.20)$$

and

$$\chi_2 = |\chi|^2 \exp(v_n^2 \langle h_s h'_s \rangle) \quad (2.21)$$

At the specular point $\bar{n} = \bar{n}_s$ and

$$|\chi|^2 + |\chi|_\infty^2 = \exp[-v^2 \langle h_s^2 \rangle] = \exp[-\beta \cos^2(\phi'/2) \cos^2 \theta_o^i] \quad (2.22)$$

The surface height autocorrelation function $\langle hh' \rangle$ (which is not Gaussian) is the Fourier transform of the surface height spectral density function W (Rice 1951)

$$\frac{W(k)}{4} = \frac{1}{2\pi} \int_{-\infty}^{\infty} \langle h_s h'_s \rangle \exp(ik\tau) d\tau \quad (2.23)$$

In (2.23) $\langle h_s h'_s \rangle$ is assumed to be a function of the distance τ measured along the cylinder's circumference. The normalized scattering cross section (2.15) is expressed as a weighted sum of two cross sections (Bahar 1981b, Bahar and Barrick 1983)

$$\langle \sigma^{PQ} \rangle = |\chi|_\infty^2 \langle \sigma_\infty^{PQ} \rangle + \langle \sigma_s^{PQ} \rangle \quad (2.24)$$

The first term in (2.24) is the physical optics contribution $\langle \sigma^{PQ} \rangle$ modified by the coefficient $|\chi|^2$. It can be shown (using the steepest descent method) that for a conducting circular cylinder

$$\langle \sigma_\infty^{PQ} \rangle = \frac{k_o}{\pi a \cos \theta_o^i} \left| \int_{-a}^a \frac{D^{PQ}}{(\bar{n} \cdot \bar{a}_y)} \exp(iv_x x + iv_y y) dx \right|^2 = \frac{\cos(\phi'/2)}{\cos^2 \theta_o^i} \left| \frac{D^{PQ}}{\bar{n} \cdot \bar{a}_y} \right|_{\bar{n}=\bar{n}_s}^2 \quad (2.25)$$

When the planes of incidence and scatter are taken to be normal to $\vec{n}^i \times \vec{n}^f$ (2.25) reduces to

$$\langle \sigma_{\infty}^{PQ} \rangle = \cos(\phi'/2) |R_p|^2 \delta_{PQ} \quad (2.26)$$

in which R_p is the Fresnel reflection coefficient for the specular angle γ given by $\cos \gamma = -\vec{n}^i \cdot \vec{n}_s = \cos \theta_o^i \cos(\phi'/2)$ and δ_{PQ} is the Kronecker delta.

Due to the surface roughness, the physical optics contribution (specular scattering) is decreased by the factor $|\chi|^2$ (2.20). The surface roughness also gives rise to the diffuse scattering term

$$\langle \sigma_{\infty}^{PQ} \rangle_s = \frac{k_o}{\pi a \cos \theta_o^i} \int_{A_i} \int_{-\infty}^{\infty} |D^{PQ}|^2 \exp(iv_T \tau) (\chi_2 - |\chi|^2) d\tau \frac{dx}{\vec{n} \cdot \vec{a}_y} \quad (2.27)$$

in which A_i is the illuminated and visible portion of the surface. In (2.27), it is assumed that the rough surface correlation distance $\tau = l_c$ (where $\langle h_s^2 \rangle$ is equal to $\langle h_s^2 \rangle / e$) is very small compared to the circumference of the cylinder. The quantity $\chi_2 - |\chi|^2$ vanishes for $\tau \gg l_c$ (justifying the limits $(-\infty, \infty)$ in (2.27)).

On expressing it as an infinite series and on noting that for the unperturbed cylinder $\vec{n} = \vec{a}_r$, $\vec{n} \cdot \vec{a}_y = \cos \gamma$ and $dx/(\vec{n} \cdot \vec{a}_y) = a d\gamma$, (2.27) reduces to

$$\langle \sigma_{\infty}^{PQ} \rangle_s = \sum_{m=1}^{\infty} \langle \sigma_{\infty}^{PQ} \rangle_{sm} = \frac{2k_o}{\cos \theta_o^i} \int |D^{PQ}|^2 Q(v_n, v_T) d\gamma \quad (2.28)$$

in which v_n and v_T are the components of \vec{v} (2.7) normal and tangential to the surface of the unperturbed circular cylinder and

$$\begin{aligned} Q(v_n, v_T) &= \frac{1}{2\pi} \int (\chi_2 - |\chi|^2) \exp(iv_T \tau) d\tau \\ &= |\chi(v_n)|^2 \sum_m \left(\frac{v_n}{2} \right)^{2m} \frac{W_m(v_T)}{m!} \end{aligned} \quad (2.29)$$

in which $W_1 = W$ and for $m \geq 2$

$$\begin{aligned} W_m &= \frac{2^{2m}}{2\pi} \int_{-\infty}^{\infty} \langle h_s^2 \rangle^m \exp(iv_T \tau) d\tau \\ &= W_{m-1} \otimes W \equiv \int_{-\infty}^{\infty} W_{m-1}(k - v_T) W(k) dk \end{aligned} \quad (2.30)$$

Thus for $\beta = 4k_o^2 \langle h_s^2 \rangle \ll 1$, (2.28) reduces to the perturbation solution

$$\langle \sigma_{\infty}^{PQ} \rangle_s = \frac{k_o}{2 \cos \theta_o^i} \int |D^{PQ}|^2 v_n^2 W(v_T) d\gamma \quad (2.31).$$

The full wave solution (2.24) is valid in both the high frequency physical optics limit as well as the low frequency perturbation limit and it bridges the wide gap between them.

3. Illustrative Examples

In this section two different sets of physical and electrical parameters are considered for the illustrative examples. For case (1) (visual band) $\lambda = 0.555 \times 10^{-4}$ cm, the radius of the cylinder is $a = 10\lambda$ and the complex dielectric coefficient is $\epsilon = -40 - i12$ (aluminum; Ehrenreich, 1965). For case (2) (infrared band) $\lambda = 10 \times 10^{-4}$ cm, $a = 2.5\lambda$ and $\epsilon = -6000(1+i)$.

The random rough (homogeneous) surface height autocorrelation function $\langle hh' \rangle$ is assumed to be a function of distance τ measured around the circumference of the unperturbed cylinder. The corresponding surface height spectral density function $W(v_T)$ (2.23) is assumed to be given by

$$W(k) = \begin{cases} \frac{2B}{\pi k^4} & , \quad k_d < |k| < k_c \\ 0 & , \text{ elsewhere} \end{cases}$$

$$k_d = \pi/a \quad \text{and} \quad k_c = 4.5 \times 10^5 \text{ cm}^{-1}$$

for case (1) and

$$W(k) = \begin{cases} \frac{2B(k-k_d)^4}{\pi[(k-k_d)^2 + \kappa^2]^4} & , \quad k_d < |k| < k_c \\ 0 & , \text{ elsewhere} \end{cases}$$

$$k_d = 2/a \quad , \quad k_c = 4k_o \quad \text{and} \quad \kappa = 0.3k_d$$

for case (2).

The constants B in the above expressions for $W(k)$ are determined such that the roughness parameter $\beta = 4k_o^2 \langle h_s^2 \rangle = 1$, where the mean square height is given by

$$\langle h_s^2 \rangle = \int_{-\infty}^{\infty} \frac{W(k)}{4} dk = \beta/4k_o^2$$

Thus $B = 33.3 \text{ cm}^{-1}$ for case (1) and $B = 2.80 \text{ cm}^{-1}$ for case (2).

For case (1), the surface height spectral density function $W(k)$ decreases monotonically as $1/k^4$ and is maximum at $k=k_d$. For case (2), $W(k)$ vanishes at $k=k_d$ and it is maximum at $k=k_d + \kappa$. For $k > k_c$, (the spectral density cut off wavelength), the roughness scales are too small to affect the scattering cross sections (Brown 1978). Case (2) represents a surface with characteristic scales of roughness, relative to k_o , that are smaller than those for case (1). The mean square slopes σ_s^2 are (1) 0.00015 and (2) 0.01. The corresponding correlation length to circumference ratios $l_c/2\pi a = (\langle h_s^2 \rangle / 2)^{1/2} \pi a \sigma_s$ are (1) 0.015 and (2) 0.07.

In figures 3 and 4 $\langle \sigma^{VV} \rangle$ and $\langle \sigma^{HH} \rangle$ are plotted as functions of ϕ' for $\theta_o^i = 0$ and case (1). The corresponding plots for case (2) are shown in figures 5 and 6. The normals to the incident and scatter planes are given by $-\bar{n}^i \times \bar{a}_y$ and $-\bar{n}^f \times \bar{a}_y$ respectively. Note that for case (1) ($a/\lambda = 10$), there is very little difference between the two polarizations $\langle \sigma^{VV} \rangle$ and $\langle \sigma^{HH} \rangle$ however; for case (2) ($a/\lambda = 2.5$), the diffuse scattering contributions to the cross sections are polarization dependent. In figures 3 through 6, the contributions due to specular point scattering $\langle \sigma_{\infty}^{PP} \rangle \cdot |\chi|^2$ and the diffuse scattering terms $\langle \sigma^{PP} \rangle_{s1}$ and $\langle \sigma^{PP} \rangle_{s2}$ are also shown separately. For $\theta_o^i = 0$ there is no cross polarization ($\langle \sigma^{PQ} \rangle = 0 \text{ } P \neq Q$).

In figures 7, 8 and 9, the like and cross polarized total normalized cross sections $\langle \sigma^{VV} \rangle$, $\langle \sigma^{HH} \rangle$ and $\langle \sigma^{VH} \rangle = \langle \sigma^{HV} \rangle$ are plotted as functions of ϕ' for $\theta_o^i = 30^\circ$ and case (2). Cross sections for both smooth and rough cylinders are shown and the incident and scatter planes are normal to $-\bar{n}^i \times \bar{a}_y$ and $-\bar{n}^f \times \bar{a}_y$, respectively. Note that for the smooth cylinders $\langle \sigma^{VV} \rangle$ and $\langle \sigma^{HH} \rangle$ approach unity for the specular direction $\phi' = 0$ and become vanishingly small for $\phi' = \pi/2$. However for the rough cylinder the like cross sections do not display the sharp nulls near $\phi' = \pi/2$ and

for the specular direction, $\phi' = 0$, the normalized cross sections are significantly smaller than unity. On the other hand, for the smooth cylinder, the cross polarized cross sections are vanishingly small near the specular direction and peak around $\phi' = \pi/2$. For the rough cylinder however, no sharp null occurs near the specular direction. Thus, we observe that the scattering cross sections become more isotropic as one introduces surface roughness.

In figures 10, 11 and 12 the like and cross polarized total cross sections $\langle \sigma^{VV} \rangle$, $\langle \sigma^{HH} \rangle$ and $\langle \sigma^{HV} \rangle = \langle \sigma^{VH} \rangle$ are plotted as functions of ϕ' for $\theta_0^i = 30^\circ$ and case (2). In these plots however, the incident and scatter planes are defined as normal to the vector $\vec{n}^i \times \vec{n}^f$ (Barrick 1970). Cross sections for both smooth and rough cylinders are shown in figures 10 and 11. For the smooth cylinder there is no depolarization in the specular scatter plane normal to $\vec{n}^i \times \vec{n}^f$ (2.26) (Barrick 1970). It should be noted that for figures 10, 11 and 12 the definition of the incident plane depends on the scatter direction while it is fixed (normal to $\vec{n}^i \times \vec{a}_y$) in the context of figures 3 through 9.

The normalized extinction cross sections σ_{ext} , the albedo for smooth ($\beta=0$) and rough cylinders ($\beta=1$) are shown in Table I for case (1) and case (2) when the incident wave is either vertically (V) or horizontally polarized (H) and $\theta_0^i = 0$. Also shown in this table is the computed value of the albedo for $\beta=1$ when one does not account for the contribution due to diffuse scattering $\langle \sigma^{PQ} \rangle_s$. Clearly even for $\beta=1$, the contributions due to diffuse scattering are not negligible. As β increases, additional terms in the expansion (2.28) need to be considered and the solution based on perturbation analyses becomes inadequate (Barrick 1970).

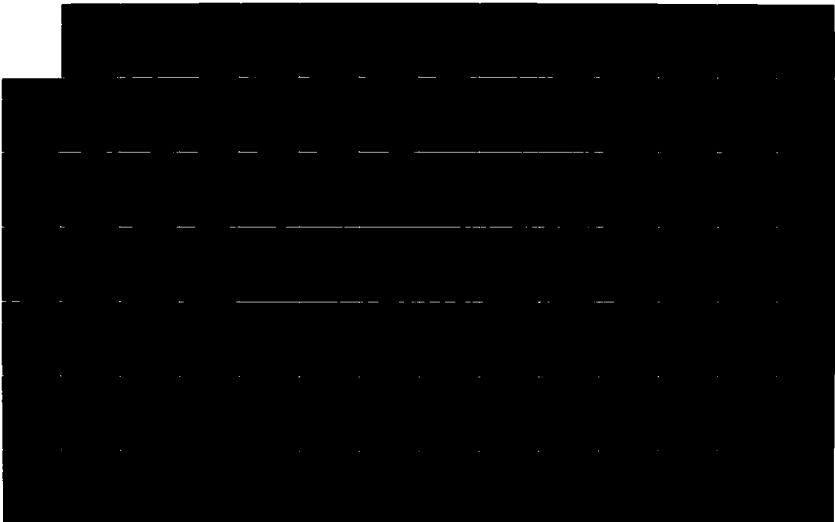
AD-A171 218

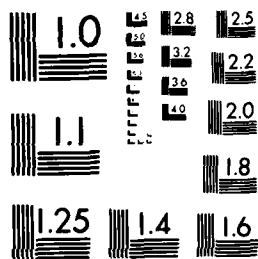
DEPOLARIZATION AND SCATTERING OF ELECTROMAGNETIC WAVES
APPENDICES (U) NEBRASKA UNIV LINCOLN 1 BAHAR 30 JUN 86
ARO-18128.17-EL-APP DRAC29-82-K-0123

3/3

UNCLASSIFIED

F/G 28/14 NL





MICROCOPY RESOLUTION TEST CHART
NATIONAL BUREAU OF STANDARDS 1963-A

In Table II, the corresponding values for the normalized extinction cross sections and the albedos are given for the case of oblique incidence $\theta_0^i = 30^\circ$.

It should be pointed out that in order to compute the albedo (the total scattered power in all directions divided by the extinction cross section for a given incident polarization), the plane of incidence is assumed to be normal to $-\hat{n} \times \hat{a}_y$. The total scattered power is obtained by averaging over the azimuthal angle, ϕ , the expression $\langle \sigma^{PP} \rangle_M |\chi|^2 + \langle \sigma^{PP} \rangle_S + \langle \sigma^{QP} \rangle_M |\chi|^2 + \langle \sigma^{QP} \rangle_S$ in which $\langle \sigma^{PP} \rangle_M$ and $\langle \sigma^{QP} \rangle_M$ are the like and cross polarized normalized Mie solutions (Barrick 1970), for the smooth cylinders and P/Q. The albedos for case (2) are larger mainly because $|\epsilon|$ is larger for $\lambda = 0.555 \times 10^{-4}$ cm than for $\lambda = 10 \times 10^{-4}$ cm.

4. Concluding Remarks

From the computed values of the like and cross polarized cross sections and albedos, it is obvious that even for roughness scales corresponding to $\beta=1$ the effects of surface roughness cannot be ignored and the diffuse scattering contribution is very significant. Using a perturbation approach to the problem, one is restricted to values of $\beta < 0.1$ (Brown 1978). In this case the perturbation diffuse scattering terms reduce to the first term in (2.28) $\langle \sigma^{PQ} \rangle_{sl}$. This term for $\beta < 0.1$ is negligibly small compared to the contribution due to specular scattering ($\langle \sigma^{PQ} \rangle |\chi|^2$). Thus the perturbation solutions for the albedo are not adequate when the effects of the surface roughness are significant.

Using the full wave approach, the surface roughness of the cylinder is characterized by its surface height autocorrelation function $\langle hh' \rangle$ or its Fourier transform $W(v_T)$. In this work diffuse scattering due to different forms of $W(v_T)$ (namely roughness

scales) is investigated. In the scattering plane normal to $\vec{n}^i \times \vec{n}^f$, the cross polarized cross section is only due to diffuse scattering, thus $\langle \sigma^{VH} \rangle$, as defined in Fig. 12, is most sensitive to the characteristics of the surface roughness. The dominant effect of surface roughness is to flatten out the peaks and dips in the scattering patterns and to make the scatterers more isotropic.

The albedos of the cylinders are computed for vertically and horizontally polarized waves at normal and oblique incidence. The results for both smooth and rough cylinders are given. It is shown in Tables I and II that the contribution due to diffuse scattering is significant, however, perturbation theory cannot adequately account for diffuse scattering when $\beta=1$.

Acknowledgments

This investigation was sponsored by the U.S. Army Research Office, Contract No. DAAG-29-82-K-0123. The authors wish to thank D. Barrick, F. G. Ullman and S. Chakrabarti for reading the manuscript and Mrs. E. Everett for preparing the manuscript.

References

1. Bahar, E. (1973a), "Depolarization of electromagnetic waves excited by distributions of electric and magnetic sources in inhomogeneous multilayered structures of arbitrarily varying thickness. Generalized field transforms," J. Math. Phys., Vol. 14, No. 11, pp. 1502-1509.
2. Bahar, E. (1973b), "Depolarization of electromagnetic waves excited by distributions of electric and magnetic sources in inhomogeneous multilayered structures of arbitrarily varying thickness. Full Wave solutions," J. Math. Phys., Vol. 14, No. 11, pp. 1510-1515.
3. Bahar, E. (1981a), "Full Wave Solutions for the Depolarization of the Scattered Radiation Fields by Rough Surfaces of Arbitrary Slope," IEEE Transactions on Antennas and Propagation, Vol. AP-29, No. 3, pp. 443-454.
4. Bahar, E. (1981b), "Scattering Cross Sections for Composite Random Surfaces--Full Wave Analysis," Radio Science, 16 (6), pp. 1327-1335.
5. Bahar, E. (1982), "Depolarization of the scattered radiation fields by conducting objects of irregular shape above rough land and sea: Full Wave Solutions," Radio Science, Vol. 17, No. 5, pp. 1055-1066.
6. Bahar, E., D. E. Barrick (1983), "Scattering Cross Sections for Composite Surfaces that Cannot be Treated as Perturbed Physical Optics Problems," Radio Science, Vol. 18, No. 2, pp. 129-137.

7. Bahar, E., G. G. Rajan (1979), "Depolarization and Scattering of Electromagnetic Waves by Irregular Boundaries for Arbitrary Incident and Scatter Angles, Full Wave Solutions," IEEE Transactions on Antennas and Propagation, AP-27 (2), pp. 214-225.
8. Barrick, D. E. (1970), Rough Surfaces in "Radar Cross Section Handbook," Chapter 8, Plenum Press, New York.
9. Beckmann, P., and A. Spizzichino (1963), The Scattering of Electromagnetic Waves from Rough Surfaces, MacMillan, New York.
10. Brown, G. S. (1978), "Backscattering from Gaussian-Distributed Perfectly Conducting Rough Surfaces," IEEE Transactions on Antennas and Propagation, AP-26 (3), pp. 472-482.
11. Ehrenreich, H. (1965), "The Optical Properties of Metals," IEEE Spectrum 2 (3), pp. 162-170.
12. Morse, P. M. and H. Feshbach (1953), Methods of Theoretical Physics, McGraw-Hill, New York.
13. Rice, S. O. (1951), "Reflection of Electromagnetic Waves from a Slightly Rough Surface," Communication of Pure and Applied Math, Vol. 4, pp. 351-378.

TABLE I $\theta_o^1 = 0^\circ$

	V case 1	H case 1	V case 2	H case 2
σ_{ext}	1.310	1.359	1.373	1.189
albedo $\beta = 0$.945	.915	.952	.926
albedo $\beta = 1$.894	.866	.924	.898
albedo $\beta = 1$ no $\langle \sigma^{PQ} \rangle_s$.759	.734	.776	.746

TABLE II $\theta_o^1 = 30^\circ$

	V case 1	H case 1	V case 2	H case 2
σ_{ext}	1.281	1.348	1.381	1.179
albedo $\beta = 0$.958	.911	.960	.956
albedo $\beta = 1$.923	.878	.942	.936
albedo $\beta = 1$ no $\langle \sigma^{PQ} \rangle_s$.797	.759	.816	.789

Figure Captions

- Fig. 1. Incident and scattered waves in the x-y plane.
- Fig. 2. Plane wave incident in the y-z plane.
- Fig. 3. $\langle \sigma^{VV} \rangle$, (2.24), case 1, $\theta_0^1 = 0^\circ$,
total(-), $|\chi|^2 \langle \sigma_\infty^{VV} \rangle (X)$, $\langle \sigma^{VV} \rangle_{s1}$ (\square), $\langle \sigma^{VV} \rangle_{s2}$ (Δ).
- Fig. 4. $\langle \sigma^{HH} \rangle$, (2.24), case 1, $\theta_0^1 = 0^\circ$,
total(-), $|\chi|^2 \langle \sigma_\infty^{HH} \rangle (X)$, $\langle \sigma^{HH} \rangle_{s1}$ (\square), $\langle \sigma^{HH} \rangle_{s2}$ (Δ).
- Fig. 5. $\langle \sigma^{VV} \rangle$, (2.24), case 2, $\theta_0^1 = 0^\circ$,
total(-), $|\chi|^2 \langle \sigma_\infty^{VV} \rangle (X)$, $\langle \sigma^{VV} \rangle_{s1}$ (\square), $\langle \sigma^{VV} \rangle_{s2}$ (Δ).
- Fig. 6. $\langle \sigma^{HH} \rangle$, (2.24), case 2, $\theta_0^1 = 0^\circ$,
total(-), $|\chi|^2 \langle \sigma_\infty^{HH} \rangle (X)$, $\langle \sigma^{HH} \rangle_{s1}$ (\square), $\langle \sigma^{HH} \rangle_{s2}$ (Δ).
- Fig. 7. $\langle \sigma^{VV} \rangle$, (2.24), case 2, $\theta_0^1 = 30^\circ$,
smooth cylinder (+), rough cylinder (\square).
- Fig. 8. $\langle \sigma^{HH} \rangle$, (2.24), case 2, $\theta_0^1 = 30^\circ$,
smooth cylinder (+), rough cylinder (\square).
- Fig. 9. $\langle \sigma^{HV} \rangle = \langle \sigma^{VH} \rangle$, (2.24), case 2, $\theta_0^1 = 30^\circ$,
smooth cylinder (+), rough cylinder (\square).
- Fig. 10. $\langle \sigma^{VV} \rangle$, (2.24), case 2, $\theta_0^1 = 30^\circ$, scatter plane,
smooth cylinder (+), rough cylinder (\square).
- Fig. 11. $\langle \sigma^{HH} \rangle$, (2.24), case 2, $\theta_0^1 = 30^\circ$, scatter plane,
smooth cylinder (+), rough cylinder (\square).
- Fig. 12. $\langle \sigma^{HV} \rangle = \langle \sigma^{VH} \rangle$, (2.24), case 2, $\theta_0^1 = 30^\circ$, scatter plane,
smooth cylinder (+), rough cylinder (\square).

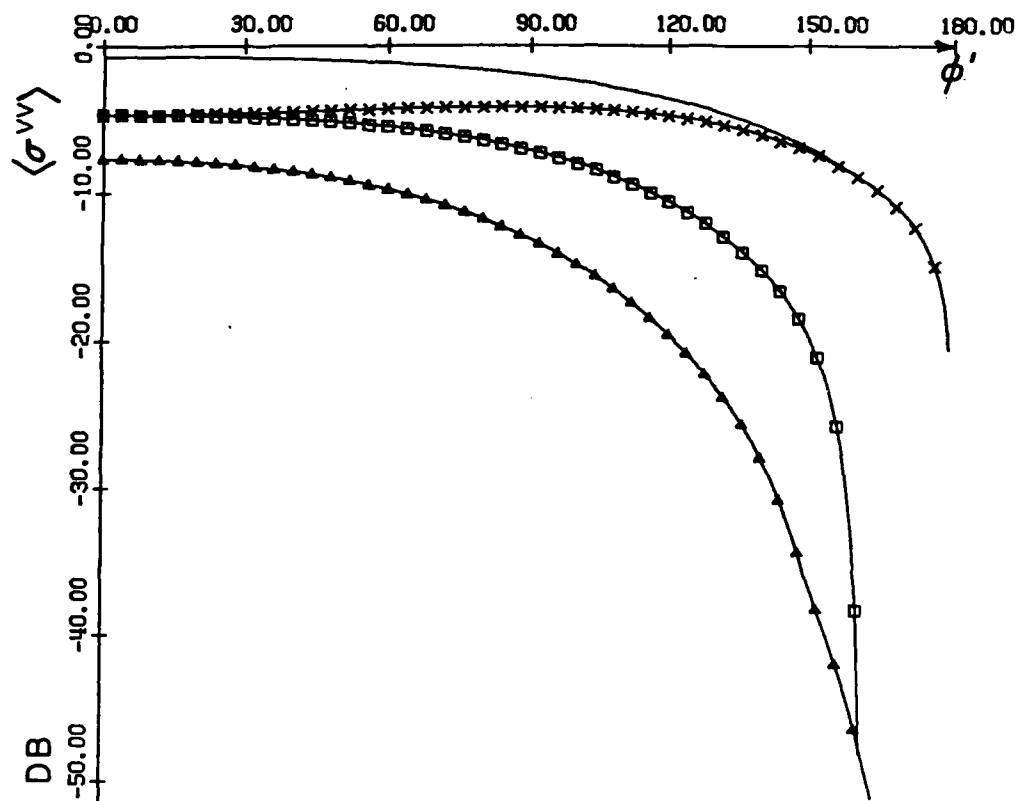


Fig. 3

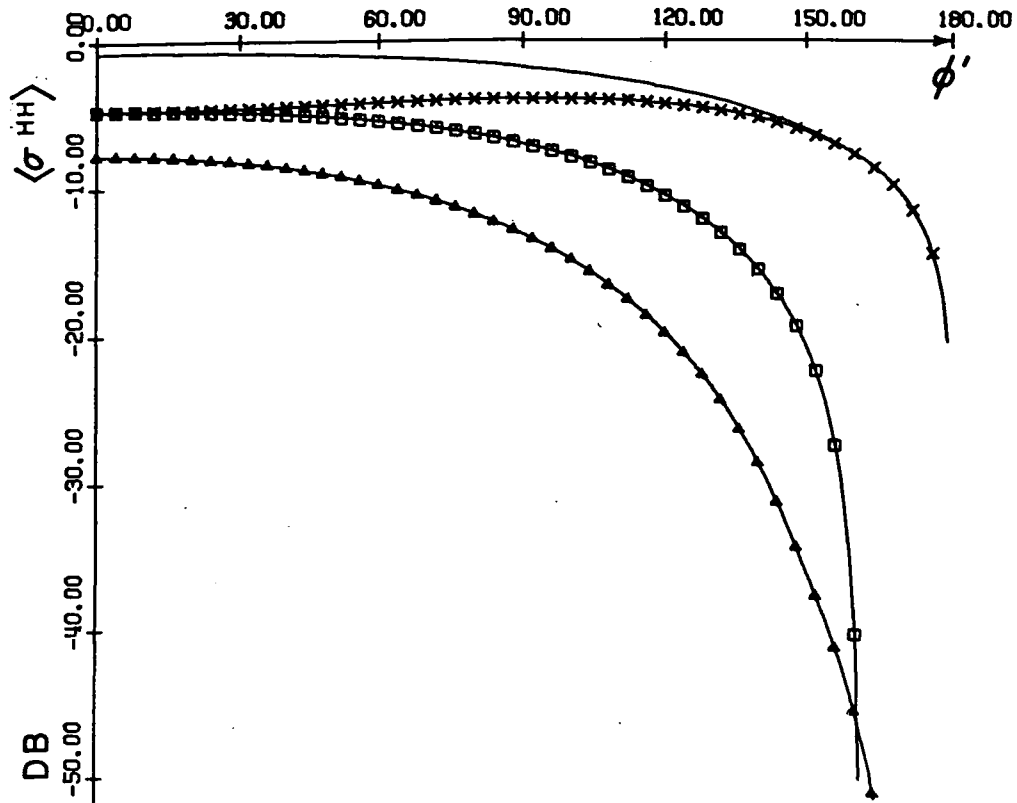


Fig. 8

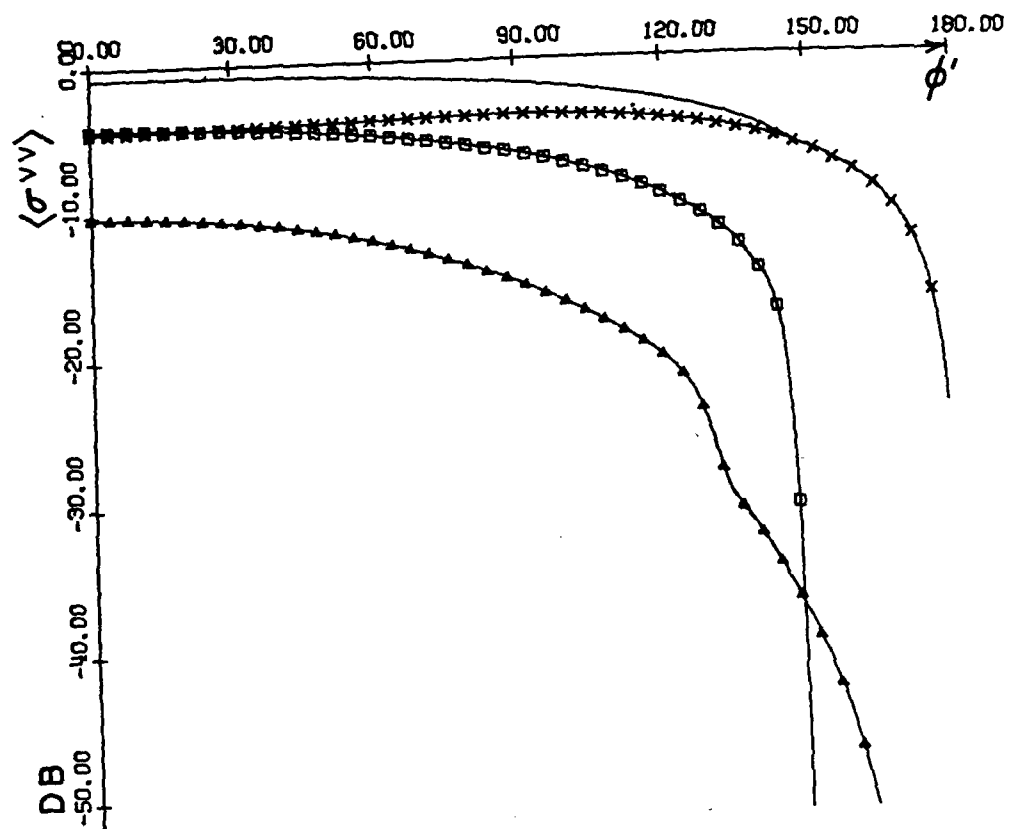


Fig. 5

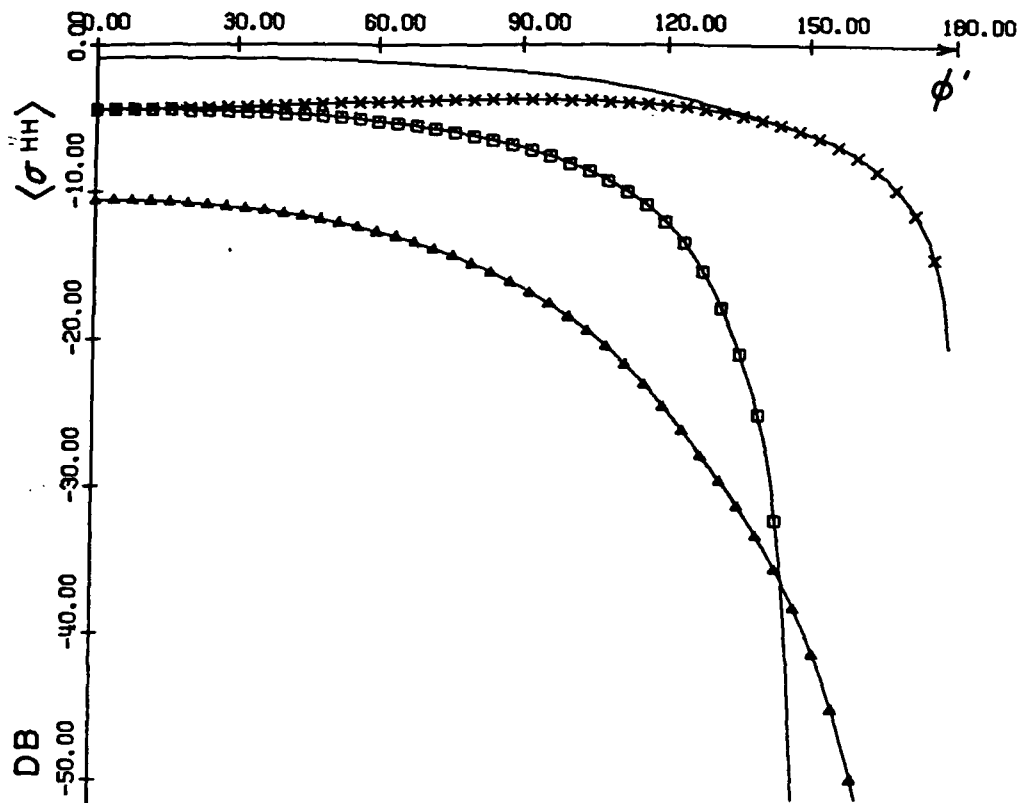


Fig. 6

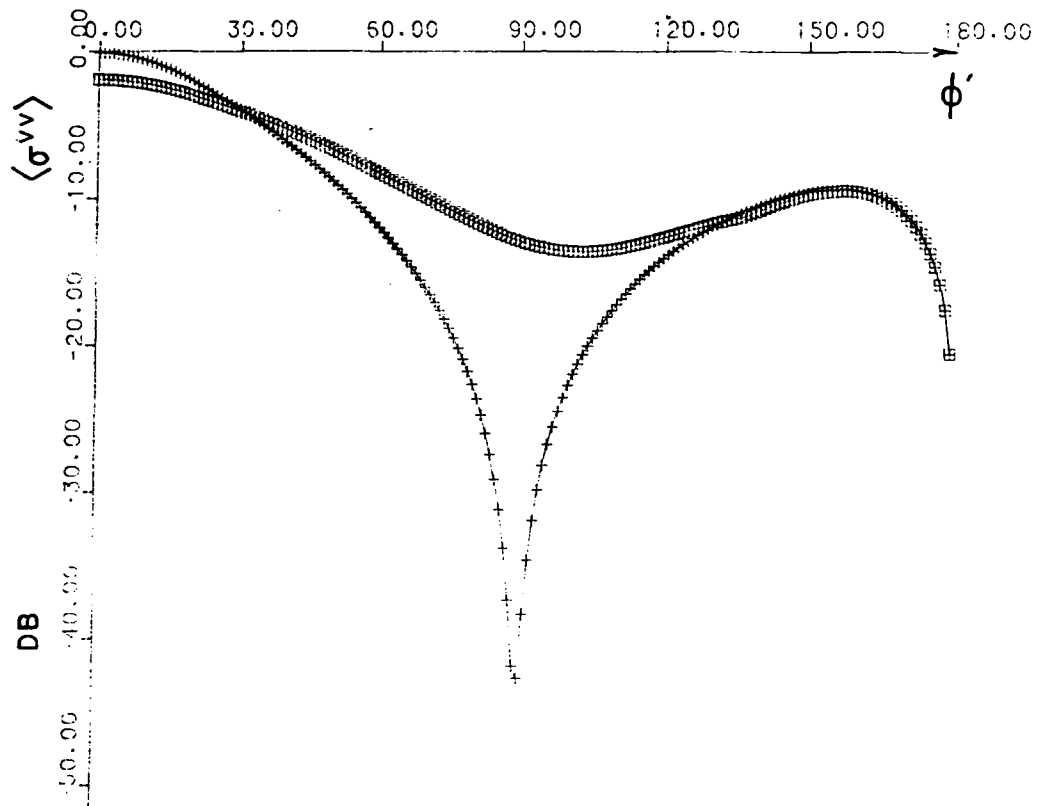


Fig. 7

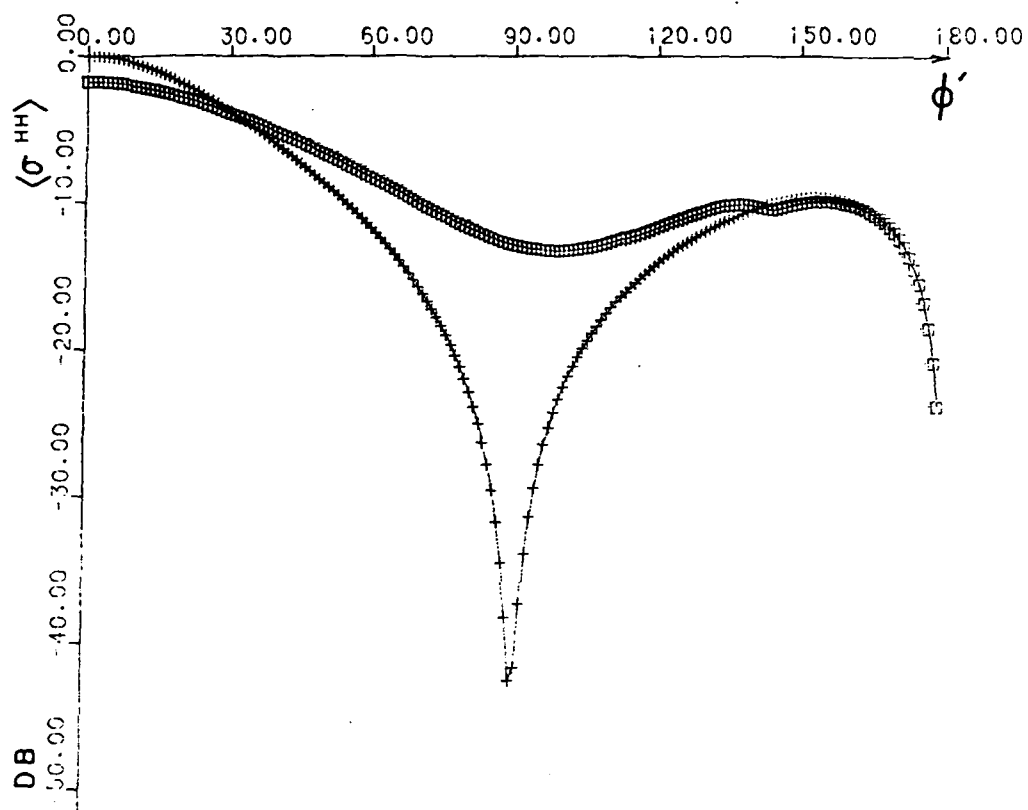


Fig. 8

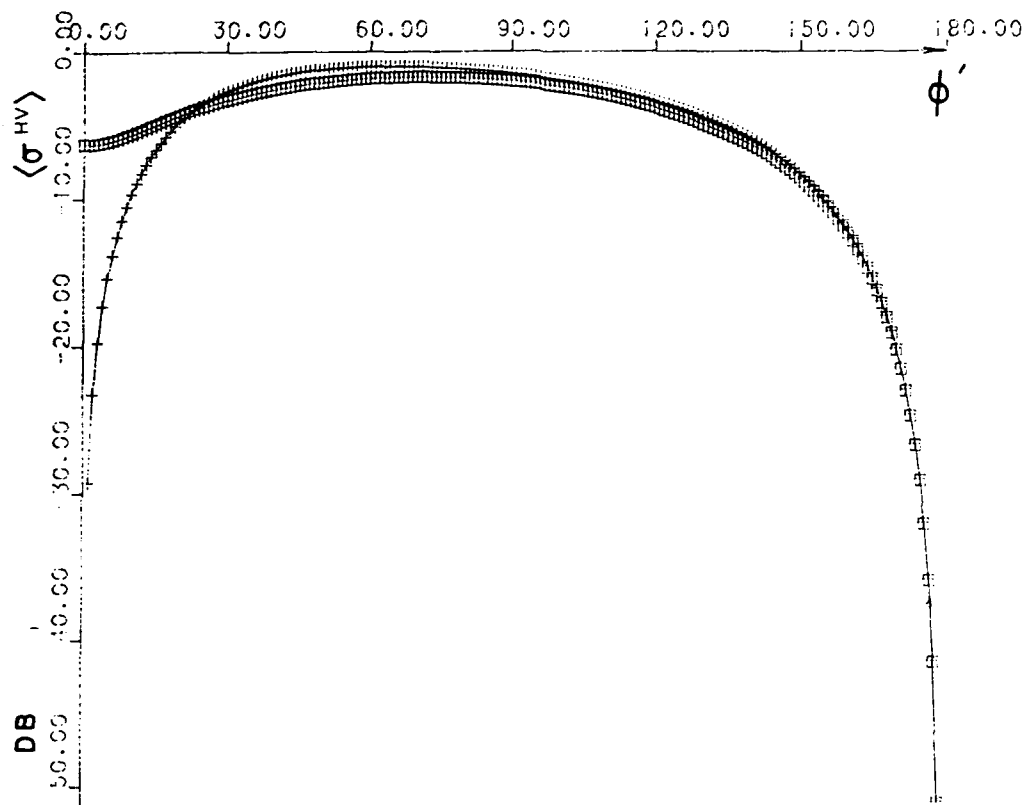


Fig. 2

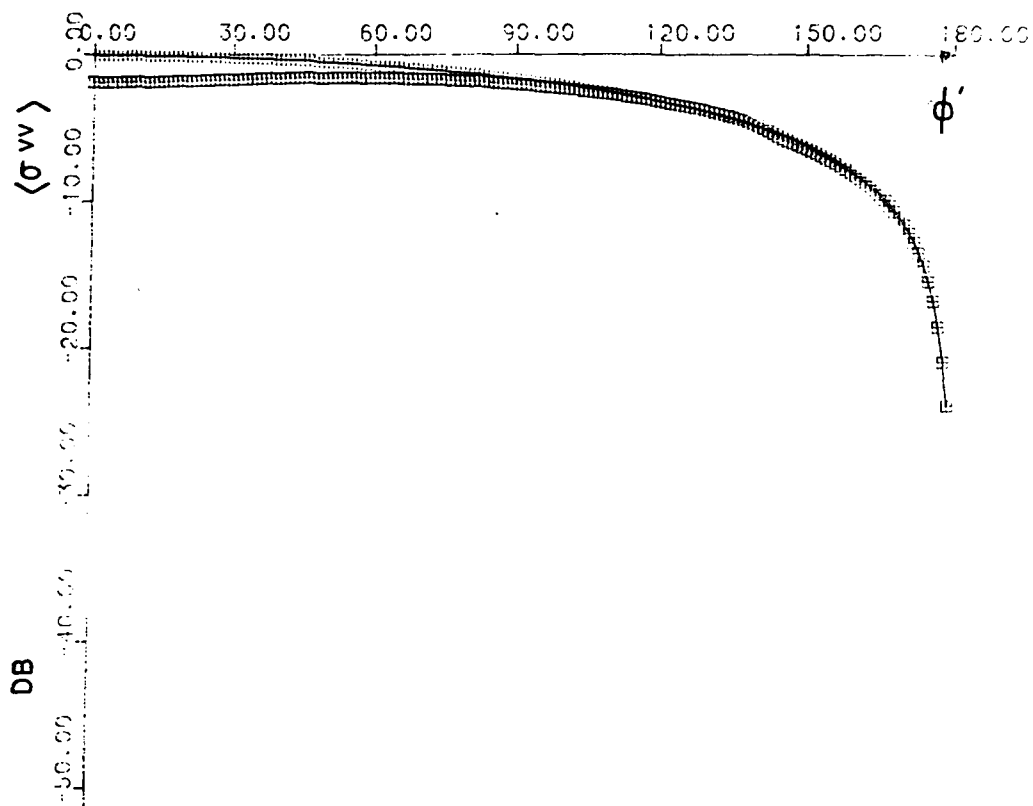


Fig. 10

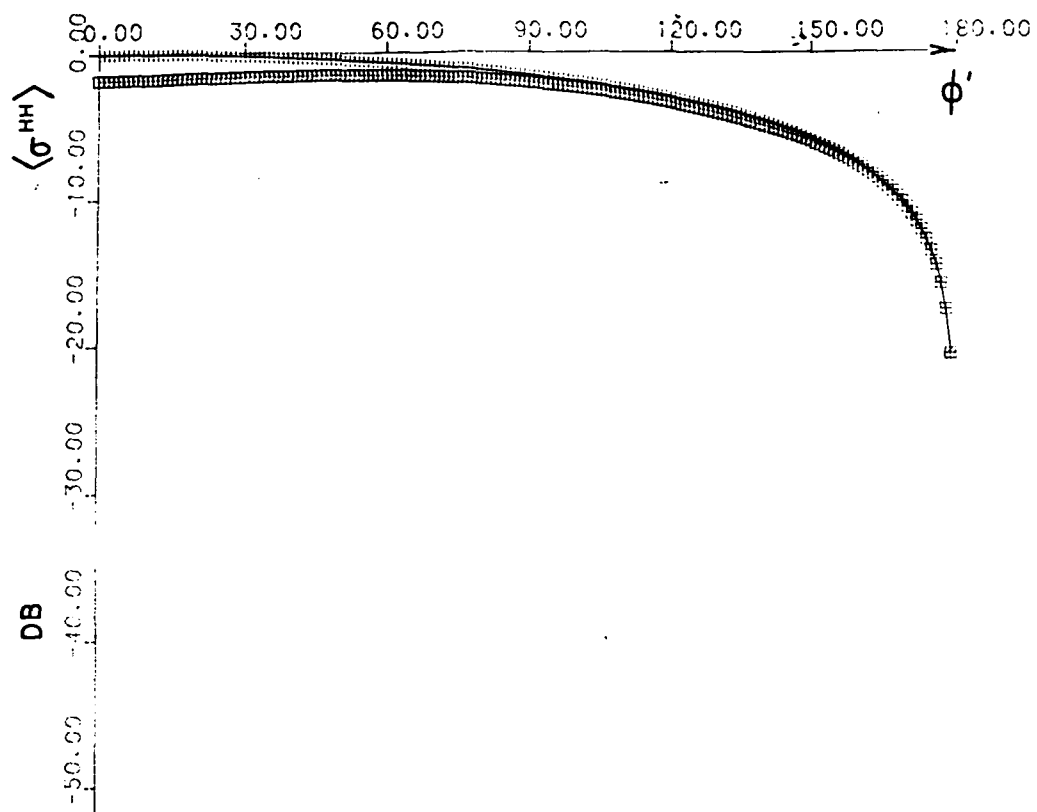


Fig. 11

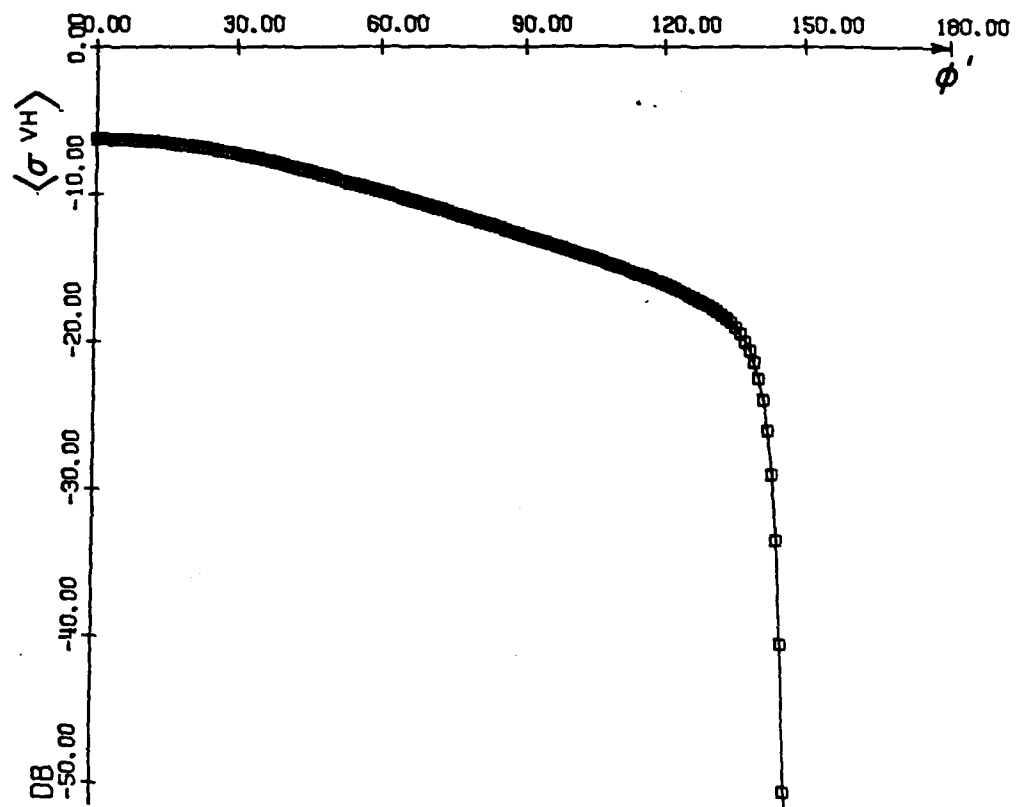


Fig. 12

MULTIPLE SCATTERING BY FINITELY CONDUCTING PARTICLES
WITH RANDOM ROUGH SURFACES AT INFRARED AND OPTICAL FREQUENCIES

Ezekiel Bahar

and

Mary Ann Fitzwater

Electrical Engineering Department
University of Nebraska--Lincoln
Lincoln, Nebraska 68588-0511

Abstract

The incoherent specific intensities for the waves scattered by a random distribution of particles with rough surfaces are derived. Since large roughness scales are considered, the diffuse scattering contributions to the like and cross polarized scattering cross sections are given by the full wave solutions. The scattering matrix in the expression for the equation of transfer is given by a weighted sum of the scattering matrix for the smooth particle and the diffuse contribution due to the rough surface of the particle. Illustrative examples are presented for the propagation of a circularly polarized wave normally incident upon a parallel layer of particles. Particles with different surface height spectral density functions, roughness scales, complex permittivities and sizes are considered. Both first order (single scatter) and multiple scatter solutions are provided and the results for particles with smooth and rough surfaces are compared.

\

1. Introduction

Scattering of electromagnetic waves in media consisting of random distributions of particles has been investigated extensively using the equation of transfer (Chandrasekhar 1950, Ishimaru 1978). The main difficulty in setting up the equation of transfer lies in the determination of the elements of the 4×4 scattering matrix for the individual particles. Thus most of the work has been done for particles of idealized shapes such as spheres.

In this work a method is presented for the modification of the results derived for particles with idealized shapes to account for the random surface roughness of the particles. To this end the full wave approach was used to determine the rough surface contributions to the like and cross polarized scattering cross sections and the elements of the scattering matrix are given in terms of a weighted sum of the Mie solutions and the diffuse scattering terms due to the particle surface roughness (See Section 2). For convenience in this work a circularly polarized wave is assumed to be normally incident upon a parallel layer consisting of a random distribution of irregular shaped particles. Different particle sizes with different complex dielectric coefficients are considered. The rough surface height is characterized by different surface height spectral density functions (the Fourier transform of the surface height autocorrelation function), and different roughness scales.

For the illustrative examples presented in Section 3 both first order (single scatter) and multiple scatter results are presented for smooth particles and for particles with rough surfaces. Layers with different optical thicknesses are considered and the results are presented for both the forward and backward scattered incoherent diffuse scattering intensities. The matrix characteristic value technique is used to account for multiple scattering (Ishimaru and Cheung 1980).

2. Formulation of the Problem

In this section the principal elements of the full wave solutions for the like and cross polarized differential scattering cross sections of non-spherical particles are summarized. The contributions of these cross sections to the familiar equation of transfer (Ishimaru 1978), in a medium consisting of a random distribution of nonspherical particles are also indicated explicitly.

The radius vector from the center to the irregular surface of the particle is given by (see Fig. 1)

$$\vec{r}_s = h_0 \vec{a}_r + h_s \vec{a}_r \quad (2.1)$$

in which \vec{a}_r is the unit vector in the direction of the radius vector, h_0 is the radius of the unperturbed sphere and h_s is the random rough surface height measured in the direction normal to the surface of the unperturbed sphere.

In this work it is assumed that the mean square of the rough surface height, $\langle h_s^2 \rangle$, can be sufficiently large such that standard perturbation techniques are not applicable (Barrick 1970). Thus the rough surface parameter, $\beta = 4k_0^2 \langle h_s^2 \rangle$, considered in this work is in the range $0 < \beta < 10$. (Smooth particle $\beta=0$, moderately rough particle $\beta=1$, very rough particle $\beta=10$). To apply the standard perturbation technique it is necessary to restrict the mean square height such that $\beta \leq 0.1$ (Brown 1978).

The full wave solutions for the normalized scattering cross sections $\langle \sigma^{ij} \rangle$ per unit cross sectional area ($A_y = \pi h_0^2$) are expressed as a weighted sum (Bahar and Chakrabarti 1985)

$$\langle \sigma^{ij} \rangle = \langle \sigma^{ij} \rangle_u + \langle \sigma^{ij} \rangle_s \quad (2.2)$$

the symbol $\langle \cdot \rangle$ denotes the statistical average. In the above expression the first and second superscripts indicate the polarizations of the scattered and incident waves respectively. Thus $i, j = 1$ denotes Vertical polarization and $i, j = 2$ denotes Horizontal polarization. The cross section $\langle \sigma^{ij} \rangle_u$ is the modified cross section associated with the unperturbed sphere...

$$\langle \sigma^{ij} \rangle_L = |\chi^S(v)|^2 \langle \sigma^{ij} \rangle_{Mie} \quad (2.3)$$

In (2.3) $\langle \sigma^{ij} \rangle_{Mie}$ is the Mie solution (Ishimaru 1978), for the like and cross polarized cross sections of the unperturbed sphere. For large spheres, $k_0 h_0 > 20$, (k_0 is the free space wavenumber), the most significant parts of the solution are the specularly reflected wave and the shadow forming wave (Morse and Feshbach 1954). The coefficient of $\langle \sigma^{ij} \rangle_{Mie}$ is the rough surface height characteristic function

$$\chi^S(v) = \langle \exp i v h_s \rangle \quad (2.4)$$

in which v is the magnitude of the vector

$$\vec{v} = k_0 (\vec{n}^f - \vec{n}^i) \quad (2.5)$$

where \vec{n}^f and $\vec{n}^i = -\vec{a}_y$ (see Fig. 1) are unit vectors in the direction of the scattered and incident wave normals. For a rough surface h_s with a Gaussian probability density

$$|\chi^S(v)|^2 = \exp[-4k_0^2 \langle h_s^2 \rangle \cos^2(\theta_0^f/2)] = \exp(-v^2 \langle h_s^2 \rangle) \leq 1 \quad (2.6)$$

in which $\theta_0^f/2$ is equal to the angle of incidence at the specular point. The coefficient $|\chi^S|^2$ accounts for the degradation of the reflected wave due to surface roughness. The coefficient is minimum for backscatter and approaches unity for forward scattering.

The second term in (2.2) $\langle \sigma^{ij} \rangle_s$ is the contribution to the total scattering cross section due to the surface roughness. It is expressed as (Bahar and Chakrabarti 1985)

$$\langle \sigma^{ij} \rangle_s = \int A^{ij}(\vec{n}^f, \vec{n}^i, \vec{n}) (\vec{n} \cdot \vec{a}_y) Q_s(\vec{n}^f, \vec{n}^i, \vec{n}) p(\vec{n}) d\vec{n} \quad (2.7)$$

in which \vec{n} is a unit vector normal to the surface of the scatterer,

$$A^{ij}(\vec{n}^f, \vec{n}^i, \vec{n}) = \frac{1}{\pi} \left| \frac{k_0 D^{ij}}{(\vec{v} \cdot \vec{a}_r)(\vec{a}_y \cdot \vec{n})} \right|^2 P_2(\vec{n}^f, \vec{n}^i | \vec{n}) \quad (2.8)$$

$$Q_s(\vec{n}^f, \vec{n}^i, \vec{n}) = (\vec{v} \cdot \vec{a}_r)^2 \int_{-\infty}^{\infty} (\chi_2^S(\vec{v} \cdot \vec{a}_r) - |\chi^S(\vec{v} \cdot \vec{a}_r)|^2) \exp(i\vec{v} \cdot \vec{r}_d) d\vec{x}_d d\vec{z}_d \quad (2.9)$$

and $p(\vec{n})$ is the probability density function for the slope of the surface of the scatterer. Thus for a sphere

$$p(\bar{n})d\bar{n} + \frac{\sin\gamma \cos\gamma}{\pi} dyd\delta, \quad 0 < \gamma < \pi/2, \quad 0 < \delta < 2\pi \quad (2.10)$$

where γ and δ are the polar and azimuth angles. In (2.10) it is assumed that

the rough surface (h_s) mean square slope is small compared to unity ($\bar{n} \approx \bar{a}_r$).

In (2.8), D^{ij} is the scattering coefficient which depends on the polarizations and the directions of the wave normals for the incident and scattered waves

as well as \bar{n} , the normal to the particle surface and the complex electromagnetic parameters (ϵ, μ) of the particle (Bahar 1981a). Since D^{ij} is not very sensitive to small fluctuations in \bar{n} , in the expression for D^{ij} , \bar{n} is approximated by \bar{a}_r . This does not mean that the effects of rough surface slope is neglected, since it is also contained in the expression for χ_2^s which depends on the surface height autocorrelation function. (See Table I). The term $P_2(\bar{n}^f, \bar{n}^i | \bar{n})$ is the probability that a point on the rough surface is both illuminated by the source and visible to the observer given the slopes (\bar{n}) of the surface of the scatterer (Smith 1967, Sancer 1969). Since $\bar{n} \approx \bar{a}_r$, and P_2 is also not very sensitive to small fluctuations in the slope, thus $P_2 \approx u(-\bar{n}^i \cdot \bar{n})u(\bar{n} \cdot \bar{n})$ where $u(\cdot)$ is the unit step function.

In (2.9) $\chi^s(\bar{v} \cdot \bar{a}_r)$ and $\chi_2^s(\bar{v} \cdot \bar{a}_r)$ are the rough surface height characteristic function and joint characteristic function respectively

$$\chi^s(\bar{v} \cdot \bar{a}_r) = \langle \exp(i\bar{v} \cdot \bar{h}_s) \rangle \quad (2.11)$$

and

$$\chi_2^s(\bar{v} \cdot \bar{a}_r) = \langle \exp[i\bar{v} \cdot (\bar{h}_s - \bar{h}_s')] \rangle \quad (2.12)$$

in which $\bar{v}_r = \bar{v} \cdot \bar{a}_r$. For Gaussian surfaces

$$|\chi^s(\bar{v} \cdot \bar{a}_r)|^2 = \exp(-v_r^2 \langle h_s^2 \rangle) \quad (2.13a)$$

and

$$\chi_2^s(\bar{v} \cdot \bar{a}_r) = \exp(-v_r^2 \langle h_s^2 \rangle + v_r^2 \langle h_s h_s' \rangle) = \exp(v_r^2 \langle h_s h_s' \rangle) |\chi^s(\bar{v} \cdot \bar{a}_r)|^2 \quad (2.13b)$$

The distance between two neighboring points \bar{r} and \bar{r}' on the surface of the unperturbed sphere is given by the vector

$$\bar{r}_d = \bar{r} - \bar{r}' = x_d \bar{n}_1 + z_d \bar{n}_3, \quad |\bar{r}_d| = r_d = (x_d^2 + z_d^2)^{1/2} \quad (2.14)$$

in which \bar{n}_1 and \bar{n}_3 are any pair of orthogonal unit vectors tangent to the surface of the unperturbed sphere. It is assumed in this work that the rough surface h_s is homogeneous and isotropic, thus the surface height autocorrelation function $\langle h_s h_s' \rangle$ is only a function of the distance r_d between \bar{r} and \bar{r}' and independent of direction. Hence Q_s (2.9) can be reduced to a one dimensional integral

$$Q_s(\bar{n}^f, \bar{n}^i, \bar{n}) = v_r^2 \int_0^\infty \int_0^{2\pi} (\chi_2^s(v_r) - |\chi^s(v_r)|^2) J_0[(v_x^2 + v_z^2)^{1/2} r_d] r_d dr_d \quad (2.15)$$

in which J_0 is the Bessel function of the first kind. It is also assumed that the rough surface correlation distance r_{dc} (where the correlation coefficient $R(r_d) = \langle h_s h'_s \rangle / \langle h_s^2 \rangle \exp(-1)$) is small compared to the circumference of the sphere.

The general expression for the equation of transfer (Ishimaru 1978) can be written as follows for a plane parallel slab consisting of rough spherical particles (see Fig. 2)

$$\mu \frac{d[I]}{d\tau} = -[I] + \int [S][I'] d\mu' d\phi' + [I_i] \quad (2.16)$$

In (2.16) τ is the optical distance in the z direction (normal to the plane parallel slab)

$$\tau = \rho[\sigma_t]z \equiv \int \sigma_t n(D) dD \quad , \quad D = 2h_0 \quad (2.17)$$

where $n(D)$ is the particle size distribution and σ_t is the extinction coefficient. Since $\langle \sigma^{ij} \rangle_s$ vanishes in the forward direction, the extinction matrix (Ishimaru and Cheung 1980) for the rough sphere, can be represented by a scalar quantity as in the case for the smooth sphere. However, if the unperturbed particle is non-spherical, the first term on the right hand side of equation (2.16) is multiplied by the extinction matrix. In general $\langle \sigma^{ij} \rangle_s$ vanishes in the forward direction due to the term P_2 in (2.8). The matrices $[I]$ and $[I']$ are the (4×1) incoherent specific diffuse intensity matrices for waves scattered from the particles in the direction $\theta = \cos^{-1}\mu$ and ϕ and for waves incident in the direction $\theta' = \cos^{-1}\mu'$ and ϕ' , respectively. The elements of $[I]$ are the modified Stokes' parameters

$$[I] = \begin{bmatrix} I_1 \\ I_2 \\ U \\ V \end{bmatrix} = \begin{bmatrix} \langle E_1 E_1^* \rangle \\ \langle E_2 E_2^* \rangle \\ 2\text{Re}\langle E_1 E_2^* \rangle \\ 2\text{Im}\langle E_1 E_2^* \rangle \end{bmatrix} \quad (2.18)$$

where the symbol $*$ denotes the complex conjugate and E_1 and E_2 are the vertically and horizontally polarized components of the electric field. The (4×4) scattering

matrix $[S]$ in the reference coordinate system can be expressed in terms of the scattering matrix $[S']$ in the scattering plane as follows:

$$[S] = [\mathcal{L}(-\pi + \alpha)][S'][\mathcal{L}(\alpha')] \quad (2.19)$$

in which

$$[S'] = |\chi^s(\vec{v} \cdot \vec{a}_r)|^2 [S_{Mie}] + [S_g] \quad (2.20)$$

In (2.20) $[S_{Mie}]$ is given by

$$[S_{Mie}] = \frac{1}{\rho[\sigma_r]} \begin{bmatrix} \rho[|f_{11}|^2] & \rho[|f_{12}|^2] & \rho\text{Re}[f_{11}f_{12}^*] & -\rho\text{Im}[f_{11}f_{12}^*] \\ \rho[|f_{21}|^2] & \rho[|f_{22}|^2] & \rho\text{Re}[f_{21}f_{22}^*] & -\rho\text{Im}[f_{21}f_{22}^*] \\ \rho 2\text{Re}[f_{11}f_{21}^*] & \rho 2\text{Re}[f_{12}f_{22}^*] & \rho\text{Re}[f_{11}f_{22}^* + f_{12}f_{21}^*] & -\rho\text{Im}[f_{11}f_{22}^* - f_{12}f_{21}^*] \\ \rho 2\text{Im}[f_{11}f_{21}^*] & \rho 2\text{Im}[f_{12}f_{22}^*] & \rho\text{Im}[f_{11}f_{22}^* + f_{12}f_{21}^*] & \rho\text{Re}[f_{11}f_{22}^* - f_{12}f_{21}^*] \end{bmatrix} \quad (2.21)$$

where f_{ij} are elements of the 2×2 scattering amplitude matrix $[f]$ and $\rho[\cdot]$ denotes integration over the particle size distribution $n(D)$ (2.17)

$$\begin{bmatrix} E_\theta \\ E_r \end{bmatrix} = \begin{bmatrix} f_{11} & f_{12} \\ f_{21} & f_{22} \end{bmatrix} \begin{bmatrix} E'_\theta \\ E'_r \end{bmatrix} \frac{\exp(-ik_o r)}{r} \quad (2.22)$$

In (2.22) E_θ and E_r are the vertically and horizontally polarized field components in the scattering plane and r is the distance from the center of the sphere to the field point. An $\exp(i\omega t)$ time dependence is assumed in this work.

For a smooth sphere the elements f_{ij} are given by the Mie solution (Barrick 1970, Ishimaru 1978) and $[f]$ is a diagonal matrix. The transformation matrix $[\mathcal{L}]$ in (2.19) is

$$[\mathcal{L}(\alpha)] = \begin{bmatrix} \cos^2 \alpha & \sin^2 \alpha & \frac{1}{2} \sin 2\alpha & 0 \\ \sin^2 \alpha & \cos^2 \alpha & -\frac{1}{2} \sin 2\alpha & 0 \\ -\sin 2\alpha & \sin 2\alpha & \cos 2\alpha & 0 \\ 0 & 0 & 0 & 1 \end{bmatrix} \quad (2.23)$$

where α' is the angle between the reference plane of incidence and the scattering plane (containing the wave normals \vec{n}^f and \vec{n}^i) and α is the angle between the reference plane of scatter and the scattering plane (see Fig. 2).

In (2.20) the coefficient $|\chi^s(\vec{v} \cdot \vec{a}_r)|^2$ accounts for the fact that the specular point contributions to the scattering cross sections is decreased because of the rough surface ($|\chi^s|^2 \leq 1$ and $|\chi^s|^2 \rightarrow 1$ as $\beta \rightarrow 0$). The diffuse scattering matrix $[S_s]$ due to the random rough surface h_s is given by

$$[S_s] = \begin{bmatrix} [S_{11}^s] & [S_{12}^s] & 0 & 0 \\ [S_{21}^s] & [S_{22}^s] & 0 & 0 \\ 0 & 0 & [S_{33}^s] & [S_{34}^s] \\ 0 & 0 & [S_{43}^s] & [S_{44}^s] \end{bmatrix} \quad (2.24)$$

where

$$[S_{ij}^s] = \frac{A_y}{4\pi\rho[\sigma_t]} \rho[\langle\sigma^{ij}\rangle_s], \text{ for } i, j = 1, 2 \quad (2.25a)$$

and $\langle\sigma^{ij}\rangle_s$ is given by the full wave solution (2.7)

Furthermore for $i = 3$ and 4

$$[S_{ii}^s] = \rho[\text{Re}[\langle\sigma_{22}^{11}\rangle_s \pm \langle\sigma_{21}^{12}\rangle_s]] A_y / 4\pi\rho[\sigma_t] \quad (2.25b)$$

(upper and lower signs for $i = 3$ and 4 respectively) and for $i \neq j$

$$[S_{ij}^s] = \rho[\text{Im}[\pm \langle\sigma_{22}^{11}\rangle_s + \langle\sigma_{21}^{12}\rangle_s]] A_y / 4\pi\rho[\sigma_t] \quad (2.25c)$$

(upper and lower signs for $i, j = 4, 3$ and $i, j = 3, 4$ respectively)

In the above expressions

$$\langle\sigma_{kl}^{ij}\rangle = \frac{1}{\pi} \int \frac{k_o^2 D^{ij} D^{kl*}}{(\vec{v} \cdot \vec{a}_r)^2 (\vec{n} \cdot \vec{a}_y)} P_2 Q_s p(\vec{n}) d\vec{n} \quad (2.25d)$$

The remaining eight terms of the matrix $[S_s]$ vanish since D^{ii} and $D^{ij}(i \neq j)$ are symmetric and antisymmetric respectively with respect to the azimuth angle δ .

In order to simplify the solution of the transfer equation (2.16), it is assumed in this work that the normally incident wave is circularly polarized. Thus the incident Stokes matrix at $z = 0$ is given by

$$[I_{inc}] = \begin{bmatrix} 1 \\ 1 \\ 0 \\ 2 \end{bmatrix} \delta(\mu' - 1) \delta(\phi') \equiv I_o \delta(\mu' - 1) \delta(\phi') \quad (2.26)$$

where the - and + signs correspond to the right and left circularly polarized waves and $\mu' = \cos\theta'$. The reduced incident intensity is therefore,

$$[I_{ri}] = [I_{inc}] \exp(-\tau) \quad (2.27)$$

In (2.16) the (4x1) excitation matrix $[I_i]$ is given by

$$[I_i] = \int [S][I_{ri}] d\mu' d\phi' = \left[[S][I_o] \right]_{\substack{\mu'=1 \\ \phi'=0}} \cdot \exp(-\tau) \quad (2.28)$$

where I_o , the incident Stokes' matrix is defined by (2.26).

Since the normally incident circularly polarized wave is independent of the azimuth angle ϕ , the Stokes' matrices for the incoherent specific intensities are also independent of ϕ . The elements of the scattering matrix $[S]$ (2.16) are functions of $\phi - \phi'$ only. Upon integration with respect to ϕ' over a range of 2π the scattering matrix $[S]$ reduces to the following form (Ishimaru and Cheung 1980).

$$[S] = \begin{bmatrix} S_{11} & S_{12} & 0 & 0 \\ S_{21} & S_{22} & 0 & 0 \\ 0 & 0 & S_{33} & S_{34} \\ 0 & 0 & S_{43} & S_{44} \end{bmatrix} \quad (2.29)$$

Since f_{11} and f_{22} are even functions of $\phi - \phi'$ while f_{21} and f_{12} are odd functions of $\phi - \phi'$. As a result there is no coupling between I_1, I_2 and U, V in (2.16) and the equation of transfer for the normally incident, circularly polarized wave decouples into the following two matrix equations

$$\mu \frac{d}{d\tau} \begin{bmatrix} I_1 \\ I_2 \end{bmatrix} = - \begin{bmatrix} I_1 \\ I_2 \end{bmatrix} + \int \begin{bmatrix} S_{11} & S_{12} \\ S_{21} & S_{22} \end{bmatrix} \begin{bmatrix} I_1' \\ I_2' \end{bmatrix} d\mu' + \begin{bmatrix} I_{11} \\ I_{12} \end{bmatrix} \quad (2.30a)$$

$$\text{and} \quad \mu \frac{d}{d\tau} \begin{bmatrix} U \\ V \end{bmatrix} = - \begin{bmatrix} U \\ V \end{bmatrix} + \int \begin{bmatrix} S_{33} & S_{34} \\ S_{43} & S_{44} \end{bmatrix} \begin{bmatrix} U' \\ V' \end{bmatrix} d\mu' + \begin{bmatrix} U_1 \\ V_1 \end{bmatrix} \quad (2.30b)$$

in which I_{11} and I_{12} are the first two elements of the excitation matrix $[I_i]$ (2.28) while U_1 and V_1 are the third and fourth elements of the excitation matrix.

3. Illustrative Examples

For the illustrative examples considered in this section, the random rough surface height h_s (measured normal to the surface of the unperturbed spherical particle of diameter $D = 2h_0$) is assumed to be homogeneous and isotropic. Different forms of the surface height spectral density function $W(v_x, v_z)$ (which is the two dimensional Fourier Transform of the surface height autocorrelation function $\langle h_s h'_s \rangle$) are considered.

$$\begin{aligned} W(v_T) &= W(v_x, v_z) = \frac{1}{\pi^2} \int_{-\infty}^{\infty} \langle h_s h'_s \rangle \exp(iv_x x_d + iv_z z_d) dx_d dz_d \\ &= \frac{2}{\pi} \int_0^{\infty} \langle h_s h'_s \rangle J_0(v_T r_d) r_d dr_d \end{aligned} \quad (3.1)$$

where v_x and v_z are components of \bar{v} in the directions of the unit vectors \bar{n}_1, \bar{n}_3 tangent to the surface of the unperturbed sphere. Thus

$$v_T = (v_x^2 + v_z^2)^{1/2} = (v^2 - v_r^2)^{1/2} \quad (3.2)$$

Similarly the surface height autocorrelation function $\langle h_s h'_s \rangle$ is given by the inverse formula

$$\begin{aligned} \langle h_s h'_s \rangle &= \int_{-\infty}^{\infty} \frac{W(v_x, v_z)}{4} \exp(-iv_x x_d - iv_z z_d) dv_x dv_z \\ &= \frac{\pi}{2} \int_0^{\infty} W(v_T) J_0(v_T r_d) v_T dv_T \end{aligned} \quad (3.3)$$

For case (a) (see Table I), the specific expression for the surface height spectral density function is

$$\begin{aligned} W(v_T) &= \frac{2C}{\pi} \left[\frac{(v_T - v_d)}{(v_T - v_d)^2 + v_m^2} \right]^n \quad v_d < v_T < v_c \\ &= 0 \quad \text{elsewhere} \end{aligned} \quad (3.4)$$

In (3.4) the smallest spatial wavenumber is

$$v_d = 4/D \quad (3.5a)$$

and the cutoff wavenumber is

$$v_c = 4k_o \quad (3.5b)$$

where k_o is the wavenumber for the electromagnetic wave. The constant C is chosen such that the scale of the random rough surface is

$$\beta = 4k_o^2 \langle h_s^2 \rangle = 1 \quad (3.6)$$

In (3.6) $\langle h_s^2 \rangle$ is the mean square height

$$\langle h_s^2 \rangle = \frac{\pi}{2} \int_0^\infty W(v_T) v_T^2 dv_T \quad (3.7)$$

The corresponding value for the mean square slope

$$\sigma_s^2 = \frac{\pi}{2} \int_0^\infty W(v_T) v_T^3 dv_T \quad (3.8)$$

is $\sigma_s^2 = 0.013$. The parameter v_m where $W(v_T)$ is maximum is $v_m = 1.2/D$.

The exponent in (3.4) is $n = 4$ and the material of the particle is aluminum.

For wavelengths $\lambda = 10 \mu\text{m}$ the relative (complex) dielectric coefficient is

$\epsilon_r = -6000(1+i)$ (Ehrenreich 1965). The diameter of the unperturbed spherical particle is $D = 5 \lambda$ (See Table I case (a)).

For surfaces with small scale roughnesses $\beta \leq 1$, the contribution (2.7) to the total scattering cross sections due to surface roughness h_s can also be expressed as a series

$$\begin{aligned} \langle \sigma^{ij} \rangle_s &= \sum_m 4\pi k_o^2 \frac{|D^{ij}|^2 P_2(\bar{n}^f, \bar{n}^i | \bar{n})}{(\bar{a}_r \cdot \bar{a}_y)} \left(\frac{v_r}{2} \right)^{2m} \frac{W_m(v_T)}{m!} \chi(v_r) \\ &= \sum_m 4k_o^2 \int_0^{2\pi} \int_0^{\pi/2} |D^{ij}|^2 P_2(\bar{n}^f, \bar{n}^i | \bar{n}) \left(\frac{v_r}{2} \right)^{2m} \frac{W_m(v_T) \chi(v_r)}{m!} \sin \gamma d\gamma d\delta \end{aligned} \quad (3.9)$$

in which $W_m(v_T)/2^{2m}$ is the two dimensional Fourier transform of $\langle h_s h'_s \rangle^m$ and the integration is over the polar angle γ and azimuthal angle δ . The Fourier transform W_m can also be expressed as

$$\begin{aligned} \frac{W_m(v_x, v_z)}{2^{2m}} &= \frac{1}{(2\pi)^2} \int (h_s h'_s)^m \exp(iv_x x_d + iv_z z_d) dx_d dz_d \\ &= \frac{1}{2^{2m}} \int W_{m-1}(v'_x, v'_z) W_1(v_x - v'_x, v_z - v'_z) dv'_x dv'_z \\ &= \frac{1}{2^{2m}} W_{m-1}(v_x, v_z) \otimes W_1(v_x, v_z) \end{aligned} \quad (3.10)$$

In (3.10) the symbol \otimes denotes the two dimensional convolution of W_{m-1} with $W_1 = W$. For $\beta \ll 1$ only the first term in (3.9) is non-negligible. This term corresponds to first order Bragg scattering from rough surfaces (Bahar 1981a,b). For case (a) ($\beta=1$), it is necessary to evaluate only two terms of the series in (3.9). For large values of roughness scales ($\beta \gg 1$) it is more convenient to evaluate $\langle \sigma^{ij} \rangle_s$ using (2.7).

For cases (b) (c) and (d) the specific form of the surface height spectral density function considered is

$$W(v_T) = \frac{2C}{\pi} \left[\frac{v_T}{v_T^2 + v_m^2} \right]^n, \quad v_T > 0 \quad (3.11)$$

where the exponent is assumed to be $n = 8$. For case (b) the roughness parameter is $\beta = 1$ and for cases (c) and (d) it is $\beta = 10$. The corresponding values for v_m , σ_s^2 , λ , ϵ_r and D are shown in Table I cases (b) (c) and (d). For these cases, the surface height autocorrelation coefficient $R(\zeta) \equiv \langle h_s h'_s \rangle / \langle h_s^2 \rangle$ can be expressed in closed form

$$\begin{aligned} R(\zeta) &= \left[1 - \frac{3\zeta^2}{8} + \frac{3\zeta^4}{32} + \frac{\zeta^6}{3072} \right] \zeta K_1(\zeta) \\ &+ \left[\frac{1}{2} - \frac{\zeta^2}{4} - \frac{\zeta^4}{96} \right] \zeta^2 K_0(\zeta) \end{aligned} \quad (3.12)$$

In (3.12) K_0 and K_1 are modified Bessel functions of the second kind of order zero and one respectively (Abramowitz and Stegun 1964) and the dimensionless parameter ζ is

$$\zeta \equiv \frac{v}{m} r_d \quad (3.13)$$

For all the illustrative examples, it is assumed that a right circularly polarized wave is normally incident at $\tau = 0$ ($z = 0$) upon a parallel layer of optical thickness τ_0 (see Fig. 2). The equation of transfer for the azimuthally independent modified Stokes' parameters (2.30) are solved using the matrix characteristic (eigen) value technique (Ishimaru and Cheung 1980). For case (b) ($D/\lambda=10$) the scattering cross sections are more sharply peaked in the forward direction, thus it is necessary to use a Gaussian quadrature formula of order 32 (Abramowitz and Stegun 1964). The boundary conditions for the incoherent specific diffuse intensities are

$$[I] = 0 \quad \text{for} \quad 0 \leq \mu \leq 1 \quad \text{at} \quad \tau = 0 \quad (3.14)$$

transmitted incoherent diffuse intensities are zero at $\tau = 0$) and

$$[I] = 0 \quad \text{for} \quad 0 \geq \mu \geq -1 \quad \text{at} \quad \tau = \tau_0 \quad (3.15)$$

reflected incoherent diffuse intensities are zero at $\tau = \tau_0$).

For case (a) (see Table I) I_1 (vertical polarization) and I_2 (horizontal polarization) are plotted in Figs. 3 and 4, respectively, as functions of the scatter angle θ (0.90°) (transmitted $\tau \geq \tau_0$) for $\tau_0 = 10$. The solid curves correspond to first order scattering solutions only (Ishimaru 1978) for the smooth (unperturbed spherical) particles and particles with rough surfaces. The surface roughness of the particles tends to smooth out the incoherent diffuse intensities as function of θ . Note that the vertically polarized intensity is more oscillatory than the horizontally polarized intensity.

The corresponding solutions that account for multiple scatter are also given for the smooth (+) and rough (Δ) particles. We note that since the albedos for the rough particles are slightly lower than the albedos for the smooth particles (see Table I), the incoherent diffuse intensities are somewhat lower for the

rough particles. For optically very thick layers of particles, the diffuse intensities I_1 and I_2 are practically equal and rather flat functions of θ . Multiple scattering cannot be neglected in these cases.

For case (b) (see Table I), the incoherent diffuse intensities I_1 and I_2 are plotted in Figs. 5 and 6 as functions of θ ($0^\circ, 90^\circ$) (transmitted $\tau \geq \tau_0$) for $\tau_0 = 1$. The first order solutions are closer to the multiple scattering solutions for $\tau_0 = 1$ than for $\tau_0 = 10$, however multiple scattering does tend to make the incoherent intensities more monotonic functions of the scatter angle θ . For optical thickness $\tau_0 = 1$, the surface roughness has a smaller effect on the incoherent intensities and I_1 and I_2 are not equal in the intermediate range of angles between 10° and 40° .

In Figs. 7 and 8 the incoherent diffuse intensities I_1 and I_2 are plotted as functions of θ ($90^\circ, 180^\circ$ reflected $\tau \leq 0$) (case b with optical thickness $\tau_0 = 10$). Note again the oscillatory nature of the first order solutions for I_1 (vertical polarization).

For case (c) (see Table I), the incoherent diffuse intensities I_1 and I_2 are plotted in Figs. 9 and 10 as functions of θ ($0^\circ, 90^\circ$) (transmitted $\tau \geq \tau_0$) for $\tau_0 = 10$. For smaller particle sizes ($D=5\lambda$), the first order intensities are less oscillatory than for large particle sizes ($D=10\lambda$). Note also that for dissipative plastic materials, there is a more significant difference between the intensities for the smooth and rough particles.

For the final case considered (d) (see Table I), the incoherent intensities I_1 and I_2 are plotted in Figs. 11 and 12 as functions of θ ($0^\circ, 90^\circ$) (transmitted $\tau \geq \tau_0$) for $\tau_0 = 10$. The only difference between case (c) and case (d) is the relative complex permittivity ϵ of the particles. Since the particles for cases (a) and (d) are highly conducting there is a smaller difference in the specific incoherent intensities for the smooth and rough particles. This is because the corresponding albedos are not significantly different for highly conducting particles (see Table I). Nevertheless, it should be pointed out that for optically thin layers ($\tau_0 < 1$) the principal effect of particle surface roughness is to smooth out the undulations in the diffuse specific (incoherent) intensities as functions of the scatter angle. The effect of particle surface roughness is more pronounced for highly dissipative particles with small albedos, case (c).

The effect of surface roughness on forward scatter ($\theta=0$) is less pronounced since $\langle \sigma^{ij} \rangle_s$ (2.7) vanishes and $|\chi^s|^2 \rightarrow 1$ for forward scattering.

4. Concluding Remarks

In this work scattering of electromagnetic waves by particles with moderate ($\beta=1$) to very large ($\beta=10$) roughness scales (that cannot be accounted for using the standard perturbation methods) has been considered. The incoherent diffuse scattering intensities for the rough particles have been compared with the corresponding results for smooth particles. Both first order (single scatter) and multiple scatter results have been presented for a set of four different cases listed in Table I. Particles of different sizes, complex dielectric coefficients, and surface height spectral density functions are considered.

As the scale of roughness $\beta = 4k_0^2 \langle h_s^2 \rangle$ increases, the scattering coefficients as well as the incoherent diffuse scattering intensities become practically independent of the scattering angle. In addition, for large τ_0 , the incoherent scattering intensities decrease as the roughness scale increases. This effect is more pronounced for particles made of very dissipative materials. As the optical thickness of the layer increases, the incoherent diffuse scattering intensities become less dependent on scatter angle.

ACKNOWLEDGMENTS

This investigation is sponsored by the U. S. Army Research Offices, Contract No. DAAG-29-82-K-0123. The authors wish to thank S. Chakrabarti for his assistance in documenting the computer programs.

TABLE I

	case a	case b	case c	case d
n	4	8	8	8
β	1	1	10	10
v_m	1.2/D	15.9/D	4/D	4/D
σ_s^2	.0131	.10	.10	.10
λ	10 μ	.555 μ	10 μ	10 μ
ϵ_r	-6000-16000	-40-112	1.5-18	-6000-16000
Material	aluminum	aluminum	dissipative plastic	aluminum
$2h_0 = D$	5 λ	10 λ	5 λ	5 λ
σ_t , smooth	2.059	2.259	2.370	2.059
σ_t , rough	2.059	2.313	2.333	2.198
albedo, smooth	.9885	.9356	.6434	.9885
albedo, rough	.9732	.8999	.6043	.9724
$\frac{r_{dc}}{\pi D} = \frac{2}{\pi D} \left(\frac{\langle h_s^2 \rangle}{\sigma_s^2} \right)^{1/2}$.089	.016	.102	.102

Table I. Values of parameters for the surface height spectral density function W , wavelength λ , dielectric coefficient ϵ_r and diameter D for the scattering particles.

5. References

1. Abramowitz, M., and I. A. Stegun (1964), Handbook of Mathematical Functions with Formulas, Graphs, and Mathematical Tables, Appl. Math. Ser. 55, National Bureau of Standards, Washington, D.C.
2. Bahar, E. (1981a), "Scattering Cross Sections for Random Rough Surfaces-Full Wave Analysis," Radio Science, Vol. 16, No. 3, 331.
3. Bahar, E. (1981b), "Scattering Cross Sections for Composite Random Surfaces-Full Wave Analysis," Radio Sci., Vol. 16, No. 6, 1327.
4. Bahar, E., and Swapan Chakrabarti (1985), "Scattering and Depolarization by Large Conducting Spheres with Rough Surfaces," Applied Optics, Vol. 24, No. 12, 1820.
5. Barrick, D. E. (1970), Rough Surfaces, in Radar Cross Section Handbook (Plenum, New York), Chapter 9.
6. Brown, G. S. (1978), "Backscattering from a Gaussian-Distributed Perfectly Conducting Rough Surface," IEEE Trans. Antennas Propag. AP-26, 472.
7. Chandrasekhar, S. (1950), Radiative Transfer. Dover, Publ., New York.
8. Ehrenreich, H. (1965), "The Optical Properties of Metals," IEEE Spectrum 2, 162.
9. Ishimaru, A. (1978), Wave Propagation and Scattering in Random Media, Academic, New York.
10. Ishimaru, A., and R. L.-T. Cheung (1980), "Multiple Scattering Effects in Wave Propagation Due to Rain," Ann. Telecommun., 35, 373.
11. Morse, P. M., and H. Feshbach (1953), Methods of Theoretical Physics, McGraw-Hill, New York.
12. Sancer, M. H. (1969), "Shadow-Corrected Electromagnetic Scattering from a Randomly Rough Surface," IEEE Trans. Antennas Propag. AP-17, 577.
13. Smith, B. G. (1965), "Geometrical Shadowing of a Randomly Rough Surface," IEEE Trans. Antennas and Propag. AP-15, 668.

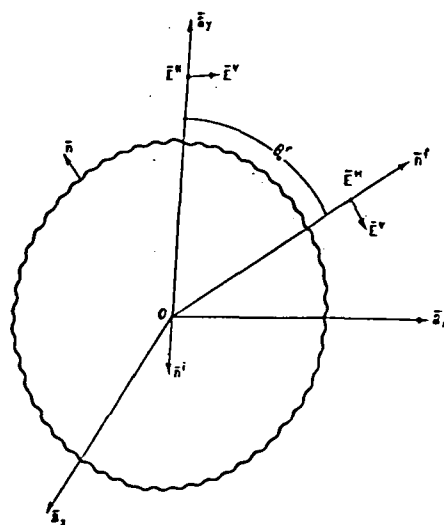


Fig. 1. Scattering geometry for a rough conducting sphere.

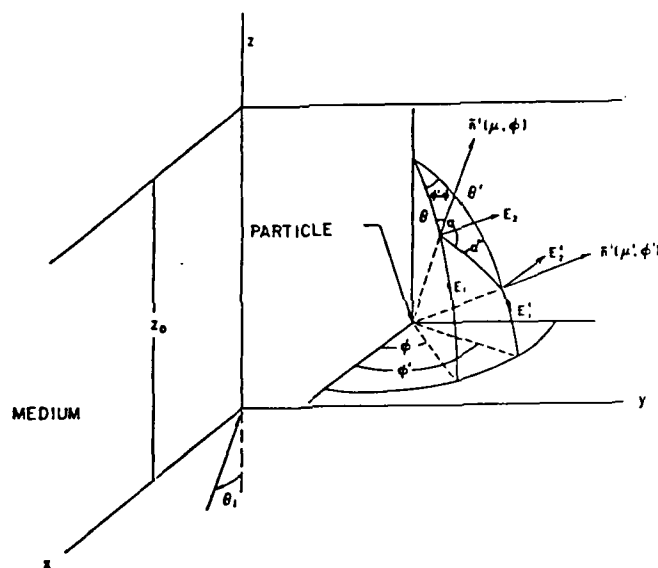


Fig. 2. Scattering geometry indicating incident and scattering wave normals \vec{n}^i and \vec{n}^r and corresponding field components E_1 parallel (vertical) and E_2 perpendicular (horizontal) polarizations.

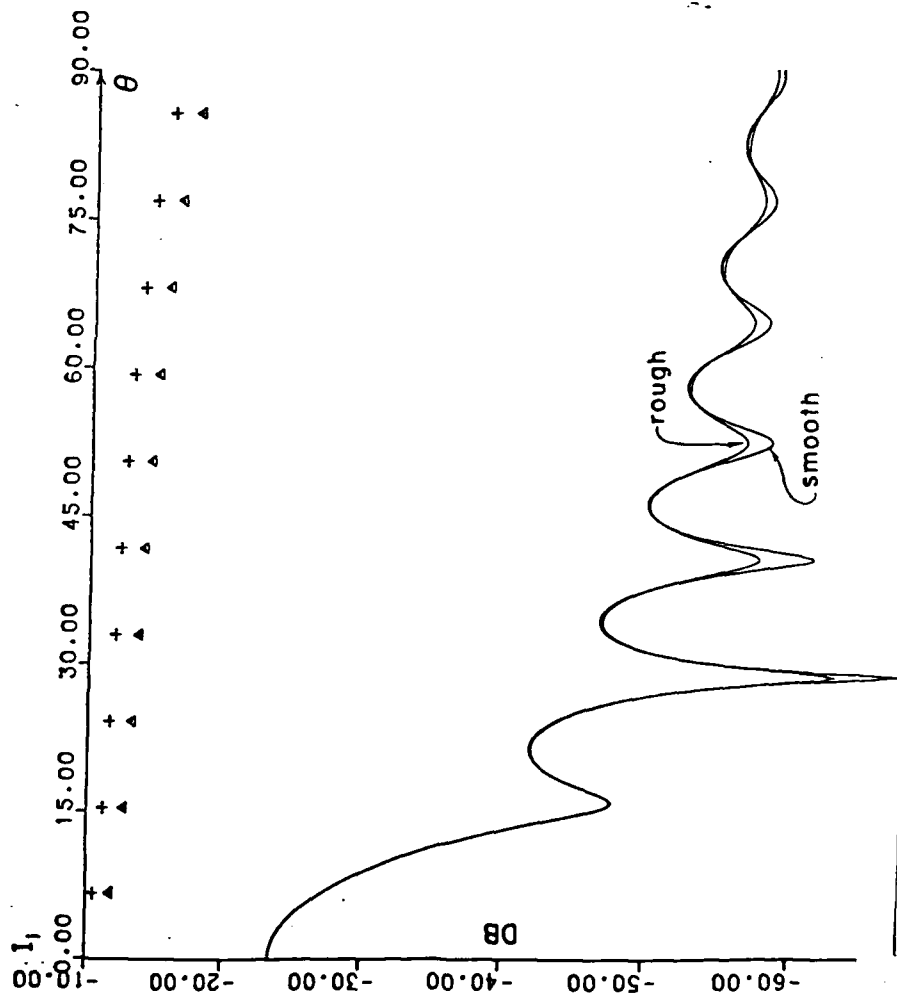


Fig. 3. Specific incoherent intensity I_1 for a right circularly polarized wave normal incidence, $\beta = 1$, $v_m = 1.2/\eta$, $\lambda = 10 \mu$, $\epsilon = -6000(1+i)(AL)$, $D = 5\lambda$, transmitted, $\tau_0 = 10$. First order (solid line), smooth and rough particles. Multiple scatter: (plus), smooth; (triangle), rough.

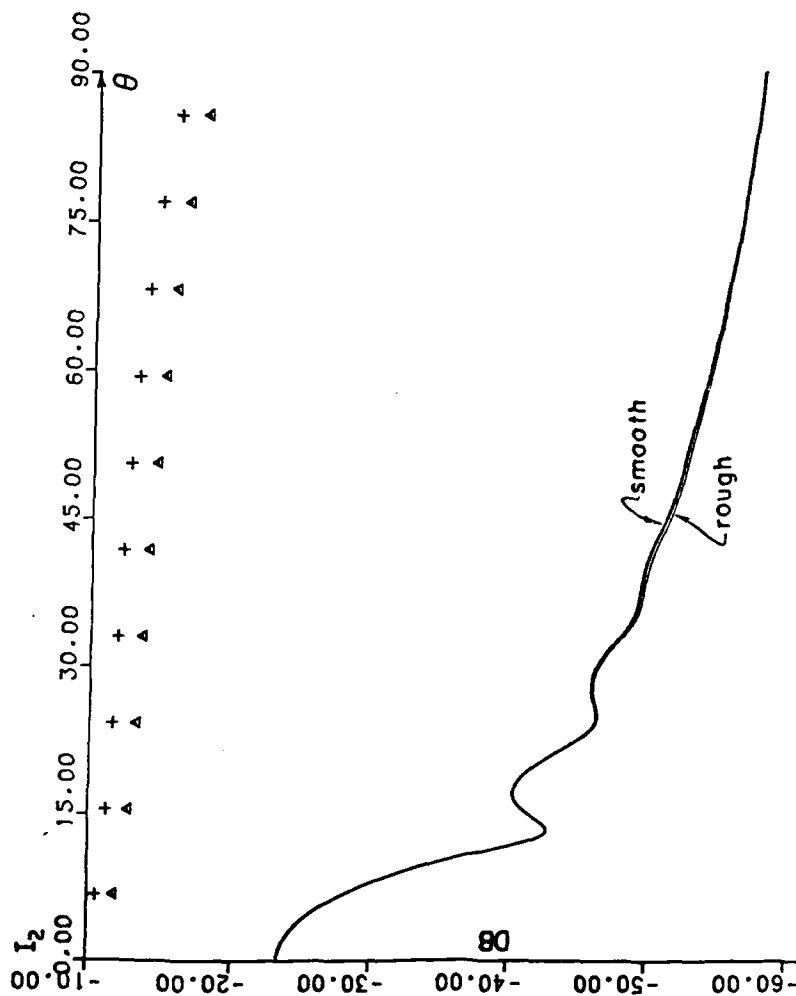


Fig. 4. Specific incoherent intensity I_2 for a right circularly polarized wave normal incidence, $\beta = 1$, $v_m = 1.2/D$, $\lambda = 10$ μ , $\epsilon = -6000(1+i)(AL)$, $D = 5\lambda$, transmitted, $\tau_0 = 10$. First order (solid line), smooth and rough particles. Multiple scatter: (+), smooth; (Δ), rough.

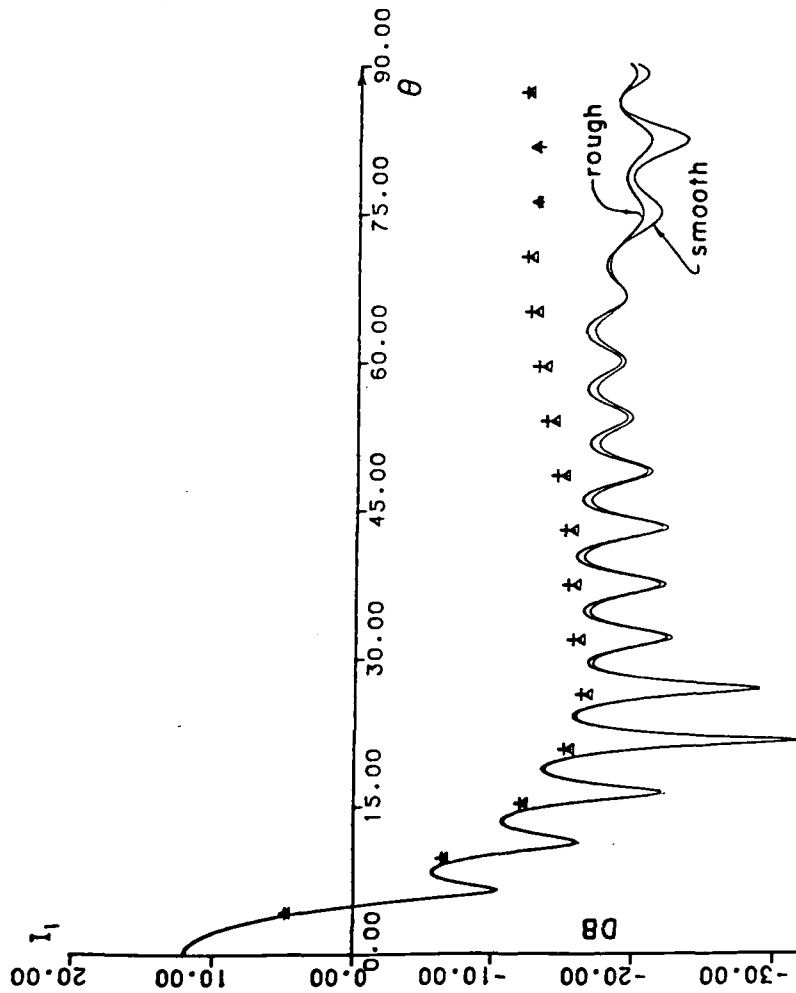


Fig. 5. Specific incoherent intensity I_1 for a right circularly polarized wave normal incidence, $\beta = 1$, $v_m = 15.9/D$, $\lambda = 0.555 \mu$, $\epsilon = -40 - i12$ (AL), $D = 10\lambda$. Transmitted, $\tau_0 = 1$, $\phi = 0$. First order (solid line), smooth and rough particles. Multiple scatter: (plus), smooth; (triangle), rough.

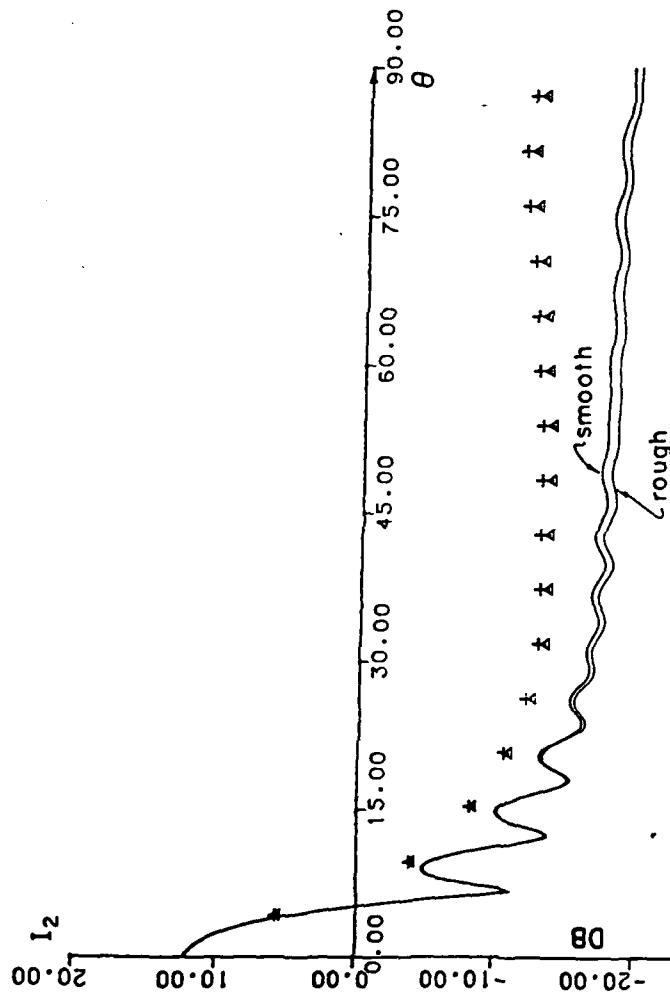


Fig. 6. Specific incoherent intensity I_2 for a right circularly polarized wave normal incidence, $\beta = 1$, $v_m = 15.9/D$, $\lambda = 0.555 \mu$, $\epsilon = -40 - i12$ (AL), $D = 10\lambda$. Transmitted, $\tau = 1$, $\phi = 0$. First order (solid line), smooth and rough particles. Multiple scatter: (plus), smooth; (triangle), rough.

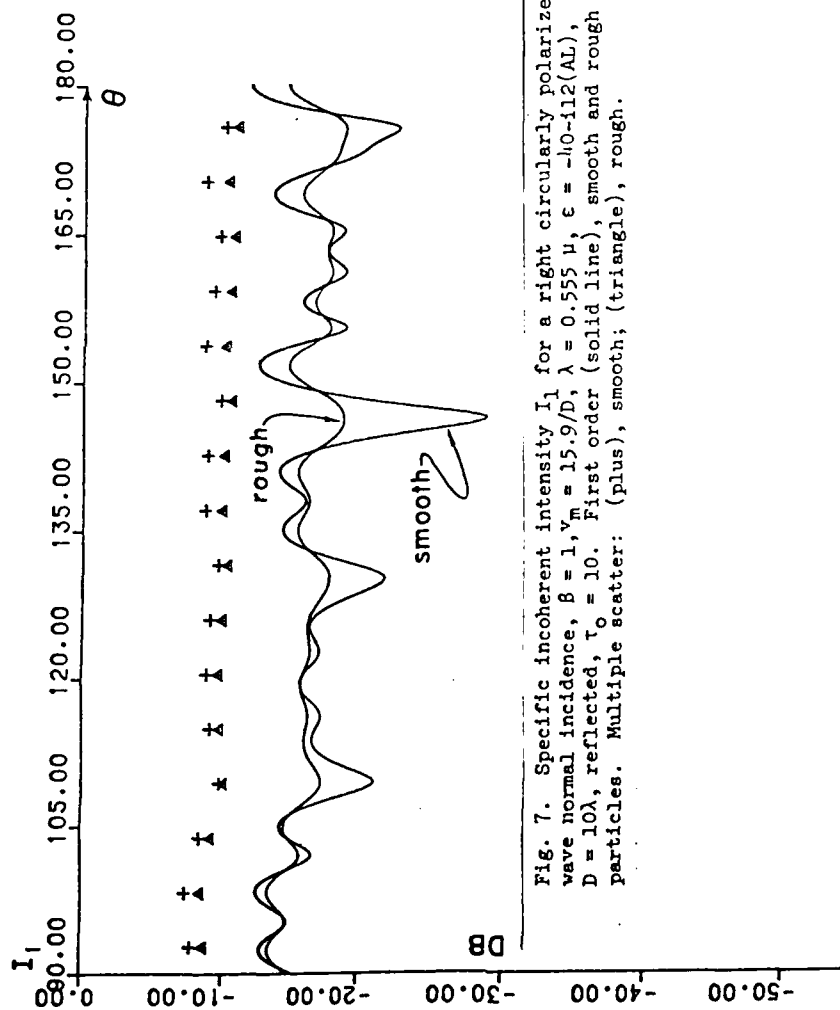


Fig. 7. Specific incoherent intensity I_1 for a right circularly polarized wave normal incidence, $\beta = 1$, $v_m = 15.9/D$, $\lambda = 0.555 \mu$, $\epsilon = -40 - i12(4L)$, $D = 10\lambda$, reflected, $v_0 = 10$. First order (solid line), smooth and rough particles. Multiple scatter: (plus), smooth; (triangle), rough.

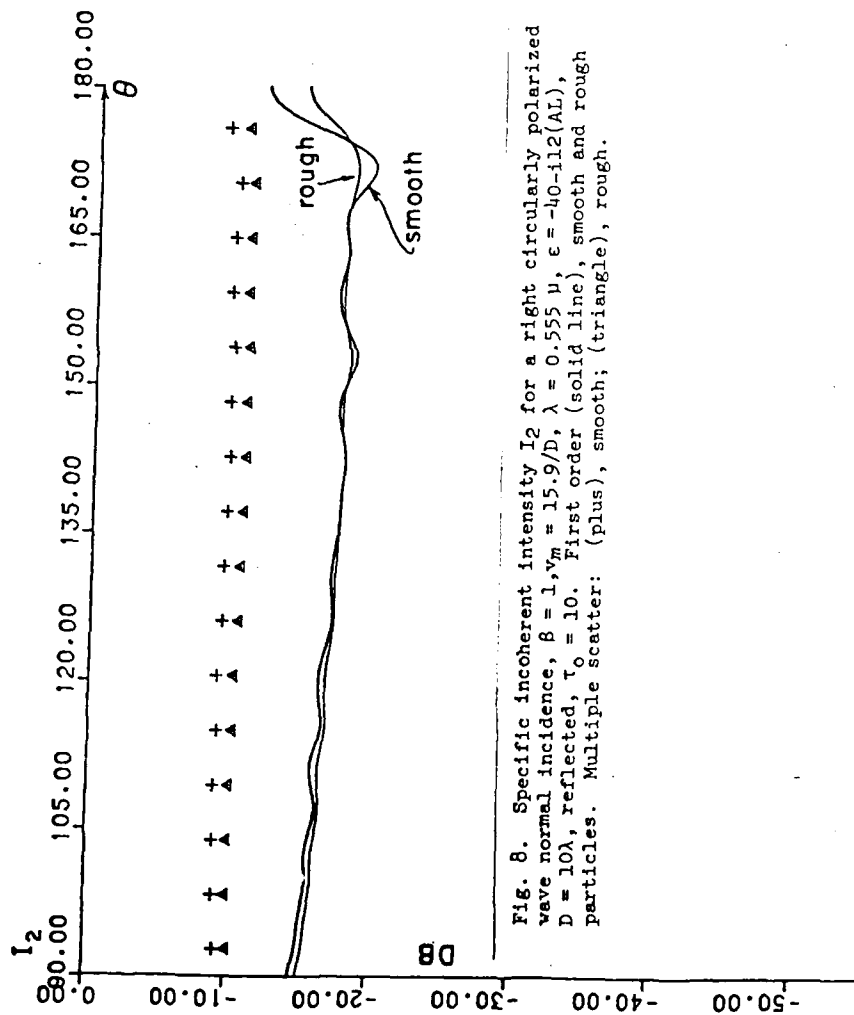


Fig. 8. Specific incoherent intensity I_2 for a right circularly polarized wave normal incidence, $\beta = 1$, $v_m = 15.9/D$, $\lambda = 0.555 \mu$, $\epsilon = -40 - i12(4L)$, $D = 10\lambda$, reflected, $\tau_0 = 10$. First order (solid line), smooth and rough particles. Multiple scatter: (plus), smooth; (triangle), rough.

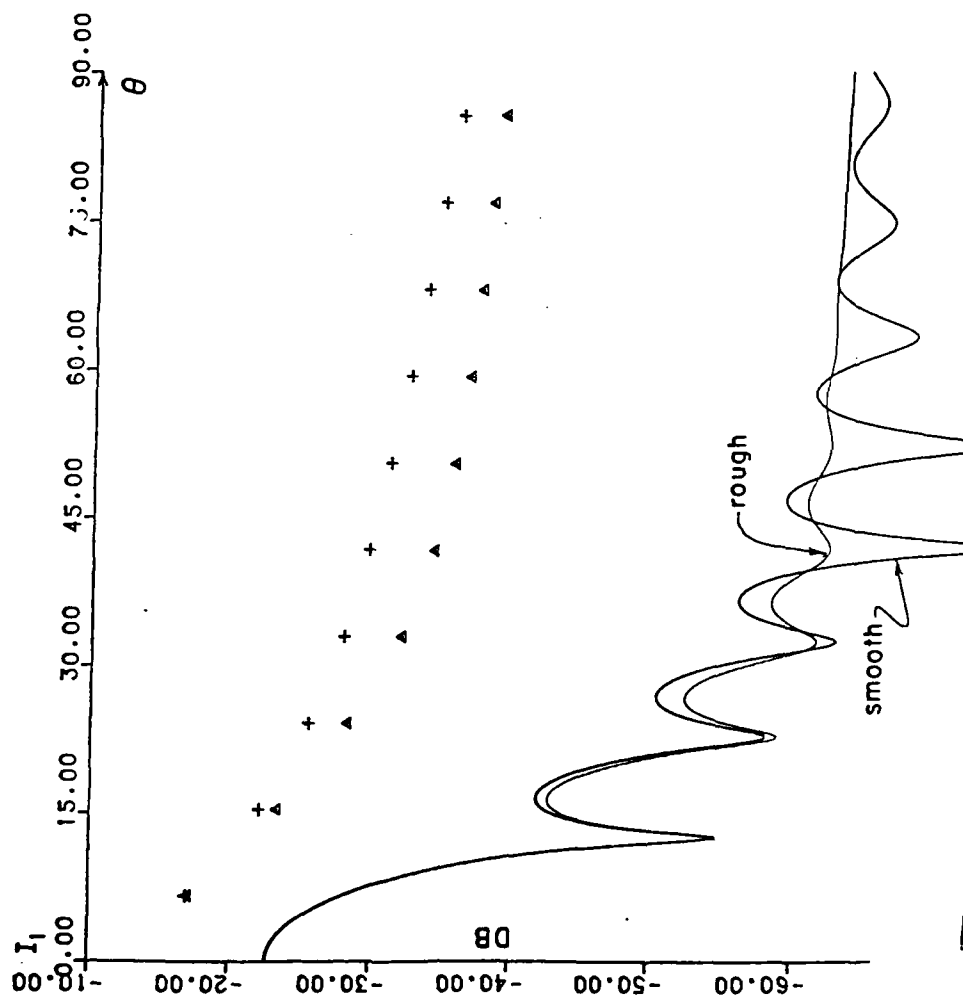


Fig. 9. Specific incoherent intensity I_1 for a right circularly polarized wave normal incidence, $\beta = 10$, $v_m = 4/D$, $\lambda = 10 \mu$, $\epsilon = 1.5-18$ (plastic), $D = 5\lambda$, transmitted, $t_0 = 10$. First order (solid line), smooth and rough particles. Multiple scatter: (plus), smooth (triangle), rough.

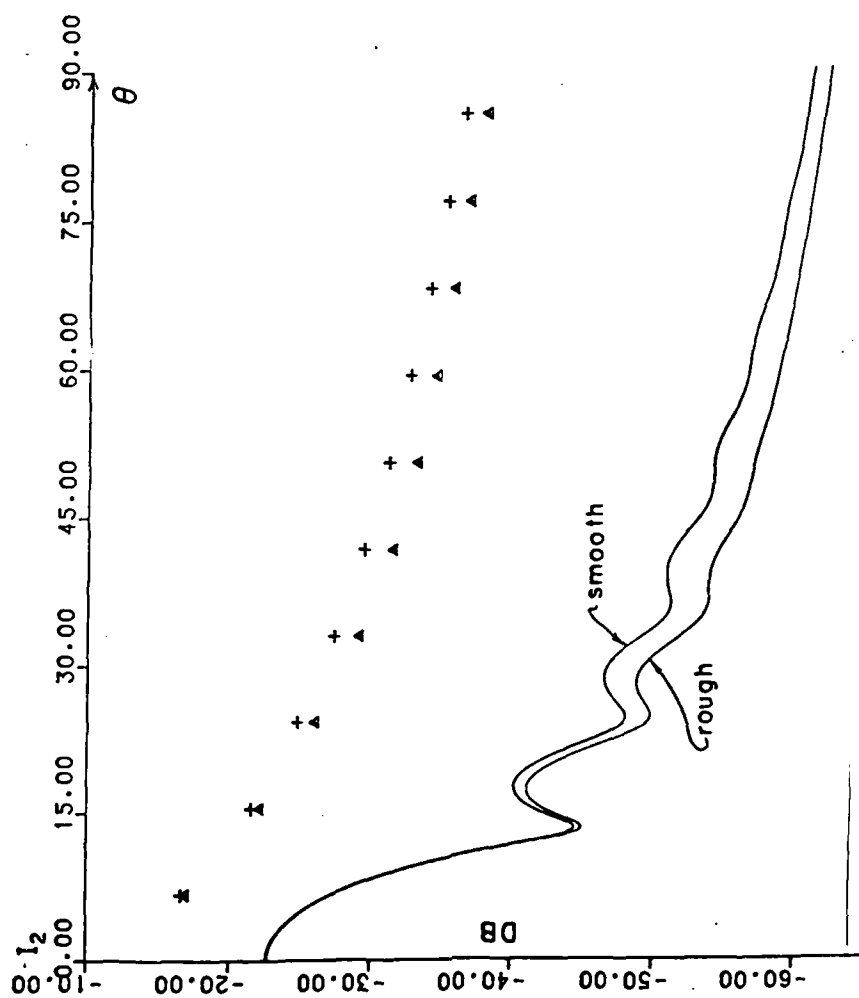


Fig. 10. Specific incoherent intensity I_2 for a right circularly polarized wave normal incidence, $\beta = 10$, $v_m = 4/D$, $\lambda = 10 \mu$, $\epsilon = 1.5-i8$ (plastic), $D = 5\lambda$, transmitted, $\tau_0 = 10$. First order (solid line), smooth and rough particles. Multiple scatter: (plus), smooth; (triangle), rough.

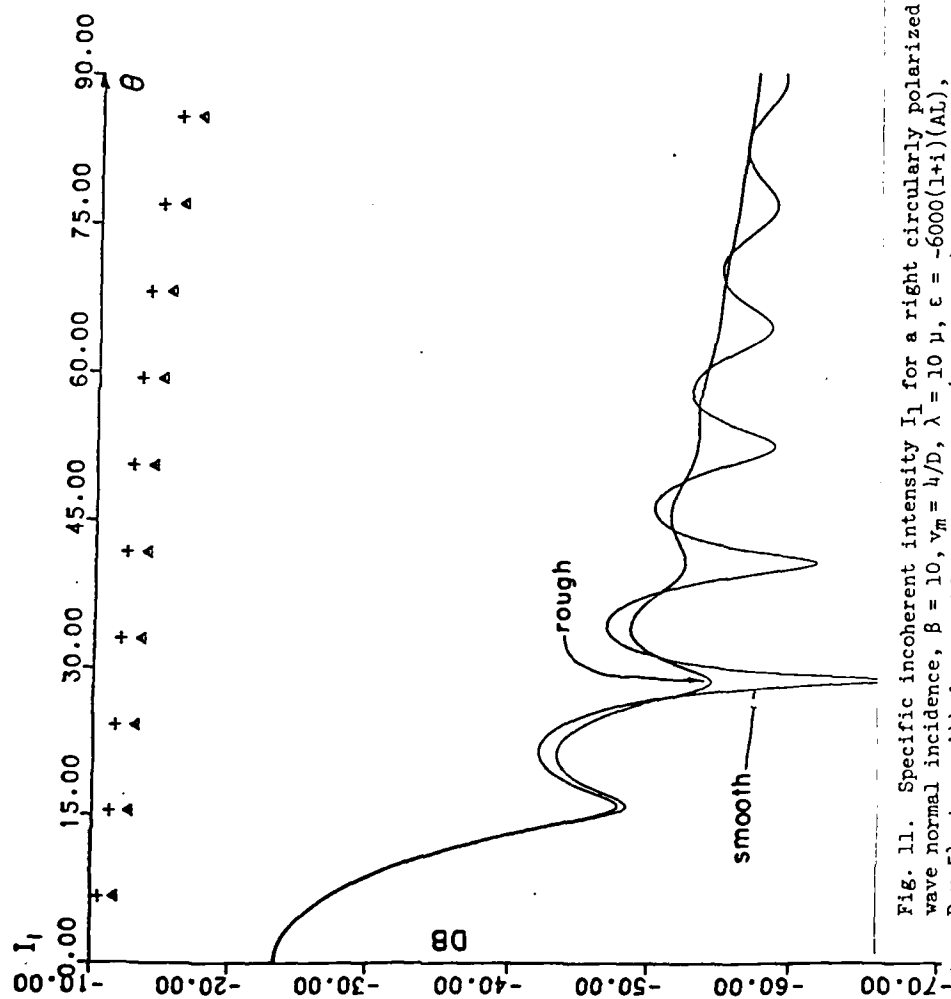


Fig. 11. Specific incoherent intensity I_1 for a right circularly polarized wave normal incidence, $\beta = 10$, $v_m = 4/D$, $\lambda = 10 \mu$, $\epsilon = -6000(1+i)(\text{AL})$, $D = 5\lambda$, transmitted, $T_0 = 10$. First order (solid line), smooth and rough particles. Multiple scatter: (plus), smooth; (triangle), rough.

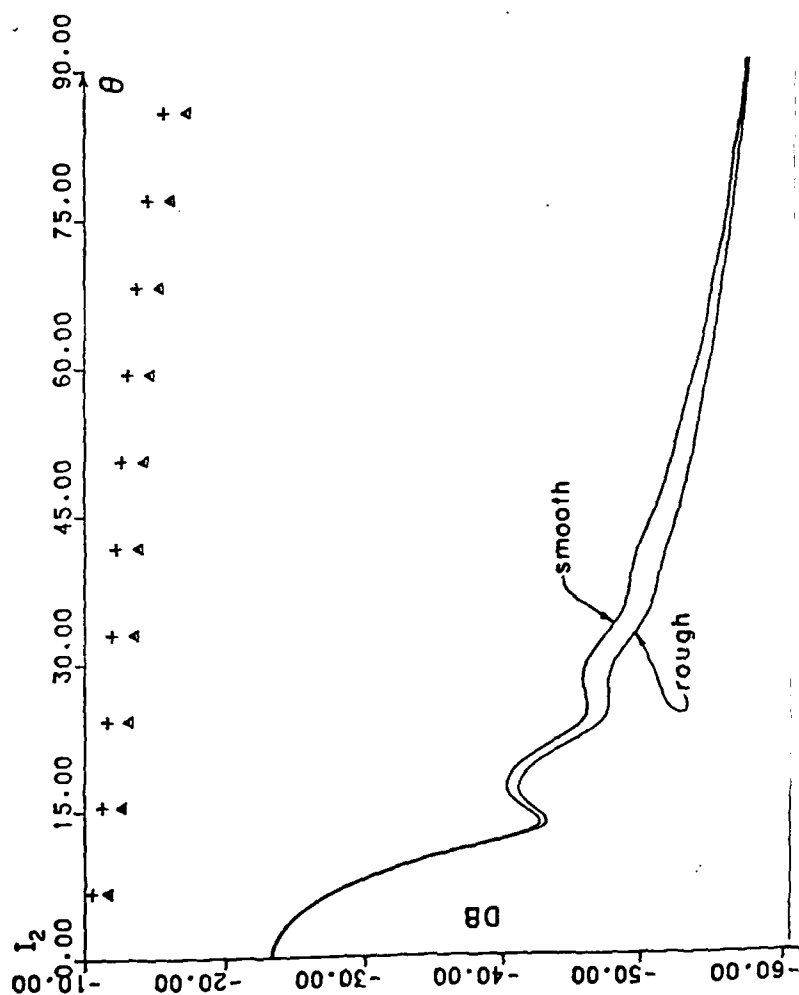


Fig. 12. Specific incoherent intensity I_2 for a right circularly polarized wave normal incidence, $\beta = 10$, $v_m = 4/D$, $\lambda = 10 \mu$, $\epsilon = -6000(1+i)(AL)$, $D = 5\lambda$, transmitted, $\tau = 10$. First order (solid line), smooth and rough particles. Multiple scatter: (plus), smooth; (triangle), rough.

SCATTERING AND DEPOLARIZATION OF LINEARLY POLARIZED
WAVES BY FINITELY CONDUCTING PARTICLES OF IRREGULAR SHAPE

Ezekiel Bahar

and

Mary Ann Fitzwater

Electrical Engineering Department
University of Nebraska--Lincoln
Lincoln, Nebraska 68588-0511

Abstract

In this work a layer consisting of a large variety of randomly distributed finitely conducting particles with irregular shapes is assumed to be excited at infrared and optical frequencies by a linearly polarized wave. The resulting incoherent specific intensities as well as the co-polarized and cross polarized intensities are evaluated. Both single scatter and multiple scatter results are presented for particles with smooth and rough surfaces and the effects of particle surface roughness on the degree of polarization are considered in detail.

1. Introduction

In this work the scattering and depolarization of linearly polarized waves by a random distribution of finitely conducting particles of irregular shape are presented. Infrared and optical excitations of a large variety of particles with different sizes, shapes and complex dielectric coefficients (see Table I) are considered in detail. The random rough surface of the particle is characterized by its surface height spectral density function (or its Fourier transform the surface height autocorrelation function).

The full wave approach is used to account for both specular point scattering as well as diffuse scattering by the particle in a self-consistent manner¹, and the equation of transfer^{2,3} for the modified Stokes parameters is solved using the matrix characteristic value method⁴. Both single scatter and multiple scatter results are given for particles with smooth and rough surfaces and the effects of particle surface roughness are considered in detail.

Both the co-polarized and cross polarized incoherent diffuse intensities are plotted as functions of the azimuth angle and the optical thickness of the layer of particles. The degree of polarization of the scattered waves is also evaluated as a function of the azimuth angle.

2. Formulation of the Problem

In this section we present the analytical solutions for the modified Stokes incoherent specific diffuse intensity matrix $[I]$. A linearly polarized wave is assumed to be normally incident upon a parallel layer of randomly distributed non-spherical particles. Thus the like and cross polarized incoherent intensities are azimuthally dependent. Special consideration is given to the effects of the surface roughness of the particles of finite conductivity. Since the roughness parameter $\beta = 4k_0^2 \langle h_s^2 \rangle$ (where k_0 is the free space wavenumber of the electromagnetic wave and $\langle h_s^2 \rangle$ is the mean square height of the particle rough surface) is assumed to be large ($0 < \beta < 10$), the full wave solutions¹ are used to determine the elements of the scattering matrix for the equation of transfer^{2,3}.

$$\mu \frac{d[I]}{d\tau} = -[I] + \int [S][I'] d\mu' d\phi' + [I_i] \quad (2.1)$$

In (2.1) τ is the optical distance in the z direction (normal to the plane of the slab, (see Figs. 1 and 2)

$$\tau = \rho[\sigma_t]z \equiv \int \sigma_t n(D) dD \quad (2.2)$$

where D is the diameter of the unperturbed spherical particle, $n(D)$ is the particle size distribution and σ_t is the extinction coefficient. The symbol $\rho[\cdot]$ denotes integration over the size distribution. Since the effects of the particle surface roughness are vanishingly small in the forward direction, the extinction matrix^{5,4}

for the rough sphere can be represented by a scalar quantity. The (4×1) matrices $[I]$ and $[I']$ are the incoherent diffuse intensity matrices for waves scattered by the particles in the direction $\theta = \cos^{-1}\mu$ and ϕ and for waves

incident in the direction $\theta' = \cos^{-1} \mu'$ and ϕ' respectively. The elements of $[I]$ are the modified Stokes parameters³.

$$[I] = \begin{bmatrix} I_1 \\ I_2 \\ U \\ V \end{bmatrix} = \begin{bmatrix} \langle E_1 E_1^* \rangle \\ \langle E_2 E_2^* \rangle \\ 2\text{Re}\langle E_1 E_2^* \rangle \\ 2\text{Im}\langle E_1 E_2^* \rangle \end{bmatrix} \quad (2.3)$$

where the symbol * denotes the complex conjugate (an $\exp(i\omega t)$ time dependent excitation is assumed) and E_1 and E_2 are the vertically and horizontally polarized components of the electric field. The (4x4) scattering matrix $[S]$ in the reference coordinate system is expressed in terms of the scattering matrix $[S']$ in the scattering plane through the following transformation

$$[S] = [\mathcal{L}(-\pi + \alpha)][S'][\mathcal{L}(\alpha)] \quad (2.4)$$

in which $[S']$ is the weighted sum of two matrices

$$[S'] = |\chi^s(\vec{v} \cdot \vec{e}_r)|^2 [S_{\text{Mie}}] + [S_s] \quad (2.5)$$

In (2.5) $[S_{\text{Mie}}]$ is given by

$$[S_{\text{Mie}}] = \frac{1}{\rho[\sigma_t]} \begin{bmatrix} \rho[|f_{11}|^2] & \rho|f_{12}|^2 & \rho\text{Re}[f_{11}f_{12}^*] & -\rho\text{Im}[f_{11}f_{12}^*] \\ \rho[|f_{21}|^2] & \rho|f_{22}|^2 & \rho\text{Re}[f_{21}f_{22}^*] & -\rho\text{Im}[f_{21}f_{22}^*] \\ \rho 2\text{Re}[f_{11}f_{21}^*] & \rho 2\text{Re}[f_{12}f_{22}^*] & \rho\text{Re}[f_{11}f_{22}^* + f_{12}f_{21}^*] & -\rho\text{Im}[f_{11}f_{22}^* - f_{12}f_{21}^*] \\ \rho 2\text{Im}[f_{11}f_{21}^*] & \rho 2\text{Im}[f_{12}f_{22}^*] & \rho\text{Im}[f_{11}f_{22}^* + f_{12}f_{21}^*] & \rho\text{Re}[f_{11}f_{22}^* - f_{12}f_{21}^*] \end{bmatrix} \quad (2.6)$$

where f_{ij} are the elements of the 2x2 scattering matrix $[f]$ for the unperturbed (spherical) particle.

$$\begin{bmatrix} E_l \\ E_r \end{bmatrix} = \begin{bmatrix} f_{11} & f_{12} \\ f_{21} & f_{22} \end{bmatrix} \begin{bmatrix} E_l' \\ E_r' \end{bmatrix} \frac{\exp(-ik_0 r)}{r} \quad (2.7)$$

In (2.7) E_v and E_h are the vertically and horizontally polarized field components (in the scattering plane which contains the unit vectors \bar{n}^i and \bar{n}^f in the directions of the incident and scattered waves), and r is the distance from the center of the spherical particles. For a smooth sphere f_{ij} are given by the Mie solution^{6,3} and $[f]$ is a diagonal matrix. The transformation matrix $[\mathcal{A}]$ in (2.4) is

$$[\mathcal{A}(\alpha)] = \begin{bmatrix} \cos^2 \alpha & \sin^2 \alpha & \frac{1}{2} \sin 2\alpha & 0 \\ \sin^2 \alpha & \cos^2 \alpha & -\frac{1}{2} \sin 2\alpha & 0 \\ -\sin 2\alpha & \sin 2\alpha & \cos 2\alpha & 0 \\ 0 & 0 & 0 & 1 \end{bmatrix} \quad (2.8)$$

where α' is the angle between the reference plane of incidence and the scattering plane and α is the angle between the reference plane of scatter and the scattering plane (see Fig. 2). In (2.5) $\chi^s(\bar{v} \cdot \bar{a}_r)$ is the particle random rough surface characteristic function

$$\chi^s(\bar{v} \cdot \bar{a}_r) = \langle \exp(i\bar{v} \cdot \bar{a}_r h_s) \rangle \quad (2.9a)$$

in which

$$\bar{v} = k_0(\bar{n}^f - \bar{n}^i) \quad (2.9b)$$

and \bar{n}^f and \bar{n}^i are unit vectors in the directions of the scattered and incident wave normals. The random rough surface h_s is measured normal to the unperturbed (spherical) particle. Thus, the radius vector to the surface of the irregular particle is (see Fig. 1),

$$\bar{r}_s = h_0 \bar{a}_r + h_s \bar{a}_r \quad (2.9c)$$

The radius of the unperturbed sphere is h_0 . The coefficient $|\chi^s|^2$ in (2.5) accounts for the degradation of the specular point contributions to the scattered fields by the rough surface ($|\chi^s|^2 \leq 1$ and $|\chi^s|^2 \rightarrow 1$ as $\beta \rightarrow 0$). The diffuse scattering contribution to the matrix $[S']$ due to surface roughness is given by

$$[S_s] = \begin{bmatrix} [S_{11}^s] & [S_{12}^s] & 0 & 0 \\ [S_{21}^s] & [S_{22}^s] & 0 & 0 \\ 0 & 0 & [S_{33}^s] & [S_{34}^s] \\ 0 & 0 & [S_{43}^s] & [S_{44}^s] \end{bmatrix} \quad (2.10)$$

where

$$[S_{ij}^s] = \frac{A_y}{4\pi\rho[\sigma_t]} \rho[\langle\sigma^{ij}\rangle_s], \text{ for } i,j = 1,2 \quad (2.11a)$$

in which $A_y = \pi h_0^2$ is the cross sectional area of the unperturbed particle and $\langle\sigma^{ij}\rangle_s$ are the full wave solutions for the like and cross polarized normalized scattering cross sections.¹

The first and second superscripts i,j denote the polarizations (V vertical, H horizontal) of the scattered and incident fields respectively.

$$\langle\sigma^{ij}\rangle_s = \int_0^{2\pi} \int_0^\pi |k_o D^{ij}|^2 P_2 Q_s \sin\gamma \, d\gamma d\delta / \pi^2 \quad (2.11b)$$

where

$$Q_s = \int_{-\infty}^{\infty} (\chi_2^s(\vec{v} \cdot \vec{a}_r) - |\chi_2^s(\vec{v} \cdot \vec{a}_r)|^2) \exp(i\vec{v} \cdot \vec{r}_d) dx_d dz_d \quad (2.11c)$$

The joint characteristic function χ_2 for the rough surface h_s is only a function of distance $r_d = (x_d^2 + z_d^2)^{1/2}$ measured along the surface of the unperturbed sphere.

Furthermore for $i = 3$ and 4

$$[S_{ii}^s] = \rho[\text{Re}[\langle\sigma_{22}^{11}\rangle_s \pm \langle\sigma_{21}^{12}\rangle_s]] A_y / 4\pi\rho[\sigma_t] \quad (2.11d)$$

(upper and lower signs for $i = 3$ and 4 respectively) and for $i \neq j$

$$[S_{ij}^s] = \rho[\text{Im}[\pm \langle\sigma_{22}^{11}\rangle_s + \langle\sigma_{21}^{12}\rangle_s]] A_y / 4\pi\rho[\sigma_t] \quad (2.11e)$$

(upper and lower signs for $i,j=4,3$ and $i,j=3,4$ respectively). In the above expressions

$$\langle\sigma_{kl}^{ij}\rangle = \int_0^{2\pi} \int_0^\pi k_o^2 D^{ij} D^{kl*} P_2 Q_s \sin\gamma \, d\gamma d\delta / \pi^2 \quad (2.11f)$$

In (2.11) P_2 is the shadow function and the scattering coefficients D^{ij} are functions of \vec{n}^i, \vec{n}^f and \vec{n} the normal to the unperturbed surface of the particle as well as its electromagnetic parameters ϵ, μ . The remaining eight terms of the matrix $[S_s]$ vanish since D^{ii} and $D^{ij} (i \neq j)$ are symmetric and antisymmetric respectively with respect to δ , the azimuth angle of the sphere.

In this work it is assumed that a linearly polarized wave is normally incident upon a parallel layer (of optical thickness τ_o) containing a random distribution of irregular particles. Thus the incident Stokes matrix at $z=0$ (Fig. 2) is

$$[I_{inc}] = \begin{bmatrix} 1 \\ 0 \\ 0 \\ 0 \end{bmatrix} \delta(\mu'-1) \delta(\phi') \equiv [I_o] \delta(\mu'-1) \delta(\phi') \quad (2.12)$$

in which $\delta(\cdot)$ is the Dirac delta function.

Thus the reduced incident intensity is

$$[I_{ri}] = [I_{inc}] \exp(-\tau) \quad (2.13)$$

and the (4x1) excitation matrix in (2.1) is

$$[I_i] = \int [S][I_{ri}] d\mu' d\phi' = [F] \exp(-\tau) \quad (2.14)$$

in which the (4x1) matrix F is

$$[F] = [S][I_o] \Big|_{\substack{\mu'=1 \\ \phi'=0}} \quad (2.15)$$

and the matrix $[I_o]$ is defined by (2.12). The matrix $[F]$ contains terms that are azimuthally independent as well as terms that are proportional to $\cos 2\phi$ and $\sin 2\phi$. Thus $[F]$ is expressed as follows⁴

$$[F] = [F]_o + [F]_a \cos 2\phi + [F]_b \sin 2\phi \quad (2.16)$$

in which, for a rough sphere,

$$[F]_o = \frac{1}{2} \begin{bmatrix} F_{01} \\ F_{02} \\ 0 \\ 0 \end{bmatrix}, \quad [F]_a = \frac{1}{2} \begin{bmatrix} F_{a1} \\ F_{a2} \\ 0 \\ 0 \end{bmatrix}, \quad [F]_b = \begin{bmatrix} 0 \\ 0 \\ -S_{33} \\ -S_{43} \end{bmatrix} \quad (2.17)$$

and $F_{\alpha i} = S_{i1} \pm S_{i2}$ (upper and lower signs for $\alpha=0$ and $\alpha=a$ respectively.)

The solution of the equation of transfer (2.1) for the incoherent specific intensity matrix can be expressed in terms of the Fourier series

$$[I] = \sum_{m=0}^{\infty} [I]_m^a \cos m\phi + \sum_{m=1}^{\infty} [I]_m^b \sin m\phi \quad (2.18)$$

Since the elements of the scattering matrix $[S]$ are functions of $\phi' - \phi$ it is expressed as follows

$$[S] = \frac{1}{2\pi} [S]_o^a + \frac{1}{\pi} \sum_{m=1}^{\infty} \left[[S]_m^a \cos m(\phi' - \phi) + [S]_m^b \sin m(\phi' - \phi) \right] \quad (2.19)$$

Furthermore, since in (2.7) f_{11} and f_{22} are even functions while f_{12} and f_{21} are odd functions of $\phi' - \phi$, for $m=0, 1, 2, \dots$

$$[S]_m^a = \begin{bmatrix} [S_1]_m^a & 0 \\ 0 & [S_4]_m^a \end{bmatrix} \text{ and } [S]_m^b = \begin{bmatrix} 0 & [S_2]_m^b \\ [S_3]_m^b & 0 \end{bmatrix} \quad (2.20)$$

in which $[S_i]_m^a$ and $[S_i]_m^b$ are 2×2 matrices

$$[S_i]_m^a = \int_0^{2\pi} [S_i] \cos m(\phi' - \phi) d(\phi' - \phi) \quad i=1,4 \quad (2.21a)$$

and

$$[S_i]_m^b = \int_0^{2\pi} [S_i] \sin m(\phi' - \phi) d(\phi' - \phi) \quad i=2,3 \quad (2.21b)$$

and $[S_i]$ are the (2×2) submatrices

$$[S] = \begin{bmatrix} [S_1] & [S_2] \\ [S_3] & [S_4] \end{bmatrix} \quad (2.22)$$

In view of the excitation, (2.14) through (2.17), the only non-vanishing Fourier terms are $m=0$ and $m=2$.⁴ The equation of transfer for the $m=0$ Stokes matrix is

$$\mu \frac{d}{d\tau} [I]_0^a = -[I]_0^a + \int_{-1}^1 [S]_0^a [I]_0^a d\mu' + [F]_0 \exp(-\tau) \quad (2.23)$$

Since the third and fourth elements of $[F]_0$ (2.17) are zero, and in view of the special form of $[S]_0^a$, the third and fourth terms of $[I]_0^a$ vanish.

The equation of transfer for the $m=2$ term is

$$\mu \frac{d}{d\tau} [I]_2 = -[I]_2 + \int_{-1}^1 [S]_2 [I]_2 d\mu' + [F]_2 \exp(-\tau) \quad (2.24)$$

in which

$$[S]_2 = \begin{bmatrix} [S_1]_2^a & [S_2]_2^b \\ -[S_3]_2^b & [S_4]_2^a \end{bmatrix} \text{ and } [F]_2 = [F]_a + [F]_b \quad (2.25)$$

The boundary conditions for the Stokes matrix are

$$[I]_0 = [I]_2 = 0 \quad \text{for } 0 \leq \mu \leq 1 \text{ at } \tau = 0 \quad (2.26a)$$

and

$$[I]_0 = [I]_2 = 0 \quad \text{for } 0 \geq \mu \geq -1 \text{ at } \tau = \tau_0. \quad (2.26b)$$

Equations (2.23) and (2.24) together with the associated boundary conditions (2.26) are solved for the specific incoherent diffuse scattering intensities using the Gaussian quadrature method (to discretize the angles $\theta = \cos^{-1}\mu$) and the matrix characteristic value technique.³

The diffuse scattering intensities I_1 and I_2 correspond to the vertically polarized (E_θ) and horizontally polarized (E_ϕ) waves. However in practice, the polarization of the receiver is either parallel (E_x) or perpendicular (E_y) to the polarization of the incident wave. The corresponding specific intensities I_x and I_y are called the co-polarized and cross polarized incoherent intensities respectively.⁴

They are related to the intensities I_1 and I_2 through the linear transformation

$$\begin{bmatrix} I_x \\ I_y \\ U_{xy} \\ V_{xy} \end{bmatrix} = \begin{bmatrix} \langle E_x E_x^* \rangle \\ \langle E_y E_y^* \rangle \\ 2\langle \text{Re}(E_x E_y^*) \rangle \\ 2\langle \text{Im}(E_x E_y^*) \rangle \end{bmatrix} = [R][I] \quad (2.27)$$

where

$$[R] = \begin{bmatrix} \cos^2\theta \cos^2\phi & \sin^2\phi & -\frac{1}{2} \sin 2\phi \cos\theta & 0 \\ \cos^2\theta \sin^2\phi & \cos^2\phi & \frac{1}{2} \sin 2\phi \cos\theta & 0 \\ \cos^2\theta \sin 2\phi & -\sin 2\phi & \cos 2\phi \cos\theta & 0 \\ 0 & 0 & 0 & \cos\theta \end{bmatrix} \quad (2.28)$$

The degree of polarization of scattered waves is given by³

$$m = \frac{[(I_1 - I_2)^2 + U^2 + V^2]^{\frac{1}{2}}}{I_1 + I_2} \quad (2.29)$$

All the specific intensities as well as the parameter m are symmetric about the $\phi = 0, \pi$ plane and the $\phi = \pi/2, 3\pi/2$ plane.

3. Illustrative Examples

The random rough surface height h_s (2.9) (measured normal to the surface of the unperturbed spherical particle of radius h_0 , see Fig. 2), is assumed to be homogeneous and isotropic for the illustrative examples considered in this section. The rough surface is characterized by its surface height spectral density function $W(v_x, v_z) = W(v_T)$, the Fourier transform of the surface height autocorrelation function $\langle h_s h'_s \rangle$.

$$\begin{aligned} W(v_T) = W(v_x, v_z) &= \frac{1}{\pi^2} \int_{-\infty}^{\infty} \langle h_s h'_s \rangle \exp(i v_x x_d + i v_z z_d) dx_d dz_d \\ &= \frac{2}{\pi} \int_0^{\infty} \langle h_s h'_s \rangle J_0(v_T r_d) r_d dr_d \end{aligned} \quad (3.1)$$

in which $J_0(v_T r_d)$ is the zero order Bessel function of the first kind and v_x and v_z are components of the vector \bar{v} (2.9b) in the directions of the unit vectors \bar{n}_1 and \bar{n}_3 tangent to the surface of the unperturbed sphere. Thus

$$v_T = (v_x^2 + v_z^2)^{\frac{1}{2}} = (v^2 - v_r^2)^{\frac{1}{2}} \quad (3.2a)$$

and

$$v^2 = \bar{v} \cdot \bar{v}, \quad v_r = \bar{v} \cdot \bar{a}_r \quad (3.2b)$$

The surface height autocorrelation function $\langle h_s h'_s \rangle$ is only a function of the distance r_d measured along the unperturbed surface

$$\begin{aligned} \langle h_s h'_s \rangle &= \int_{-\infty}^{\infty} \frac{W(v_x, v_z)}{4} \exp(-i v_x x_d - i v_z z_d) dv_x dv_z \\ &= \frac{\pi}{2} \int_0^{\infty} W(v_T) J_0(v_T r_d) v_T dv_T \end{aligned} \quad (3.3)$$

Different forms of the surface height spectral density function W and different roughness parameters $\beta = 4k_0^2 \langle h_s^2 \rangle$ are considered for particles of different sizes $D = 2h_0$ and relative complex permittivities ϵ_r excited at infrared and optical frequencies (see Table I). Thus for case (a) (Table I), the specific form of the surface height spectral density function is

$$W(v_T) = \frac{2C}{\pi} \left[\frac{(v_T - v_d)}{(v_T - v_d)^2 + v_m^2} \right]^n \quad v_d < v_T < v_c \quad (3.4a)$$

$$= 0 \text{ elsewhere}$$

In (3.4a) the smallest spatial wavenumber is

$$v_d = 4/D \quad (3.4b)$$

and the cut-off wavenumber is

$$v_c = 4k_0 \quad (3.4c)$$

in which k_0 is the wavenumber for the electromagnetic wave. The constant C is determined by the choice of the roughness parameter (Table I).

$$\beta = 4k_0^2 \langle h_s^2 \rangle \quad (3.5)$$

In (3.5) $\langle h_s^2 \rangle$ is the mean square height

$$\langle h_s^2 \rangle = \frac{\pi}{2} \int_0^\infty W(v_T) v_T dv_T \quad (3.6)$$

The corresponding value for the mean square slope is (Table I)

$$\langle \sigma_s^2 \rangle = \frac{\pi}{2} \int_0^\infty W(v_T) v_T^3 dv_T \quad (3.7)$$

For case (a) the parameter $v_m = 1.2/D$ ($W(v_T \rightarrow v_m + v_d)$ is the maximum value of W), the exponent n (3.4a) is $n = 4$ and the diameter of the particle is $D = 5\lambda$ (Table I). For wavelength $\lambda = 10\mu$ the relative (complex) dielectric coefficient of aluminum is $\epsilon_r = -6000(1+i)$.⁸

For cases (b) through (d), (Table I), the specific form of the surface height spectral density function is

$$W(v_T) = \frac{2C}{\pi} \left[\frac{v_T}{v_T^2 + v_m^2} \right]^D, \quad v_T > 0 \quad (3.8)$$

in which the exponent is assumed to be $n = 8$. For case (b) the roughness parameter is $\beta = 1$ and for cases (c) through (e) $\beta = 10$. The corresponding values for v_m , $W(v_m) = (W_{\text{maximum}})$, σ_s^2 , λ , ϵ_r and $D = 2h_0$ are shown in Table I. The analytical expression for the surface height autocorrelation function for cases (b) through (e) is

$$R(\zeta) = \left[1 - \frac{3\zeta^2}{8} + \frac{3\zeta^4}{32} + \frac{\zeta^6}{3072} \right] \zeta K_1(\zeta) + \left[\frac{1}{2} - \frac{\zeta^2}{4} - \frac{\zeta^4}{96} \right] \zeta^2 K_0(\zeta) \quad (3.9)$$

In (3.9) K_0 and K_1 are modified Bessel functions of the second kind of order zero and one respectively⁹ and the dimensionless argument is

$$\zeta \equiv v_m r_d \quad (3.10)$$

For all the illustrative examples it is assumed that the normally incident wave is linearly polarized with the electric field in the direction of the x axis (in the $\phi=0$ plane, see Fig. 2). The equation of transfer for the Stokes parameters (2.23) and (2.24) together with the associated boundary conditions (2.26) are solved using the matrix characteristic value technique.³

For case (b) ($D/\lambda=10$), the scattering cross sections are very sharply peaked in the forward direction, thus it is necessary to use a Gaussian quadrature formula⁹ of order 32.

In Figs. 3 and 4, the incoherent diffuse transmitted intensities I_1 (vertical polarization) and I_2 (horizontal polarization) for case (a) are plotted as functions of $\theta(0,90^\circ)$ with $\phi=0$ and $\tau_0=10$. The solid curves correspond to first order scattering solutions only³ for the smooth (unperturbed

spherical) particles and particles with rough surfaces ($I_2 \neq 0$, for single scatter smooth particle). The corresponding solutions that account for multiple scattering are also plotted in these figures. The albedo for highly conducting particles with roughness parameter $\beta = 1$ is 0.9732 and the albedo for smooth particles is 0.9885 (see Table I). Thus for case (a) there is only a 2 db difference between the diffuse intensities for the rough and smooth particles. Note also that for $\tau_0 = 10$ except for scattering in the forward direction $I_1 \approx I_2$ (degree of polarization $m \approx 0$.)

In Figs. 5 and 6 the transmitted incoherent intensities I_1 and I_2 for case (b) are plotted as functions of $\theta(0,90^\circ)$ with $\phi = 0$ and $\tau_0 = 10$. At $\lambda = 0.555\mu$ the dielectric coefficient is $\epsilon_r = -40 - i12$ for aluminum. In this case there is a more significant difference between the albedoes for the rough and smooth particles (see Table I). Consequently there is a larger difference between the results for the smooth and rough particles for this case than for case (a) where $\lambda = 10\mu$. Note again that $I_1 \approx I_2$ except for the near forward direction.

In Figs. 7 and 8 the transmitted specific intensities I_1 and I_2 for case (c) are plotted as functions of $\theta(0,90^\circ)$ with $\phi = 0$ and $\tau_0 = 1$. The particle surface roughness tends to smooth out the first order solution (solid line). In this case $\lambda = 10\mu$ and $\epsilon_r = -6000(1+i)$, the albedoes for both the smooth and rough particles are near unity however surface roughness does have a very significant effect on the specific intensity I_2 . For $\tau_0 = 1$ $I_1 > I_2$ particularly in the forward direction. The corresponding results (case (c)) for the co-polarized and cross polarized incoherent specific intensities I_x and I_y respectively are plotted as functions of ϕ in Figs. 9 and 10 with $\theta = 15.4^\circ$.

In Figs. 11 and 12 the reflected co-polarized and cross polarized specific intensities I_1 and I_2 are plotted for case (d) as functions of the azimuth angle $\phi(0,180^\circ)$ with $\theta = 164.6^\circ$ and $\tau_0 = 1$. It is interesting to note

that the co-polarized intensity I_x is smaller for the rough particle than for the smooth particle since the albedo for the rough particle is smaller. However the cross polarized intensity I_y is smaller for the smooth particle than for the rough particle in this case. This is because the rough particles tend to depolarize the incident wave more strongly. As τ_0 becomes very large ($\tau_0 > 10$) I_y for the rough particle becomes smaller than I_y for the smooth particle.

In Figs. 13 and 14 the transmitted specific intensities I_1 and I_2 are plotted for case (e) as a function of θ with $\phi = 0$ and $\tau_0 = 1$. In this case particles of varying sizes ranging from $D = 5\lambda$ to $D = 8\lambda$ are considered. As a result the plots for I_1 do not exhibit the sharp undulations present in the corresponding plots of I_1 for particles of uniform size. Furthermore in the near forward direction ($\theta < 10^\circ$) multiple scattering and the rough surface effects on I_1 are small. From these plots it follows that the degree of polarization is largest in the near forward direction and it becomes very small for near grazing angles.

In Fig. 15 the transmitted co-polarized and cross polarized specific incoherent intensities I_x and I_y are plotted as functions of the optical thickness τ_0 for case (c) with $\theta = 6.7^\circ$ and $\phi = 0$. For $\tau < 2$ the results for the smooth and rough particles are practically the same, however for $\tau > 15$ $I_x \approx I_y$ (degree of polarization m becomes very small), and the effects of surface roughness become very significant.

In Fig. 16 the transmitted co-polarized and cross polarized specific incoherent intensities I_x and I_y are plotted as functions of τ_0 for case (d) with $\theta = 6.7^\circ$ and $\phi = 0$. In this case the particles are more dissipative than for case (c). The effect of surface roughness is more pronounced on I_y than on I_x . Both I_x and I_y peak around $\tau_0 = 2$.

In Figs. 17 and 18 the degree of polarization (2.29) is plotted for case (a) as a function of azimuth angle ϕ with $\theta = 6.7^\circ$, $\theta = 15.4^\circ$, $\theta = 24.2^\circ$ and $\theta = 33^\circ$. For near forward scattering $\theta = 6.7^\circ$, the degree of polarization m for the smooth and rough particles is close to unity for all angles ϕ . For $\theta = 15.4^\circ$ the degree

of polarization m undulates strongly as a function of ϕ . It is smaller for the rough particles. As the angle θ increases (see Fig. 18) the degree of polarization decreases and becomes more dependent on particle surface roughness.

The extinction cross sections σ_T and the albedoes for the different smooth and rough particles considered are given in Table I.

4. Concluding Remarks

The specific incoherent diffuse intensities I_1 and I_2 as well as the co-polarized and cross polarized intensities are evaluated for a layer of randomly distributed finitely conducting particles of irregular shape. A variety of particle sizes with different complex dielectric coefficients are considered. The rough surfaces of the particles are characterized by different surface height spectral density functions and roughness parameters β . The layer of particles is assumed to be excited by normally incident linearly polarized waves at wavelengths $\lambda = 10\mu$ and $\lambda = 0.555\mu$.

The rough particles will generally depolarize the incident waves more than the smooth particles and the specific intensities tend to be less oscillatory functions of θ for the rough particles. Since the albedoes for the rough particles are smaller than those for the smooth particles (the difference increases for more dissipative particles), hence for very thick layers the specific intensities are smaller for the rough particles. Both single scatter and multiple scatter solutions are given. For small optical thickness $\tau \leq 1$ I_1 is smaller for the rough particles than for the smooth particles (since the albedo for the rough particle is smaller). However I_2 is larger for the rough particles since the rough particles more strongly depolarize the incident waves (see Figs. 11 and 12). The reflected specific intensities I_1 and I_2 are generally less dependent on angle θ than the transmitted specific intensities. The particle surface roughness has a very significant effect on the degree of polarization m especially as the particle roughness parameter β increases.

ACKNOWLEDGMENTS

This work was supported by the U. S. Army Research Office under Contract DAAG-29-82-K-0123. The authors wish to thank Swapan Chakrabarti for his comments.

References

- ¹E. Bahar and Swapan Chakrabarti, "Scattering and depolarization by large conducting spheres with rough surfaces," Applied Optics, 24 (12), 1820 (1985).
- ²S. Chandrasekhar, Radiative Transfer, (Dover, Publ., New York, 1950).
- ³A. Ishimaru, Wave Propagation and Scattering in Random Media, (Academic, New York, 1978).
- ⁴R.L.-T. Cheung and A. Ishimaru, "Transmission, backscattering, and depolarization of waves in randomly distributed spherical particles," Applied Optics, 21 (20), 3792 (1982).
- ⁵A. Ishimaru and R.L.-T. Cheung, "Multiple scattering effects in wave propagation due to rain," Ann. Telecommun., 35, 373 (1980).
- ⁶D. E. Barrick, Rough Surfaces, in Radar Cross Section Handbook (Plenum, New York, 1970), Chapter 9.
- ⁷E. Bahar and M. Fitzwater, "Multiple scattering by irregular shaped particles of finite conductivity at infrared and optical frequencies," Radio Science - in press.
- ⁸H. Ehrenreich, "The optical properties of metals," IEEE Spectrum, 2, 162 (1965).
- ⁹M. Abramowitz and I. A. Stegun, Handbook of Mathematical Functions with Formulas, Graphs, and Mathematical Tables, Appl. Math. Ser. 55, (National Bureau of Standards, Washington, D. C., 1964).

TABLE I

	case a	case b	case c	case d	case e
n	4	8	8	8	8
β	1	1	10	10	10
v_m	1.2/D	15.9/D	4/D	4/D	4/D
$\langle \sigma_s^2 \rangle$	0.0131	0.10	0.10	0.10	0.065
λ	10 μ	0.555 μ	10 μ	10 μ	10 μ
ϵ_r	-6000-16000	-40-112	-6000-16000	1.5-18	1.5-18
Material	aluminum	aluminum	aluminum	dissipative plastic	dissipative plastic
$2h_0 = D$	5 λ	10 λ	5 λ	5 λ	average of sizes*
σ_T , smooth	2.059	2.259	2.059	2.370	2.320
σ_T , rough	2.059	2.313	2.198	2.333	2.285
albedo, smooth	0.9885	0.9356	0.9885	0.6434	0.6502
albedo, rough	0.9732	0.8999	0.9724	0.6043	0.6216

*mixture of 7 sizes (equal densities)

D = 5 λ , D = 5.5 λ , D = 6 λ , D = 6.5 λ , D = 7 λ , D = 7.5 λ , D = 8 λ TABLE I. Values of parameters for the surface height spectral density function W, wavelength λ , dielectric coefficient ϵ_r and diameter D for the scattering particles.

Figure Captions

FIG. 1. Scattering geometry for a rough conducting sphere.

FIG. 2. Scattering geometry indicating incident and scattered wave normals \vec{n}^i and \vec{n}^f and corresponding field components E_1 parallel (vertical) and E_2 perpendicular (horizontal) polarizations.

FIG. 3. Specific incoherent intensity I_1 , $\beta = 1$, $v_m = 1.2/D$, $\lambda = 10\mu$,

$\epsilon_r = -6000 - i6000(AL)$, $D = 5\lambda$, case (a), transmitted, $\tau_0 = 10$, $\phi = 0$.

First order (—), smooth and rough particles. Multiple scatter:

(+) smooth, (Δ) rough.

FIG. 4. Specific incoherent intensity I_2 , $\beta = 1$, $v_m = 1.2/D$, $\lambda = 10\mu$,

$\epsilon_r = -6000 - i6000(AL)$, $D = 5\lambda$, case (a), transmitted, $\tau_0 = 10$, $\phi = 0$.

First order (—), rough particles. Multiple scatter: (+) smooth,

(Δ) rough.

FIG. 5. Specific incoherent intensity I_1 , $\beta = 1$, $v_m = 15.9/D$, $\lambda = .555\mu$,

$\epsilon_r = -40 - i12(AL)$, $D = 10\lambda$, case (b), transmitted, $\tau_0 = 10$, $\phi = 0$. First

order (—), smooth and rough particles. Multiple scatter: (+) smooth,

(Δ) rough.

FIG. 6. Specific incoherent intensity I_2 , $\beta = 1$, $v_m = 15.9/D$, $\lambda = .555\mu$,

$\epsilon_r = -40 - i12(AL)$, $D = 10\lambda$, case (b), transmitted, $\tau_0 = 10$, $\phi = 0$. First

order (—), rough particles. Multiple scatter: (+) smooth, (Δ) rough.

FIG. 7. Specific incoherent intensity I_1 , $\beta = 10$, $v_m = 4/D$, $\lambda = 10\mu$,

$\epsilon_r = -6000 - i6000(AL)$, $D = 10\lambda$, case (c), transmitted, $\tau_0 = 1$, $\phi = 0$.

First order (—), smooth and rough particles. Multiple scatter:

(+) smooth, (Δ) rough.

FIG. 8. Specific incoherent intensity I_2 , $\beta = 10$, $v_m = 4/D$, $\lambda = 10\mu$,

$\epsilon_r = -6000 - i6000(AL)$, $D = 10\lambda$, case (c), transmitted, $\tau_0 = 1$, $\phi = 0$.

First order (—), rough particles. Multiple scatter: (+) smooth,

(Δ) rough.

FIG. 9. Specific incoherent intensity I_x , $\beta = 10$, $v_m = 4/D$, $\lambda = 10\mu$, $\epsilon_r = -6000-i6000(\text{AL})$, $D = 5\lambda$, case (c), transmitted, $\tau_0 = 1$, $\theta = 15.4^\circ$. First order (—), smooth and rough particles. Multiple scatter: (X) smooth, (X) rough.

FIG. 10. Specific incoherent intensity I_y , $\beta = 10$, $v_m = 4/D$, $\lambda = 10\mu$, $\epsilon_r = -6000-i6000(\text{AL})$, $D = 5\lambda$, case (c), transmitted, $\tau_0 = 1$, $\theta = 15.4^\circ$. First order (—), smooth and rough particles. Multiple scatter: (X) smooth, (X) rough.

FIG. 11. Specific incoherent intensity I_x , $\beta = 10$, $v_m = 4/D$, $\lambda = 10\mu$, $\epsilon_r = 1.5-i8(\text{PLASTIC})$, $D = 5\lambda$, case (d), reflected, $\tau_0 = 1$, $\theta = 164.6^\circ$. First order (—), smooth and rough particles. Multiple scatter: (X) (X) rough.

FIG. 12. Specific incoherent intensity I_y , $\beta = 10$, $v_m = 4/D$, $\lambda = 10\mu$, $\epsilon_r = 1.5-i8(\text{PLASTIC})$, $D = 5\lambda$, case (d), reflected, $\tau_0 = 1$, $\theta = 164.6^\circ$. First order (—), smooth and rough particles. Multiple scatter: (X) (X) rough.

FIG. 13. Specific incoherent intensity I_1 , $\beta = 10$, $v_m = 4/D$, $\lambda = 10\mu$, $\epsilon_r = 1.5-i8(\text{PLASTIC})$, $D = \text{average of sizes}$, case (e), transmitted, $\tau_0 = 1$, $\phi = 0$. First order (—), smooth and rough particles. Multiple scatter: (+) smooth, (Δ) rough.

FIG. 14. Specific incoherent intensity I_2 , $\beta = 10$, $v_m = 4/D$, $\lambda = 10\mu$, $\epsilon_r = 1.5-i8(\text{PLASTIC})$, $D = \text{average of sizes}$, case (e), transmitted, $\tau_0 = 1$, $\phi = 0$. First order (—), rough particles. Multiple scatter: (+) smooth, (Δ) rough.

FIG. 15. Specific incoherent intensity I_x and I_y , $\beta = 10$, $v_m = 4/D$, $D = 5\lambda$, $\lambda = 10\mu$, $\epsilon_r = -6000(1+i)(\text{AL})$, case (c), $\theta = 6.7^\circ$ and $\phi = 0^\circ$. (O) I_x smooth, (Δ) I_y smooth, (+) I_x rough, (X) I_y rough.

FIG. 16. Specific incoherent intensity I_x and I_y , $\beta = 10$, $v_m = 4/D$,

$D = 5\lambda$, $\lambda = 10\mu$, $\epsilon_r = 1.5-i8$ (PLASTIC), case (d), $\theta = 6.7^\circ$ and $\phi = 0$.

(0) I_x smooth, (Δ) I_y smooth, (+) I_x rough, (X) I_y rough.

FIG. 17. Degree of polarization m , $\beta = 1$, $v_m = 1.2/D$, $D = 5\lambda$, $\lambda = 10\mu$,

$\epsilon_r = -6000(1+i)$, case (a), $\tau_0 = 1$, $\theta = 6.7^\circ$ (+) smooth, (X) rough;

$\theta = 15.4^\circ$ (0) smooth, (Δ) rough.

FIG. 18. Degree of polarization m , $\beta = 1$, $v_m = 1.2/D$, $D = 5\lambda$, $\lambda = 10\mu$,

$\epsilon_r = -6000(1+i)$, case (a), $\tau_0 = 1$, $\theta = 24.2^\circ$ (+) smooth, (X) rough;

$\theta = 33.0^\circ$ (0) smooth, (Δ) rough.

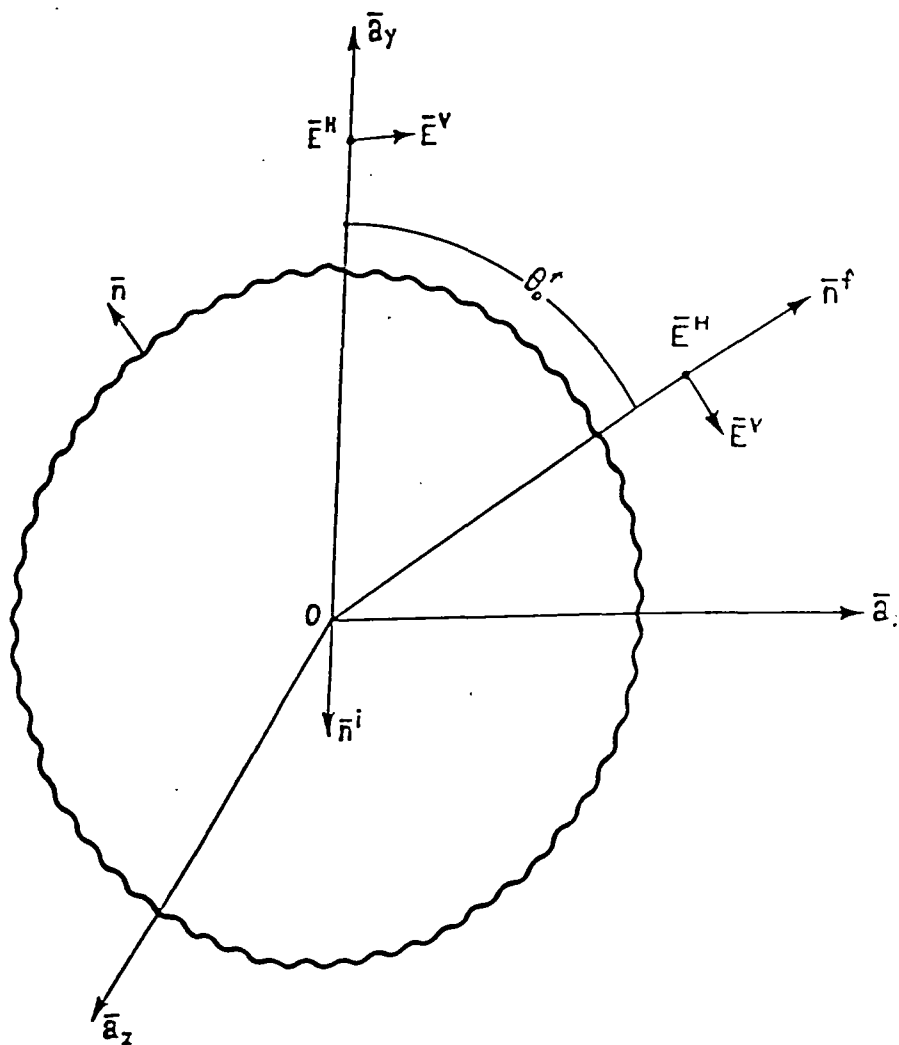


Figure 1.

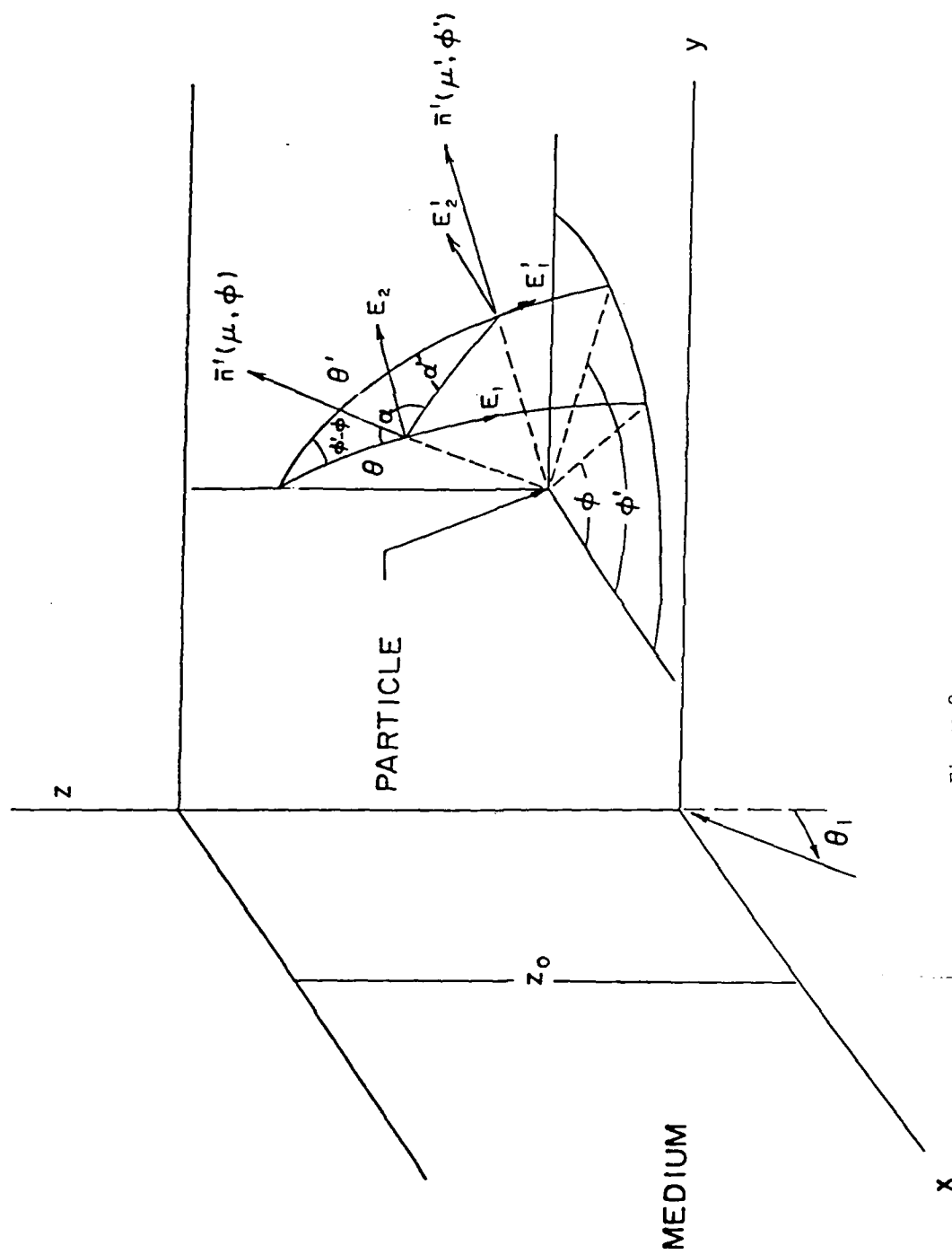


Figure 2.

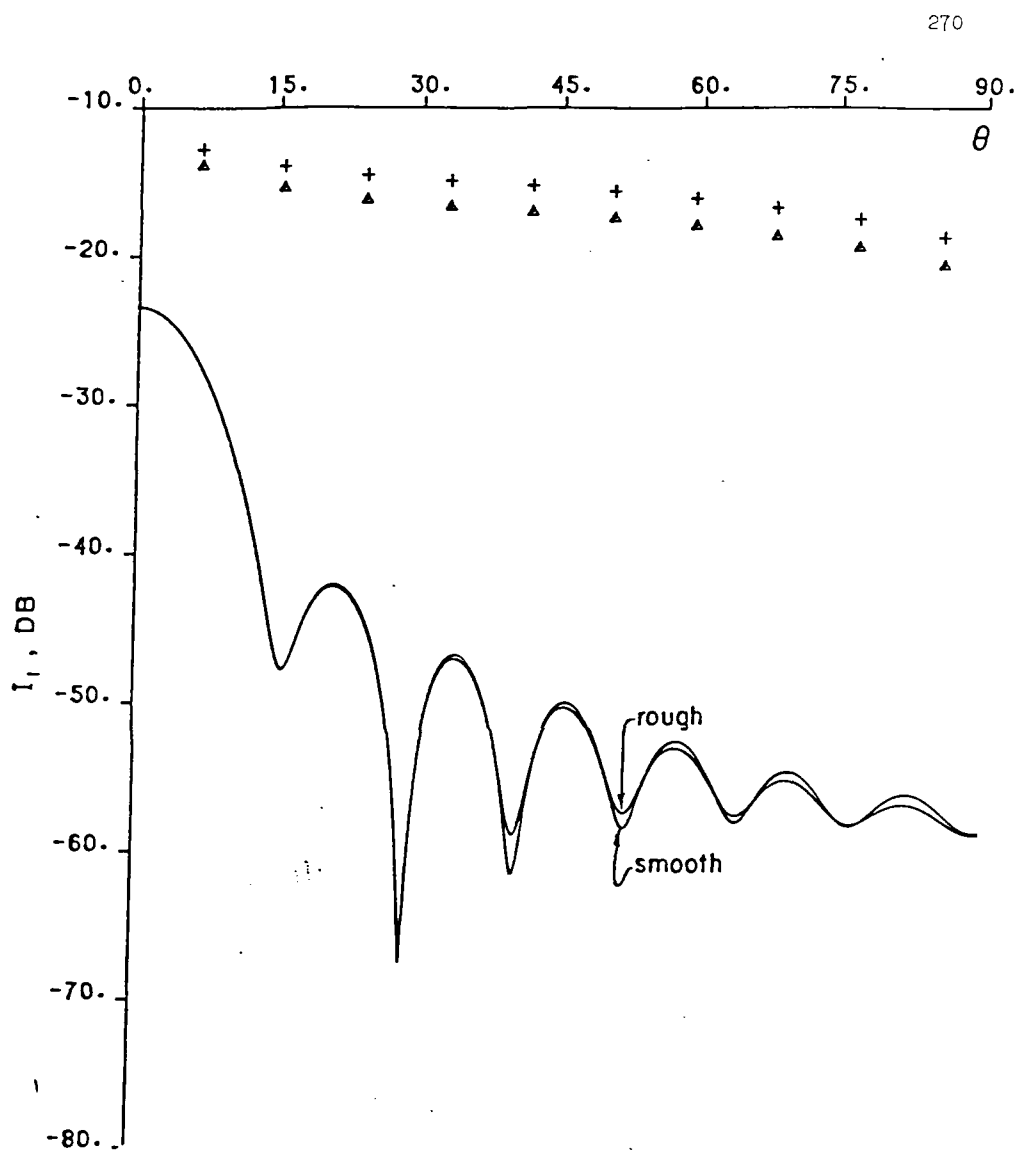


Figure 3.

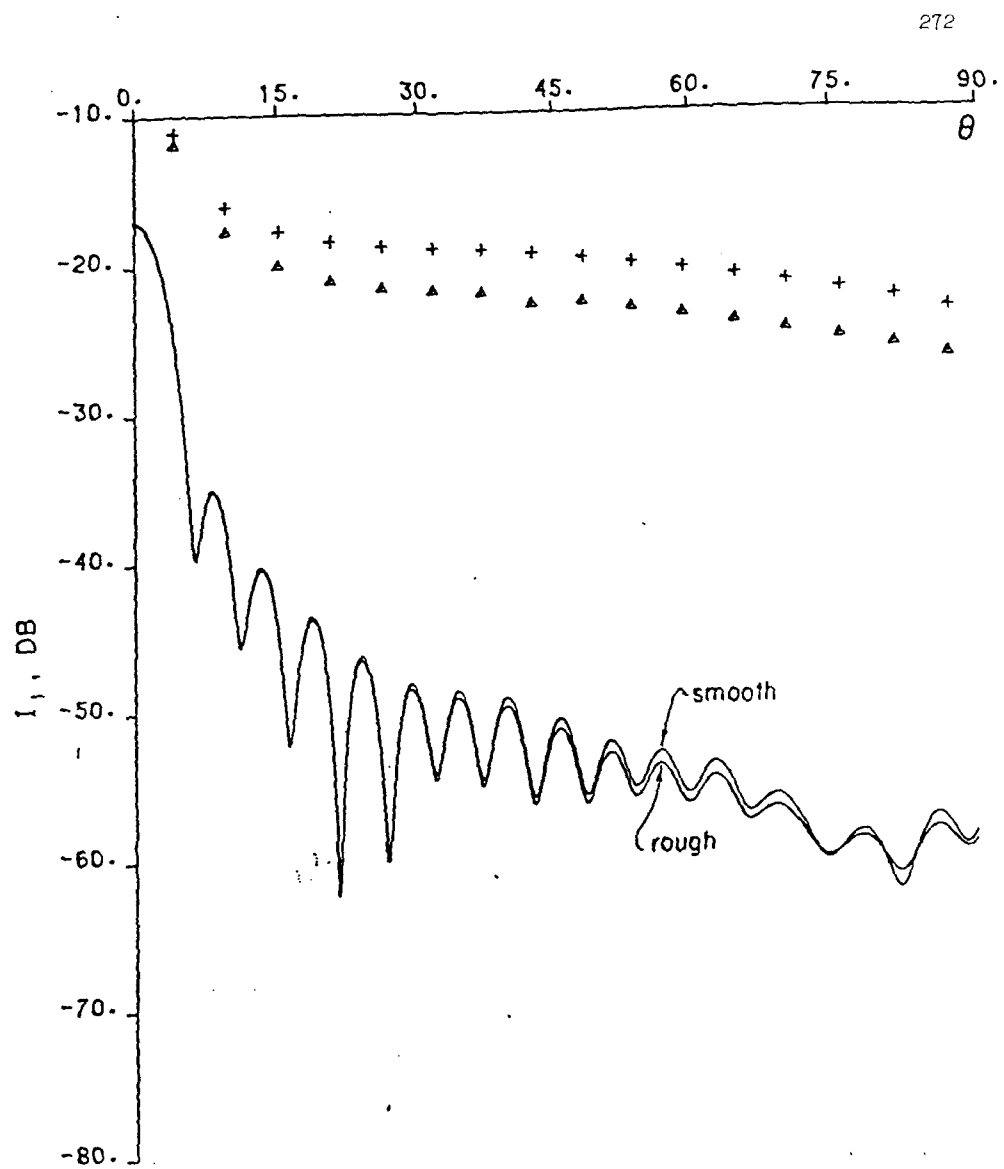


Figure 5.

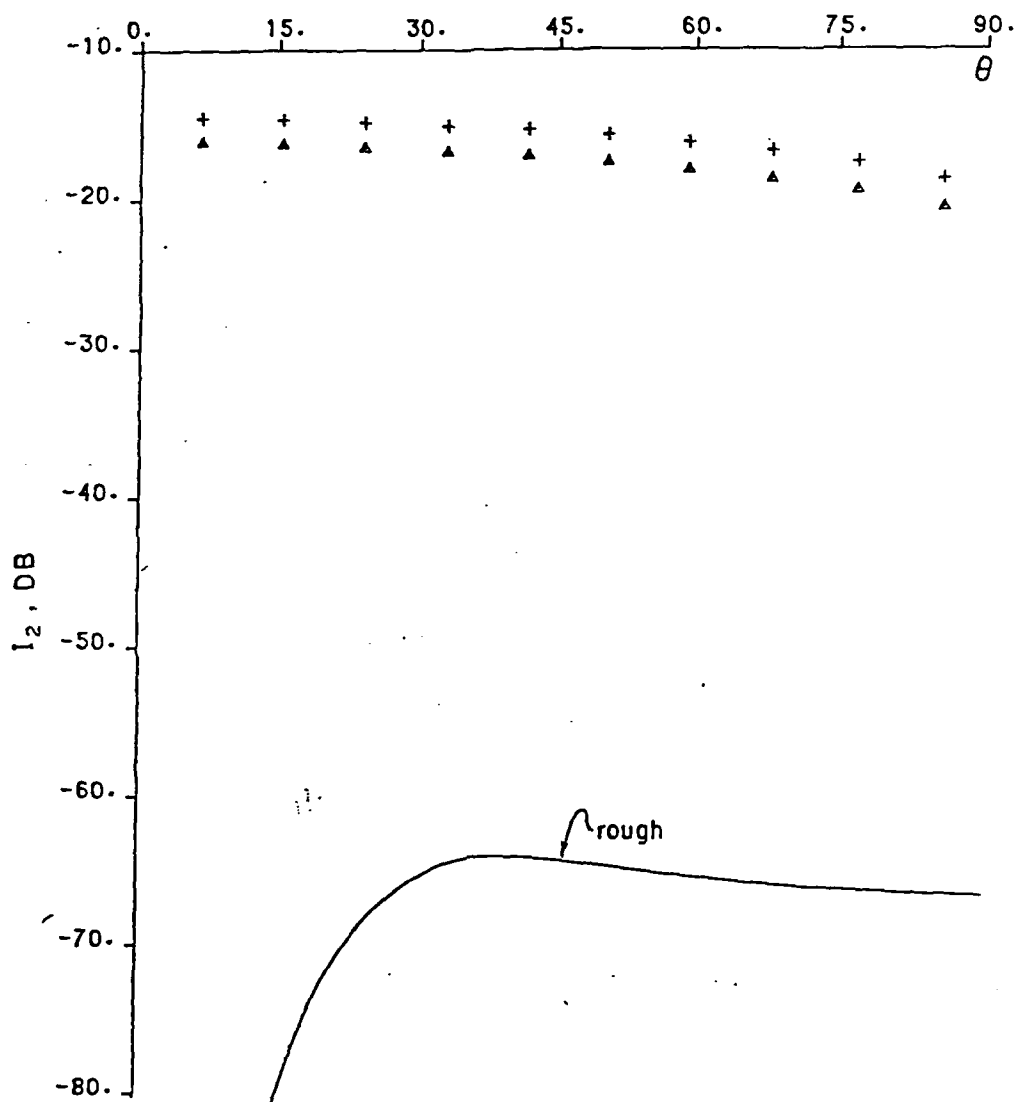


Figure 4.

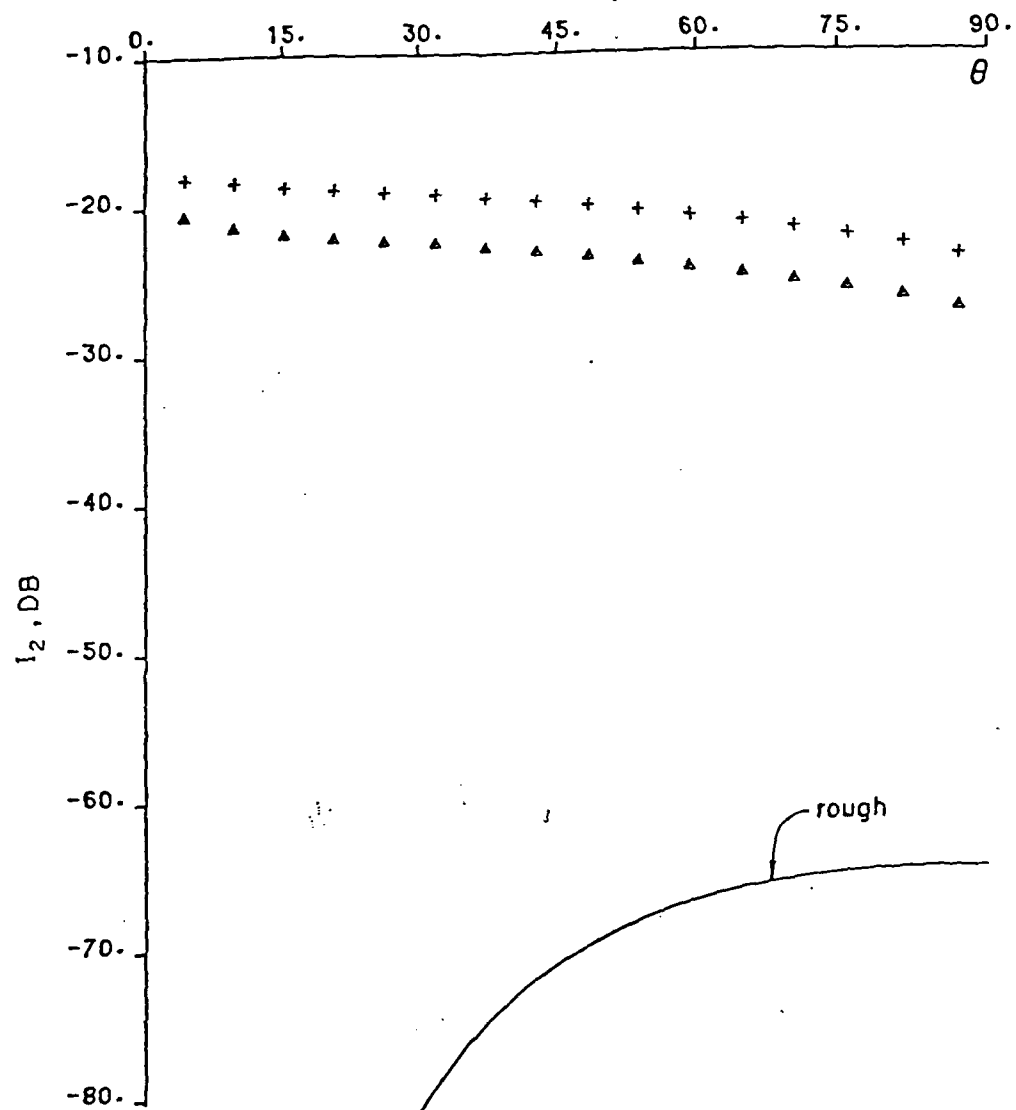


Figure 6.

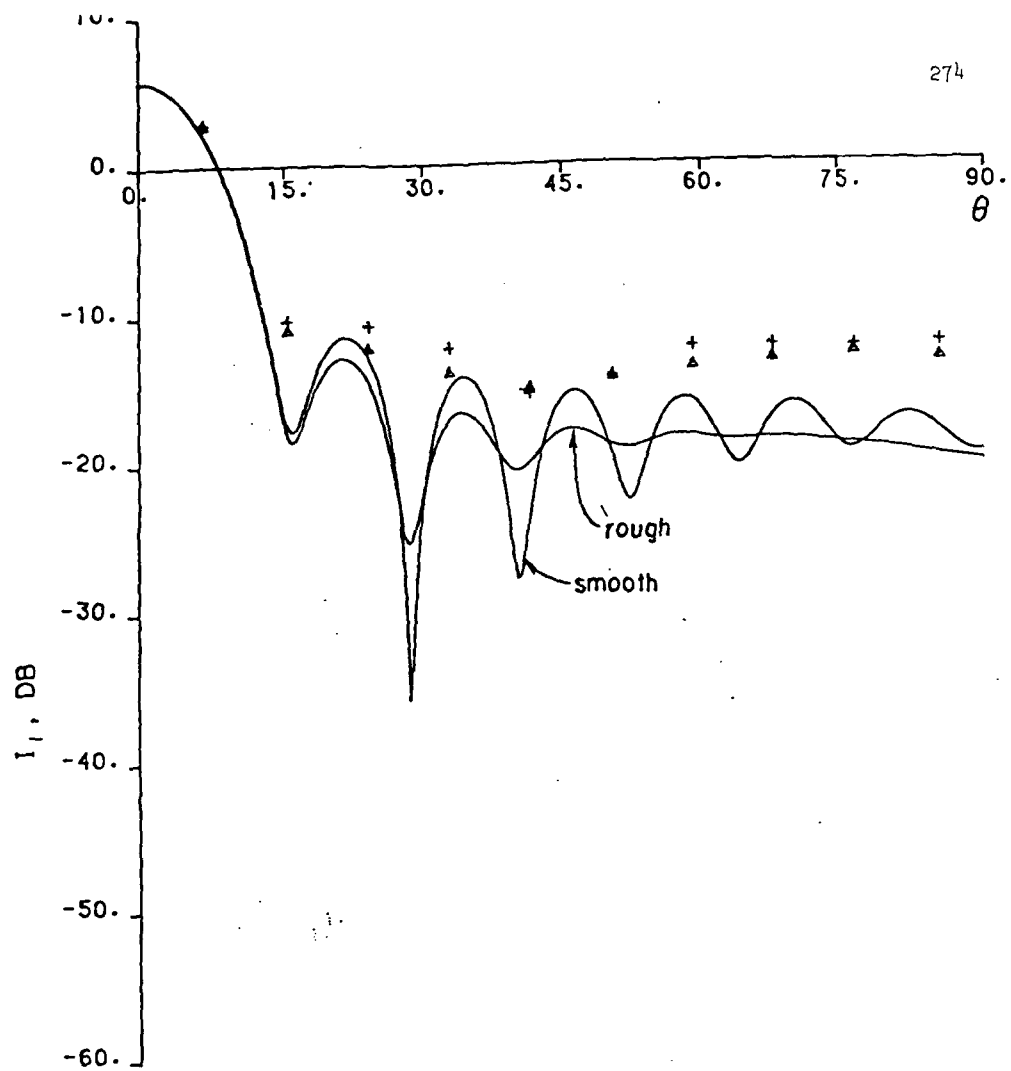


Figure 7.

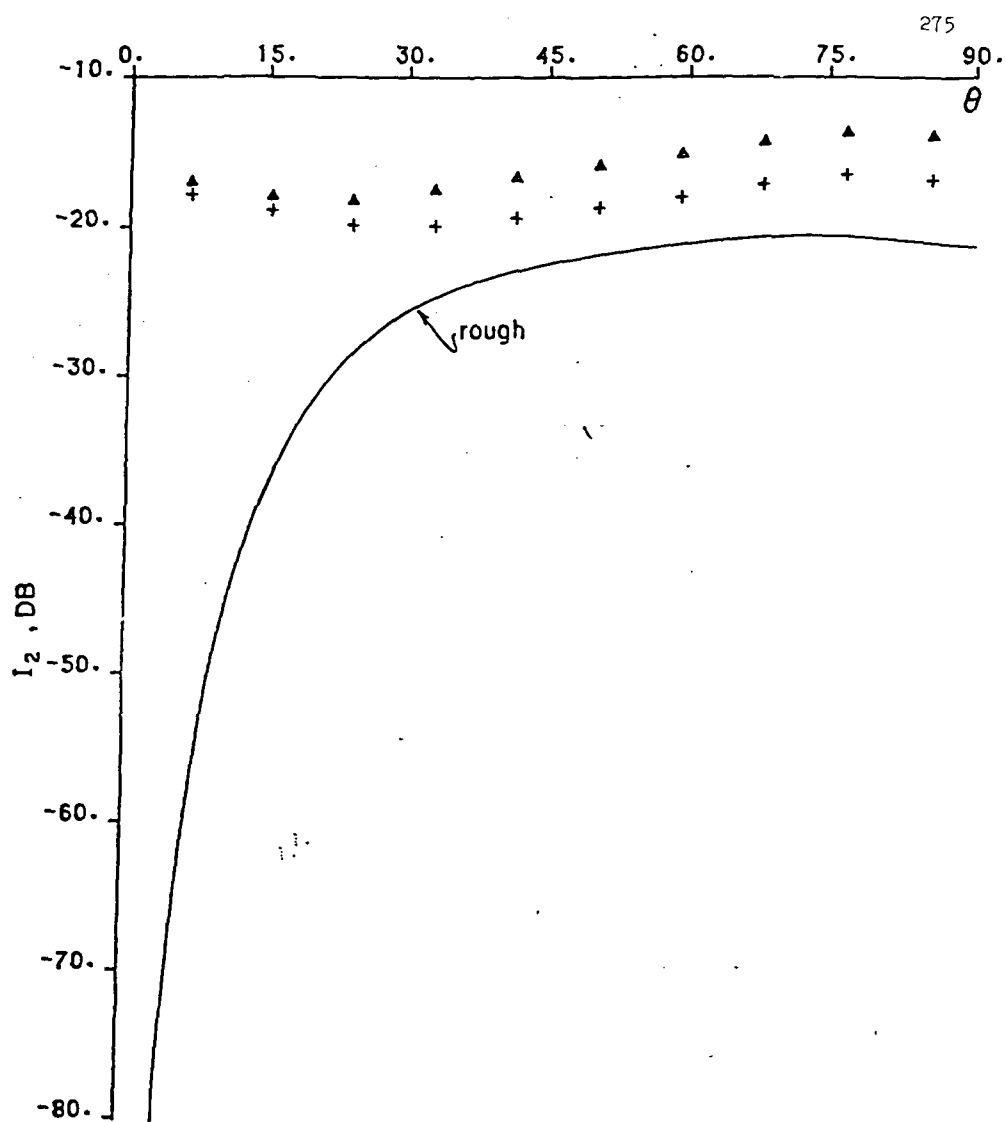


Figure 8.

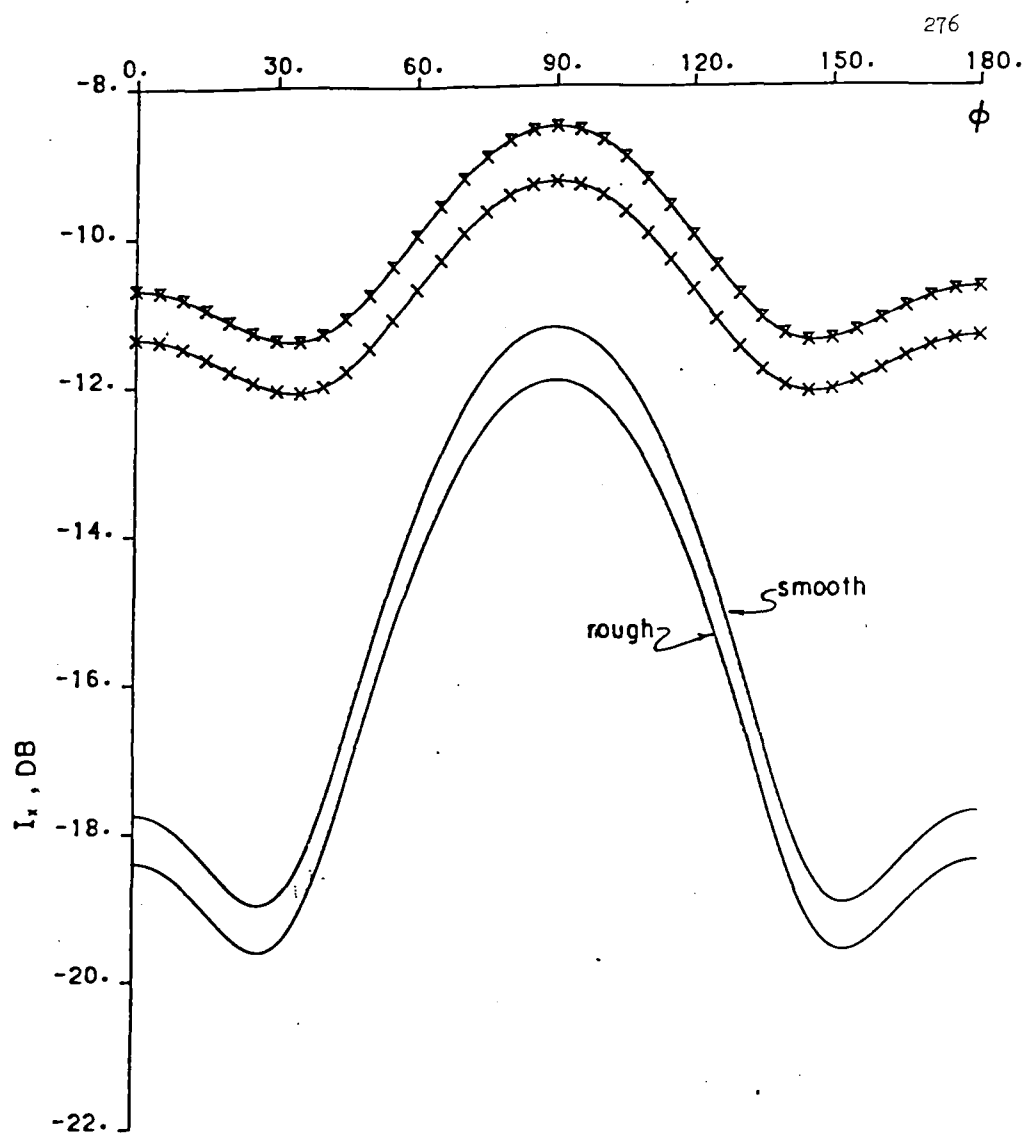


Figure 9.

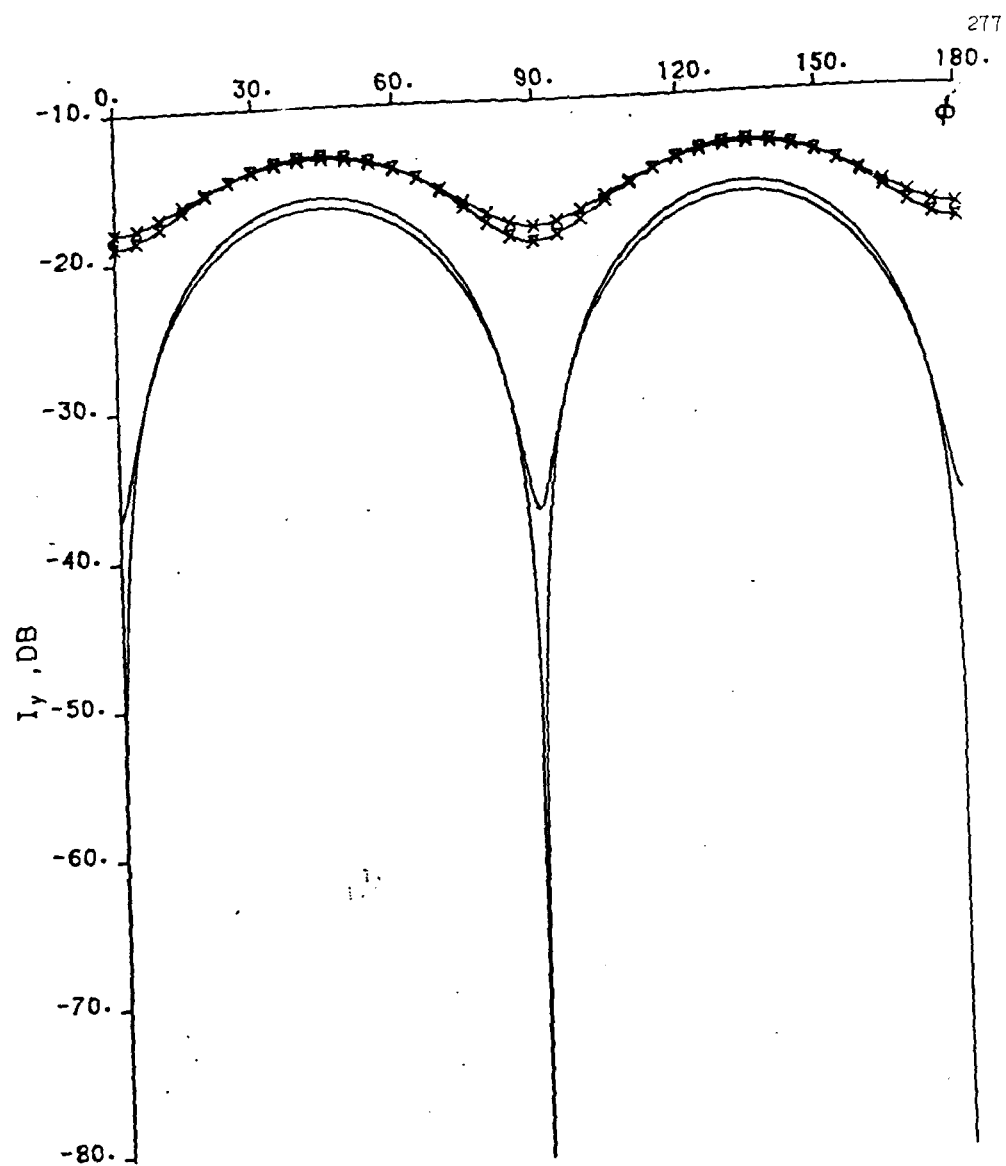


Figure 10.

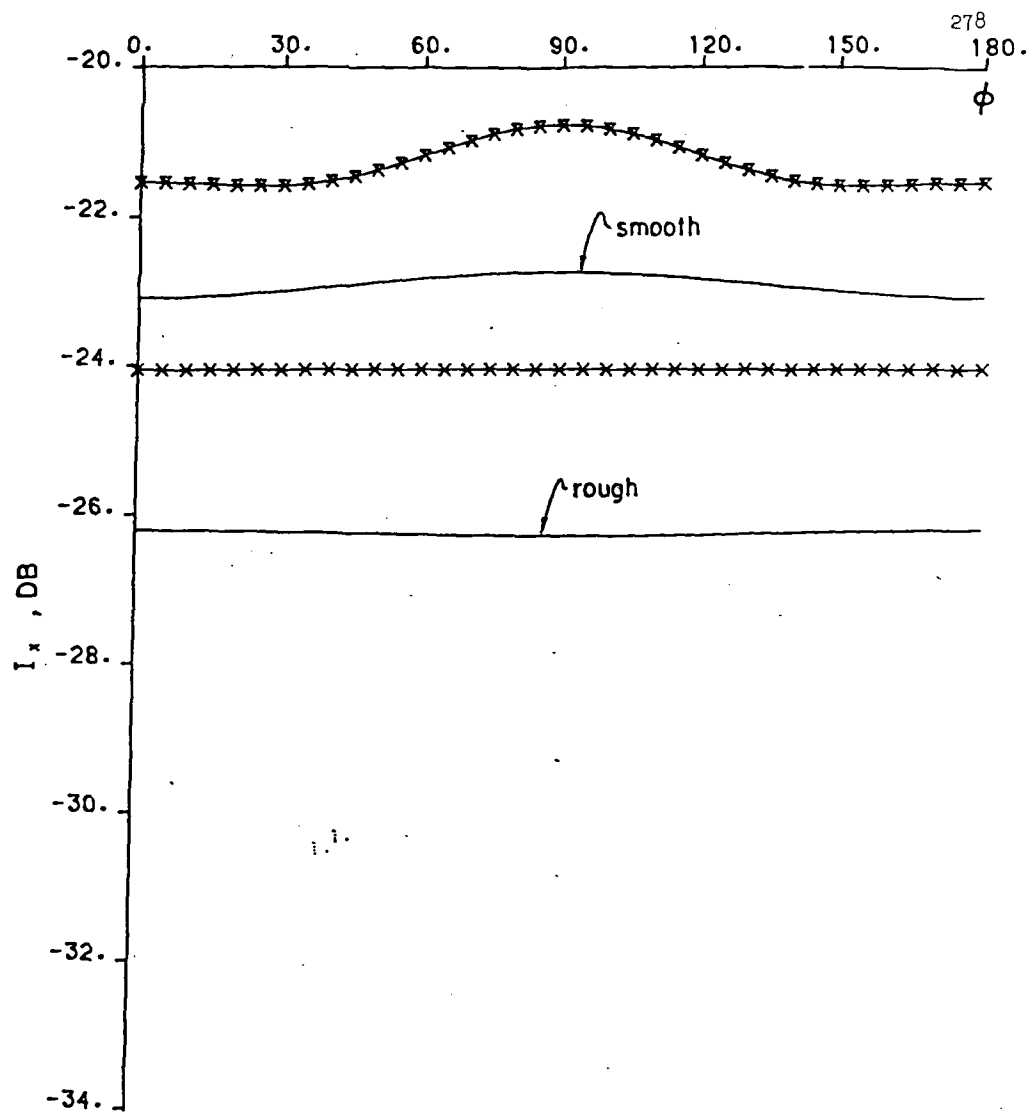


Figure 11.

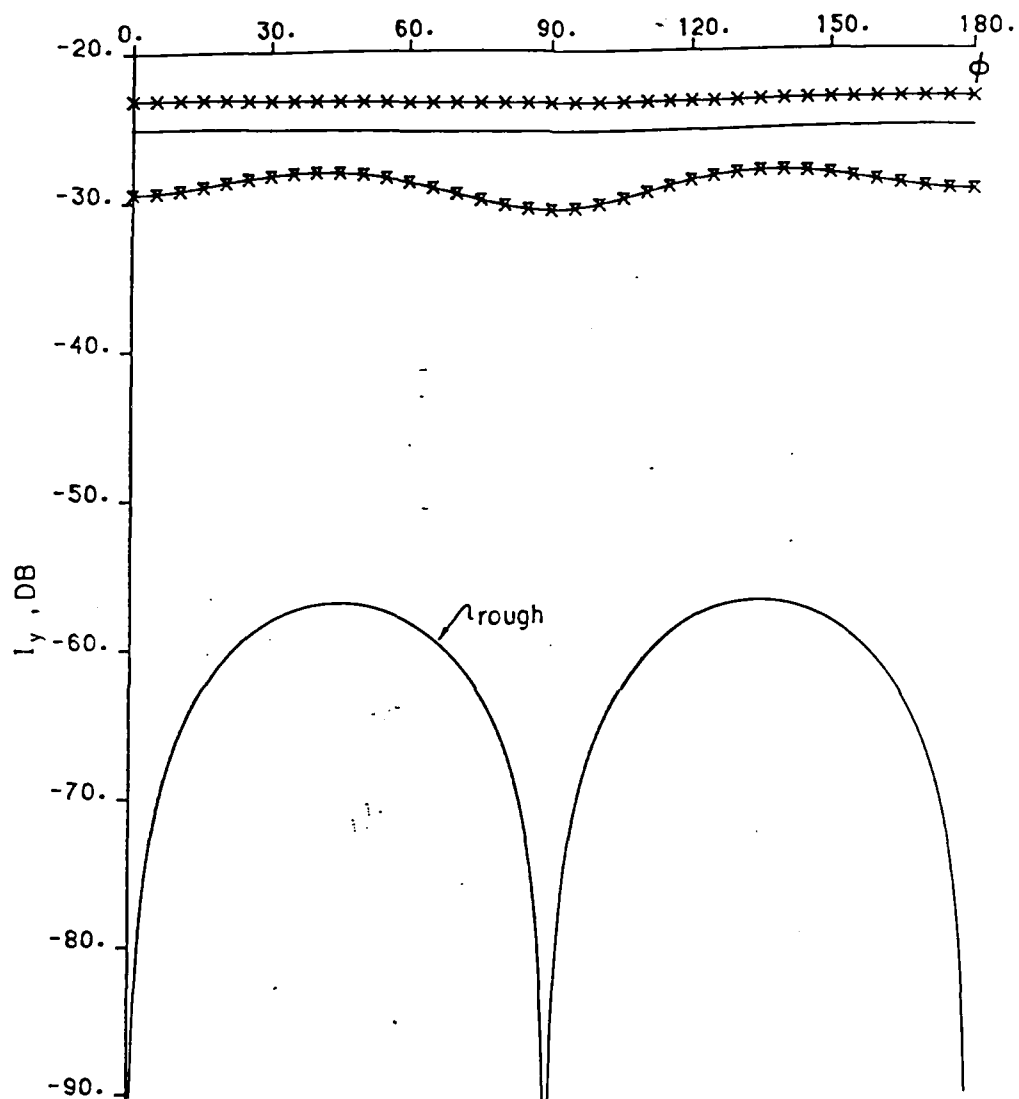


Figure 12.

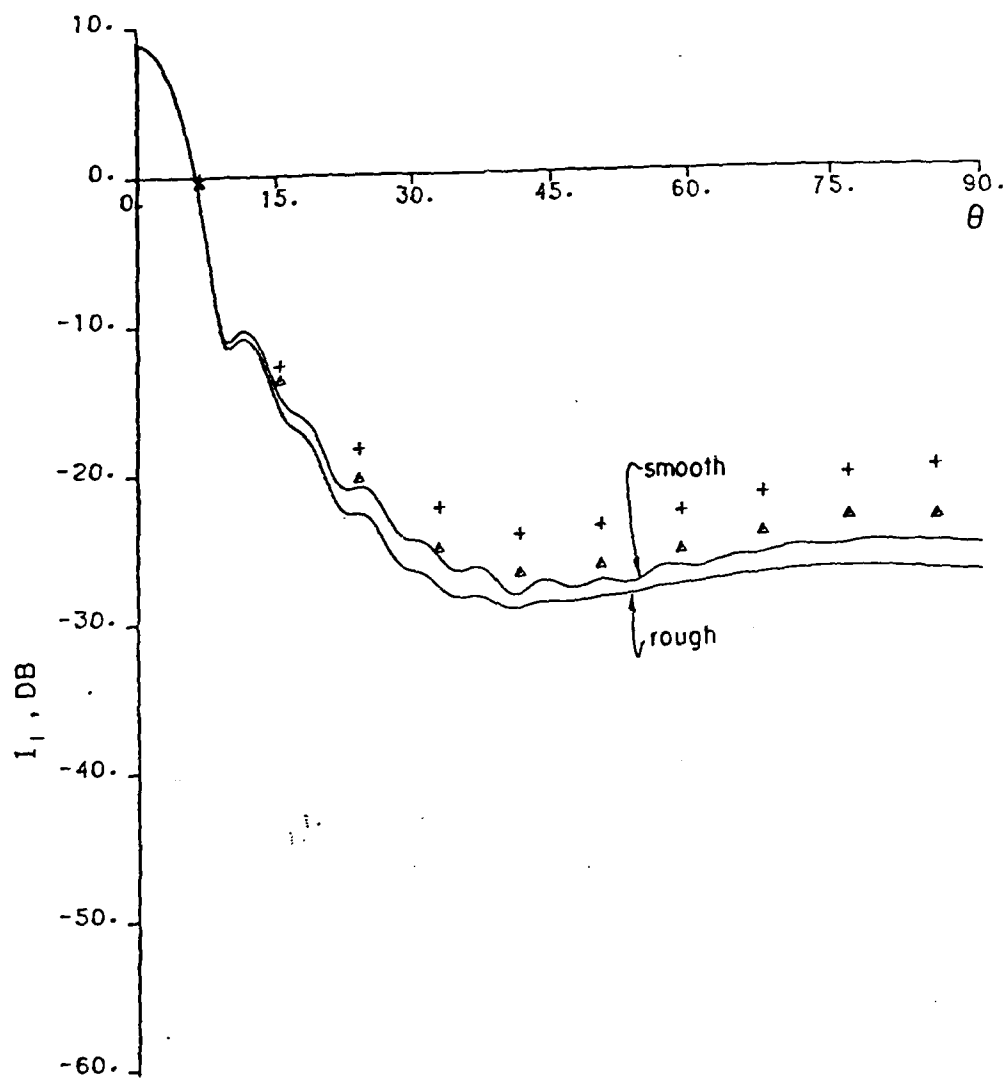


Figure 13.

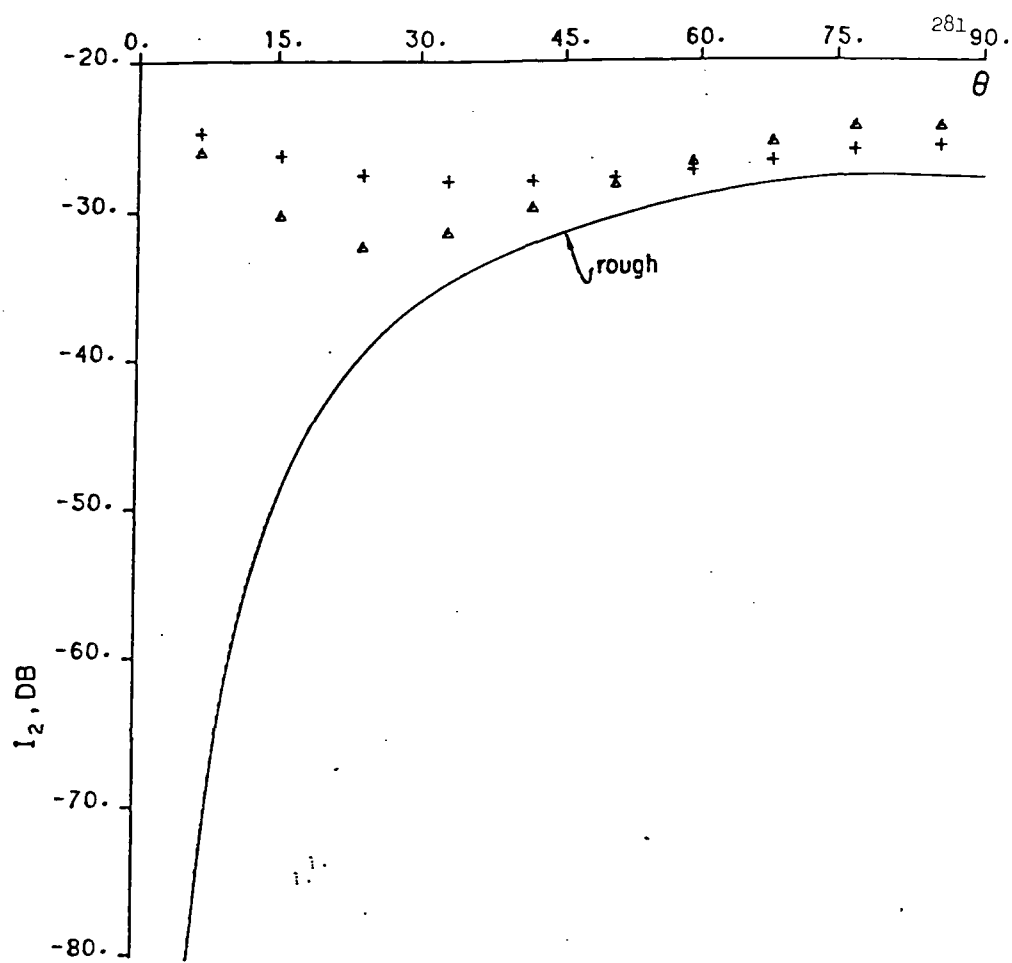


Figure 14.

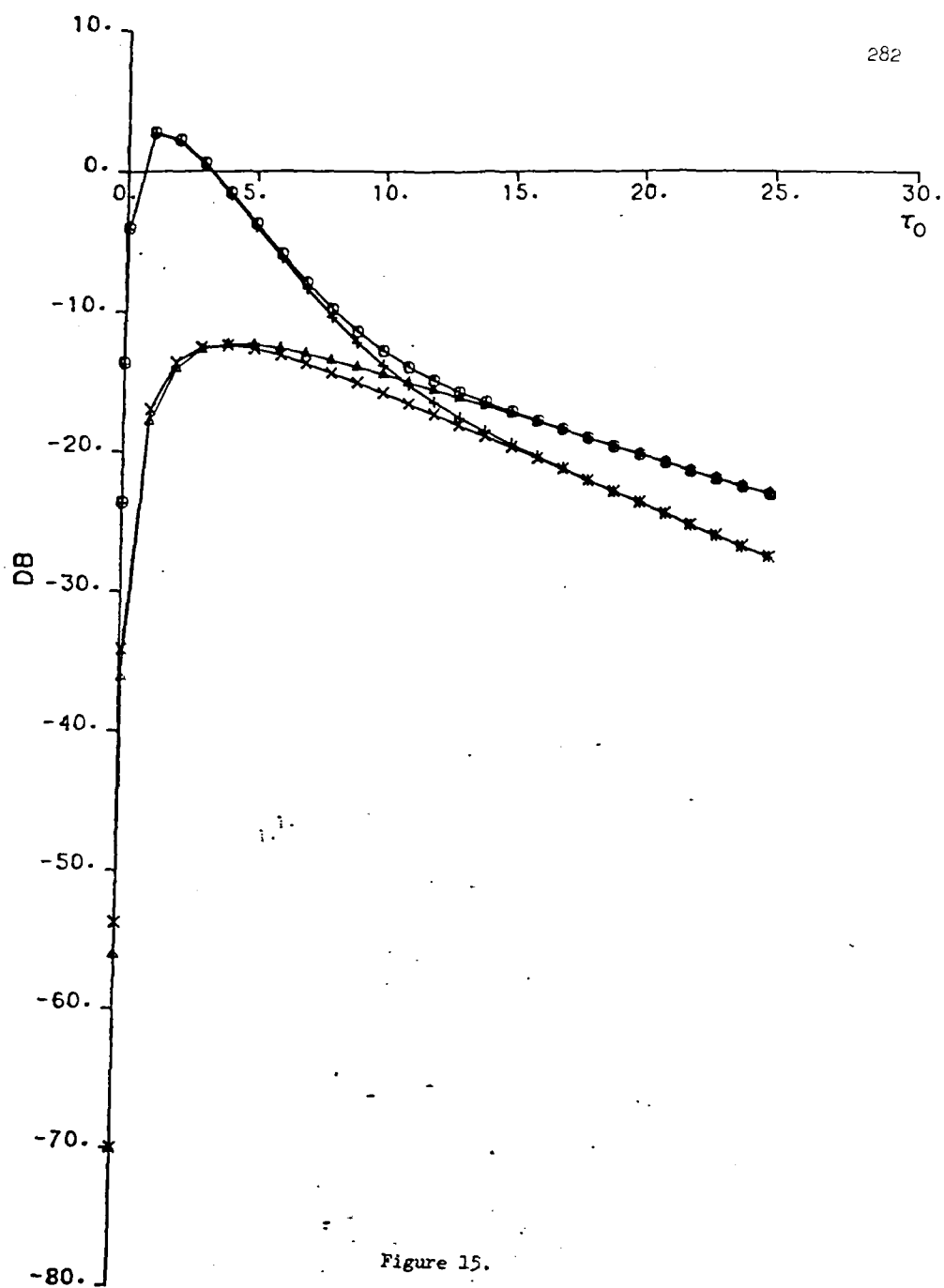


Figure 15.

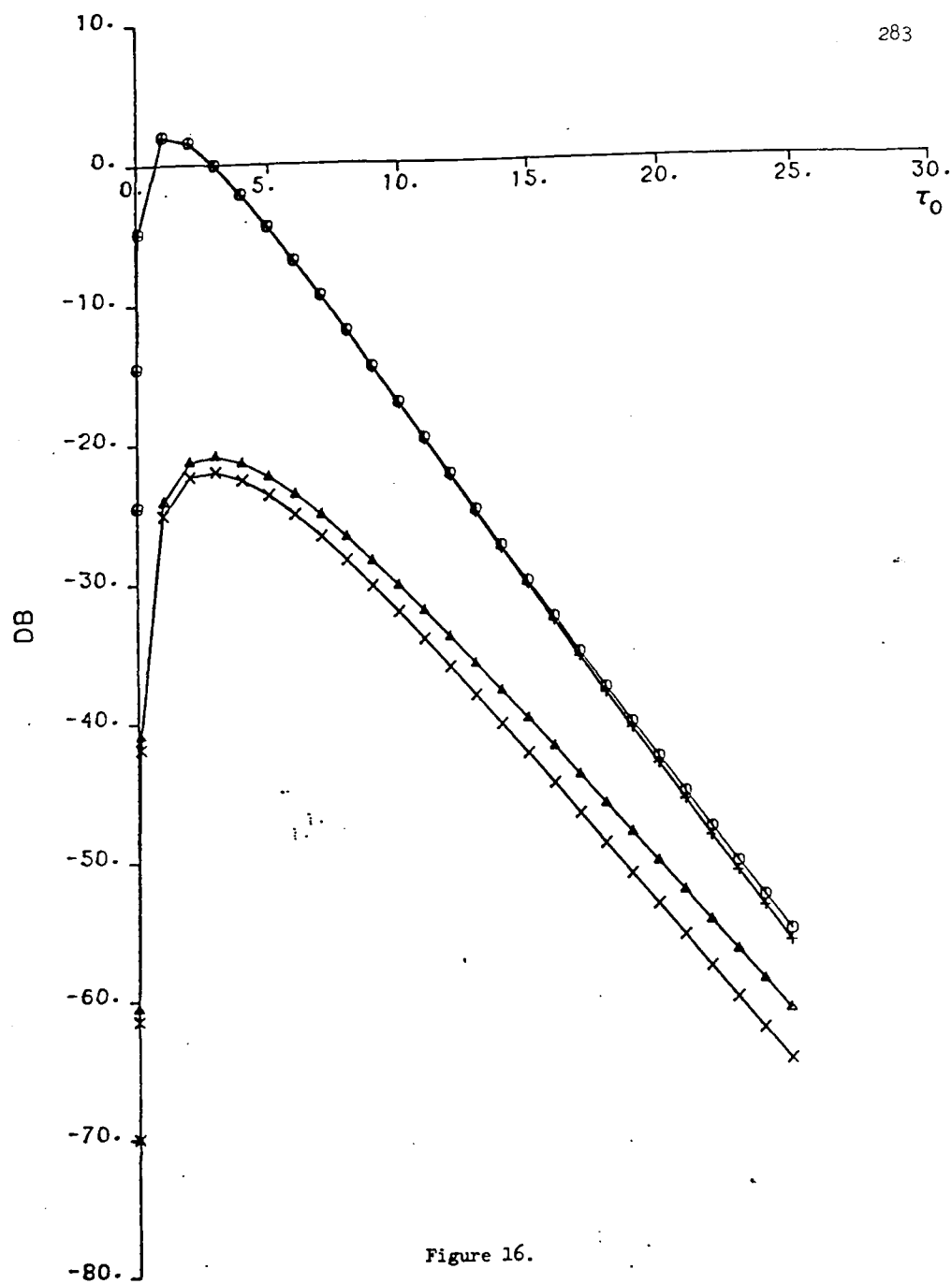


Figure 16.

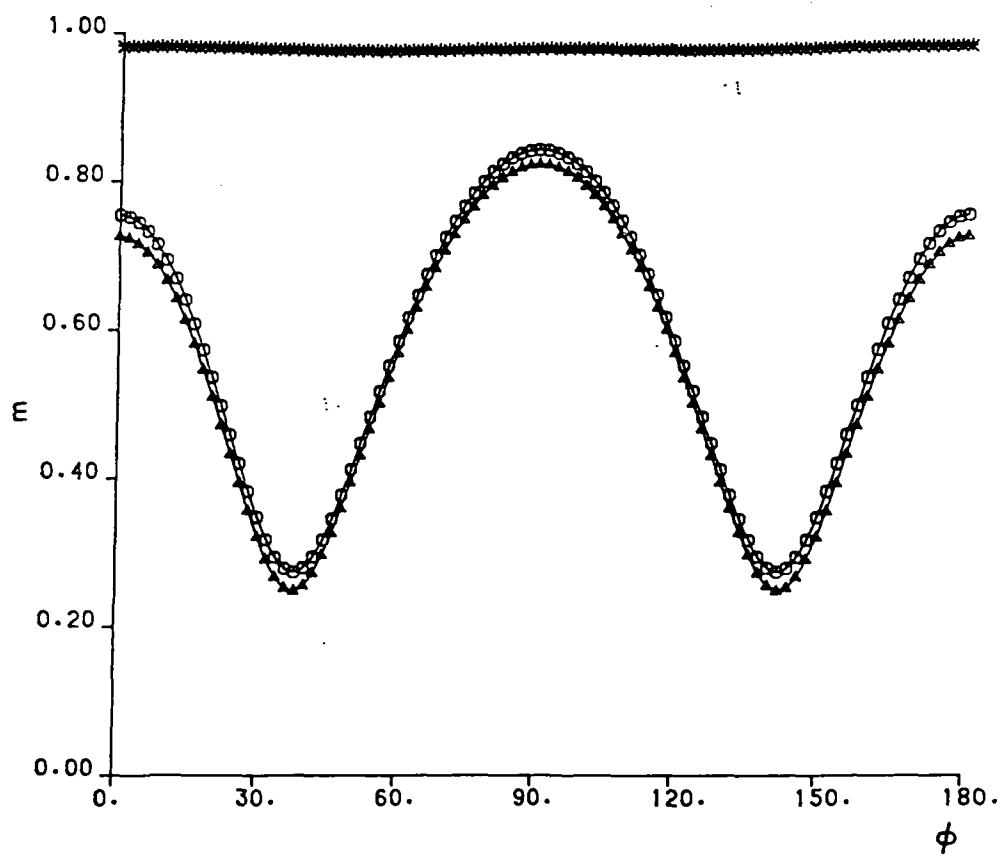


Figure 17.

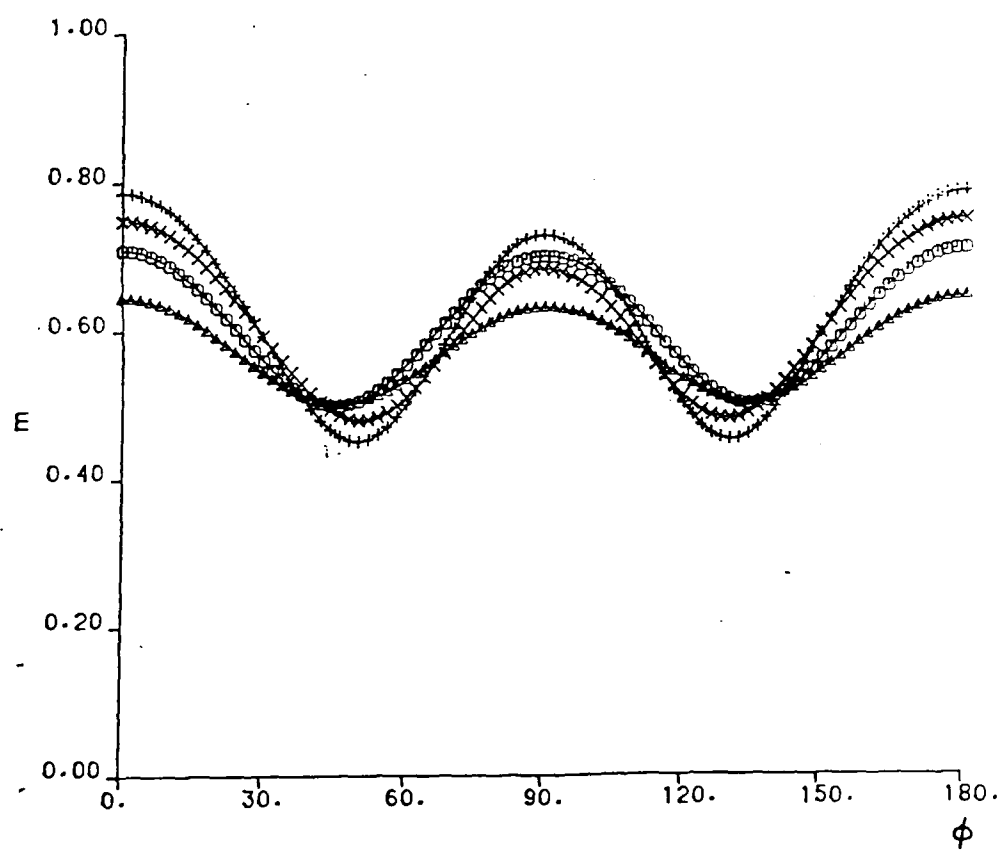


Figure 18.

INTERPRETATION OF BACKSCATTER CROSS SECTIONS FOR NORMAL INCIDENCE
USING UNIFIED AND TWO-SCALE FULL WAVE ANALYSES OF ROUGH SURFACES

E. Bahar

Electrical Engineering Department
University of Nebraska-Lincoln 68588-0511

D. E. Barrick

Ocean Surface Research, Boulder, Colorado 80303

M. A. Fitzwater

Electrical Engineering Department
University of Nebraska-Lincoln 68588-0511

ABSTRACT

The like and cross polarized backscattered scattering cross sections are evaluated for random rough surfaces using the full wave analysis. The resulting cross sections are also expressed in terms of a weighted sum of two cross sections in keeping with previous two-scale interpretations of scatter. The first is associated with the cross section for the large scale filtered surface and the second is the diffuse scattering term associated with the small scale surface component. Special attention is given to waves at normal incidence. Both perfectly and finitely conducting boundaries are considered. The random rough interface is characterized by its surface height spectral density function and detailed consideration is given to the choice of the wavenumber where spectral splitting (between the small and large scale surfaces) is assumed to occur.

Brown's and Tyler's criteria for decomposing the rough surface cannot be satisfied simultaneously. Neither reconciles the observed discrepancy at normal incidence for sea return and the resulting values of the slopes of the large scale surface (producing the specular echo) are considerably different.

The full-wave solution for rough-surface scattering reduces to an integral similar in form to the physical optics or perturbation solutions (Bahar 1981). In its derivation from the exact telegraphists' equations, multiple scattering is neglected. The full wave solution has been shown to reduce to the specular-point result in the high frequency limit, and to the perturbational result (with the correct polarization dependence) in the low frequency limit. Since it is valid across the spectrum for all roughness scales, it is not necessary to adopt the two-scale model to analyze rough surface scattering problems. In recent work however, (Bahar and Barrick 1983), the full wave solution has been artificially decomposed into two components to elucidate the mechanisms at play in the two-scale models discussed above. For the like polarized case the sum of the two terms of the full wave solution is approximately constant as the break point between the large and small roughness scales varies as β ranges from 1 to 2. For normal incidence the values of like polarized cross sections based on the unified and two-scale solutions are the same for $\beta = 0.25$. For this case the specular point contribution from the large scale surface is the only significant contribution. Thus through a judicious choice of the break point (between the large and small scale surfaces) corresponding to $\beta = 0.25$ a single-term large-scale specular-point model can be used at normal incidence for microwave like polarized backscatter cross sections of the sea.

1. Introduction

A specific and important application of rough-surface scattering at normal incidence concerns short-pulse satellite microwave altimeter return from the sea surface. In addition to its use to measure ocean waveheight at nadir as on Seasat (Barrick and Lipa 1985), the altimeter has also been employed to infer wind speed from the backscattered signal intensity, since the roughness statistics depend strongly on surface wind. Up to now, attempts to establish a quantitative connection between altimeter nadir backscattered cross section (per projected area) and wind speed have employed a physical-optics derived specular-point model that (i) relates the backscatter cross section to rms surface slopes, and subsequently (ii) relates surface slopes to wind speed in some manner (Barrick 1974). Unfortunately, the returns predicted thereby are several dB greater than the measured (Brown 1979), leading to use of empirical rather than theory-based models to establish the connection (Chelton and McCabe 1985). This discrepancy can only be due to the inadequacy of the simple, specular-point model, as it has been used, to describe the backscattered return even from a gently sloping sea at normal incidence.

Composite rough-surface models (Barrick and Peake, 1968; Wright, 1968; Brown, 1978) break the surface roughness into two scales: large and small. Brown formulated the first detailed analysis of this model, describing the small-scale surface component as riding on the large-scale surface, while allowing the large-scale slope statistics to modulate the smaller component's return. He proposed one method for spectrally dividing the surface into large-scale and small-scale regions, based on the criterion that the mean square height $\langle h_s^2 \rangle$ of the small-scale component be small enough ($\beta = 4k_0^2 \langle h_s^2 \rangle < 0.1$ where k_0 is the free space wavenumber) to guarantee the satisfaction of the perturbation approximation. Tyler (1976) suggested that the rough surface height spectral components (that contribute to the large scale slopes) should be determined by the requirement that the mean of the large scale surface radius of curvature be larger than a wavelength. This is also a physically reasonable proposition since it is inherent in the tangent-plane approximation of physical optics. However, in general

The illustrative examples of the individual terms contributing to the solution are given as a function of the parameter β for like and cross-polarized returns. It should also be noted that the previously mentioned approximate methods produce a zero cross-polarized backscatter component at normal incidence, although measurements clearly indicate a non-vanishing contribution which is close to the value predicted by full-wave theory (Bahar and Fitzwater, 1984).

2. Formulation of the Problem

On adopting the two-scale model of the rough surface, the full wave solutions for the normalized like and cross polarized scattering cross sections (per unit projected area) reduce to a weighted sum of two cross sections (Bahar and Barrick 1983).

$$\langle \sigma^{PQ} \rangle = \langle \sigma^{PQ} \rangle_L + \langle \sigma^{PQ} \rangle_S \quad P, Q = V \text{ or } H \quad (2.1)$$

in which the first and second superscripts P and Q denote the polarizations of the scattered and incident waves (V vertical, H horizontal). The first term in (2.1) is the modified cross section associated with the large scale filtered surface h_L

$$\langle \sigma^{PQ} \rangle_L = \left| \chi^S(\vec{v} \cdot \vec{n}_S) \right|^2 \langle \sigma_{\infty}^{PQ} \rangle \quad (2.2)$$

in which $\langle \sigma_{\infty}^{PQ} \rangle$ is the physical optics expression for the scattering cross section of the large scale surface and $\chi^S(\vec{v} \cdot \vec{n}_S)$ is the small scale surface characteristic function. For rough surfaces with Gaussian height distributions

$$\left| \chi^S(\vec{v} \cdot \vec{n}) \right|^2 = \left| \langle \exp(i\vec{v} \cdot \vec{n}_S h_S) \rangle \right|^2 = \exp(-(\vec{v} \cdot \vec{n}_S)^2 \langle h_S^2 \rangle) \quad (2.3)$$

in which $\langle h_S^2 \rangle$ is the mean square of the small scale surface height h_S ,

$$\vec{v} = k_0 (\vec{n}^f - \vec{n}^i) \quad , \quad v = |\vec{v}| \quad (2.4)$$

where k_0 is the free space wavenumber, \vec{n}^f and \vec{n}^i are unit vectors in the directions of the scattered and incident wave normals. The unit vector normal to the actual rough surface is \vec{n} and \vec{n}_S is its value at the specular points

$$\bar{n} + \bar{n}_s = \bar{v}/v \quad (2.5)$$

The coefficient $|\chi^s|^2$ in (2.2) accounts for the degradation of the physical optics scattering cross section due to the small scale surface h_s that rides on the large scale surface. The second term in (2.1) is the diffuse scattering cross section due to the small scale surface h_s . It can be expressed as an infinite sum as follows

$$\langle \sigma^{PQ} \rangle_s = \sum_{m=1}^{\infty} \langle \sigma^{PQ} \rangle_{sm} \quad (2.6)$$

where

$$\langle \sigma^{PQ} \rangle_{sm} = 4\pi k_0^2 \left\langle \frac{|D^{PQ}|^2 P_2(\bar{n}^f, \bar{n}^i | \bar{n})}{\bar{n} \cdot \bar{a}_y} \left(\frac{v_y}{2} \right)^{2m} \frac{W_m(v_{\bar{x}}, v_{\bar{z}})}{m!} \right\rangle |\chi^s|^2 \quad (2.7)$$

The symbol $\langle \cdot \rangle$ denotes the statistical average over the slopes $\bar{n}(h_x, h_z)$ of the large scale rough surface ($h_x = \partial h_0 / \partial x$, $h_z = \partial h_0 / \partial z$). In (2.7) $v_{\bar{x}}, v_{\bar{y}}$ and $v_{\bar{z}}$ are components of the vector \bar{v} (2.4) in the local coordinate system

$$\bar{v} = v_{\bar{x}} \bar{n}_1 + v_{\bar{y}} \bar{n}_2 + v_{\bar{z}} \bar{n}_3 \quad (2.8)$$

in which $\bar{n}_2 = \bar{n}$ is the unit vector normal to the large scale rough surface, \bar{n}_1 and \bar{n}_3 are unit vectors tangent to the large scale rough surface. The unit vector \bar{a}_y is normal to the mean surface (the reference plane). Note that $\langle h_s \rangle$ is assumed to be zero and that h_s is measured normal to the large scale surface. The scattering coefficients D^{PQ} depend upon the incident and scattered wave polarizations and wave normals \bar{n}^i and \bar{n}^f as well as the electromagnetic parameters of the medium (Bahar 1981). The two dimensional function W_m is the Fourier transform of the m th power of the small scale surface height autocorrelation function $\langle h_s h'_s \rangle$

$$\begin{aligned}
\frac{W_m(v_{\bar{x}}, v_{\bar{z}})}{2^{2m}} &= \frac{1}{(2\pi)^2} \int \langle h_s h'_s \rangle^m \exp(i v_{\bar{x}} x_{\bar{d}} + i v_{\bar{z}} z_{\bar{d}}) dx_{\bar{d}} dz_{\bar{d}} \\
&= \frac{1}{2^{2m}} \int W_{m-1}(v_{\bar{x}}', v_{\bar{z}}') W_1(v_{\bar{x}} - v_{\bar{x}}', v_{\bar{z}} - v_{\bar{z}}') dv_{\bar{x}}' dv_{\bar{z}}' \\
&= \frac{1}{2^{2m}} W_{m-1}(v_{\bar{x}}, v_{\bar{z}}) \otimes W_1(v_{\bar{x}}, v_{\bar{z}}) \quad (2.9)
\end{aligned}$$

In (2.9) the symbol \otimes denotes the two dimensional convolution of W_{m-1} with W_1 and $(x_{\bar{d}}^2 + z_{\bar{d}}^2)^{1/2} = r_{\bar{d}}$ is the distance between two points $\bar{r} - \bar{r}'$ measured along the large scale surface. In this work the rough surface is assumed to be homogeneous and isotropic, thus the surface height spectral density function (the Fourier transform of the rough surface height autocorrelation function $h_s h'_s$) is only a function of

$$v_T = (v_{\bar{x}}^2 + v_{\bar{z}}^2)^{1/2} = (v^2 - v_y^2)^{1/2} \quad (2.10)$$

and the autocorrelation function depends only upon the distance r_d measured along the large scale surface. It is also assumed that the width of the illuminated patch of the rough surface is much large than the rough surface correlation length. The shadow function $P_2(\bar{n}^f, \bar{n}^i | \bar{n})$ is the probability that a point on the rough surface is both illuminated and visible given the slopes at the point (Smith 1967, Sancer 1969).

To facilitate the adoption of the two-scale model of the composite rough surface it is assumed that the filtered large scale surface h_l is associated with that part of the surface height spectral density function for which $v_T \leq v_d$ and the small scale surface h_s is associated with the remaining part of the surface height spectral density function ($v_T > v_d$) (Brown 1978).

In a recent investigation of scattering by composite perfectly conducting rough surfaces based upon a perturbed-physical optics approach, Brown obtains the following solution

$$\langle \sigma^{PQ} \rangle = \langle \sigma_{\infty}^{PQ} \rangle + \langle \sigma_p^{PQ} \rangle \quad (2.11)$$

in which $\langle \sigma_{\infty}^{PQ} \rangle$ is the physical optics scattering cross section for the filtered large scale surface and

$$\langle \sigma_p^{PQ} \rangle = 4\pi k_o^2 \left\langle \left| \frac{D^{PQ} \mathbf{v}}{2} \right|_{\bar{\mathbf{n}} + \bar{\mathbf{a}}_y}^2 P_2(\bar{\mathbf{n}}^f, \bar{\mathbf{n}}^i | \bar{\mathbf{n}}) W_1(v_x, v_z) \right\rangle \quad (2.12)$$

In (2.12) v_x, v_y and v_z are components of the vector $\bar{\mathbf{v}}$ (2.4) in the fixed reference coordinate system

$$\bar{\mathbf{v}} = v_x \bar{\mathbf{a}}_x + v_y \bar{\mathbf{a}}_y + v_z \bar{\mathbf{a}}_z \quad (2.13)$$

in which $\bar{\mathbf{a}}_x$ and $\bar{\mathbf{a}}_z$ are unit vectors tangent to the mean plane. The results obtained by Brown (1978) on using (2.11) to compute the scattering cross sections is shown to depend very strongly upon the choice of the wavenumber v_d where spectral splitting is assumed to occur. Since Brown uses Burrows' (1967) perturbation approach in his work he concludes that the appropriate value of v_d must be based on the choice of the roughness parameter for the small scale surface

$$\beta = 4k_o^2 \langle h_s^2 \rangle = 0.1 \quad (2.14)$$

However, in the work by Tyler (1976) the specification of v_d is assumed to be based on the characteristics of the large scale surface (radii of curvature) and for backscatter near normal incidence Tyler neglects the second term in (2.11). In general however, the conditions specified by Brown and Tyler for the choice v_d cannot be satisfied simultaneously. In an effort to resolve these discrepancies, computations of the scattering cross sections based on the two-scale full wave approach (2.1) were performed (Bahar et al. 1983). Note that for surface with small slopes ($\bar{\mathbf{n}} \approx \bar{\mathbf{a}}_y$) and with $\beta \ll 1$, $|\chi^s(\bar{\mathbf{v}} \cdot \bar{\mathbf{n}})|^2 + 1$, the full wave solution (2.1) reduced to Brown's perturbed physical optics solution (2.11).

In this work we evaluate the backscattered like and cross polarized cross sections for normal incidence as the parameter v_d is varied. Both perfectly conducting and finitely conducting media are considered.

The contributions of the individual terms of the full wave solution (2.1) and the perturbed-physical optics solution (2.11), are examined in detail.

Since the full wave approach accounts for specular point and diffuse scattering in a unified self-consistent manner, it is not necessary to adopt the two-scale model of the rough surface. It is done here in order to elucidate the interpretation of rough-surface scattering in terms of the two-scale (or composite) models that have been in use for nearly two decades and in order to see whether through a judicious choice of the break point v_d (between the large and small scale surfaces) a single-term large-scale specular point model could be used to determine the like polarized backscatter cross sections for the sea at normal incidence. In addition to the numerical solutions based on the two-scale model, the results corresponding to the unified full wave solutions are also presented (Bahar and Fitzwater 1984). The unified full wave solution for the incoherent scattering cross sections can be expressed as:

$$\langle \sigma^{PQ} \rangle_U = \frac{Q(\bar{n}^f, \bar{n}^i)}{\pi} \int \left| \frac{k_o D^{PQ}}{\bar{n} \cdot \bar{a}_y} \right|^2 P_2(\bar{n}^f, \bar{n}^i, \bar{n}) p(\bar{n}) d\bar{n} \quad (2.15a)$$

in which

$$Q(\bar{n}^f, \bar{n}^i) = \int (\chi_2 - |\chi|^2) \exp(i\bar{v} \cdot \bar{r}_d) d\bar{x}_d d\bar{z}_d \quad (2.15b)$$

where χ_2 and χ are the joint characteristic function and the characteristic function respectively for the total rough surface h and $r_d = (x_d^2 + z_d^2)^{1/2}$ is the distance measured along the reference surface $y = 0$. The two dimensional slope distribution of the total rough surface is $p(\bar{n})$.

3. Illustrative Examples

For the illustrative examples considered in this section, the specific form of the surface height spectral density function is a polynomial approximation of the Pierson-Moskowitz spectrum for the steady-state response of the ocean surface to a surface wind of speed V (m/s) (Brown 1978).

$$W(v_x, v_z) = \left(\frac{2}{\pi}\right) S(v_x, v_z) = \begin{cases} \frac{2}{\pi} B v_T^4 / (v_T^2 + \kappa^2)^4 & v_T \leq v_c \\ 0 & v_T > v_c \end{cases} \quad (3.1)$$

in which W is the notation originally used by Rice (1951) and S is the notation used by Brown (1978). For the above isotropic model of the ocean surface, we select as an example a typical, moderate wind speed sea, and radar frequency corresponding to space borne altimeters such as Seasat's:

$$B = 0.0046 \quad V = 4.3 \text{ (m/s)} \quad (3.2)$$

$$\kappa = (335.2 V^4)^{-1/2} (\text{cm})^{-1} \quad v_c = 12 (\text{cm})^{-1} \quad (3.3)$$

The wavelength of the electromagnetic wave is

$$\lambda_o = 2.22 (\text{cm}) \quad (k_o = 2.83 (\text{cm})^{-1}) \quad (3.4)$$

The mean square height of the small scale surface h_s is

$$\langle h_s^2 \rangle = \int_0^{2\pi} \int_{v_d}^{v_c} \frac{W(v_T)}{4} v_T dv_T d\phi = \frac{B}{2} \left[\frac{1}{v_d^2} - \frac{1}{v_c^2} \right] = B/4k_o^2 \quad (3.5)$$

and the total mean square slope for the large scale filtered surface is

$$\begin{aligned} \sigma_{ls}^2 = \langle h_{ls}^2 \rangle &= \int_0^{2\pi} \int_0^{v_d} \frac{W(v_T)}{4} v_T^3 dv_T d\phi \\ &= \frac{B}{2} \left[\frac{-11}{6} + \ln \left(\frac{v_d^2 + \kappa^2}{\kappa^2} \right) \right] \end{aligned} \quad (3.6)$$

In (3.5) and (3.6) it is assumed that $v_d \gg \kappa$. The wavenumber where spectral splitting is assumed to occur, v_d , is determined by the choice of the roughness

parameter $\beta = 4k_o^2 \langle h_s^2 \rangle$. Thus,

$$\frac{1}{v_d^2} = \frac{1}{v_c^2} + \frac{1}{2Bk_o^2} \beta, \quad 0.1 \leq \beta \leq 2.0 \quad (3.7)$$

The slope distribution is assumed to be Gaussian

$$p(\bar{n}) = p(h_x, h_z) = \frac{1}{\pi \sigma_{ls}^2} \exp \left[-\frac{h_x^2 + h_z^2}{\sigma_{ls}^2} \right] \quad (3.8)$$

For backscatter with normal incidence, the wave normals are

$$\bar{n}^f = -\bar{n}^i = \bar{a}_y \quad (3.9)$$

and

$$\bar{v} = 2k_o \bar{n}^f = 2k_o \bar{a}_y, \quad \bar{n}_s = \bar{a}_y \quad (3.10)$$

The relative permeability is assumed to be $\mu_r = 1$ and the ocean is characterized by (i) a perfect conductor $|\epsilon_r| \rightarrow \infty$ and (ii) a relative complex (dissipative) dielectric coefficient representative of ocean water (Stogryn 1971)

$$\epsilon_r = 42 - i39 \quad (3.11)$$

The functions $W_m(v_T)$ are evaluated numerically for $m=2$ and 3 since for the range of values of β considered only three terms of the series expansion (2.6) are non-negligible.

For the range of values of β considered ($0.1 \leq \beta \leq 2$) the corresponding values for the wavenumber v_d (3.7) (where spectral splitting is assumed to occur), the mean square height for the small scale surface $\langle h_s^2 \rangle$ (3.5) and the mean square slope for the large scale surface σ_{ls}^2 (3.6) are listed in Table I.

In Figures 1 through 4, the backscatter cross sections $\langle \sigma^{PQ} \rangle$ and the individual contributions $\langle \sigma^{PQ} \rangle_l$, $\langle \sigma^{PQ} \rangle_{s1}$, $\langle \sigma^{PQ} \rangle_{s2}$ and $\langle \sigma^{PQ} \rangle_{s3}$ are plotted as functions of the roughness parameter β . When the characteristic function χ^s (2.3) is set equal to unity in (2.2) and (2.7), the corresponding results are denoted by the superscript o. The results for $\langle \sigma^{PQ} \rangle_o$, $\langle \sigma^{PQ} \rangle_l^o$, $\langle \sigma^{PQ} \rangle_{s1}^o$

$\langle \sigma^{PQ} \rangle_{s2}^o$ and $\langle \sigma^{PQ} \rangle_{s3}^o$ are also plotted in Figures 1 through 4. It should be pointed out that

$$\langle \sigma^{PQ} \rangle_{\ell}^o = \langle \sigma_{\infty}^{PQ} \rangle \quad (3.12)$$

corresponds to the physical optics contribution to the cross section (from the large scale surface) in Brown's formulation (2.11), and

$$\langle \sigma^{PQ} \rangle_{s1}^o = \langle \sigma_p^{PQ} \rangle \quad (3.13)$$

corresponds to the perturbation (small scale) contribution to the cross section in Brown's formulation. The dashed horizontal lines in all of these figures correspond to the unified full wave solutions (2.15) that are not artificially split into two components.

In Figures 1 and 2, the like polarized backscatter cross sections $\langle \sigma^{PP} \rangle = \langle \sigma^{VV} \rangle = \langle \sigma^{HH} \rangle$ for normal incidence are plotted as functions of β with $\epsilon \rightarrow \infty$ (perfect conductor) and $\epsilon_r = 42 - i39$ respectively. In Figures 3 and 4 the cross polarized backscatter cross sections $\langle \sigma^{PQ} \rangle = \langle \sigma^{VH} \rangle = \langle \sigma^{HV} \rangle$ for normal incidence are plotted as functions of β with $\epsilon \rightarrow \infty$ (perfect conductor) and $\epsilon_r = 42 - i39$ respectively. Note that $\langle \sigma^{PQ} \rangle_{\ell} = 0$ for the cross polarized case.

In all the plots we find that for the range of values $1 \leq \beta \leq 2$ the full wave solutions for the (total) backscatter cross sections $\langle \sigma^{PQ} \rangle$ is relatively independent of β even though the individual contributions to $\langle \sigma^{PQ} \rangle$ are very sensitive to variations in β . Significant variations in the cross sections occur only for $\beta < 0.25$. On the other hand, Brown's solutions for the backscatter cross sections are very sensitive to the choice of $\beta(v_d)$. He notes that on the basis of the two-scale perturbed physical optics approach he used, v_d should be chosen such that $\beta = 0.1$. For $\beta = 0.1$ and small surface slopes the full wave solutions reduce to Brown's solution (with only one significant term needed in (2.6)). For normal incidence the unified full wave

solutions $\langle \sigma^{PP} \rangle_U$ (2.15) intersect the full wave solutions based on the two-scale model $\langle \sigma^{PP} \rangle$ (2.1) at points corresponding to $\beta = 0.25$. For the cross polarized case however, $\langle \sigma^{PQ} \rangle_U$ is about 15 dB above the corresponding values based on the two-scale approach. This is because for backscatter $\langle \sigma_{\infty}^{PQ} \rangle \rightarrow 0$ ($P \neq Q$) even though the large scale surface h_L does depolarize the backscattered wave.

It is also interesting to point out that for normal incidence, the backscattered like polarized cross sections

$$\langle \sigma^{PP} \rangle \approx \langle \sigma^{PP} \rangle_L^0 \quad (3.14)$$

and that for $1 < \beta < 2$ these results are relatively insensitive to variations in β . As noted above, for normal incidence the unified full wave solution for $\langle \sigma^{PP} \rangle_U$ intersects the results based on the two-scale model $\langle \sigma^{PP} \rangle$ at $\beta = 0.25$. However, the point of intersection of the two results will in general depend upon the angle of incidence θ . For the like polarized case, the main drawback in the analysis based on the two-scale model is due to the assumption that the large and small scale surfaces (which are spectrally separated at the wavenumber v_d) are statistically independent. Note that the value of v_d is selected in order to conform with the mathematical two-scale model and not with any physical feature of the rough surface. For the cross polarized case this drawback is compounded by the fact that $\langle \sigma_{\infty}^{PQ} \rangle \rightarrow 0$ while the large scale surface is also responsible for depolarization.

For the isotropic surface height spectral density function assumed here (3.1), the mean square radius of curvature $\langle \rho^2 \rangle$ is given by

$$\frac{1}{\langle \rho^2 \rangle} = \pi \int \frac{W(v_T)}{2} v_T^5 dv_T \approx B v_d^2 / 2 \quad (3.15)$$

Thus on imposing the condition (for the decomposition of the rough surface) suggested by Tyler (1976), $B v_d^2 / 2 k_0^2 \approx 1$. However, in view of (3.5) $\beta = 4 k_0^2 \langle h_s^2 \rangle = 2 B k_0^2 / v_d^2$. Thus $\beta = B^2 = 2.116 \times 10^{-5}$. The corresponding value for $\langle \sigma^{PP} \rangle$ is about 2 dB below $\langle \sigma^{PP} \rangle_U$.

There are two ways in which the full-wave two-scale solution for like-polarized backscatter at normal incidence differs from the previous composite models (Brown 1978). First, the large-scale term for the full-wave solution is multiplied by $|\chi^s|^2$ (2.2) accounting for the fact that the specular-point regions are roughened by the small-scale surface component. Hence, the Fresnel reflection for specular return is reduced exactly in the amount predicted by Rice (1951) from perturbation theory, due to the energy scattered away from the specular direction by this small-scale roughness. Second, the full-wave contribution due to the small-scale roughness (which also contains the term $|\chi^s|^2$) is actually an infinite series in which more terms become significant as β increases, while for the perturbed-physical optics two-scale model β is kept low enough so that the perturbation criteria is satisfied by the small scale surface. Therefore, interpretation of the full-wave two-scale mathematical solution elucidates the physical mechanisms one would expect to occur when the surface is broken artificially into two scales of roughness. It is interesting that for backscatter at normal incidence and for the gently sloping sea-surface examined here, the choice by Brown of $\beta = 0.1$ as the break between the roughness scales produces results for the like polarized cross sections that are only about 1 dB below the full-wave solutions indicating the soundness of that approach. Such agreement however, does not hold for the cross polarized cross sections off normal or for surfaces with larger slopes. Tyler's criterion (1976) for using the radius of curvature condition to locate the break point is somewhat less suitable for the sea surface considered here, although it may be more suitable for more irregular planetary surfaces.

As mentioned earlier, there is no need to split the full-wave solution into two components; the integral (2.15) represents the entire solution. It can and has been evaluated as one term (dashed lines in illustrations). Since the splitting is artificial, the validity of the full-wave two-scale approach can be tested by checking (i) whether the weighted sum (2.1) varies significantly with the splitting parameter, β ; (ii) whether the two-scale full-wave solutions agree with the unified full-wave solutions. The curves for the like polarized cases (Figs. 1

and 2) show that the sum of all terms of the two-scale full-wave solution is nearly constant over large variations in the break point, i.e., for $1 < \beta < 2$. For normal incidence it agrees exactly with the unified, full-wave solution at $\beta = 0.25$ and differs from it at most by about 2 dB at $\beta = 2$. On the other hand, the results based on the perturbed physical optics model begin to vary significantly from the full-wave solutions for $\beta > 0.25$. The reason for the small disagreement between the unified and two-scale full-wave results stems primarily from the fact that on artificially splitting the surface it is assumed that the small scale rough surface is statistically independent of the large scale rough surface. This assumption becomes decreasingly valid as β increases. The unified full-wave solution is self-consistent; no such assumption is made and in fact it is the only valid solution for the cross polarized return, where the asymptotically evaluated "specular" contribution from the large scale surface is meaningless.

A final conclusion is that, for backscatter from the sea at normal incidence, the simple Gaussian-slope specular-point solution $\langle \sigma^{PP}_l \rangle^0 = |R(0)|^2 / (2s_x s_z)$. (Eq. (9) of Barrick and Lipa (1985)) can be used with reasonable accuracy, ($R(0)$ is the normal incidence Fresnel reflection coefficient of sea water and s_x, s_z are the rms slopes of the sea surface along the major and minor roughness axes). Although this specular-point result $\langle \sigma^{PP}_l \rangle^0$ (which neglects the small-scale characteristic-function factor) is observed in Figs. 1 and 2 to be almost independent of the split point for $1 < \beta < 2$, the correct value for β is shown to be 0.25 at the intersection with the unified full-wave solution. The value β enters the above equation implicitly (through v_d) in the expression for the rms slopes of the large scale surface. They are logarithmic functions of v_d the wave-number where spectral splitting is assumed to occur (3.6) for the idealized sea-surface waveheight spectrum assumed here (3.1).

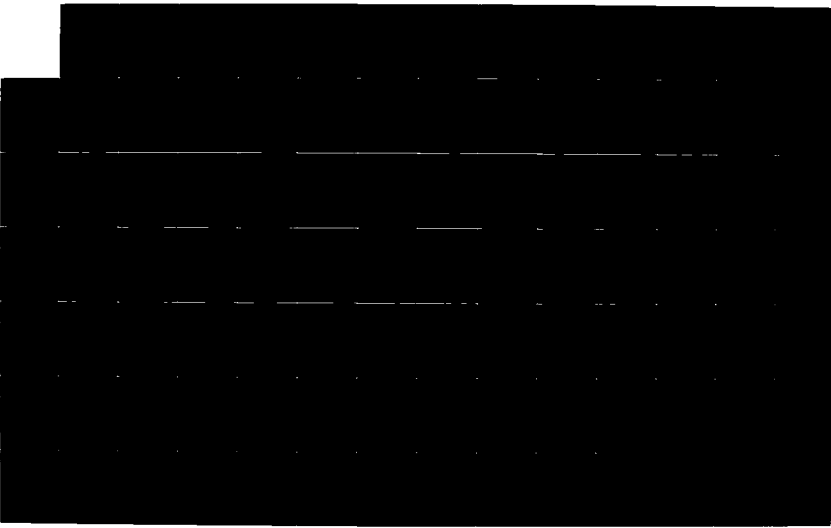
AD-A171 218

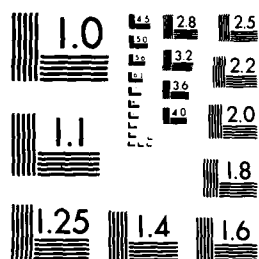
DEPOLARIZATION AND SCATTERING OF ELECTROMAGNETIC WAVES
APPENDICES (U) NEBRASKA UNIV LINCOLN E BANAR 30 JUN 86
ARO-18120.17-EL-APP DAAG29-82-K-0123

4/3

UNCLASSIFIED

F/G 20/14 NL





MICROCOPY RESOLUTION TEST CHART
NATIONAL BUREAU OF STANDARDS 1963-A

5. References

1. Bahar, E. (1981), "Scattering Cross Section for Random Rough Surfaces: Full Wave Analysis," Radio Science, Vol. 16, No. 3, pp. 331-341.
2. Bahar, E. and D. E. Barrick (1983), "Scattering Cross Sections for Composite Rough Surfaces that Cannot be Treated as Perturbed Physical Optics Problems," Radio Science, Vol. 18, No. 2, pp. 129-137.
3. Bahar, E., D. E. Barrick and M. A. Fitzwater (1983), "Computations of Scattering Cross Sections for Composite Surfaces and the Specification of the Wavenumber Where Spectral Splitting Occurs," IEEE Transactions on Antennas and Propagation, Vol. AP-31, No. 5, pp. 698-709.
4. Bahar, E. and M. A. Fitzwater (1984), "Scattering Cross Sections for Composite Rough Surfaces Using the Unified Full Wave Approach," IEEE Trans. Antennas and Propagation, Vol. AP-32, No. 7, pp. 730-734.
5. Barrick, D. E. (1974), "Wind Dependence of Quasi-Specular Microwave Sea Scatter," IEEE Trans. Antennas Propagat., Vol. AP-22, pp. 135-136.
6. Barrick, D. E. and B. J. Lipa (1985), "Analysis and Interpretation of Altimeter Sea Echo," Advances in Geophysics, Vol. 27, ed. B. Saltzman, New York: Academic Press, pp. 61-100.
7. Barrick, D. E. and W. H. Peake (1968), "A Review of Scattering from Surfaces with Different Roughness Scales," Radio Science, Vol. 3, pp. 865-868.
8. Brown, G. S. (1978), "Backscattering from a Gaussian-Distributed Perfectly Conducting Rough Surface," IEEE Trans. Antennas Propagat., Vol. AP-26, No. 3, pp. 472-482.
9. Brown, G. S. (1979), "Estimation of Surface Wind Speeds Using Satellite-Borne Radar Measurements of Normal Incidence," J. Geophys. Res., Vol. 84, pp. 3974-3978.
10. Burrows, M. L. (1967), "On the Composite Model for Rough Surface Scattering," IEEE Trans. Antennas Propagat., Vol. AP-21, No. 2, pp. 241-243.
11. Chelton, D. B. and P. J. McCabe (1985), "A Review of Satellite Altimeter Measurement of Sea Surface Wind Speed: With a Proposed New Algorithm," J. Geophys. Res., Vol. 90, (C3), pp. 4707-4720.
12. Rice, S. O. (1951), "Reflection of Electromagnetic Waves from Slightly Rough Surfaces," Theory of Electromagnetic Waves, ed. M. Kline, New York: Interscience Pubs., pp. 351-378.
13. Sancer, M. I. (1968), "Shadow-Corrected Electromagnetic Wave Propagation Over a Nonparallel Stratified Conducting Medium," Can. J. Phys., Vol. 45, pp. 3697-3720.

14. Smith, B. G. (1967), "Geometrical Shadowing of a Randomly Rough Surface," IEEE Trans. Antennas Propagat., Vol. AP-15, No. 5, pp. 668-671.
15. Stogrun, A. (1971), "Equations for Calculating the Dielectric Constant of Saline Water," IEEE Trans. on Microwave Theory and Techniques, Vol. MTT-19, No. 8, pp. 734-736.
16. Tyler, G. L. (1976), "Wavelength Dependence in Radio Wave Scattering and Specular-Point Theory," Radio Science, Vol. 11, No. 2, pp. 83-91.
17. Wright, J. W. (1968), "A New Model for Sea Clutter," IEEE Trans. Antennas Propagat., Vol. AP-16, pp. 217-233.

ACKNOWLEDGMENTS

This work has been supported in part by U.S. Army Research Office Contract No. DAAG-29-K-0123.

Figure Captions


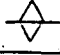

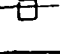
- Fig. 1. Like polarized backscattered cross sections for normal incidence as a function of the roughness parameter β or v_d ; $\epsilon_r \rightarrow \infty$ (perfectly conducting boundary). P=V or H (vertical or horizontal polarization).
- Fig. 2. Like polarized backscatter cross sections for normal incidence as a function of the roughness parameter β or v_d ; $\epsilon_r = 42-139$ (finitely conducting boundary). P=V or H (vertical or horizontal polarization).
- Fig. 3. Cross polarized (P \neq Q) backscattered cross sections for normal incidence as a function of the roughness parameter β or v_d ; $\epsilon_r \rightarrow \infty$ (perfectly conducting boundary). P,Q=V or H scattered and incident polarizations respectively.
- Fig. 4. Cross polarized (P \neq Q) backscattered cross sections for normal incidence as a function of the roughness parameter β or v_d ; $\epsilon_r = 42-139$ (finitely conducting boundary). P,Q=V or H scattered and incident polarizations respectively.

TABLE I

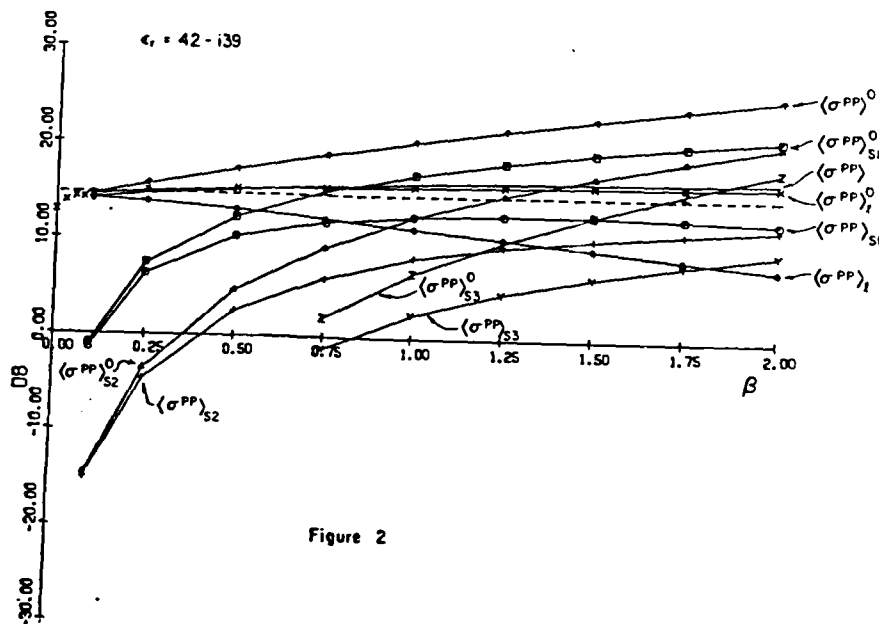
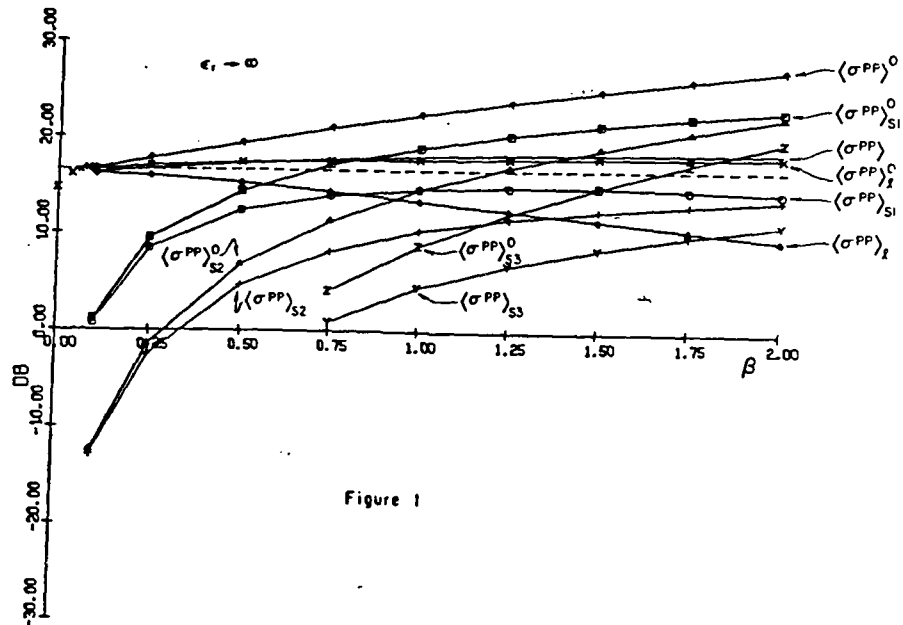
β	v_d (cm ⁻¹)	$\langle h_s^2 \rangle$ (cm ²)	σ_{ls}^2
.1	.856	.00312	.0219
.25	.542	.00780	.0178
.50	.384	.0156	.0182
.75	.313	.0234	.0172
1.00	.271	.0312	.0166
1.25	.243	.0390	.0161
1.50	.222	.0468	.0156
1.75	.205	.0546	.0153
2.00	.192	.0624	.0150

Table I. List of the values of v_d , $\langle h_s^2 \rangle$ and $\langle \sigma_s^2 \rangle$ for different values of the roughness parameter β .

List of Symbols and Notations in
Illustrations 1 Through 4.

Symbol	Notation	Cross Section	Symbol	Notation	Modified Cross Section ($\chi^s + 1$)
—	$\langle \sigma^{PP} \rangle$	total two-scale		$\langle \sigma^{PP,o} \rangle$	total two-scale
	$\langle \sigma^{PP} \rangle_l$	large scale	—x—	$\langle \sigma^{PP,o} \rangle_l$	large scale (Brown)
	$\langle \sigma^{PP} \rangle_{s1}$	small scale m=1		$\langle \sigma^{PP,o} \rangle_{s1}$	small scale m=1 (Brown)
—+—	$\langle \sigma^{PP} \rangle_{s2}$	small scale m=2	—Δ—	$\langle \sigma^{PP,o} \rangle_{s2}$	small scale m=2
—x—	$\langle \sigma^{PP} \rangle_{s3}$	small scale m=3	—B—	$\langle \sigma^{PP,o} \rangle_{s3}$	small scale m=3

— — — — Unified Full Wave Solutions



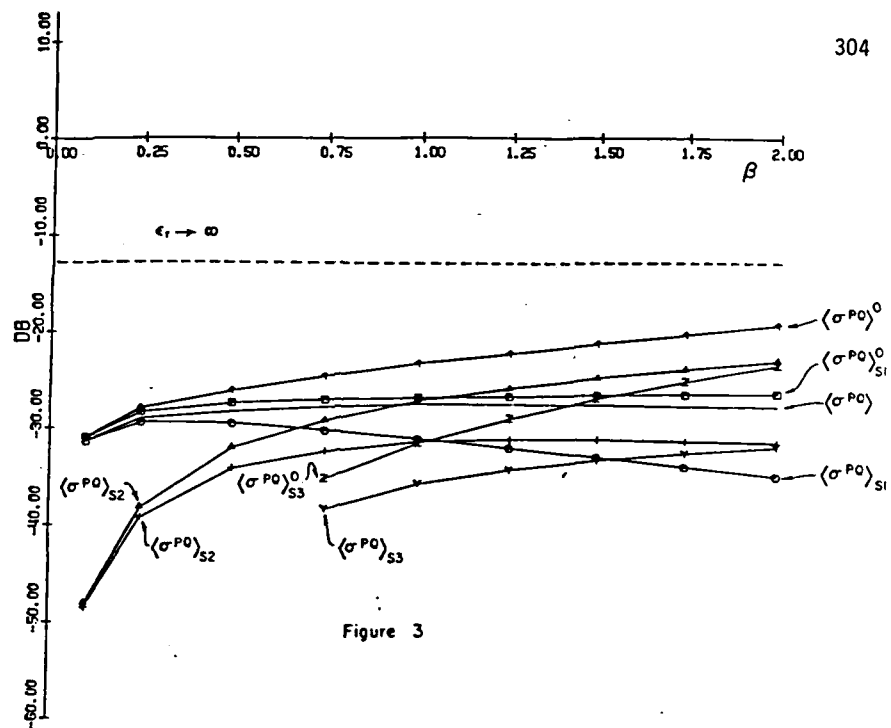


Figure 3

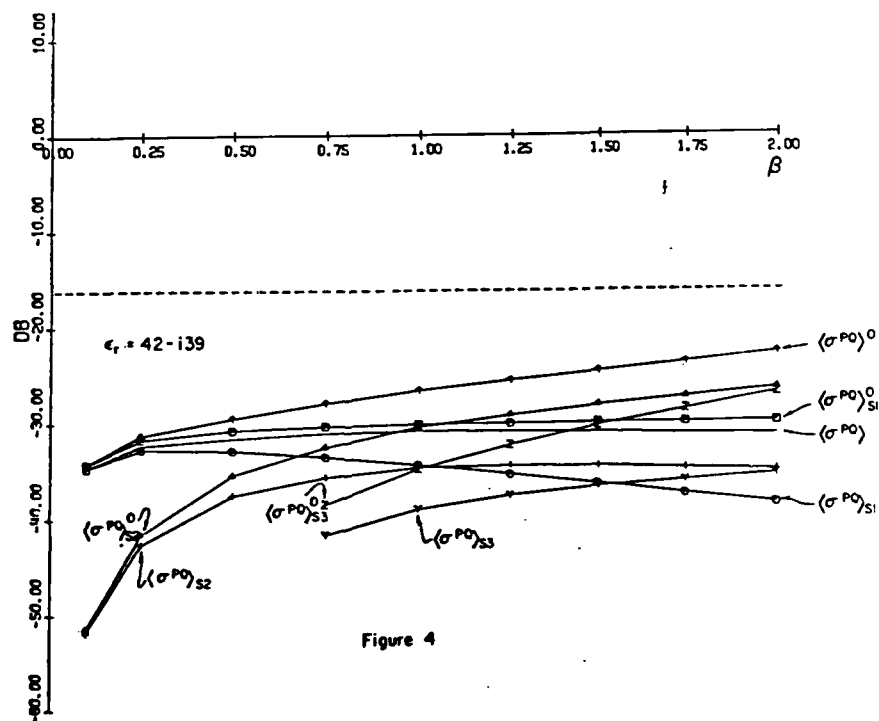


Figure 4

Ezekiel Bahar
Mary Ann Fitzwater
Electrical Engineering Department
University of Nebraska--Lincoln
Lincoln, Nebraska 68588-0511

ABSTRACT

The incoherent diffuse scattering intensities (Stokes parameters) are evaluated for infrared and optical excitations of a layer consisting of random distributions of finitely conducting irregular shaped particles. The full wave approach is used to determine the elements of the phase matrix and the extinction cross sections appearing in the equation of transfer. The rough surface height of the particles is characterized by different surface height spectral density functions.

1. INTRODUCTION

Scattering of electromagnetic waves in media consisting of random distributions of particles has been investigated extensively using the equation of transfer.^{1,2} The main difficulty in setting up the equation of transfer lies in the determination of the elements of the 4×4 scattering matrix for the individual particles. Thus, most of the work has been done for particles of idealized shapes such as spheres.

In this work a method is presented for the modification of the results derived for particles with idealized shapes to account for the random surface roughness of the particles. To this end, the full wave approach³ was used to determine the rough surface contributions to the like and cross polarized scattering cross sections. Different particle sizes with different complex dielectric coefficients are considered. The rough surface height is characterized by different surface height spectral density functions (the Fourier transforms of the surface height autocorrelation functions).

2. FORMULATION OF THE PROBLEM

The full wave solutions for the normalized scattering cross sections $\langle \sigma^{ij} \rangle$ per unit cross sectional area ($A_y = \pi h_0^2$) are expressed as a weighted sum³

$$\langle \sigma^{ij} \rangle = \langle \sigma^{ij} \rangle_s + \langle \sigma^{ij} \rangle_u \quad (1)$$

the symbol $\langle \rangle$ denotes the statistical average. In the above expression the first and second superscripts indicate the polarizations of the scattered and incident waves respectively. Thus $i, j=1$ denotes Vertical polarization and $i, j=2$ denotes Horizontal polarization. The cross section $\langle \sigma^{ij} \rangle_s$ is the modified cross section associated with the unperturbed sphere.

$$\langle \sigma^{ij} \rangle_s = |\chi(v)|^2 \langle \sigma^{ij} \rangle_{\text{Mie}} \quad (2)$$

In (2) $\langle \sigma^{ij} \rangle_{\text{Mie}}$ is the Mie solution,² for the like and cross polarized cross sections of the unperturbed sphere. The coefficient of $\langle \sigma^{ij} \rangle_{\text{Mie}}$ is the rough surface height characteristic function

$$\chi^s(v) = \langle \exp i v h_s \rangle \quad (3)$$

in which v is the magnitude of the vector

$$\vec{v} = k_0 (\vec{n}^f - \vec{n}^i) \quad (4)$$

where \vec{n}^f and \vec{n}^i are unit vectors in the direction of the scattered and incident wave normals. The coefficient $|\chi^s|^2$ accounts for the degradation of the reflected wave due to surface roughness.

The second term in (1) $\langle \sigma^{ij} \rangle_u$ is the contribution to the total scattering cross section due to the surface roughness. It is expressed as⁴

$$\langle \sigma^{ij} \rangle_u = \int A^{ij}(\vec{n}^f, \vec{n}^i, \vec{n}) (\vec{n} \cdot \vec{a}_y) Q_s(\vec{n}^f, \vec{n}^i, \vec{n}) p(\vec{n}) d\vec{n} \quad (5)$$

in which \vec{n} is a unit vector normal to the surface of the scatterer,

$$A^{ij}(\vec{n}^f, \vec{n}^i, \vec{n}) = \frac{1}{\pi} \left| \frac{k_0 D^{ij}}{(\vec{v} \cdot \vec{a}_y)(\vec{a}_y \cdot \vec{n})} \right|^2 P_2(\vec{n}^f, \vec{n}^i | \vec{n}) \quad (6)$$

$$Q_s(\vec{n}^f, \vec{n}^i, \vec{n}) = (\vec{v} \cdot \vec{a}_r)^2 \int_{-\infty}^{\infty} (\chi_2^s(\vec{v} \cdot \vec{a}_r) - |\chi(\vec{v} \cdot \vec{a}_r)|^2) \cdot \exp(i\vec{v} \cdot \vec{r}_d) d\vec{r}_d \quad (7)$$

and $p(\vec{n})$ is the probability density function for the slope of the surface of the scatterer. In (6), D^{ij} is the scattering coefficient which depends on the polarizations and the directions of the wave normals for the incident and scattered waves as well as the complex electromagnetic parameters (ϵ, μ) of the scatterers. The term $P_2(\vec{n}^f, \vec{n}^i | \vec{n})$ is the probability that a point on the rough surface is both illuminated by the source and visible to the observer given the slopes (\vec{n}) of the surface of the scatterer.⁵

In (7) $\chi^s(\vec{v} \cdot \vec{a}_r)$ and $\chi_2^s(\vec{v} \cdot \vec{a}_r)$ are the rough surface height characteristic function and joint characteristic function respectively,

$$\chi^s(\vec{v} \cdot \vec{a}_r) = \langle \exp(i\vec{v} \cdot \vec{h}_s) \rangle \quad (8)$$

$$\text{and } \chi_2^s(\vec{v} \cdot \vec{a}_r) = \langle \exp(i\vec{v}_r \cdot (\vec{h}_s - \vec{h}_s')) \rangle \quad (9)$$

in which $\vec{v}_r = \vec{v} \cdot \vec{a}_r$.

With the above expressions for the scattering cross sections (1), the general expression for the equation of transfer² can be written as follows for a plane parallel slab consisting of rough spherical particles

$$\mu \frac{d[I]}{d\tau} = -[I] + f[S][I'] d\mu' d\phi' + [I_1] \quad (10)$$

In (10), τ is the optical distance in the z direction (normal to the plane parallel slab). Since $\langle \sigma^{ij} \rangle_s$ vanishes in the forward direction, the extinction matrix⁶ for the rough sphere can be represented by a scalar quantity. The matrices $[I]$ and $[I']$ are the (4×1) incoherent specific diffuse intensity matrices for waves scattered from the particles in the direction $\theta = \cos^{-1} \mu$ and ϕ and for waves incident in the direction $\theta' = \cos^{-1} \mu'$ and ϕ' , respectively. The (4×4) scattering matrix $[S]$ in the reference coordinate system can be expressed in terms of the scattering matrix $[S']$ in the scattering plane as follows:

$$[S] = [Z(-\phi, \phi)][S'] [Z(\phi, -\phi)] \quad (11)$$

in which $[Z]$ is a transformation matrix and

$$[S'] = |\chi^s(\vec{v} \cdot \vec{a}_r)|^2 [S_{\text{Mie}}] + [S_u] \quad (12)$$

In (12) $[S_{\text{inc}}]$ is the scattering matrix for the unperturbed sphere. The coefficient $|\chi^s(\vec{v}, \vec{a}_r)|^2$ accounts for the fact that the specular point contributions to the scattering cross sections is decreased because of the rough surface. The diffuse scattering matrix $[S_s]$ due to the random rough surface height h_s of the particle is given by

$$[S_s] = \begin{bmatrix} [S_{11}^s] & [S_{12}^s] & 0 & 0 \\ [S_{21}^s] & [S_{22}^s] & 0 & 0 \\ 0 & 0 & [S_{33}^s] & [S_{34}^s] \\ 0 & 0 & [S_{43}^s] & [S_{44}^s] \end{bmatrix} \quad (13)$$

where

$$[S_{ij}^s] = \frac{A}{4\pi p[\sigma_t]} \rho [\langle \sigma_{ij}^s \rangle_s] \quad (14)$$

in which $\langle \sigma_{ij}^s \rangle_s$ is given by the full wave solution (5), σ_t is the total cross section and $\rho[\cdot]$ denotes average over particle size.

Furthermore for $i=3$ and 4

$$[S_{ij}^s] = \rho[\text{Re}[\langle \sigma_{22}^{11} \rangle_s \pm \langle \sigma_{21}^{12} \rangle_s]] A_y / 4\pi p[\sigma_t] \quad (15)$$

(upper and lower signs for $i=3$ and 4 respectively) and for $i \neq j$

$$[S_{ij}^s] = \rho[\text{Im}[\langle \sigma_{22}^{11} \rangle_s + \langle \sigma_{21}^{12} \rangle_s]] A_y / 4\pi p[\sigma_t] \quad (16)$$

(upper and lower signs for $i, j=3, 4$ and $i, j=3, 4$ respectively). In the above expressions

$$\langle \sigma_{kl}^{ij} \rangle_s = \frac{1}{\pi} \int_0^{2\pi} \frac{k^2 D^{ij}(\phi, \phi')}{(\vec{v} \cdot \vec{a}_r)^2 (\vec{n} \cdot \vec{a}_y)} P_2 Q_s P(\vec{n}) d\vec{n} \quad (17)$$

The remaining eight terms of the matrix $[S_s]$ vanish since D^{11} and $D^{12}(ij)$ are symmetric and antisymmetric respectively with respect to the azimuth angle ϕ .

In order to simplify the solution of the transfer equation (10), it is assumed in this work that the normally incident wave is circularly polarized. Thus the incident Stokes matrix at $z=0$ is given by

$$[I_{\text{inc}}] = \begin{bmatrix} 1 \\ 1 \\ 0 \\ 0 \end{bmatrix} \delta(\mu'-1) \delta(\phi') \approx I_0 \delta(\mu'-1) \delta(\phi') \quad (18)$$

where the $-$ and $+$ signs correspond to the right and left circularly polarized waves and $\mu' = \cos \theta'$. The reduced incident intensity is therefore,

$$[I_{r1}] = [I_{\text{inc}}] \exp(-\tau) \quad (19)$$

In (10) the $(kx1)$ excitation matrix $[I_1]$ is given by

$$[I_1] = \int [S][I_{r1}] d\mu' d\phi' = [S][I_0] \int_{\mu'=1}^{\mu'=1} \exp(-\tau) d\mu' \quad (20)$$

where I_0 , the incident Stokes matrix is defined by (18).

For the illustrative examples considered in this section, the random rough surface height h_s (measured normal to the surface of the unperturbed spherical particle of diameter $D=2a_0$) is assumed to be homogeneous and isotropic. Different forms of the surface height spectral density function $W(v_x, v_y)$ (which is the two dimensional Fourier Transform of the surface height autocorrelation function $\langle h_s h_s' \rangle$) are considered.

For cases (a) and (b) the specific form of the surface height spectral density function considered is

$$W(v_x, v_y) = \frac{2C}{\pi} \left[\frac{v_T}{v_T^2 + v_x^2 + v_y^2} \right]^B, \quad v_T > 0 \quad (21)$$

where the exponent is assumed to be $n=8$. For case (a) the roughness parameter is $\beta=4$, $\langle h_s^2 \rangle = 1$ and for case (b) it is $\beta=10$. This sets the value of the constant C in (21) since

$$\langle h_s^2 \rangle = \frac{\pi}{C} \int_0^\infty W(v_T) v_T dv_T \quad (22)$$

The corresponding values for v_T, λ, C , and D are in Figs. 1-4. For these cases, the surface height autocorrelation coefficient $R(\zeta) = \langle h_s h_s' \rangle / \langle h_s^2 \rangle$ can be expressed in closed form

$$R(\zeta) = \left[1 - \frac{3\zeta^2}{8} + \frac{3\zeta^4}{32} + \frac{\zeta^6}{3072} \right] K_1(\zeta) + \left[\frac{3}{2} - \frac{\zeta^2}{4} - \frac{\zeta^4}{96} \right] \zeta^2 K_0(\zeta) \quad (23)$$

In (23) K_0 and K_1 are modified Bessel functions of the second kind of order zero and one respectively and the dimensionless parameter ζ is

$$\zeta \equiv \frac{v_T}{\lambda} D \quad (24)$$

For all the illustrative examples, it is assumed that a right circularly polarized wave is normally incident at $\tau=0$ ($z=0$) upon a parallel layer of optical thickness τ_0 . The equation of transfer for the azimuthally independent modified Stokes parameters are solved using the matrix characteristic (eigen) value technique.⁶ For case (a) ($D/\lambda=10$) the scattering cross sections are more sharply peaked in the forward direction, thus it is necessary to use a Gaussian quadrature formula of order 32.⁷ The boundary conditions for the incoherent specific diffuse intensities are

$$[I] = 0 \quad \text{for } 0 \leq \mu \leq 1 \quad \text{at } \tau=0 \quad (25)$$

(transmitted incoherent diffuse intensities are zero at $\tau=0$) and

$$[I] = 0 \quad \text{for } 0 \geq \mu \geq -1 \quad \text{at } \tau=\tau_0 \quad (26)$$

(reflected incoherent diffuse intensities are zero at $\tau=\tau_0$).

For case (a), the incoherent diffuse intensities I_1 and I_2 are plotted in Figs. 1 and 2 as functions of $\theta(0^\circ, 90^\circ)$ (transmitted $\tau \geq \tau_0$) for $\tau_0=1$. The solid curves correspond to first order scattering solutions only for the smooth (unperturbed spherical) particles and particles with rough surfaces. The first order solutions are close to the multiple scattering solutions for $\tau_0=1$, however multiple scattering does tend to make the incoherent intensities more monotonic functions of the scatter angle θ . For optical thickness $\tau_0=1$, the surface roughness has a

smaller effect on the incoherent intensities and I_1 and I_2 are not equal in the intermediate range of angles between 10° and 40° .

For case (b), the incoherent intensities I_1 and I_2 are plotted in Figs. 3 and 4 as functions of $\theta(0^\circ, 90^\circ)$ (transmitted $\tau \geq \tau_0$) for $\tau_0 = 10$. Since the particles are highly conducting there is a smaller difference in the specific incoherent intensities for the smooth and rough particles. This is because the corresponding albedos are not significantly different for highly conducting particles. Nevertheless, it should be pointed out that for optically thin layers ($\tau_0 < 1$) the principal effect of particle surface roughness is to smooth out the undulations in the diffuse specific (incoherent) intensities as functions of the scatter angle. The effect of particle surface roughness is more pronounced for highly dissipative particles with small albedos. The effect of surface roughness on forward scatter ($\theta = 0$) is less pronounced since $\langle \sigma^2 \rangle$ (5) vanishes and $|X^s| \rightarrow 1$ for forward scattering.

ACKNOWLEDGMENTS

This investigation was sponsored by the U. S. Army Research Office, Contract No. DAAG-29-82-K-0123.

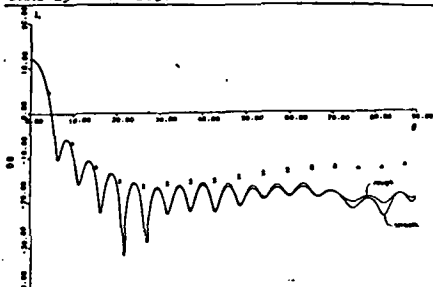


Fig. 1. Specific intensity I_1 case (a), $B=1, \sigma_s^2=.1$, $v_D=15.9$, $\lambda=.555$, $\epsilon=-40-i12$ (AL), $D=10\lambda$, $\tau_0=1$, $\phi=0$. First order (—), multiple scatter: (+) smooth, (Δ) rough.

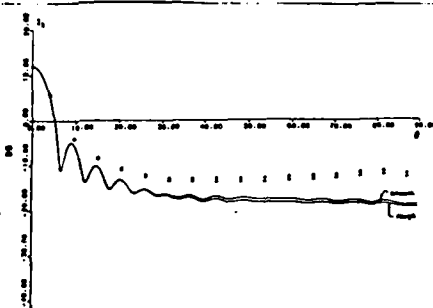


Fig. 2. Specific intensity I_2 case (a), $B=1, \sigma_s^2=.1$, $v_D=15.9$, $\lambda=.555$, $\epsilon=-40-i12$ (AL), $D=10\lambda$, $\tau_0=1$, $\phi=0$. First order (—), multiple scatter: (+) smooth, (Δ) rough.

REFERENCES

307

1. Chandrasekhar, S. (1960), Radiative Transfer. Dover, Publ., New York.
2. Ishimaru, A. (1978), Wave Propagation and Scattering in Random Media. Academic, New York.
3. Bahar, E., and Swapn Chakrabarti (1985), *Applied Optics*, Vol. 24, No. 12, 1820.
4. Bahar, E., and M. A. Fitzwater (1985), *Journal of the Optical Society of America*, Vol. 2, No. 12, pp. 2295-2303.
5. Sancer, M. I. (1968), *IEEE Trans. on Antennas and Propagation*, Vol. AP-17, No. 5, pp. 577-585.
6. Ishimaru, A., and R.L.-T. Cheung (1980), *Ann. Telecommun.*, 35, 373.
7. Abramowitz, M., and I. A. Stegun (1968), *Handbook of Mathematical Functions*, Applied Math. Series 55, National Bureau of Standards, Washington, D.C.

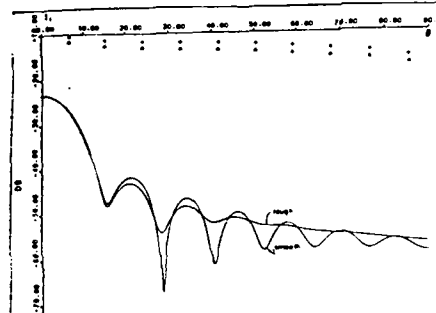


Fig. 3. Specific intensity I_1 case (b), $B=10, \sigma_s^2=.1$, $v_D=4$, $\lambda=10\mu$, $\epsilon=-6000(1+i)$ (AL), $D=5\lambda$, $\tau_0=10$. First order (—), multiple scatter: (+) smooth (Δ) rough.

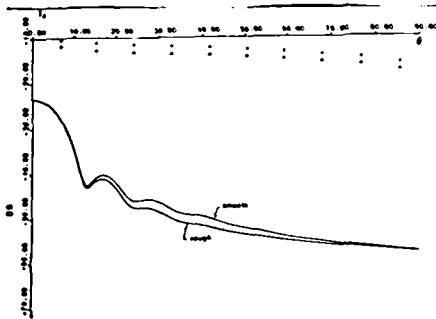


Fig. 4. Specific intensity I_2 case (b), $B=10, \sigma_s^2=.1$, $v_D=4$, $\lambda=10\mu$, $\epsilon=6000(1+i)$ (AL), $D=5\lambda$, $\tau_0=10$. First order (—), multiple scatter: (+) smooth, (Δ) rough.

EXTINCTION CROSS SECTIONS AND ALBEDOS FOR
PARTICLES WITH VERY ROUGH SURFACES

Ezekiel Bahar

Swapam Chakrabarti

and

Mary Ann Fitzwater

Electrical Engineering Department
University of Nebraska--Lincoln
Lincoln, Nebraska 68588-0511

Abstract

Using the full wave approach, the scattering cross sections for finitely conducting particles with very rough surfaces are expressed as weighted sums of specular point (physical optics) and diffuse scattering cross sections. Through a judicious use of the forward scattering theorem and the observation that for large particles the forward scattered, "shadow forming wave is the same for all surfaces which have the same shadow line," the albedos and the extinction cross sections for particles with rough surfaces are evaluated. These computations are essential to solve the equation of radiative transfer for the specific intensities (Stokes parameters) in media consisting of random distributions of particles with rough surfaces. The particle surface roughness has a significant effect on the diffuse specific intensities.

I. INTRODUCTION

The problem of electromagnetic wave scattering by random distributions of particles has been studied extensively by researchers in a broad range of disciplines such as atmospheric aerosols, smoke, and dust in planetary atmospheres (Chandrasekhar 1950, Ishimaru 1978). However, in most of the work, the scattering particles are assumed to be of idealized shapes such as spheres, oblate and prolate spheroids and circular cylinders for which rigorous separable solutions are known (Ruck et al. 1970). In many physical problems of interest however, the individual scatterers are of irregular shapes such as flakes, spheres and cylinders with random rough surfaces (Greenberg 1960, Chylek 1977a, Scheurman 1980, Bahar and Fitzwater 1983, Bahar and Chakrabarti 1985). Several theoretical and experimental techniques used in the study of scattering and absorption by irregularly shaped particles have been reported in the proceedings on the workshop on light scattering (Scheurman 1980). A survey of several analytical and numerical techniques including their respective pros and cons has been presented by Yeh and Mei (1980). For example, if the mean square height of the surface roughness $\langle h^2 \rangle$ is small ($\beta = 4k_0^2 \langle h^2 \rangle \ll 1$, where k_0 is the free space wavenumber) a perturbation approach can be used to account for diffuse scattering attributable to the rough surface (Rice 1951, Ruck et al. 1970, Kiehl et al. 1980). However for $\beta \ll 1$ the effects of the rough surface upon the scattered specific intensities is negligible.

For problems of practical interest with $\beta > 1$, the perturbation solutions are not suitable and a full wave solution, which accounts for

physical optics and diffuse scattering in a self-consistent manner, can be used to express the scattering cross sections as weighted sums of the physical optics and the diffuse scattering cross sections.

To facilitate the analysis, it is assumed here that the radius of the sphere is not only large compared to the wavelength λ_0 , but also large compared to the rough surface height correlation length. However, the radii of curvature of the rough surfaces need not be small compared to the wavelength. Multiple scattering between the different elements of the surface of the sphere is neglected. The random rough surface (assumed here to have Gaussian statistics) is characterized by its surface height (isotropic) spectral density function and a corresponding non-Gaussian autocorrelation function. These full wave expressions may be used to determine the elements of the phase matrix appearing in the equation of radiative transfer for a medium consisting of a random distribution of irregularly shaped particles (Bahar and Fitzwater 1985). Since the albedo of the particle is an important factor in radiative transfer it is also necessary to determine the albedo and the extinction coefficient for the irregularly shaped particles, in order to solve the equation of transfer (Ishimaru and Cheung 1980). When "equivalent" spheres, spheroids or cylinders do not reasonably represent the basic scattering characteristics of irregularly shaped particles, experimental microwave techniques developed by Greenberg (1960) can be used to determine the albedo for particles for which no theoretical method yet exists (Chylek 1977b, Scheurman 1980).

In this paper, the values of the extinction coefficients and the albedos are determined for spherical particles of finite conductivity with very rough surfaces ($\beta \rightarrow 10$). This is done using the full wave approach. In addition, judicious use is made of the forward scattering theorem (Born and Wolf 1964) and the very perceptive observation that for large scatterers (physical dimensions large compared to a wavelength) the forward scattered "shadow forming wave" is the same for all surfaces which have the same shadow line" (Morse and Feshbach 1953).

The problem is formulated in Section 2 and the analytical approach is given in Section 3. Several illustrative examples are presented in Section 4. Using the results presented in this work, it can be shown that particle surface roughness results in the blocking of transmission windows that appear in problems of propagation through thin layers of randomly distributed particles of idealized (spherical, circular cylindrical) shapes.

2. FORMULATION OF THE PROBLEM

Using the equation of transfer (Chandrasekhar 1950, Ishimaru 1978)

$$\frac{d[I]}{ds} = -[T][I] + \int [S][I'] d\mu' d\phi' + [I_i] \quad , \quad (2.1)$$

the scattering and depolarization of electromagnetic waves in media consisting of random distributions of particles has been investigated extensively. However, most of this work has been conducted for particles of idealized shapes such as spheres for which rigorous solutions are known for all the sixteen elements of the phase (Mueller) matrix $[S]$ as well as for the extinction matrix $[T]$. In (2.1) the elements of the $[4 \times 1]$ specific intensity column matrices $[I]$ and $[I']$ are the Stokes parameters for the scattered and incident waves respectively.

Thus for instance, for spheres, the elements of the phase matrix $[S]$ can be expressed in terms of the Mie solutions (Ishimaru 1978) for the scattering coefficients f_{ij} that relate the scattered vertically and horizontally polarized wave amplitudes E_ℓ and E_r to the incident vertically and horizontally wave amplitudes E'_ℓ and E'_r

$$\begin{bmatrix} E_\ell \\ E_r \end{bmatrix} = \begin{bmatrix} f_{11} & f_{12} \\ f_{21} & f_{22} \end{bmatrix} \begin{bmatrix} E'_\ell \\ E'_r \end{bmatrix} \frac{\exp(-ik_0 r)}{r} \quad (2.2)$$

In (2.2) k_0 is the free space wavenumber and r is the distance from the center of the sphere to the observation point.

The integration in (2.1) is over the solid angle $d\Omega' = \sin\theta' d\theta' d\phi' = -d\mu' d\phi'$ where $\mu' = \cos\theta'$ and θ' and ϕ' are the polar and azimuthal angles of the unit vector \hat{n}^i in the direction of the incident wave normal. The unit vector in the direction of the scattered wave normal (θ, ϕ) is \hat{n}^f . The excitation matrix $[I_i]$ is

$$[I_i] = \int [S][I_{ri}] d\mu d\phi, \quad (2.3)$$

where $[I_{ri}]$ is the reduced incident intensity (Ishimaru 1978). The differentiation in (2.1) is with respect to the displacement. For spherical particles the extinction matrix $[T]$ (Ishimaru and Cheung 1980) is replaced by a scalar quantity, the extinction coefficient (or total cross section) σ_t . The "forward scattering theorem" (Born and Wolf 1964) relates the total cross section to the imaginary part of the scattering amplitude in the forward direction $f_{ii}(\hat{n}^f, \hat{n}^i)$ (where $\hat{n}^f = \hat{n}^i$). Thus for a spherical particle, the normalized total cross section (per unit area of the cross section; πa^2) is given by

$$\sigma_t = \frac{4}{k_0^2 a^2} \text{Im}[f_{ii}(\hat{n}^f, \hat{n}^i)], \quad i=1 \text{ or } 2 \quad (2.4)$$

In general however, for particles of irregular shape such as finitely conducting flakes or spheroids with random rough surfaces, it is more difficult to determine the scattering coefficients f_{ij} . When the surface roughness of the particles is small ($\beta = 4k_0^2 \langle h^2 \rangle \ll 1$, where $\langle h^2 \rangle$ is the mean square height of the surface roughness measured normal to the unperturbed surface), perturbation theory can be used to determine the diffuse scattering contribution due to the surface roughness (Rice 1951, Ruck et al. 1970). In this case σ_t can be approximated by its corresponding unperturbed value since the diffuse scattering contributions for large particles vanishes in the forward direction and the shadow boundary is practically unchanged. For the cases covered by the perturbation restriction ($\beta \ll 1$) however, the effects of surface roughness upon the specific intensities (Stokes parameters) is very small.

In this work, scattering by particles with very rough surfaces is considered ($10 > \beta > 1$) and perturbation theory cannot be used to determine the elements of the scattering matrix f_{ij} . Thus, the effects of surface roughness on the specific intensities cannot be ignored.

For the cases considered in this manuscript, the full wave approach (Bahar 1981) (which accounts for specular point scattering as well as diffuse scattering in a self-consistent manner) is used to determine the elements of the phase matrix $[S]$ as well as values for the total cross sections σ_t and the albedos for spherical particles with very rough surfaces. Thus the phase matrix for the rough particles (in the scattering plane) $[S']$ is expressed as a weighted sum of two matrices (Bahar and Fitzwater 1986)

$$[S'] = |\chi(\bar{v} \cdot \bar{a}_r)|^2 [S_{Mie}] + [S_R] \quad , \quad (2.5)$$

in which χ is the characteristic function for the rough surface height h measured along the normal ($\bar{n} = \bar{a}_r$) to the unperturbed (spherical) surface of the particle. For surface height probability density functions that are Gaussian

$$|\chi(v_r)|^2 = \exp[-(v_r^2 \langle h^2 \rangle)] \quad (2.6a)$$

and

$$\bar{v} = k_0(\bar{n}^f - \bar{n}^i), \quad v_r = \bar{v} \cdot \bar{a}_r \quad (2.6b)$$

The elements of the matrix S_{Mie} are determined by the Mie solutions for f_{ij} for a smooth spherical particle and the diffuse scattering contributions $[S_R]$ due to the rough surface are given by the full wave solutions. It is assumed in this work that the correlation length τ_c of the surface roughness is smaller than the particle radius a and that $k_0 a > 15$. Thus the full wave solution (2.5) represents the degradation of the specular point contribution to scattering (since $|\chi|^2 < 1$) along with diffuse scattering $[S_R]$ that is due to the surface roughness. For very small surface roughness ($\beta \ll 1$), $|\chi|^2 \rightarrow 1$ and the diffuse scattering term reduces to Bragg scattering (Bahar and Chakrabarti 1985).

The problem of determining the total cross section σ_t also becomes more complicated as the surface roughness increases. It has been shown that for large particles ($k_0 a > 15$) the forward scattered "shadow forming wave is the same for all surfaces which have the same shadow line." (Morse and Feshbach 1953). Thus for small surface roughness ($\beta < 1$) the shadow line (that distinguishes the illuminated surfaces of the particle from the non-illuminated surface) is practically the same as that for the unperturbed sphere and the value for the total cross section is for all practical purposes unmodified for $\beta \ll 1$. However, as the value of β increases ($\beta > 1$), the shadow line becomes significantly distorted and σ_t cannot be approximated by the corresponding value for the unperturbed sphere. Furthermore, analytical expressions for the forward scattered, shadow forming waves $f_{ii}(\bar{n}^i, \bar{n}^i)$ are not readily obtained for particles with irregular shape (Scheurman 1980).

In the next section, expressions are derived for the total cross sections and the albedos for spherical particles with very rough surfaces,

making judicious use of the observation that the "shadow forming wave is the same for all surfaces which have the same shadow line" (Morse and Feshbach 1953) and physical implications of the "forward scattering theorem" (Born and Wolf 1964).

3. THE TOTAL CROSS SECTIONS AND ALBEDOS FOR SPHERICAL PARTICLES WITH ROUGH SURFACES

The albedos for particles with rough surfaces are given by

$$A = \sigma_S / \sigma_t = \sigma_S / (\sigma_S + \sigma_a) \quad , \quad (3.1)$$

in which σ_a is the normalized absorption cross section and σ_S is the normalized scattering cross section (per unit cross sectional area)

$$\begin{aligned} \sigma_S &= \frac{1}{\pi a^2} \int |\chi|^2 \sigma_M d\Omega + \frac{1}{4\pi} \int \sigma_R d\Omega \\ &\equiv \sigma_{S1} + \sigma_{S2} \quad , \end{aligned} \quad (3.2)$$

the rough surface height characteristic function is χ , and σ_M is the Mie solution for the differential scattering cross section (per unit solid angle) for the smooth (unperturbed) sphere (Ruck et al 1970, Ishimaru 1978). Thus

$$\sigma_{S1} = (k_0 a)^{-2} \int |\chi|^2 [|S_1(\theta)|^2 + |S_2(\theta)|^2] \sin\theta d\theta \quad . \quad (3.3)$$

Explicit expressions for the terms S_1 and S_2 in the Mie solution are given by Ishimaru (1978). Furthermore σ_R is the diffuse scattering contribution to the cross section. Thus

$$\sigma_{S2} = 0.25 \int (\sigma_R^{VV} + \sigma_R^{VH} + \sigma_R^{HV} + \sigma_R^{HH}) \sin\theta d\theta \quad , \quad (3.4)$$

in which σ_R^{PQ} ($P=V,H$) are the like and cross-polarized diffuse differential scattering contributions to the cross sections (Bahar and Chakrabarti 1985, Bahar and Fitzwater 1985). The above full wave solution represents a weighted sum of two cross sections. The first, σ_{S1} is the modified Mie solution. The degradation of the physical optics contribution is manifested by the factor $|\chi|^2 < 1$ in the integrand of σ_{S1} . The degradation of the physical

optics contribution due to the effects of the rough surface is accompanied by the diffuse scattering term. This term corresponds to Bragg scattering (as predicted by perturbation theory) for $\beta \ll 1$ (Rice 1951). When $B = 0$ (smooth sphere), σ_S reduces to the Mie solution and the integration with respect to the solid angle $d\Omega$ can be performed analytically (Ishimaru 1978).

In order to facilitate the solution of (3.1), it is rewritten as follows

$$A = \frac{\sigma_S}{\sigma_t} = \frac{\sigma_S}{\sigma_{to}} \frac{\sigma_{to}}{\sigma_t} = \frac{\sigma_S}{\sigma_{to}} \left(\frac{\sigma_{to}}{\sigma_t} \right)_{P.C.} \quad (3.5)$$

In (3.5) σ_{to} is the total cross section for the smooth particle. In (3.5) use has been made of the "forward scattering theorem" (making σ_t proportional to the forward scattered field) and the fact that for large particles ($ka > 1$), the forward scattered, shadow-forming wave is the same for all surfaces which have the same shadow line (Morse and Feshbach 1953). Thus the ratio (σ_{to}/σ_t) in (3.5) is approximated by the value of the ratio for perfectly conducting particles $(\sigma_{to}/\sigma_t)_{P.C.}$. Therefore, implicit in (3.5) is the approximation, that for conducting particles, the above ratio (related to the forward scattered field intensities that extinguish the incident fields in the forward direction) does not critically depend upon the conductivity of the particle. The expressions for σ_{to} and $(\sigma_{to})_{P.C.}$ are given by the corresponding Mie solutions (Ishimaru 1978) for finitely and perfectly conducting spherical particles. To obtain the value for $(\sigma_t)_{P.C.}$ use is made of the fact that

$$(\sigma_t)_{P.C.} = (\sigma_S)_{P.C.}, \quad (3.6)$$

where $(\sigma_S)_{P.C.}$ is the normalized scattering cross section for the perfectly conducting particle with the same rough surface as the one under consideration. Thus $(\sigma_S)_{P.C.}$ is given by (3.2) for the corresponding

perfectly conducting particle and (3.5) is evaluated as follows

$$A = \left(\frac{\sigma_S}{\sigma_{to}} \right) / \left(\frac{\sigma_S}{\sigma_{to}} \right)_{P.C.} = A_1/A_2 \quad (3.7)$$

Examine (3.7) for two limiting cases of particular interest. As the conductivity of the particle increases $A_1 \rightarrow A_2$ and $A \rightarrow 1$. Furthermore as $\beta \rightarrow 0$ (small roughness) $A_2 \rightarrow 1$ since $(\sigma_S)_{PC} = (\sigma_t)_{PC} + (\sigma_{to})_{PC}$ and $A \rightarrow A_1 = \sigma_S/\sigma_{to}$. As expected, the albedo approaches unity for highly conducting particles and approaches the corresponding value for smooth particles as $\beta \rightarrow 0$.

4. ILLUSTRATIVE EXAMPLES

For the illustrative examples considered in this work, the random rough surface height h is assumed to be homogeneous and isotropic. Thus, the surface height autocorrelation function $\langle h(\vec{r})h(\vec{r}') \rangle$ is only a function of the distance $r_d = |\vec{r} - \vec{r}'|$ measured along the surface of the (unperturbed) spherical particle of radius a . It is also assumed that the rough surface correlation length τ_c is smaller than the circumference of the particle. ($\tau_c = 2(\langle h^2 \rangle / \langle \sigma_s^2 \rangle)^{1/2}$).

The surface height spectral density function $W(v_T)$ (which is the Fourier transform of the autocorrelation function $\langle hh' \rangle$) is assumed to be

$$W(v_T) = 2C/\pi v_T^4 \quad v_d < v_T < v_c, \quad (4.1)$$

for the case presented in Table I. In this case, the roughness parameter $\beta = 4k_0^2 \langle h^2 \rangle$ is varied between 0 and 1. The value of the constant C in (4.1) is determined by the parameter β since the mean square height is

$$\langle h^2 \rangle = \frac{\pi}{2} \int_{v_d}^{v_c} W(v_T) v_T dv_T = \frac{C}{2} \left(\frac{1}{v_d^2} - \frac{1}{v_c^2} \right) \quad (4.2)$$

The upper bound of v_T is usually chosen such that $v_c \geq 2k_0$ since the spectral components $v_T > 2k_0$ do not contribute to Bragg scatter. The lower bound of v_T is $v_d = 2\pi/D$ such that the largest spectral component (in wavelengths) of the rough surface is equal to the particle diameter.

The values for v_d and v_c as well as the relative dielectric coefficient ϵ_r (aluminum Ehrenreich, et al., 1963) the diameter of the particle D and the wavelength of the incident excitation λ are given in Table I. The values of σ_{S1} , the modified physical optics contribution, σ_{S2} the diffuse scattering contribution (Bahar and Chakrabarti 1985), and the sum σ_S , the normalized scattering cross section, are given in Table I, together with the corresponding values for A_1 , A_2 and the albedo A . The total cross section $\sigma_t = \sigma_s / A$ is also given in Table I. If the diffuse scattering contribution σ_{S2} is neglected (Abdelazeez 1983) the value of the albedo is given by $A_{S1} = \sigma_{S1} / \sigma_{t0}$. This quantity is also shown in Table I.

The mean square slope of the rough surface with respect to the (unperturbed) spherical surface

$$\langle \sigma_s^2 \rangle = \frac{\pi}{2} \int_{v_d}^{v_c} W(v_T) v_T^3 dv_T = C \ln(v_c/v_d) \quad , \quad (4.3)$$

and the ratios of the correlation length to the circumference of the particle, $\tau_c / \pi D$, are also given in Table I. The surface height characteristic function χ

for a Gaussian height distribution and the values of the scattering and total cross sections for the unperturbed particle, σ_{S0} and σ_{t0} are also listed in Table I. In Figure 1, σ_{S1} and σ_{S2} and σ_S as functions of β are plotted. As β increases, the physical optics contribution σ_{S1} decreases while σ_{S2} , the diffuse scattering term, increases. Since as β increases, σ_S decreases more than σ_t decreases, the albedo also decreases as the roughness parameter increases (see Fig. 2). Thus the absorption cross section $\sigma_a = \sigma_t - \sigma_S$ increases slightly as β increases.

For the cases considered in Tables II, III and IV, the surface height spectral density function is given by

$$W(v_T) = \frac{2C}{\pi} \left[\frac{v_T}{v_T^2 + v_m^2} \right]^8 \quad (4.4)$$

Thus the corresponding expressions for the normalized surface height autocorrelation function $R = \langle hh' \rangle / \langle h^2 \rangle$ is

$$R(\xi) = \left[1 - \frac{3\xi^2}{8} + \frac{3\xi^4}{32} + \frac{\xi^6}{3072} \right] \xi K_1(\xi) + \left[\frac{1}{2} - \frac{\xi^2}{4} - \frac{\xi^4}{96} \right] \xi^2 K_0(\xi) \quad (4.5)$$

In (4.5) K_0 and K_1 are modified Bessel Functions of the second kind, of order zero and one respectively (Abramowitz and Stegun 1964) and the dimensionless argument is

$$\xi = v_m r_d \quad (4.6)$$

For the case considered in Table II, the mean square slope of the rough surface is $\langle \sigma_s^2 \rangle = 0.101$ and the roughness parameter β is varied from one to ten. Using the relationships between $\langle h^2 \rangle$ and $\langle \sigma_s^2 \rangle$ and $W(v_T)$, it follows that

$$\langle h^2 \rangle = C/210 v_m^6, \quad \langle \sigma_s^2 \rangle = C/84 v_m^4 \quad (4.7)$$

Thus the values of C and v_m are determined. Since $W(v_T)$ is maximum at $v_T = v_m$, an increase in v_m corresponds to an increase in the high frequency component of the surface roughness. In Table II, the values of the wavelength λ , the diameter D , the relative dielectric coefficient ϵ_r (aluminum) and the scattering and the total cross sections σ_{S0} and σ_{t0} for the smooth (unperturbed) particles are listed.

The values of σ_{S1} , σ_{S2} , σ_S , A_1 and A_2 together with the corresponding values for the albedo A and the total cross sections σ_t are given in Table II. Clearly it cannot be assumed that $\sigma_t = \sigma_{t0}$. Such an assumption would result in values for A greater than unity as the values of A_1 indicate.

In Fig. 3, plots of σ_{S1} , σ_{S2} and σ_S as functions of β are given.

while the corresponding values for A and σ_t are plotted in Fig. 4. Since for $\lambda = 10\mu$, aluminum is highly reflecting $|\epsilon_r| \gg 1$, the albedo A decreases only slightly as β increases. The absorption cross section σ_a increases very slightly with increasing β .

For the case presented in Table III, λ , D and ϵ_r and the form of the surface height spectral density function $W(v_m)$ (4.4) are the same as in the case presented in Table II. However, instead of maintaining a constant mean square slope $\langle \sigma_s^2 \rangle$, the location of the peak of the spectral density function $v_T = v_m$ is fixed ($v_m D = 4$ and $\tau_c / \pi D = 0.101$). Thus, as β is varied from 0 to 10, $\langle \sigma_s^2 \rangle$ also increases (see Table III). In Table III, the values for σ_{S1} , σ_{S2} , σ_S , A_1 , A_2 as well as for σ_t and A are given for $0 \leq \beta \leq 10$. Note that the last columns in Tables II and III are identical. In Figure 5, σ_{S1} , σ_{S2} and the sum σ_S are plotted as functions of β while σ_t and A are plotted as functions of β in Figure 6. There is a somewhat larger variation in σ_a as β increases when the mean square slope varies (Table III) than where the mean square slope is fixed (Table II). The variations in σ_t and A are more moderate for the cases presented in Tables II and III (where $|\epsilon_r|$ is very large) than for the case presented in Table I. Note also that for cases presented in Tables II and III, A varies more rapidly for small values of β and levels off for larger values of β .

The data presented in Tables II and III (and the corresponding figures) clearly indicate that while the scattering cross section σ_s depends primarily on the roughness parameter β , the absorption cross section $\sigma_a = \sigma_t - \sigma_s$ depends upon both β and the mean square slope $\langle \sigma_s^2 \rangle$. Thus for particles with the same value of β the absorption cross section σ_a increases (and the albedo decreases) as the mean square slope increases.

For the case presented in Table IV, the roughness parameter β is fixed at 10 and the quantity $v_m D$ is set equal to 4 as in Table III. However, since $\lambda = 10\mu$ and D/λ varies from 5 to 8 the mean square height is fixed ($\langle h^2 \rangle = 2.5/k_0^2$) but the mean square slope $\langle \sigma_s^2 \rangle$ varies (see Table III).

The material of the particle is a dissipative dielectric with $\epsilon_r = 1.5 - i8$.

The values of σ_{S1} , σ_{S2} , σ_S , σ_{S0} as well as σ_t , σ_{t0} , A and $A_0 = \sigma_{S0}/\sigma_{t0}$ are given in Table IV. In Figure 7, σ_{S1} , σ_{S2} , σ_S and σ_{S0} (the scattering cross section for the smooth particle) are plotted as functions of D/λ while σ_t , σ_{t0} , A and A_0 are plotted as functions of D/λ in Figure 8.

Note that while the plots for the scattering cross sections in Figure 7 are relatively flat, the values for σ_t and σ_{t0} (and therefore σ_a) decrease with increasing D/λ (they asymptotically approach 2 for very large D/λ).

The corresponding values of A and A_0 increase as D/λ increases; they also tend to level off as D/λ becomes large. Both the total cross sections, σ_t and albedo A , for the rough particles ($\beta = 10$) are smaller than the corresponding values, σ_{t0} and A_0 , for the smooth particles ($\beta = 0$).

5. CONCLUDING REMARKS

In the illustrative examples considered, it is shown that surface roughness results in a small but significant decrease in the values of the albedos of spherical particles. For particles made of aluminum, this effect is more pronounced at optical frequencies (0.555μ) (Table I) than at infrared frequencies (10μ) (Tables II, III and IV). The effects of varying the roughness parameter $\beta = 4k_0^2 \langle h^2 \rangle$, the mean square slope and the surface height spectral density function (varying v_m changes the location of the peak value of $W(v_m)$) have also been investigated in detail (Tables II and III). The effects of surface roughness on the extinction cross sections and the albedos of particles are also presented as functions of particle size (D/λ) (Table IV). Both aluminum particles (at 10μ and 0.555μ) and particles made of dissipative dielectric materials are considered.

On examining the results, it is clear that except for $\beta \ll 1$, the extinction cross sections for the rough particles cannot be approximated by the value of the extinction coefficient for the corresponding smooth

particle ($\beta \rightarrow 0$). In some cases this would lead to values greater than unity for the albedos (see Table II $A_1 = \sigma_S/\sigma_{to}$).

When the optical thickness of the layers with random distribution of particles is very small (compared to unity), several sharp windows of transmission may exist if the particles have smooth surfaces. These windows of transmission are blocked when the surface of the particle is very rough ($\beta = 10$).

Acknowledgments

This investigation was sponsored by the U.S. Army Research Office contract DAAG-29-82-K-0123. The authors also acknowledge the National Science Foundation Engineering Supercomputer Grant ECS 8515794/5. They wish to thank F.G. Ullman for reading the manuscript and C. Bohren for his suggestions. The manuscript was typed by Mrs. E. Everett.

References

1. Abdelazeez, M. K. (1983), "Wave Scattering from a Large Sphere with Rough Surface," IEEE Trans. Antennas Propag. AP-31, p. 375.
2. Abramowitz, M. and I. A. Stegun (1964), Handbook of Mathematical Functions with Formulas, Graphs, and Mathematical Tables, Appl. Math. Ser. 55, National Bureau of Standards, Washington, D. C.
3. Bahar, E. (1981), "Full Wave Solutions for the Depolarization of the Scattered Radiation Fields by Rough Surfaces of Arbitrary Slope," IEEE Trans. Antennas and Propag., AP-24, No. 3, May 1981, pp. 443-454.
4. Bahar, E. and S. Chakrabarti (1985), "Scattering and Depolarization by Large Conducting Spheres with Very Rough Surfaces," Applied Optics, Vol. 24, No. 12, p. 1820.
5. Bahar, E. and M. A. Fitzwater, (1983), "Backscatter Cross Sections for Randomly Oriented Metallic Flakes at Optical Frequencies--Full Wave Approach," Applied Optics, Vol. 22, pp. 3813-3819.
6. Bahar, E. and M. Fitzwater (1986), "Multiple Scattering by Finitely Conducting Particles with Random Rough Surfaces at Infrared and Optical Frequencies," Radio Science, in press.
7. Born, M. and E. Wolf (1964), Principles of Optics, Pergamon Press, New York.
8. Chandrasekhar, S. (1950), Radiative Transfer, Dover Publ., New York.

9. Chylek, Petr (1977a), "Depolarization of Electromagnetic Radiation Scattered by Nonspherical Particles," Opt. Soc. Am., Vol. 67, No. 2, pp. 175-178.
10. Chylek, Petr (1977b), "Extinction Cross Sections of Arbitrarily Shaped Randomly Oriented Nonspherical Particles," Opt. Soc. Am., Vol. 67, No. 10, pp. 1348-1350.
11. Ehrenreich, H., H.R. Philipp, and B. Segall (1963), "Optical Properties of Aluminum," Physical Review, Vol. 132, No. 5, pp. 1918-1922.
12. Greenberg, J.M. (1960), "Scattering by Nonspherical Particles," Journal of Applied Physics, Vol. 31, p. 82.
13. Ishimaru, A. (1978), Wave Propagation and Scattering in Random Media, Academic, New York.
14. Ishimaru, A. and R.L.-T. Cheung (1980), "Multiple Scattering Effects in Wave Propagation Due to Rain," Ann. Telecommun., Vol. 35, p. 373.
15. Kiehl, J.T., M.W. Ko, A. Mugnai and Petr Chylek (1980), Perturbation Approach to Light Scattering by Nonspherical Particles, chapter in Light Scattering by Irregular Shaped Particles (Editor D.W. Scheurman), Plenum Press, New York.
16. Morse, P.M., and H. Feshbach (1953), Methods of Theoretical Physics, McGraw-Hill, New York.
17. Rice, S.O. (1951), "Reflection of Electromagnetic Waves from a Slightly Rough Surface," Communication of Pure and Applied Math., Vol. 4, pp. 351-378.
18. Ruck, G.T., D.E. Barrick, W.D. Stuart and C.K. Krichbaum (1970), "Radar Cross Section Handbook", Plenum, New York.
19. Scheurman, D.W. (1980), Editor, Light Scattering by Irregular Shaped Particles, Plenum Press, New York.
20. Yeh, C. and K.K. Mei (1980), On the Scattering from Arbitrarily Shaped Inhomogeneous Particles, chapter in Light Scattering by Irregular Shaped Particles, (Editor D.W. Scheurman) Plenum Press, New York.

Table I. Extinction Cross Sections and Albedos
for Spheres with Rough Surfaces ($0 \leq \beta \leq 1$)

$$\begin{aligned}\sigma_{S0} &= 2.093 \quad (\beta=0) \\ \sigma_{t0} &= 2.237 \quad (\beta=0) \\ |\chi|^2 &= e^{-(\beta \cos^2 \theta_0^f / 2)}\end{aligned}$$

$\beta = 4k_0^2 h_s^2$	0.0	0.1	0.5	1.0
$\sigma_{S1} = \frac{1}{\pi a^2} \int \sigma_m \chi ^2 d\Omega$	2.093	2.048	1.892	1.746
$\sigma_{S2} = \frac{1}{4\pi} \int \sigma_R d\Omega$	0.0	0.04351	0.1891	0.3103
$\sigma_S = \sigma_{S1} + \sigma_{S2}$	2.093	2.091	2.081	2.056
A_1	0.9356	0.9348	0.9303	0.9190
A_2	1.0000	1.0002	0.9978	0.9874
$A = A_1/A_2$	0.9356	0.9346	0.9323	0.9307
$A_{S1} = \frac{\sigma_{S1}}{\sigma_{t0}}$	0.9356	0.9342	0.9191	0.8876
$\sigma_t = \sigma_S/A$	2.237	2.237	2.232	2.209
$\langle \sigma_s^2 \rangle$	0.0	0.0017	0.0086	0.0172

$$\lambda = 0.555\mu, \quad D = 20\lambda, \quad \epsilon_r = -40 - i12, \quad v_d = 2\pi/D, \quad v_c = 8\pi/\lambda = 4k_0$$

$$\tau_c/\pi D = 0.019 \quad W = \frac{2C}{\pi v_T} \quad v_d < v_T < v_c$$

Table II. Extinction Cross Sections and Albedos
for Spheres with Rough Surfaces ($1 \leq \beta \leq 10$)

$$\langle \sigma_s^2 \rangle = 0.101$$

$$\sigma_{S0} = 2.035 \quad (\beta=0)$$

$$\sigma_{t0} = 2.059 \quad (\beta=0)$$

$$|\chi|^2 = e^{-(\beta \cos^2 \theta_0^f/2)}$$

$\beta = 4k_0^2 \langle h_s^2 \rangle$	1	2	4	8	10
$\sigma_{S1} = \frac{1}{\pi a^2} \int \sigma_m \chi ^2 d\Omega$	1.659	1.451	1.246	1.095	1.057
$\sigma_{S2} = \frac{1}{4\pi} \int \sigma_R d\Omega$.4048	.6027	.7863	.9039	.9278
$\sigma_S = \sigma_{S1} + \sigma_{S2}$	2.064	2.053	2.033	1.999	1.985
$A_1 = \sigma_S / \sigma_{t0}$	1.003	.9974	.9874	.9711	.9641
$A_2 = (\sigma_S / \sigma_{t0})_{P.C.}$	1.020	1.015	1.006	.9915	.9844
$A = A_1 / A_2$.9833	.9825	.9814	.9794	.9794
$c_t = \sigma_S / A$	2.099	2.090	2.071	2.041	2.027
$v_{\pi} D$	12.60	8.92	6.32	4.48	4.00
$\tau_c / \pi D$	0.032	0.045	0.064	0.09	0.101

$$\lambda = 10\mu, \quad D = 5\lambda, \quad \epsilon_r = -6000 - 16000i$$

$$W = \frac{2C}{\pi} \left[\frac{v_T}{v_T^2 + v_m^2} \right]^8$$

Table III. Extinction Cross Sections and Albedos
for Spheres with Rough Surfaces ($0 \leq \beta \leq 10$)

$$v_m D = 4$$

$$\sigma_{S0} = 2.035 \quad (\beta=0)$$

$$\sigma_{t0} = 2.059 \quad (\beta=0)$$

$$|\chi|^2 = e^{-(\beta \cos^2 \theta_o^f / 2)}$$

$\beta = 4k_o^2 \langle h_s^2 \rangle$	0	1	2	4	8	10
$\sigma_{S1} = \frac{1}{\pi a^2} \int \sigma_m \chi ^2 d\Omega$	2.035	1.659	1.451	1.246	1.095	1.057
$\sigma_{S2} = \frac{1}{4\pi} \int \sigma_R d\Omega$	0	.3654	.5658	.7581	.8944	.9278
$\sigma_S = \sigma_{S1} + \sigma_{S2}$	2.035	2.025	2.017	2.004	1.990	1.985
$A_1 = \sigma_S / \sigma_{t0}$.9885	.9835	.9795	.9737	.9665	.9641
$A_2 = (\sigma_S / \sigma_{t0})_{P.C.}$	1.000	.9961	.9932	.9891	.9852	.9844
$A = A_1 / A_2$.9885	.9873	.9863	.9844	.9810	.9794
$\sigma_t = \sigma_S / A$	2.059	2.051	2.045	2.036	2.028	2.027
$\langle \sigma_s^2 \rangle$	0	.010	.020	.041	.081	.101

$$\lambda = 10\mu, \quad D = 5\lambda, \quad \epsilon_r = -6000 - 16000i, \quad \tau_c / \pi D = 0.101$$

$$W = \frac{2C}{\pi} \left[\frac{v_T}{v_T^2 + v_m^2} \right]^8$$

Table IV. Extinction Cross Sections and Albedos
for Spheres with Rough Surfaces ($5\lambda \leq D \leq 8\lambda$)

$$v_m D = 4$$

D/λ	5	5.5	6	6.5	7	7.5	8
$\sigma_{S1} = \frac{1}{\pi a^2} \int \sigma_m \chi ^2 d\Omega$	1.116	1.118	1.119	1.120	1.120	1.120	1.120
$\sigma_{S2} = \frac{1}{4\pi} \int \sigma_R d\Omega$.2942	.2973	.3000	.3023	.3043	.3060	.3075
$\sigma_S = \sigma_{S1} + \sigma_{S2}$	1.410	1.415	1.419	1.422	1.424	1.426	1.427
σ_S	1.525	1.518	1.513	1.507	1.503	1.499	1.495
$A_1 = \sigma_S / \sigma_{to}$.5959	.6022	.6084	.6137	.6184	.6224	.6261
$A_2 = (\sigma_S / \sigma_{to})_{P.C.}$.9844	.9843	.9845	.9848	.9852	.9856	.9861
$A = A_1 / A_2$.6043	.6118	.6179	.6232	.6276	.6315	.6349
$\sigma_t = \sigma_S / A$	2.333	2.313	2.296	2.282	2.269	2.258	2.248
$A_o = \sigma_{So} / \sigma_{to}$.6434	.6462	.6486	.6507	.6526	.6543	.6558
σ_{to}	2.370	2.350	2.332	2.317	2.303	2.290	2.279
$\langle \sigma_s^2 \rangle$.101	.0837	.0704	.0600	.0517	.0450	.0396

$$\tau_c / \pi D = 0.1, \quad \lambda = 10\mu, \quad \epsilon_r = 1.5 - i8, \quad \beta = 10$$

$$W = \frac{2C}{\pi} \left[\frac{v_T}{v_T^2 + v_m^2} \right]^8$$

Figure Captions

- Figure 1. Scattering cross sections σ_{S1} , σ_{S2} , and σ_S versus β (roughness parameter) (Table I).
- Figure 2. Extinction cross section σ_t , σ_{to} , albedos A and A_1 versus β (roughness parameter) (Table I).
- Figure 3. Scattering cross sections σ_{S1} , σ_{S2} , and σ_S versus β (roughness parameter) (Table II).
- Figure 4. Extinction cross section σ_t and albedo A versus β (roughness parameter) (Table II).
- Figure 5. Scattering cross sections σ_{S1} , σ_{S2} , and σ_S versus β (roughness parameter) (Table III).
- Figure 6. Extinction cross section σ_t and albedo A versus β (roughness parameter) (Table III).
- Figure 7. Scattering cross section σ_{S1} , σ_{S2} , σ_S , and σ_{So} versus D/λ (Table IV).
- Figure 8. Extinction cross section σ_t , σ_{to} , albedos A and A_o versus D/λ (Table IV).

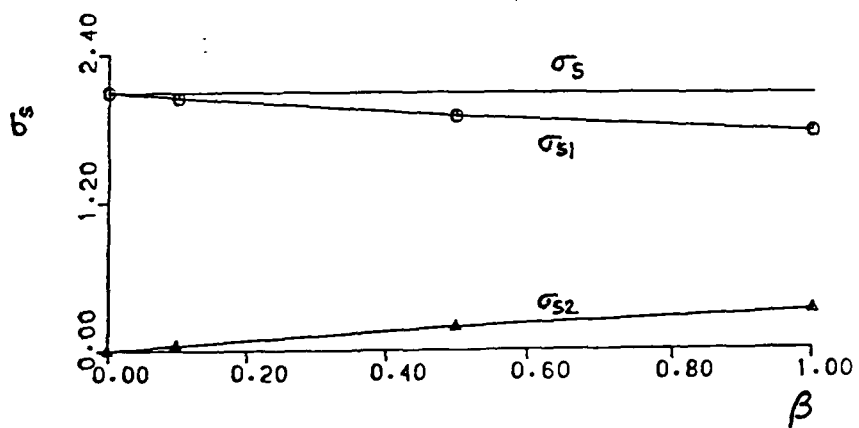


Figure 1.

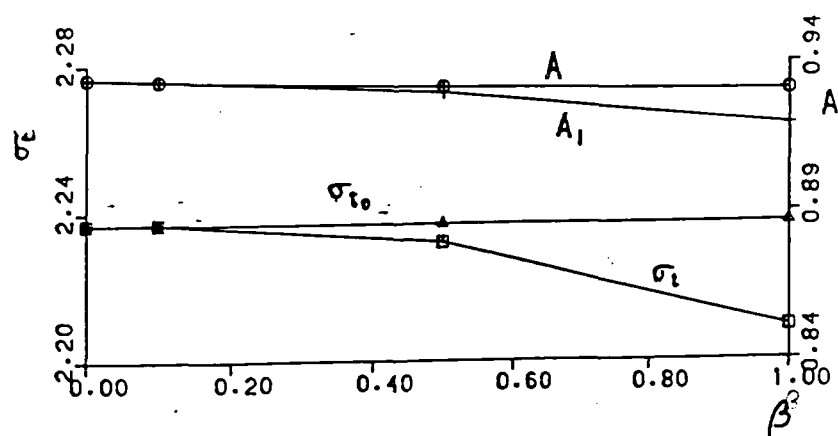


Figure 2.

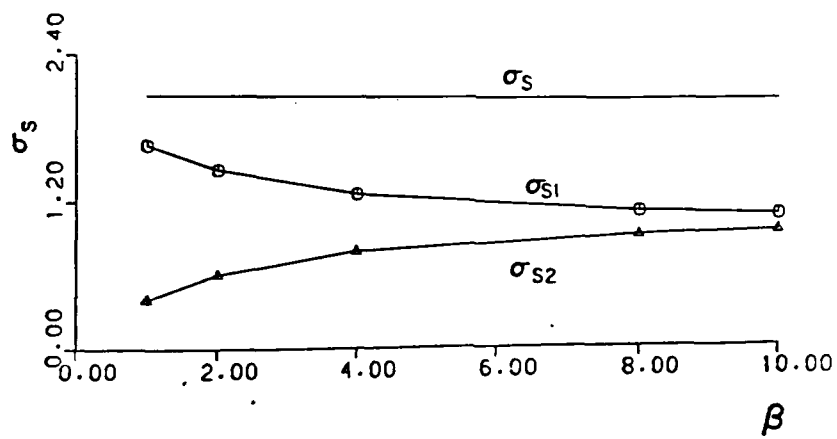
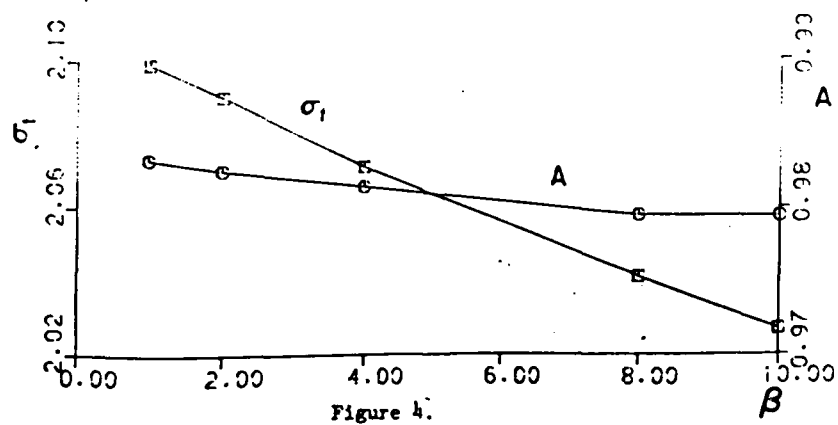


Figure 3.



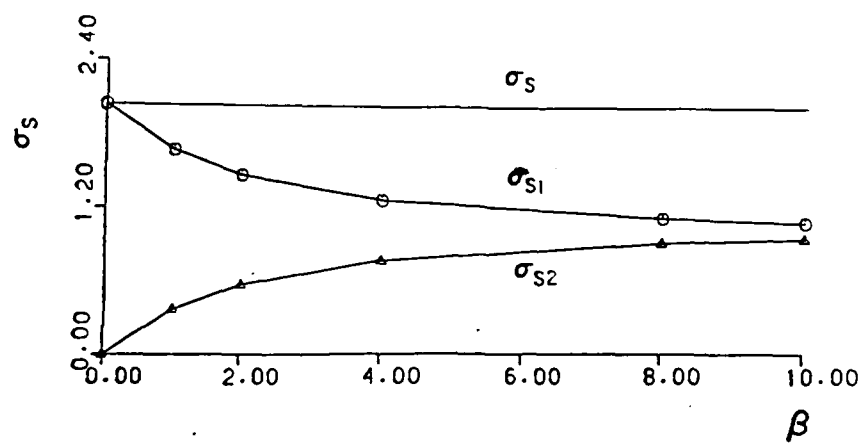


Figure 5.

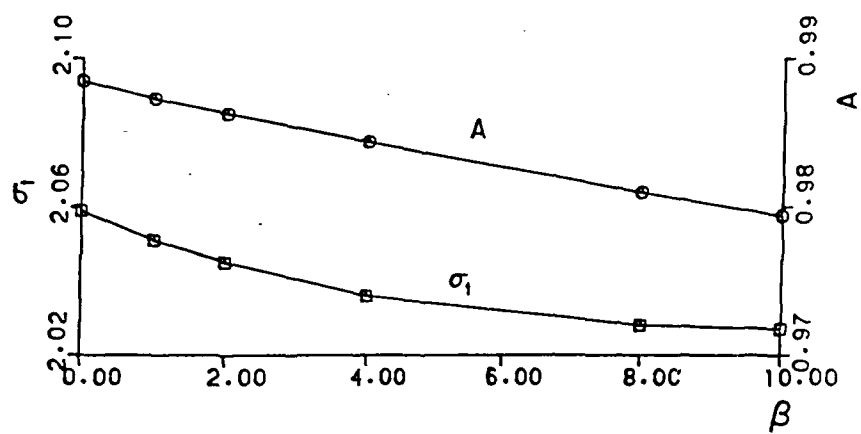


Figure 6.

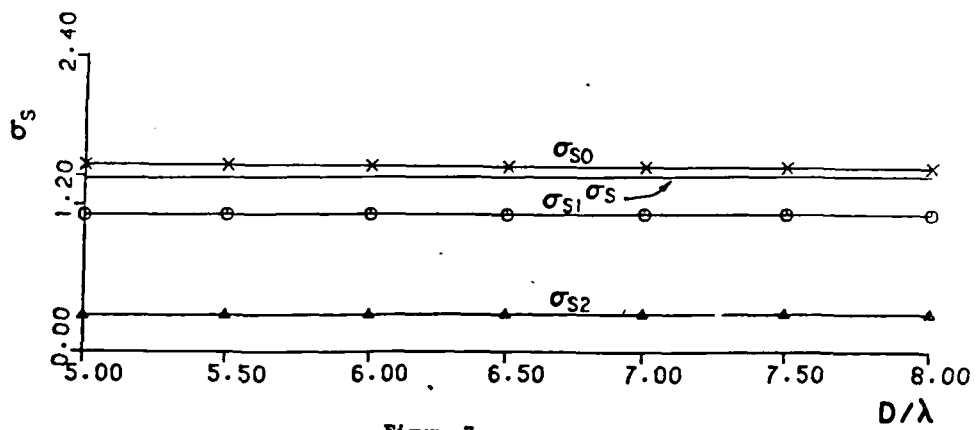


Figure 7.

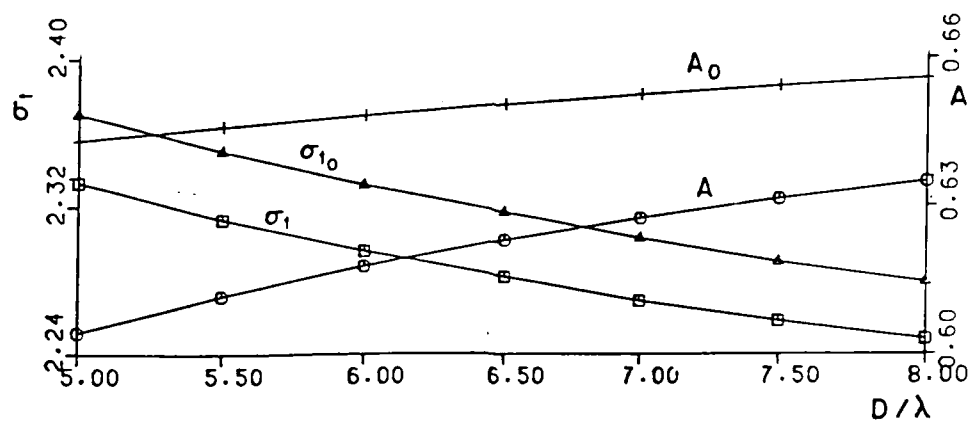


Figure 8.

CO-POLARIZED AND CROSS-POLARIZED INCOHERENT SPECIFIC
INTENSITIES FOR WAVES AT OBLIQUE INCIDENCE UPON LAYERS
OF FINITELY CONDUCTING PARTICLES OF IRREGULAR SHAPE

Ezekiel Bahar
and
Mary Ann Fitzwater

Electrical Engineering Department
University of Nebraska-Lincoln
Lincoln, Nebraska 68588-0511

ABSTRACT

Optical and infrared electromagnetic scattering and depolarization by layers of randomly distributed particles of irregular shape and finite conductivity are determined through the use of the equation of transfer. The irregular shaped particles are characterized by their random rough surface height spectral density function or autocorrelation function.

The extinction cross section and the elements of the scattering matrix in the equation of transfer are evaluated using a full wave approach which accounts for specular point and diffuse scattering in a self-consistent manner. Both single scatter and multiple scatter incoherent specific intensities are evaluated for particles with smooth and rough surfaces.

1. INTRODUCTION

Optical and infrared electromagnetic scattering and depolarization by random distributions of particles of irregular shape and finite conductivity are determined by solving the equation of transfer (Chandrasekar 1950, Ishimaru 1978). In this work excitations of both vertically and horizontally polarized waves obliquely incident upon parallel layers of particles are considered. The irregular shaped particles are characterized by their random rough surface height spectral density function W or its Fourier transform the rough surface height autocorrelation function $\langle hh' \rangle$.

The full wave approach (Bahar and Fitzwater 1983, 1985; Bahar and Chakrabarti 1985) which accounts for specular point scattering as well as diffuse scattering in a self-consistent manner is used to evaluate the elements of the scattering matrix and the extinction cross section (Bahar et al. 1986) that appear in the equation of transfer. The equation of transfer is solved for the incoherent specific intensities using Gaussian quadrature and the matrix characteristic value techniques (Ishimaru et al. 1982). Both single scatter as well as multiple scatter results for the co-polarized and cross-polarized incoherent specific intensities are presented for particles with smooth as well as rough surfaces. Thus the effects of particle surface roughness upon the co-polarized and cross-polarized intensities are investigated in detail. Special consideration is given to the degree of polarization of the incoherent specific intensities (modified Stokes parameters).

2. FORMULATION OF THE PROBLEM

In this section, we formulate the solution for the incoherent diffuse specific intensity matrix $[I]$. The elements of the matrix $[I]$ are the modified Stokes parameters (Chandrasekhar 1950, Ishimaru 1978)

$$[I] = \begin{bmatrix} I_1 \\ I_2 \\ U \\ V \end{bmatrix} = \begin{bmatrix} \langle E_1 E_1^* \rangle \\ \langle E_2 E_2^* \rangle \\ 2\text{Re}\langle E_1 E_2^* \rangle \\ 2\text{Im}\langle E_1 E_2^* \rangle \end{bmatrix} \quad (2.1)$$

in which the symbol $\langle \cdot \rangle$ denotes the statistical average and $*$ denotes the complex conjugate (a suppressed $\exp(i\omega t)$ time dependent excitation is assumed). The vertically and horizontally polarized components of the electric field are E_1 and E_2 respectively. A linearly polarized electromagnetic wave is assumed to be obliquely incident upon a parallel layer of randomly distributed particles of finite conductivity and irregular shape. Specifically, in this work the particles are assumed to be spheres whose surfaces are randomly perturbed (see Fig. 1). Thus if h is the random surface height of the particle measured normal to the unperturbed sphere of radius a , the radius vector to the surface of the irregular shaped particle is

$$\bar{r}_s = (a + h)\bar{a}_r \quad (2.2)$$

in which \bar{a}_r is the unit radius vector. The mean square height of the rough surface $\langle h^2 \rangle$ is assumed to be such that the roughness parameter $\beta = 4k_0^2 \langle h^2 \rangle$ (where k_0 is the free space wavenumber) is large ($1 < \beta < 40$). Thus the small perturbation method (Rice

1951; Ruck et al. 1970; Kiehl et al. 1980) cannot be used to analyze the scattering by the very rough particles considered. The small perturbation method is restricted to particles with small roughness parameters $\beta \leq 0.1$, for which the incoherent diffuse specific intensities are not significantly different from those for the corresponding smooth (spherical) particles. Theoretical and experimental techniques used in the study of scattering and absorption by irregular shaped particles have been presented in the proceedings on the workshop on light scattering (Scheurman 1980). A survey of analytical and numerical techniques including their pros and cons has been presented by Yeh and Mie (1980).

The full wave method that accounts for specular point scattering and diffuse scattering in a unified, self-consistent manner has been used in this work to determine the scattering and depolarization by particles with rough surfaces (Bahar and Fitzwater 1983; Bahar and Chakrabarti 1985). The random rough surface height h is characterized by its surface height spectral density function W or its Fourier transform, the surface height autocorrelation function $\langle hh' \rangle$.

The incoherent diffuse specific intensity matrix $[I]$ satisfies the equation of transfer (Chandrasekhar 1950; Ishimaru 1978)

$$\mu \frac{d[I]}{d\tau} = -[I] + \int [S][I'] d\mu d\phi + [I_i] \quad (2.3)$$

in which τ is the optical distance in the z direction (normal to the plane of the slab, see Fig. 2).

$$\tau = z\rho[\sigma_t] \equiv z\int \sigma_t n(D) dD \quad (2.4)$$

where D is the diameter of the unperturbed spherical particle, $n(D)$ is the particle size distribution and σ_t is the total cross section (extinction coefficient). The symbol $\rho[\cdot]$ denotes integration over the size distribution. The effects of the particle surface roughness (which is assumed to be isotropic and homogeneous) are vanishingly small in the forward direction, thus the extinction matrix (Ishimaru and Cheung 1980; Cheung and Ishimaru 1982) for the particle with the rough surface can be represented by a scalar quantity. The matrices $[I]$ and $[I']$ are the incoherent diffuse intensities for waves scattered by the particles in the direction $\theta = \cos^{-1}\mu$ and ϕ and for waves incident in the direction $\theta' = \cos^{-1}\mu'$ and ϕ' respectively. The (4×4) scattering (phase) matrix $[S]$ in the reference coordinate system is expressed in terms of the scattering matrix $[S']$ in the scattering plane (that contains the incident and scatter wave normals \tilde{n}^i and \tilde{n}^f respectively, see Fig. 2) through the following transformation

$$[S] = \mathcal{L}(-\pi + \alpha)[S']\mathcal{L}(\alpha') \quad (2.5)$$

in which $[S']$ is the weighted sum of two matrices

$$[S'] = |\chi(\tilde{v} \cdot \tilde{a}_r)|^2 [S_{Mie}] + [S_D] \quad (2.6)$$

In (2.6) $[S_{Mie}]$ is given by

$$[S_{Mie}] = \frac{1}{\rho[\sigma_t]} \times \begin{bmatrix} \rho[|f_{11}|^2] & \rho[|f_{12}|^2] & \rho\text{Re}[f_{11}f_{12}^*] & -\rho\text{Im}[f_{11}f_{12}^*] \\ \rho[|f_{21}|^2] & \rho[|f_{22}|^2] & \rho\text{Re}[f_{21}f_{22}^*] & -\rho\text{Im}[f_{21}f_{22}^*] \\ \rho 2\text{Re}[f_{11}f_{21}^*] & \rho 2\text{Re}[f_{12}f_{22}^*] & \rho\text{Re}[f_{11}f_{22}^* + f_{12}f_{21}^*] & \rho\text{Re}[f_{11}f_{22}^* - f_{12}f_{21}^*] \\ \rho 2\text{Im}[f_{11}f_{21}^*] & \rho 2\text{Im}[f_{12}f_{22}^*] & \rho\text{Im}[f_{11}f_{22}^* + f_{12}f_{21}^*] & \rho\text{Im}[f_{11}f_{22}^* - f_{12}f_{21}^*] \end{bmatrix} \quad (2.7)$$

where f_{ij} are elements of the 2x2 scattering matrix for the unperturbed (spherical) particle

$$\begin{bmatrix} E_l \\ E_r \end{bmatrix} = \begin{bmatrix} f_{11} & f_{12} \\ f_{21} & f_{22} \end{bmatrix} \begin{bmatrix} E'_l \\ E'_r \end{bmatrix} \frac{\exp(-ik_o r)}{r} \quad (2.8)$$

In (2.8) E'_l , E'_r and E_l , E_r are the incident and scattered vertically and horizontally polarized electric field components in the scattering plane and r is the distance to the field point from the center of the spherical particle. For a smooth sphere f_{ij} are given by the Mie solution (Ruck et al. 1970; Ishimaru 1978) and $[f]$ is a diagonal matrix. The transformation matrices $[L]$ in (2.5) are given in terms of the angle α' between the reference plane of incidence and the scattering plane and the angle α between the scattering plane and the reference plane of scatter (see Fig. 2)

$$[L(\alpha)] = \begin{bmatrix} \cos^2 \alpha & \sin^2 \alpha & \frac{1}{2} \sin 2\alpha & 0 \\ \sin^2 \alpha & \cos^2 \alpha & -\frac{1}{2} \sin 2\alpha & 0 \\ -\sin 2\alpha & \sin 2\alpha & \cos 2\alpha & 0 \\ 0 & 0 & 0 & 1 \end{bmatrix} \quad (2.9)$$

The quantity χ in (2.6) is the particle random rough surface characteristic function.

$$\chi(\bar{v} \cdot \bar{a}_r) = \langle \exp(i\bar{v} \cdot \bar{a}_r h) \rangle \quad (2.10)$$

in which

$$\bar{v} = k_o (\bar{n}^f - \bar{n}^i) \quad (2.11)$$

Thus the coefficient $|\chi|^2$ in (2.6) accounts for the degradation of the specular point contributions to the scattered fields by the rough surface ($|\chi|^2 \leq 1$ and as $\beta \rightarrow 0$ $|\chi|^2 \rightarrow 1$). The diffuse

scattering contribution to the matrix S' due to the particle rough surface is given by

$$[S_D] = \begin{bmatrix} [S_{11}^D] & [S_{12}^D] & 0 & 0 \\ [S_{21}^D] & [S_{22}^D] & 0 & 0 \\ 0 & 0 & [S_{33}^D] & [S_{34}^D] \\ 0 & 0 & [S_{43}^D] & [S_{44}^D] \end{bmatrix} \quad (2.12)$$

where

$$[S_{ij}^D] = \frac{A_y}{4\pi\rho[\sigma_t]} \rho \langle \sigma^{ij} \rangle_D, \quad \text{for } i, j = 1, 2 \quad (2.13)$$

in which $A_y = \pi a^2$ is the average cross sectional area of the unperturbed particle and $\langle \sigma^{ij} \rangle_D$ are the full wave solutions for the like ($i=j$) and cross polarized ($i \neq j$) scattering cross sections (Bahar and Fitzwater 1983, Bahar and Chakrabarti 1985). The first and second superscripts i, j denote the polarizations (V vertical and H horizontal) of the scattered and incident waves respectively

$$\langle \sigma^{ij} \rangle_D = \int_0^{2\pi} \int_0^\pi |k_o^D{}^{ij}|^2 P_2 Q \sin\gamma d\gamma d\delta / \pi^2 \quad (2.14)$$

where

$$Q = \int_{-\infty}^{\infty} (\chi_2(\bar{v} \cdot \bar{a}_r) - |\chi(\bar{v} \cdot \bar{a}_r)|^2) \exp(i\bar{v} \cdot \bar{r}_d) dx_d dz_d \quad (2.15)$$

Since the rough surface height h is assumed to be isotropic and homogeneous, the surface height autocorrelation function $\langle hh' \rangle$ and the joint characteristic function χ_2 are only functions of the distance $r_d = (x_d^2 + z_d^2)^{1/2}$ measured along the surface of the unperturbed sphere. For rough surface heights with Gaussian distributions

$$|\chi(\vec{v} \cdot \vec{a}_r)|^2 = \exp[-(\vec{v} \cdot \vec{a}_r)^2 \langle h^2 \rangle] \quad (2.16)$$

and

$$\chi_2(\vec{v} \cdot \vec{a}_r) = \langle \exp i \vec{v} \cdot \vec{a}_r (h-h') \rangle = \exp[(\vec{v} \cdot \vec{a}_r)^2 \langle hh \rangle] |\chi(\vec{v} \cdot \vec{a}_r)|^2 \quad (2.17)$$

In (2.15) it is assumed that the surface height correlation length r_c is small compared to the particle circumference πD .

For $i = 3$ and 4

$$[S_{ii}^D] = \rho [\text{Re}[\langle \sigma_{22}^{11} \rangle_D \pm \langle \sigma_{21}^{12} \rangle_D]] A_y / 4\pi \rho [\sigma_t] \quad (2.18)$$

(upper and lower signs for $i = 3$ and 4 respectively). For $i \neq j$

$$[S_{ij}^D] = \rho [\text{Im}[\pm \langle \sigma_{22}^{11} \rangle_D + \langle \sigma_{21}^{12} \rangle_D]] A_y / 4\pi \rho [\sigma_t] \quad (2.19)$$

(upper sign for $i = 4, j = 3$ and lower sign for $i = 3, j = 4$ respectively).

In the above expressions

$$\langle \sigma_{kl}^{ij} \rangle = \int_0^{2\pi} \int_0^\pi k_0^2 D^{ij} D^{kl*} P_2 Q \sin \gamma d\gamma d\delta / \pi^2 \quad (2.20)$$

In (2.14) and (2.20), P_2 , the shadow function, is the probability that a point on the surface of the particle is both illuminated and visible given the slope of the surface at the given point (Sancer 1964). The scattering coefficients D^{ij} are functions of \vec{n}^i, \vec{n}^f and \vec{n} the normal to the unperturbed surface of the particle as well as its electromagnetic parameters ϵ, μ . The remaining eight terms of the matrix $[S_D]$ vanish since D^{ii} and D^{ij} ($i \neq j$) are symmetric and antisymmetric respectively with respect to δ the azimuth angle for the sphere.

In this work it is assumed that a linearly polarized wave (vertical or horizontal) is obliquely incident upon a parallel layer

of optical thickness τ_0 containing a random distribution of particles with rough surfaces. The incident Stokes matrix at $z = 0$ is (see Fig. 2)

$$[I_{inc}] = I_O^P \delta(\mu' - \mu^i) \delta(\phi') \quad (2.21)$$

in which $\mu^i = \cos \theta^i$, the direction of the incident wave is $(\theta^i, 0)$ and

$$I_O^V = \begin{bmatrix} 1 \\ 0 \\ 0 \\ 0 \end{bmatrix} \quad \text{and} \quad I_O^H = \begin{bmatrix} 0 \\ 1 \\ 0 \\ 0 \end{bmatrix} \quad (2.22)$$

for $P = V$ (vertical) and $P = H$ (horizontal). In (2.21) $\delta(\cdot)$ is the Dirac delta function. Thus the reduced incident intensity is

$$[I_{ri}] = [I_{inc}] \exp(-\tau/\mu^i) \quad (2.23)$$

and the (4×1) excitation matrix (2.3) is

$$[I_i] = \int [S][I_{ri}] d\mu' d\phi' \equiv [F] \exp(-\tau/\mu^i) \quad (2.24)$$

in which the (4×1) matrix $[F]$ is

$$[F] = [S][I_O^P] \Big|_{\substack{\mu' = \mu^i \\ \phi' = 0}} \quad (2.25)$$

and the matrix $[I_O^P]$ is defined in (2.22). The matrix $[F]$ can be expressed as a Fourier series (Ishimaru et al. 1982)

$$[F] = \sum_{m=0}^{\infty} [F]_m^a \cos m\phi + \sum_{m=1}^{\infty} [F]_m^b \sin m\phi \quad (2.26)$$

in which

$$[F]_m^a = \begin{bmatrix} F_{m1} \\ F_{m2} \\ 0 \\ 0 \end{bmatrix}, \quad [F]_m^b = \begin{bmatrix} 0 \\ 0 \\ F_{m3} \\ F_{m4} \end{bmatrix} \quad (2.27)$$

For normally incident ($\theta^i=0$) linearly polarized waves, the terms $m=0$ and $m=2$ are the only non-vanishing terms and for normally incident circularly polarized waves the only non-vanishing term is $m=0$. However, for the obliquely incident linearly polarized waves considered in this work, the number of terms of the infinite series needed to be considered depends on the desired accuracy of the numerical results (see Section 3).

From (2.26) it follows that

$$[F]_0^a = \frac{1}{2\pi} \int_0^{2\pi} [F] d\phi \quad (2.28a)$$

and for $m \geq 1$

$$[F]_m^a = \frac{1}{\pi} \int_0^{2\pi} [F] \cos m\phi d\phi, [F]_m^b = \frac{1}{\pi} \int_0^{2\pi} [F] \sin m\phi d\phi \quad (2.28b)$$

The incoherent specific intensity matrix $[I]$ can also be expressed in terms of the Fourier series

$$[I] = \sum_{m=0}^{\infty} [I]_m^a \cos m\phi + \sum_{m=1}^{\infty} [I]_m^b \sin m\phi \quad (2.29)$$

Since the elements of the scattering matrix $[S]$ are functions of $\phi' - \phi$ it is expressed as follows

$$[S] = \frac{1}{2\pi} [S]_0^a + \frac{1}{\pi} \sum_{m=1}^{\infty} \left[[S]_m^a \cos(\phi' - \phi) + [S]_m^b \sin(\phi' - \phi) \right] \quad (2.30)$$

Furthermore, for the rough sphere f_{ii} are even functions and f_{ij} ($i \neq j$) are odd functions of $\phi' - \phi$, for $m=0,1,2 \dots$, thus

$$[S]_m^a = \begin{bmatrix} [S_1]_m^a & 0 \\ 0 & [S_4]_m^a \end{bmatrix}, [S]_m^b = \begin{bmatrix} 0 & [S_2]_m^b \\ [S_3]_m^b & 0 \end{bmatrix} \quad (2.31)$$

where

$$[S_1]_m^a, [S_4]_m^a, [S_2]_m^b \text{ and } [S_3]_m^b \quad (2.32)$$

are (2x2) matrices given by

$$[S_i]_m^a = \int_0^{2\pi} [S_i] \cos m(\phi' - \phi) d(\phi' - \phi) \quad , i=1,4 \quad , \quad (2.32a)$$

$$[S_i]_m^b = \int_0^{2\pi} [S_i] \sin m(\phi' - \phi) d(\phi' - \phi) \quad , i=2,3 \quad (2.32b)$$

and $[S_i]$ are the (2x2) matrices defined by

$$[S] = \begin{bmatrix} [S_1] & [S_2] \\ [S_3] & [S_4] \end{bmatrix} \quad (2.33)$$

It therefore follows that the first two elements of the Stokes matrix, I_1 and I_2 , are even functions of $\phi' - \phi$ while the last two elements, U and V , are odd functions of $\phi' - \phi$ (Ishimaru et al. 1982).

Thus for $m=0,1,2 \dots$

$$[I]_m^a = \begin{bmatrix} I_{m1} \\ I_{m2} \\ 0 \\ 0 \end{bmatrix} \quad \text{and} \quad [I]_m^b = \begin{bmatrix} 0 \\ 0 \\ U_m \\ V_m \end{bmatrix} \quad \text{where} \quad [I]_0^b = [0] \quad (2.34)$$

The equation of transfer for each of the Fourier components can be written as follows

$$\mu \frac{d}{d\tau} [I]_m = -[I]_m + \int_{-1}^1 [S]_m [I']_m d\mu' + [F]_m \exp(-\tau/\mu^i) \quad (2.35)$$

in which

$$[I]_m = [I]_m^a + [I]_m^b, \quad [F]_m = [F]_m^a + [F]_m^b \quad (2.36)$$

and

$$[S]_m = \begin{bmatrix} [S_1]_m^a & [S_2]_m^b \\ -[S_3]_m^b & [S_4]_m^a \end{bmatrix} \quad (2.37)$$

Note that since $[I]_0^b = [0]$, $[S_i]_0^b = [0]$ ($i=2,3$) and $[F]_0^b = [0]$ the last two elements of the matrix equation (2.35) vanish for the case $m=0$.

The boundary conditions for the Stokes matrix $[I]$ are

$$[I]_m = 0 \quad \text{for } 0 \leq \mu \leq 1 \quad \text{at } \tau = 0 \quad (2.38a)$$

and

$$[I]_m = 0 \quad \text{for } 0 \geq \mu \geq -1 \quad \text{at } \tau = \tau_0 \quad (2.38b)$$

Equation (2.35) together with the associated boundary conditions (2.38) are solved for $[I]_m$ using the Gaussian quadrature method (to discretize the angle θ) and the matrix characteristic value technique (Ishimaru 1978).

It is also necessary to determine the extinction coefficient (total cross section) σ_t in order to solve the equation of transfer (2.3). When "equivalent" spheres do not reasonably represent the basic scattering characteristics of irregular shaped particles, Greenberg has developed experimental microwave techniques to determine the albedos of particles for which no theoretical method existed (Greenberg 1960, Chylek 1977, Scheurman 1980). In this work the full wave approach (which unlike the small perturbation method is not restricted to small values of β) is used to evaluate σ_t (Bahar et al. 1986) by making judicious use of the forward scattering theorem (Born and Wolf 1964) and the very perceptive observation that for large scatterers (compared to wavelength) the forward scatter "shadow forming wave is the same for all surfaces which have the same shadow line" (Morse and Feshbach 1953).

The diffuse specific scattering intensities I_1 and I_2 correspond to vertically polarized (E_θ) and horizontally polarized (E_ϕ) waves respectively. In practice, however, the polarization of the receiver is either parallel (E_x) or perpendicular (E_y) to the polarization of the incident wave. The corresponding diffuse specific intensities I_x and I_y are the co-polarized and cross polarized incoherent specific intensities (Cheung and Ishimaru 1982). They are obtained from I_1 and I_2 through a linear transformation.

The degree of polarization m of the scattered wave is (Ishimaru 1978),

$$m = \frac{[(I_1 - I_2)^2 + U^2 + V^2]^{\frac{1}{2}}}{I_1 + I_2} \leq 1 \quad (2.39)$$

3. ILLUSTRATIVE EXAMPLES

For the illustrative examples considered in this work, the particle random rough surface height h (measured normal to the unperturbed surface) is assumed to be homogeneous and isotropic and the unperturbed surface is assumed to be spherical (2.2). Thus, the rough surface height autocorrelation function $\langle h(\vec{r})h(\vec{r}') \rangle$ is only a function of the distance $r_d = |\vec{r} - \vec{r}'| = (x_d^2 + z_d^2)^{\frac{1}{2}}$ measured along the surface of the (unperturbed) spherical particle of radius a . It is also assumed that the rough surface correlation distance r_c (where $\langle hh' \rangle + \langle h^2 \rangle \exp(-1)$) is smaller than the circumference of the particle. The correlation length is related to the mean square height $\langle h^2 \rangle$ and the total mean square slope

$\langle \sigma_s^2 \rangle$ through the expression

$$r_c = 2(\langle h^2 \rangle / \langle \sigma_s^2 \rangle)^{1/2} \quad (3.1)$$

The surface height spectral density function $W(v_x, v_z)$ is the two dimensional Fourier transform of the surface height autocorrelation function $\langle hh' \rangle$. Since the rough surface is assumed to be homogeneous and isotropic the spectral density function is only a function of

$$v_T = (v_x^2 + v_z^2)^{1/2} \quad (3.2)$$

Thus

$$\begin{aligned} W(v_x, v_z) &= \frac{1}{\pi^2} \int_{-\infty}^{\infty} \langle hh' \rangle \exp(i v_x x_d + i v_z z_d) dx_d dz_d \\ &= \frac{2}{\pi} \int_0^{\infty} \langle hh' \rangle J_0(v_T r_d) r_d dr_d \end{aligned} \quad (3.3)$$

in which $J_0(v_T r_d)$ is the zero order Bessel function of the first kind and v_x and v_z are components of the vector $\bar{v} = k_0(\bar{n}^f - \bar{n}^i)$ in the direction of the unit vectors \bar{n}_1 and \bar{n}_3 tangent to the surface of the unperturbed sphere. In view of the Fourier transform

relationship between $\langle hh' \rangle$ and W

$$\begin{aligned} \langle hh' \rangle &= \int_{-\infty}^{\infty} \frac{W(v_x, v_z)}{4} \exp(-i v_x x_d - i v_z z_d) dv_x dv_z \\ &= \frac{\pi}{2} \int_0^{\infty} W(v_T) J_0(v_T r_d) v_T dv_T \end{aligned} \quad (3.4)$$

The following special form is assumed in this work for the surface height spectral density function

$$W(v_T) = \frac{2C}{\pi} \left[\frac{v_T}{v_T^2 + v_m^2} \right]^8 \quad (3.5)$$

Thus the surface height autocorrelation function is

$$R(\zeta) = \left[1 - \frac{3\zeta^2}{8} + \frac{3\zeta^4}{32} + \frac{\zeta^6}{3072} \right] \zeta K_1(\zeta) + \left[\frac{1}{2} - \frac{\zeta^2}{4} + \frac{\zeta^4}{96} \right] \zeta^2 K_0(\zeta) \quad (3.6)$$

in which K_0 and K_1 are the modified Bessel functions of the second kind of order zero and one respectively (Abramowitz and Stegun 1964) and the dimensionless argument is

$$\zeta = v_m r_d \quad (3.7)$$

The dominant roughness scale (where $W(v_T)$ is maximum) is $v_T = v_m$ and $W(v_m) = C/128\pi v_m^4$. The mean square height is

$$\langle h^2 \rangle = \frac{\pi}{2} \int_0^\infty W(v_T) v_T^3 dv_T = C/210 v_m^6 \quad (3.8)$$

and the total mean square slope is

$$\langle \sigma_s^2 \rangle = \frac{\pi}{2} \int_0^\infty W(v_T) v_T^5 dv_T = C/84 v_m^4 \quad (3.9)$$

Thus

$$r_c = 1.26/k_m \quad (3.10)$$

Two special cases are considered in detail at infrared and optical frequencies.

Case (a) $\lambda = 10\mu$ $D = 5\lambda$ $\epsilon_r = 1.5-i8$ (dissipative dielectric)

$$v_m D = 4, \langle \sigma_s^2 \rangle = 0.101, \beta = 4k_0^2 \langle h^2 \rangle = 10, r_c/\pi D = 0.101$$

Case (b) $\lambda = 0.555\mu$ $D = 10\lambda$ $\epsilon_r = -40-i12$ (aluminum, Ehrenreich 1965)

$$v_m D = 4, \langle \sigma_s^2 \rangle = 0.101, \beta = 40, r_c/\pi D = 0.101.$$

For case (a) ($D = 5\lambda$) it is necessary to use a Gaussian quadrature formula of order 20 to discretize the angle θ (Abramowitz and Stegun 1964) and for case (b) ($D = 10\lambda$) since the differential

scattering cross sections are very sharply peaked in the forward direction it is necessary to use a Gaussian quadrature formula of the order 32. The number of terms needed in the Fourier series expansions for the incoherent specific diffuse intensities depends on the angle of incidence θ^i . As was noted, for normal incidence all the terms of the Fourier series except $m=0$ and $m=2$ vanish. For case (a) it is necessary to account for the terms $m=0,1,\dots,16$ when $\theta^i=15^\circ$ and when $\theta^i=30^\circ$ it is necessary to account for the terms $m=0,1,2,\dots,24$ to get a two significant figure accuracy for the excitation matrix F (2.25).

In Figures 3 and 4 I_1 and I_2 are plotted as functions of θ for a vertically polarized wave incident at an angle $\theta^i=15^\circ$ upon a parallel layer of optical thickness $\tau_0=0.1$. In Figures 5 and 6 the corresponding results are shown for a horizontally polarized incident wave. Both first order and multiple scattering results are shown for the smooth spherical particles as well as the particles with rough surfaces. For a vertically polarized incident wave the main lobe of the scattered intensity I_1 is in the forward direction $\theta=15^\circ$. Since the diffuse scattering contributions $[S_D]$ is negligible in the near forward direction, the effects of the particle surface roughness is also negligible in the near forward direction. Moreover, since the Mie solution for the scattered field has a very large lobe in the forward direction, for $\tau_0=0.1$ multiple scattering effects are not significant in the forward direction. Away from the forward direction the effects of particle surface roughness become significant. The effects of particle

surface roughness are primarily manifested in the smoothing out of the large undulations in the specific intensities for the smooth spherical particles. The effects of multiple scattering are more pronounced away from the near forward directions. The multiple scattering effects increase as the optical thickness τ_0 increases. The effects of particle surface roughness are more strongly manifested in the results for the cross polarized specific intensity I_2 (Fig. 4). The single scatter results are zero for the smooth particle. However, for the rough particle the single scatter results are in agreement with the multiple scatter results except in the near forward direction where the single scatter results are negligible. This is again because the diffuse scattering contribution $[S_D]$ is negligible in the forward direction. For the same reason in the near forward direction the multiple scatter results are the same for both the smooth particles and the particles with rough surfaces.

The principal difference between the results for the horizontally polarized excitations and the results for the vertically polarized excitations is that the like polarized intensity I_2 (Fig. 6) for a horizontally polarized excitation undulates less strongly. This results directly from the behavior of the corresponding Mie solutions.

In Figs. 7 and 8 the incoherent specific intensities I_1 and I_2 are shown for the case considered in Figs. 3 and 4 (vertically polarized excitation) except that here the optical thickness is $\tau_0 = 20$. As the optical thickness of layer of particles increases,

the incoherent specific intensities become more isotropic and the levels of the like (I_1) and cross (I_2) polarized intensities approach each other. Multiple scattering cannot be ignored and the effects of particle surface roughness increase away from the near forward scattering direction. The specific intensities are lower for the particle with rough surfaces than for the smooth spherical particles since the albedos for the rough particles are smaller than the albedos for the smooth particles (Table I). The corresponding results for horizontally polarized excitations (not shown) are similar to those for vertically polarized excitations. As the optical thickness of the layer of particles τ_0 increases the multiple scatter results become more independent of polarization.

In Figs. 9 and 10 the incoherent specific intensities I_1 and I_2 are plotted as functions of θ for vertically polarized waves incident at an angle $\theta^i = 30^\circ$, $\phi^i = 0$ ($\lambda = 10\mu$, case (a)). The optical thickness of the layer is $\tau_0 = 1$. The effects of particle roughness on both I_1 and I_2 are negligible in the near forward scatter direction. However, away from the forward scatter direction the effects of particle surface roughness is very significant. The incoherent specific intensities become more isotropic. Moreover, it should be noted that for $\tau_0 = 1$ while the particle surface roughness reduces the level of I_1 (like polarized intensity) it increases the level of I_2 (cross-polarized intensity). This is because the albedos for the particles with rough surfaces are smaller than the albedos for the smooth particles, and the cross-

polarized scattering cross sections are not zero for the particles with rough surfaces. As a result the degree of polarization is smaller for the layer containing particles with rough surfaces. The single scatter results, also shown in Fig. 9 indicate the effect of the particle rough surface is to reduce the sharp undulations in the specific intensity I_1 .

In Figs. 11 and 12 the co-polarized (I_y) and cross-polarized (I_x) incoherent specific intensities are plotted as functions of the azimuth angle ϕ for horizontally polarized waves incident at an angle $\theta^i = 30^\circ, \phi^i = 0$ ($\lambda = 10\mu$, case (a)). The optical thickness of the layer is $\tau_0 = 0.1$ and the (forward) scatter angle is $\theta = 68.1^\circ$. The first order and multiple scatter results for the specific intensities I_x and I_y are less than 1/2 db apart for the particles with rough surfaces. On the other hand, the corresponding results for the smooth particles are far more oscillatory and there are significant differences between the first order and multiple scatter results especially for the cross-polarized intensities (I_x) in the neighborhood of $\phi = 0$ and $\phi = \pi$.

The co-polarized (I_x) and cross-polarized (I_y) incoherent specific intensities for vertically polarized waves incident at an angle $\theta = 30^\circ, \phi^i = 0$ ($\lambda = 10\mu$, case (a)) are plotted as functions of the azimuth angle ϕ in Figures 13 and 14. The optical thickness of the layer is $\tau_0 = 0.1$ and the (back) scatter angle is $\theta = 111.9^\circ$. The co-polarized reflected incoherent specific intensity I_x is larger for the smooth particles than for the rough particles,

however since $\tau_0 = 0.1$, the multiple scatter and single scatter results are less than 0.5 db apart. The reflected flux of the cross-polarized incoherent specific intensity I_y is larger for the particles with rough surfaces than for the smooth particles and I_y is more isotropic for the particles with rough surfaces. The difference between the single and multiple scatter results is significantly larger for the smooth particles. The co-polarized and cross-polarized specific intensities are even functions of ϕ (2.34).

In Figs. 15 and 16 the incoherent specific intensities I_1 and I_2 are plotted as functions of θ ($\phi = 0$) for vertically polarized waves incident at an angle $\theta^i = 15^\circ$, $\phi^i = 0$ ($\lambda = 0.555\mu$, case (b)). The optical thickness of the layer $\tau_0 = 2$. Since $D = 10\lambda$ for case (b) the plot of the specific intensity I_1 is strongly peaked in the forward direction and the first order, single scatter results for the smooth particle oscillate rapidly. In this case it is necessary to account for the terms $m = 0, 1, 2 \dots 26$ to get a two significant figure accuracy. The multiple scatter results for the smooth particle do not undulate as strongly since $\tau_0 = 2$. For the particles with rough surfaces, both the single scatter and multiple scatter results for I_1 are similar to the corresponding near forward scatter results for the smooth particles. However, away from the near forward direction both the single and multiple scatter specific intensity I_1 for the particles with rough surfaces are significantly different from the corresponding results for the

smooth particles. The effects of particle surface roughness are to significantly smooth out the undulations in I_1 away from the forward scatter direction. Since the albedo for the particles with rough surfaces is smaller than for smooth particles generally I_1 for the smooth particles is larger. This is not the case for I_2 (the cross polarized specific intensity). For small values of τ_0 , I_2 is larger for the particles with rough surfaces (since their cross-polarized cross sections $\langle \sigma^{PQ} \rangle_D$ $P \neq Q$ are not zero). However for layers with very large optical thickness τ_0 , the reverse is true since the albedos for the smooth particles are larger. The cross-over occurs at about $\tau_0 = 2$ where the multiple scatter results for I_2 are approximately the same for the particles with rough and smooth surfaces (see Fig.16). The single scatter results I_2 for the smooth particles are zero for the $\phi = 0$ plane.

In Figures 17 and 18 the co-polarized and cross-polarized incoherent specific intensities I_y and I_x are plotted as functions of the azimuth angle ϕ for a horizontally polarized wave incident at an angle $\theta^i = 15^\circ$, $\phi^i = 0^\circ$ ($\lambda = 0.555\mu$, case (b)). The scatter polar angle in these figures is $\theta = 59.5^\circ$ (forward scatter) and the optical thickness of the layer is $\tau_0 = 0.1$. In view of the excitation I_x and I_y are even functions of ϕ . For this excitation the co-polarized intensity is I_y (Fig. 18). For the smooth particles both I_x and I_y undulate very strongly, the major difference between the multiple scatter and single scatter results occur only at the sharp nulls. For particles with rough

surfaces both I_x and I_y are significantly more isotropic (with respect to ϕ) and the difference between the single scatter and multiple scatter results is less than 1 db.

In Figs. 19 and 20 the co-polarized and cross-polarized incoherent specific intensity I_y and I_x are plotted as functions of ϕ for the scatter polar angle $\theta = 164.7^\circ$ (backward scatter). The excitation is the same as for the case considered in Figs. 17 and 18. The effect of particle surface roughness is to smooth out the undulations in the specific intensities for the smooth particles. Thus the backward scattered incoherent specific intensities for the particles with rough surfaces are practically isotropic as well as polarization independent even for layers of small optical thickness $\tau_0 = 0.1$. As τ_0 increases, the difference between the single and multiple scatter results saturate at about 0.7 db for the particles with rough surfaces.

In Figs. 21 and 22 the degree of polarization m (2.39) is plotted as a function of the azimuth angle ϕ . The excitation is a horizontally polarized wave incident at an angle $\theta^i = 15^\circ$, $\phi^i = 0$ ($\lambda = 0.555\mu$ case (b)). The optical thickness of the layer is $\tau_0 = 2$. In Fig. 21 the scatter angles are $\theta = 4.2^\circ$ and $\theta = 9.7^\circ$. Multiple scatter results are plotted for particles with both smooth and rough surfaces. For the near forward scatter direction ($\theta = 9.7^\circ$, $\phi = 0$) m is the same for both smooth and rough particles, however as ϕ increases to π the difference becomes very significant. The results for $\theta = 4.2^\circ$ do not undulate as strongly as the results for $\theta = 9.7^\circ$ since the main

scatter lobe is in the direction $\theta = \theta^i = 15^\circ$, $\phi^i = 0$. The degree of polarization m is smaller for particles with rough surfaces. For the case plotted in Figure 22, the (backward) scatter angles are $\theta = 148.1^\circ$ and $\theta = 153.7^\circ$. The backward scattered waves have a degree of polarization $m < 0.1$ for the particles with rough surfaces. However, for particles with smooth surfaces m oscillates around the value $m = 0.5$.

Since the degree of polarization is $m \leq 1$, this parameter together with the single scatter data provide valuable checks on the numerical results.

4. CONCLUDING REMARKS

The illustrative examples presented in Section 3 vividly describe the effects of particle surface roughness on the co-polarized and cross-polarized incoherent specific intensities for optical and infrared electromagnetic excitations at oblique incidence.

Since the diffuse scattering contributions due to particle surface roughness are negligible in the near forward direction, the primary effect of the surface roughness is to smooth out the side lobe undulations of the specific intensities for the corresponding smooth particles. Furthermore, the particles with rough surfaces more strongly depolarize the incident wave. Thus since the albedos are smaller for the particles with rough surfaces than for the smooth particles, the co-polarized specific intensities are smaller for the rough particles while the cross-polarized specific intensities are smaller for the smooth particles when the optical thickness of

the layer of particles is small $\tau < 1$. However, as the optical thickness of the layer increases ($\tau > 1$) both the co-polarized and cross-polarized specific intensities are smaller for the particles with rough surfaces.

In general as the optical thickness increases and multiple scattering effects become significant, the layer consisting of particles with rough surfaces tend to scatter the incident waves in a more isotropic manner. The sharp undulations in the specific intensities are smoothed out and the results become more polarization independent. Thus the degree of polarization for the particles with rough surfaces is significantly smaller than for the smooth particles when the layers of particles with rough surfaces are optically thin, the first order single scatter results and the multiple scatter results for the co-polarized and cross-polarized intensity are in very good agreement.

5. References

1. Abramowitz, M., and I. A. Stegun (1964), Handbook of Mathematical Functions with Formulas, Graphs, and Mathematical Tables, Appl. Math. Ser. 55, National Bureau of Standards, Washington, D. C.
2. Bahar, E., and S. Chakrabarti (1985), "Scattering and Depolarization by Large Conducting Spheres with Rough Surfaces," Applied Optics, 24, No. 12, p. 1620.
3. Bahar, E., S. Chakrabarti, and M. A. Fitzwater (1986), "Extinction Cross Sections and Albedos for Particles with Very Rough Surfaces," submitted for review.
4. Bahar, E., and M. A. Fitzwater (1983), "Backscatter Cross Sections for Randomly Oriented Metallic Flakes at Optical Frequencies--Full Wave Approach," Applied Optics, Vol. 23, pp. 3813-3819.
5. Bahar, E., and M. A. Fitzwater (1985), "Like- and Cross-Polarized Scattering Cross Sections for Random Rough Surfaces: Theory and Experiment," Journal of the Optical Society of America A, Vol. 2, pp. 2295-2303.
6. Born, M., and E. Wolf (1964), Principles of Optics, Pergamon Press, New York.
7. Chandrasekhar, S. (1950), Radiative Transfer. Dover, Publ., New York.
8. Cheung, R.L.-T., and A. Ishimaru (1982), "Transmission, Backscattering, and Depolarization of Waves in Randomly Distributed Spherical Particles," Applied Optics, 21, No. 20, p. 3792.
9. Chylek, Petr (1977), "Extinction Cross Sections of Arbitrarily Shaped Randomly Oriented Nonspherical Particles," Journal of the Optical Society of America, Vol. 67, No. 10, pp. 1348-1350.
10. Ehrenreich, H. (1965), "The Optical Properties of Metals," IEEE Spectrum, 2, p. 162.
11. Greenberg, J. M. (1960), "Scattering by Nonspherical Particles," Journal of Applied Physics, Vol. 31, p. 82.
12. Ishimaru, A. (1978), Wave Propagation and Scattering in Random Media, Academic, New York.

13. Ishimaru, A., and R.L.-T. Cheung (1980), "Multiple Scattering Effects in Wave Propagation Due to Rain," Ann. Telecommun., Vol. 35, p. 373.
14. Ishimaru, A., R. Woo, J. W. Armstrong, and D. C. Blackman, "Multiple Scattering Calculations of Rain Effects," Radio Science, Vol. 17, No. 6, pp. 1425-1433.
15. Kiehl, J. T., M. W. Ko, A. Mugnai, and Petr Chylek (1980), Perturbation Approach to Light Scattering by Nonspherical Particles, chapter in Light Scattering by Irregular Shaped Particles (Editor D. W. Scheurman), Plenum Press, New York.
16. Morse, P. M., and H. Feshbach (1953), Methods of Theoretical Physics, McGraw-Hill, New York.
17. Rice, S. O. (1951), "Reflection of Electromagnetic Waves from a Slightly Rough Surface," Communication of Pure and Applied Math., Vol. 4, pp. 351-378.
18. Ruck, G. T., D. E. Barrick, W. D. Stuart, and C. K. Krichbaum (1970), "Radar Cross Section Handbook", Plenum, New York.
19. Sancer, M. H. (1969), "Shadow-Corrected Electromagnetic Scattering from a Randomly Rough Surface," IEEE Trans. Antennas Propag. AP-17, p. 577.
20. Scheurman, D. W. (1980), Editor, Light Scattering by Irregular Shaped Particles, Plenum Press, New York.
21. Yeh, C., and K. K. Mie (1980), On the Scattering from Arbitrarily Shaped Inhomogeneous Particles, chapter in Light Scattering by Irregular Shaped Particles, (Editor D. W. Scheurman) Plenum Press, New York.

ACKNOWLEDGMENTS

This investigation was sponsored by the U. S. Army Research Office Contract DAAG-29-82-K-0123. The authors acknowledge the National Science Foundation Engineering Supercomputer Grant ECS 8515794/5. The manuscript was typed by Mrs. E. Everett.

Table I

	Case a	Case b
β	10	40
λ	10μ	$.555\mu$
ϵ_r	$1.5-i8$	$-40-i12$
$2a = D$	5λ	10λ
σ_t , smooth	2.370	2.259
σ_t , rough	2.333	2.213
albedo, smooth	.6434	.9356
albedo, rough	.6043	.8579

$$W(v_T) = \frac{C}{2\pi} \left[\frac{v_T}{v_T^2 + v_m^2} \right]^8, \quad v_m D = 4, \quad \langle \sigma_s^2 \rangle = .101, \quad r_c / \pi D = .101$$

Table I. Values of parameters for the surface height spectral density function W , wavelength λ , dielectric coefficient ϵ_r and diameter D for the scattering particles.

6. Figure Captions

1. Scattering geometry for a rough conducting sphere.
2. Scattering geometry indicating incident and scattered wave normals \vec{n}^i and \vec{n}^f and corresponding field components E_1 parallel (vertical) and E_2 perpendicular (horizontal) polarizations.
3. Incoherent specific intensity I_1 for a vertically polarized wave incident at $\theta^i = 15^\circ$, $\phi^i = 0$, case (a), $\tau_0 = 0.1$. First order smooth and rough (—). Multiple scatter (+) smooth, (Δ) rough.
4. Incoherent specific intensity I_2 for a vertically polarized wave incident at $\theta^i = 15^\circ$, $\phi^i = 0$, case (a), $\tau_0 = 0.1$. First order smooth and rough (—). Multiple scatter (+) smooth, (Δ) rough.
5. Incoherent specific intensity I_1 for a horizontally polarized wave incident at $\theta^i = 15^\circ$, $\phi^i = 0$, case (a), $\tau_0 = 0.1$. First order smooth and rough (—). Multiple scatter (+) smooth, (Δ) rough.
6. Incoherent specific intensity I_2 for a horizontally polarized wave incident at $\theta^i = 15^\circ$, $\phi^i = 0$, case (a), $\tau_0 = 0.1$. First order smooth and rough (—). Multiple scatter (+) smooth, (Δ) rough.
7. Incoherent specific intensity I_1 for a vertically polarized wave incident at $\theta^i = 15^\circ$, $\phi^i = 0$, case (a), $\tau_0 = 20$. First order smooth and rough (—). Multiple scatter (+) smooth, (Δ) rough.
8. Incoherent specific intensity I_2 for a vertically polarized wave incident at $\theta^i = 15^\circ$, $\phi^i = 0$, case (a), $\tau_0 = 20$. First order smooth and rough (—). Multiple scatter (+) smooth, (Δ) rough.

9. Incoherent specific intensity I_1 for a vertically polarized wave incident at $\theta^i = 30^\circ$, $\phi^i = 0$, case (a), $\tau_0 = 1$.
First order smooth and rough (—). Multiple scatter (+) smooth, (Δ) rough.
10. Incoherent specific intensity I_2 for a vertically polarized wave incident at $\theta^i = 30^\circ$, $\phi^i = 0$, case (a), $\tau_0 = 1$.
First order smooth and rough (—). Multiple scatter (+) smooth, (Δ) rough.
11. Co-polarized specific intensity I_y for a horizontally polarized wave incident at $\theta^i = 30^\circ$, $\phi^i = 0$, case (a), $\tau_0 = 0.1$, $\theta = 68.1^\circ$. First order smooth and rough (—). Multiple scatter (\bar{X}) smooth, (X) rough.
12. Cross-polarized specific intensity I_x for a horizontally polarized wave incident at $\theta^i = 30^\circ$, $\phi^i = 0$, case (a), $\tau_0 = 0.1$, $\theta = 68.1^\circ$. First order smooth and rough (—). Multiple scatter (\bar{X}) smooth, (X) rough.
13. Co-polarized specific intensity I_x for a vertically polarized wave incident at $\theta^i = 30^\circ$, $\phi^i = 0$, case (a), $\tau_0 = 0.1$, $\theta = 111.9^\circ$. First order smooth and rough (—). Multiple scatter (\bar{X}) smooth, (X) rough.
14. Cross-polarized specific intensity I_y for a vertically polarized wave incident at $\theta^i = 30^\circ$, $\phi^i = 0$, case (a), $\tau_0 = 0.1$, $\theta = 111.9^\circ$. First order smooth and rough (—). Multiple scatter (\bar{X}) smooth, (X) rough.
15. Incoherent specific intensity I_1 for a vertically polarized wave incident at $\theta^i = 15^\circ$, $\phi^i = 0^\circ$, case (b), $\tau_0 = 2$.
First order smooth and rough (—). Multiple scatter (+) smooth, (Δ) rough.

16. Incoherent specific intensity I_2 for a vertically polarized wave incident at $\theta^i = 15^\circ$, $\phi^i = 0^\circ$, case (b), $\tau_0 = 2$.
First order smooth and rough (—). Multiple scatter (+) smooth, (Δ) rough.
17. Co-polarized specific intensity I_y for a horizontally polarized wave incident at $\theta^i = 15^\circ$, $\phi^i = 0$, case (b), $\tau_0 = 0.1$, $\theta = 59.5^\circ$. First order smooth and rough (—). Multiple scatter (\bar{X}) smooth, (X) rough.
18. Cross-polarized specific intensity I_x for a horizontally polarized wave incident at $\theta^i = 15^\circ$, $\phi^i = 0$, case (b) $\tau_0 = 0.1$, $\theta = 59.5^\circ$. First order smooth and rough (—). Multiple scatter (\bar{X}) smooth, (X) rough.
19. Co-polarized specific intensity I_y for a horizontally polarized wave incident at $\theta^i = 30^\circ$, $\phi^i = 0$, case (b), $\tau_0 = 0.1$, $\theta = 164.7^\circ$. First order smooth and rough (—). Multiple scatter (\bar{X}) smooth, (X) rough.
20. Cross-polarized specific intensity I_x for a horizontally polarized wave incident at $\theta^i = 30^\circ$, $\phi^i = 0$, case (b), $\tau_0 = 0.1$, $\theta = 164.7^\circ$. First order smooth and rough (—). Multiple scatter (\bar{X}) smooth, (X) rough.
21. Degree of polarization m for a horizontally polarized wave incident at $\theta^i = 15^\circ$, $\phi^i = 0$, case (b), $\tau_0 = 2$, $\theta = 4.2^\circ$ (+) smooth, (X) rough, $\theta = 9.7^\circ$ (0) smooth, (Δ) rough.
22. Degree of polarization m for a horizontally polarized wave incident at $\theta^i = 15^\circ$, $\phi^i = 0$, case (b), $\tau_0 = 2$, $\theta = 148.1^\circ$ (+) smooth, (X) rough, $\theta = 153.6^\circ$ (0) smooth, (Δ) rough.

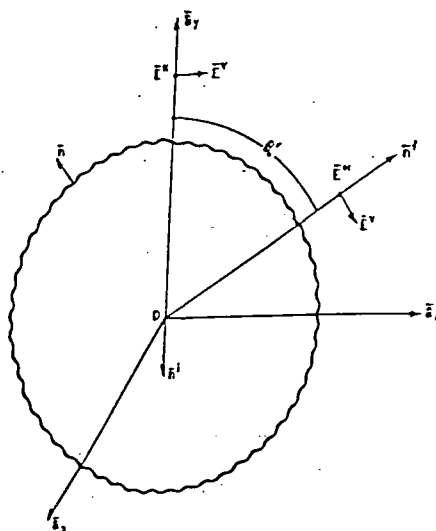


FIG. 1

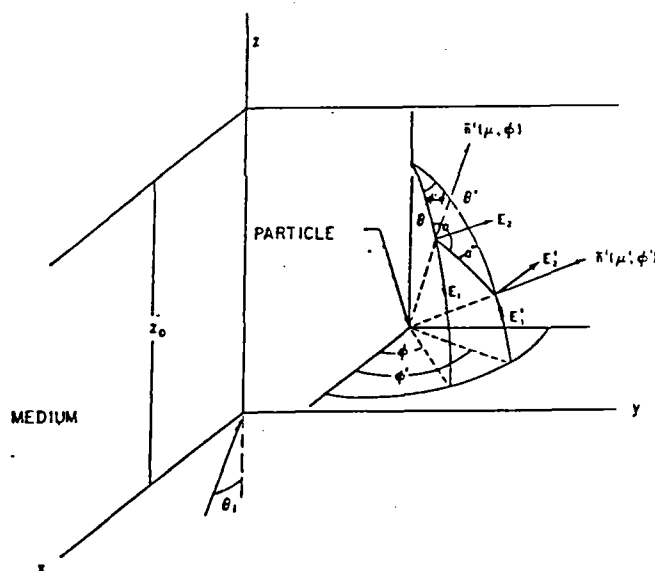


Fig. 2

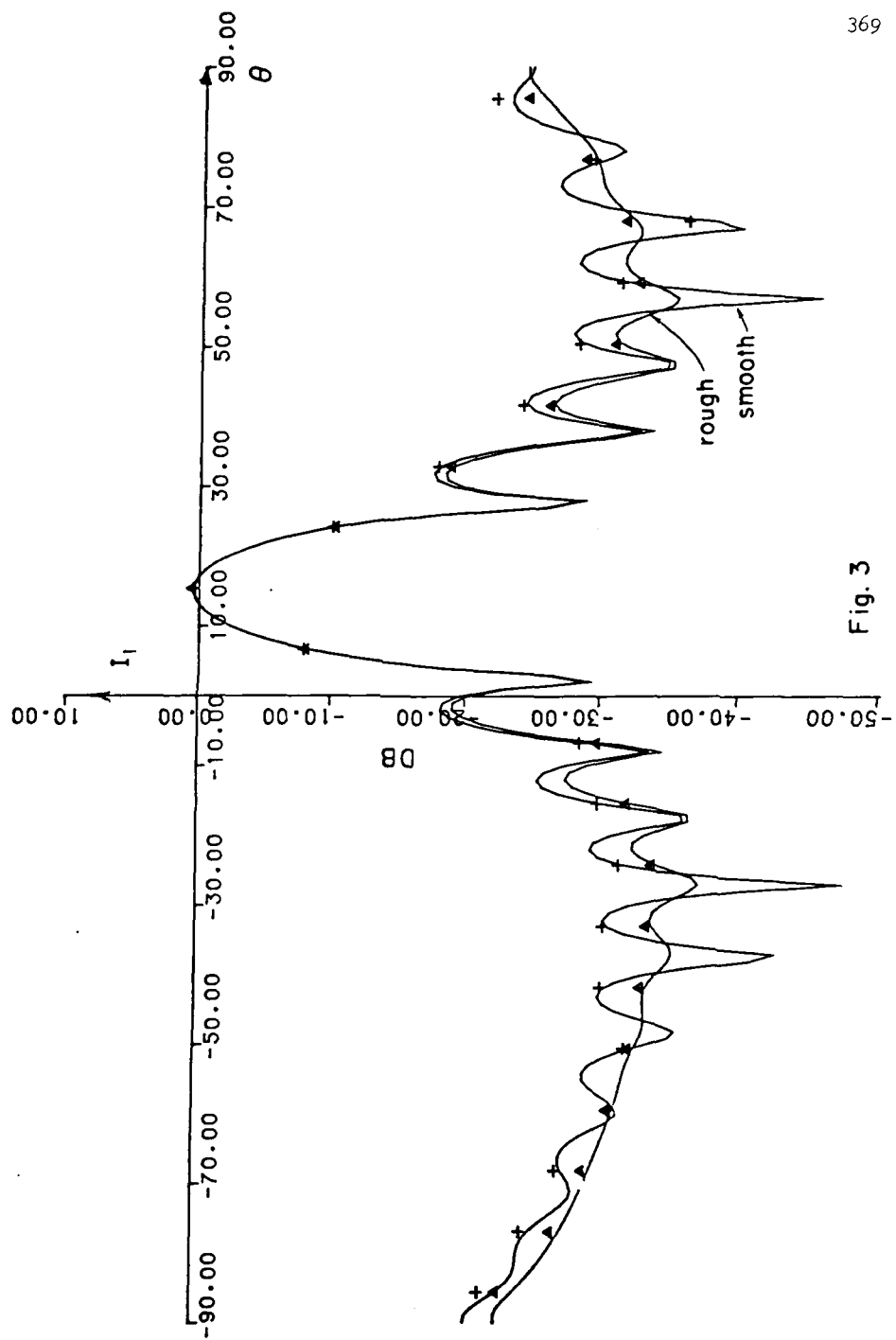


Fig. 3

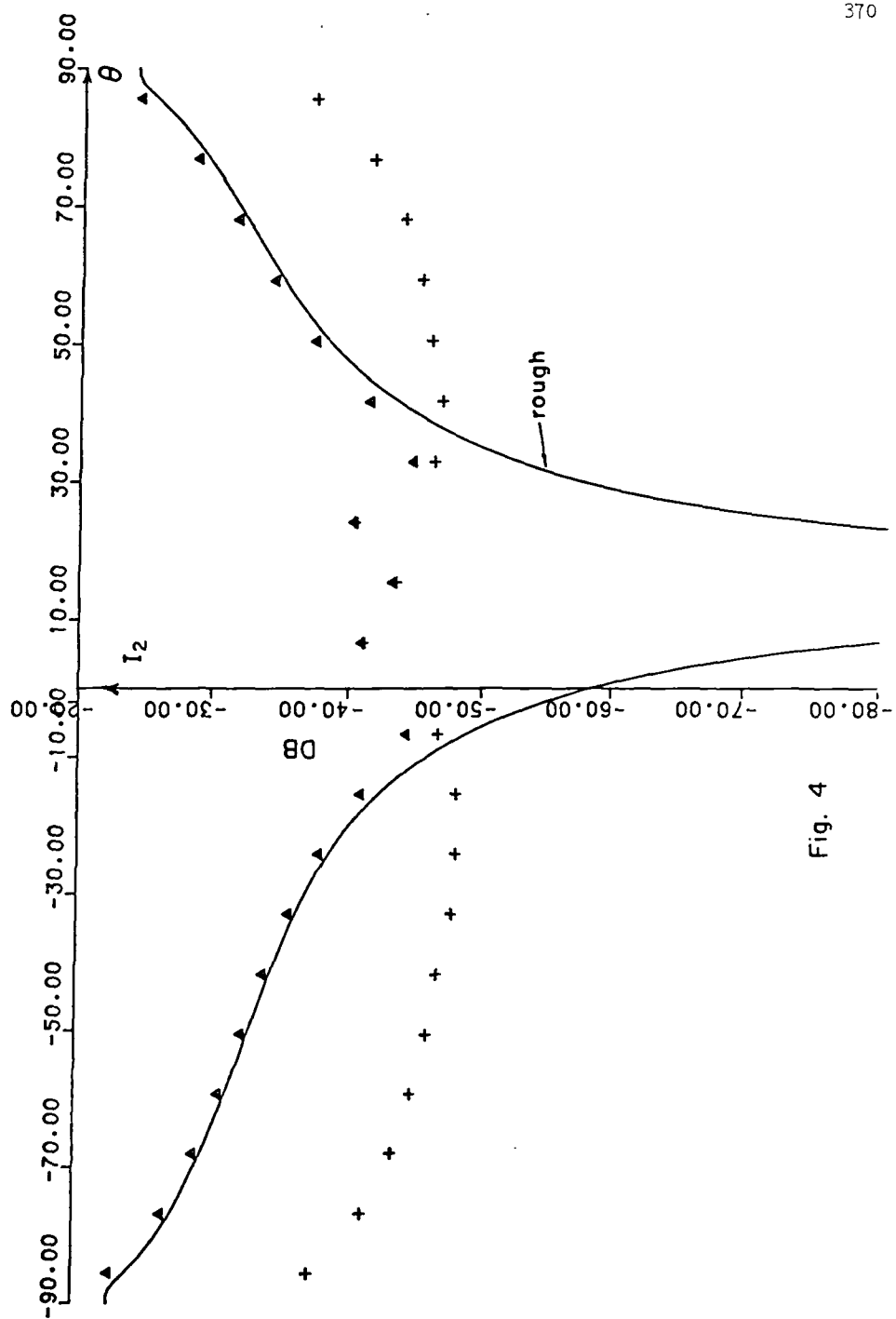


Fig. 4

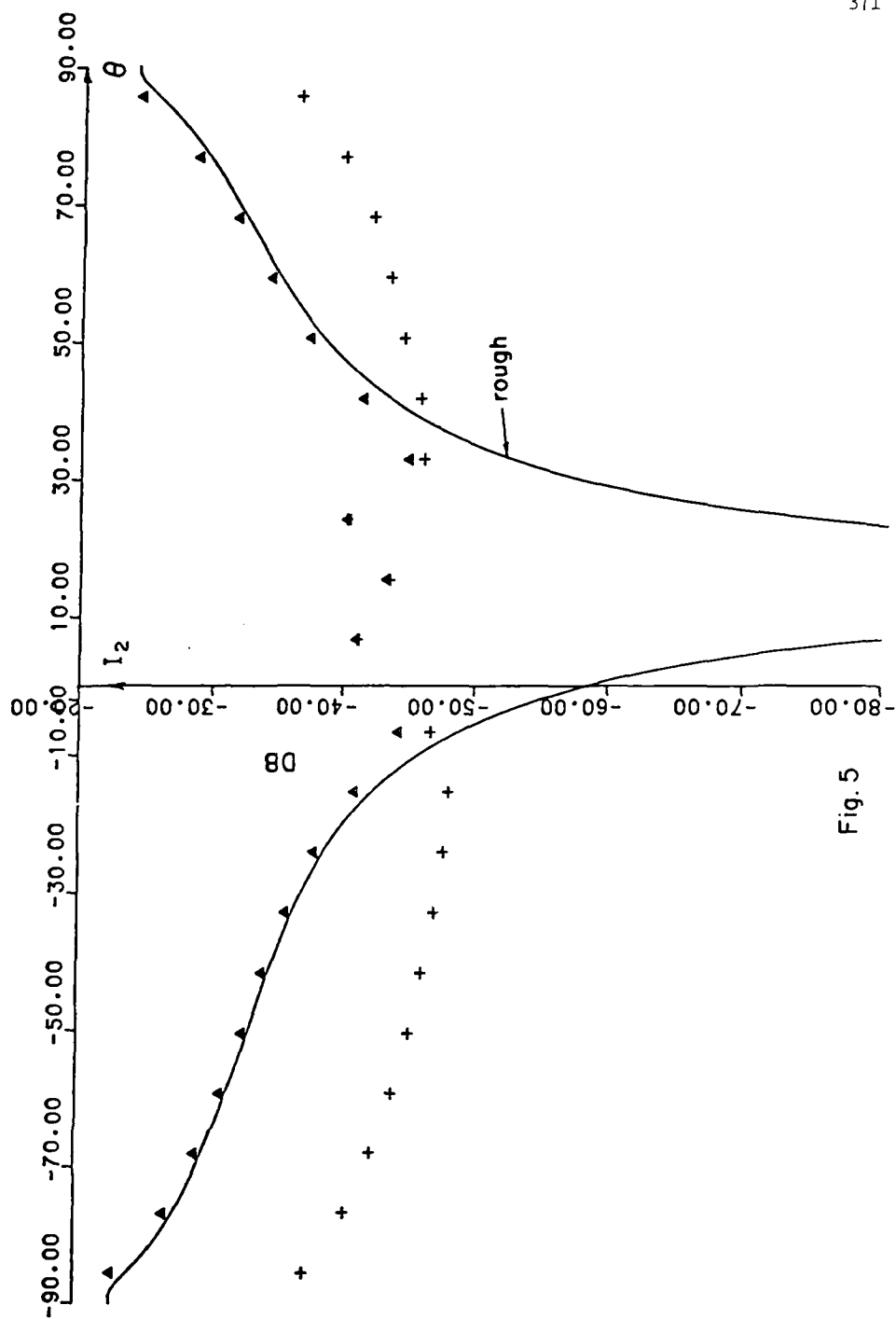


Fig. 5

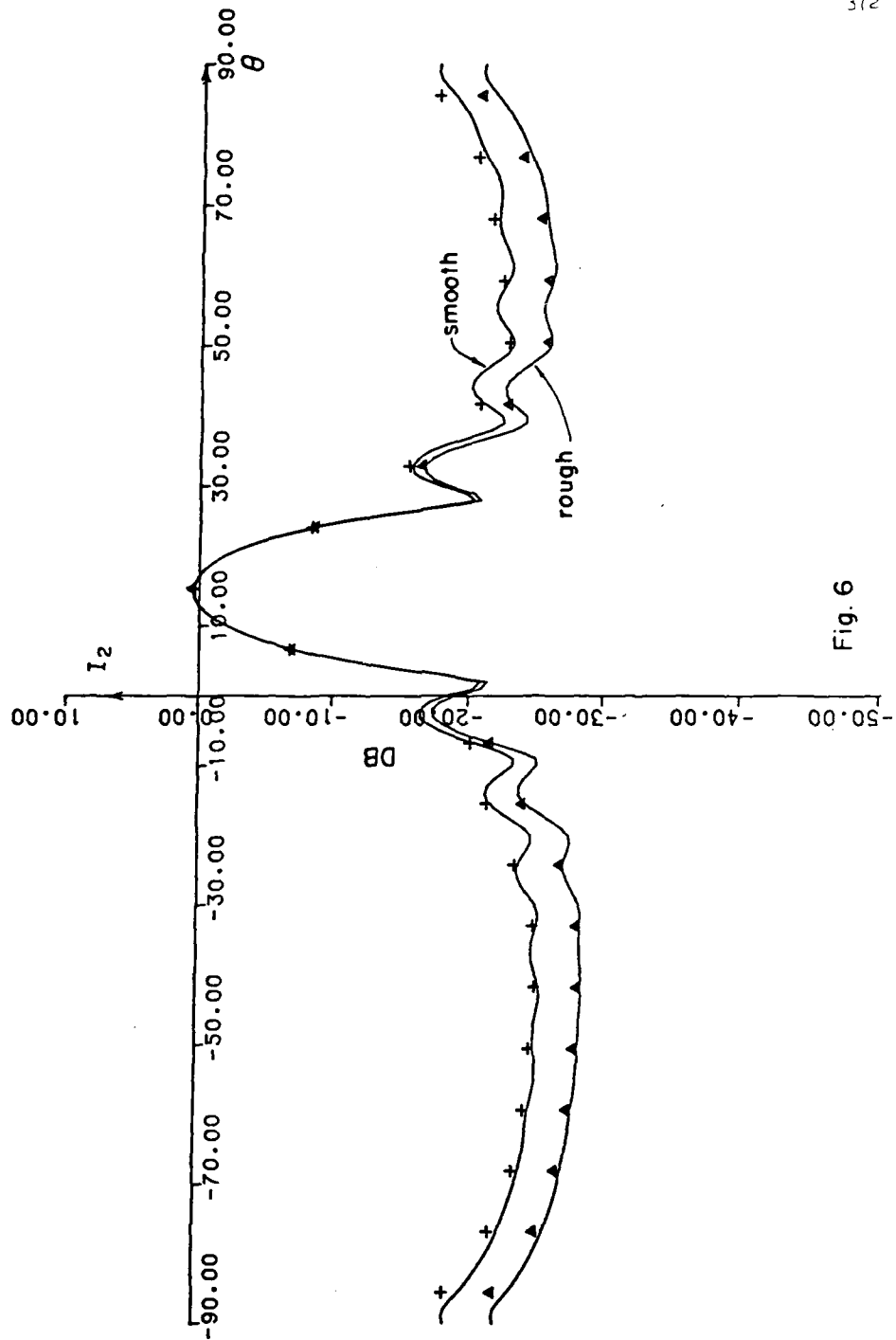


Fig. 6

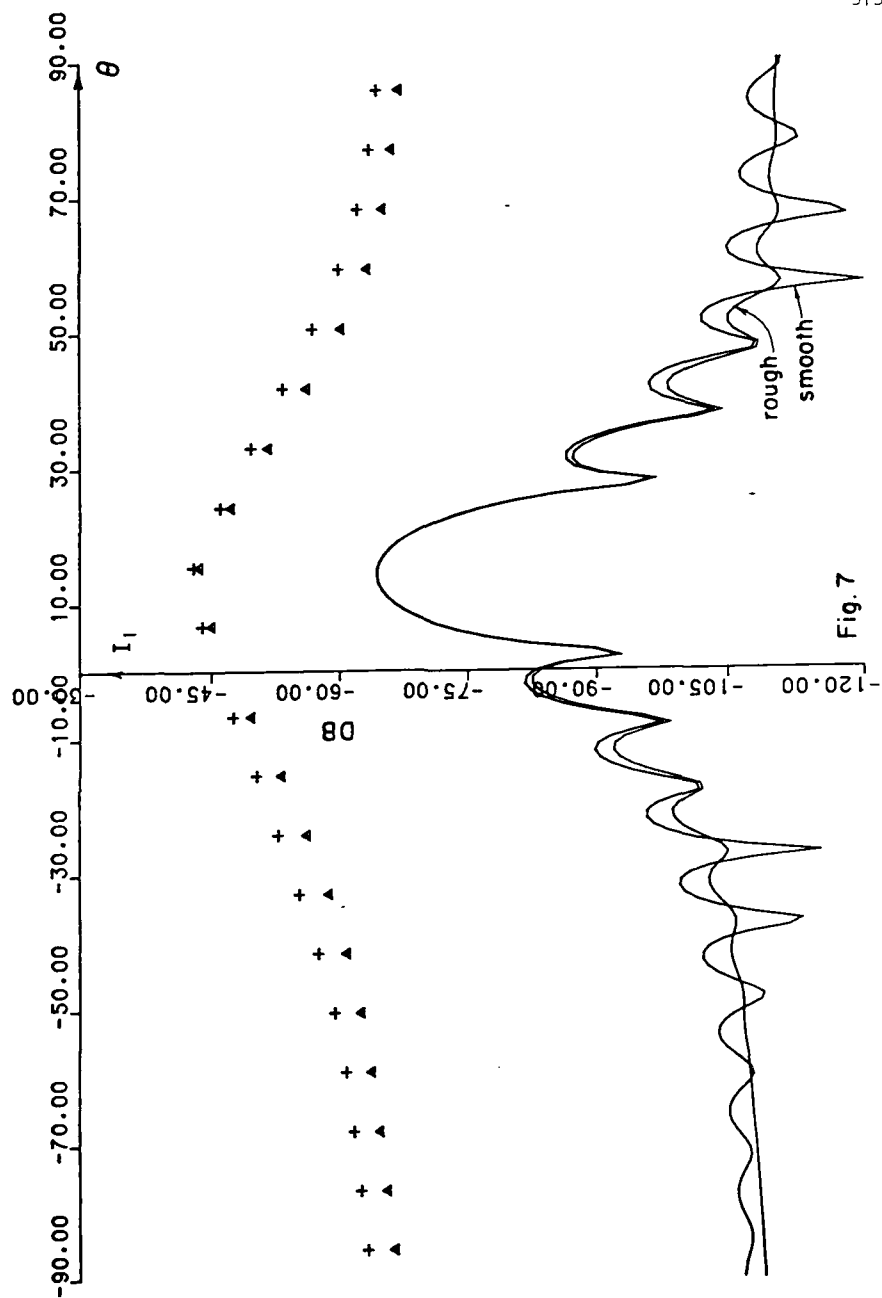


Fig. 7

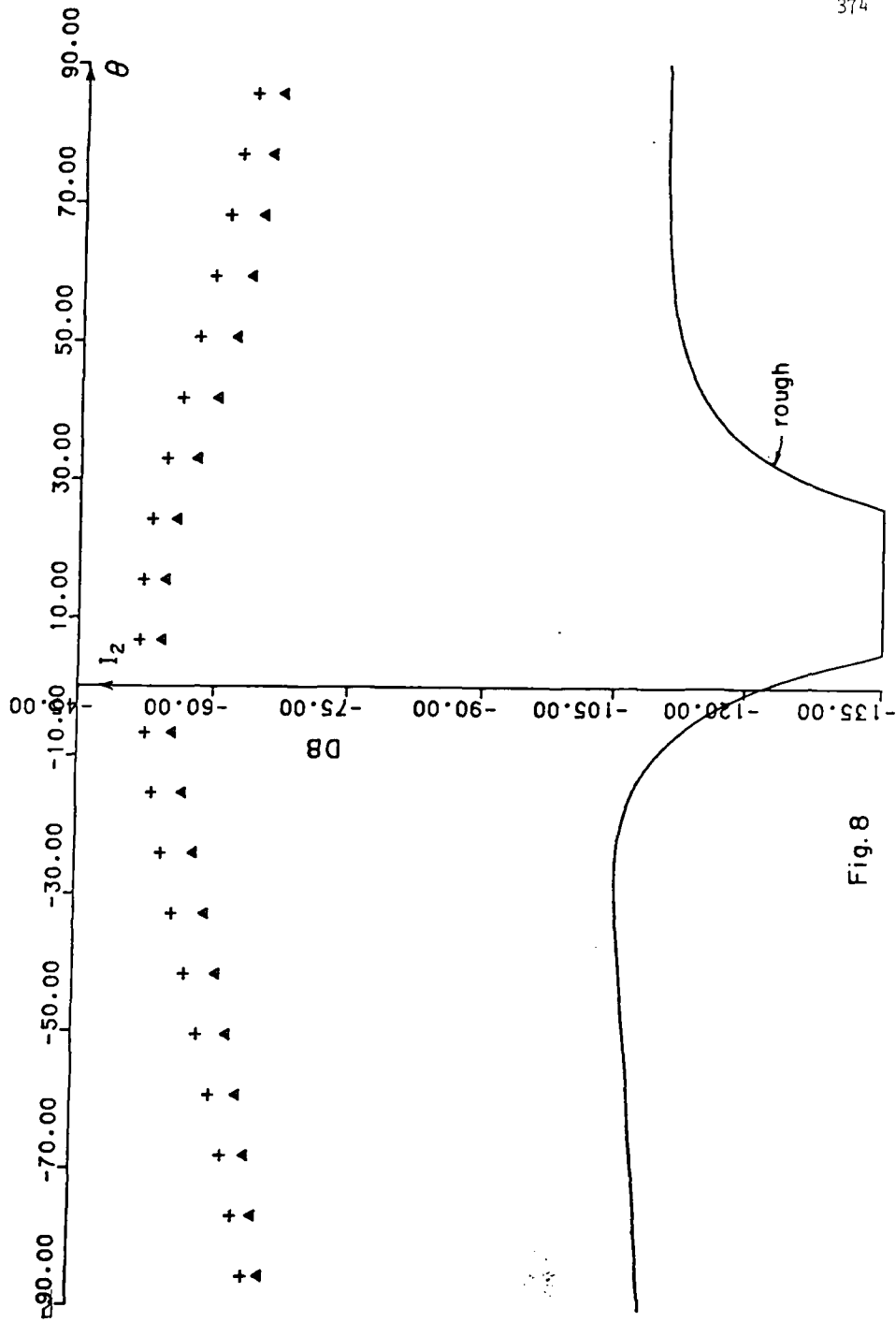


Fig. 8

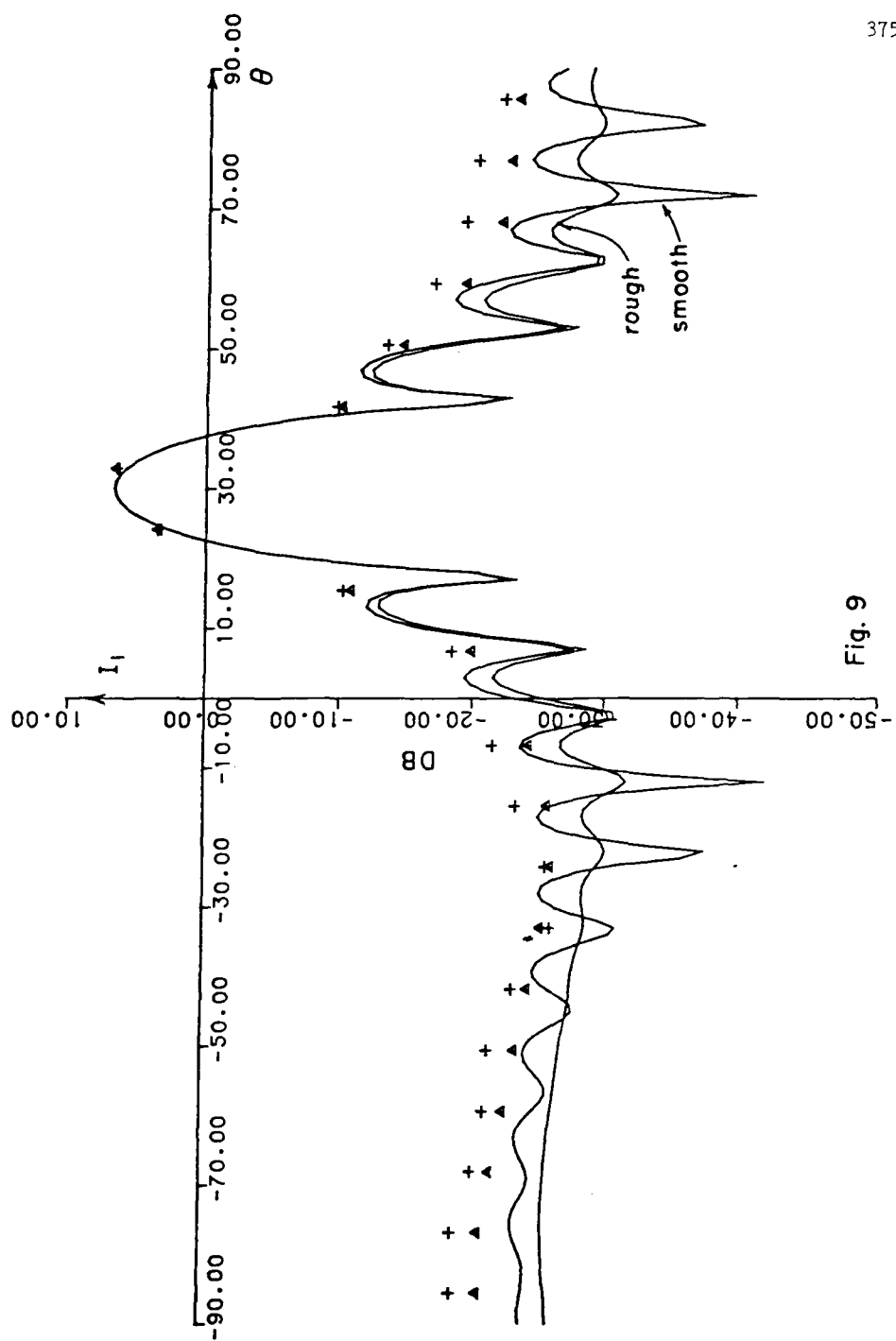


Fig. 9

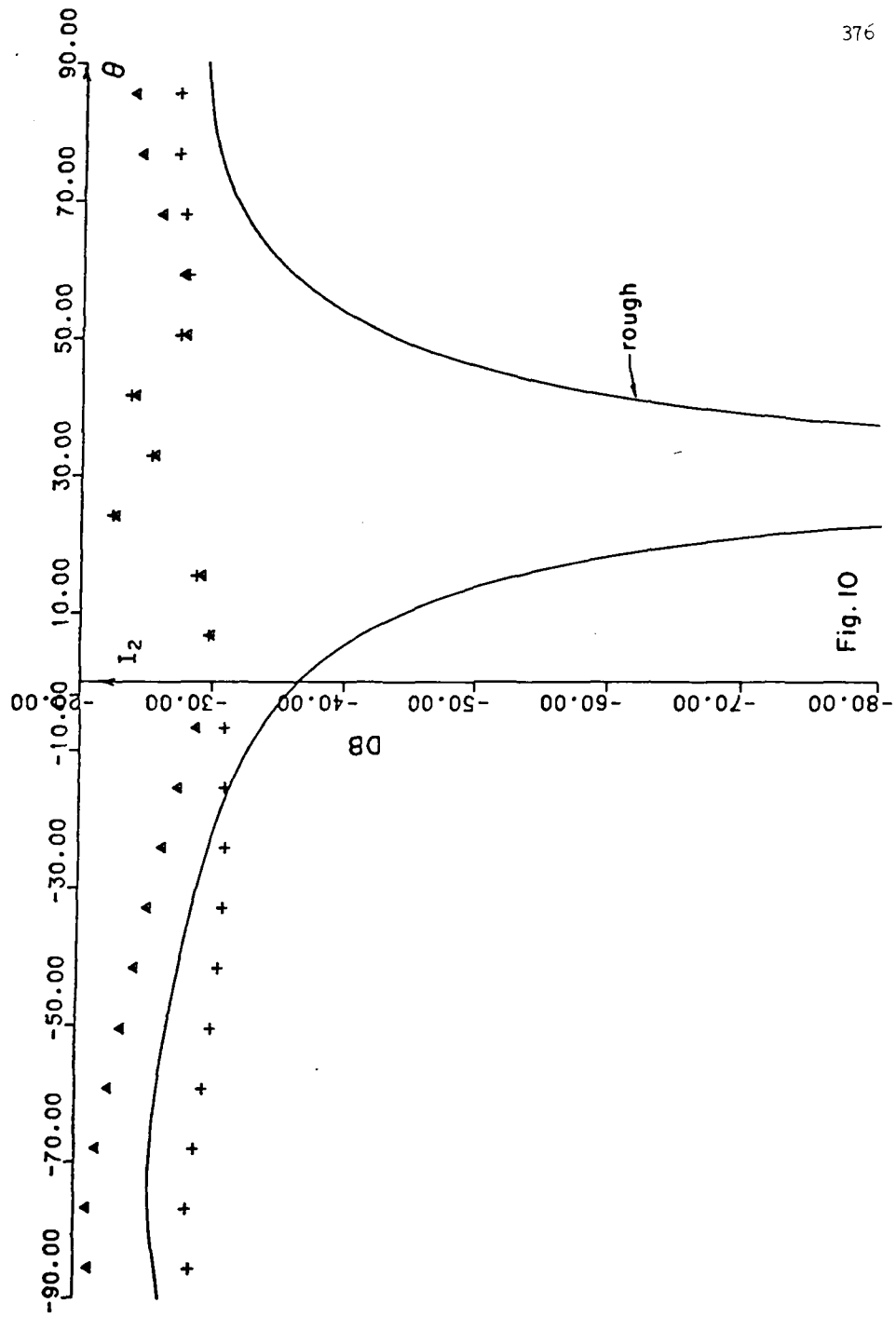


Fig. 10

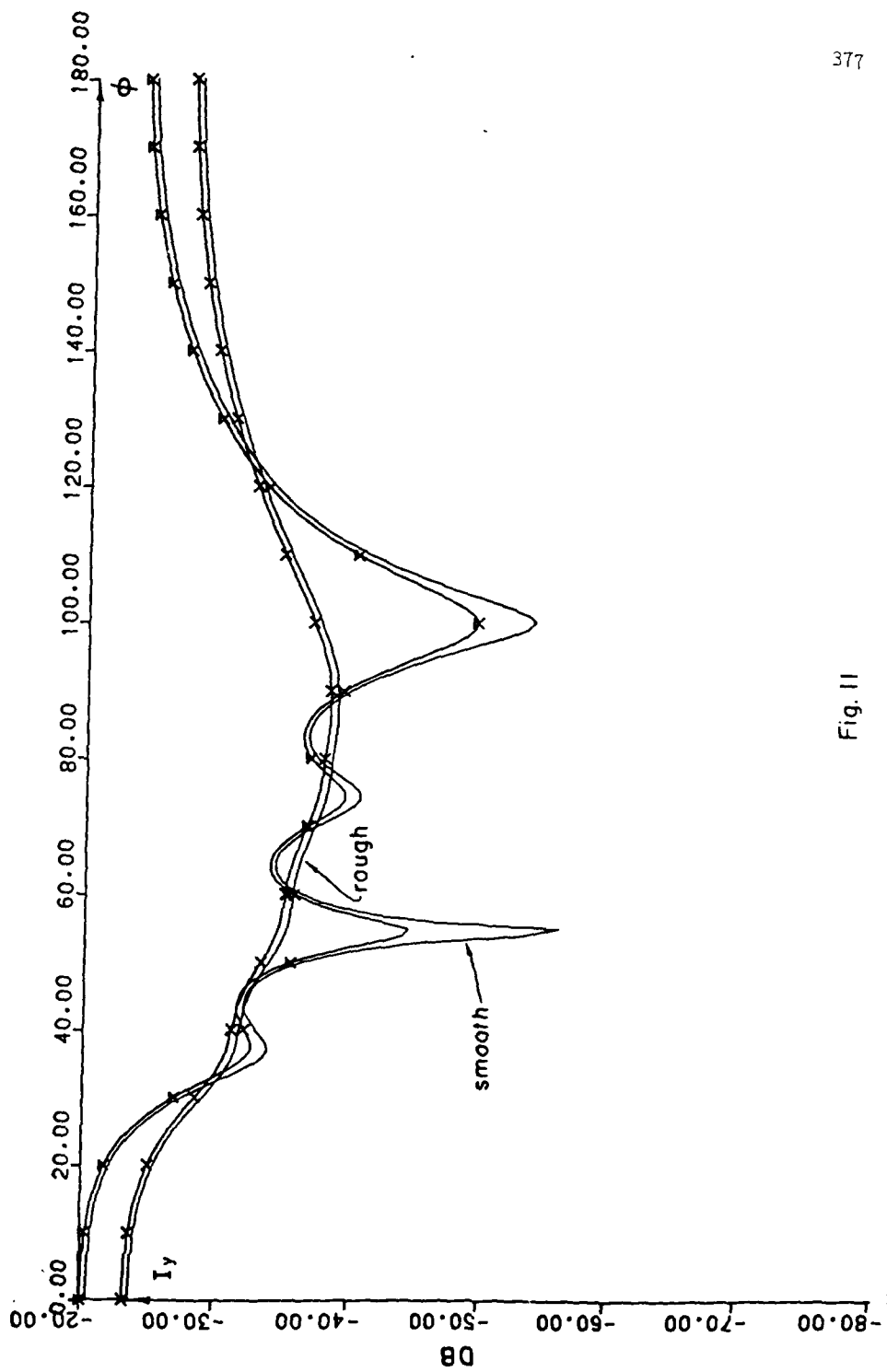


Fig. II

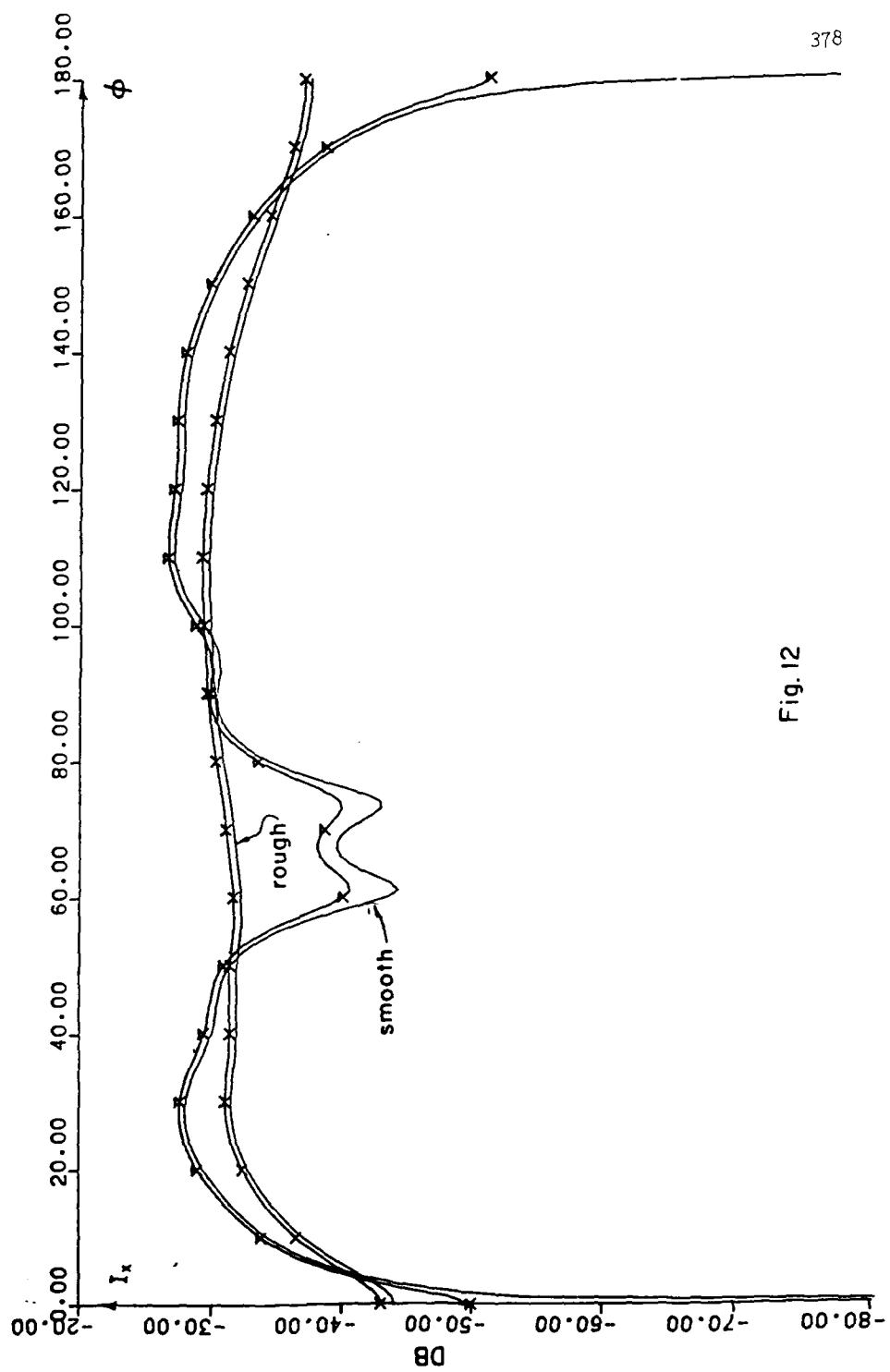


Fig.12

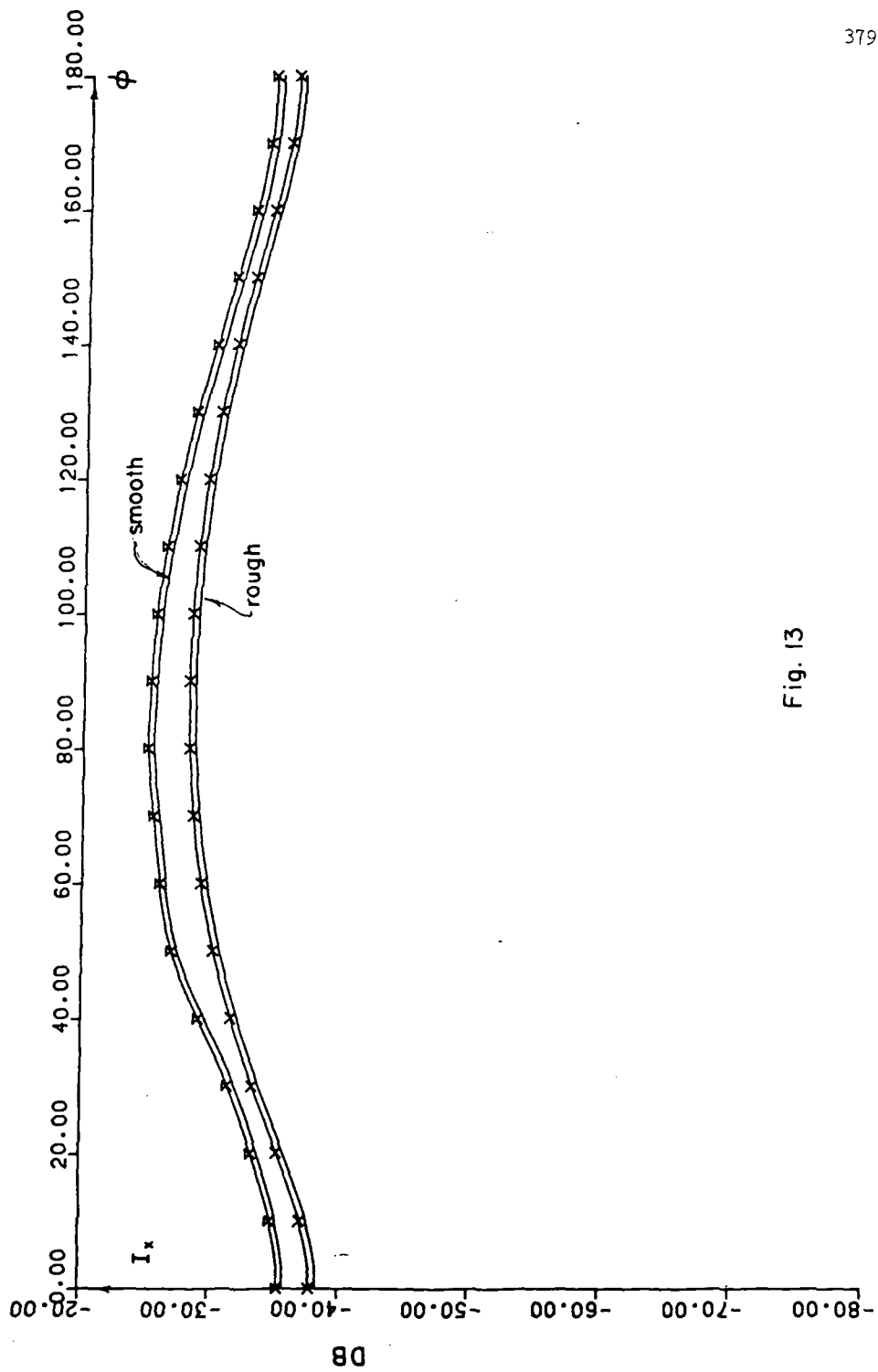


Fig. 13

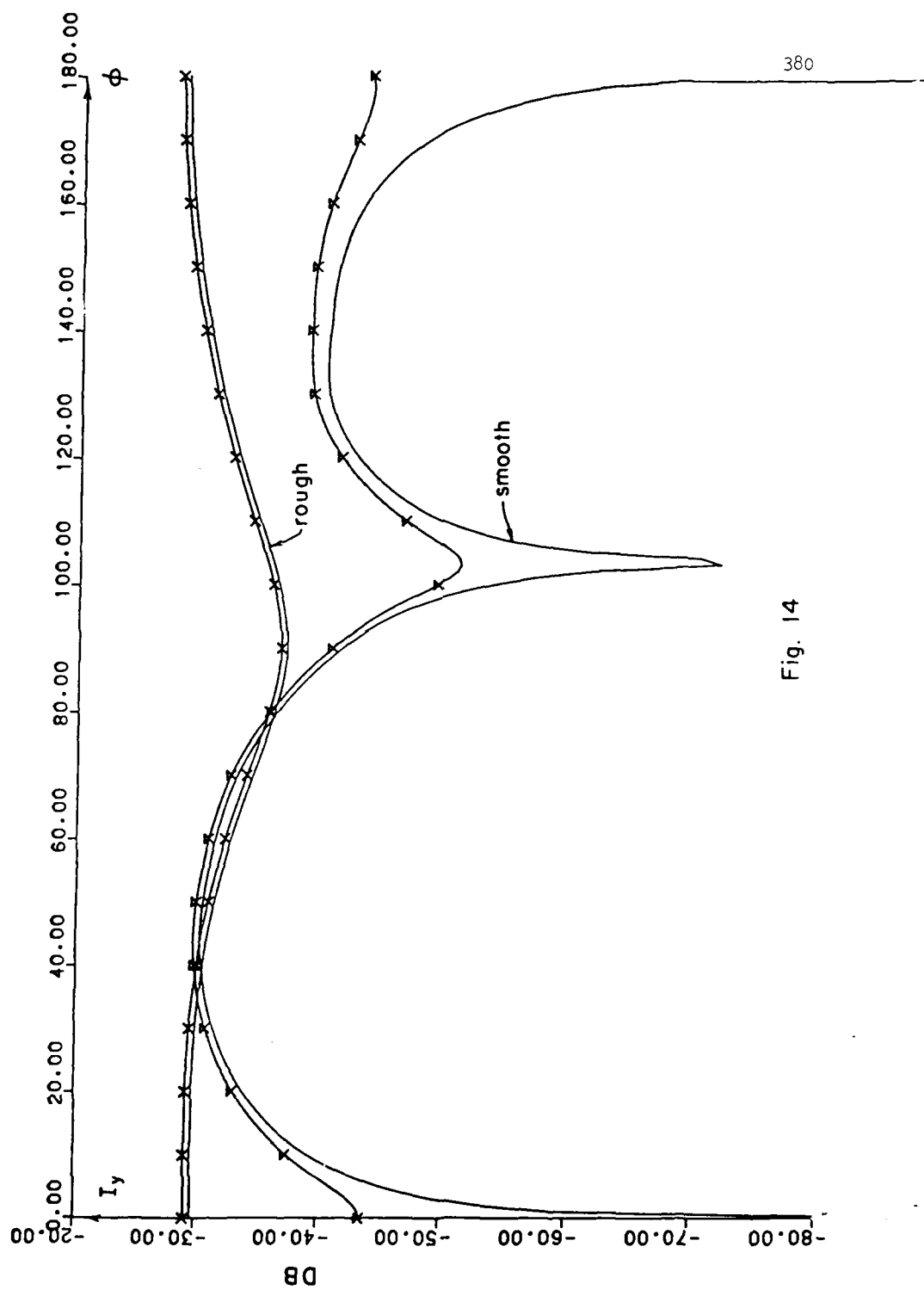


Fig. 14

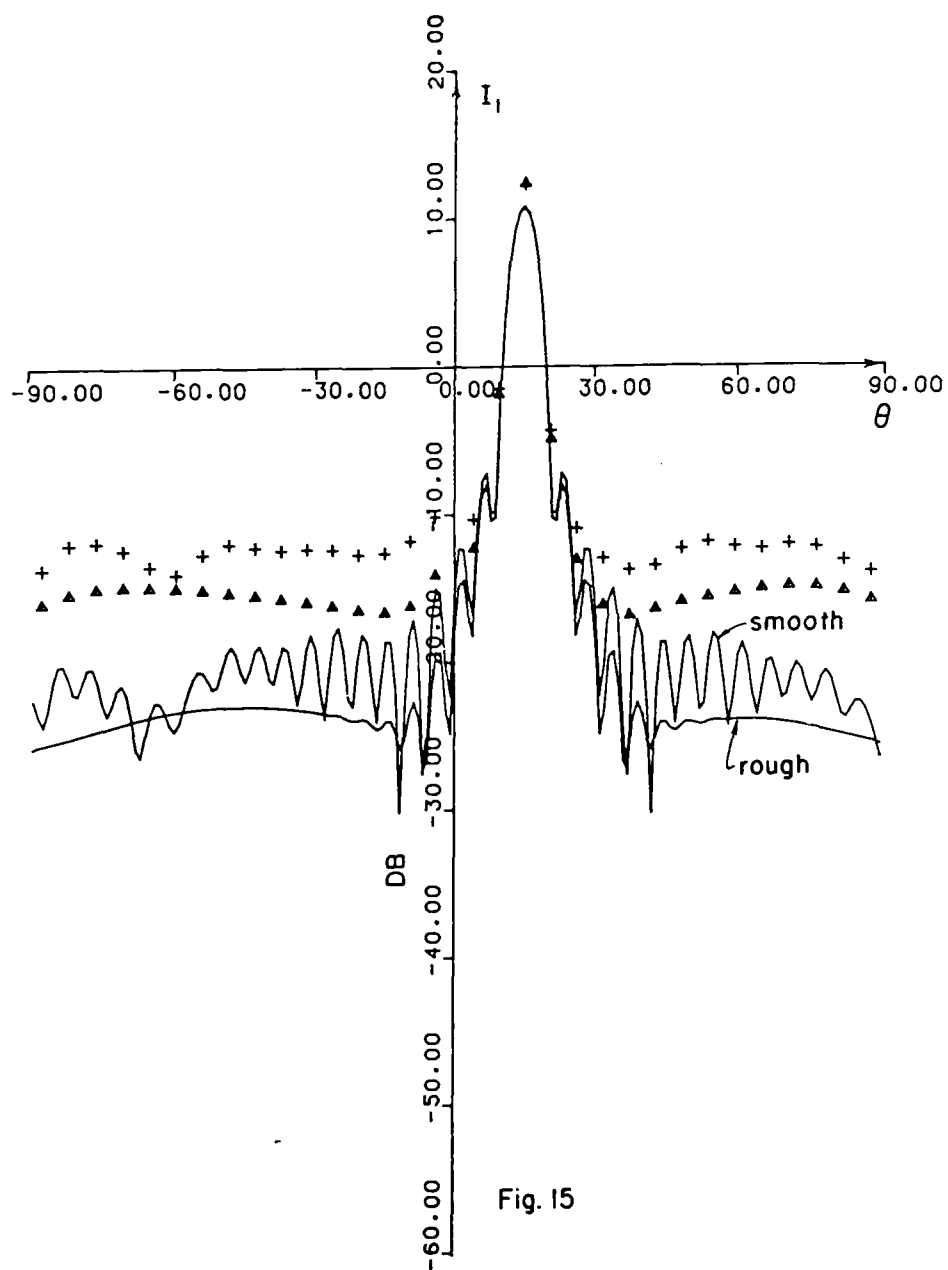


Fig. 15

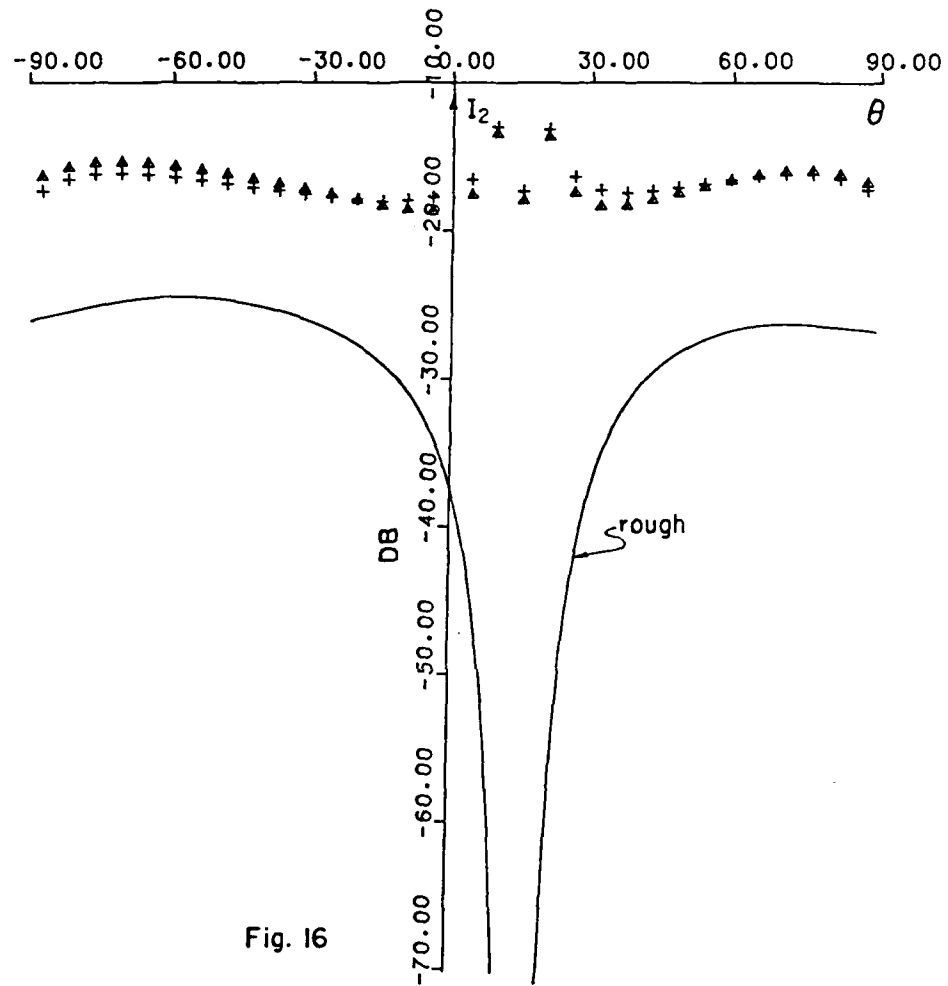


Fig. 16

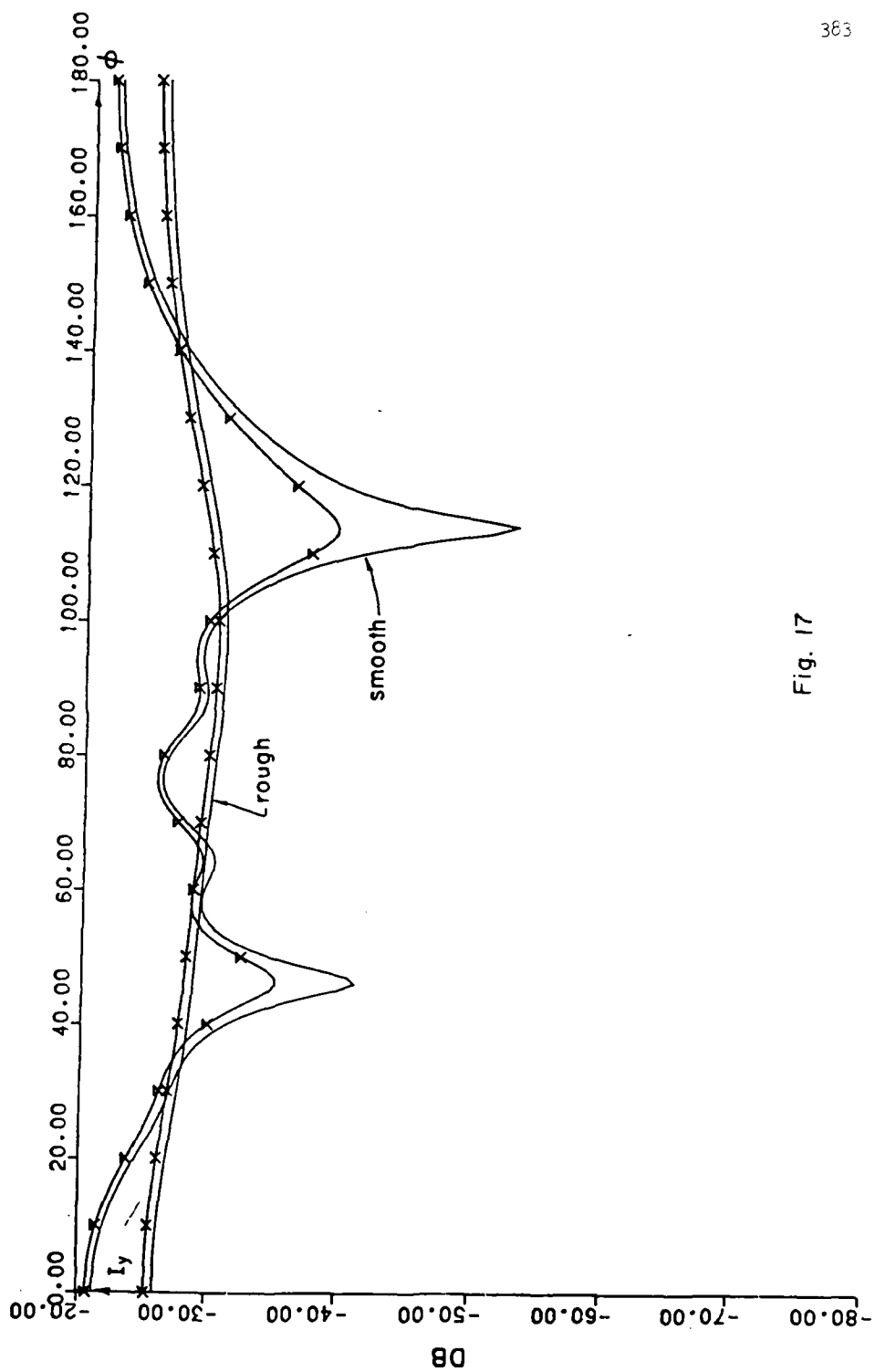


Fig. 17

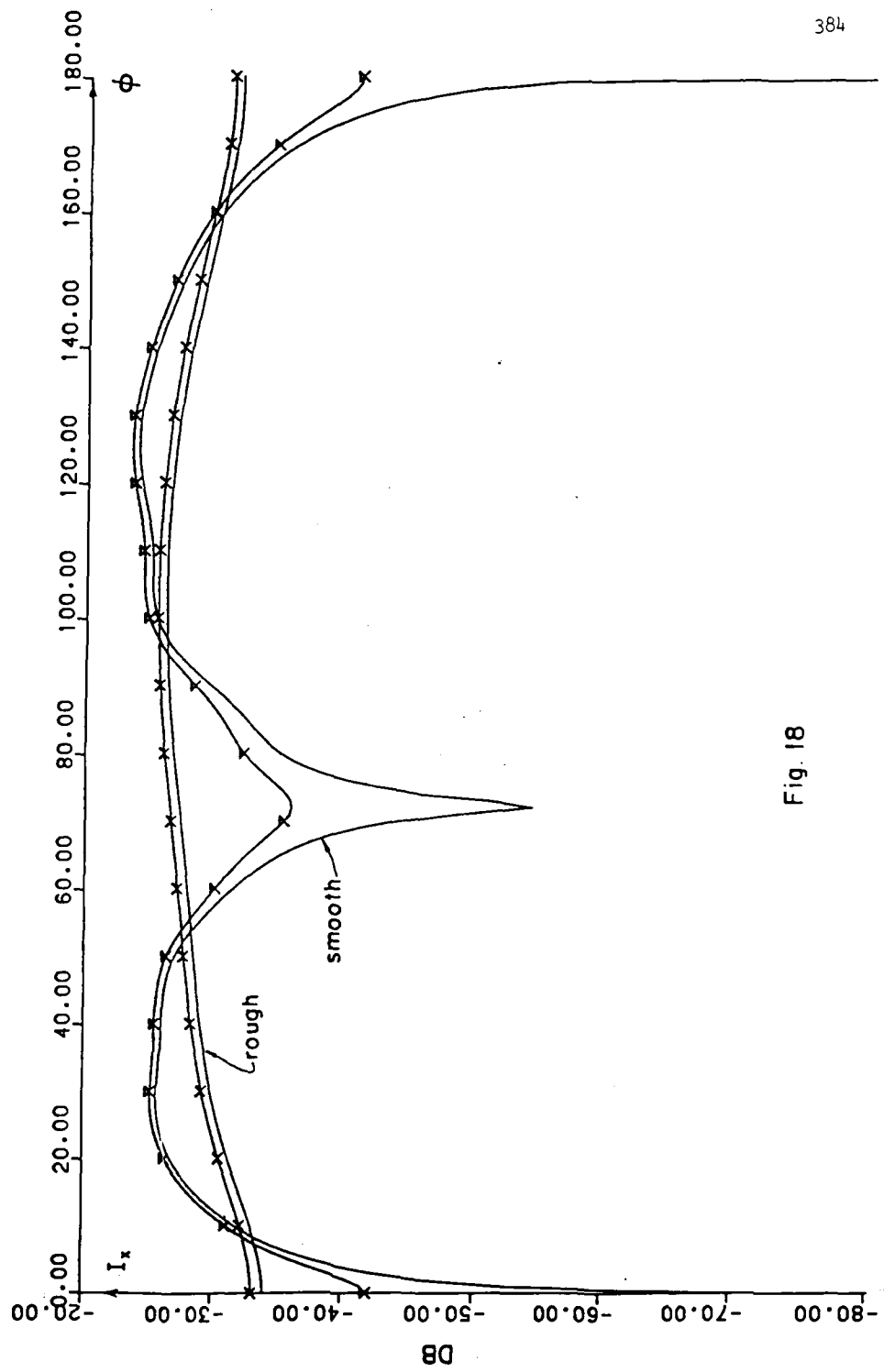


Fig. 18

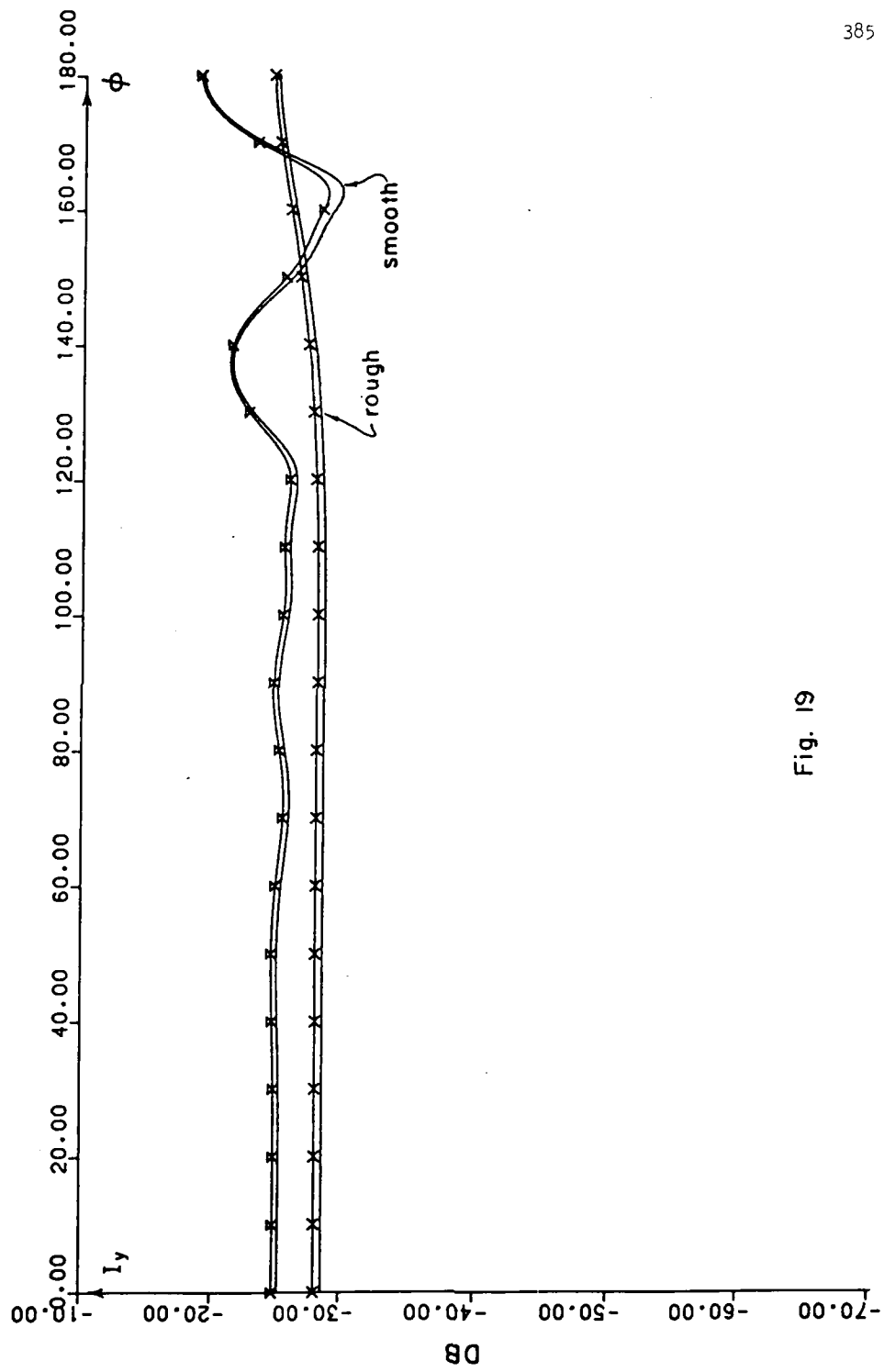


Fig. 19

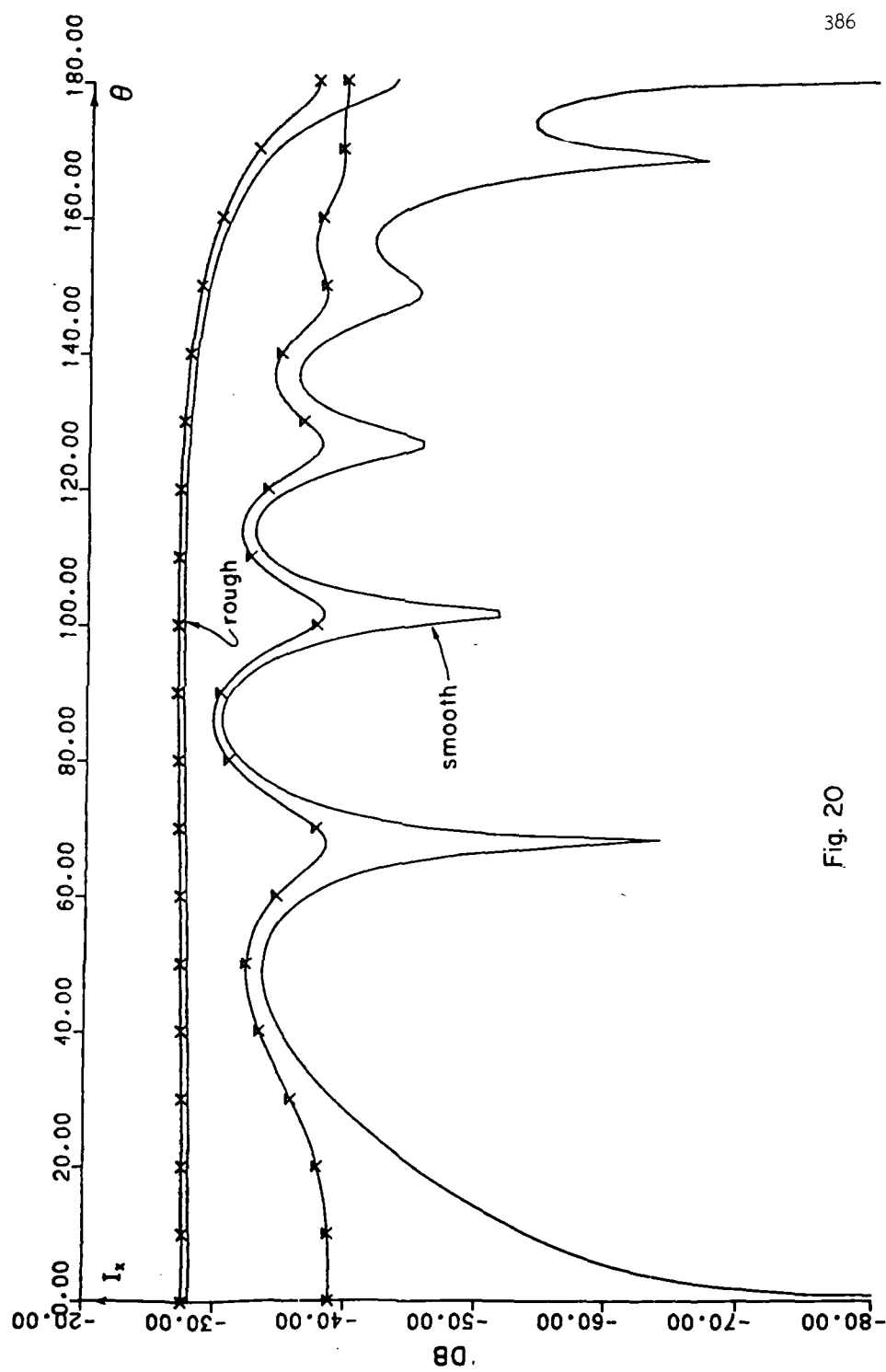


Fig. 20

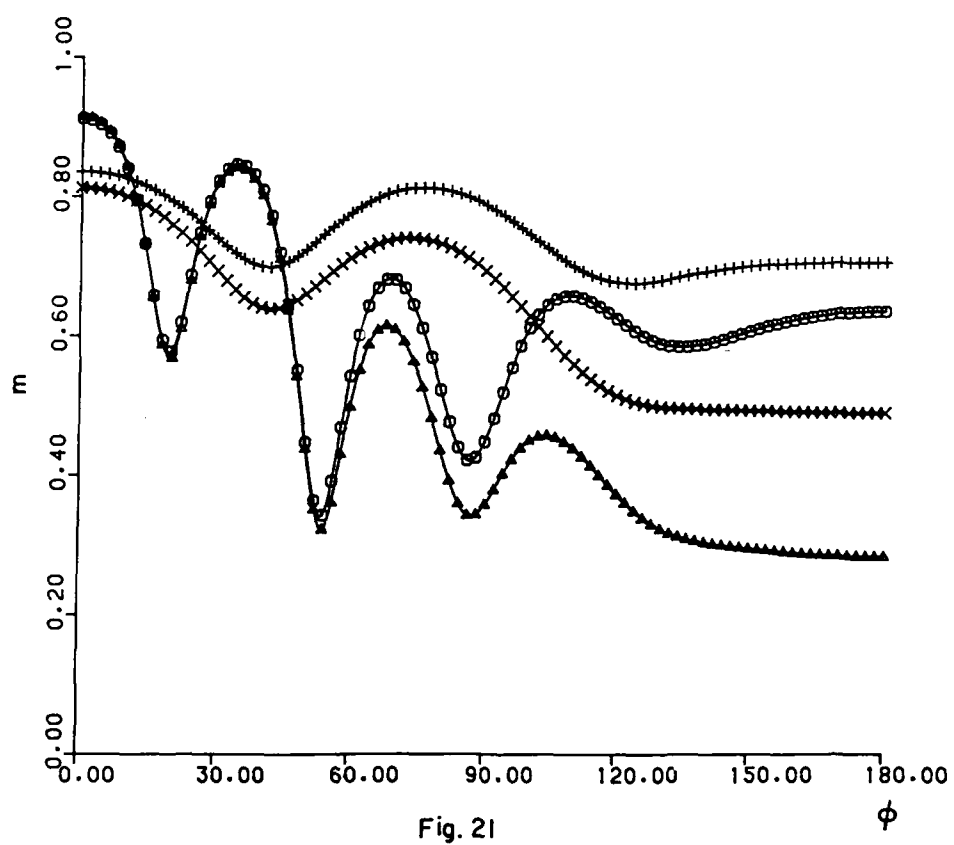
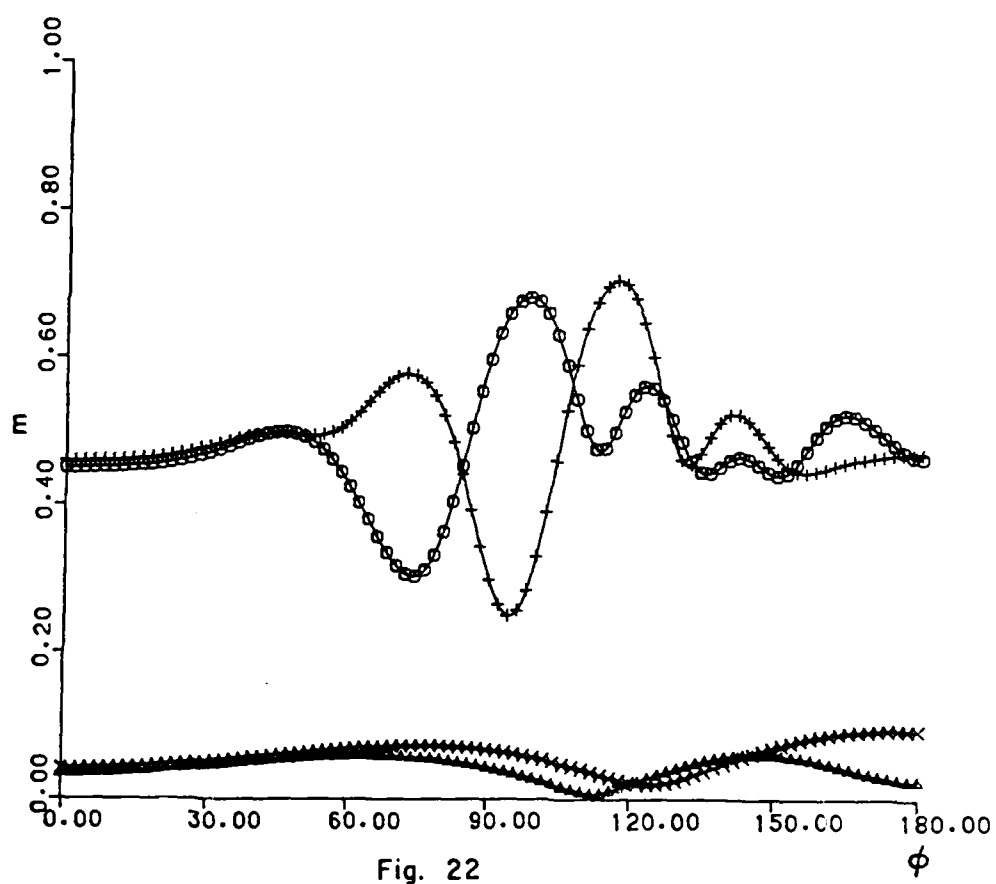


Fig. 21



COMPUTER AIDED GRAPHICS FOR THREE DIMENSIONAL OBJECTS
BASED ON FULL WAVE THEORY

Ezekiel Bahar

and

Swapan Chakrabarti

Department of Electrical Engineering
University of Nebraska-Lincoln
Lincoln NE 68588-0511

ABSTRACT

A new reflection model for computer generated synthetic images of metallic objects is developed. This model is based on a full wave analysis of electromagnetic scattering by rough surfaces. The full wave approach accounts for specular point scattering and diffuse scattering in a self-consistent manner. The model presented here is compared with earlier models. It is shown that the practical application of the new reflection model to computer aided geometric design of manufactured objects is relatively easy to implement.

I. INTRODUCTION

Over the period of the last decade the reflection models for computer generated synthetic images have been improved in order to produce very realistic images of three dimensional objects on a two dimensional screen. Phong [18] began by computing the intensity of each pixel as a linear combination of diffuse and specularly reflected components. Diffuse reflection was simulated using Lambert's cosine law. While specular reflection was accounted for by using the cosine function raised to the n^{th} power (typically n ranges from 1 to 10) with its peak at the specular point. Blinn [7,8] modified this model by adopting the specular reflection model described in the work of Torrance and Sparrow [7]. In their model the simulated rough surface is assumed to be composed of mirror-like microfacets which are oriented randomly all over a smooth surface. Later Whitted [19] introduced an enhanced ray tracing model, in which the intensity at each pixel is computed from the global illumination information. Cook and Torrance [13, 14] applied their reflectance model to computer graphics. Their model took into account the effect of the spectral distribution of the energy of the incident light and the reflectance spectra of the object to display the color of the object. Recently Kajiya [17] introduced an anisotropic reflection model for surfaces which exhibit anisotropy in their scattering pattern. However, in

practically all the above mentioned models the specular reflection component is characterized by the Fresnel reflection coefficient and the diffuse contribution is assumed to be Lambertian.

In this paper scattering from rough surfaces based on full wave theory is reviewed. The full wave theory is based on the complete spectral representation of the scattered fields and upon the imposition of exact boundary conditions at the irregular surface. This theory accounts for both specular reflection and diffuse reflection. A reflection model for computer generated synthetic images is derived from the full wave analysis.

In this investigation the rough surface is assumed to be isotropic and homogeneous. In addition the mean square slope of the random rough surface, which is superimposed on the unperturbed surface, is assumed to be small ($\langle \sigma_s^2 \rangle \leq 0.1$). Hence for convex shapes (as in cylinders, spheres or cones) multiple scattering between different surface elements of the object is ignored.

In Section II the problem is formulated and the principal elements of the full wave solutions are obtained. Expressions for the total reflected intensities are evaluated in Section III for objects illuminated by unpolarized light. In Section IV the diffuse and specular scattering contributions from different surface elements of the objects are examined in detail. and the full wave reflection model for computer generated synthetic images is derived. In Section V the full wave reflection model is used to generate the three dimensional primitives for computer aided geometric design by locating isointensity contours.

II. FORMULATION OF THE PROBLEM

For the purpose of computer aided graphics of manufactured objects, it has been shown [15] that almost 95% of the surfaces of the manufactured objects can be described as combinations of planes, cones, cylinders and spheres. In general these primitives have some measure of roughness and therefore it is necessary to examine in detail scattering from rough surfaces. The objective of this research is to develop realistic models in order to generate these primitives for computer graphics. In this presentation spherical scatterers are considered in detail and in the analysis, it is assumed initially that the spheres are illuminated by vertically or horizontally polarized light [3].

Consider a large spherical surface perturbed by a superimposed random rough surface. The height of the random rough surface h is measured along the normal to the unperturbed spherical surface. It is characterized by its spectral density function. The position vector \bar{r}_s to a point on the rough surface is given by

$$\bar{r}_s = a \hat{a}_r + h \hat{a}_r \quad (1)$$

where \hat{a}_r is the unit radius vector and the radius of the unperturbed sphere, a , is assumed to be large compared to the wavelength, λ_0 , of the incident wave.

The normal to the unperturbed sphere $\hat{n} = \hat{a}_r$ is

$$\hat{n} = \sin\gamma \cos\delta \hat{a}_x + \sin\gamma \sin\delta \hat{a}_y + \cos\gamma \hat{a}_z \quad (2)$$

where γ and δ are polar and azimuthal angles respectively (Fig. 1). In view of the spherical symmetry, the coordinate system is chosen such that unit vectors \hat{n}^i and \hat{n}^f in the direction of the incident and scattered waves are (see Fig. 1).

$$\hat{n}^i = \sin\theta_o^i \hat{a}_y - \cos\theta_o^i \hat{a}_z \quad (3)$$

$$\hat{n}^f = \sin\theta_o^f \hat{a}_y + \cos\theta_o^f \hat{a}_z \quad (4)$$

in which $\theta_o^i = \theta_o^f$. The vector \bar{v} which bisects the angle between the incident and scattered wave normals is

$$\bar{v} = k_o (\hat{n}^f - \hat{n}^i) = 2k_o \cos\theta_o^f / \hat{a}_z = |\bar{v}| \hat{v} \quad (5)$$

and

$$\hat{v} = \frac{\bar{v}}{|\bar{v}|} = \hat{a}_z \quad (6)$$

For a Gaussian random rough surface height h , with mean square height $\langle h^2 \rangle$ the characteristic function is

$$\chi(v_z) = \exp\{-v_z^2 \langle h^2 \rangle / 2\}, \quad (v_z = \bar{v} \cdot \hat{n}) \quad (7)$$

in which v_z is the component of \bar{v} normal to the unperturbed surface.

The total normalized differential scattering cross section per unit projected area A_z of the object is given by [16]

$$\langle \sigma^{PQ} \rangle = \frac{4\pi(r^f)^2}{A_z} \left\langle \left| \frac{E^{Pf}}{E^{Qi}} \right|^2 \right\rangle \quad (8)$$

In (8) the second superscript Q corresponds to the polarization of the incident field and the first superscript P corresponds to the polarization of the scattered wave. Pursuant to the choice of the coordinate system, the plane of incidence (normal to $\hat{x}\hat{a}_z$) and the plane of scatter (normal to $\hat{n}^f \hat{x} \hat{a}_z$) are in the scattering plane (normal to $\hat{n}^i \times \hat{n}^f$). E^{Pf} and E^{Qi} are the scattered

and incident electric fields respectively [12]. The distance to the observation point from origin is r^f .

Using the full wave approach $\langle \sigma^{PQ} \rangle$ is expressed as a weighted sum [2]

$$\langle \sigma^{PQ} \rangle = \langle \sigma^{PQ} \rangle_L + \langle \sigma^{PQ} \rangle_R \quad (9)$$

in which $\langle \sigma^{PQ} \rangle_L$ is the cross section associated with the large scale unperturbed surface and $\langle \sigma^{PQ} \rangle_R$ is the cross section associated with the rough surface h that is superimposed on the large scale spherical surface. Using a steepest descent or stationary phase approximation [5] $\langle \sigma^{PQ} \rangle_L$ reduces to the form

$$\langle \sigma^{PQ} \rangle_L = |\chi(v)|^2 |R_P|^2 \delta_{PQ} \quad (10)$$

where R_P is the Fresnel reflection coefficient for vertically ($P=V$) or horizontally ($P=H$) polarized waves and δ_{PQ} is the Kronecker delta. The unit vector normal to the unperturbed surface at the specular point is given by

$$\left. \begin{aligned} \hat{n}_s &= \hat{v} \approx \hat{a}_z \\ \hat{v} \cdot \hat{n}_s &= v \end{aligned} \right\} \quad \text{and} \quad (11)$$

Hence equation (10) reduces to

$$\langle \sigma^{PQ} \rangle_L = e^{-4k_o^2 \langle h^2 \rangle \cos^2 \theta_o^f} |R_P|^2 \delta_{PQ} \quad (12)$$

In equation (10) $|\chi|^2$ represents the degradation of specular point, physical optics, scattering cross section of the large

scale smooth sphere due to the rough surface superimposed on its surface. This decrease in the specular point scattering is accompanied by the diffuse scattering contribution $\langle \sigma^{PQ} \rangle_R$ due to the rough surface h.

Using the full wave approach [4] it is shown that

$$\langle \sigma^{PQ} \rangle_R = k_o^2 \int_0^{2\pi} \int_{-1}^1 |D^{PQ}|^2 Q_R(v, v_T) P_2 \, d\mu d\delta \quad (13)$$

where $d\mu d\delta = -d(\cos\gamma) d\delta$ is the differential solid angle. The function P_2 is unity for the illuminated and visible portions of the sphere and it is zero elsewhere. Furthermore,

$$\begin{aligned} Q_R(v, v_T) &= \int_{-\infty}^{+\infty} (\chi_2 - |\chi|^2) \exp(i\bar{v} \cdot \bar{r}_d) d\chi_d dy_d \\ &= 2\pi \int_0^{\infty} (\chi_2 - |\chi|^2) J_0(v_T r_d) r_d dr_d \end{aligned} \quad (14a)$$

where J_0 is the Bessel function of the first kind of order 0 and χ_2 , the joint surface height characteristic function for Gaussian surfaces, is given by [6]

$$\chi_2 = |\chi|^2 \exp(-\langle hh' \rangle v_z^2) \quad (14b)$$

in which $\langle hh' \rangle$ is the rough surface height autocorrelation function. The component of \bar{v} tangent to the unperturbed surface is

$v_T = \sqrt{v_x^2 + v_y^2}$ and the distance $r_d = \sqrt{x_d^2 + y_d^2}$ is measured along the surface of the unperturbed sphere. In equation (13) D^{PQ} is

an element of a 2×2 scattering matrix whose elements are functions

AD-A171 218

DEPOLARIZATION AND SCATTERING OF ELECTROMAGNETIC WAVES
APPENDICES (U) NEBRASKA UNIV LINCOLN E SAHAR 30 JUN 86
ARO-18120.17-EL-APP DAAG29-82-K-0123

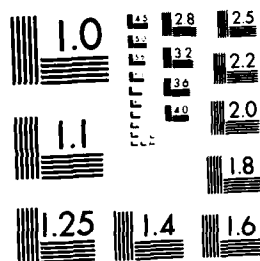
5/5

UNCLASSIFIED

F/G 20/14

ML

END
DATE
FILMED
9-86
DTIC



MICROCOPY RESOLUTION TEST CHART
NATIONAL BUREAU OF STANDARDS-1963-A

of \hat{n}^i , \hat{n}^f , \hat{n} , the complex electric permittivity and permeability of the particle [12].

Hence from equations (9) and (10) one obtains

$$\begin{aligned}\langle \sigma^{VV} \rangle &= \langle \sigma^{VV} \rangle_R + |\chi(v)|^2 |R_V|^2 \\ \langle \sigma^{VH} \rangle &= \langle \sigma^{VH} \rangle_R \\ \langle \sigma^{HV} \rangle &= \langle \sigma^{HV} \rangle_R \\ \langle \sigma^{HH} \rangle &= \langle \sigma^{HH} \rangle_R + |\chi(v)|^2 |R_H|^2\end{aligned}\tag{15}$$

The above equations imply that there are no physical optics (specular point) contributions to the cross polarized cross sections (where the planes of incidence and scatter are in the scatter plane). It is assumed in (14a) that the rough surface height correlation distance τ_c (where $\langle hh' \rangle$ reduces to $\exp(-1) \langle h^2 \rangle$) is smaller than the particle circumference.

III. COMPUTATIONS OF SCATTERED INTENSITY FOR UNPOLARIZED EXCITATIONS

Metallic objects are visible due to the light that is reflected primarily from their surfaces [13]. In this section the full wave expressions for the scattered intensities from surfaces illuminated by unpolarized excitations are derived.

For single scatterers the incident and scattered intensities I^i and I^f are related by the 4×4 phase matrix S . Thus [16]

$$[I^f] = \frac{1}{(r^f)^2} [S][I^i] \quad (16)$$

in which the elements of the 4×1 column matrices $[I^i]$ and $[I^f]$ are the modified Stokes parameters (watts/m²) for incident and scattered waves respectively.

$$[I^k] = \begin{bmatrix} I_1^k \\ I_2^k \\ U^k \\ V^k \end{bmatrix} = \begin{bmatrix} \langle |E^{V_k}|^2 \rangle \\ \langle |E^{H_k}|^2 \rangle \\ \text{Re} \langle (2E^{V_k} E^{H_k*}) \rangle \\ \text{Im} \langle (2E^{V_k} E^{H_k*}) \rangle \end{bmatrix} \quad (17)$$

In (17) $k = i$ or f and the ensemble average is denoted by the symbol $\langle \rangle$.

For natural light, which is unpolarized, the intensities of the electromagnetic fields are the same for all directions perpendicular to the direction of propagation of the wave and there is no correlation between the orthogonal components of the fields. Hence, if the total incident intensity is unity, the incident modified

Stokes parameters are $I_1^i = I_2^i = \frac{1}{2}$ and $U^i = V^i = 0$. Thus, for unpolarized light equation (16) reduces to [4]

$$\begin{bmatrix} I_1^f \\ I_2^f \end{bmatrix} = \frac{1}{(r^f)^2} \begin{bmatrix} S_{11} & S_{12} \\ S_{21} & S_{22} \end{bmatrix} \begin{bmatrix} 1/2 \\ 1/2 \end{bmatrix} \quad (18)$$

where

$$\begin{aligned} S_{11} &= \frac{A_z}{4\pi} \langle \sigma^{VV} \rangle \\ S_{12} &= \frac{A_z}{4\pi} \langle \sigma^{VH} \rangle \\ S_{21} &= \frac{A_z}{4\pi} \langle \sigma^{HV} \rangle \\ S_{22} &= \frac{A_z}{4\pi} \langle \sigma^{HH} \rangle \end{aligned} \quad (19)$$

and the scattering cross sections $\langle \sigma^{PQ} \rangle$ are defined in equation (15). Since scattering in the near specular direction from the surface element of the conducting object is practically independent of polarization it is assumed that the incident unpolarized light remains unpolarized upon reflection by the object. Thus, $U^f = V^f = 0$ and the total unpolarized scattered intensity is

$$\begin{aligned} I_T = I_1^f + I_2^f &= \frac{A_z}{4\pi(r^f)^2} [(\langle \sigma^{VV} \rangle_R + \langle \sigma^{VH} \rangle_R + \langle \sigma^{HV} \rangle_R + \langle \sigma^{HH} \rangle_R)/2 \\ &+ |X|^2 |R|^2] \end{aligned} \quad (20)$$

where $|R|^2 = (|R_V|^2 + |R_H|^2)/2$ is referred to as the Fresnel power reflection coefficient for unpolarized light.

Equation (20) is rewritten for convenience as follows

$$I_T = \frac{A_2}{4\pi f_i^2} (\sigma_d + \sigma_{PO}) \quad (21)$$

where σ_d is the total normalized diffuse differential scattering cross section. It is given by

$$\sigma_d = (\langle \sigma^{VV} \rangle_R + \langle \sigma^{VH} \rangle_R + \langle \sigma^{HV} \rangle_R + \langle \sigma^{HH} \rangle_R) / 2 \quad (22)$$

The corresponding specular point contribution is given by

$$\sigma_{PO} = |X(v)|^2 |R|^2 \quad (23)$$

IV. DEVELOPMENT OF THE FULL WAVE REFLECTION

MODEL FOR DIFFUSE AND SPECULAR SCATTERING

For the illustrative examples used in the development of the full wave reflection model, the rough surface height spectral density function is assumed to be

$$W(v_T) = \frac{2C}{\pi} \left[\frac{v_T}{v_T^2 + v_m^2} \right]^8 \quad (24)$$

The peak value of $W(v_T)$ is $W(v_T = v_m) = \frac{C}{128\pi v_m^8}$. The corresponding mean square rough surface height $\langle h^2 \rangle$ and the mean square slope $\langle \sigma_s^2 \rangle$ are given by

$$\langle h^2 \rangle = C/(210 v_m^6) \quad (25a)$$

$$\langle \sigma_s^2 \rangle = C/(84 v_m^4) \quad (25b)$$

The wavelength of the monochromatic illumination is

$$\lambda_o = 0.555 \times 10^{-4} \text{ cm} \quad (26a)$$

and

$$k_o = \frac{2\pi}{\lambda_o} \quad (26b)$$

The diameter of the unperturbed sphere is

$$D = 10\lambda_o \quad (27a)$$

and

$$v_m = 4/D = 0.4/\lambda_o \quad (27b)$$

The relative dielectric coefficient is $\epsilon_r = -40 - j12$ (aluminum) [3].

The random rough surface height (Rayleigh) parameter is defined by

$$\beta = 4k_0^2 \langle h^2 \rangle \quad (27c)$$

The constant C in (24) is related to the roughness parameter β through (25a). In Fig. (2), the spectral density function $W(v_T)$ (equation (24)) is plotted for several values of β .

The diffuse and specular scattering contributions to the total reflected intensity are considered separately in this section. Using equations (22) and (13), the diffuse scattering contribution is expressed as follows

$$\begin{aligned} \sigma_d &= k_0^2 \int_0^{2\pi} \int_{-1}^1 [|D^{VV}|^2 + |D^{VH}|^2 + |D^{HV}|^2 + |D^{HH}|^2] \\ &\quad \cdot Q_R \cdot P_2 \, d\mu d\delta \\ &= \int \sigma_\Omega^d(\gamma, \delta) d\Omega \end{aligned} \quad (28)$$

where $d\Omega = -d\mu d\delta$ is the differential solid angle and the integrand σ_Ω^d in equation (28) is the normalized diffuse intensity scattered by an element of the surface of the sphere subtended by the solid angle $d\Omega$.

For the backscatter case ($\theta_o^i = \theta_o^f = 0$) the normalized diffuse scattering cross section (per unit solid angle) σ_Ω^d (28) is plotted in Figures (3) and (4) as a function of the polar angle γ and the azimuthal angle δ (see Figure (1)). In Figure (3) the roughness parameter is $\beta = 10$ and in Figure (4), $\beta = 40$. Note that

σ_{Ω}^d is azimuthally symmetric for backscatter since $\hat{v} = \hat{a}_z$. In Figure (5) σ_{Ω}^d is plotted for the bistatic case, with $\theta_o^i = \theta_o^f = 40^\circ$ and $\beta = 40$. Here, too, σ_{Ω}^d is practically independent of δ . It is apparent from Figures (3), (4) and (5), that the diffuse scattering contribution σ_{Ω}^d decreases more rapidly as a function of γ than predicted by Lambert's cosine law. Indeed it is shown in this section that the dependence of σ_{Ω}^d upon γ is very nearly Gaussian for $\beta \geq 7$.

It is interesting to note that using a physical optics (Kirchhoff) approach [5,6] it has been shown that the mean power reflection coefficient is proportional to the probability density for the rough surface slopes at the specular point. Thus, since \hat{n} is the normal to the unperturbed reference surfaces (\hat{a}_z in Beckmann's work) the angle between the bisector of the incident and scattered waves and the normal to the unperturbed reference surface is

$$\alpha = \cos^{-1}(\hat{n} \cdot \hat{v}) = \gamma \quad (\text{for } \hat{v} = \hat{a}_z) \quad (29a)$$

Thus Cook and Terrence [14] who adopted Beckmann's results obtained images of three dimensional metallic objects that are more realistic than the images obtained on assuming Lambert's cosine law.

In view of the azimuthal symmetry of σ_{Ω}^d for arbitrary $\theta_o^i = \theta_o^f$ only the backscatter case $\theta_o^i = \theta_o^f = 0$ is considered here in detail and σ_{Ω}^d is plotted as a function of α only. In Figure (6) the normalized quantity $\sigma_{\Omega}^d / \sigma_{\Omega}^d(0)$ is plotted as a function of

$\alpha(0 \leq \alpha \leq \pi/2)$. For all the plots in this figure, the mean square slope of the rough surface is constant ($\langle \sigma_s^2 \rangle = 0.1$) while the roughness parameter β is 1, 5, 7, 10 and 40. For $\beta \geq 7$ the plots of $\sigma_\Omega^d(\alpha)/\sigma_\Omega^d(0)$ are rather insensitive to variations in β .

As β decreases below 7 the diffuse scattering contribution from regions around the specular point decreases. However, as β decreases the diffuse scattering contribution becomes less significant than the physical optics contribution (equation (21)). Hence, the total (diffuse + specular) scattered intensity is maximum at the specular points even for small β . In Figure (7) $\sigma_\Omega^d/\sigma_\Omega^d(0)$ is plotted as a function of α for mean square slopes 0.1, 0.05 and 0.025, respectively.

In all these plots the correlation length is fixed and $\tau_c/\pi D = 0.032$. In Figures (8), (9), (10), σ_Ω^d are plotted as functions of α for the three cases shown in Figure (7). In these figures the full wave solutions for σ_Ω^d are compared with the analytical expression $\exp(-(\alpha^2/\langle \sigma_s^2 \rangle))$. It is apparent from Figures (6) through (10) that the angular dependence of the diffuse component is primarily a function of the mean square slope of the rough surfaces.

In Figure (11) $\sigma_\Omega^d(0)/\sigma_\Omega^d(0)|_{\epsilon_r \rightarrow \infty}$ is plotted as a function of β for the backscatter case ($\hat{n}^f = -\hat{n}^i$). The permittivity of the scatterer is assumed to be (a) $|\epsilon_r| \rightarrow \infty$ (perfect conductor) (b) $\epsilon_r = -40 - i12$ (aluminum) [3] and (c) $\epsilon_r = 1.5 - i8$ (dissipative plastic). For $\beta \geq 7$ $\sigma_\Omega^d(\alpha)$ is maximum at $\alpha = 0$ (see Figure (6)).

An approximate analytical formula of the form

$$f(\beta) = \frac{1}{1+0.1 \ln(\beta/\beta_{\min})} = \sigma_{\Omega}^d(0)/\sigma_{\Omega}^d(0)_{\beta=\beta_{\min}} \quad (29b)$$

is found to approximate the analytical results (obtained using the full wave approach) reasonably well for $\beta > \beta_{\min} = 7$.

In Figure (12) the ratio $\sigma_{\Omega}^d(0)/\left[\sigma_{\Omega}^d(0)\right]_{\langle\sigma_s^2\rangle=0.1}$ is plotted as a function of the mean square slope $\langle\sigma_s^2\rangle$ for $\beta = 20$. It is found to be in good agreement with the formula $f(\langle\sigma_s^2\rangle) = \frac{0.1}{\langle\sigma_s^2\rangle}$.

Using the above result based on full wave theory, the following simplified analytical model of the diffuse reflection contribution to the backscattered power is proposed

$$\sigma_{\Omega}^d(\alpha) = \sigma_{\Omega_0}^d f(\beta) \exp(-\alpha^2/\langle\sigma_s^2\rangle) \quad (30a)$$

since $f(\beta) = 1$ for $\beta = \beta_{\min} = 7$ and $\exp(-\alpha^2/\langle\sigma_s^2\rangle) = 1$ for $\alpha = 0$, the coefficient $\sigma_{\Omega_0}^d$ is equal to $\sigma_{\Omega}^d(0)$ evaluated for $\beta = 7$. Thus using (28)

$$\sigma_{\Omega}^d(0) = 2k_o^2 |R|^2 Q_R \quad (30b)$$

Where Q_R reduces to (for $|X|^2 \ll 1$)

$$Q_R = 2\pi \int \exp[-v_z^2 \langle h^2 \rangle (1-R_c(r_d))] \cdot J_0(v_T r_d) r_d dr_d \quad (31a)$$

in which the normalized autocorrelation function is

$$R_c(r_d) = \langle hh' \rangle / \langle h^2 \rangle \quad (31b)$$

For the surface height spectral density function assumed (24)

$$R_c(r_d = \xi/v_m) = [1 - \frac{3\xi^2}{8} + \frac{3\xi^4}{32} + \frac{\xi^6}{3072}] K_1(\xi) + [\frac{1}{2} - \frac{\xi^2}{4} - \frac{\xi^4}{96}] \xi^2 K_0(\xi) \quad (32)$$

where K_0 and K_1 are defined as Bessel functions of the second kind of order zero and one respectively. However to evaluate (32) for $\beta \gg 1$ it is sufficient to retain the first two terms of the Taylor series expansion of $R_c(r_d)$. Thus

$$R_c(r_d) = 1 - \left(\frac{r_d}{\tau_c}\right)^2 \quad (33)$$

where

$$\tau_c^2 = 2/R_c''(0) \quad (34)$$

Since $J_0''(0) = -v_T^2/2$ it follows that

$$R_c''(0) = -\frac{\langle \sigma_s^2 \rangle}{2\langle h^2 \rangle} \quad (35)$$

Hence

$$\tau_c^2 = 4\langle h^2 \rangle / \langle \sigma_s^2 \rangle = \left(\frac{1.265}{v_m} \right)^2 \quad (36)$$

and $\sigma_\Omega^d(0)$ for the backscatter at normal incidence ($v_T = 0$) reduces to

$$\begin{aligned} \sigma_\Omega^d(0) &= 2\pi k_o^2 \int_0^\infty \exp\left(-\beta \left(\frac{r_d}{\tau_c}\right)^2\right) r_d dr_d |R|^2 \\ &= \frac{2\pi k_o^2 \tau_c^2 |R|^2}{2\beta} = \frac{\pi |R|^2}{\langle \sigma_s^2 \rangle} + \sigma_{\Omega 0}^d \end{aligned} \quad (37)$$

This result is in complete agreement with the slope dependence of $\sigma_\Omega^d(0)$ shown in Figure (12). Note that the above analytical approximation for $\sigma_\Omega^d(0)$ is independent of β . However, the exact numerical results obtained from the full wave analysis show

that $\sigma_{\Omega}^d(0)$ is weakly dependent on the roughness parameter β (see Figure (11)). As β increases (above 7) $\sigma_{\Omega}^d(0)$ decreases slightly since there is a small increase in the power absorbed by the rough surface as the roughness parameter β increases [3]. Note also that the level of the curves for $\sigma_{\Omega}^d(0)/\sigma_{\Omega}^d(0)|_{\epsilon \rightarrow \infty}$ (see $\beta=7$ Figure (11)) depends on $|R|^2$ as predicted by equation (37).

The physical optics (specular point) contribution to the full wave reflection model σ_{PO} (equation (23)) is considered now in detail. It is expressed in a similar way as the diffuse scattering contribution σ_d (equation (28)). Thus defining σ_{Ω}^P as the normalized physical optics intensity scattered by an element of the surface of the rough sphere subtended by the solid angle $d\Omega$, the total physical optics contribution σ_{PO} is given by

$$\sigma_{PO} = \int \sigma_{\Omega}^P(\alpha) d\Omega = |\chi|^2 |R|^2 \quad (38)$$

where

$$\alpha = \cos^{-1}(\hat{n} \cdot \hat{v}) = \gamma \text{ for } (\hat{v} = \hat{a}_z)$$

and

$$\sigma_{\Omega}^P(\alpha) = \sigma_{\Omega}^P(0) e^{-\left(\frac{\alpha}{\alpha_0}\right)^2} \quad (39)$$

Thus

$$\sigma_{\Omega}^P(0) = \frac{|\chi|^2 |R|^2}{\pi \alpha_0^2} \quad (40)$$

The angle α_0 is the value of α where $\sigma_{\Omega}^P(\alpha) = \sigma_{\Omega}^P(0)/\exp(1)$. It is obtained on expanding the exponent in the integral expression for the physical optics contribution to the scattered field [5] in a Taylor series about the saddle (specular) point. Thus it can be shown that

$$\alpha_o^2 = \frac{1}{va} \quad (41)$$

where $a = \frac{D}{2}$, is the radius of the sphere. For nonspherical objects "a" should be replaced by the geometric mean of the principal radii of curvature of the specular points. It is interesting to note that the area of the first Fresnel zone around the specular point [10]

$$A = \pi a \lambda \quad (42)$$

The polar angle θ_o subtended by the first Fresnel zone is given by the following expression

$$A = \pi a \lambda = a^2 \int_0^{\theta_o} \sin \theta d\theta d\phi = 2\pi a^2 (1 - \cos \theta_o) \approx \pi a^2 \theta_o^2 \quad (43)$$

Thus

$$\theta_o = \sqrt{\lambda/a} = \sqrt{4\pi} \alpha_o \quad (44)$$

The ratio $\sigma_{\Omega}^P(0)/\sigma_{\Omega}^d(0)$ is given by equations (37) and (40).

Thus for $\beta > 7$

$$\frac{\sigma_{\Omega}^P(0)}{\sigma_{\Omega}^d(0)} \approx \frac{|\chi| \langle \sigma_s^2 \rangle}{\pi^2 \alpha_o^2} \quad (45)$$

For the parameters of the sphere with the rough surface assumed in this section ($a = 5\lambda_o$, $\langle \sigma_s^2 \rangle = 0.1$ and $\beta \geq 7$).

$$\frac{\sigma_{\Omega}^P(0)}{\sigma_{\Omega}^d(0)} \leq 0.6 \times 10^{-3} \quad (46)$$

Thus in order to compute the backscattered intensity at each pixel I_p of constant area on the image plane, the reduced physical optics contribution $\sigma_{\Omega}^P(\alpha)$ is neglected and the following expression is used (30a)

$$I_p = \frac{\pi |R|^2 f(\beta) \exp(-(\alpha^2 / \langle \sigma_s^2 \rangle))}{(\hat{n} \cdot \hat{n}^f) \langle \sigma_s^2 \rangle} + P_a \quad (47)$$

where the constant P_a represents the contribution due to ambient illumination. For backscatter from convex objects, P_a can be set equal to zero for the purpose of computer graphics. The factor $\hat{n} \cdot \hat{n}^f = \cos \alpha$ in the denominator relates the area on the surface of the sphere to the (constant) projected area of the pixel on the image plane. For backscatter $\hat{n} \cdot \hat{n}^f = \hat{n} \cdot \hat{v}$.

$$x^2 + y^2 = z^2 \sin^2 \alpha = r^2 \quad (52)$$

Thus for metallic spheres ($\beta = 10$, $\langle \sigma_s^2 \rangle = 0.1$) of the ball bearing (Figure (13)) as the value of r is varied from $r_{\max} = a$ to zero the corresponding values of α are evaluated using (52) in order to derive the normalized intensity I_p at the pixel on the image plane. Bresenham's algorithm is used in this work to generate the circles. The unshaded areas that appear between two consecutive circles (due to the digitization of the coordinates) are shaded with an intensity I_p equal to that of an adjacent pixel.

For the bistatic case ($\hat{n}^f \neq -\hat{n}^i$) the loci of constant I_p does not coincide with the loci of $\alpha = \text{constant}$. This is due to the term $\hat{n} \cdot \hat{n}^f$ in the denominator of I_p (equation (47)). It is interesting to note that if the term $\hat{n} \cdot \hat{n}^f$ is ignored the loci of constant I_p on the image plane becomes ellipses. As a result, however the quality of the image is reduced significantly. For cones and cylinders where \hat{n} is constant along straight lines on the surface, [9,11], I_p will also be constant along these lines for the general bistatic case (since $\hat{n} \cdot \hat{v}$ and $\hat{n} \cdot \hat{n}^f$ are constant along these contours). The simplified analytical form of I_p (equation (47)) based on the full wave solutions is very easy to use in order to generate all the primitives (planes, cones, spheres and cylinders) for computer aided design of complex three dimensional objects.

The computer generated image of the model shown in Figure (14) is for $\beta = 10$ and $\langle \sigma_s^2 \rangle = 0.1$. The principal primitives in

this image are cylinders. In Figure (15) idealized renditions of missiles are presented ($\beta = 10$, $\langle \sigma_s^2 \rangle = 0.1$). The primitives for these images are cylinders, cones, and planes.

Assuming a two-scale composite model of the rough surface the full wave solution can also be decomposed into a weighted sum of the two contributions [1]. Thus for a two-scale model, the total normalized reflected intensity I_p of each pixel can be expressed as

$$I_p = |R|^2 (P_{dl} \exp(-\alpha^2 / \langle \sigma_{sl}^2 \rangle) + P_{ds} \exp(-\alpha^2 / \langle \sigma_{ss}^2 \rangle)) \quad (53)$$

In equation (53) the first term is the contribution to I_p from the large scale rough surface while the second term is the contribution to I_p from the small scale rough surface. The surface with the large scale roughness is given by $W(v_T)$ (equation (24)) for $v_T \leq v_d$ while the surface with small scale roughness is given by $W(v_T)$ for $v_T > v_d$. For the images shown in Figures (16) and (17) the mean square slopes are $\langle \sigma_{sl}^2 \rangle = 0.01$ (for the large scale surface) and $\langle \sigma_{ss}^2 \rangle = 0.1$ (for the small scale surface). The coefficients P_{dl} and P_{ds} are dependent on the values of β , $\langle \sigma_s^2 \rangle$ and v_d (where the spectral splitting between the large scale and small scale rough surface is assumed to occur). For the illustrative examples (Figures (16) and (17)) $P_{dl} = 0.7$ and $P_{ds} = 0.3$. It is interesting to note that equation (53) strongly resembles the empirical formula used by Cook and Torrence [14].

VI. CONCLUDING REMARKS

A simple reflection model for computer generated synthetic images of three dimensional objects is developed in this work. It is based on a rigorous full wave analysis of electromagnetic scattering by rough surfaces. The full wave analysis accounts for physical optics-specular point reflection as well as diffuse scattering in a self-consistent manner and its use is not limited by the small perturbation restriction. Thus using the full wave approach, it is not necessary to adopt two scale models of rough surfaces even when the Rayleigh parameter $\beta = 4k_0^2 \langle h^2 \rangle$ is not very small compared to unity.

For the roughness parameter $\beta > 7$ it is shown that the physical optics contribution $\sigma_{\Omega}^p(\alpha)$ is negligible compared to the diffuse scattering contribution $\sigma_{\Omega}^d(\alpha)$. In this case, it is only necessary to choose the rough surfaces parameters $\langle h^2 \rangle$, $\langle \sigma_s^2 \rangle$ and the Fresnel reflection coefficients R_v and R_h for specular reflection (corresponding to normal incidence for backscatter) and to locate the loci of the isointensity contours (for backscatter $\alpha = \text{const}$).

The reflection model based on the full wave analysis has been compared to earlier semi-empirical models used in computer aided graphics. It is found to be very practical, efficient and easy to use.

VII. REFERENCES

1. E. Bahar. Scattering and depolarization by random rough surfaces, Unified Full Wave Approach--An overview. Wave Material Interaction--in press (January 1986).
2. E. Bahar and S. Chakrabarti. Scattering and depolarization by large conducting spheres with rough surfaces. Applied Optics, Vol. 24, No. 12, 15 June 1985, pp. 1820-1825.
3. E. Bahar, S. Chakrabarti, M. A. Fitzwater. Extinction cross-sections and albedos for particles with very rough surfaces.
4. E. Bahar and M. A. Fitzwater. Multiple scattering by finitely conducting particles with random rough surfaces at infrared and optical frequencies. Radio Science
5. D. E. Barrick. Rough surfaces, in Radar Cross Section Handbook. (Plenum, New York, 1973).
6. P. Beckmann and A. Spizzichino. The scattering of electromagnetic waves from rough surfaces. (Macmillan, New York, 1963).
7. J. F. Blinn. Models of light reflection for computer synthesized pictures. Computer Graphics, 11, 2, (1977), pp. 192-198.
8. J. F. Blinn. Computer display of curved surfaces. Ph.D. dissertation, University of Utah, Salt Lake City, 1978.
9. R. M. Boole and D. B. Cooper. Bayesian recognition of local 3-D shape by approximating image intensity functions with quadratic polynomials. IEEE Transactions on Pattern Analysis and Machine Intelligence. Vol. PAMI-6, No. 4, July 1984, pp. 418-429.
10. M. Born and E. Wolf. Principles of Optics. (Pergamon Press, 1965).
11. Bruno Cernuschi-Frias and D. B. Cooper. 3-D Space location and orientation parameter estimation of Lambertian spheres and cylinders from a single 2-D image by fitting lines and ellipses to thresholded data. IEEE Transactions on Pattern Analysis and Machine Intelligence. Vol. PAMI-6, No. 4, July 1984, pp. 430-441.

12. S. Chakrabarti. Scattering cross-sections and incoherent specific intensities for particles of irregular shape and finite conductivity, Full Wave Approach. Ph.D. dissertation, University of Nebraska-Lincoln, 1986.
13. R. L. Cook. A reflection model for realistic image synthesis. Master's Thesis, Cornell University, Ithaca, New York, 1981.
14. R. L. Cook and K. E. Torrance. A reflectance model for computer graphics. ACM Transactions on Graphics, Vol. 1, No. 1, January 1982, pp. 7-24.
15. D. G. Hakala, R. C. Hillyard, P. J. Malraison and B. F. Noore. Natural quadrics in mechanical design. SIGGRAPH/81, Seminar: Solid Modeling, Dallas, TX, August 1981.
16. A. Ishimaru. Wave propagation and scattering in a random media, chapter 2 and chapter 21. (Academic, New York, 1978).
17. J. T. Kajiya. Anisotropic reflection models. SIGGRAPH 1985, San Francisco, July 22-26, pp. 15-21.
18. B. T. Phong. Illumination for computer generated pictures. CACM, 18, 6, June 1975, pp. 311-317.
19. T. Whitted. An improved illumination model for shaded display. CACM, 23, 6, June 1980, pp. 343-349.

ACKNOWLEDGMENT

This investigation was sponsored in part by the U.S. Army Research office contract DAAG-29-82-K-0123 and the National Science Foundation Engineering Supercomputer grant ECS8515794/5. The computations were carried out on the Cyber 205 at Colorado State University. The authors wish to thank M. A. Fitzwater and E. Everett for their assistance in the preparation of the manuscript.

VIII. LIST OF FIGURES

- Fig. 1. Scattering geometry for a rough conducting sphere.
- Fig. 2. Plot of spectral density function (24) $\beta = 10, 20, 40$.
- Fig. 3. Normalized diffuse intensity σ_{Ω}^d (28) scattered by an element of the sphere as a function of polar angle (γ) and azimuthal angle (δ) for $\beta = 10$ (backscatter $\hat{n}^f = -\hat{n}^i$).
- Fig. 4. Normalized diffuse intensity σ_{Ω}^d (28) scattered by an element of the sphere as a function of polar angle (γ) and azimuthal angle (δ) for $\beta = 40$ (backscatter $\hat{n}^f = -\hat{n}^i$).
- Fig. 5. Normalized diffuse intensity σ_{Ω}^d (28) scattered by an element of the sphere as a function of polar angle (γ) and azimuthal angle (δ) for $\beta = 40$ (bistatic, $\theta_o^i = \theta_o^f = 40^\circ$).
- Fig. 6. Normalized diffuse intensity $\sigma_{\Omega}^d/\sigma_{\Omega}^d(0)$ (28) as a function of polar angle $\alpha = \gamma$ where $0 \leq \alpha \leq \pi/2$ for $\beta = 1, 5, 7, 10$ and 40 . Mean square slope ($\langle \sigma_s^2 \rangle$) is constant at 0.1 .
- Fig. 7. $\sigma_{\Omega}^d/\sigma_{\Omega}^d(0)$ (28) as a function of α for $\langle \sigma_s^2 \rangle = 0.025, 0.05, 0.1$.
- Fig. 8. $\sigma_{\Omega}^d/\sigma_{\Omega}^d(0)$ (28) as a function of α (—).
 $\exp(-\alpha^2/\langle \sigma_s^2 \rangle)$ as a function of α (----).
 $\langle \sigma_s^2 \rangle = 0.025$.

Fig. 9. $\sigma_{\Omega}^d/\sigma_{\Omega}^d(0)$ (28) as a function of α (—).
 $\exp(-\alpha^2/\langle\sigma_s^2\rangle)$ as a function of α (----).
 $\langle\sigma_s^2\rangle = 0.05$.

Fig. 10. $\sigma_{\Omega}^d/\sigma_{\Omega}^d(0)$ (28) as a function of α (—).
 $\exp(-\alpha^2/\langle\sigma_s^2\rangle)$ as a function of α (----).
 $\langle\sigma_s^2\rangle = 0.1$.

Fig. 11. $\sigma_{\Omega}^d(0)/\sigma_{\Omega}^d(0)|_{\epsilon \rightarrow \infty}$ (28) as a function of β for backscatter case ($\hat{n}^f = -\hat{n}^i$). $f(\beta)$ (6.296) (---).

Fig. 12. $\sigma_{\Omega}^d(0)/[\sigma_{\Omega}^d(0)|_{\langle\sigma_s^2\rangle=0.1}]$ (28) as a function of the mean square slope $\langle\sigma_s^2\rangle$ for $\beta = 20$. $f(\langle\sigma_s^2\rangle) \frac{0.1}{\langle\sigma_s^2\rangle}$ (----).

Fig. 13. Ball bearings (using only diffuse reflection component).

Fig. 14. Metallic valve (using only diffuse reflection component).

Fig. 15. Missiles (using only diffuse reflection component).

Fig. 16. Ball bearings (using two-scale model).

Fig. 17. Metallic valve (using two-scale model).

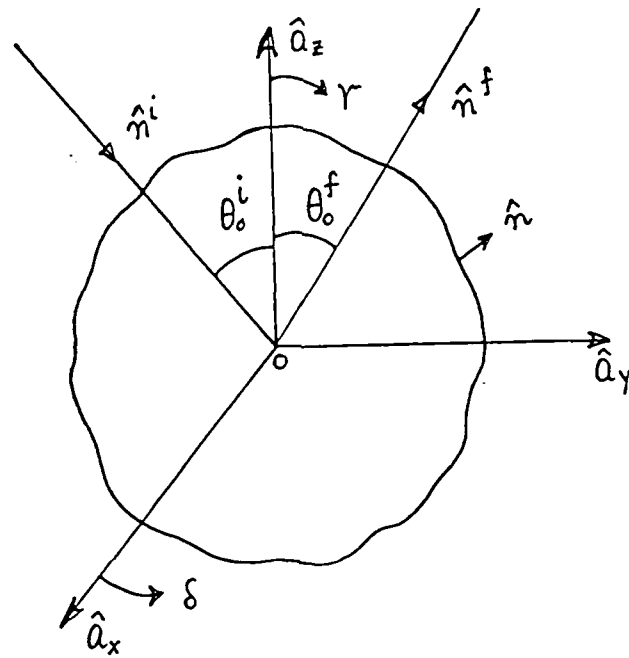


Fig 1.

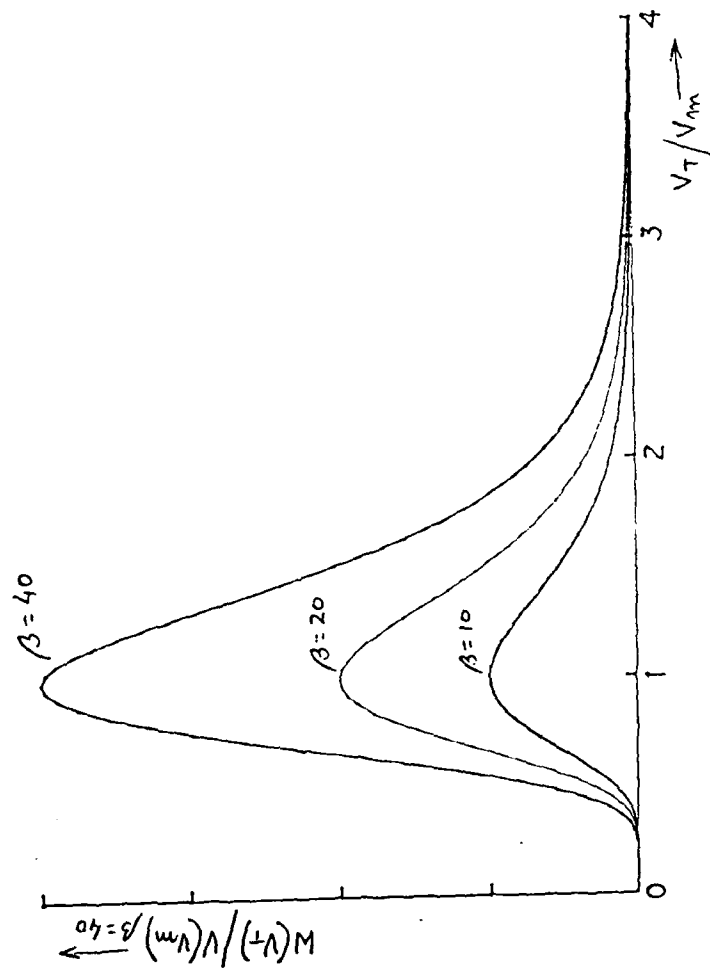


FIG. 2

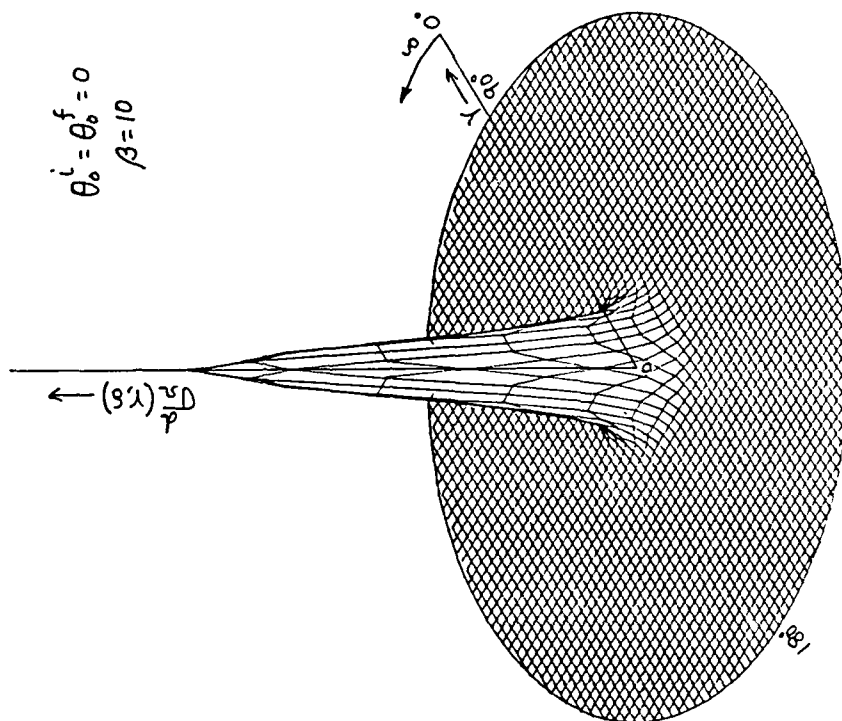


FIG 3

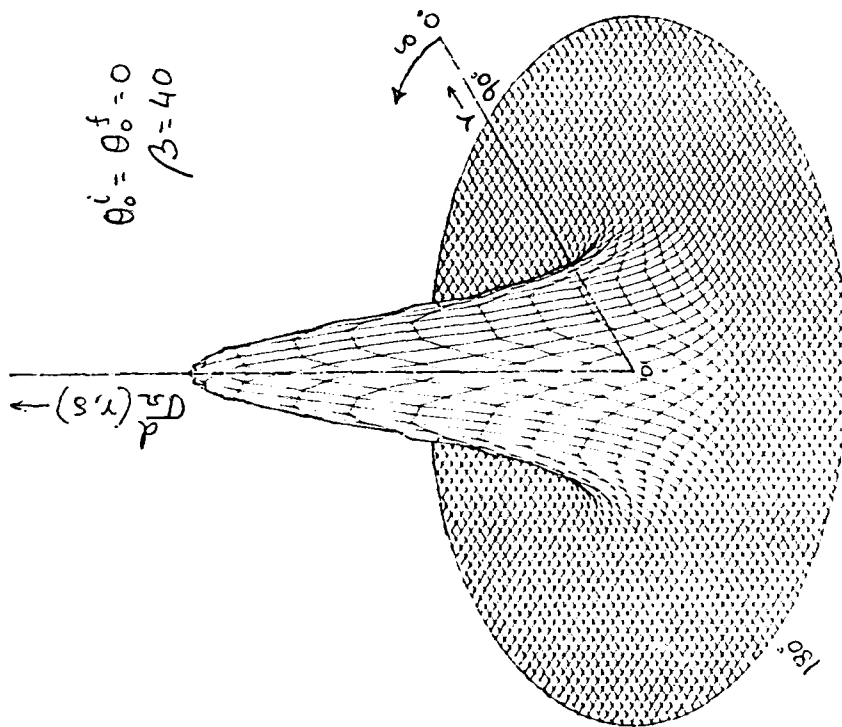


FIG 4

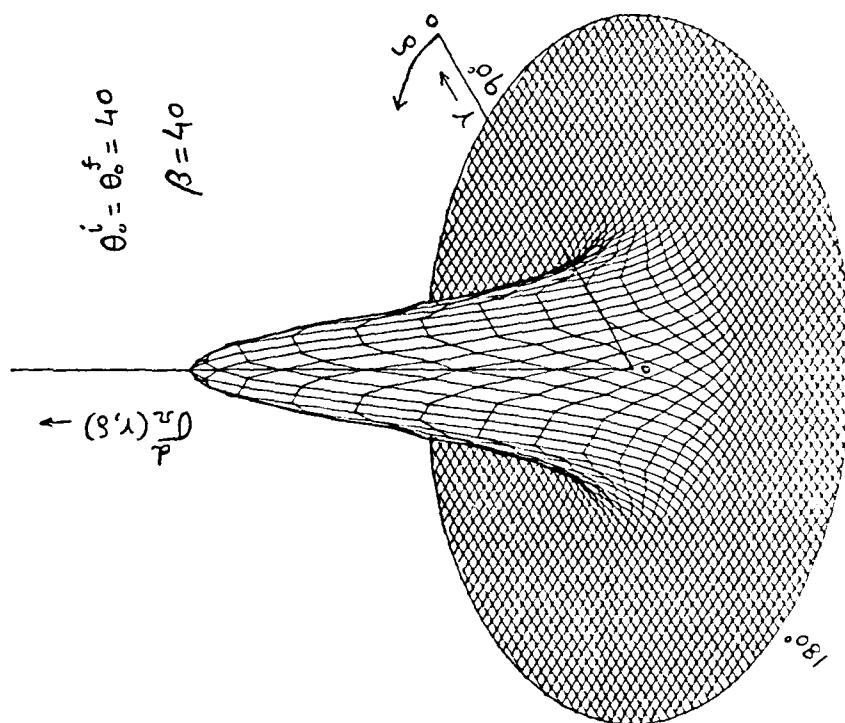


FIG 5

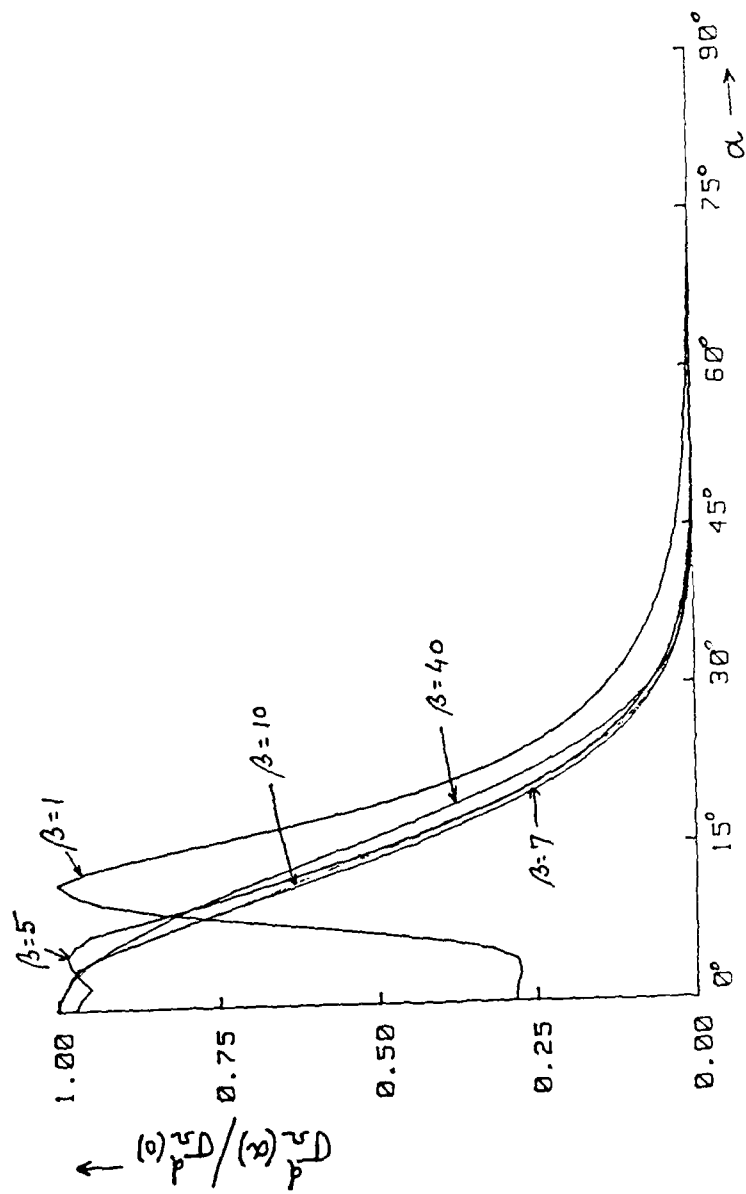


FIG 6

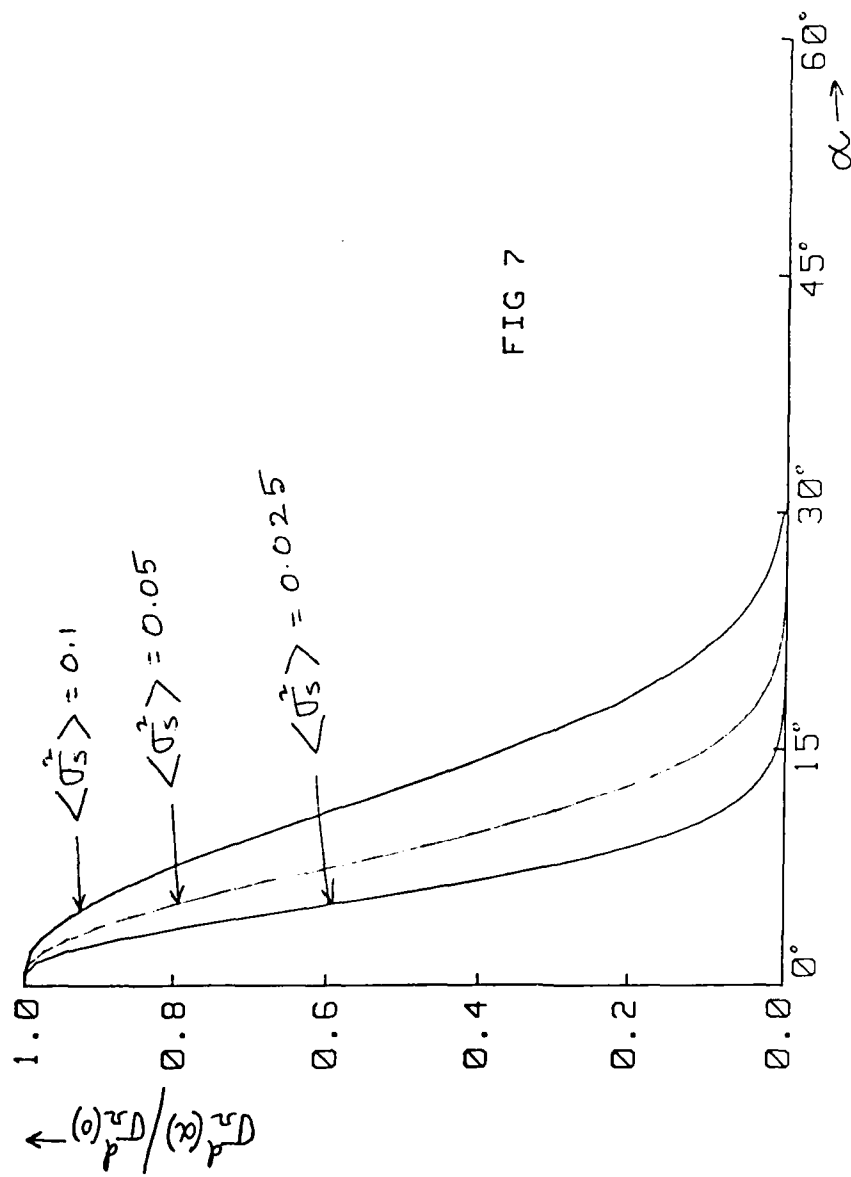


FIG 7

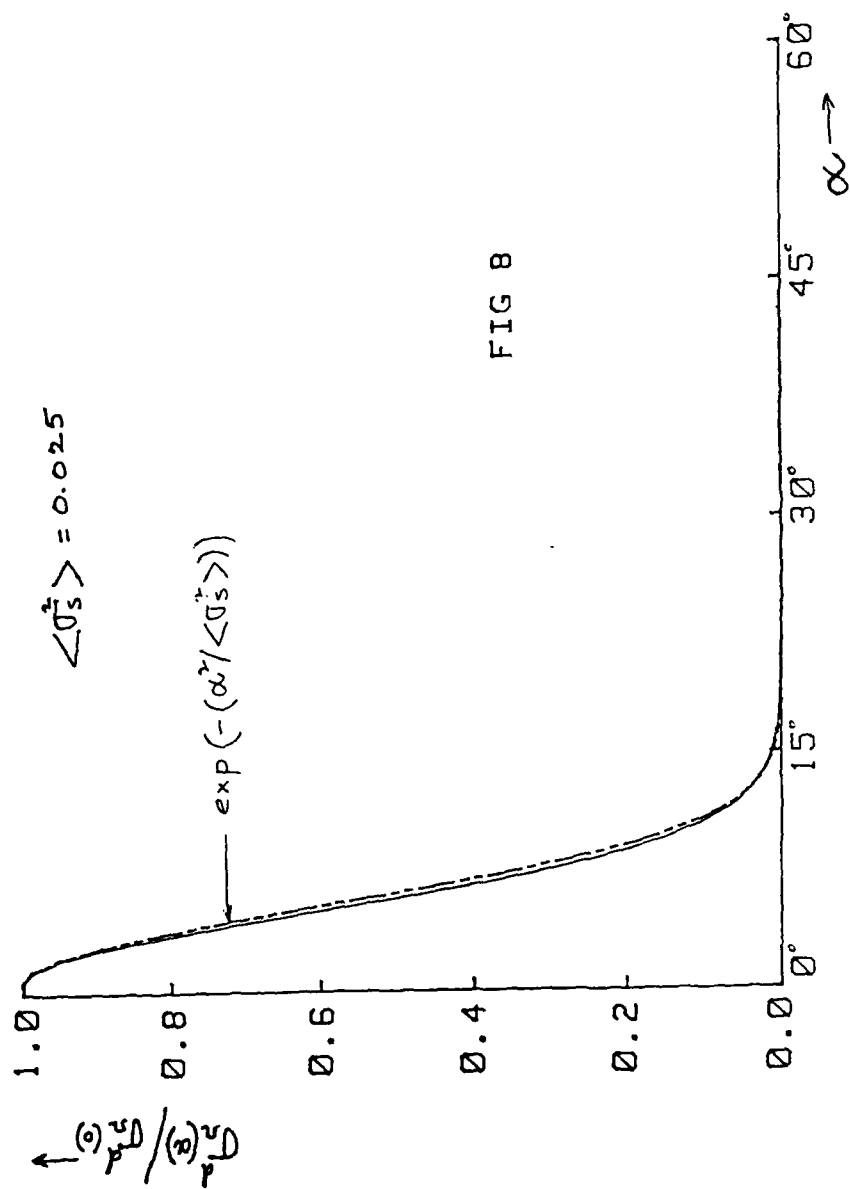


FIG 8

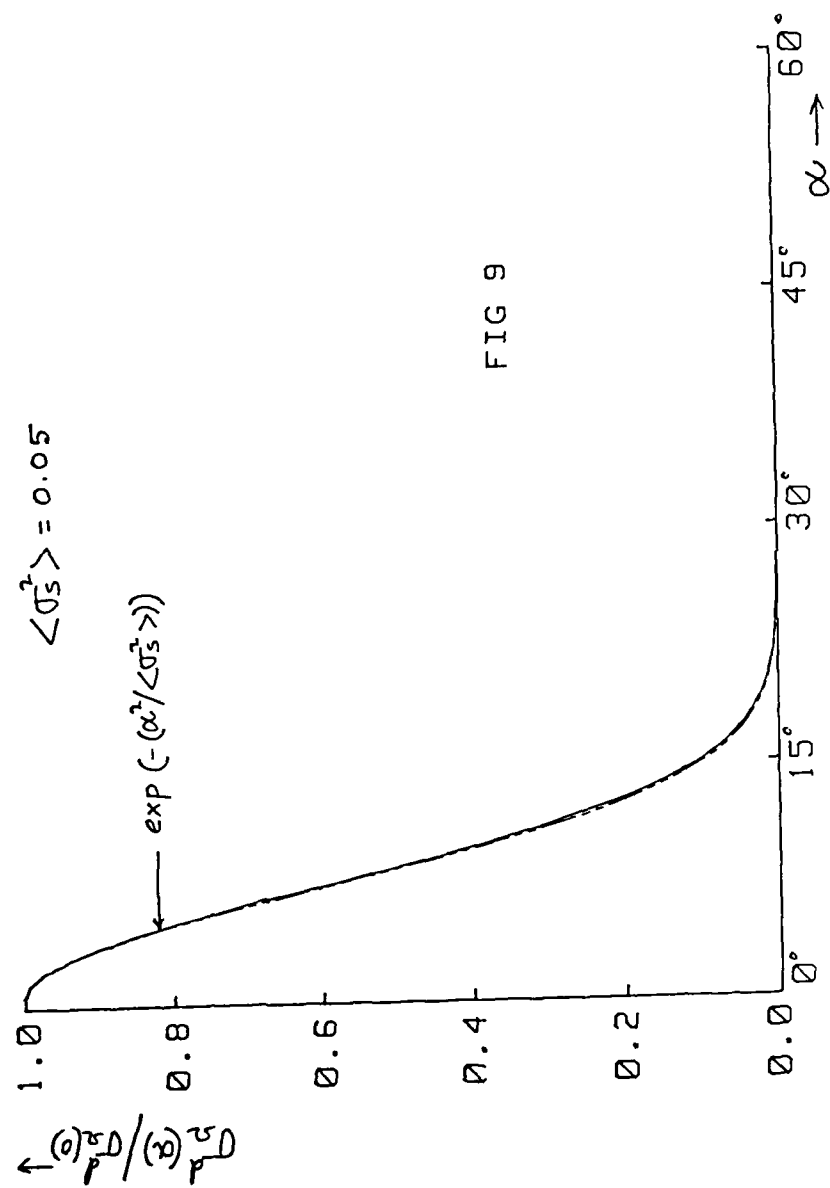


FIG 9

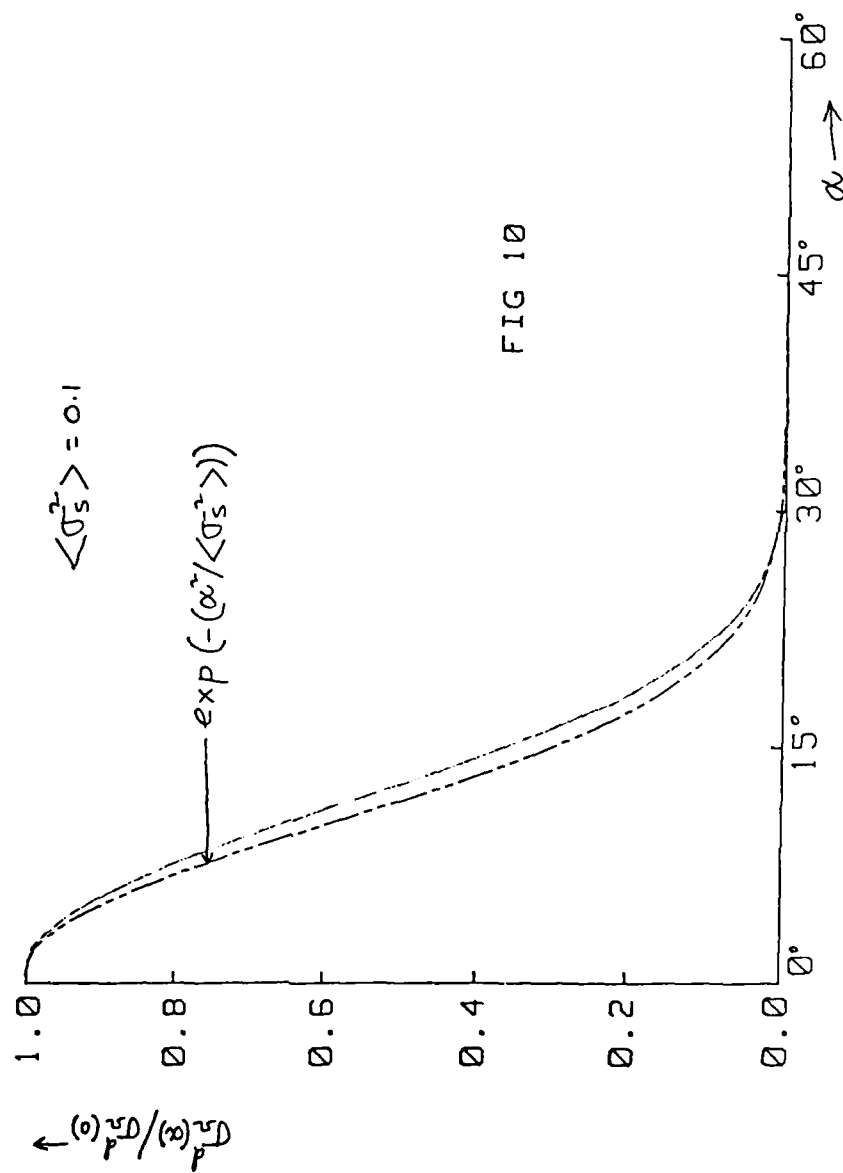


FIG 10

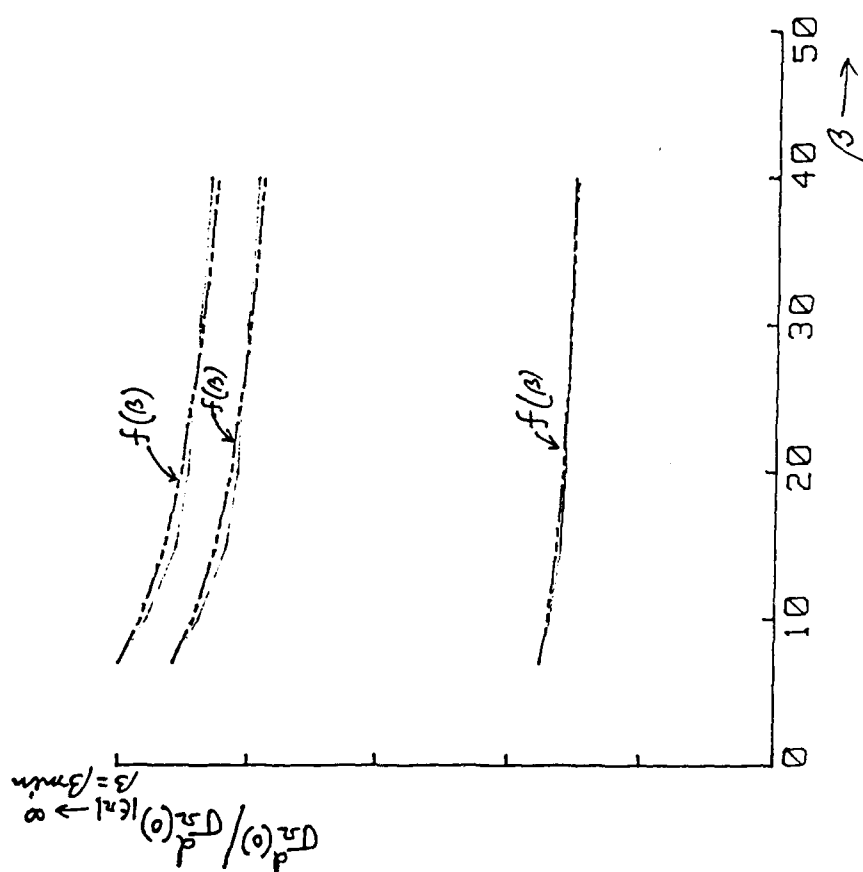


FIG 11

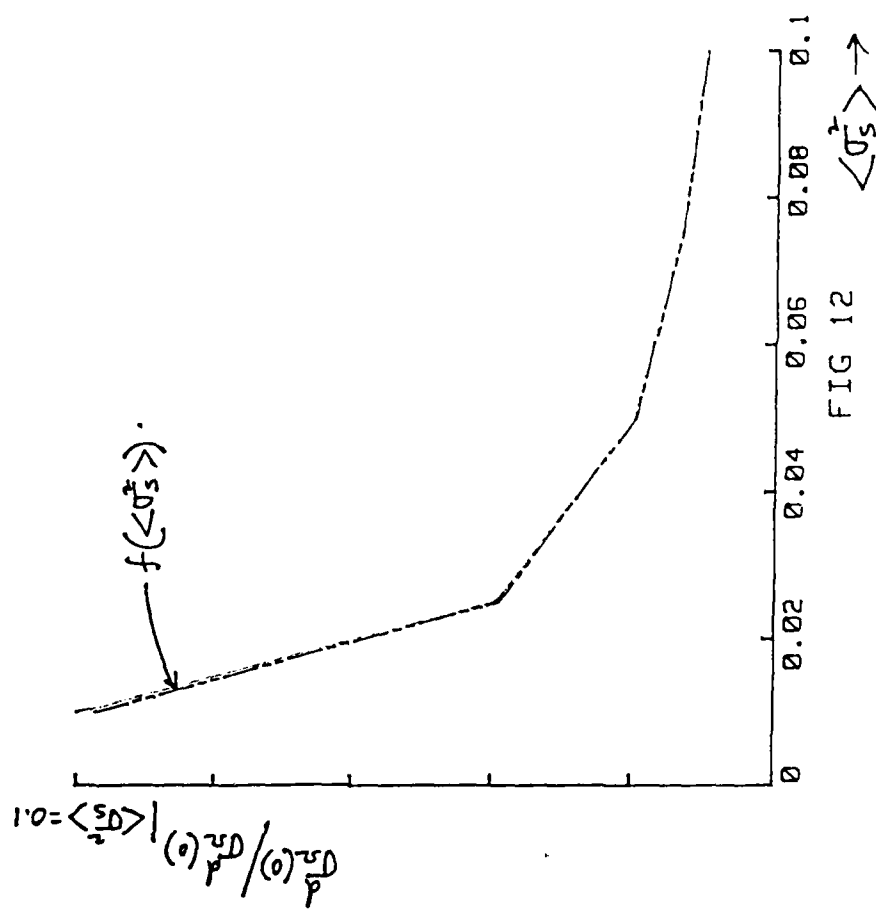


FIG 12

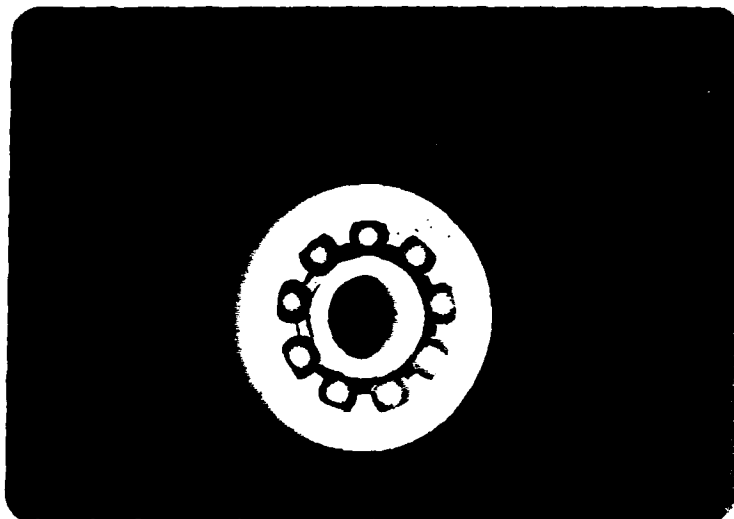


FIG 13

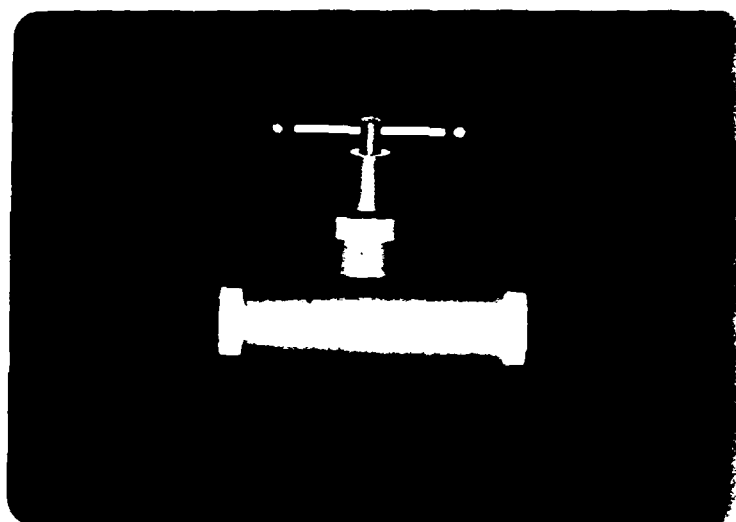


FIG 14

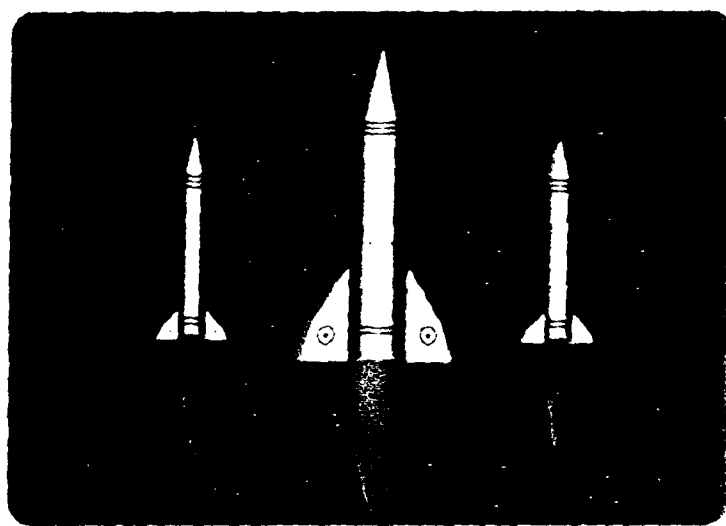


FIG 15

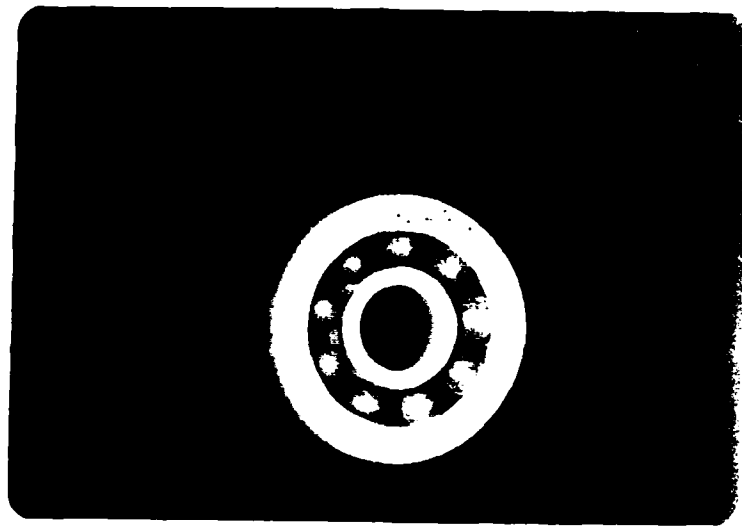


FIG 16

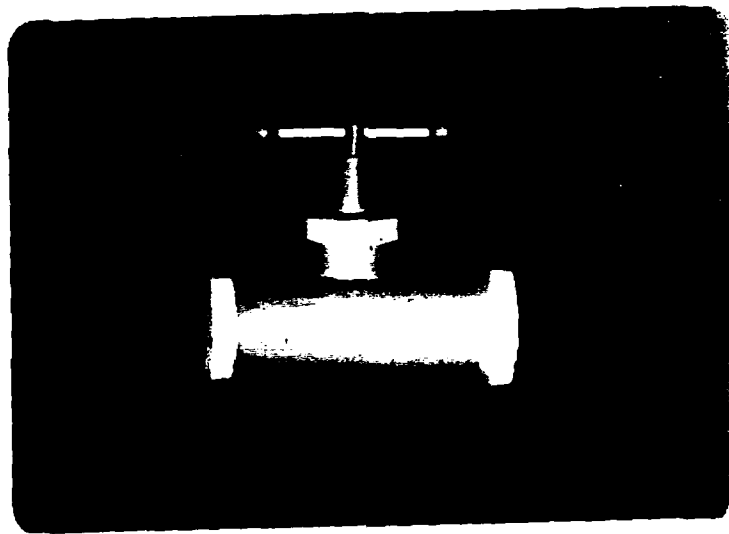


FIG 17

SEASAT MICROWAVE ALTIMETER MEASUREMENT OF THE OCEAN GRAVITY WAVE EQUILIBRIUM-RANGE SPECTRAL BEHAVIOR USING FULL-WAVE THEORY

D. E. Barrick

Ocean Surface Research
1131 Cranbrook Court
Boulder, Colorado 80303 USA

I. Bahar

Electrical Engineering Dept
University of Nebraska
Lincoln, Nebraska 68586 USA

ABSTRACT

A new spectral law for the equilibrium region of the waveheight spatial spectrum is derived from the extensive SEASAT altimeter data set. Applicable to the open ocean under all conditions of wave development, the result is a $k^{-4.25}$ power-law dependence rather than the classic k^{-4} . This spectral model is established using the specular-point result for backscatter supported by full-wave theory to determine the proper upper wavenumber limit for the slope spectrum.

1. INTRODUCTION

Microwave backscatter (of the expected polarization state) from the sea near normal incidence has long been known to be explainable by a specular-point model (Refs. 1,2). According to this model, backscatter comes from smoothly curving "specular points" distributed over the waves, i.e., facets tilted normal to the line of sight. (By the same specular-scattering mechanism, however, this model fails completely for the cross-polarized scatter component, which it predicts to be zero. Since altimeters to date have been constructed to receive only the expected same-sense polarized component, we need not be concerned with this limitation here.) The specular-point model gives the backscattering cross section per unit surface area, σ^0 , as the Fresnel power reflection coefficient divided by the mean-square slope of the sea as seen by the radar. This mean-square slope should be obtainable by integrating the height spectrum -- times wavenumber squared -- between a lower and upper limit. The lower limit depends on wind speed in a known manner. The frequency in some way determines the upper limit of the spatial roughness scales that the radar can discern. Since classic wind-wave wave spec-

tral models have been available for nearly three decades (e.g., the Phillips spectrum, Ref. 3), it was recognized some time ago that one should be able to produce a valid theoretical model for the wind-speed dependence of microwave (nadir-looking) altimeter return. Although such models indeed show the correct shape of σ^0 vs wind speed (Ref. 4), extensive and carefully calibrated data sets from GEOS and SEASAT show a persistent discrepancy in amplitude of -3 dB (Refs. 5,6).

Full-wave theory (Ref. 7) produces an exact solution for scatter from rough surfaces for which multiple scatter is not significant; this solution is an integral that is no more complex than classical physical optics. Its power lies in the fact that the surface does not have to be split artificially into two scales of roughness (e.g., Refs. 8,9), although it does allow examination of the validity of such composite models. In particular, it shows that indeed, at normal incidence for the sea, backscatter is well predicted by the specular point model for the same-sense polarization as was transmitted, and it gives the upper limit for the waveheight spectrum required in the expression for mean-square slope (Refs. 10-12).

Hence, (i) having a valid model for altimeter scatter, i.e., the specular-point model; (ii) knowing the lower limit for the spectrum, (iii) having determined the correct upper limit to use from full-wave theory, we reason that the 3 dB discrepancy in σ^0 must be due to the inadequacy of the classic waveheight spectral models in the equilibrium region. The equilibrium region is defined as the wavenumber (k) portion far removed from the peak at lower end, which is strongly wind-speed dependent; it is this equilibrium region that has the greatest influence on mean-square slope. In fact, for the classic Phillips k^{-4} dependence that overpredicts σ^0 by 3 dB, the mean-square slope depends logarithmically on the upper limit used for the spectrum, and hence the equilibrium region contributes very strongly. If σ^0 is overpredicted by the k^{-4}

equilibrium region, this implies that the mean-square slope derived therefrom is too small. Therefore, we maintain by this argument that the classic inverse-4th spectral dependence on the open ocean is too strong; the dependence should be less than k^{-4} . Interestingly, Phillips very recently has used energy balance arguments to show the same thing (Ref. 13): the spectral dependence he deduces in the equilibrium region (far from the peak) is $k^{-3.4}$. We employ the extensive SEASAT data set (and empirical wind-speed fit to it) given by Chelton and McCabe (Ref. 6) to derive a power-law spectral model in this paper, and find that $k^{-3.2}$ fits best.

2. SPECULAR-POINT MODEL

The specular-point model refers to a high-frequency asymptotic approximation for the return from a rough surface. It is derivable from either physical optics or geometrical optics formulations. The assumptions made in use of this model are that the average incoherent scattered power originates from separate facets of the surface that are smoothly curving and separated in phase (on the average) by at least 180° . The former approximation (that the radius of curvature of the specular facet be large in terms of wavelength) allows one to write the total field at the surface in terms of the incident field and a reflection coefficient, and is also called the "tangent-plane" approximation. The latter approximation, sometimes called the "deep-phase" condition, requires that the surface be "very rough," i.e., its rms height be large in terms of wavelength. The sea surface in the microwave region satisfies both of these conditions. Scatter according to this model, then, is produced by facets (or specular points) whose normals bisect the incidence and scatter directions, for backscatter, the normal points toward the radar. Since specular points must exist in order to produce scatter at given angles with respect to the surface, one intuitively sees that the intensity of the return will depend on the probability density of surface slopes with the required normals. The derived solutions (Refs. 1,2) indeed exhibit this dependence.

For normally incident backscatter (the condition for satellite altimeters), the directionality of ocean waves is irrelevant (i.e., it is integrated out), and the specular-point expression reduces to $\sigma^0 = |R(0)|^2 / S^2$, where $R(0)$ is the Fresnel reflection coefficient for a smooth plane at normal incidence (for the sea at the 13.5 GHz SEASAT altimeter frequency, $|R(0)|^2 = 0.61$), and S^2 is the mean-square slope of the sea as seen by the radar. As one expects for normally incident backscatter, the rougher the sea (i.e., the higher the slopes), the less power is returned because the more highly tilted specular points scatter in other directions; as roughness disappears and $S^2 \rightarrow 0$, the return increases to the point where one abandons the specular-point model (the deep-phase criterion fails), and treat the earth as a smooth sphere.

The dependence of altimeter intensity on roughness is therefore contained in the slope. The mean-square slope in turn can be obtained from the integral of the slope spectrum (vs spatial wavenumber), and the latter expressed in terms of the more familiar height spectrum $S(k)$, as $k^2 S(k)$. The classic Phillips model for fully developed seas, for example, has $S(k) = B/k^4$, for $k = |k|$ greater than $k_1 =$

g/U^2 , where g is the acceleration of gravity (9.806 m/s^2), U is the wind speed in meters per second, and B is a dimensionless constant estimated experimentally to be 0.005. Below this lower limit, the spectrum is zero. Although more sophisticated models are presently favored for the shape of the spectrum's lower end (rather than the sharp Phillips cutoff), this issue is largely irrelevant to slope calculations because the slope integral is highly insensitive to the detail of how the spectral energy is distributed at the lower end (in contrast to the mean-square height). This is easily seen by integrating the Phillips model to obtain the slope: $S^2 = \int k^2 S(k) dk = B \ln(k_2/k_1)$. This illustrates two points: (i) one must specify a non-infinite upper limit to the spectrum, k_2 , otherwise the slope becomes infinite, and (ii) it is the vast expanse of the spectrum between the upper and lower limits that has more influence on slope, and hence backscatter, than the detailed shape at either end.

According to the specular-point model, therefore, the mean-square sea slope and hence backscattered return, depend on (i) the lower end of the spectrum, which is inversely proportional to the square of the wind speed (higher winds cause rougher seas, decreasing the scattering cross section), (ii) the spectral behavior between the upper and lower limits, (iii) the upper limit. Full-wave theory will be used to determine the third item, the upper limit. Hence, the second item, the wave spectral shape between the upper and lower limits is the remaining quantity to be determined in this study.

3. USE OF FULL-WAVE THEORY

As mentioned previously, full-wave theory is the most exact, tractable theory available to date applicable to rough surfaces where multiple scattering can be neglected. Its power lies in the fact that one can integrate the full-wave solution for backscatter numerically without splitting the roughness and its spectrum artificially into separate components. However, it has been used (Refs. 10,12) to examine the older, less accurate "composite" theories that hypothesize a splitting of the roughness into two components: a quasi-specular term and the "diffuse" scatter. At nadir, only the quasi-specular term is important. In Ref. 12 it is shown that the simplest version of the quasi-specular term, i.e., that given above for σ^0 , remains very close to the result predicted by full-wave theory (when the two are applied to the same surface) over a fairly wide variation of the upper spectral limit. This fact suggests that the simple

specular-point model above can in fact be used reliably for predicting altimeter return. Furthermore, the full-wave solution provides guidance as to precisely what upper limit to use in evaluating the slope for the specular-point model. Over the range of observed SEASAT surface wind speeds from 3.5 m/s to 16 m/s, the values of σ^0 obtained both from the full-wave solution and the specular-point model differed from each other by less than 0.1 dB for an upper limit $k_0 = 85 \text{ m}^{-1}$. Hence this upper limit is to be used with the simple specular-point model, along with the lower limit given earlier, to derive a general ocean waveheight spatial spectrum (valid in the equilibrium region) based on observed SEASAT σ^0 vs wind speed.

4. A PARAMETRIC MODEL FOR THE WAVEHEIGHT SPATIAL SPECTRUM

We now propose a parametric model for the waveheight spatial spectrum, and then derive its parameters based on SEASAT altimeter return. The equilibrium region for radar-observed spectral scales extends over a large range, i.e., from k_1 (e.g., $= 0.1 \text{ m}^{-1}$ for $U = 10 \text{ m/s}$ wind) to $k_0 = 85 \text{ m}^{-1}$. We select a power-law spectrum, such that $S(k) = K/(k^{4-\alpha} \cdot k_1^\alpha)$, where K is a dimensionless constant and α is the power-law departure from the classic Phillips model. Such a spectrum has a constant shape when normalized to the lower-end, and hence should represent fully developed seas with any wind speed. To illustrate this parametric shape, we normalize wavenumbers such that $K \approx k/k_1$, and note that the normalized spectrum is now $K/K^{4-\alpha}$ for $1 < K$, which is the parametric version we want. Therefore, the unknown constants, to be determined from the SEASAT altimeter data and specular-point model are K and α .

5. DETERMINATION OF MODEL PARAMETERS FROM SEASAT DATA

Chelton and McCabe (Ref. 6) established a new model for altimeter σ^0 vs wind speed by employing winds measured by the SEASAT scatterometer with σ^0 obtained from the SEASAT altimeter. It is accepted that the scatterometer measurement of wind beneath the satellite is more accurate because of more extensive calibration of that instrument. With nearly 2000 applicable points that were collected by the altimeter over the oceans during the satellite lifetime, they established an empirical relationship for altimeter σ^0 vs U , the wind speed. They fitted a power law over the range $3.5 \text{ m/s} < U < 16 \text{ m/s}$, and obtained $\sigma^0 = 32U^{1.44}$; error bounds for the two constants appearing in this model were derived, and their implications on the present analysis will be discussed subsequently. Using this in the specular-point model for slope, we obtain $S_1 = (0.61/32)U^{1.44}$. The superscript 1 on S^2 is

used here to denote this as the input to our analysis.

Using the waveheight spatial waveheight spectral model specified in the previous section, then, and integrating this between the lower and upper limits, we obtain $S_2 = (K/\alpha)(k_0 U^2/g)^{\alpha-1}$ as the model to be fitted to the input to determine the two unknowns, K and α . We do this by a least-squares fitting of S_2 to S_1 , summing over wind-speed samples equally incremented at $\Delta U = 0.5 \text{ m/s}$ from $3.5 \text{ m/s} < U < 16 \text{ m/s}$. The value for k_0 that we employ is 85 m^{-1} , as determined from full-wave theory. Since the model is linear in K and nonlinear in α , we eliminate K from the least-squares sum by differentiating with respect to K , solving for it, and replacing it. Then the minimum is sought over α at increments $\Delta\alpha = 0.0005$. The solutions are $K = 0.00512$ and $\alpha = 0.1355$. Hence, the spectral model that describes the equilibrium region based on SEASAT altimeter data is $S(k) = 0.00512/(k^{3.86} \cdot k_1^{0.14})$.

6. VALIDATION OF WAVE AND SCATTER MODELS

Two arguments can be used to establish the soundness of the spectral model derived here from SEASAT altimeter data. The first has to do with the uncertainties in the empirical wind-speed model fitted by Chelton and McCabe to the SEASAT altimeter data. If these are sufficiently large, they might produce spectral model uncertainties that would encompass the older, classic k^{-4} law. If this were the case, then the $k^{-3.86}$ would not be statistically significant, and any claim for its acceptance would be weak. To show that the result derived here is indeed statistically significant, we plot σ^0 from the Chelton/McCabe model $\sigma^0 = 32U^{1.44}$ in Fig. 1; shown in shading around it is the uncertainty region represented by using the standard deviations in their derived model parameters 32 and -1.468, which we added so as to produce the greatest departures. The line at the center of the shading is also of course identically the specular-point model applied to our newly derived $k^{-3.86}$ spectrum with $k_0 = 85 \text{ m}^{-1}$ as the upper limit, because the input S_1 matches the fitted model S_2 in the least-squares fitting to within $\pm 0.05 \text{ dB}$. Also plotted in the figure is the older spectrum $0.005/k^4$ used in the specular-point model, also out off at the same upper limit $k_0 = 85 \text{ m}^{-1}$. The 2-3 dB mentioned earlier is in evidence here, but more important, the older model clearly lies well beyond the uncertainty region of the SEASAT-based model derived here. Reference to Fig. 13 of Chelton and McCabe (Ref. 6) also shows that the individual 2000 altimeter points for σ^0 all lie well within 3 dB of their empirical fit, supporting our claim that the older spectral model cannot produce a scattering law that fits measured data. Finally, we note

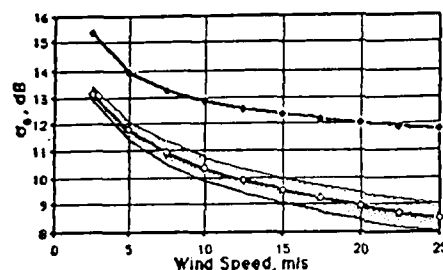


Figure 1. Radar backscatter cross section at 13.5 GHz at normal incidence. Lower curve is empirical law fitted to SEASAT data (Ref. 6), where shaded region represents statistical uncertainty to this law from fitted parameters. Lower curve also represents specular-point scattering model upon use of k^2 wave spectrum for required slope. Upper curve is specular-point model with the older, classic k^{-4} spectrum employed instead.

that the older k^{-4} law cannot be made to fit very well merely by taking a different upper limit to the spectrum (even if that step could be physically justified somehow), a higher upper limit will essentially slide the upper curve lower, but its slope still differs throughout the plotted range, so that it still does not convincingly fit the measured data.

A second validation of our model has to do with "closure." We started with the claim that the more approximate specular-point model was a sufficiently accurate representation of radar altimeter scatter that we could use it to derive a wave spectral model from SEASAT data. We then invoked the full-wave scatter solution to find the proper upper limit $k_0 = 85 \text{ m}^{-1}$ to use in the specular-point model for all wind speeds. If this process all holds together, we ought to be able to now put our new wave spectral model back into full-wave theory for scatter and produce the same result as the specular-point model across the wind-speed range we worked with, i.e., $3.5 \text{ m/s} < U < 16 \text{ m/s}$. We have done this, and the differences (in dB) for σ_0 between the two at wind speeds of 3, 5, 10, 15, 20 m/s are (respectively) +0.07, +0.04, -0.02, -0.05, and +0.01 dB. Since these are well below the noise level of the original model, and since they are essentially due to numerical roundoff errors, we maintain that the arguments that invoked full-wave theory to validate the use of the specular-point model are indeed proven.

7. DISCUSSION

We have employed SEASAT altimeter data along with a demonstrated consistent scattering model to formulate a new equilibrium-range law for the waveheight spatial spectrum on the open ocean. This law is not significantly different from the older classic Phillips law

0.005/ k^4 law near the lower end, but departs markedly at wavenumbers an order of magnitude or more beyond. We illustrate this for the newer model $S(k) = 0.00512/(k^{2.86} \cdot k_{-1}^{1.14})$ and

older model $S(k) = 0.005/k^4$ at $k_0 = 85 \text{ m}^{-1}$ (for wind speed 10 m/s); the two differ by a factor of 2.64. If one is willing to extrapolate both models out to the capillary region where $k_c = 360 \text{ m}^{-1}$, this factor becomes 3.23. The method used involving surface slope precludes saying much about the shape of the spectrum near the lower end. In addition, we have not demonstrated that the new spectral law holds out to the capillary break $k_c = 360 \text{ m}^{-1}$ since our fitting stopped at $k_0 = 85 \text{ m}^{-1}$; on the other hand, we have no reason to suspect that it should not be valid in this gravity-wave region as well.

It deserves mention that the two SEASAT instruments (altimeter and scatterometer) used to establish the wind-speed law for the former do not observe the ocean at the same place and time. Chel and McCabe indicated that they employed a matching process so that only data from the two that were within 100 km and less than one hour apart on the sea were used. We suggest that any errors resulting from the remaining mismatch should be randomly distributed about the mean values, rather than a bias one way or the other; hence they will tend to average out for the analysis performed here.

In addition to the oceanographic implications of the new wave spectrum, the present findings constitute validation of a physically-based scattering algorithm for return from the sea at and near normal incidence: the specular-point model, along with a slope spectrum and upper "radar" wavenumber limit for the slope integral. This should prove to be useful for both algorithm development and system studies associated with implementation of future satellite microwave ocean sensors.

It has been normal practice to convert between spatial and temporal waveheight spectra (and *vice versa*) through the gravity-wave dispersion relation: $k = \sigma^2/g$. Although this works well near the dominant part of the wave spectrum (i.e., the peak), it is not clear that it holds well out in the equilibrium region (Ref. 14). Thus we hesitate to say that our findings imply a temporal dependence $\sigma^{-1.72}$, as the dispersion relation would suggest.

The model derived here, with a lower equilibrium-range wavenumber falloff than -4, is in qualitative agreement with the very recent findings of Phillips (Ref. 13). He postulates -3.5 compared to the -3.86 derived here. Phillips' arguments are based on energy balance at a constant ratio among three factors: energy input from the wind, energy dissipation (from the equilibrium region) by wave breaking, and energy transfer away from the equilibrium region by wave-wave interaction processes. The reason for the difference between the two values may well be the

fact that global, open-ocean SEASAT observations include all states of wave development and decay. One should expect the greatest departure from the -4 law when nonlinearities are the strongest, which occurs during "fully developed" (or steady-state) conditions. When this latter condition ceases, the maintenance of a constant ratio among the three energy processes will no longer hold, e.g., wind may die first, followed later by cessation of breaking, and finally by a variation in the rate of intra-spectral wave-wave energy transfer. A given point on the ocean observed by SEASAT is likely to be in a fully developed condition only a fraction of the time. Hence, the SEASAT-derived -3.86 -law would apply to an average over all possible wave development/decay conditions, whereas the -3.5 -law applies during steady-state fully developed conditions.

In calling the -4 -law the "classic Phillips" spectral model, we apologize and emphasize again that it was Phillips (Ref. 13) who presented a convincing case for a re-evaluation based on measured data, and was the first to produce a physical model that refutes this law. We can only welcome his statement "The matter clearly deserves reconsideration - 25 years is a pretty good lifetime for the simple ideas underlying (1.1) and (1.2) [i.e., the k^{-4} and O^3 laws], and if they are found to be no longer viable, they should be saluted and interred with dignity."

8. REFERENCES

1. Barrick D E 1968, Rough surface scattering based on the specular point theory, *IEEE Trans. Antennas Propagat.* AP-16, 449-454.
2. Barrick D E & E Bahar 1981, Rough surface scattering using specular point theory, *IEEE Trans. Antennas Propagat.* AP-29, 798-800.
3. Phillips O M 1966, *Dynamics of the Upper Ocean*, Cambridge, University Press.
4. Barrick D E 1974, Wind-dependence of quasi-specular sea scatter, *IEEE Trans. Antennas Propagat.* AP-22, 135-136.
5. Brown G S 1978, Estimation of surface wind speeds using satellite-borne radar measurements of normal incidence, *J. Geophys. Res.* 84, 3974-3978.
6. Chelton D B & P J McCabe 1985, A review of satellite altimeter measurement of sea surface wind speed, *J. Geophys. Res.* 90(C3), 4707-4720.
7. Bahar E 1981, Scattering cross section for random rough surfaces: full wave analysis, *Radio Sci.* 16, 331-341.
8. Barrick D E & W N Peake 1968, A review of scattering from surfaces with different roughness scales, *Radio Sci.* 3, 865-868.
9. Brown G S 1978, Backscattering from a Gaussian-distributed perfectly conducting rough surface, *IEEE Trans. Antennas Propagat.* AP-26, 472-482.
10. Bahar E, D E Barrick, & M A Fitzwater 1983, Computations of scattering cross sections for composite surfaces and the specification of the wavenumber where spectral splitting occurs, *IEEE Trans. Antennas Propagat.* AP-31, 698-709.
11. Bahar E & M A Fitzwater 1984, Scattering cross sections for composite rough surfaces using the unified full wave approach, *IEEE Trans. Antennas Propagat.* AP-32, 730-734.
12. Bahar E, D E Barrick, & M A Fitzwater 1986, Interpretation of backscatter cross sections for normal incidence using unified and two-scale full wave analyses of rough surfaces, *IEEE Trans. Geosci. Remote Sensing*, in review.
13. Phillips O M 1985, Spectral and statistical properties of the equilibrium range in wind-generated gravity waves, *J. Fluid Mech.* 156, 505-531.
14. Barrick D E 1986, The role of the gravity-wave dispersion relation when interpreting HF radar measurements, *IEEE J. Ocean. Eng.* 11(2).

CO-POLARIZED AND CROSS-POLARIZED INCOHERENT DIFFUSE INTENSITIES
SCATTERED BY FINITELY CONDUCTING PARTICLES OF IRREGULAR SHAPE

Ezekiel Bahar
and
Mary Ann Fitzwater
Electrical Engineering Department
University of Nebraska--Lincoln
Lincoln, Nebraska 68588-0511

ABSTRACT

In this work, a layer consisting of a large variety of randomly distributed finitely conducting particles with irregular shapes is assumed to be excited at infrared and optical frequencies by a normally incident linearly polarized wave. The resulting incoherent specific intensities as well as the co-polarized and cross-polarized intensities are evaluated. Both single scatter and multiple scatter results are presented for particles with smooth and rough surfaces.

1. Introduction

In this work, the scattering and depolarization of linearly polarized waves by a random distribution of finitely conducting particles of irregular shape are presented. The random rough surface of the particle is characterized by its surface height spectral density function (or its Fourier transform the surface height autocorrelation function).

The full wave approach is used to account for both specular point scattering as well as diffuse scattering by the particle in a self-consistent manner (Bahar and Chakrabarti 1985), and the equation of transfer (Chandrasekhar 1950 and Ishimaru 1978) for the modified Stokes parameters is solved using the matrix characteristic value method (Cheung and Ishimaru 1982). Both single scatter and multiple scatter results are given for particles with smooth and rough surfaces and the effects of particle surface roughness are considered in detail.

2. Formulation of the Problem

The analytical solutions for the modified Stokes incoherent specific diffuse intensity matrix $[I]$ are presented in this section. A linearly polarized wave is assumed to be normally incident upon a parallel layer of randomly distributed non-spherical particles. Thus the like and cross polarized incoherent intensities are azimuthally dependent. Special consideration is given to the effects of the surface roughness of the particles of finite conductivity. Since the roughness parameter $\beta = k_0 \langle h_s^2 \rangle$ (where k_0 is the free space wavenumber of the electromagnetic wave and $\langle h_s^2 \rangle$ is the mean square height of the particle rough surface) is assumed to be large ($\beta = 40$), the full wave solutions (Bahar and Chakrabarti 1985) are used to determine the elements of the scattering matrix for the equation of transfer (Chandrasekhar 1950, Ishimaru 1978).

$$\mu \frac{d[I]}{d\tau} = -[I] + f[S][I'] d\mu' d\phi' + [I_1] \quad (2.1)$$

In (2.1) τ is the optical distance in the z direction (normal to the plane of the slab),

$$\tau = \rho [\sigma_t] z \int_0^z \int_0^z n(D) dD \quad (2.2)$$

where D is the diameter of the unperturbed spherical particle, $n(D)$ is the particle size distribution and σ_t is the extinction coefficient. The symbol $\rho[\cdot]$ denotes integration over the size distribution. Since the effects of the particle surface roughness are vanishingly small in the forward direction, the extinction matrix (Ishimaru and Cheung 1980, Cheung and Ishimaru 1982) for the rough sphere can be represented by a scalar quantity. The (4×1) matrices $[I]$ and $[I']$ are the incoherent diffuse intensity matrices for waves scattered by the particles in the direction $\theta = \cos^{-1} \mu$ and ϕ and for waves incident in the direction $\theta' = \cos^{-1} \mu'$ and ϕ' respectively. The elements of $[I]$ are the modified Stokes parameters (Ishimaru 1978). The (4×4) scattering matrix $[S]$ in the reference coordinate system is expressed in terms of the scattering matrix $[S']$ in the scattering plane through the following transformation

$$[S] = [\mathcal{L}(-\pi + \alpha)][S'][\mathcal{L}(\alpha)] \quad (2.3)$$

in which \mathcal{L} is a transformation matrix and $[S']$ is the weighted sum of two matrices

$$[S'] = |\chi^S(\vec{v} \cdot \vec{a}_r)|^2 [S_{Mic}] + [S_s] \quad (2.4)$$

In (2.4) $[S_{Mic}]$ is the scattering matrix for the unperturbed sphere (Ishimaru 1978) and $\chi^S(\vec{v} \cdot \vec{a}_r)$ is the particle random rough surface characteristic function

$$\chi^S(\vec{v} \cdot \vec{a}_r) = \langle \exp(i\vec{v} \cdot \vec{a}_r h_s) \rangle \quad (2.5a)$$

in which

$$\vec{v} = k_0 (\vec{n}^f - \vec{n}^i) \quad (2.5b)$$

and \vec{n}^f and \vec{n}^i are unit vectors in the direction of the scattered and incident wave normals. The random rough surface h_s is measured normal to the unperturbed (spherical) particle. Thus, the radius vector to the surface of the irregular particle is

$$\vec{r}_s = h_0 \vec{a}_r + h_s \vec{a}_r \quad (2.5c)$$

The radius of the unperturbed sphere is h_0 . The coefficient $|\chi^S|^2$ in (2.4) accounts for the degradation of the specular point contributions to the scattered fields by the rough surface ($|\chi^S|^2 \leq 1$ and $|\chi^S|^2 \rightarrow 1$ as $\beta \rightarrow 0$). The diffuse scattering contribution to the matrix $[S']$ due to surface roughness is given by

$$[S_s] = \begin{bmatrix} [S_{11}^s] & [S_{12}^s] & 0 & 0 \\ [S_{21}^s] & [S_{22}^s] & 0 & 0 \\ 0 & 0 & [S_{33}^s] & [S_{34}^s] \\ 0 & 0 & [S_{43}^s] & [S_{44}^s] \end{bmatrix} \quad (2.6)$$

where

$$[S_{ij}^s] = \frac{A_y}{4\pi p[\sigma_t]} \rho \langle \sigma^{ij} \rangle_s, \text{ for } i, j=1, 2 \quad (2.7a)$$

in which $A_y = \pi h_0^2$ is the cross sectional area of the unperturbed particle and $\langle \sigma^{ij} \rangle_s$ are the full wave solutions for the like and cross polarized normalized scattering cross sections (Bahar and Chakrabarti 1985). The first and second superscripts i, j denote the polarizations (V vertical, H horizontal) of the scattered and incident fields respectively.

$$\langle \sigma^{ij} \rangle_s = \int_0^{2\pi} \int_0^\pi |k_o^{ij}|^2 P_2 Q_s \sin y dy d\phi / \pi^2 \quad (2.7b)$$

where

$$Q_s = \int_{-\infty}^{\infty} (\chi_2^s(\vec{r} \cdot \vec{a}_r) - |\chi_2^s(\vec{r} \cdot \vec{a}_r)|^2) \exp(i\vec{r} \cdot \vec{r}_d) dx_d dz_d \quad (2.7c)$$

The joint characteristic function χ_2 for the rough surface h_s is only a function of distance $r_d = (\chi_d^2 + z_d^2)^{1/2}$ measured along the surface of the unperturbed sphere.

Furthermore for $i=3$ and 4 (Bahar and Fitzwater 1985)

$$[S_{11}^s] = \rho [Re \langle \sigma_{22}^{11} \rangle_s + \langle \sigma_{21}^{12} \rangle_s] A_y / 4\pi p[\sigma_t] \quad (2.7d)$$

(upper and lower signs for $i=3$ and 4 respectively) and for $i \neq j$

$$[S_{ij}^s] = \rho [Im \langle \sigma_{22}^{11} \rangle_s + \langle \sigma_{21}^{12} \rangle_s] A_y / 4\pi p[\sigma_t] \quad (2.7e)$$

(upper and lower signs for $i, j=4, 3$ and $i, j=3, 4$ respectively). In the above expressions

$$\langle \sigma_{kk}^{ij} \rangle_s = \int_0^{2\pi} \int_0^\pi k_o^{2ij} D^{kk*} P_2 Q_s \sin y dy d\phi / \pi^2 \quad (2.7f)$$

In (2.7) P_2 is the shadow function and the scattering coefficients D^{ij} are functions of \vec{n}^i, \vec{n}^j and \vec{n} the normal to the unperturbed surface of the particle as well as its electromagnetic parameters ϵ, μ . The remaining eight terms of the matrix $[S_s]$ vanish since D^{ii} and $D^{ij}(i \neq j)$ are symmetric and antisymmetric respectively with respect to ϕ , the azimuth angle of the sphere.

In this work it is assumed that a linearly polarized wave is normally incident upon a parallel layer (of optical thickness τ_0) containing a random distribution of irregular particles. Thus the incident Stokes matrix at $z=0$ is

$$[I_{inc}] = \begin{bmatrix} 1 \\ 0 \\ 0 \\ 0 \end{bmatrix} \delta(\mu'-1) \delta(\phi') \equiv [I_0] \delta(\mu'-1) \delta(\phi') \quad (2.8)$$

in which $\delta(\cdot)$ is the Dirac delta function. Thus the reduced incident intensity is

$$[I_{r1}] = [I_{inc}] \exp(-\tau) \quad (2.9)$$

and the (4×1) excitation matrix in (2.1) is

$$[I_1] = \int [S] [I_{r1}] d\mu' d\phi' = [F] \exp(-\tau) \quad (2.10)$$

in which the (4×1) matrix F is

$$[F] = [S] [I_0] \Big|_{\substack{\mu=1 \\ \phi=0}}^{\mu=1} \quad (2.11)$$

and the matrix $[I_0]$ is defined by (2.8). The matrix $[F]$ contains terms that are azimuthally independent as well as terms that are proportional to $\cos 2\phi$ and $\sin 2\phi$. Thus $[F]$ is expressed as follows (Cheung and Ishimaru 1982)

$$[F] = [F]_0 + [F]_a \cos 2\phi + [F]_b \sin 2\phi \quad (2.12)$$

in which, for a rough sphere,

$$[F]_0 = \frac{1}{2} \begin{bmatrix} F_{01} \\ F_{02} \\ 0 \\ 0 \end{bmatrix}, [F]_a = \frac{1}{2} \begin{bmatrix} F_{a1} \\ F_{a2} \\ 0 \\ 0 \end{bmatrix}, [F]_b = \begin{bmatrix} 0 \\ 0 \\ -S_{33} \\ -S_{43} \end{bmatrix} \quad (2.13)$$

and $F_{01} = S_{11} \pm S_{22}$ (upper and lower signs for $a=0$ and $a=a$ respectively). The solution of the equation of transfer (2.1) for the incoherent specific intensity matrix can be expressed in terms of the Fourier series

$$[I] = \sum_{m=0}^{\infty} [I]_m^a \cos m\phi + \sum_{m=1}^{\infty} [I]_m^b \sin m\phi \quad (2.14)$$

Since the elements of the scattering matrix $[S]$ are functions of $\phi' - \phi$ it is expressed as follows

$$S = \frac{1}{2\pi} [S]_0^a + \frac{1}{\pi} \sum_{m=1}^{\infty} \{ [S]_m^a \cos m(\phi' - \phi) + [S]_m^b \sin m(\phi' - \phi) \} \quad (2.15)$$

In view of the excitation, (2.10) through (2.13), the only non-vanishing Fourier terms are $m=0$ and $m=2$ (Cheung and Ishimaru 1982). The equation of transfer for the $m=0$ Stokes matrix is

$$\mu \frac{d}{d\tau} [I]_0^a = -[I]_0^a + \int_{-1}^1 [S]_0^a \mu' [I]_0^a d\mu' + [F]_0 \exp(-\tau) \quad (2.16)$$

Since the third and fourth elements of $[F]_0$ (2.13) are zero, and in view of the special form of $[S]_0^a$, the third and fourth terms of $[I]_0^a$ vanish.

The equation of transfer for the $m=2$ term is

$$\mu \frac{d}{d\tau} [I]_2 = -[I]_2 + \int_{-1}^1 [S]_2 [I]_2 d\mu' + [F]_2 \exp(-\tau) \quad (2.17)$$

in which

$$[S]_2 = \begin{bmatrix} [S_1]_2^a & [S_2]_2^b \\ -[S_3]_2^b & [S_4]_2^a \end{bmatrix} \text{ and } [F]_2 = [F]_a + [F]_b \quad (2.18)$$

in which $[S_1]_m^a$ and $[S_4]_m^b$ are 2×2 matrices

$$[S_1]_m^a = \int_{-1}^1 [S_1] \cos m(\phi' - \phi) d(\phi' - \phi) \quad i=1, 4 \quad (2.19a)$$

and

$$[S_4]_m^b = \int_{-1}^1 [S_4] \sin m(\phi' - \phi) d(\phi' - \phi) \quad i=2, 3 \quad (2.19b)$$

and $[S_1]$ are the (2×2) submatrices

$$[S] = \begin{bmatrix} [S_1] & [S_2] \\ [S_3] & [S_4] \end{bmatrix} \quad (2.20)$$

The boundary conditions for the Stokes matrix are

$$[I]_0 = [I]_2 = 0 \text{ for } 0 \leq \mu \leq 1 \text{ at } \tau=0 \quad (2.21a)$$

and

$$[I]_0 = [I]_2 = 0 \text{ for } 0 \geq \mu \geq -1 \text{ at } \tau=\tau_0. \quad (2.21b)$$

Equations (2.16) and (2.17) together with the

associated boundary conditions (2.21) are solved for the specific incoherent diffuse scattering intensities using the Gaussian quadrature method (to discretize the angles $\theta = \cos^{-1}\mu$) and the matrix characteristic value technique (Ishimaru 1978).

The diffuse scattering intensities I_1 and I_2 correspond to the vertically polarized (E_0) and horizontally polarized (E_0) waves. However, in practice, the polarization of the receiver is either parallel (E_x) or perpendicular (E_y) to the polarization of the incident wave. The corresponding specific intensities I_x and I_y are called the co-polarized and cross polarized incoherent intensities respectively (Cheung and Ishimaru 1982).

3. Illustrative Examples

The random rough surface height h_s (2.5c) measured normal to the surface of the unperturbed spherical particle of radius h_0 , is assumed to be homogeneous and isotropic. The rough surface is characterized by its surface height spectral density function $W(v_x, v_y) = W(v_T)$, the Fourier transform of the surface height autocorrelation function $\langle h_s h_s^* \rangle$, where v_T is the component of \bar{v} (2.5b) tangent to the surface of the unperturbed sphere,

$$v_T = (v_x^2 + v_y^2)^{1/2} \quad (3.1)$$

The specific form of the surface height spectral density function is

$$W(v_T) = \frac{2C}{\pi} \left[\frac{v_T}{v_m^2 + v_T^2} \right]^8, \quad v_T > 0 \quad \begin{matrix} v_m = 4D \\ D = 10\lambda \\ \lambda = 0.55\mu \end{matrix} \quad (3.2)$$

The constant C is determined by the choice of the roughness parameter.

$$\beta = 4k^2 \langle h_s^2 \rangle = 40 \quad (3.3)$$

In (3.3) $\langle h_s^2 \rangle$ is the mean square height

$$\langle h_s^2 \rangle = \frac{\pi}{2} \int_0^\infty W(v_T) v_T dv_T = C/210 v_m^6 \quad (3.4)$$

The corresponding value for the mean square slope is

$$\langle \sigma_s^2 \rangle = \frac{\pi}{2} \int_0^\infty W(v_T) v_T^3 dv_T = C/84 v_m^4 = 10 \quad (3.5)$$

Thus the correlation length is

$$r_c = 2(\langle h_s^2 \rangle / \langle \sigma_s^2 \rangle)^{1/2} = 1.26/v_m = 10 \quad (3.6)$$

The corresponding values for the extinction cross sections and the albedos are shown in Table I. The analytical expression for the surface height autocorrelation function $R(\zeta) = \langle h_s h_s^* \rangle / \langle h_s^2 \rangle$ is

$$R(\zeta) = \left[1 - \frac{3\zeta^2}{8} + \frac{3\zeta^4}{32} + \frac{\zeta^6}{3072} \right] K_1(\zeta) + \left[\frac{1}{2} - \frac{\zeta^2}{4} - \frac{\zeta^4}{96} \right] \zeta^2 K_0(\zeta) \quad (3.7)$$

In (3.7) K_0 and K_1 are modified Bessel functions of the second kind of order zero and one respectively (Abramowitz and Stegun 1964) and the dimensionless argument is

$$\zeta = v_m r_d \quad (3.8)$$

For all the illustrative examples it is assumed that the normally incident wave is linearly polarized with the electric field in the direction

of the x axis (in the $\phi=0$ plane). The equation of transfer for the Stokes parameters (2.16) and (2.17) together with the associated boundary conditions (2.21) are solved using the matrix characteristic value technique (Ishimaru 1978). The scattering cross sections are very sharply peaked in the forward direction, thus it is necessary to use a Gaussian quadrature formula of order 32 (Abramowitz and Stegun 1964).

In Figs. 1 and 2 the incoherent diffuse transmitted intensities I_1 (vertical polarization) and I_2 (horizontal polarization) for case (a) (aluminum) are plotted as functions of $\theta(0,90^\circ)$ with $\phi=0$ and $v_0=1$. The solid curves correspond to first order scattering solutions only (Ishimaru 1978), for the smooth (unperturbed spherical) particles and particles with rough surfaces (I_2+C , for single scatter smooth particle). The corresponding solutions that account for multiple scattering are also plotted in these figures.

In Figs. 3 and 4 the transmitted incoherent intensities I_1 and I_2 for case (b) (plastic) are plotted as functions of $\theta(0,90^\circ)$ with $\phi=0$ and $v_0=1$. There is a larger difference between the results for the smooth and rough particles for this case than for case (a).

4. Concluding Remarks

The specific incoherent diffuse intensities I_1 and I_2 as well as the co-polarized and cross polarized intensities are evaluated for a layer of randomly distributed finitely conducting particles of irregular shape. The rough surfaces of the particles are characterized by different surface height spectral density functions and roughness parameters β . The layer of particles is assumed to be excited by normally incident linearly polarized waves at wavelength $\lambda=0.55\mu$.

The rough particles will generally depolarize the incident waves more than the smooth particles and the specific intensities tend to be less oscillatory functions of θ for the rough particles. Since the albedos for the rough particles are smaller than those for the smooth particles (the difference increases for more dissipative particles), hence for very thick layers the specific intensities are smaller for the rough particles. Both single scatter and multiple scatter solutions are given. For small optical thickness $r \ll 1$ I_1 is smaller for the rough particles than for the smooth particles (since the albedo for the rough particle is smaller). However I_2 is larger for the rough particles since the rough particles more strongly depolarize the incident waves.

ACKNOWLEDGMENTS

This work was supported by the U.S. Army Research Office under Contract DAAG-29-82-K-0123. The authors wish to thank Swapan Chakrabarti for his comments.

References

1. Abramowitz, M., and I.A. Stegun (1964), *Handbook of Mathematical Functions*, Appl. Math. Ser. 55, Nat. Bur. of Stand., Washington, D.C.
2. Bahar, E., and Swapan Chakrabarti (1985), Appl. Optics, **24**, No. 12, 1820.
3. Bahar, E., and M. Fitzwater (1985), Radio Science - in press.
4. Chandrasekhar, S. (1950), Radiative Transfer, Dover, Publ., New York.

5. Cheung, R.L.-T., and A. Ishimaru (1982), *Applied Optics*, 21, No. 20, 3792.
6. Ehrenreich, H. (1965), "The Optical Properties of Metals," *IEEE Spectrum*, 2, 162.
7. Ishimaru, A. (1978), *Wave Propagation and Scattering in Random Media*, Academic, New York.
8. Ishimaru, A., and R.L.-T. Cheung (1980), *Ann. Telecommun.*, 35, 373.

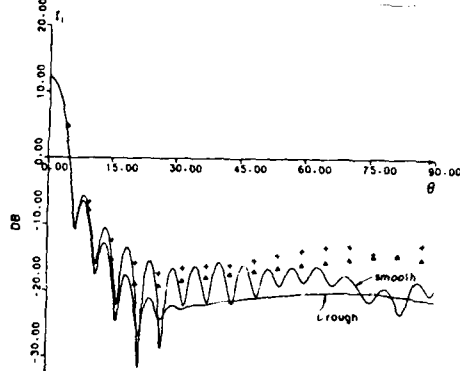


Fig. 1. Specific incoherent intensity I_1 case (a), transmitted, $\tau_0=1$, $\phi=0$. First order (—), smooth and rough particles. Multiple scatter: (+) smooth, (Δ) rough. $\epsilon_r = -40-i12$ (Ehrenreich, 1965).

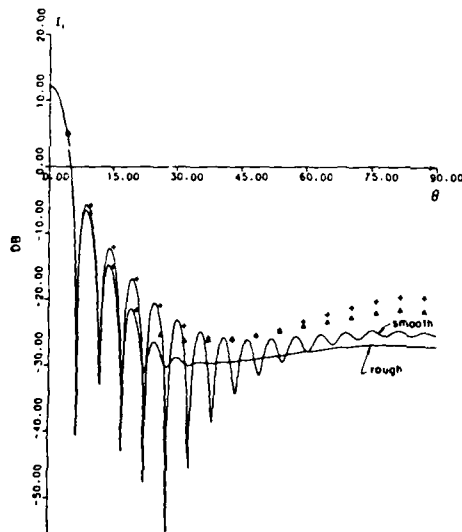


Fig. 3. Specific incoherent intensity I_1 , case (b), transmitted, $\tau_0=1$, $\phi=0$. First order (—), smooth and rough particles. Multiple scatter: (+) smooth, (Δ) rough. $\epsilon_r = 1.5-i8$.

	case a	case b
ϵ_r	-40-i12	1.5-i8
material	aluminum	dissipative plastic
σ_t , smooth	2.2592	2.2432
σ_t , rough	2.2126	2.1959
albedo, smooth	.9356	.6607
albedo, rough	.8579	.6105

Table 1. The dielectric coefficient ϵ_r , the extinction cross section and the albedos for the scattering particles.

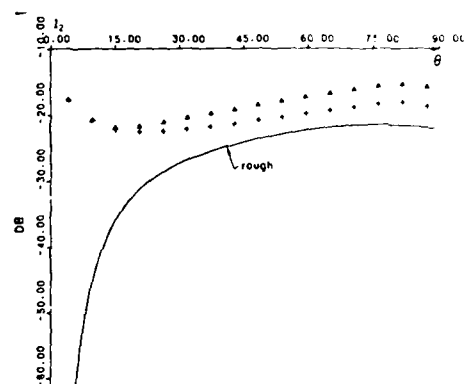


Fig. 2. Specific incoherent intensity I_2 case (a), transmitted, $\tau_0=1$, $\phi=0$. First order (—), smooth and rough particles. Multiple scatter: (+) smooth, (Δ) rough. $\epsilon_r = -40-i12$.

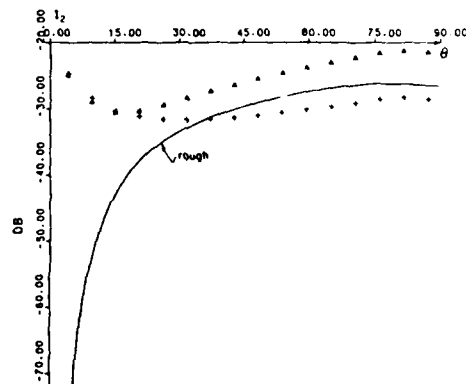


Fig. 4. Specific incoherent intensity I_2 , case (b), transmitted, $\tau_0=1$, $\phi=0$. First order (—), smooth and rough particles. Multiple scatter: (+) smooth, (Δ) rough. $\epsilon_r = 1.5-i8$.



CHEMICAL
SYSTEMS
LABORATORY

US Army Armament Research and Development Command
Aberdeen Proving Ground, Maryland 21010

SPECIAL PUBLICATION ARCSL-SP-83011

PROCEEDINGS

OF THE

1982

CHEMICAL SYSTEMS LABORATORY

SCIENTIFIC CONFERENCE

ON

OBSCURATION AND AEROSOL RESEARCH

Edited by

Ronald H. Kohl & Associates
Tullahoma, Tennessee 37388

June 1983



Distribution limited to US Government agencies only because of test and evaluation; June 1983. Other requests for this document must be referred to Commander, Chemical Systems Laboratory, ATTN: DRDAR-CLJ-IR, Aberdeen Proving Ground, Maryland 21010.

SCATTERING CROSS SECTIONS FOR PARTICLES OF IRREGULAR SHAPE

Ezekiel Bahar
Electrical Engineering Department
University of Nebraska-Lincoln, Lincoln, Nebraska 68588-0511

ABSTRACT

The full wave approach recently applied to the problem of electromagnetic scattering by a two scale model of random rough surfaces has been shown to account for both Bragg scattering and Specular Point scattering in a self-consistent manner. Thus scattering cross sections can be expressed as weighted sums of two cross sections. The first is associated with a smooth, filtered surface consisting of the large scale spectral components of the rough surface and the second is associated with its small scale spectral components.

In a similar manner the scattering cross sections for a particle of irregular shape can be characterized by weighted sums of two cross sections. The first is related to the cross section for a "smooth" particle of arbitrary shape and the second accounts for the small scale surface roughness of the particle. To apply such an approach to the scattering problem, it is necessary to assume that the principal dimensions of the particle are larger than both the wavelength of the scattered fields and the small scale surface height correlation distance.

Both the depolarized and like polarized components of the scattered fields are accounted for in the full wave analysis. These solutions are consistent with reciprocity and realizability relationships in electromagnetic theory and they are invariant to coordinate transformations.

NATIONAL ACADEMIES OF SCIENCE AND ENGINEERING

NATIONAL RESEARCH COUNCIL

of the

UNITED STATES OF AMERICA

UNITED STATES NATIONAL COMMITTEE
International Union of Radio Science



National Radio Science Meeting
5-7 January 1983

Sponsored by USNC/IURSI
in cooperation with
Institute of Electrical and Electronics Engineers

University of Colorado
Boulder, Colorado
U.S.A.

Commission B Session 5

B5-5
1510

BACKSCATTER CROSS SECTIONS FOR
RANDOMLY ORIENTED METALLIC FLAKES
AT OPTICAL FREQUENCIES - FULL
WAVE APPROACH

E. Bahar and Mary Ann Fitzwater,
U. of Nebraska, Lincoln, NE

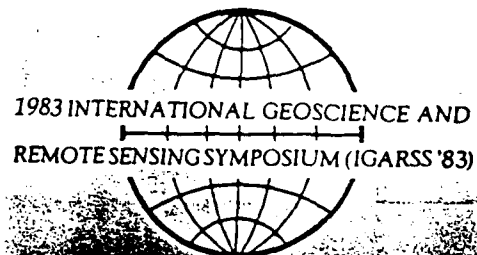
The backscatter cross sections for randomly oriented metallic flakes are derived using the full wave approach. The metallic flakes are characterized by their surface height spectral density function. Both specular point and Bragg scattering at optical frequencies are accounted for in a self-consistent manner. It is shown that the average normalized backscatter cross sections (per unit area) for the randomly oriented metallic flakes are larger than that of a perfectly conducting sphere.

Handwritten signature

1983 Joint Meeting of the
IEEE Geoscience and Remote Sensing Society
and URSI/USNC - Commission F



REMOTE SENSING: EXTENDING MAN'S HORIZON



August 31 - September 2, 1983
San Francisco, California

FINAL PROGRAM



Ezekiel Bahar
Electrical Engineering Department
University of Nebraska, Lincoln, Nebraska 68588

Clifford L. Rufenach and Donald E. Barrick
NOAA/ERL/Wave Propagation Laboratory
Boulder, Colorado 80303

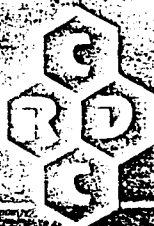
and

Mary Ann Fitzwater
Electrical Engineering Department
University of Nebraska, Lincoln, Nebraska 68588

ABSTRACT

As a synthetic aperture radar scans different portions of a rough surface, the direction of the unit vector normal to the mean surface of the effective illuminated area (resolution cell) fluctuates. In this paper the modulations of the scattering cross sections of the resolution cell are determined as the normal to it tilts in planes that are in and perpendicular to the fixed reference plane of incidence. Using the full wave approach, the scattering cross sections are expressed as a weighted sum of two cross sections. The first cross section is associated with scales of roughness within the resolution cell that are large compared to the radar wavelength, and the second cross section is associated with small-scale spectral components within the resolution cell. Thus, both specular point scattering and Bragg scattering are accounted for in a self-consistent manner. The results are compared with earlier solutions based on first order Bragg scattering theory.

AD



CHEMICAL
RESEARCH &
DEVELOPMENT
CENTER

CRDC-SP-84009

PROCEEDINGS OF THE
1983 SCIENTIFIC CONFERENCE
ON
OBSCURATION AND AEROSOL RESEARCH

Edited by JAN FARMER
RONALD H. KOHL

RONALD H. KOHL & ASSOCIATES
Tullahoma, TN 37388

JULY 1984

US Army Armament, Munitions & Chemical Command
Aberdeen Proving Ground, Maryland 21010

SCATTERING CROSS SECTIONS FOR LARGE FINITELY CONDUCTING SPHERES
WITH ROUGH SURFACES-FULL WAVE SOLUTIONS

Ezekiel Bahar
and
Swapn Chakrabarti
Electrical Engineering Department
University of Nebraska-Lincoln
Lincoln, NE 68588-0511

ABSTRACT

The scattering cross sections for large finitely conducting spheres with very rough surfaces are determined for optical frequencies using the full wave approach. For the roughness scales considered the scattering cross sections differ significantly from those of smooth conducting spheres. Several illustrative examples are presented and the results are compared with earlier solutions to the problem.

NATIONAL ACADEMIES OF SCIENCE AND ENGINEERING
NATIONAL RESEARCH COUNCIL
of the
UNITED STATES OF AMERICA

UNITED STATES NATIONAL COMMITTEE
International Union of Radio Science



National Radio Science Meeting
11-13 January 1984

Sponsored by USNC/URSI
in cooperation with
Institute of Electrical and Electronics Engineers

University of Colorado
Boulder, Colorado
U.S.A.

074 00000

02-3
1-00

SCATTERING AND DEPOLARIZATION
BY LARGE CONDUCTING SPHERES
WITH VERY ROUGH SURFACES
Ezekiel Bahar and Swapan Chakrabarti
Electrical Engineering Department
University of Nebraska
Lincoln, NE 68588-0511

The purpose of this investigation is to determine the like and cross polarized scattering cross sections for large conducting spheres with very rough surfaces. Perturbation theory has been used to determine EM scattering by spheres with random rough surfaces provided that the parameter $\beta = k_0 \langle h \rangle$ is much smaller than unity (where k_0 is the wave number and $\langle h \rangle$ is the mean square height of the rough surface of the sphere (D. E. Barrick, Radar Cross Section Handbook, Ch. 9, Plenum Press 1970). For large conducting spheres with $\beta \ll 1$, the total scattering cross sections are not significantly different from the physical optics cross sections for the smooth conducting spheres. In this paper the full wave approach is used to determine the scattering cross sections for spheres with roughness scales that significantly modify the total cross sections. The full wave approach accounts for specular point scattering and Bragg scattering in a self consistent manner and the total cross section are expressed as weight sums of two cross sections. (E. Bahar and D. E. Barrick, Radio Science, 18, No. 2, 129-137, 1983).

NASA Conference Publication 2303

Frontiers of Remote Sensing of the Oceans and Troposphere from Air and Space Platforms

Proceedings of the URSI Commission F
Symposium and Workshop
Shoresh, Israel
May 14-23, 1984

NASA

OPTIMUM BACKSCATTER CROSS SECTION OF THE OCEAN
AS MEASURED BY SYNTHETIC APERTURE RADARS

Ezekiel Bahar

Electrical Engineering Department
University of Nebraska-Lincoln, NE 68588-0511

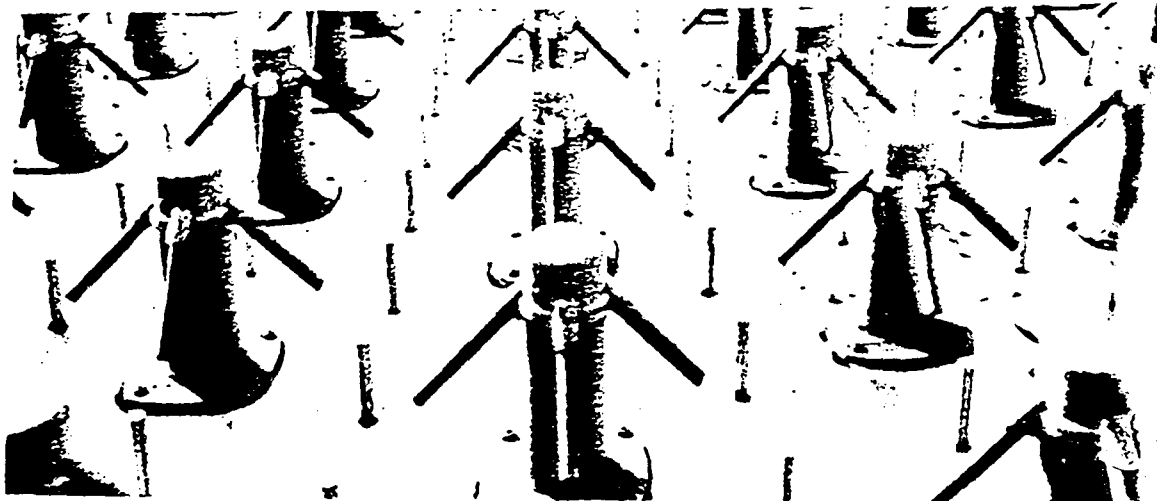
Clifford L. Rufenach and Donald E. Barrick
NOAA/ERL/Wave Propagation Laboratory, Boulder, CO 80303

Mary Ann Fitzwater

Electrical Engineering Department
University of Nebraska-Lincoln, NE 68588-0511

ABSTRACT

Microwave remote sensing of rough surfaces (both land and ocean), using moving platforms (aircraft and satellite), as well as ground based measurements has illustrated the need for a better understanding of the interaction of the radar signals with these surfaces. This interaction is particularly important for the ocean surface where the radar modulation can yield information about the long ocean wave field. Radar modulation measurements from fixed platforms have been made in wavetanks and the open oceans. The surfaces have been described in terms of two-scale models. The radar modulation is considered to be principally due to: (1) geometrical tilt due to the slope of the long ocean waves and (2) the straining of the short waves (by hydrodynamic interaction). For application to moving platforms, Synthetic Aperture Radar (SAR) and Side Looking Airborne Radar (SLAR), this modulation needs to be described in terms of a general geometry for both like- and cross-polarization since the long ocean waves, in general, travel in arbitrary directions. In the present work, the finite resolution of the radar is considered for tilt modulation with hydrodynamic effects neglected.



ANTENNAS AND PROPAGATION

VOLUME I

JUNE 25-29
1984

WESTIN HOTEL

BOSTON
MASSACHUSETTS



IEEE ANTENNAS
AND PROPAGATION
SOCIETY

MACQUENON 2

APS-2-2

SCATTERING CROSS SECTIONS FOR COMPOSITE MODELS OF NON-GAUSSIAN ROUGH SURFACES FOR WHICH DECORRELATION IMPLIES STATISTICAL INDEPENDENCE

Ezekiel Bahar
and
Mary Ann Fitzwater
Electrical Engineering Department
University of Nebraska-Lincoln, NE 68586

SUMMARY

In this work the full wave approach is used to determine the scattering cross sections for composite models of non-Gaussian rough surfaces. In particular, it is assumed here that the rough surface is characterized by a family of joint height probability densities that have been developed by Beckmann (IEEE Trans. Antennas Propag., AP-21(2), 189-175, 1973) for non-Gaussian surfaces. These joint height probability densities are expressed as an infinite sum of powers of the correlation coefficient and it is assumed that decorrelation of surface heights implies statistical independence. Using these joint probability density functions Beckmann derives physical optics and geometrical optics approximations for the scattering cross sections.

By considering a very broad family of non-Gaussian rough surfaces with marginals that include in the limits the exponential and the Gaussian surfaces, it is possible to derive the full wave solutions for the backscatter cross sections for more realistic models of rough surfaces. Since it is assumed in this work that decorrelation of the surface heights implies statistical independence, no delta function type specular terms are obtained in these results. It is found that for angles of incidence $\theta_i, 25^\circ$, the backscatter cross section for the horizontally polarized waves are more sensitive to the specific form of the joint height probability density assumed. For near normal incidence both the backscatter cross sections for vertically and horizontally polarized waves exhibit the same dependence on the specific form of the joint height probability density assumed. For convenience in this work the rough surface height $h(x,y)$ is decomposed into a large scale filtered surface h_L and a small scale surface h_s . The incident and scattered wave normals are in the directions of the unit vectors \hat{n}_i and \hat{n}_s respectively. The scattering cross section for the composite surface which accounts for both specular scatter and Bragg scatter in a self-consistent manner is given by the weighted sum of two cross sections (Bahar, E., D.E. Barrick and M.A. Fitzwater, IEEE Trans. Antennas Propag., AP-31(5), 698-702, 1983)

$$\langle \sigma^p \rangle_T = \langle \sigma^p \rangle_0 + \langle \sigma^p \rangle_R \quad (1)$$

CITIZENSHIP/000000000000000000 0 1984 IEEE



CHEMICAL
RESEARCH &
DEVELOPMENT
CENTER

CRDC-SP-85007

**PROCEEDINGS OF THE
CHEMICAL RESEARCH AND DEVELOPMENT
CENTER'S 1984 SCIENTIFIC CONFERENCE
ON OBSCURATION AND AEROSOL
RESEARCH**

Edited by Ronald H. Kohl
Deborah Stroud

RONALD H. KOHL & ASSOCIATES
Tullahoma, Tennessee 37388

June 1985

Army Ammunition Operations Chemical Command
Gordon, Pennsylvania Maryland 21010-5423

SCATTERING AND DEPOLARIZATION BY CONDUCTING CYLINDERS
WITH VERY ROUGH SURFACES

Ezekiel Bahar
and
Mary Ann Fitzwater
Electrical Engineering Department
University of Nebraska--Lincoln
Lincoln, NE 68588-0511

ABSTRACT

Like- and cross-polarized scattering cross sections are determined at optical frequencies for conducting cylinders with very rough surfaces. Both normal and oblique incidence with respect to the cylinder axis are considered. The full-wave approach is used to account for both the specular point scattering and the diffuse scattering. For the roughness scales considered, the scattering cross sections differ significantly from those derived for smooth conducting cylinders. Several illustrative examples are presented.

INTERNATIONAL
UNION OF RADIO SCIENCE



XXIst General Assembly

ABSTRACTS

OS 3: Radio Techniques in Planetary Exploration

September 3, 1984

August 28 - September 5, 1984

Session 2

2.1 SCATTERING AND DEPOLARIZATION OF RADIO WAVES BY ROUGH PLANETARY SURFACES

Ezekiel Bahar
Department of Electrical Engineering
University of Nebraska, Lincoln, Nebraska

Traditionally physical optics and perturbation theories have been used to derive the like and cross polarized scattering cross sections for rough planetary surfaces. To this end, two-scale models have been adopted and the rough surfaces are regarded as small scale surface perturbations that are superimposed on large scale, flat surfaces. Thus the scattering cross sections are expressed as a sum of the physical optics cross section for the large scale surface and the diffuse cross section for the small scale surface.

It is necessary to apply the perturbed-physical optics approach splitting is assumed to be the wavenumber k , where spectral scale spectral components of the rough surface. However, the results based on this approach critically depend upon the specification of k . Furthermore it is also necessary to assume that (a) the large and small scale surfaces are statistically independent, (b) the mean square slope for the total surface is approximately equal to the mean square slope of the large scale surface, (c) the mean square height of the total surface is large compared to a wavelength, and (d) the physical optics approximation for the cross polarized backscatter is zero.

In this paper the full wave approach is used to derive a unified formulation for the like and cross polarized cross sections for all angles of incidence. Since the full wave approach accounts for Bragg scattering and specular point scattering in a self consistent manner it is not necessary to decompose the rough surface. (E. Bahar and D.E. Barrick, Radio Science 18, 129-137, 1983) Thus it is not necessary to assume (a) or to make the above assumptions. These full wave solutions are compared with earlier solutions based on the two-scale model. The diffuse cross sections and the problems associated with the scattering of k are carefully examined. The full wave solutions for the cross polarized cross sections differ significantly from the corresponding solutions based on the two-scale model of the rough surface.

1985 NORTH AMERICAN RADIO SCIENCE MEETING

International Union of Radio Science



L'Union Radio-Scientifique Internationale

RÉUNION RADIO-SCIENTIFIQUE

NORD-AMÉRICAIN 1985

June/juin 17-21, 1985

University of British Columbia
Vancouver, Canada

B-3-9

SCATTERING BY ANISOTROPIC MODELS OF COMPOSITE ROUGH SURFACES-FULL WAVE SOLUTION

E. Behar
Electrical Engineering Department
University of Nebraska--Lincoln
Lincoln, NE 68588

ABSTRACT

Various combinations of physical optics theory and perturbation theory have been used to determine the scattering cross sections for composite models of rough surfaces. These solutions are based on a two-scale model of the rough surface. Physical optics accounts for specular point scattering from the large scale surface while perturbation theory accounts for Bragg scattering from the small scale surface. However, the results based on the perturbed-physical optics approach critically depend upon the manner in which the composite surface is decomposed into a large and a small scale surface.

Since the full wave approach accounts for specular point scattering and Bragg scattering in a unified self-consistent manner, the solutions for the scattering cross sections can be derived from a single integral. However, the two-scale model can also be adopted when the full wave approach is used and the results are shown to be independent of the wavenumber k_0 where spectral splitting is assumed to occur, provided that the large scale surface satisfies the criteria for deep phase modulation (E. Behar, et al., IEEE Trans. on Antennas and Propagation, AP-31, 5, 698-709, 1983).

In this work, the full wave approach is applied to a rough surface characterized by an anisotropic slope probability density function. The full wave solutions based on the unified and two-scale model are presented. Backscatter cross sections for both vertically and horizontally polarized waves are evaluated for all angles of incidence and it is shown that the results are most sensitive to wind direction for angles of incidence around 40° . On examining the individual terms for the total cross sections based on the two-scale model, it is shown that the cross sections become insensitive to wind direction for near grazing incidence.

DRAFT FOR PRESENTERS AND CRDC USE ONLY

VOLUMES I & II
Proceedings of the
1985 CRDC SCIENTIFIC CONFERENCE
on
OBSCURATION AND AEROSOL RESEARCH

This draft is to be superseded
by the published Proceedings.

This draft has not been cleared for public release.

RHK&A

RONALD H. KOHL & ASSOCIATES
Tullahoma, Tennessee 37388

MULTIPLE SCATTERING IN MEDIA CONSISTING OF NONSPHERICAL
FINITELY CONDUCTING PARTICLES

Ezekiel Bahar and Mary Ann Fitzwater
Electrical Engineering Department
University of Nebraska--Lincoln
Lincoln, Nebraska 68588-0511

RECENT PUBLICATIONS, SUBMITTALS FOR PUBLICATION AND PRESENTATIONS:

- A) E. Bahar, "Scattering and Depolarization by Very Long Finitely Conducting Cylinders with Rough Surfaces," 1984 CRDC Scientific Conference on Obscuration and Aerosol Research, Aberdeen, Maryland, June 25-29, 1984.
- B) E. Bahar, "Scattering and Depolarization of Radio Waves by Rough Planetary Surfaces," International Union of Radio Science Symposium on Radio Techniques in Planetary Exploration, in conjunction with the XXI General Assembly of URSI, Florence, Italy, August 26-September 6, 1984.
- C) E. Bahar and M. A. Fitzwater, "Scattering Cross Sections for Composite Rough Surface Using the Unified Full Wave Approach," IEEE Transactions on Antennas and Propagation, Vol. AP-32, No. 7, pp. 730-734, July 1984.
- D) E. Bahar, "Scattering by Anisotropic Models of Composite Rough Surface--Full Wave Solutions," IEEE Transactions on Antennas and Propagation, Vol. AP-33, No. 1, pp. 106-112, January 1985.
- E) E. Bahar and S. Chakrabarti, "Scattering and Depolarization by Large Conducting Spheres with Very Rough Surfaces," Applied Optics, Vol. 24, No. 12, pp. 1820-1825, June 1985.
- F) E. Bahar, "Scattering by Anisotropic Models of Composite Rough Surfaces--Full Wave Solutions," International IEEE/APS-Symposium and 1985 North American Radio Science Meeting, Vancouver, Canada, June 17-21, 1985.
- G) E. Bahar, "Multiple Scattering in Media Consisting of Nonspherical, Finitely Conducting Particles, 1985 CRDC Scientific Conference on Obscuration and Aerosol Research, Aberdeen, Maryland, June 17-21, 1985.
- H) E. Bahar, "Scattering and Depolarization by Random Rough Surfaces--Unified Full Wave Approach," Symposium/Workshop on Multiple Scattering of Waves in Random Media and by Random Rough Surfaces," Pennsylvania State University, University Park, Pennsylvania, July 29-August 1, 1985.
- I) E. Bahar, "Unified Full Wave Solutions for Electromagnetic Scattering by Rough Surfaces--Comparison with Physical Optics, Geometric Optics and Perturbation Solutions Using Two-Scale Models of Rough Surfaces," Schlumberger Doll Research Workshop on Waves in Inhomogeneous Media, August 8-9, 1985.
- J) E. Bahar, "Scattering and Depolarization by Conducting Cylinders with Rough Surfaces," DRSAC-CLJ-IR, pp. 365-371, January 1985.
- K) E. Bahar and M. A. Fitzwater, "Like and Cross Polarized Scattering Cross Sections for Random Rough Surfaces--Theory and Experiment," Journal of the Optical Society of America Special Issue on Wave Propagation and Scattering in Random Media--in press.
- L) E. Bahar and M. A. Fitzwater, "Scattering and Depolarization by Conducting Cylinders with Rough Surfaces," submitted for review.
- M) E. Bahar and M. A. Fitzwater, "Multiple Scattering by Irregular Shaped Particles of Finite Conductivity at Infrared and Optical Frequencies," submitted for review.

ABSTRACT

The incoherent specific intensities for the waves scattered by a random distribution of particles with rough surfaces are derived. Since large roughness scales are considered, the diffuse scattering contributions to the like and cross polarized scattering cross sections are given by the full wave solutions. The scattering matrix in the expression for the equation of transfer is given by a weighted sum of the scattering matrix for the smooth particle and the diffuse contribution due to the rough surface of the particle. Illustrative examples are presented for the propagation of a circularly polarized wave normally incident upon a parallel layer of particles. Particles with different surface height spectral density functions, roughness scales, complex permittivities and sizes are considered. Both first order (single scatter) and multiple scatter solutions are provided and the results for particles with smooth and rough surfaces are compared.

**MULTIPLE SCATTERING OF WAVES
IN
RANDOM MEDIA AND RANDOM ROUGH SURFACES**

AN INTERNATIONAL SYMPOSIUM

July 29 - August 2, 1985

ABSTRACTS



Sponsored by :

U.S. Office of Naval Research

U.S. Army Research Office

Host :

The Pennsylvania State University

University Park, Pennsylvania

Thursday(XVI), 5:20 p.m.

SCATTERING AND DEPOLARIZATION BY RANDOM ROUGH SURFACES-
UNIFIED FULL WAVE APPROACH

Ezekiel Bahar
Electrical Engineering Department
University of Nebraska
Lincoln, NE 68588-0511

The recent impetus to produce rigorous solutions to more realistic models of pertinent propagation problems over a very wide frequency range has generated the need to derive full wave solutions to problems of radio wave propagation in dispersive, inhomogeneous, anisotropic and dissipative media with irregular boundaries.

To perform the full wave analyses, it is necessary to develop generalized field transforms that provide the basis for the complete expansions for the electromagnetic fields in irregular multilayered structures with varying thickness and electromagnetic parameters. These complete expansions consist of the vertically and horizontally polarized radiation fields, lateral waves and guided surface waves. The generalized field transforms are used to reduce Maxwell's equations, in conjunction with the associated exact boundary conditions for the electromagnetic fields, into sets of first order coupled differential equations for the forward and backward traveling wave amplitudes.

The full wave solutions, that have been derived for the scattered radiation fields from rough surfaces with arbitrary slope and electromagnetic parameters, bridge the wide gap that exists between the perturbational solutions for rough surfaces with small slopes and the Physical Optics solutions.

UNIFIED FULL WAVE SOLUTIONS
FOR ELECTROMAGNETIC SCATTERING BY ROUGH SURFACES--
COMPARISON WITH PHYSICAL OPTICS, GEOMETRIC OPTICS AND
PERTURBATION SOLUTIONS USING TWO-SCALE
MODELS OF ROUGH SURFACES

presented by

Dr. E. Bahar

at

The Schlumberger Workshop on
Waves in Inhomogeneous Media

August 8-9, 1985

Ridgefield, Connecticut

National Academies of Science and Engineering
National Research Council
of the
United States of America

UNITED STATES NATIONAL COMMITTEE
International Union of Radio Science



Commission F Meeting

October 7-9, 1985

Sponsored by USNC/URSI Commission F
held jointly with
1985 International Geoscience and
Remote Sensing Symposium (IGARSS '85)
Institute of Electrical and Electronics Engineers
University of Massachusetts
Amherst, Massachusetts
U.S.A.

**LIKE AND CROSS POLARIZED SCATTERING CROSS SECTIONS
FOR RANDOM ROUGH SURFACES--FULL WAVE THEORY AND EXPERIMENT**

Ezekiel Bahar
and

Mary Ann Fitzwater
Electrical Engineering Department
University of Nebraska-Lincoln
Lincoln, NE 68588-0311

ABSTRACT

Solutions for the like and cross polarized scattered radiation fields are presented for rough surfaces using the full wave approach (Bahar 1981). The full wave solutions account for specular point scattering and diffuse scattering for the like and cross sections. Unified full wave expressions for the like and cross sections are also presented for random rough surfaces. In addition, on adopting a two-scale model of the rough surface, the cross sections are expressed as a weighted sum of two cross sections. The like section for specular point scattering from the large scale filiform surface is shown to be consistent with the two-scale model. The solutions for diffuse scattering from the small scale surface h_2 that rides on the large scale surface h_1 . The solutions for diffuse scattering from the large scale surface h_1 are shown to be consistent with the corresponding perturbation, physical optics and geometric optics solutions.

Several illustrative examples are presented using both the unified full wave expressions and those based on the two-scale model. The discrepancy between the two solutions for the like and cross polarized backscatter cross sections is examined in detail. In particular near normal incidence ($\theta_i = 15^\circ$) there is a difference of about 15 db between the two computed values of the cross sections. The like to cross polarized cross sections σ_{HH}/σ_{VV} (V.H. correspond to vertical and horizontal). The unified full wave solution for the ratio is consistent with experimental data.

BL1/F4-3 SCATTERING AND DEPOLARIZATION BY CONDUCTING
0920 CYLINDERS WITH ROUGH SURFACES
Ezekiel Bahar and Mary Ann Fitzwater
Electrical Engineering Department
University of Nebraska--Lincoln
Lincoln, NE 68588-0511

ABSTRACT

The problem of electromagnetic scattering by finitely conducting cylinders or spheres has been dealt with extensively in the technical literature. Perturbation theory has been used to extend these results to scattering by slightly rough circular cylinders or spheres (D. E. Barrick et al., Radar Cross Section Handbook, Chapter 8, Plenum Press, 1970). However, perturbation theory is limited to surfaces for which the roughness parameter $\beta = 4k_0 \langle h^2 \rangle < 0.1$ (k_0 is the electromagnetic wavenumber and $\langle h^2 \rangle$ is the mean square height of the rough surface (G. S. Brown, IEEE Trans. Ant. and Prop. AP-26 (3) 472-482, 1978). For $\beta < 0.1$ the scattering cross sections are not significantly different from those for smooth conducting circular cylinders.

In this work the full wave approach (E. Bahar, Radio Sci., 16(6), 1327-1335, 1981), is used to determine the like and cross polarized scattering cross sections at optical frequency for finitely conducting cylinders with roughness scales that significantly modify the scattering cross sections. The radii of curvature of the unperturbed cylinders considered are large compared to wavelength λ . (However, the cross section of the unperturbed cylinder need not be circular). Both specular point scattering and diffuse scattering are accounted for in the analysis in a self-consistent manner and the scattering cross sections are expressed as a weighted sum of two

The full wave solutions are presented for long cylinders with mean circular cross sections and both the specular point and diffuse contributions are identified. Several illustrative examples are considered for cylinders with roughness parameter $\beta = 1$. The rough surface is characterized by its surface height spectral density function. The like and cross polarized cross sections as well as the albedos for smooth and rough cylinders are compared.

NATIONAL ACADEMIES OF SCIENCE AND ENGINEERING

NATIONAL RESEARCH COUNCIL

of the

UNITED STATES OF AMERICA

UNITED STATES NATIONAL COMMITTEE

International Union of Radio Science



National Radio Science Meeting

13-16 January 1986

Sponsored by USNC/URSI
in cooperation with
Institute of Electrical and Electronics Engineers

University of Colorado
Boulder, Colorado
U.S.A



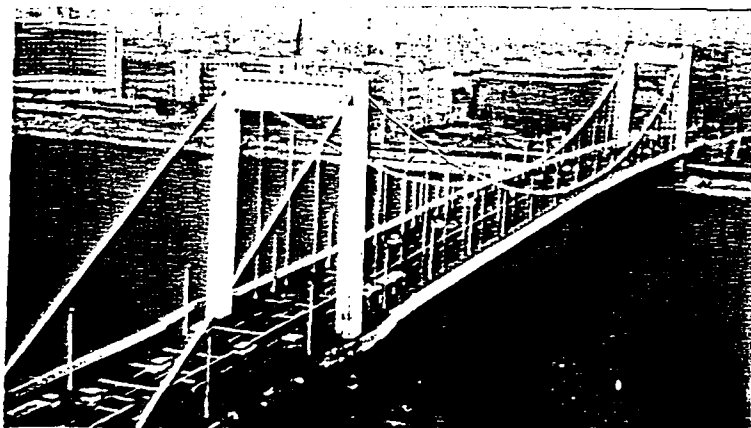
SECOND
ANNOUNCEMENT
and Program

URSI
INTERNATIONAL SYMPOSIUM
ON
ELECTROMAGNETIC THEORY

8TH
COLLOQUIUM ON
MICROWAVE
COMMUNICATION

Budapest — Hungary
25—29 August, 1986

Budapest — Hungary
25—29 August, 1986



Ezekiel Bahar
Mary Ann Fitzwater
Electrical Engineering Department
University of Nebraska--Lincoln
Lincoln, Nebraska 68588-0511

ABSTRACT

The incoherent diffuse scattering intensities (Stokes parameters) are evaluated for infrared and optical excitations of a layer consisting of random distributions of finitely conducting irregular shaped particles. The full wave approach is used to determine the elements of the phase matrix and the extinction cross sections appearing in the equation of transfer. The rough surface height of the particles is characterized by different surface height spectral density functions.

1986 NATIONAL RADIO SCIENCE MEETING

International Union of Radio Science



PROGRAM AND ABSTRACTS

June 8-13, 1986

Wyndham Franklin Plaza Hotel
Philadelphia, PA

INTERPRETATION OF BACKSCATTER CROSS SECTIONS FOR NORMAL INCIDENCE USING UNIFIED AND TWO-SCALE FULL WAVE ANALYSES OF ROUGH SURFACES

Z. Bahar, Electrical Engineering Department
University of Nebraska-Lincoln NE 68588-0511
D.E. Barrick, Ocean Surface Research, Boulder CO 80303
M.A. Fitzwater, Electrical Engineering Department
University of Nebraska-Lincoln NE 68588-0511

A specific and important application of rough-surface scattering at normal incidence concerns short-pulse satellite microwave altimeter return from the sea surface. In addition to its use to measure ocean waveheight at nadir as on Seasat, the altimeter has also been employed to infer wind speed from the backscattered signal intensity, since the roughness statistics depend strongly on surface wind. Up to now, attempts to establish a quantitative connection between altimeter nadir backscattered cross section (per projected area) and wind speed have employed a physical-optics derived specular-point model that (i) relates the backscatter cross section to rms surface slopes, and subsequently (ii) relates surface slopes to wind speed in some manner. Unfortunately, the returns predicted thereby are several db greater than the measured, leading to use of empirical rather than theory-based models to establish the connection. This discrepancy can only be due to the inadequacy of the simple, specular-point model, as it has been used, to describe the backscattered return even from a gently sloping sea at normal incidence.

The full wave solution for rough-surface scattering reduces to an integral similar in form to the physical optics or perturbation solutions (Z. Bahar, Radio Science, 16, No. 3, 331-344, 1981). In its derivation from the exact representation of the surface, multiple scattering is neglected. The full wave solution has been shown to reduce to the specular-point result in the high frequency limit, and to the perturbation result with the correct polarization dependence in the low frequency limit. Since it is valid across the spectrum from all roughness scales, it is not necessary to adopt the perturbation model to analyze rough surface scattering problems (Z. Bahar and M.A. Fitzwater, IEEE Trans. Antennas and Prop. AP-32, No. 7, 730-734, 1984). In recent work however (Z. Bahar and D.E. Barrick, Radio Science, 18, No. 2, 129-137, 1983), the full wave solution has been artificially decomposed into two components to elucidate the mechanisms at play in the two-scale models discussed above.

SEASAT MICROWAVE ALTIMETER MEASUREMENT
OF THE OCEAN GRAVITY-WAVE EQUILIBRIUM-RANGE
SPECTRAL BEHAVIOR USING FULL WAVE THEORY

by

Dr. Donald E. Barrick
and
Dr. Ezekiel Bahar

at

The 1986 International Geoscience
and Remote Sensing Symposium (IGARSS'86)

September 8-11, 1986

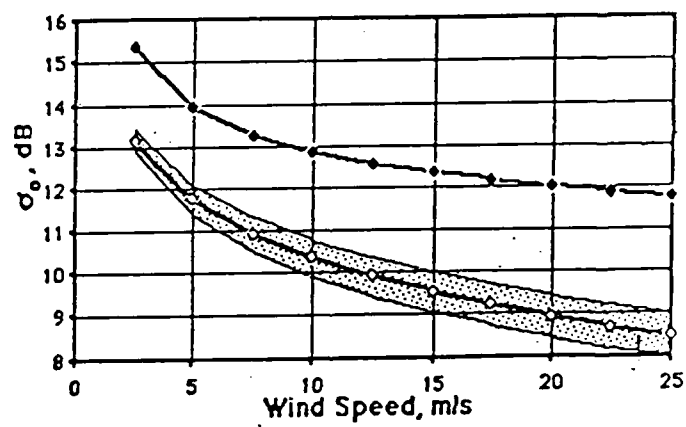
Zurich-Irchel, Switzerland

SEASAT Microwave Altimeter Measurement of the Ocean Gravity-Wave Equilibrium-Range Spectral Behavior Using Full-Wave Theory

Donald E. Barrick	Ezekiel Bahar
Ocean Surface Research	University of Nebraska
1131 Cranbrook Court	W194 Nebraska Hall
Boulder, Colorado 80303	Lincoln, Nebraska 68588
(303) 494-9103	(402) 472-1966

Models for the deep-water ocean gravity-wave spatial spectrum fully developed by the wind have classically tended to follow an inverse fourth power dependence on wavenumber beyond the spectral peak (which translates to an inverse fifth power dependence on wave frequency through the gravity-wave dispersion relation). Such behavior is predicted if all wave scales can linearly and independently develop to a maximum, constant slope before breaking. Recent theoretical and experimental oceanographic results, however, demonstrate the importance of nonlinearities in determining the characteristics of the shorter gravity waves. Most conventional instruments are incapable of measuring the wave spectral dependence well into the equilibrium region, i.e., a factor of 10 or more in wavenumber beyond the peak.

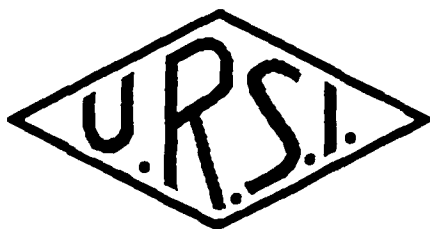
Full-wave theory for scattering from rough surfaces sheds light on the wave scales that contribute to backscatter at normal incidence. In particular, it shows how the simple specular-point model can be interpreted in terms of the upper limit on the waveslope spatial spectrum. This is then used to establish an empirical model for the wind-developed ocean waveheight spatial spectrum, based on 2000 independent measurements by the SEASAT microwave altimeter of nadir backscatter cross section vs wind speed. Although not accurate near the spectral peak, the resulting model gives its equilibrium behavior, valid for three orders of magnitude beyond its peak but still considerably short of the capillary-wave region. The wavenumber dependence follows a -3.77 power law instead of the inverse-fourth. The confidence in this value is well above the statistical uncertainty of the data, and other sources of error in this calculation (such as the presence of swell) are examined and found to be negligible. This departure from inverse-fourth is sufficient to produce a factor of three higher spectral level two orders of magnitude beyond the peak, demonstrating the importance of nonlinearities in characterizing the spectrum of shorter ocean-wave scales.



INTERNATIONAL UNION OF RADIO SCIENCE

COMMISSION F

WAVE PROPAGATION AND REMOTE SENSING



PROGRAM

OPEN SYMPOSIUM

**WAVE PROPAGATION: REMOTE SENSING AND
COMMUNICATIONS**

JULY 28 - AUGUST 1, 1986

**UNIVERSITY OF NEW HAMPSHIRE
DURHAM, NEW HAMPSHIRE, USA**

SCATTERING AND DEPOLARIZATION OF LINEARLY POLARIZED
WAVES BY FINITELY CONDUCTING PARTICLES OF IRREGULAR SHAPE

Ezekiel Bahar and Mary Ann Fitzwater
Electrical Engineering Department
University of Nebraska-Lincoln NE 68588-0511

In this work the scattering and depolarization of linearly polarized waves by random distributions of finitely conducting particles of irregular shape are presented. Infrared and optical excitations of a large variety of particles with different sizes, shapes and complex dielectric coefficients are considered in detail. The random rough surface of the particle is characterized by its surface height spectral density function (or its Fourier transform the surface height autocorrelation function).

The full wave approach is used to account for both specular point scattering as well as diffuse scattering by the particle in a self-consistent manner (Bahar and Chakrabarti, *Applied Optics*, 24, No. 12, 1820, 1985), and the equation of transfer (Chandrasekar, *Radiative Transfer*, Dover, NY, 1950 and Ishimaru, *Wave Propagation and Scattering in Random Media*, Academic Press, 1978) for the modified Stokes parameters is solved using the matrix characteristic value method (Cheung and Ishimaru, *Applied Optics*, 21, No. 20, 3792, 1982). Both single scatter and multiple scatter results are given for particles with smooth and rough surfaces and the effects of particle surface roughness are considered in detail.

Both the co-polarized and cross polarized incoherent diffuse intensities are plotted as functions of the azimuth angle and the optical thickness of the layer of particles. The degree of polarization of the scattered waves is also evaluated as a function of the azimuth angle.

AGARD

ADVISORY GROUP FOR AEROSPACE RESEARCH & DEVELOPMENT

7 RUE ANCELLE 92200 NEUILLY SUR SEINE FRANCE

FALL 1986 ELECTROMAGNETIC WAVE PROPAGATION PANEL SYMPOSIUM

on

"TERRESTRIAL PROPAGATION CHARACTERISTICS IN MODERN SYSTEMS
OF COMMUNICATIONS, SURVEILLANCE, GUIDANCE AND CONTROL"

to be held in
Ottawa, Canada
20-24 October 1986

NORTH ATLANTIC TREATY ORGANIZATION



Scattering and Depolarization by Rough Terrain
and Vegetation Covered Terrain-Unified Full Wave Approach

Ezekiel Bahar
Electrical Engineering Department
University of Nebraska-Lincoln, NE 68588

ABSTRACT

Traditionally physical optics and perturbation theories have been used to derive the like and cross polarized scattering cross sections for composite random rough surfaces. To this end two-scale models have been adopted and the rough surfaces are regarded as small scale surface perturbations that are superimposed on large scale, filtered surfaces. Thus the physical optics cross section accounts for scattering by the filtered surface consisting of the large scale spectral components and the perturbation cross section accounts for scattering by the surface consisting of the small scale spectral components that ride on the filtered surface.

On applying the perturbed-physical optics approaches it is necessary to specify the wavenumber where spectral splitting is assumed to occur between the large and small scale spectral components of the rough surface. In general the restrictions on both the large and small scale surfaces cannot be satisfied simultaneously and using the perturbed-physical optics approaches the evaluation of the scattering cross sections critically depends on the specification of the wave numbers where spectral splitting is assumed to occur.

More recently the full wave approach has been used to determine the scattering cross sections for composite random rough surfaces of finite conductivity. Since the full wave solutions, which are based on a complete expansion of the fields and the imposition of exact boundary conditions, account for Bragg scattering and specular point scattering in a self-consistent manner, it is not necessary to decompose the surface into two surfaces with small and large roughness scales. However, on applying the full wave approach to evaluate the like and cross polarized scattering cross sections for two-scale models of composite rough surfaces, several assumptions were made to facilitate the computations. The assumptions are: the large and

small scale surfaces are statistically independent, the mean square slope for the total surface is approximately equal to the mean square slope for the filtered large scale surface, the mean square height of the total rough surface is large compared to a wavelength, the physical optics approximation for the cross polarized backscatter cross section is zero.

A unified formulation has also been derived for the like and cross polarized cross sections for all angles of incidence and the simplifying assumptions, that are common to all the earlier solutions based on two-scale models of the rough surface, are carefully examined.

The unified full wave solutions are formulated in terms of an integral (not integral equation) similar to the perturbation and physical optics solutions. They are shown to reduce to the physical optics solution in the high frequency limit and to the perturbation solution in the low frequency limit. The unified full wave solutions which are derived from the rigorous telegraphists' equations for wave amplitudes can also be used to account for multiple scattering by the rough surface and for the contributions to the scattered fields from the non-illuminated or non-visible portions of the rough surface.

The full wave approach has also been applied recently to problems of scattering and depolarization by arbitrarily oriented discrete scatterers of finite conductivity characterized by their surface height spectral density functions. Therefore using the unified full wave approach it is possible to analyze more realistic models of propagation paths over the earth's surface. At microwave frequencies the vegetation that covers the terrain can be represented by distributions of discrete randomly oriented scatterers rather than by a dielectric layer with an "effective complex permittivity" or an "effective surface impedance."

29th Midwest Symposium on Circuits and Systems

August 11-12, 1986

Lincoln, Nebraska

APPLICATION OF FULL WAVE THEORY
TO COMPUTER AIDED GEOMETRIC DESIGN

Ezekiel Bahar
and
Swapan Chakrabarti

Department of Electrical Engineering
194 W Nebraska Hall
University of Nebraska-Lincoln
Lincoln NE 68588

Over the period of the last decade, reflection models, for computer generated synthetic images, have been considerably improved in order to generate very realistic images of three dimensional objects on two dimensional screens. In almost all of the existing models the reflecting surface is assumed to be a small-scale, random rough surface superimposed upon a smooth large-scale surface. Reflection from the smooth large-scale surface is characterized by the Fresnel reflection coefficients and scattering from the small scale rough surface is accounted for by Lambert's cosine law.

In this presentation a full wave scattering theory is reviewed and the corresponding reflection model for computer generated synthetic images is presented.

The full wave theory is based on a complete spectral representation of the scattered vertically and horizontally polarized fields and the imposition of exact boundary conditions at the irregular surface. This theory accounts for both specular reflection and diffuse reflection in a unified self-consistent manner.

The height of the random rough surface is measured normal to the large-scale, smooth, deterministic surface and the mean square height

of the random rough surface, $\langle h^2 \rangle$, need not be restricted by the perturbation condition $\beta = 4k_0^2 \langle h^2 \rangle \ll 1$ (where k_0 is the free space wave number). However, the mean square slope of the random rough surface (relative to the large scale smooth surface) is assumed to be small ($\sigma_s^2 \leq 0.1$). Hence for convex shapes (as in cylinders, spheres or cones) multiple scattering between different surface elements of the object is ignored.

The scattering model based on the full wave theory significantly reduces computation time of the simulated image without any loss in the image quality. Use of the full wave theory facilitates the location of the isointensity lines. This is a very important asset to computer aided geometric design of manufactured objects.

Since the model is based on a rigorous full wave approach to electromagnetic scattering, it is applicable to the inverse scattering, computer vision problem in which three dimensional surfaces are identified by analyzing their two dimensional images.

CO-POLARIZED AND CROSS-POLARIZED
INCOHERENT DIFFUSE SPECIFIC INTENSITIES
FOR LINEARLY POLARIZED EXCITATIONS
OF IRREGULARLY SHAPED PARTICLES

by

Dr. E. Bahar

at

1986 CRDC Scientific Conference
on Obscuration and Aerosol Research

June 23-27, 1986

Aberdeen, Maryland

EXTINCTION CROSS SECTIONS AND ALBEDOS
FOR PARTICLES WITH VERY ROUGH SURFACES

presented by

Dr. E. Bahar

at

1986 CRDC Scientific Conference
on Obscuration and Aerosol Research

June 23-27, 1986

Aberdeen, Maryland

END

DATE
FILMED

9 - 86

DTIC